ENVIRONMENTAL MONITORING AND REMEDIATION USING MICROBIOTECHNOLOGY

EDITED BY: Tian Li, Lean Zhou, Xiaojing Li, Li Yuan and Wei Zhi

PUBLISHED IN: Frontiers in Microbiology and
Frontiers in Environmental Science

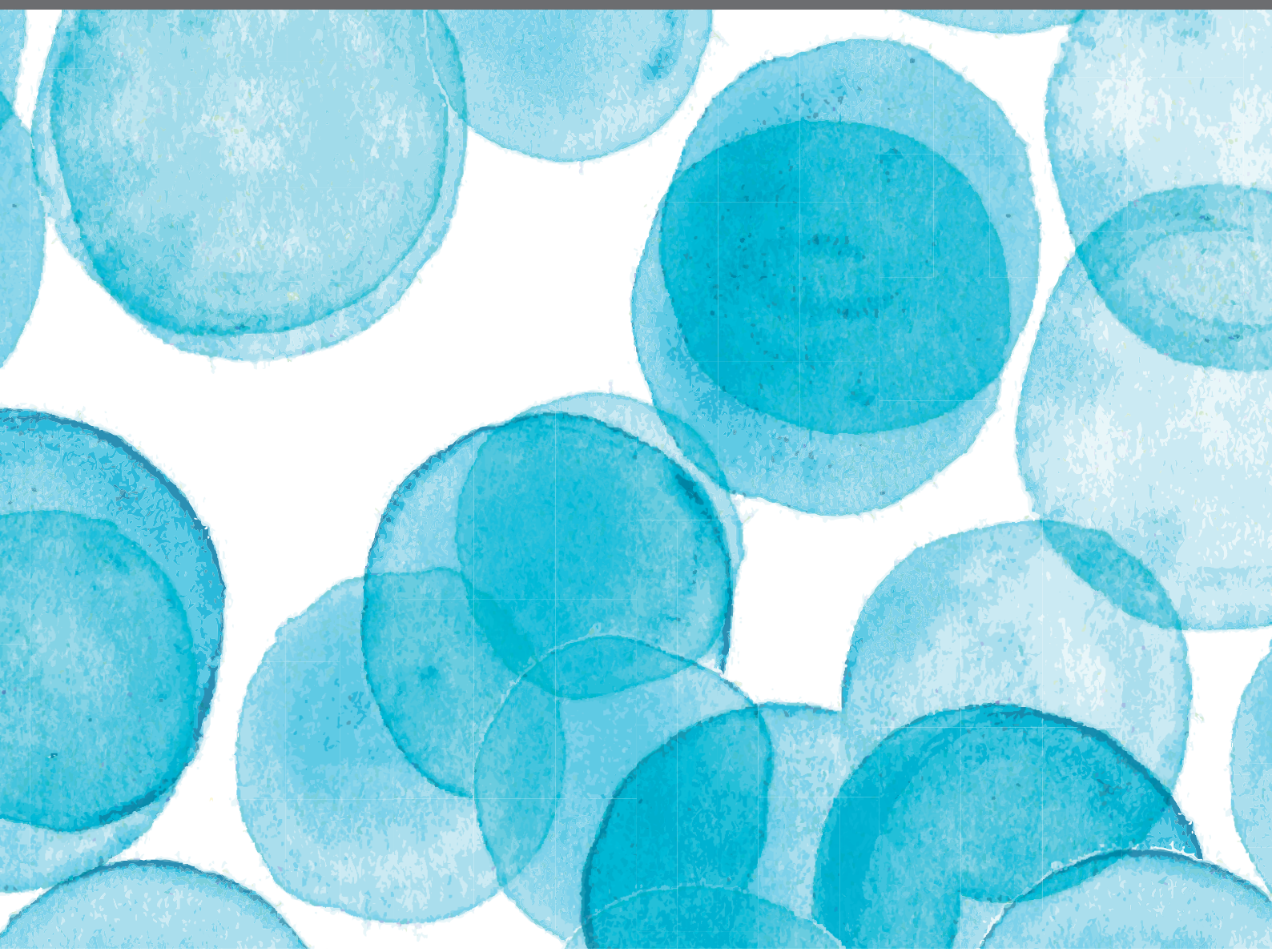

frontiers Research Topics

frontiers

ISSN 1664-8714
ISBN 978-2-88976-282-8
DOI 10.3389/978-2-88976-282-8

About Frontiers

Frontiers is more than just an open-access publisher of scholarly articles: it is a pioneering approach to the world of academia, radically improving the way scholarly research is managed. The grand vision of Frontiers is a world where all people have an equal opportunity to seek, share and generate knowledge. Frontiers provides immediate and permanent online open access to all its publications, but this alone is not enough to realize our grand goals.

Frontiers Journal Series

The Frontiers Journal Series is a multi-tier and interdisciplinary set of open-access, online journals, promising a paradigm shift from the current review, selection and dissemination processes in academic publishing. All Frontiers journals are driven by researchers for researchers; therefore, they constitute a service to the scholarly community. At the same time, the Frontiers Journal Series operates on a revolutionary invention, the tiered publishing system, initially addressing specific communities of scholars, and gradually climbing up to broader public understanding, thus serving the interests of the lay society, too.

Dedication to Quality

Each Frontiers article is a landmark of the highest quality, thanks to genuinely collaborative interactions between authors and review editors, who include some of the world's best academicians. Research must be certified by peers before entering a stream of knowledge that may eventually reach the public - and shape society; therefore, Frontiers only applies the most rigorous and unbiased reviews.
Frontiers revolutionizes research publishing by freely delivering the most outstanding research, evaluated with no bias from both the academic and social point of view. By applying the most advanced information technologies, Frontiers is catapulting scholarly publishing into a new generation.

What are Frontiers Research Topics?

Frontiers Research Topics are very popular trademarks of the Frontiers Journals Series: they are collections of at least ten articles, all centered on a particular subject. With their unique mix of varied contributions from Original Research to Review Articles, Frontiers Research Topics unify the most influential researchers, the latest key findings and historical advances in a hot research area! Find out more on how to host your own Frontiers Research Topic or contribute to one as an author by contacting the Frontiers Editorial Office: frontiersin.org/about/contact

ENVIRONMENTAL MONITORING AND REMEDIATION USING MICROBIOTECHNOLOGY

Topic Editors:
Tian Li, Nankai University, China
Lean Zhou, Changsha University of Science and Technology, China
Xiaojing Li, Agro-Environmental Protection Institute (CAAS), China
Li Yuan, University of Science and Technology of China, China
Wei Zhi, The Pennsylvania State University (PSU), United States

Citation: Li, T., Zhou, L., Li, X., Yuan, L., Zhi, W., eds. (2022). Environmental Monitoring and Remediation Using Microbiotechnology.
Lausanne: Frontiers Media SA. doi: 10.3389/978-2-88976-282-8

Table of Contents

frontiers | Frontiers in Microbiology

EDITORIAL
published: 13 May 2022
doi: 10.3389/fmicb.2022.927867

Editorial: Environmental Monitoring and Remediation Using Microbiotechnology

Tian Li[1]*, *Lean Zhou*[2], *Xiaojing Li*[3], *Li Yuan*[4] and *Wei Zhi*[5]

[1] Ministry of Education (MOE) Key Laboratory of Pollution Processes and Environmental Criteria/Tianjin Key Laboratory of Environmental Remediation and Pollution Control/College of Environmental Science and Engineering, Nankai University, Tianjin, China, [2] School of Hydraulic and Environmental Engineering, Changsha University of Science and Technology, Changsha, China, [3] Agro-Environmental Protection Institute, Ministry of Agriculture and Rural Affairs/Key Laboratory of Original Agro-Environmental Pollution Prevention and Control, Ministry of Agriculture and Rural Affairs (MARA)/Tianjin Key Laboratory of Agro-Environment and Agro-Product Safety, Tianjin, China, [4] Chinese Academy of Sciences (CAS) Key Laboratory of Urban Pollutant Conversion, Department of Environmental Science and Engineering, University of Science and Technology of China, Hefei, China, [5] Department of Civil and Environmental Engineering, Pennsylvania State University, University Park, PA, United States

Keywords: environmental monitoring, environmental remediation, microbiotechnology, wastewater treatment, modeling design

Editorial on the Research Topic

Environmental Monitoring and Remediation Using Microbiotechnology

With the continuous improvement of the level of scientific and technological innovation, many emerging materials and chemicals have come into our lives, which has brought great pressure to the environment and caused an increasing number of contamination problems (Atashgahi et al., 2018; Escher Beate et al., 2020; Johnson Andrew et al., 2020). Microbiotechnology is considered to be environmentally friendly and sustainable when dealing with contaminants and has been attracting tremendous attention (Ahmed et al., 2021; Li et al., 2021, 2022b). Considering the degradation period of contaminants and the mechanism conducted by microbes, oxidation and reduction reactions occur all the time, providing the most basic support for early warning and remediation using microbiotechnology (Li et al., 2018, 2022a; Zhang et al., 2021). The appearance of contaminants is bound to break the balance of the original ecological environment, so how to monitor the existence of contaminants online, *in situ*, and quickly will become one of the key issues in the early warning field, and how to realize the efficient degradation of contaminants by microbes will become one of the key difficulties in remediation field.

In this special issue, we set up the Research Topic of *Environmental Monitoring and Remediation Using Microbiotechnology* in the journal of *Front. Microbiol.*, which had attracted a lot of attention from researchers. This topic mainly focuses on the monitoring and remediation of contaminants in water, sediment, and soil using microbes and the mechanisms of the interaction between microbes and the surrounding environment. For early warning of contamination using microbes, various signals can be collected: bioelectrical signals through electron transfer, biochemical signals through material coupling, or biophysical signals through matrix changes. As for the remediation using microbes, pure bioremediation, phyto-bioremediation, electrically/chemically driven bioremediation and other improved bioremediations are well described. The continuous challenge is to design the processes to include nutrient recovery, which will be aided by further exploration through the interface between microbes and contaminants.

Specifically, 18 papers were accepted and published on this Research Topic, which was contributed by 118 authors from around the world. The papers that were viewed more than 2,000 times were from *Transcriptome-Guided Insights Into*

Edited and reviewed by:
William James Hickey, University of Wisconsin-Madison, United States

***Correspondence:**
Tian Li
tianli1@nankai.edu.cn

Specialty section:
This article was submitted to Microbiotechnology, a section of the journal Frontiers in Microbiology

Received: *25 April 2022*
Accepted: *02 May 2022*
Published: *13 May 2022*

Citation:
Li T, Zhou L, Li X, Yuan L and Zhi W (2022) Editorial: Environmental Monitoring and Remediation Using Microbiotechnology. Front. Microbiol. 13:927867. doi: 10.3389/fmicb.2022.927867

Plastic Degradation by the Marine Bacterium contributed by Kumari et al., *Advances in Studies on Microbiota Involved in Nitrogen Removal Processes and Their Applications in Wastewater Treatment* contributed by Mai et al. and *An Ultrafast One-Step Quantitative Reverse Transcription–Polymerase Chain Reaction Assay for Detection of SARS-CoV-2* contributed by Milosevic et al. The research directions of these papers were the hot spot in the current environment. The first paper focused on microplastic degradation by microorganisms. Through the detection of PET hydrolysates, the genes of degraded PET were identified and cloned as an environmentally friendly solution to improve the utilization of PET by microbial systems. The second paper reviewed the microflora, pathways and related functional genes involved in nitrogen removal, and discussed the methods to improve nitrogen removal efficiency in the microbial treatment of industrial wastewater (Mai et al.). The third paper developed an ultrafast one-step RT-qPCR assay for SARS-CoV-2 detection, which significantly reduces the running time of conventional RT-qPCR (Milosevic et al.). Meanwhile, other papers also included the studies on modeling design, pollutant degradation and greenhouse gas emissions, which also covered water, soil and constructed wetlands involved with microorganisms. There was only one review paper among the remaining 15 papers, entitled *A Review on Microorganisms in Constructed Wetlands for Typical Pollutant Removal: Species, Function, and Diversity*. In this review, an in-depth bibliometric analysis of microbial studies in constructed wetlands (CWs) was performed to evaluate research trends and identify the most studied pollutants, which could provide new ideas and directions for the research of microorganisms in CWs (Wang et al.).

Four papers focus on bacterial isolates against different contaminants and harmful substances, including atrazine, Nitrogen, *Karenia mikimotoi*, and Roxarsone. In the study of Jia et al., *Paenarthrobacter* sp. AT-5, an atrazine-degrading strain, was inoculated into agricultural soils contaminated with atrazine to investigate the bioaugmentation process and the reassembly of the soil microbiome. They reported that the inoculation of strain AT-5 significantly affected the community structure of the soil microbiome, and the abundances of bacteria associated with atrazine degradation were improved (Jia et al.). Sun et al. prepared biochar/clay composite particle (BCCP) as the carrier to immobilize *Ochrobactrum* sp. to consume ammonium nitrogen (NH_4^+-N), and the effects of the calcined program and immobilizing material were investigated. Ding et al. investigated the biochemical and physiological responses of *K. mikimotoi* to the algicidal bacterium *Paracoccus homiensis* O-4. The effects on the levels of reactive oxygen species (ROS), malondialdehyde content, multiple antioxidant systems and metabolites, photosynthetic pigments, and photosynthetic index were also examined. This research provides insights into the prophylaxis and control of harmful algal blooms *via* interactions between harmful algae and algicidal bacteria (Ding et al.). In the study of Li W. et al., wheat-straw-derived biochar was used to investigate how biochar amendment affected *Shewanella oneidensis* MR-1 growth and roxarsone transformation in water under anaerobic conditions. Their results suggested that wheat-straw-derived biochar may be an important agent for activating microbial growth and can be used to accelerate the transformation of roxarsone, which could be a novel strategy for roxarsone remediation (Li W. et al.). In addition to studies of pure bacteria, there are also studies of mixed bacteria. Mao et al. assessed the microbiological effects of black carbon (BC) by using a fluorescent fingerprinting assay based on flow cytometry (FCM) of bacterial communities with low (LNA) and high (HNA) nucleic acid-content bacteria. They also investigated a high-resolution temporal variation of bacterial abundance and LNA/HNA ratio in Tibetan ice cores and revealed that bacterial abundance was proportional to the atmospheric BC on the glaciers. In the study of Song et al., the biodiversity and functional characteristics of microplastic-attached biofilms originating from two freshwater bacterial communities were reported. The results from 16S rRNA amplicon sequencing showed that the dynamic biofilm successions on different microplastics were highly dissimilar. This study also speculated that more symbionts and parasites colonized microplastics in the tap water than in the lake water (Song et al.). Fungal research is also reflected in this special issue. Zhou et al. demonstrated the effect of Arbuscular mycorrhizal fungi (AMF) on the uptake and transport of Stibium (Sb) in the soil–rice system, facilitating future research on the related mechanism in the soil–rice system under Sb stress. Zhong et al. reported that fungi were dominant in N_2O production processes followed by archaea in Northern Chinese grasslands and the key variables of N_2O production and the nitrogen (N) cycle depended on the dominant microbial functional groups in the N-cycle in soils. Moreover, the study of Liu et al. explored the effects of environmental factors on the longitudinal plankton patterns, through a 5-year-long study on the environmental factors and communities of phytoplankton and zooplankton in an alpine cascade reservoir system located upstream of the Yellow River region.

Different pollutants are also discussed as research priorities, including chemical oxygen demand (COD), polycyclic aromatic hydrocarbons (PAHs), crystal violet, methylene blue, etc. In the research of Huang et al., a mathematical simulation model was established to investigate the performance of a full-scale anaerobic biochemical system for treating the COD in deinking pulp wastewater. Wang et al. investigated the adsorption mechanism of crystal violet and methylene blue and performed the extraction of activated carbon (AC) and AC-based ZVI by solid-phase and liquid-phase reduced approaches. Huang et al. explored the performance of denitrification deep-bed filter (DN-DBF) to treat municipal sewage and investigated the metabolic pathway for meeting a more stringent discharge standard of total nitrogen (TN). Li Y. et al. explained the influence mechanism of soil salinity on PAH biodegradation from the perspective of degradation genes and soil enzyme activities. In the study of Guo et al., a colorimetric enzyme biosensor was developed for one-step detection of hypoxanthine (Hx), which provided a robust advantage in the economic reaction system, ease of preparation, short time consumption, and moderate reaction temperature compared with other methods.

With the emergence of new pollutants and the continuous improvement of environmental standards, environmental pollution monitoring and remediation will be paid more and more attention. How to realize *in-situ* monitoring and efficient remediation will be a problem worthy of attention in the future.

AUTHOR CONTRIBUTIONS

TL wrote this editorial note. All authors edited the final text and contributed to the article and approved the submitted version.

ACKNOWLEDGMENTS

We thank all authors and reviewers for their contributions, as well as the Journal Committee for providing the opportunity to establish the Research Topic.

REFERENCES

Ahmed, S. F., Mofijur, M., Nuzhat, S., Chowdhury, A. T., Rafa, N., Uddin, M. A., et al. (2021). Recent developments in physical, biological, chemical, and hybrid treatment techniques for removing emerging contaminants from wastewater. *J. Hazard. Mater.* 416, 125912. doi: 10.1016/j.jhazmat.2021.125912

Atashgahi, S., Sánchez-Andrea, I., Heipieper Hermann, J., van der Meer Jan, R., Stams Alfons, J. M., and Smidt, H. (2018). Prospects for harnessing biocide resistance for bioremediation and detoxification. *Science* 360, 743–746. doi: 10.1126/science.aar3778

Escher Beate, I., Stapleton Heather, M., and Schymanski Emma, L. (2020). Tracking complex mixtures of chemicals in our changing environment. *Science* 367, 388–392. doi: 10.1126/science.aay6636

Johnson Andrew, C., Jin, X., Nakada, N., and Sumpter John, P. (2020). Learning from the past and considering the future of chemicals in the environment. *Science* 367, 384–387. doi: 10.1126/science.aay6637

Li, R., Li, T., Wan, Y., Zhang, X., Liu, X., Li, R., et al. (2022a). Efficient decolorization of azo dye wastewater with polyaniline/graphene modified anode in microbial electrochemical systems. *J. Hazard. Mater.* 421, 126740. doi: 10.1016/j.jhazmat.2021.126740

Li, R., Wang, J., Li, T., and Zhou, Q. (2022b). Recent advances in improving the remediation performance of microbial electrochemical systems for contaminated soil and sediments. *Crit. Rev. Environ. Sci. Technol.* 1–24. doi: 10.1080/10643389.2022.2040327

Li, T., Li, R., and Zhou, Q. (2021). The application and progress of bioelectrochemical systems (BESs) in soil remediation: a review. *Green Energy Environ.* 6, 50–65. doi: 10.1016/j.gee.2020.06.026

Li, T., Wang, X., Zhou, Q., Liao, C., Zhou, L., Wan, L., et al. (2018). Swift acid rain sensing by synergistic rhizospheric bioelectrochemical responses. *ACS Sensors* 3, 1424–1430. doi: 10.1021/acssensors.8b00401

Zhang, X., Li, R., Song, J., Ren, Y., Luo, X., Li, Y., et al. (2021). Combined phyto-microbial-electrochemical system enhanced the removal of petroleum hydrocarbons from soil: a profundity remediation strategy. *J. Hazard. Mater.* 420, 126592. doi: 10.1016/j.jhazmat.2021.126592

Conflict of Interest: The authors declare that the research was conducted in the absence of any commercial or financial relationships that could be construed as a potential conflict of interest.

Publisher's Note: All claims expressed in this article are solely those of the authors and do not necessarily represent those of their affiliated organizations, or those of the publisher, the editors and the reviewers. Any product that may be evaluated in this article, or claim that may be made by its manufacturer, is not guaranteed or endorsed by the publisher.

frontiers in Microbiology

ORIGINAL RESEARCH
published: 21 September 2021
doi: 10.3389/fmicb.2021.755398

Modeling the Performance of Full-Scale Anaerobic Biochemical System Treating Deinking Pulp Wastewater Based on Modified Anaerobic Digestion Model No. 1

Yifeng Huang[1], Yongwen Ma[1,2,3], Jinquan Wan[1,2,3] and Yan Wang[1,3]*

[1] School of Environment and Energy, South China University of Technology, Guangzhou Higher Education Mega Center, Guangzhou, China, [2] Sino-Singapore International Joint Research Institute, Guangzhou, China, [3] Guangdong Plant Fiber High-Valued Cleaning Utilization Engineering Technology Research Center, Guangzhou, China

The deinking pulp (DIP) is a main resource for paper making, and the wastewater from DIP process needs to be treated. Anaerobic biochemical technique has been widely applied in DIP wastewater treatment, due to the remarkable capability in reducing high chemical oxygen demand (COD). In this study, a mathematical simulation model was established to investigate the performance of a full-scale anaerobic biochemical system for treating DIP wastewater. The model was based on Anaerobic Digestion Model No. 1 (ADM1), which was modified according to the specific anaerobic digestion process for DIP wastewater treatment. The hydrodynamic behavior of a full-scale anaerobic biochemical system was considered in this model. The characteristics of the influent DIP wastewater were assessed, and then, the substrate COD proportion was divided successfully for the necessity of ADM1 applying. The Monte Carlo technique was implemented to distinguish the most sensitive parameters that influenced the model output indicators comprising effluent COD and biogas production. The sensitive parameters were estimated and optimized. The optimized value of $k_{\_m\_pro}$ is 12.02, $K_{\_S\_pro}$ is 0.35, $k_{\_m\_ac}$ is 4.26, $K_{\_S\_ac}$ is 0.26, $k_{\_m\_h2}$ is 16.62, and $K_{\_S\_h2}$ is 3.21×10^{-5}. The model was calibrated with 150 days operation values measured in the field. The subsequent 100 days on-site values were used to validate the model, and the results obtained by the simulations were in good agreement. This study provides a meaningful and theoretical model guidance for full-scale wastewater anaerobic biochemical treatment simulation.

Keywords: anaerobic digestion, deinking pulp wastewater, full-scale anaerobic reactor, Anaerobic Digestion Model No. 1 (ADM1), anaerobic biochemical treatment

OPEN ACCESS

Edited by:
Lean Zhou,
Changsha University of Science and Technology, China

Reviewed by:
Fansheng Meng,
Tianjin Chengjian University, China
Xizi Long,
National Institute for Materials Science, Japan

****Correspondence:***
Yongwen Ma
ppywma@scut.edu.cn

Specialty section:
This article was submitted to Microbiotechnology, a section of the journal Frontiers in Microbiology

Received: *08 August 2021*
Accepted: *30 August 2021*
Published: *21 September 2021*

Citation:
Huang Y, Ma Y, Wan J and Wang Y (2021) Modeling the Performance of Full-Scale Anaerobic Biochemical System Treating Deinking Pulp Wastewater Based on Modified Anaerobic Digestion Model No. 1. Front. Microbiol. 12:755398. doi: 10.3389/fmicb.2021.755398

INTRODUCTION

Due to the shortage of raw fiber from wood, wastepaper recycling has become an important source of pulp and paper production (Saxena and Singh Chauhan, 2017; Ozgun, 2019). The deinking pulp (DIP) process is an essential component of wastepaper recycling, which involves the removal of ink from printed paper (Xu et al., 2011). Large amounts of wastewater are inevitably produced by the deinking process, which needs to be treated carefully (Song et al., 2018). The amount of wastewater

produced by pulp and wastepaper treatment was estimated to have grown by 60% from 2012 to 2020 (Meyer and Edwards, 2014). It was estimated that 400 million tons of paper were produced annually, and the wastewater is 10∼100 m^3 per ton of pulp and paper production (Irizar et al., 2018). Various strategies such as flotation, sedimentation, filtration, and aerobic activated sludge have been utilized to DIP wastewater treatment (Simstich et al., 2012; Irizar et al., 2018). In last two decades, the application of anaerobic digestion (AD) to the treatment of wastewater with high organic contents has grown rapidly, including wastewater produced from pulp and paper making. AD is a biological process that involves the transformation of organic compounds into biogas under an oxygen-free state, where the reduction in the chemical oxygen demand (COD) is up to 80% (Buzzini and Pires, 2002). In addition, the biogas, a byproduct from AD process, is a profitable green fuel (Kamali et al., 2016; Wu et al., 2019, 2020).

Previous researches showed that, because of the difficulty of biochemical degradation or decomposition of ingredients in high organic wastewater, pre-acidification process was employed to promote biodegradability with a short hydraulic residence time (HRT) in anoxia state (Çalışkan and Azbar, 2017; Diamantis and Aivasidis, 2018; Wu et al., 2020). After pre-acidification, the high organic wastewater will always be treated by the anaerobic biochemical reactor, which plays a key role in the removal of COD concentration (Sarathai et al., 2010). The internal circulation (IC) reactor is a specific representative type of high-rate anaerobic biochemical reactor, which can be viewed as two upflow anaerobic sludge blanket (UASB) reactors stacked together. In contrast to the 15 kg COD m^{-3} d^{-1} loading of UASB, the organic loading rate capacity of IC is up to 20–50 kg COD m^{-3} d^{-1} (Rajagopal et al., 2013; Karadag et al., 2015; Wang et al., 2015; Hamza et al., 2016). The IC reactor has been widely utilized in industrial wastewater anaerobic treatment, such as beer production (Chen et al., 2021), cotton pulp manufacturing (Cui et al., 2011), food processing (Guo et al., 2018), and paper making (Irizar et al., 2018), etc.

Mathematical models have been applied broadly in wastewater treatment for simulation (Feldman et al., 2017), design (Flores-Alsina et al., 2012), supervision (Rodriguez-Roda et al., 2002), optimization (Rivas et al., 2008), and even benchmark control (Gernaey et al., 2014). Compared with aerobic biochemical process, AD process is much more complicated and often easily disrupted by several adverse factors, for example, organic overload, acute temperature variance, or the presence of inhibitory substances, etc. For these reasons, the wastewater plants have to adopt a larger reactor, or to utilize on-site monitoring device. But the larger reactor needs more cost, and the lack of reliable, unfeasible and cost saving limits the application of on-site device. Therefore, AD models have been used to indirectly provide profitable information about the operation condition of the reactor (Irizar et al., 2018). Several types of models have been proposed for describing the details of the AD process (Diez Blanco et al., 1995; Chen et al., 2016). In particular, Anaerobic Digestion Model No. 1 (ADM1) published by the International Water Association (IWA) task group in 2002 (Batstone et al., 2002), has expanded rapidly to even became a *de facto* standard model for AD simulation (Lier et al., 2015). ADM1 is a structural model that comprises 19 steps for defining biochemical processes, where physico-chemical equations are used to describe ion association/dissociation and gas–liquid phase transfer (Batstone et al., 2015; Rubio et al., 2020).

The originally reported example of the application of ADM1 involved a completely stirring tank with a constant volume and unidirectional influent–effluent stream (Batstone et al., 2002). Most of previous studies that used ADM1 were conducted at the lab-scale, where it was assumed that the ingredients were uniformly or homogeneously distributed in the AD devices (Naessens et al., 2012; Yu et al., 2012; Van Hulle et al., 2014; Chen et al., 2015; Poblete et al., 2020). The hydraulic behavior of these reactors could be simplified as complete stirring because of their small size (Lauwers et al., 2013). However, Batstone et al. (2005) found a scaling effect between a lab-scale UASB reactor and a full-scale one. Van Hulle et al. (2014) stated that a corrected description of the mixing behavior of a full-scale AD reactor is required to simulate the reactor's performance in an appropriate manner. An incorrect description of the hydraulic behavior of a full-scale reactor would lead to over-calibration of the stoichiometric and kinetic parameters of the model, thereby affecting the experimental results (Uggetti et al., 2010; Liotta et al., 2015). Consequently, the hydraulic behavior of the full-scale AD reactor should be considered when ADM1 is applied for simulation. As far as now, most previous applications of ADM1 focused on lab-scale studies and few have considered full plant-wide application of ADM1.

In the present study, we aimed to develop a simulation method to model the performance of an anaerobic biochemical system treating DIP wastewater. The system comprised an anaerobic pre-acidification tank connected to a full-scale IC reactor at a pulp and paper mill that is located in Guangzhou City (Guangdong Province, China; **Supplementary Figure 1**). The model of pre-acidification process has few been fully research.

According to the running status of this anaerobic biochemical system and some previous researches (Feldman et al., 2017, 2019; Irizar et al., 2018), a single continuous stirred tank reactor (CSTR) was used to represent the hydrodynamics of the pre-acidification tank and a series of CSTRs was applied to represent that of the full-scale IC reactor. ADM1 was integrated with these hydrodynamic models in the simulation method, which we utilized to simulate the reduction of the COD content and biogas production in this system. Furthermore, components of the influent DIP wastewater were classified based on the theoretical assumptions of the IWA task group. The results showed that this model was effective at simulating the performance of a full plant-wide anaerobic biochemical system treating wastewater. As far as we know, no similar study has been published previously.

MATERIALS AND METHODS

Overview of Deinking Pulp Wastewater Treatment Plant

The DIP process of this pulp and paper mill is based on a commonly used chemical deinking technique. According to the actual production condition, a maximum 20,000 m^3 day^{-1} of

high-concentration DIP wastewater need to be treated, the COD of which is over 2000 mg L^{-1}.

The DIP wastewater treatment plant has four main sections. Firstly, large particulate pollutants are removed from the DIP wastewater in the physical pre-treatment section. Next, fine particles and dissolved pollutants are absorbed, converted, and reduced in the anaerobic biochemical treatment section that includes an anaerobic pre-acidification tank and an anaerobic biochemical IC reactor. The COD content of the DIP wastewater is mostly converted and degraded there. Then, the wastewater enters an aerobic treatment system section followed by an advanced oxidation section for further treatment. Finally, the wastewater satisfies the local effluent standard and it is discharged.

Deinking Pulp Wastewater Quality

This mill utilizes recycled wasted newspapers and magazines, accounted for about 80 and 20%, respectively, to produce high-end newsprint. The raw DIP wastewater has to been purified in DIP wastewater treatment plant. The main quality indicators for the raw DIP wastewater are shown in **Supplementary Table 1**.

After filtering and settling in the physical pre-treatment section, large particles such as shredded paper, large fiber particles, inorganic filler blocks, and residual ink are removed from the raw DIP wastewater. After that, the DIP wastewater that enters the anaerobic biochemical treatment section mainly comprises fine fiber particles, soluble cellulose (solubilized fiber), surfactants (fatty acid organics from deinking agents), and fine ink particles. The color of the wastewater is grayish yellow at this stage. Through long-term observations, the effluent water quality indicators after anaerobic biochemical system treatment are listed in **Supplementary Table 2**.

Wastewater Characterization

The main application objective of ADM1 developed by IWA is to model the AD process for waste activated sludge from sewage treatment plant. The input variables in the model are related to the compositions of the particulate materials. Therefore, two crucial issues must be addressed when using ADM1 to simulate the AD treatment of various types of substrates or organic wastewater. The first one is how to separate and classify the inflow components, where the input variables for the model must be determined according to the inflow substrates. The other one is how to select the values for the parameter set, where it is first necessary to estimate the sensitive kinetic parameters in the model, before then to calibrate them (Kleerebezem and Van Loosdrecht, 2006; Girault et al., 2012). In the following, we describe the theoretical assumptions of ADM1, as well as the separation and classification of the influent substrates in DIP wastewater. These classification assumptions and methods of inflow components are given in **Supplementary SI1**.

In the actual wastewater treatment process, the wastewater components are not consistent at all times. The pollutant components may differ within a certain range according to the variations in the mill's production status. Clearly, none of the assessment methods described above can provide real-time information regarding the wastewater components. In particular, the component interpretation method might not be capable of completely and accurately classifying the COD components. However, the average measurement results obtained based on multiple samples can be used to represent the actual composition. In addition, the component interpretation method is relatively simple to conduct and the detection results can be applied to determine the contents of different components, before classifying and interpreting the COD components of the reactor influent. For these reasons, the component interpretation method was applied in the present study.

Model Development

According to ADM1 released by IWA, the AD processes involve disintegration, hydrolysis, acidogenesis, acetogenesis, and methanogenesis (Batstone et al., 2002). Among these stages, disintegration and hydrolysis are extracellular processes conducted by bacteria. The actions of extracellular enzymes decompose macromolecular organic matter into proteins, carbohydrates, and lipids, which are subsequently hydrolyzed into monosaccharides, amino acids, long-chain fatty acids (LCFAs), and other molecules. Monosaccharides and amino are absorbed in the acidogenesis step, and then converted into VFAs and hydrogen. Subsequently, LCFA and VFAs are transformed into acetate at the acetogenesis step. Finally, acetate and hydrogen are transformed into CH_4 or CO_2 in methanogenesis step (**Supplementary Figure 2**).

Development of the Anaerobic Pre-acidification Tank Model

Previous research and experience of wastewater engineering have shown that pre-hydrolysis and pre-acidification before fully anaerobic biochemical treatment are beneficial of materials such as industrial organic wastewater derived from food, tanning, pulp, printing, dyeing, and pharmaceutical production (Ahn et al., 2001; Diamantis and Aivasidis, 2018; Al-Rubaye et al., 2020; Wu et al., 2020). Because an anaerobic or facultative pre-treatment section with a relatively short HRT, before subsequent fully anaerobic treatment, can enhance the biodegradability of wastewater. The explanation for anaerobic biological mechanism of pre-hydrolysis (pre-acidification) is provided in **Supplementary SI2**.

The maximum volume of the pre-acidification tank in used is 2250 m^3. The tank is equipped with a hyperboloid mixer, which forms a continuous fully mixed interior hydrodynamic state. The DIP wastewater is acidified for almost 2 h here. Due to the short HRT and hydraulic state, the retention of methanogenic bacteria and accumulation of bacteria do not occur in the tank. In general, methanogenesis does not occur in the tank. As seen in **Supplementary Figure 2**, the anaerobic biochemical processes happening in pre-acidification tank involve disintegration, hydrolysis, acidogenesis, and acetogenesis. In addition, according to ADM1 released by IWA, the equations for modeling the biochemical reactions in the pre-acidification tank are expressed as follows:

$$\frac{dS_{i,a}}{dt} = \frac{Q_{inf}}{V_a}\left(S_{i,in} - S_{i,a}\right) + \sum_{k=1}^{15} \upsilon_{i,k}\rho_k \quad (1)$$

$$\frac{dX_{i,a}}{dt} = \frac{Q_{inf}}{V_a}\left(X_{i,in} - X_{i,a}\right) + \sum_{k=1}^{15} \upsilon_{i,k}\rho_k \quad (2)$$

Where $\frac{dS_{i,a}}{dt}$ and $\frac{dX_{i,a}}{dt}$ represent the time derivatives of the soluble and particulate substrates in the tank, respectively, Q_{inf} is the feed flow rate (m^3 day^{-1}), V_a is the pre-acidification tank volume (V_a = 750 m^3), $S_{i,in}$ and $X_{i,in}$ are the soluble and particulate substrates in the feed flow (kgCOD m^{-3}), and $S_{i,a}$ and $X_{i,a}$ represent the soluble and particulate substrates in the tank (kgCOD m^{-3}). Moreover, the term $\sum_{k=1}^{15} \upsilon_{i,k}\rho_k$ represents the sum of the kinetic rates for process k multiplied by the rate coefficients ($\upsilon_{i,k}$). It is assumed that methanogenesis does not occur in the pre-acidification tank, so all of the processes proposed by IWA are involved, except for the uptake of acetate and hydrogen, and the decay of aceticlastic methanogens (X_{ac}) and hydrogen-utilizing methanogens (X_{h2}). These uptake and decay processes are considered to be related to methanogenesis.

Development of the Internal Circulation Reactor Simulation Model

Chen et al. (2021) who analyzed a full-scale IC reactor treating brewery wastewater, found that the bacterial community was significantly different at the diverse layers. The fermentation and acidification were mainly accomplished at bottom layer, but methane production was achieved at upper and middle layers. Recent studies (Feldman et al., 2017; Irizar et al., 2018) divided the hydrodynamics of the full-scale IC reactor into three CSTRs in series.

The size (height and diameter) of the full-scale IC reactor under researched is φ 24 m × 12.5 m. The design volume is 2900 m^3, and the active volume is almost 2250 m^3. The wastewater would retain approximately 8 h for anaerobic treating. Hence, we divided this reactor into three layers and CSTRs in series based on the internal state of the reactor. The bottom of the reactor retains large sludge granules. The sludge granules expand and fluidize in the middle part, and a small amount of floating sludge is present at the top part. The internally generated biogas is separated by gas–liquid–sludge separators and then collected by a gas collection tank in the headspace. The internal states of the reactor and three CSTRs in series in the separate models are illustrated in **Figure 1**.

The full ADM1 released by IWA was applied to simulate the biochemical reaction for each CSTR. The reaction equations for each CSTR and the diffusion equation for the gas phase under constant volume of gas in the gas collection tank, respectively, are given as follows:

$$\frac{dS_{i.c}}{dt} = \frac{Q_{inf}}{V_c}\left(S_{i,in} - S_{i,c}\right) + \sum_{i=1}^{19} \upsilon_{i,j}\rho_j + \text{transport terms} \quad (3)$$

$$\frac{dX_i, c}{dt} = \frac{Q_{inf}}{V_c}X_{i,in} - \frac{X_{i,c}}{t_{res,X} + \frac{V_c}{Q_{inf}}} + \sum_{i=1}^{19} \upsilon_{i,j}\rho_j \quad (4)$$

$$\frac{dS_{gas,i}}{dt} = -\frac{S_{gas,i}Q_{gas}}{V_{gas}} + \rho_{T,i}\frac{V_c}{V_{gas}}, \quad (5)$$

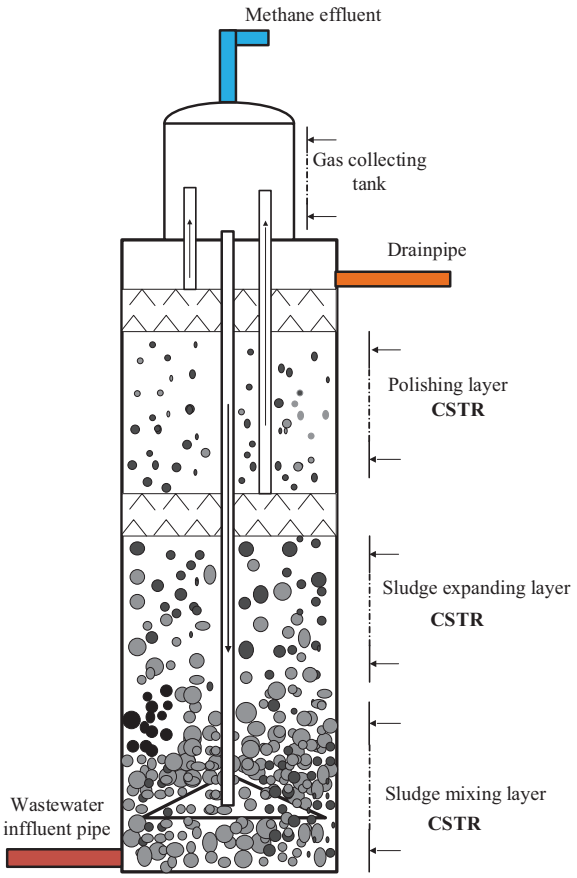

FIGURE 1 | Schematic diagram of three CSTRs in series simulating hydrodynamic of full-scale IC reactor.

Where $\frac{dS_{i,c}}{dt}$ and $\frac{dX_{i,c}}{dt}$ represent the time derivatives of the soluble substrates and particulate substrates for each CSTR part in the reactor, respectively, Q_{inf} is the feed flow rate (m^3 d^{-1}), V_c is the volume of each CSTR (V_c = 750 m^3, the whole reactor volume is 2250 m^3), $S_{i,in}$ and$X_{i,in}$ are the soluble substrates and particulate substrates in the feed flow (kgCOD m^{-3}), and $S_{i,c}$ and$X_{i,c}$ represent the soluble substrates and particulate substrates in each CSTR (kgCOD m^{-3}). The term $\sum_{j=1}^{19} \upsilon_{i,j}\rho_j$ represents the sum of the kinetic rates for process j multiplied by the rate coefficients ($\upsilon_{i,j}$). In addition, $t_{res,X}$ denotes the extended retention of solids such that Sludge Retention Time (SRT) is set above HRT ($t_{res,X}$ = 40 days) (Batstone et al., 2002). The transport term is related to dissolved insoluble gasses ($S_{gas,i}$), such as carbon dioxide, methane, and hydrogen transferring into the liquid phase. $\rho_{T,i}$ is the specific mass transfer rate of gas i at temperature T. V_{gas} represents the volume of the gas collection tank (V_{gas} = 250 m^3). $Q_{gas}$is the gas flow (N m^3 day^{-1}).

Development of the Whole Anaerobic Biochemical System Model

The overall anaerobic biochemical system treating DIP wastewater, considered in this study, includes a pre-acidification

tank and full-scale IC reactor (**Supplementary Figure 1**). The models developed for the tank and the reactor were built as isolated modules. Each module included all of the details described above and it was implemented using Matlab 2017b/Simulink. The simulation model for the whole anaerobic biochemical system combined the two separate modules as a single unit.

The simulated influent "DIP wastewater" first entered the pre-acidification tank module to undergo acidification. The "acidified wastewater" then entered the full-scale IC reactor module for full anaerobic treatment. The simulated inflow rate was based on the measured wastewater discharge rate, which varied according to the actual production status. The volume of the tank relative to that of the reactor was a ratio of 1:2. Thus, the HRT ratio was also 1:2 under the same inflow rate. Using feed pump control, the HRTs for the tank and the reactor were controlled to about 4 and 8 h, respectively. These inflow rates were also implemented in the combined simulation module for the whole AD system.

Parameters Identification

Anaerobic Digestion Model No. 1 is a complex mathematical model with numerous parameters, including stoichiometric parameters, physicochemical parameters, and biochemical parameters. All of these parameters affect the model's output but the sensitivities of parameters related to this output may vary dramatically from one to another. Sensitivity analysis has been used widely to identify significant parameters with the greatest effects on the outputs of models (Bernard et al., 2001). The approaches used to identify sensitive parameters depend on local sensitivity analysis or global one.

Most previous AD simulation studies were based on lab-scale experiments. The local sensitivity analysis method was usually applied in these studies (Tartakovsky et al., 2008; Barrera et al., 2015; Li et al., 2020). This method generally involves analyzing the different outputs obtained when an individual parameter is varied over a defined range while the other parameters remain constant. However, this method generates a linear regression equation that only represents the response of the model for a set of given points, and thus it cannot provide effective details of the correlations or aggregation errors among the various parameters (Donoso-Bravo et al., 2011).

The actual full-scale anaerobic plant reactor process is much more complicated than the lab-scale process. The lab-scale experimental condition can be precisely defined or controlled. But the characteristics of a full-scale reactor are frequently dependent on multiple factors, such as flow rate, water ingredient, temperature, which are nonlinear, time variant, and uncontrollable. The global sensitivity analysis method can cover the entire domain of the model and provide more comprehensive analysis results, thereby overcoming the deficiencies of the local sensitivity analysis method. As a result, the global sensitivity analysis method needs to be applied when modeling a full-scale anaerobic reactor. As a global sensitivity method, the Monte Carlo technique was implemented in this study. Monte Carlo technique is a mathematical method, which uses a set of representative global samples to investigate the entire model space. Monte Carlo algorithms tend to be simple, flexible, and scalable, and can reduce complex models to a set of basic events and interactions (Kroese et al., 2014). Monte Carlo technique is suitable for model analysis of full-scale anaerobic reactor.

Model Calibration and Validation Implementation

The proposed anaerobic simulation model was calibrated and validated using real samples obtained from the pulp and paper mill anaerobic treatment system. An operating period of 250 days was selected to check the model, where samples from the first 150 days were used to optimize the sensitive parameters and calibrate the model, and samples from the next 100 days were employed to validate the effectiveness of the model. The set of differential and algebraic equations in ADM1 was implemented using Matlab 2017b/Simulink with ODE45s solvers, as recommended by Rosen and Jeppsson (2006).

Sample Collection and Analysis

Water samples were taken from influence and effluence of the pre-acidification tank and full-scale IC reactor, respectively, every day. The COD concentration of the water samples was determined using the potassium dichromate method. The composition of untreated DIP wastewater was taken every week, and then sampled and analyzed according to standard methods (American Public Health Association, 2005), and the results are presented in **Table 1**. The flow rate of the biogas from the full-scale IC reactor, was acquired from the biogas flowmeter installed in methane treatment system.

RESULTS AND DISCUSSION

Influent Chemical Oxygen Demand Classification

The characteristics of the DIP wastewater that influenced the anaerobic biochemical treatment section were determined by gas chromatography-mass spectrometry. Many organic compounds that comprised the soluble COD (SCOD) were detected in the wastewater solute samples. The main compounds included polysaccharides, VFAs, and surfactants (surface active agents).

TABLE 1 | The main component content and COD concentration conversion of DIP wastewater.

	Mass concentration mg L^{-1}	Converted to COD concentration kgCOD m^{-3}
Total COD	–	934.98 ± 63.29
Soluble COD	–	862.84 ± 72.99
Soluble monosaccharide (S_{su})	354.28 ± 54.56	425.14 ± 65.47
VFAs (accounted as S_{ac})	184.88 ± 40.19	197.82 ± 42.89
Anionic surfactants (accounted as stearic acid, X_{li})	19.24 ± 6.32	51.77 ± 14.71
Inert soluble (S_I)	–	197.87 ± 19.47
ssCOD (accounted as carbohydrate, X_{ch})	–	72.14 ± 19.71

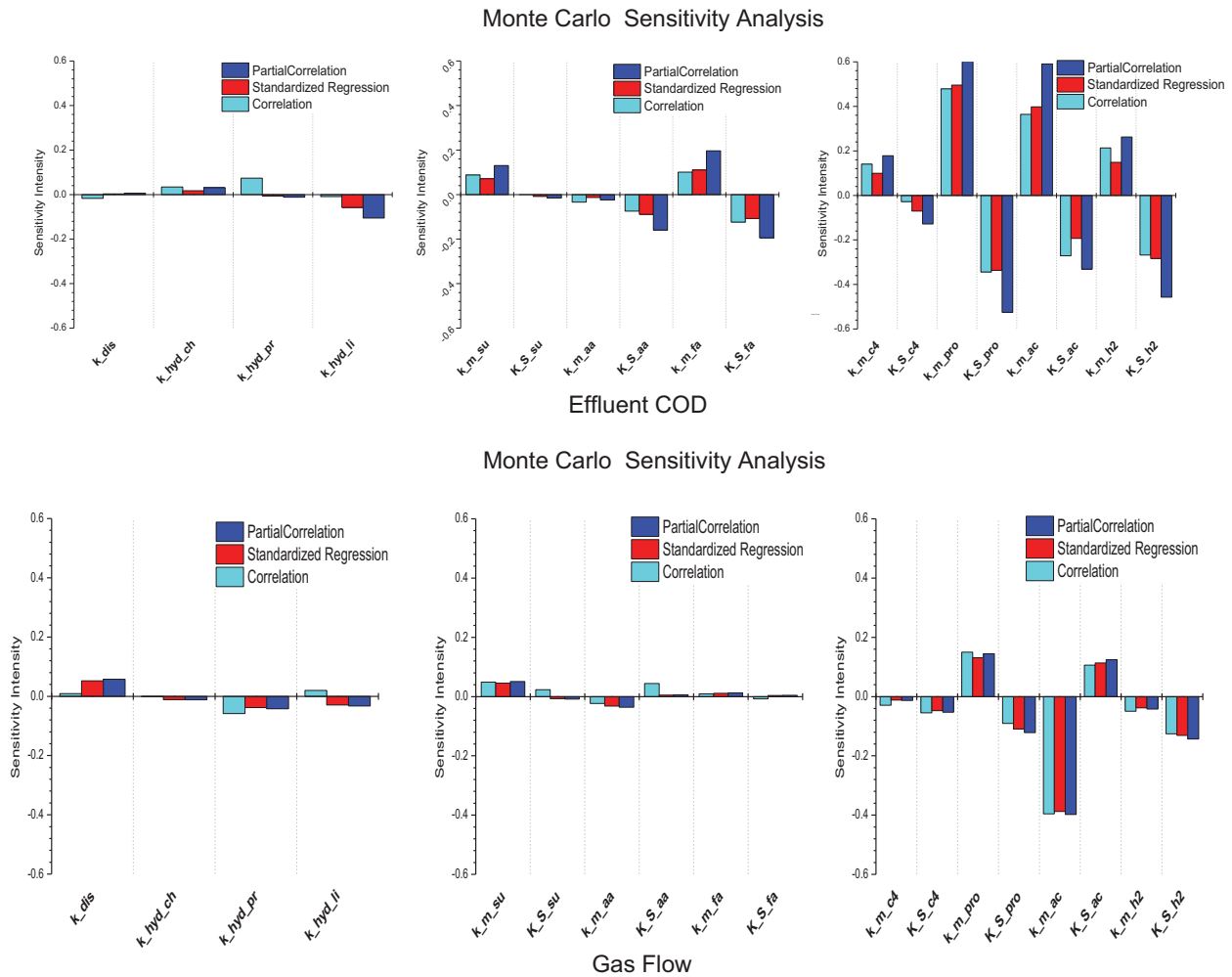

FIGURE 2 | Schematic of sensitivity analysis result of 18 kinetic parameters relating to COD_{eff} and biogas flow of AD system. Monte Carlo of Partial Correlation, Standardized Regression and Correlation for every parameter were respectively implemented in the sensitivity analysis.

The temperature of the DIP wastewater discharged from the DIP workshop usually ranged from 40 to 50°C. At this relatively high temperature, the cellulose and hemicellulose in the fine fibers obtained from wastepaper were hydrolyzed into soluble polysaccharides. The polysaccharides were then decomposed into VFAs or other small molecules such as organic acids. Due to the requirements of the DIP technique, industrial soap (mainly sodium stearate) is used as a deinking agent in the deinking process, thereby explaining why surfactants were detected. The trace amounts of soluble protein detected in the water samples indicated that microorganisms participated in the degradation of fine fibers during the transport of wastewater from the DIP workshop. The DIP wastewater was sampled and analyzed, the results of which are presented in **Table 1**.

The composition of DIP wastewater is very complicated. According to the ADM1 requirements and the detection results of DIP wastewater, also considering the flexibility of the model, the influence components of the COD distribution were simplified as followed. The carbohydrates obtained from the degradation of fibers were regarded as monosaccharides (S_{su}) and they accounted for about 49% of the influent SCOD. VFAs were calculated as acetic acid (S_{ac}) and they accounted for about 22% of the influent SCOD. Surfactants from the DIP workshop were regarded as sodium stearate (lipid X_{li}) and they accounted for about 6% of the soluble SCOD. According to the wastewater quality characterization method proposed by Ekama et al. (1986),

TABLE 2 | Parameter estimation result of the model.

	k_{m_pro}	K_{s_pro}	k_{m_ac}	K_{s_ac}	k_{m_h2}	K_{s_h2}	Relative sum of squares
Recommend values	13.0	0.3	8.0	0.15	35.0	2.5×10^{-5}	–
Estimated values	12.02	0.35	4.26	0.26	16.62	3.21×10^{-5}	5.06×10^{-4}

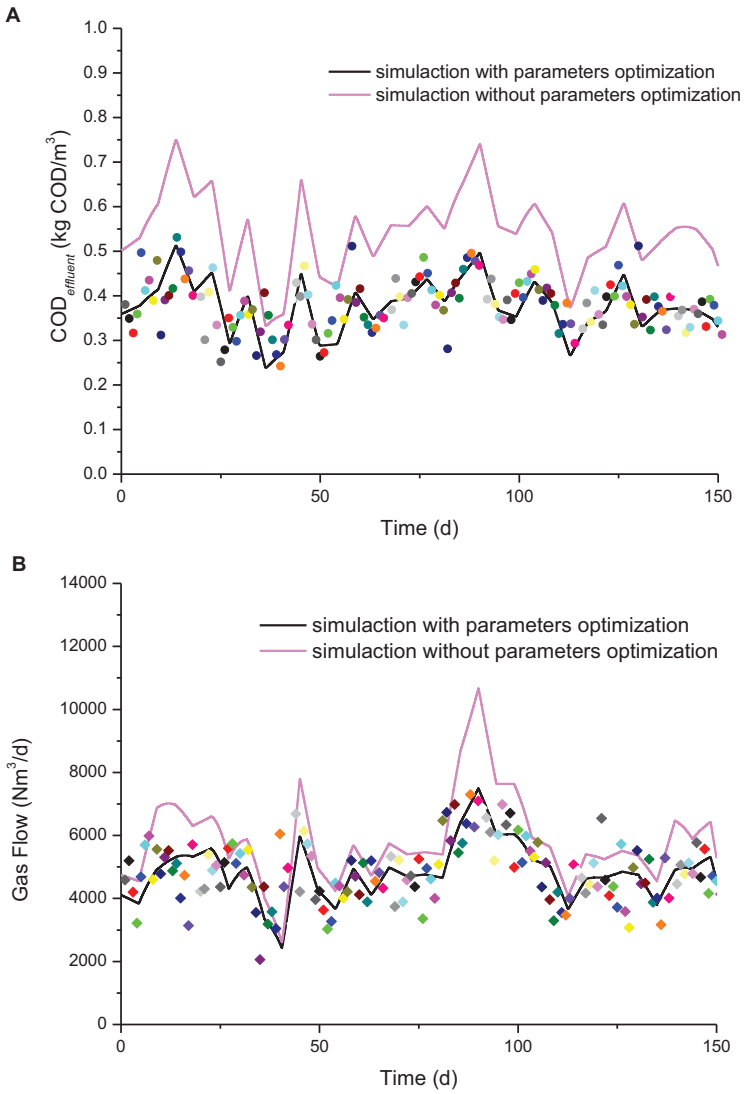

FIGURE 3 | Schematic of comparing simulation result with measured values (color oblique square dot) for IC reactors using 150 days estimation period. **(A)** Simulation comparison of COD_{eff}. **(B)** Simulation comparison of biogas production flow.

90% of the effluent COD from the subsequent aerobic system was regarded as an inert soluble component (S_I; not degradable by microorganisms) which accounted for about 23% of the influent SCOD. The effect of the suspended solids COD (ssCOD) was equal to the difference between the total COD (TCOD) and SCOD, which accounted for 7% of the influent TCOD, and it was regarded as the particulate carbohydrates X_{ch}. The proportion of the COD composition is given in **Supplementary Figure 3**.

Sensitivity Analysis Results

In total, 18 kinetic parameters are employed in ADM1. The effluent COD (COD_{eff}) and biogas production by the AD reactor are usually the main issues considered for paper and pulp mills. Therefore, our proposed model of this anaerobic biochemical system was used to simulate the changes in COD_{eff} and biogas production. A random set of parameters was generated for evaluation by using the Monte Carlo method for the model specifications. This set comprised 500 random parameter pairs. The initial values of the parameters were the values recommended by IWA in order to simulate a medium temperature and high rate reactor. Histograms illustrating the partial correlations, standardized regression, and correlations according to the sensitivity analysis evaluation results are shown in **Figure 2**.

Figures 2A–C show that the Monod absorption rates for propionate (k_{m_pro}), acetate (k_{m_ac}), and hydrogen (k_{m_h2}) had strong positive correlations with COD_{eff} for the anaerobic biochemical system, whereas the half-saturation constants of these parameters (K_{S_pro}, K_{S_ac}, and K_{S_h2}) had significant negative correlations with COD_{eff}. In addition, the Monod absorption rates for monosaccharides k_{m_su}, LCFAs (k_{m_fa}),

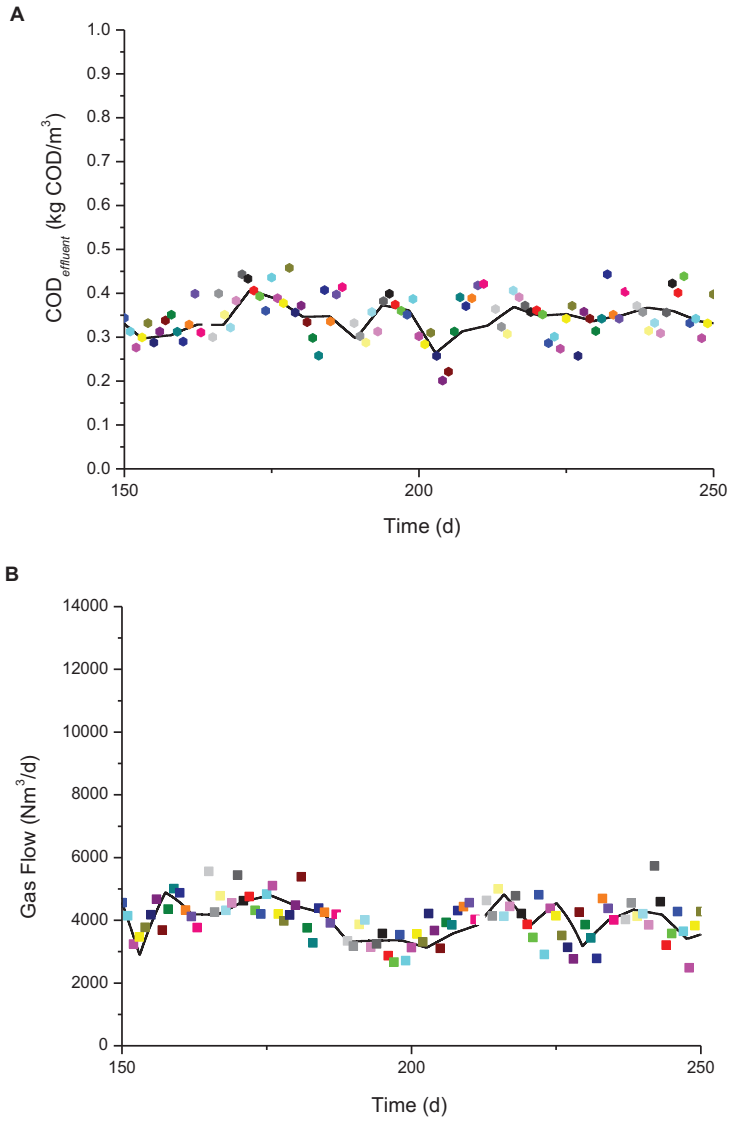

FIGURE 4 | Schematic of simulation result with measured values (color oblique square dot) for IC reactors using subsequent 100-days operation period. **(A)** Simulation comparison of COD_{eff}. **(B)** Simulation comparison of biogas production flow.

valerate and butyrate (k_m_c4) had positive correlations with COD_{eff}, whereas the half-saturation constants for amino acids (K_S_aa), LCFAs (K_S_fa), valerate and butyrate (K_S_c4) had relatively weak negative correlations.

As shown in **Figures 2D–F**, k_m_ac had a strong negative correlation with the biogas flow rate in the AD system, whereas k_m_pro and K_S_ac had positive correlations. However, K_S_pro and K_S_h2 had a negative correlation.

Thus, k_m_pro, K_S_pro, k_m_ac, K_S_ac, k_m_h2, and K_S_h2 were selected as parameters for estimating the model's outputs to assess the COD_{eff} and biogas production. Meanwhile, other 12 kinetic parameters were directly used the recommendation values by Batstone et al. (2002), which showed few correlation to the COD_{eff} and biogas production modeling result by sensitivity analysis evaluation.

Parameter Value Estimation

The sum of the squared errors (SSE) minimum function was applied for parameter estimation. SSE is also known as the "residual sum of squares" or "sum of squared residuals," and it is the sum of the squares of the residuals in statistics (a measure of the deviations between the actual data and estimated model values). A small SSE value shows that the result obtained by the model agrees closely with the actual measured data. Using the on-site COD_{eff} and biogas production data acquired from the anaerobic biochemical system for 150 days, the parameters were estimated using SSE fitting method. The results estimated for k_m_pro, K_S_pro, k_m_ac, K_S_ac, k_m_h2, and K_S_h2 are shown in **Table 2**.

Table 2 shows that the estimated values of k_m_pro and K_S_pro were close to the values recommended by IWA for high rate

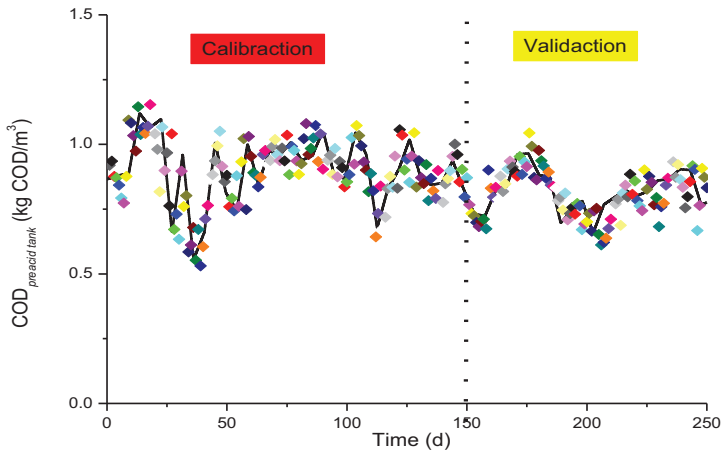

FIGURE 5 | COD_{eff} simulation curve and actual measured value of the effluent from the pre-acidification tank. Calibration part was in 150-days parameter estimation period, and validation part was in subsequent 100-days validation period.

reactor on medium temperature, which indicates the system was not affected greatly by propionate absorption. However, the estimated values of k_m_ac and k_m_h2 were about half of the values recommended by IWA, which shows that the absorption rates of k_m_ac and k_m_h2 were relatively low in this system, and the corresponding half-saturation constants of K_S_ac and K_S_h2 were slightly high. The parameter value estimation was based on the components of influent DIP wastewater. Due to the influent COD classification, the main components of the SCOD was monosaccharide and VFAs, and the ssCOD was carbohydrate. Further, the VFAs was simplified as S_{ac}. The decomposition products from monosaccharide and carbohydrate were majorly S_{ac} and S_{h2}. Because of that, the uptaking of S_{ac} and S_{h2} are the major factors of COD removing and methane producing. The high generation of S_{ac} and S_{h2} might lead to the difficulty of bacteria uptaking and removing, which resulted in the relatively low absorption rates and slightly high half-saturation constants of k_m_ac and k_m_h2.

Model Simulation and Validation

This anaerobic biochemical system treating DIP wastewater comprised an anaerobic pre-acidification tank and IC reactor. Based on the discussion above, several sensitive parameters in the simulation model were optimized using the estimated values presented in **Table 2**.

We compared the optimized parameters with the original parameters to simulate the results obtained from this anaerobic system lasting 150 days, as shown in **Figure 3**. Seeing from **Figure 3A**, after optimizing the parameters, the COD_{eff} simulating result fits much better to the data (values) acquired from IC reactor on-site, comparing with those using recommended parameters. Similar results were obtained in the simulation of IC reactor biogas production, as shown in **Figure 4B**.

COD_{eff} and biogas production data (values) were also acquired on-site from this anaerobic system over the following 100 days. These data were employed to validate the model and the simulation results are shown in **Figure 4**. The simulation results agreed well with the measured values. We concluded that the simulation results obtained using the optimized parameters were consistent with the actual COD_{eff} and biogas production values for the anaerobic system.

According to global sensitivity analysis by the Monte Carlo technique, the model developed with the optimized parameters was more suitable for modeling anaerobic biochemical treatment in the DIP wastewater plant. In contrast to lab-scale experiments, the influent DIP wastewater could not be manipulated accurately by adjusting the inflow rate in the actual plant, especially the components of the experimental water. The composition of the raw product used in the paper and pulp mill was relatively simple, where it mainly comprised cellulose from wastepaper. The manufacturing technique and production process were unique and almost constant. Thus, the composition of the influent DIP wastewater was roughly stable in the first calibration period of 150 days and the subsequent validation period of 100 days, without major fluctuations. So, the parameters optimized based on the first 150 days were still suitable for modeling COD_{eff} and biogas production by the IC reactor in the subsequent 100 days.

To further illustrate the advantages and disadvantages of the simulation model, the linear regression method was applied to quantitatively evaluate the accuracy of the simulation results. Linear fitting was performed between the predicted and measured values. The measured values were plotted on the X-axis and the predicted values on the Y-axis, and scatter plots were prepared. The slope of the fitted curve was set to 1, and the intercept was 0. The scatter plots will be distributed on or near the curve when the predicted and measured values are the same or similar.

Supplementary Figures 4, 5 show the linear fits of the measured and simulated COD_{eff} and biogas flow values during the model parameter estimation period and the subsequent validation period, respectively. The results obtained by statistical fitting curve showed that the values simulated with the optimized parameters were evenly distributed on both sides of the

fitted curve in the validation period (first 150 days) and validation period (second 100 days). By contrast, the values simulated using the recommended parameters clearly deviated from the fitted curve, where they were distributed above the curve, thereby demonstrating that the simulated values were much overestimated.

Simulation Results for Pre-acidification Tank Effluent

In this complete anaerobic biochemical system used for treating DIP wastewater, the pre-acidification tank is connected before the IC reactor. In the simulation, the pre-acidification tank and IC reactor were run simultaneously as a combined module using Matlab 2017b/Simulink. According to the settings in the simulation of the pre-acidification tank described above, methanogenesis does not occur in the pre-acidification tank model (**Supplementary Figure 2**). Thus, the entire ADM1 was applied for simulating the pre-acidification tank except for the equation describing the methanogenesis process.

As described above, the pre-acidification tank is part of the AD treatment system and its simulation was also included in the overall sensitivity analysis. Therefore, it was feasible and necessary to study the simulation outputs in terms of COD_{eff} and biogas production from the pre-acidification tank.

From theoretical perspectives, under normal conditions, COD reduction and methane production do not occur in the wastewater pre-acidification process because of the short SRT. **Figure 5** and **Supplementary Figure 6** respectively show the simulation results in terms of COD_{eff} and biogas production for the pre-acidification tank using the optimized parameters under real-time operating conditions. The results showed that the pre-acidification COD_{eff} ($COD_{preacidtank}$) obtained by the simulation was fairly consistent with the real measurements determined by sampling the pre-acidification tank effluent. In addition, the biogas production amount obtained by the simulation was maintained at zero. Therefore, the pre-acidification simulation results obtained by the model agreed well with the actual situation for the pre-acidification tank.

CONCLUSION

The model established in this study was effective at simulating the effluent COD and biogas production by a DIP wastewater treatment anaerobic biochemical system. The proposed model is based on ADM1, and it also considers the hydrodynamics of the pre-acidification tank and full-scale IC reactor. The component interpretation method was used to separate and classify the influent components according to the requirements of ADM1. Global sensitivity analysis showed that the Monod absorption rates and half-saturation constants for propionic acid, acetic acid, and hydrogen were the most sensitive parameters, which were optimized further. The modeling results of calibration and validation were both in good agreement with the on-site COD_{eff} and biogas production data. The effluent of pre-acidification tank was also fit well. The method proposed in this study may be useful for the design, operation, or monitoring of wastewater full-scale anaerobic reactors.

DATA AVAILABILITY STATEMENT

The original contributions presented in the study are included in the article/**Supplementary Material**, further inquiries can be directed to the corresponding author/s.

AUTHOR CONTRIBUTIONS

YH: methodology, investigation, software, and writing – original draft. YM: resources, supervision, conceptualization, and data curation. JW: supervision, finance supporting, and writing – review and editing. YW: writing – review and editing. All authors contributed to the article and approved the submitted version.

FUNDING

This work was supported by the National Natural Science Foundation of China (Nos. 31570568 and 31670585), Science and Technology Planning Project of Guangzhou city, China (Nos. 201607010079 and 201607020007), Science and Technology Planning Project of Guangdong Province, China (Nos. 2016A020221005 and 2017A040405022), National Key Research and Development Project (No. 2018YFE0110400), and the National Natural Science Foundation of China (Nos. 21978102 and 31670585).

SUPPLEMENTARY MATERIAL

The Supplementary Material for this article can be found online at: https://www.frontiersin.org/articles/10.3389/fmicb.2021.755398/full#supplementary-material

REFERENCES

Ahn, Y.-H., Min, K.-S., and Speece, R. E. (2001). Pre-acidification in anaerobic sludge bed process treating brewery wastewater. *Water Res.* 35, 4267–4276. doi: 10.1016/s0043-1354(01)00171-3

Al-Rubaye, H., Smith, J. D., Shivashankaraiah, M., Yu, J., Ghorbanian, M., Alembath, A., et al. (2020). The pre-acidification gas impact on upgrading the biogas produced in expanded granular sludge bed reactor. *Biofuels*. doi: 10.1080/17597269.2020.1772608

American Public Health Association (2005). "American water works association, water environment federation," in *Standard Methods for the Examination of Water and Wastewater*, eds E. W. Rice, R. B. Baird, and A. D. Eaton (Washington, D.C: APHA-AWWA-WEF).

Barrera, E. L., Spanjers, H., Solon, K., Amerlinck, Y., Nopens, I., and Dewulf, J. (2015). Modeling the anaerobic digestion of cane-molasses vinasse: extension of the Anaerobic Digestion Model No. 1 (ADM1) with sulfate reduction for a very high strength and sulfate rich wastewater. *Water Res.* 71, 42–54. doi: 10.1016/j.watres.2014.12.026

Batstone, D. J., Hernandez, J., and Schmidt, J. E. (2005). Hydraulics of laboratory and full-scale upflow anaerobic sludge blanket (UASB) reactors. *Biotechnol. Bioeng.* 91, 387–391. doi: 10.1002/bit.20483

Batstone, D. J., Keller, J., Angelidaki, I., Kalyuzhnyi, S., Pavlostathis, S., Rozzi, A., et al. (2002). The IWA anaerobic digestion model no 1 (ADM1). *Water Sci. Technol.* 45, 65–73. doi: 10.2166/wst.2002.0292

Batstone, D. J., Puyol, D., Flores-Alsina, X., and Rodríguez, J. (2015). Mathematical modelling of anaerobic digestion processes: applications and future needs. *Rev. Environ. Sci. Bio Technol.* 14, 595–613. doi: 10.1007/s11157-015-9376-4

Bernard, O., Hadj-Sadok, Z., Dochain, D., Genovesi, A., and Steyer, J.-P. (2001). Dynamical model development and parameter identification for an anaerobic wastewater treatment process. *Biotechnol. Bioeng.* 75, 424–438. doi: 10.1002/bit.10036

Buzzini, A. P., and Pires, E. C. (2002). Cellulose pulp mill effluent treatment in an upflow anaerobic sludge blanket reactor. *Process Biochem.* 38, 707–713. doi: 10.1016/s0032-9592(02)00190-5

Çalışkan, G., and Azbar, N. (2017). Energy recovery from conventional biogas digester effluent with a novel bioreactor configuration. *Waste Biomass Valorization* 8, 2371–2381. doi: 10.1007/s12649-016-9827-3

Chen, J., Liu, Y., Liu, K., Hu, L., Yang, J., Wang, X., et al. (2021). Bacterial community composition of internal circulation reactor at different heights for large-scale brewery wastewater treatment. *Bioresour. Technol.* 331:125027. doi: 10.1016/j.biortech.2021.125027

Chen, X., Chen, Z., Wang, X., Huo, C., Hu, Z., Xiao, B., et al. (2016). Application of ADM1 for modeling of biogas production from anaerobic digestion of *Hydrilla verticillata*. *Bioresour. Technol.* 211, 101–107.

Chen, Y., He, J., Mu, Y., Huo, Y.-C., Zhang, Z., Kotsopoulos, T. A., et al. (2015). Mathematical modeling of upflow anaerobic sludge blanket (UASB) reactors: simultaneous accounting for hydrodynamics and bio-dynamics. *Chem. Eng. Sci.* 137, 677–684. doi: 10.1016/j.ces.2015.07.016

Cui, P., Zhou, X., and Zhang, Y. (2011). The feasibility study of cotton pulp wastewater treatment with IC anaerobic reactor. *Procedia Environ. Sci.* 11, 686–692. doi: 10.1016/j.proenv.2011.12.107

Diamantis, V., and Aivasidis, A. (2018). Performance of an ECSB reactor for high-rate anaerobic treatment of cheese industry wastewater: effect of pre-acidification on process efficiency and calcium precipitation. *Water Sci. Technol.* 78, 1893–1900. doi: 10.2166/wst.2018.406

Diez Blanco, V., Encina, P. A. G., and Fdz-Polanco, F. (1995). Effects of biofilm growth, gas and liquid velocities on the expansion of an anaerobic fluidized bed reactor (AFBR). *Water Res.* 29, 1649–1654. doi: 10.1016/0043-1354(95)00001-2

Donoso-Bravo, A., Mailier, J., Martin, C., Rodríguez, J., Aceves-Lara, C. A., and Wouwer, A. V. (2011). Model selection, identification and validation in anaerobic digestion: a review. *Water Res.* 45, 5347–5364. doi: 10.1016/j.watres.2011.08.059

Ekama, G. A., Dold, P. L., and Marais, G. V. R. (1986). Procedures for determining influent COD fractions and the maximum specific growth rate of heterotrophs in activated sludge systems. *Water Sci. Technol.* 18, 91–114. doi: 10.2166/wst.1986.0062

Feldman, H., Flores-Alsina, X., Ramin, P., Kjellberg, K., Jeppsson, U., Batstone, D. J., et al. (2019). Assessing the effects of intra-granule precipitation in a full-scale industrial anaerobic digester. *Water Sci. Technol.* 79, 1327–1337. doi: 10.2166/wst.2019.129

Feldman, H., Flores-Alsina, X., Ramin, P., Kjellberg, K., Jeppsson, U., Batstone, D. J., et al. (2017). Modelling an industrial anaerobic granular reactor using a multi-scale approach. *Water Res.* 126, 488–500. doi: 10.1016/j.watres.2017.09.033

Flores-Alsina, X., Corominas, L., Neumann, M. B., and Vanrolleghem, P. A. (2012). Assessing the use of activated sludge process design guidelines in wastewater treatment plant projects: a methodology based on global sensitivity analysis. *Environ. Model. Softw.* 38, 50–58. doi: 10.1016/j.envsoft.2012.04.005

Gernaey, K. V., Jeppsson, U., Vanrolleghem, P. A., Copp, J. B., Steyer, J. P., Gernaey, K. V., et al. (2014). *Benchmarking of Control Strategies for Wastewater Treatment Plants*. IWA Scientific and Technical Report No. 23. London: IWA Publishing.

Girault, R., Bridoux, G., Nauleau, F., Poullain, C., Buffet, J.-P., Steyer, J. P., et al. (2012). A waste characterisation procedure for ADM1 implementation based on degradation kinetics. *Water Res.* 46, 4099–4110. doi: 10.1016/j.watres.2012.04.028

Guo, K., Shang, Y., Gao, B., Xu, X., Lu, S., and Qi, Q. (2018). Study on the treatment of soybean protein wastewater by a pilot-scale IC-A/O coupling reactor. *Chem. Eng. J.* 343, 189–197. doi: 10.1016/j.cej.2018.02.128

Hamza, R. A., Iorhemen, O. T., and Tay, J. H. (2016). Advances in biological systems for the treatment of high-strength wastewater. *J. Water Process Eng.* 10, 128–142. doi: 10.1016/j.jwpe.2016.02.008

Irizar, I., Roche, E., Beltrán, S., Aymerich, E., and Esteban-Gutiérrez, M. (2018). Model-based design of a software sensor for real-time diagnosis of the stability conditions in high-rate anaerobic reactors – Full-scale application to Internal Circulation technology. *Water Res.* 143, 479–491. doi: 10.1016/j.watres.2018.06.055

Kamali, M., Gameiro, T., Costa, M. E. V., and Capela, I. (2016). Anaerobic digestion of pulp and paper mill wastes–An overview of the developments and improvement opportunities. *Chem. Eng. J.* 298, 162–182.

Karadag, D., Koroglu, O. E., Ozkaya, B., Cakmakci, M., Heaven, S., Banks, C., et al. (2015). Anaerobic granular reactors for the treatment of dairy wastewater: a review. *Int. J. Dairy Technol.* 68, 459–470. doi: 10.1111/1471-0307.12252

Kleerebezem, R., and Van Loosdrecht, M. C. M. (2006). Waste characterization for implementation in ADM1. *Water Sci. Technol.* 54, 167–174. doi: 10.2166/wst.2006.538

Kroese, D. P., Brereton, T., Taimre, T., and Botev, Z. I. (2014). Why the Monte Carlo method is so important today. *WIREs Comput. Stat.* 6, 386–392. doi: 10.1002/wics.1314

Lauwers, J., Appels, L., Thompson, I. P., Degrève, J., Van Impe, J. F., and Dewil, R. (2013). Mathematical modelling of anaerobic digestion of biomass and waste: power and limitations. *Prog. Energy Combust. Sci.* 39, 383–402. doi: 10.1016/j.pecs.2013.03.003

Li, Z., Wan, J., Ma, Y., Wang, Y., Huang, Y., and Fan, H. (2020). A comprehensive model of N2O emissions in an anaerobic/oxygen-limited aerobic process under dynamic conditions. *Bioprocess Biosyst. Eng.* 43, 1093–1104. doi: 10.1007/s00449-020-02307-7

Lier, J. B. V., Zee, F. P. V. D., Frijters, C. T. M. J., and Ersahin, M. E. (2015). Celebrating 40 years anaerobic sludge bed reactors for industrial wastewater treatment. *Rev. Environ. Sci. Bio Technol.* 14, 681–702. doi: 10.1007/s11157-015-9375-5

Liotta, F., Chatellier, P., Esposito, G., Fabbricino, M., Van Hullebusch, E. D., Lens, P. N., et al. (2015). Current views on hydrodynamic models of nonideal flow anaerobic reactors. *Crit. Rev. Environ. Sci. Technol.* 45, 2175–2207. doi: 10.1080/10643389.2015.1010426

Meyer, T., and Edwards, E. A. (2014). Anaerobic digestion of pulp and paper mill wastewater and sludge. *Water Res.* 65, 321–349. doi: 10.1016/j.watres.2014.07.022

Naessens, W., Maere, T., and Nopens, I. (2012). Critical review of membrane bioreactor models – Part 1: biokinetic and filtration models. *Bioresour. Technol.* 122, 95–106.

Ozgun, H. (2019). Anaerobic Digestion Model No. 1 (ADM1) for mathematical modeling of full-scale sludge digester performance in a municipal wastewater treatment plant. *Biodegradation* 30, 27–36. doi: 10.1007/s10532-018-9859-4

Poblete, I. B. S., Araujo, O. D. Q. F., and de Medeiros, J. L. (2020). Dynamic analysis of sustainable biogas-combined-cycle plant: time-varying demand and bioenergy with carbon capture and storage. *Renew. Sustain. Energy Rev.* 131:109997. doi: 10.1016/j.rser.2020.109997

Rajagopal, R., Torrijos, M., Kumar, P., and Mehrotra, I. (2013). Substrate removal kinetics in high-rate upflow anaerobic filters packed with low-density polyethylene media treating high-strength agro-food wastewaters. *J. Environ. Manag.* 116, 101–106. doi: 10.1016/j.jenvman.2012.11.032

Rivas, A., Irizar, I., and Ayesa, E. (2008). Model-based optimisation of Wastewater Treatment Plants design. *Environ. Model. Softw.* 23, 435–450. doi: 10.1016/j.envsoft.2007.06.009

Rodriguez-Roda, I., Sànchez-Marrè, M., Comas, J., Baeza, J., Colprim, J., Lafuente, J., et al. (2002). A hybrid supervisory system to support WWTP operation: implementation and validation. *Water Sci. Technol.* 45, 289–297. doi: 10.2166/wst.2002.0608

Rosen, C., and Jeppsson, U. (2006). *Aspects on ADM1 Implementation Within the BSM2 Framework*. Technical report no. LUTEDX/(TEIE-7224)/1-35/(2006), Department of Industrial Electrical Engineering and Automation. Lund: Lund University.

Rubio, J. A., Garcia-Morales, J. L., Romero, L. I., and Fernandez-Morales, F. J. (2020). Modelization of anaerobic processes during co-digestion of slowly biodegradable substrates. *Chemosphere* 250:126222. doi: 10.1016/j.chemosphere.2020.126222

Sarathai, Y., Koottatep, T., and Morel, A. (2010). Hydraulic characteristics of an anaerobic baffled reactor as onsite wastewater treatment system. *J. Environ. Sci.* 22, 1319–1326. doi: 10.1016/s1001-0742(09)60257-6

Saxena, A., and Singh Chauhan, P. (2017). Role of various enzymes for deinking paper: a review. *Crit. Rev. Biotechnol.* 37, 598–612. doi: 10.1080/07388551.2016.1207594

Simstich, B., Beimfohr, C., and Horn, H. (2012). Lab scale experiments using a submerged MBR under thermophilic aerobic conditions for the treatment of paper mill deinking wastewater. *Bioresour. Technol.* 122, 11–16. doi: 10.1016/j.biortech.2012.04.029

Song, Y.-C., Kim, M., Shon, H., Jegatheesan, V., and Kim, S. (2018). Modeling methane production in anaerobic forward osmosis bioreactor using a modified anaerobic digestion model No. 1. *Bioresour. Technol.* 264, 211–218. doi: 10.1016/j.biortech.2018.04.125

Tartakovsky, B., Mu, S., Zeng, Y., Lou, S., Guiot, S., and Wu, P. (2008). Anaerobic digestion model No. 1-based distributed parameter model of an anaerobic reactor: II. Model validation. *Bioresour. Technol.* 99, 3676–3684. doi: 10.1016/j.biortech.2007.07.061

Uggetti, E., Ferrer, I., Llorens, E., and García, J. (2010). Sludge treatment wetlands: a review on the state of the art. *Bioresour. Technol.* 101, 2905–2912. doi: 10.1016/j.biortech.2009.11.102

Van Hulle, S. W. H., Vesvikar, M., Poutiainen, H., and Nopens, I. (2014). Importance of scale and hydrodynamics for modeling anaerobic digester performance. *Chem. Eng. J.* 255, 71–77. doi: 10.1016/j.cej.2014.06.041

Wang, J., Yan, J., and Xu, W. (2015). Treatment of dyeing wastewater by MIC anaerobic reactor. *Biochem. Eng. J.* 101, 179–184. doi: 10.1016/j.bej.2015.06.001

Wu, J., Jiang, B., Feng, B., Li, L., Moideen, S. N. F., Chen, H., et al. (2020). Pre-acidification greatly improved granules physicochemical properties and operational stability of Upflow anaerobic sludge Blanket (UASB) reactor treating low-strength starch wastewater. *Bioresour. Technol.* 302:122810. doi: 10.1016/j.biortech.2020.122810

Wu, J., Liu, Q., Feng, B., Kong, Z., Jiang, B., and Li, Y.-Y. (2019). Temperature effects on the methanogenesis enhancement and sulfidogenesis suppression in the UASB treatment of sulfate-rich methanol wastewater. *Int. Biodeterior. Biodegradation* 142, 182–190. doi: 10.1016/j.ibiod.2019.05.013

Xu, Q. H., Wang, Y. P., Qin, M. H., Fu, Y. J., Li, Z. Q., Zhang, F. S., et al. (2011). Fiber surface characterization of old newsprint pulp deinked by combining hemicellulase with laccase-mediator system. *Bioresour. Technol.* 102, 6536–6540. doi: 10.1016/j.biortech.2011.03.051

Yu, L., Zhao, Q., Ma, J., Frear, C., and Shulin, C. (2012). Experimental and modeling study of a two-stage pilot scale high solid anaerobic digester system. *Bioresour. Technol.* 124, 8–17. doi: 10.1016/j.biortech.2012.08.088

Conflict of Interest: The authors declare that the research was conducted in the absence of any commercial or financial relationships that could be construed as a potential conflict of interest.

Publisher's Note: All claims expressed in this article are solely those of the authors and do not necessarily represent those of their affiliated organizations, or those of the publisher, the editors and the reviewers. Any product that may be evaluated in this article, or claim that may be made by its manufacturer, is not guaranteed or endorsed by the publisher.

frontiers in Microbiology

ORIGINAL RESEARCH
published: 27 September 2021
doi: 10.3389/fmicb.2021.751571

Transcriptome-Guided Insights Into Plastic Degradation by the Marine Bacterium

Alka Kumari[1], Nasreen Bano[2,3], Sumit Kumar Bag[2,3], Doongar R. Chaudhary[1,2] and Bhavanath Jha[1]**

[1] Plant Omics Division, CSIR-Central Salt and Marine Chemical Research Institute, Bhavnagar, India, [2] Academy of Scientific and Innovative Research (AcSIR), CSIR, Ghaziabad, India, [3] Molecular Biology and Biotechnology, CSIR-National Botanical Research Institute, Lucknow, India

Polyethylene terephthalate (PET) is a common single-use plastic that accumulated in the environment because of its non-degradable characteristics. In recent years, microbes from different environments were found to degrade plastics and suggested their capability to degrade plastics under varying environmental conditions. However, complete degradation of plastics is still a void for large-scale implications using microbes because of the lack of knowledge about genes and pathways intricate in the biodegradation process. In the present study, the growth and adherence of marine *Bacillus* species AIIW2 on PET surface instigating structural deterioration were confirmed through weight loss and hydrophobicity reduction, as well as analyzing the change in bond indexes. The genome-wide comparative transcriptomic analysis of strain AIIW2 was completed to reveal the genes during PET utilization. The expression level of mRNA in the strain AIIW2 was indexed based on the log-fold change between the presence and absence of PET in the culture medium. The genes represent carbon metabolism, and the cell transport system was up-regulated in cells growing with PET, whereas sporulation genes expressed highly in the absence of PET. This indicates that the strain AIIW2 hydrolyzes PET and assimilated via cellular carbon metabolism. A protein–protein interaction network was built to obtain the interaction between genes during PET utilization. The genes traced to degrade PET were confirmed by detecting the hydrolytic product of PET, and genes were cloned to improve PET utilization by microbial system as an eco-friendly solution.

Keywords: biodegradation, polyethylene terephthalate, marine bacteria, genome, transcriptome

OPEN ACCESS

Edited by:
Lean Zhou,
Changsha University of Science and Technology, China

Reviewed by:
Qing Jiang,
Shandong University of Science and Technology, China
Junfeng Chen,
Qufu Normal University, China

****Correspondence:***
Doongar R. Chaudhary
drchuadhary@csmcri.res.in
Bhavanath Jha
jha.bhavanath@gmail.com

Specialty section:
This article was submitted to Microbiotechnology, a section of the journal Frontiers in Microbiology

Received: *01 August 2021*
Accepted: *30 August 2021*
Published: *27 September 2021*

Citation:
Kumari A, Bano N, Bag SK, Chaudhary DR and Jha B (2021) Transcriptome-Guided Insights Into Plastic Degradation by the Marine Bacterium. Front. Microbiol. 12:751571. doi: 10.3389/fmicb.2021.751571

INTRODUCTION

Polyethylene terephthalate (PET) is the most common single-use synthetic polymer, primarily used in the packaging industries such as plastic bags, bottles, and films (Andrady and Neal, 2009). Within the decades of its discovery, it has steered its spread in different ecosystems (Lithner et al., 2011; Wang et al., 2020). The need for remediation approaches is particularly urgent to combat non-degradable synthetic polymer accumulation. The biological approaches to remediate plastic wastes could provide an eco-friendly solution. The growing concerns for an efficient system meant for biodegradation of plastics are mainly due to the limitations in the conventional plastic disposal methods that cause the release of harmful chemicals in the surrounding environment that affect

the life of living organisms at various trophic levels (Tokiwa and Calabia, 2004; Hermanová et al., 2015).

In recent years, microorganisms or their enzymes are increasingly reported for degradation and decomposition of plastics. During PET degradation study, a thermophilic hydrolase from *Thermobifida fusca* had combined characteristics of lipase and esterase (Mueller, 2006). An esterase from polyester-degrading bacterium (*Thermobifida halotolerans*) was cloned in *Escherichia coli* found to hydrolyze PET and *bis*-(benzoyloxyethyl) terephthalate into terephthalic acid and mono-(2-hydroxyethyl) terephthalate (Ribitsch et al., 2012). The two-novel esterase from anaerobic *Clostridium botulinum* strain (ATCC 3502) were found to hydrolyze polyester, which was cloned in *E. coli* BL21 (Perz et al., 2016). The engineered *Comamonas testosteroni* strain can degrade PET particles under alkaline conditions (Gong et al., 2018). Subsequently, a bacterium *Ideonella sakaiensis* could utilize PET as carbon and degrade by secretion of PETase (Austin et al., 2018). The aliphatic, aromatics, polyaromatic hydrocarbon, phthalate, polyethylene, and polyisoprene degradation genes were reported in the *Rhodococcus* (Zampolli et al., 2019). Janczak et al. (2020) demonstrated the ability of rhizospheric bacterial strain (*Serratia plymuthica*) for degradation of PET in cultivated and compost soil, as well as the presence of 155 genes for xenobiotics biodegradation in the genome.

In marine environments, plastic-degrading microorganisms are often found on waste plastic surfaces. A recent study of the taxonomic pattern of microbes associated with plastics from the marine environment showed that the recurring groups and families of Erythrobacteraceae and Rhodobacteraceae (Alphaproteobacteria) bacteria, Flavobacteriaceae (Bacteriodetes), and Cyanobacteria (*Phormidium*) were documented (Roager and Sonnenschein, 2019). A carboxylic ester hydrolase from the marine *Pseudomonas aestusnigri* was identified to degrade PET, which had amino acid sequence homology with type IIa family of PET hydrolytase (Bollinger et al., 2020). Sarkhel et al. (2020) reported marine bacterium and fungus, which degraded 35 and 22% plastic waste stripes, respectively, within 6 weeks. PETase had been displayed on the yeast surface (*Pichia pastoris*) to develop the whole-cell biocatalysis for improved PET degradation efficiency at higher pH and temperature stability (Chen et al., 2020). Notably, microorganisms have a great potential to degrade plastics, which could be amplified to a higher level through an understanding of underlying pathways, ultimately to come up with novel bioremediation approaches.

The functional analysis of available genome data could provide invaluable information for developing and designing strategies to attenuate plastic non-degradability (Zampolli et al., 2019). The metabolic networks with the catabolic enzymes could be exploited from genomics and transcriptomic networking in bioremediation applications.

This study aimed to resolve the PET mineralization process by the marine *Bacillus* strain AIIW2. We used a comparative transcriptomic approach to trace genes involved in plastic degradation that will highlight potential bottlenecks in the microbial PET mineralization process, which could become preferential targets for optimizing PET degradation by environmental microorganisms. The fundamental idea of plastic degradation now shows a two-step process: the hydrolysis of polymer into shorter fragments followed by mineralization by the candidate microorganism.

MATERIALS AND METHODS

Polyethylene Terephthalate

The bacterial degradation was measured in commercially available standard PET film (Sigma-Aldrich, United States). The approximate average molecular weight of PET film was 19,500 g mol^{-1} and density 1.38 g cm^{-3} used in the present study.

Bacterial Strain and Growth Conditions

The *Bacillus* species AIIW2 (KU877334) was initially isolated from plastic waste collected from the marine environment (Kumari et al., 2019). The strain AIIW2 used in this study was previously found to degrade different plastics through extensive analytical and microscopic studies (Kumari et al., 2019). The bacterial strain was cultured and maintained in Zobell marine broth at 30°C and 120 revolutions/min (rpm) or on solid Zobell marine agar plates with 1.8% agar. For bacterial degradation study, 1 mg mL^{-1} of PET film was incubated in 30 mL of Bushnell and Haas broth (BHB) inoculated with the *Bacillus* species AIIW2, and another flask without any carbon source was taken as control incubated at 30°C under shaking condition. Before inoculation, PET film was washed with sterilized MilliQ water thrice, dried in laminar air flow, and UV-irradiated for sterilization.

Scanning Electron Microscopy Study

The morphological change on the surface of PET film due to bacterial activity was assessed using a field emission scanning electron microscope (FE-SEM, JSM-7100F, Jeol Ltd., United States). The bacterial-treated and -untreated PET films were taken out after 30 days of incubation and fixed with 2% glutaraldehyde (2 h), subsequently dehydrated with 30, 50, 70, and 100% ethanol for 30 min each, and then vacuum-dried in a desiccator. Vacuum dried films were coated with gold before scanning.

Weight Loss Assay

The bacterial degradation of PET film was evaluated through the dry weight reduction method described earlier (Kumari et al., 2019). Briefly, 1 mg mL^{-1} of preweighted PET film were extracted from the bacterial culture maintained at 30°C under shaking condition in BHB medium after every 15 days up to 90 days to measure the degradation. The extracted PET films were washed with 2% sodium dodecyl sulfate (SDS) to remove attached cells and rinsed with MilliQ water thrice. The washed PET films were dried overnight at 50°C to determine the dry weight. The biodegradation efficiency of the marine bacterium was determined through a weight loss of the PET films when offered as a sole source of carbon.

Carbon Mineralization of Polyethylene Terephthalate

The PET mineralization into carbon dioxide resulting from hydrolysis was quantified through the titrimetric method (ISO 14855, 2005; Mohee et al., 2008; Funabashi et al., 2009). The *Bacillus* species AIIW2 was grown in 300 mL of BHB medium supplemented with 1 mg mL^{-1} of PET film as a carbon source. Carbon mineralization was also studied in a bacterial culture grown without PET in BHB medium considered as a control treatment. The inoculated and control flasks were connected with 20 mL of sterilized 0.1 N sodium hydroxide through silicon tubing. The sodium hydroxide flasks were changed every 5 days of incubation, and CO_2 production was measured in the initial flask through titration against 0.1 N HCl up to 35 days of incubation at 30°C (ISO 14855, 2005; Mohee et al., 2008). The CO_2 evolution during the remineralization of PET film was calculated from the CO_2 evolved from the control flask and the initial carbon content of PET films.

Hydrophilicity Measurement of Plastic Films

Water contact angles of the PET films after incubating with bacterial strain AIIW2 were measured using a Drop Shape Analysis System DSA 100 (KRÜSS GmbH, Hamburg, Germany). The PET films were removed from the culture medium and washed with 2% SDS followed by rinsing with distilled water and oven-dried overnight at 50°C. The PET films were analyzed every 15 days of incubation up to 90 days by dropping water on the surface, and the contact angle was measured at three points in triplication (Ribitsch et al., 2012).

Bond Indexes

Structural changes were analyzed in PET films (1 mg mL^{-1}) incubated in the bacterial culture and an uninoculated control medium every 30 days after incubation for 90 days through Fourier transform infrared spectroscopy (FTIR) (Spectrum EX, PerkinElmer) in the frequency range of 400–4,000 cm^{-1} with a resolution of 1 cm^{-1}. The relative absorbance intensities of the ester carbonyl bond were evaluated using the following formula (Albertsson et al., 1987):

Keto Carbonyl Bond Index (KCBI) = $I_{1715}/I_{1465;}$ Ester Carbonyl Bond Index (ECBI) = I_{1740}/I_{1465};

Vinyl Bond Index (VBI) = I_{1650}/I_{1465}; Internal Double Bond Index (IDBI) = I_{908}/I_{1465}.

RNA Extraction and Sequencing

The *Bacillus* AIIW2 was incubated for 7 days at 30°C in a shaker incubator by supplementing with PET as treatment and without PET as control experiment in BHB medium; RNA was extracted using the RNeasy Mini Kit (Qiagen, Germany) according to the manufacturer's instructions. The flasks were maintained in triplicates and were prepared for RNA extractions. The mRNA transcripts were sequenced as forward and reversed read files. The fastq sequence file with overlapping paired-end reads was created (MedGenome Labs Pvt., Ltd.). Illumina MiSeq 2 × 100-bp paired-end libraries with multiplex adaptors were prepared with an internal PhiX control by the Genoscreen platform (Malausa et al., 2011).

Sequencing Data Filtration and Differential Expression Analysis

The raw reads from sequencing data of all the replicates were processed for the quality check using FastQC (version 0.11.2) (Andrews, 2010). The low-quality reads were removed through a quality filter from the fastq raw reads using NGS QC toolkit v2.3.3 with stringent filtering criteria (Patel and Jain, 2012). The reads with $Q < 30$ bases were removed. Cufflink (version 2.2.1) was used to assemble the reads into transcripts on the basis of the mapping results (Trapnell et al., 2012). Filtered reads were aligned with the genome using bowtie2 (version 2.3.5.1) (Langmead and Salzberg, 2012) and Cufflinks. For evaluation of gene expression levels, the FPKM (per kilobase of exon per million fragments mapped) method was used. The analysis of differential expression was carried out using the cuffdiff (Trapnell et al., 2012). Significant differentially expressed genes (DEGs) were shown through heat map using an R script, and the scale of the heat map was set according to data values.

Functional Characterization

Gene ontology (GO) of DEGs was applied to study the gene functions. The GO annotation was performed using ShinyGO v0.61 (Ge et al., 2020) and illustrated through the R studio. The GO annotation was retrieved using a singular enrichment analysis statistical test at $p < 0.05$.

Pathway Analysis

To retrieve the KO [kyoto encyclopedia of genes and genomes (KEGG) Orthology] identifiers from KAAS database,[1] entire assembled sequences were utilized (Moriya et al., 2007). These KEGG identifiers were used in KEGG[2] to retrieve all possible metabolic pathways (Kanehisa et al., 2016).

Quantitative Real-Time Polymerase Chain Reaction

The expression profile of genes from RNA-seq analysis was validated through reverse transcriptase–polymerase chain reaction (RT-PCR). The total RNA was isolated from *Bacillus* species AIIW2 which were cultured in BHB supplemented with and without PET for 7 days. Reverse transcription was performed with QuantiTect Reverse Transcription Kit (Qiagen) to obtain the corresponding cDNA library according to the manufacturer's instruction. Thirteen up-selected and 12 down-selected genes were validated by the RNA-seq differential gene expression data via RT-PCR. Amplification was performed in 20-μL volume that contained 1 μL of the reverse-transcribed RNA samples, 10 μL of SYBR Green Master Mix (Qiagen) and 20 mM of each primer (**Supplementary Table 1**). Thermocycling conditions were as follows: 30 s at 95°C, followed by 40 cycles of 5 s at 95°C, 10 s at 58°C and 45 s at 72°C, and one cycle of 15 s at 95°C,

[1]http://www.genome.jp/tools/kaas/

[2]https://www.genome.jp/kegg/mapper.html

1 min at 60°C and 15 s at 60°C for 35 cycles of amplification in Real-Time PCR Detection System (Bio-Rad). Expression of the housekeeping gene, 16S rRNA was used as a reference gene to normalize tested genes in *Bacillus* species AIIW2. The Ct value calculated from 16S rRNA reference gene was used to determine the relative abundance of target transcripts (Su et al., 2016). The RT-PCR results were compared with the transcriptome data to detect the correlation of each gene expression.

Reverse-Phase High-Pressure Liquid Chromatography

The product of PET hydrolysis was determined through reverse-phase high-pressure liquid chromatography (HPLC, RID-10A, Shimadzu, Japan). The bacterial strain AIIW2 was cultured for 30 days in 100 mL of BHB supplemented with PET film as a carbon source at 30°C under shaking conditions. After incubation, the culture supernatant was centrifuged at 10,000 rpm for 10 min and freeze-dried. The freeze-dried culture supernatant was acidified up to pH 2.5 using 2 M HCl, and hydrolysis products were extracted with ethyl acetate. The extracted hydrolyzed products were filtered with 0.2-μm filter and 20 μL injected in C_{18} column (Shimadzu, Japan). The mobile phase was 20% acetonitrile, 20% 10 mM phosphoric acid, and 60% (vol/vol) MilliQ water with a flow rate of 1 mL min^{-1} at wavelength 241 nm. The peaks were quantified through standard curves of terephthalate (TPA), mono-(2-hydroxyethyl) terephthalic acid (MHET), and *bis*(2-hydroxyethyl) terephthalate (BHET) (concentration range, 0.1–1 mM).

String Network

Carboxylesterase and aldehyde dehydrogenase genes were analyzed for their interaction network in STRING database[3] (Szklarczyk et al., 2011) using the Cytoscape 2.8 version (Smoot et al., 2011).

RESULTS

Polyethylene Terephthalate Degradation and Remineralization

To determine the degradation of standard PET film by marine *Bacillus* species AIIW2, weight reduction of PET film was observed every 15 days up to 90 days of the incubation period with the bacteria. The weight loss of PET film in percent was observed as 0.42, 0.82, 0.83, 0.94, 1.27, and 1.93% degradation after 15, 30, 45, 60, 75, and 90 days of incubation, respectively (**Figure 1**). However, no weight reduction was observed in PET film incubated without bacteria.

The CO_2 evolution was estimated to confirm PET assimilation and mineralization by bacterial strain AIIW2. It was observed that the conversion of PET into CO_2 (cumulative) was 11.78, 41.50, 74.29, 96.16, 116.49, and 128.07 mg CO_2 g^{-1} of C from days 5, 10, 15, 20, 30, and 35, respectively (**Figure 2**). The experiment was compared against control in which bacterial cultures were maintained without any carbon source.

[3]http://string-db.org/

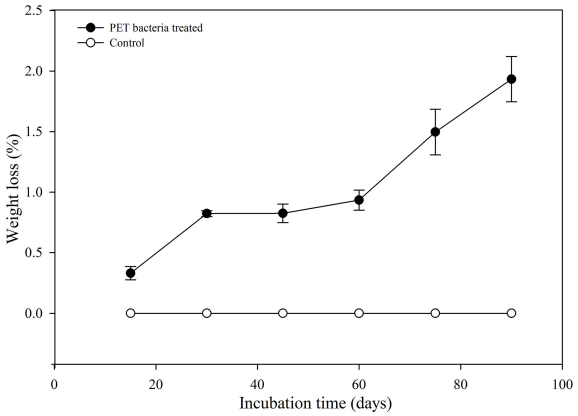

FIGURE 1 | Weight loss of PET film after incubation with *Bacillus* species AIIW2.

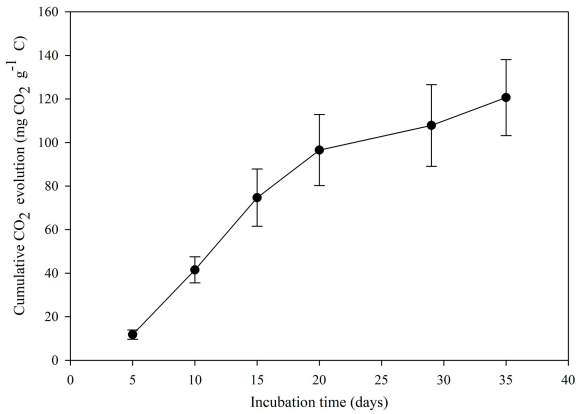

FIGURE 2 | Cumulative CO_2 evolution by bacterial strain during growth with PET.

Bacteria Adherence and Morphological Disruption

The colonization of the bacteria cells on the PET surface was confirmed through SEM after 30 days of incubation, and it was observed that the bacterial strain AIIW2 colonized and disrupted the PET surface, whereas untreated control film remains intact (**Figure 3**).

Hydrophilicity Measurement of Polyethylene Terephthalate Films

An analysis of the water contact angle on the PET film showed that after 90 days of bacterial treatment with strain AIIW2 was reduced from 77.3° (control) to 55.8° (bacteria treated) (**Supplementary Figure 1**). The results also indicated that the inoculation of bacterial strain AIIW2 decreased the hydrophobicity of the PET film and increased the surface hydrophilicity from 29.7 to 44.2% in 90 days (**Figure 4**). As the PET surface became less hydrophobic, it will be less resistant to subsequent degradation by the bacterial cells.

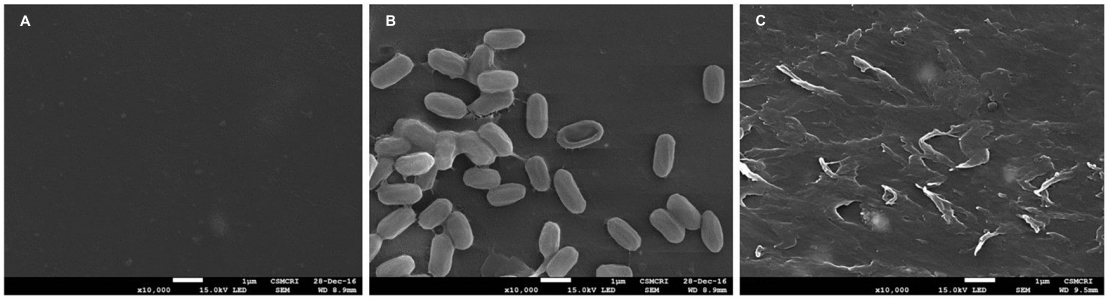

FIGURE 3 | SEM image of PET film after 30 days of incubation **(A)** control film, **(B)** with *Bacillus* species AIIW2, and **(C)** PET surface after washing off the bacterial cells.

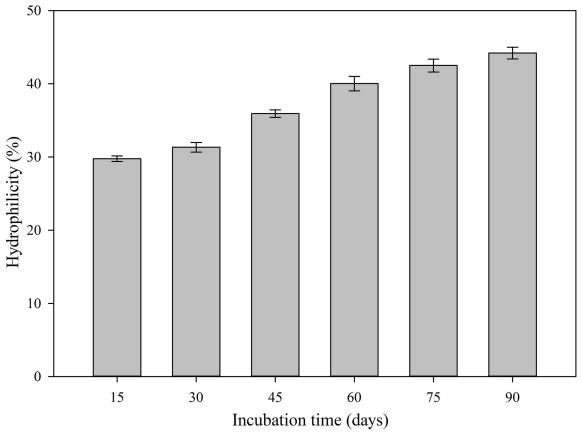

FIGURE 4 | The hydrophilicity of bacterial treated PET surface during the incubation period.

Fourier Transform Infrared Spectroscopy

Formation or disappearance of acids (1,715 cm^{-1}), ketones (1,740 cm^{-1}), and double bonds (1,640 and 908 cm^{-1}) was monitored using the FTIR to determine the mechanism of the biodegradation process. KCBI, ECBI, VBI, and IDBI were calculated and confirmed the structural transformation of PET due to bacterial action. The bond indexed was observed to be unchanged in PET during the 90 days of incubation period in BHB medium without bacteria. However, bacterial treated PET film had increased KCBI and ECBI and a reduction in VBI and IDBI over the incubation period of 90 days (**Figure 5**).

Read Quality Filtration

Misassembled transcripts from RNA-seq were filtered out with the help of genome sequence data of *Bacillus* species AIIW2 (KY694465) (Kumari et al., 2020). A total of 63,27,406 and 56,70,745 high-quality raw reads were generated out of three replicates of transcriptome sequencing data of control and treated samples, respectively. After filtration, there were a total of 63,26,176 and 56,69,934 high-quality filtered reads were retrieved in control and treated samples, respectively. The detailed description of filtered reads is given in **Supplementary Table 2**. The Short Read Achieve (SRA) data were deposited in NCBI databank with SRA identifier SRP279031 and accession number MZ322848.

Identification of Differentially Expressed Genes

The RNA-seq profiling of *Bacillus* species AIIW2 while growing with PET as carbon source and without PET was performed to unveil the genes intricate in the degradation process. The differential gene expression of bacterial culture when grown with PET was compared with that grown without PET. A total of 3,992 genes were generated via mapping of reads to the reference genome. The comprehensive information of genes and their annotations are given in **Supplementary Table 3**. Identification of differential expression of genes during PET utilization was based on FPKM calculation of each gene, and a total of 2,031 DEGs were detected, among which 1,073 genes were up-regulated and 958 genes were down-regulated (**Supplementary Table 4**). Top up-regulated and down-regulated genes are shown in **Figure 6** through heat map using the log2 FPKM values. Based on analysis of expression of these genes, enoyl-CoA hydratase (EC 4.2.1.17), acetyltransferase family (EC 2.3.1), activation of degradative enzymes, aldehyde dehydrogenase (EC 1.2.1.3), 3-oxoacyl-[acyl-carrier protein] reductase (EC 1.1.1.100), hydrolases, carboxylesterases, and putative permeases were up-regulated in bacteria-treated PET as carbon source genes. Likewise the expression of small acid-soluble spore protein beta-type SASP, acid-soluble spore protein H, cold shock protein CspD, YfhS protein, SinR regulator (post–exponential-phase responses, i.e., competence and sporulation) genes, antiholin-like protein LrgA, and sporulation-specific SASP protein were down-regulated genes. The 28.11% of hypothetical genes differentially also expressed when bacteria were grown with PET, indicating that the proteins with unknown functions were involved directly or indirectly for substrate adaptation.

Functional Analysis of Differentially Expressed Genes

There were 3,769 genes used for GO analysis for identifying the function of DEG. These DEGs are categorized into 76 functional groups and into three categories (i.e., biological

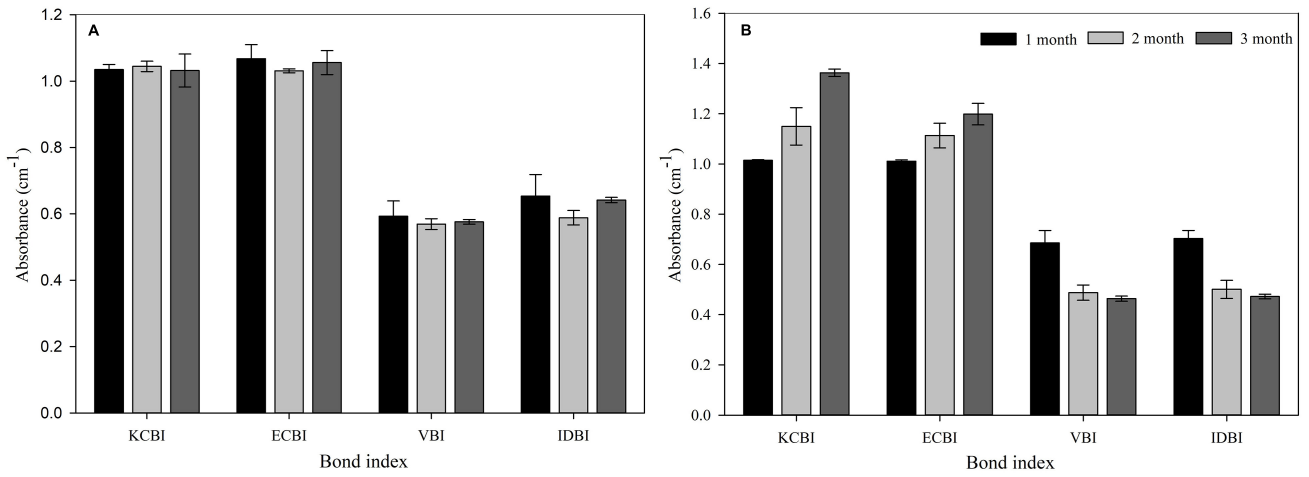

FIGURE 5 | Bond indexes of PET film after incubation **(A)** without and **(B)** with *Bacillus* species AIIW2 for 3 months. KCBI, Keto Carbonyl Bond Index; ECBI, Ester Carbonyl Bond Index; VBI, Vinyl Bond Index; IDBI, Internal Double Bond Index.

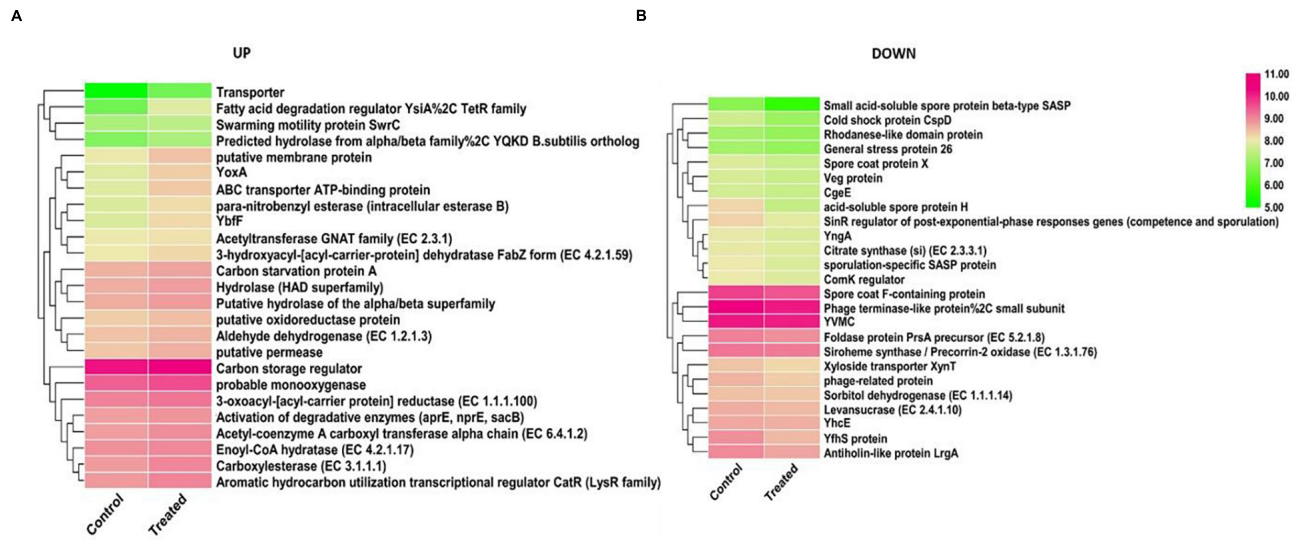

FIGURE 6 | The expression patterns of the DEGs identified between control and treated samples. The heat map represents the relative expression levels of 25 genes examined in up-regulated **(A)** and down-regulated **(B)** genes based on log2 FPKM values.

process, molecular function, and cellular component) shown in **Figure 7** with false discovery rate (FDR) value of less than 0.01 (**Supplementary Table 5**). The results of GO annotations displayed that ATPase-dependent transmembrane transport complex, ATP-binding cassette (ABC) transporter complex, Nbp35-Cfd1 ATPase complex, and transporter complex were dominant in cellular components, whereas transmembrane transport, single-organism transport, and single-organism localization were dominant in the biological process. The transmembrane transporter activity, ATPase activity, transmembrane movement of substances, primary active transmembrane transporter, and hydrolase activity act on acid anhydrides involved in the molecular function.

Kyoto Encyclopedia of Genes and Genomes Analysis

The biological pathways in the *Bacillus* species AIIW2 grown in PET treatment were mapped to the KEGG database. A total of 1,974 contigs were assigned to 218 KEGG pathways; 511 contigs (25.88%) were involved in metabolic pathways, 156 (7.90%) contigs for microbial metabolism in diverse environments, 72 contigs (3.64%) for ABC transporters, 24 contigs (1.21%) for oxidative phosphorylation, 18 contigs (0.91%) for carbon fixation pathways in prokaryotes, 8 contigs (0.40%) for benzoate degradation, and 5 contigs (0.25%) for biofilm formation (**Figure 8** and **Supplementary Table 6**). Interestingly, most up-regulated pathways were related to an

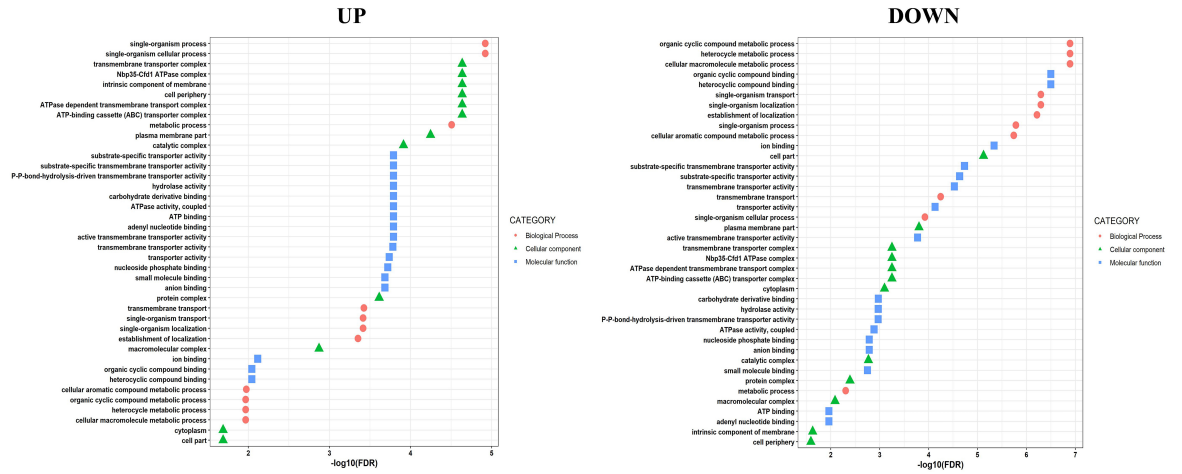

FIGURE 7 | Gene ontology classification in up-regulated and down-regulated genes during PET utilization.

intermediary pathway and quorum sensing such as the Krebs cycle and β-oxidation. However, there are voids observed within the catabolic trails, due to the limited number of enzymes annotation.

Reverse Transcriptase–Polymerase Chain Reaction Validation of Differentially Expressed Genes

For the validation of transcriptome expression profile, quantitative RT-PCR analysis (16S rRNA gene used as reference) was performed. The expression of 13 up and 12 down DGEs were validated using RT-PCR. The fold-change expressions were compared with RNA-seq expression profile data (**Figure 9** and **Supplementary Table 7**). RT-PCR showed considerable correlation with transcriptome profile between bacterial culture grown without and with PET, suggesting the consistency and accuracy of the RNA-seq expression analysis.

Network of Carboxylesterase and Aldehyde Dehydrogenases Gene

The network analysis of carboxylesterase and aldehyde dehydrogenases was performed to understand functional interactions between the expressed proteins by integrating protein–protein interaction with close species based on gene orthology. The protein–protein interaction networks were constructed for carboxylesterases and aldehyde dehydrogenases based on RT- PCR and HPLC data and illustrated pathways for PET biodegradation (**Figure 10**). The protein–protein interaction networks were constructed for carboxylesterases and aldehyde dehydrogenases based on RT-PCR and HPLC data. The significantly up-regulated genes such as carboxylesterase and aldehyde dehydrogenase that might have a crucial function in PET degradation were used to construct the protein–protein interaction networks (**Figure 11**). There were 13 nodes and 24 edges detected in carboxylesterase, whereas 7 nodes and 17 edges were detected in aldehyde dehydrogenase, at a confidence (score) cutoff 0.40. **Table 1** lists the network interactors and their description, which provided information about the physical and functional associations between proteins and pathways from the database.

DISCUSSION

The present study focused on finding PET-degrading gene in marine *Bacillus* species AIIW2 and illustrating the involved pathway. PET degradation by marine bacterial strain was determined up to 3 months by measuring weight loss and degree of mineralization. The preweighted standard and intact PET film had 1.93% of dry weight reduction after 3 months of incubation with marine *Bacillus* AIIW2 (**Figure 1**). In a previous study, hydrolase from *T. fusca was* demonstrated to degrade PET-G and PET-B by 50% weight loss in 3 weeks (Mueller, 2006). PET-GF and PET-S degraded approximately 13.5 and 27.0%, respectively, by cutinase from *Saccharomonospora viridis* (Kawai et al., 2014). The CO_2 evolution test followed up evidence for the biodegradability of a test material. Castro-Aguirre et al. (2017). Kumar et al. (2020) reported 30.52% weight reduction and mineralization of PET into CO_2 and water after incubating with *Rhodococcus* species grown with terephthalate supplementation for 132 h. The rate of PET mineralization by strain AIIW2 followed up by 128.02 mg CO_2 g^{-1} of C evolved cumulatively after 35 days and increased with the incubation period (**Figure 2**). The carbon dioxide remineralization was 0.051 and 0.046 cm^3 from cellulose filter paper and Novamont Mater-Bi (constituted 60% starch), respectively, in 5 days of incubation (Mohee et al., 2008). The bacterial colonization on the PET film is an essential prerequisite in biodegradation. The SEM images of bacteria-treated PET film support the efficient attachment and degradation of the surface compared with control film (**Figure 3**). Koshti et al. (2018) suggested that the bacterial colonization on the PET surface was an initiation of bacterial action for the degradation activity. The surface contact angle reduced from

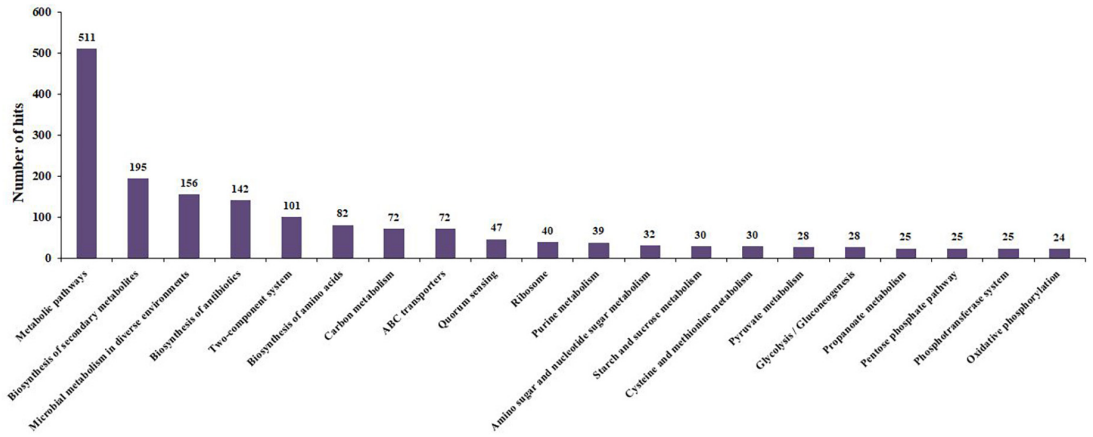

FIGURE 8 | Top 20 KEGG pathways during PET utilization by *Bacillus* species AIIW2.

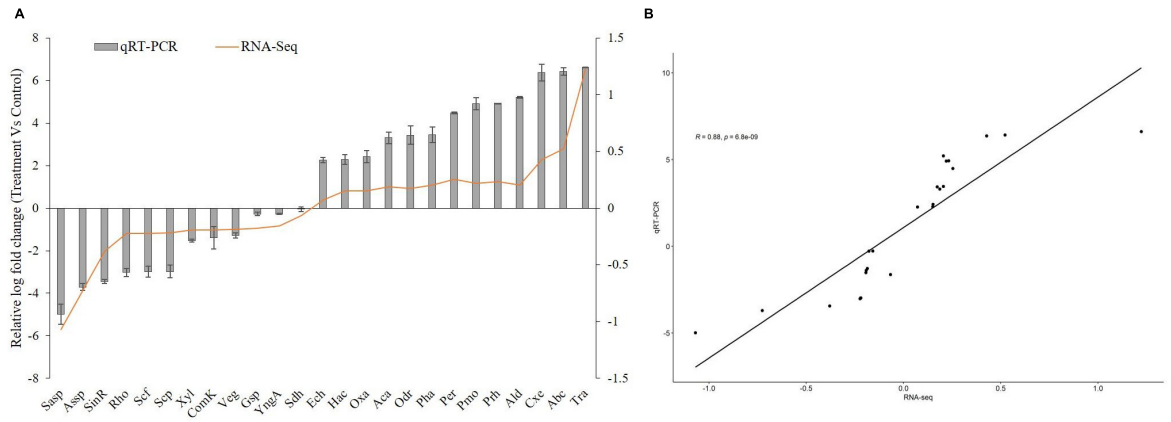

FIGURE 9 | Quantitative RT-PCR of DEGs of *Bacillus* species AIIW2 when grown with PET film compared with culture grown without PET film **(A)**. Correlation analysis between qRT-PCR and RNA-Seq data expression values **(B)**. The *R* and *p* represent the Pearson correlation coefficient and *p* value, respectively.

77.3° to 55.8° of the PET film after 90 days of bacterial incubation. The reduction in water contact angle of PET surface represents a decreased hydrophobicity and increased hydrophilicity after 90 days of incubation with *Bacillus* species AIIW2 (**Figure 4**), which is in corroboration with the observations of Radhakumary et al. (2005) and Arutchelvi et al. (2008). The contact angle of corona discharge treatment and UV-treated polyethylene was found to be reduced significantly up to 54.6% in corona discharged film and 24.56% in UV-treated film after incubation with fungal consortium (Matsunaga and Whitney, 2000). The contact angle of chitosan-blended polyethylene matrix was found to be decreased with an increase in chitosan percentage in structure due to the hydrophilic property of chitosan in comparison to unplasticized polyethylene film; moreover, the cross-linking of palm oil also added hydrophilicity in the LDPE structure incubated with *Aspergillus niger* (SunilKumar et al., 2012). The water contact angle of PET film treated with *Bacillus subtilis* was found to be reduced from 68.2° to 62.6° (Ribitsch et al., 2011).

The formation of KCBI and ECBI and reduction in IDBI and VBI were observed by FTIR spectra that confirmed the structural transformation of PET (**Figure 5**). The formation of acids (1,715 cm^{-1}) and ketones (1,740 cm^{-1}) and disappearance of double bonds (1,640 and 908 cm^{-1}) were analyzed using the FTIR to elucidate the PET biodegradation process. Notably, the appearance of hydrolyzable carbonyl functional group in the polymer structure will provide the site for hydrolytic enzyme action for biotransformation. The increase of KCBI and ECBI showed oxidoreductive enzyme activity on PET film incubated with strain AIIW2. The reduction in VBI and IDBI indicated the deformation and reduction in internal structure, whereas there was negligible variation in the bond index in PET film incubated without bacteria. The presence of carbonyls bonds as a product of degradation suggests the presence of oxidoreductive enzymes (Harshvardhan and Jha, 2013). The formation of double bonds or esters in the polymer chain may be due to the Norrish type II reaction proposed earlier (Albertsson et al., 1987). Janczak et al. (2018) reported structural changes in PET film after

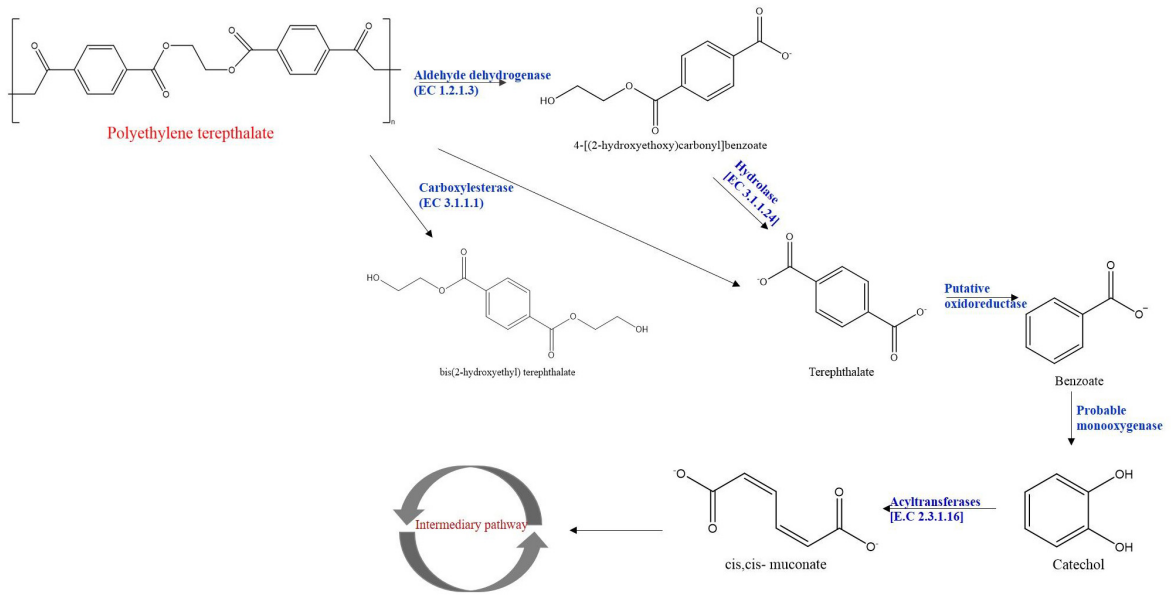

FIGURE 10 | Proposed PET metabolism by *Bacillus* species AIIW2.

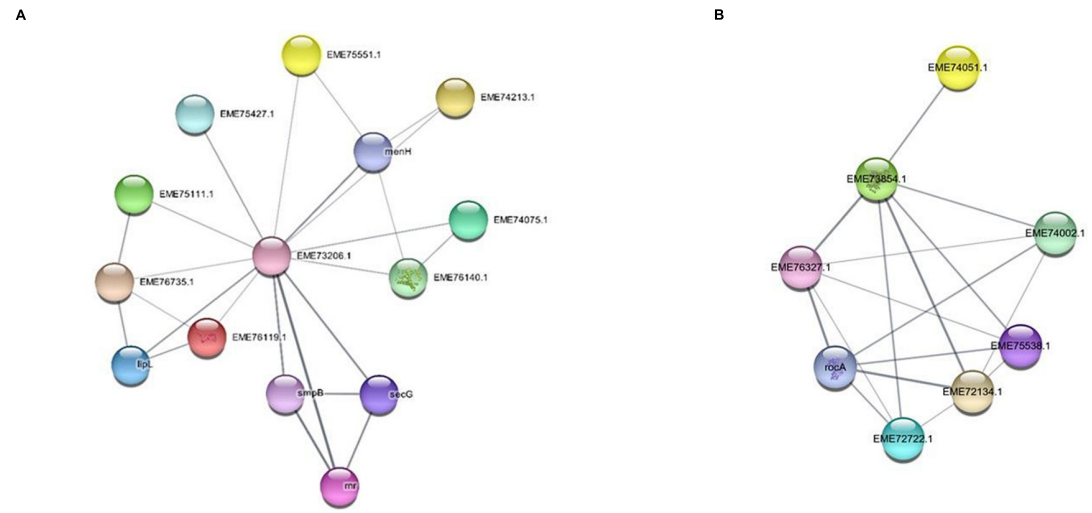

FIGURE 11 | Network analysis of **(A)** carboxylesterase and **(B)** aldehyde dehydrogenase gene. String interaction network displaying the relationship of gene clustered in a module.

incubation with rhizospheric microbe in carbonyl bond indexes. The carbonyl bond indexes, that is, KCBI, ECBI VBI, and IDBI of HDPE, were increased when incubated with *Arthrobacter* species; however, whereas in the incubation with *Pseudomonas* species KCBI, ECBI, and VBI increased, IDBI decreased compared with the control (Balasubramanian et al., 2010).

The heat map represents that the genes involved in carbon metabolism and cell transport system were up-regulated in cells growing with PET, whereas sporulation genes were expressed in the absence of PET. This observation indicates the nodes of PET assimilation via cellular carbon metabolism by strain AIIW2 (**Figure 6**). A similar pattern was also observed in GO; that is, biological processes, molecular functions, and cellular components genes were up-regulated while growing with PET film (**Figure 7**). In a study on polyethylene degradation by *Rhodococcus ruber* strain, fatty acid degradation, alkane degradation, and β-oxidation pathways were the most up-regulated pathways (Gravouil et al., 2017).

In this study, the KEGG analysis showed that supplementation of PET induces the bacterial assimilation pathway for its utilization; indeed, the *Bacillus* species AIIW2 grows when PET

TABLE 1 | Network description of carboxylesterase and aldehyde dehydrogenase of marine *Bacillus* species.

Gene	Interactor	Description of interactor
Carboxylesterase	rnr	Ribonuclease R
	smpB	SsrA-binding protein
	secG	Preprotein translocase subunit SecG
	menH	Putative 2-succinyl-6-hydroxy-2,4-cyclohexadiene-1-carboxylate synthase
	lipL	Octanoyl-[GcvH]: protein N-octanoyltransferase
	EME75427.1	Carboxylic ester hydrolase
	EME74075.1	Esterase/lipase
	EME76140.1	Enoyl-[acyl-carrier-protein] reductase (NADH)
	EME75111.1	TPR repeat-containing protein YrrB
	EME75551.1	8-Amino-7-ketopelargonate synthase
	EME74213.1	8-Amino-7-ketopelargonate synthase
	EME76735.1	UPF0354 Uncharacterized protein conserved in bacteria
	EME76119.1	Adapter protein MecA
Aldehyde dehydrogenase	EME76327.1	COG1012 NAD-dependent aldehyde dehydrogenases; belongs to the aldehyde dehydrogenase family
	EME75538.1	COG1012 NAD-dependent aldehyde dehydrogenases; belongs to the aldehyde dehydrogenase family
	rocA	L-Glutamate γ-semialdehyde dehydrogenase; COG1012 NAD-dependent aldehyde dehydrogenases; belongs to the aldehyde dehydrogenase family; RocA subfamily
	EME72722.1	COG1012 NAD-dependent aldehyde dehydrogenases; belongs to the aldehyde dehydrogenase family
	EME74002.1	COG1012 NAD-dependent aldehyde dehydrogenases
	EME73854.1	COG1012 NAD-dependent aldehyde dehydrogenases; in the C-terminal section; belongs to the iron-containing alcohol dehydrogenase family
	EME72134.1	COG1012 NAD-dependent aldehyde dehydrogenases; belongs to the aldehyde dehydrogenase family
	EME74051.1	COG1028 dehydrogenases with different specificities (related to short-chain alcohol dehydrogenases)

is provided as a carbon source (**Figure 8**). The top 13 up-regulated genes were identified as being differentially expressed in PET treated with bacterial cultures. The Ct averages and standard error were calculated to find the log-fold expression of the genes in the treated and control samples. The RT-PCR results also displayed the highest relative fold change in carboxylesterase (EC 3.1.1.1), ABC transporter, and transporter genes predicted to have 6.37, 6.48, and 6.61, respectively, in PET treated in comparison to control *Bacillus* species AIIW2 grown in the absence of PET film (**Figure 9**). The secretion of hydrolytic enzyme that hydrolyzes the PET structure results in carbonyl bond index and reduction in internal as well as vinyl bonds (Albertsson et al., 1987; Balasubramanian et al., 2010). Further, the transport system helps the subsequently hydrolyzed oligomers for cellular assimilation (Gravouil et al., 2017). The release hydrolysis product of PET during incubation with *Bacillus* species AIIW2 was quantified by reverse-phase HPLC. The presence of BHET, MHET, and TPA as a degradation product aldehyde dehydrogenase and esterase activity involved in the initial degradation step, although in combination with expression profiling (RNA-seq and RT- PCR), suggest the same. The concentrations of released BHET, MHET, and TPA were found to be 0.34, 14.01, and 107.06 mM, respectively, in 30 days of incubation by HPLC analysis. The TPA was found to be a major hydrolytic product suggesting the PET hydrolyzed into BHET, MHET, and TPA, where TPA would further hydrolyze from MHET by carboxylesterase and hydrolase (Barth et al., 2015; Yoshida et al., 2016). Yoshida et al. (2016) proposed the degradation of PET by *Ideonella sakaiensis* through hydrolysis of PET into MHET and TPA extracellularly and further transported into the cell to catabolism. In a study, TPA was released higher than MHET as a resulting product of novel esterase from *T. halotolerans*, where amorphous PET fiber was hydrolyzed into BHET (Ribitsch et al., 2012). The cutinase from *Fusarium solani* hydrolyzed PET into BHET, MHET, and TPA, although MHET and TPA ratios were higher (Vertommen et al., 2005). The degradation pathway was elucidated based on changes in the functional groups and HPLC determination. Carboxylesterase is likely to hydrolyze PET into BHET and TPA, whereas MHET by aldehyde dehydrogenase activity (**Figure 10**).

In a study, a network analysis of degrading protein obtained from the genome of *Sphingopyxis* strains deciphers interaction with the core content (Verma et al., 2020). Although carboxylesterase and aldehyde dehydrogenase genes from RNA-seq data were mapped for interaction with a relative set of hydrolytic proteins, the 13 genes of carboxylesterase were mapped, and interactors of catabolic and central metabolism were identified with both sets of genes. This determines the distant placement of proteins for growth and metabolism while growing with an unusual substrate such as PET. Interactome network analysis provided the relationship of carboxylesterase genes (EME73206.1) with the interactors, such as rnr, smpB, secG, menH, lipL, EME75427.1, EME74075.1, EME76140.1, EME75111.1, EME75551.1, EME74213.1, EME76735.1, and EME76119.1 (Barth et al., 2016), and seven genes of aldehyde dehydrogenase (EME73854.1) from the iron-containing alcohol dehydrogenase family were mapped, and their interactors were EME76327.1, EME75538.1, EME72722.1, EME74002.1, EME72134, rocA L-glutamate γ-semialdehyde dehydrogenase belonging to the aldehyde dehydrogenase family, EME74051.1 dehydrogenase with different specificities (short-chain alcohol dehydrogenases) (Reid and Fewson, 1994). The network analysis of carboxylesterase showed that interactions were present between proteins from essential cellular metabolism, such as ribonuclease R, SsrA-binding protein, preprotein translocase subunit SecG, putative 2-succinyl-6-hydroxy-2,4-cyclohexadiene-1-carboxylate synthase, N-octanoyl transferase,

carboxylic ester hydrolase, esterase/lipase, enoyl-[acyl-carrier-protein] reductase (NADH), TPR repeat-containing protein YrrB, 8-amino-7-ketopelargonate synthase, 8-amino-7-ketopelargonate synthase, UPF0354 uncharacterized protein conserved in bacteria, and adapter protein MecA. Similarly, aldehyde dehydrogenase interactors were NAD and short-chain alcohol dehydrogenases (**Figure 11**). The identification of interactions between genes and between proteins established elucidation of the functions of genes of interest or for a better understanding of a PET degradation process.

CONCLUSION

PET is the most common contributor to solid wastes in the environment. A growing body of literature supports microbial degradation of PET polymer; however, it cannot resolve how degradation occurs. Marine bacterium *Bacillus* species AIIW2 had the ability to degrade PET structure and remineralize into CO_2. The comparative transcriptome profile of strain AIIW2 suggested that hydrolytic enzymes were playing a key role during the utilization of PET film by the bacteria. The degradation product and predicted pathway have suggested the role of aldehyde dehydrogenase and carboxylesterase in PET hydrolysis. The genes traced to degrade PET were confirmed by detecting the hydrolytic product of PET and carboxylesterase gene found to be a key enzyme in the degradation process and selected for cloning. The degradation pathway had been elucidated based on changes in the functional group and HPLC determination. We provide transcriptome-based insight into the biodegradation of PET films by marine bacteria *Bacillus* species AIIW2, although the gene annotated during the degradation process could help to develop an engineered microbial system for improved degradation of PET. The study will establish an understanding of plastic biodegradation through microbial resources as eco-friendly for reducing pollution. Altogether, this study provides a map involved during the PET degradation by marine bacterial strain.

DATA AVAILABILITY STATEMENT

The datasets presented in this study can be found in online repositories. The names of the repository/repositories and accession number(s) can be found below: GenBank, MZ322848.

AUTHOR CONTRIBUTIONS

AK performed the experiments and drafting the manuscript. DC and BJ contributed to planning the experiment and manuscript preparation. NB and SB performed the bioinformatics analysis. All authors contributed to the article and approved the submitted version.

FUNDING

This work was financially supported by the Council of Scientific and Industrial Research (CSIR), New Delhi (CSC0120-Waste to Wealth) and the Department of Biotechnology (Senior Research Fellowship to AK), Government of India.

ACKNOWLEDGMENTS

We would like to thank SciGenome foundation for supporting with mRNA sequencing facility through their genome grant. CSIR-CSMCRI communication No. 141/2021.

SUPPLEMENTARY MATERIAL

The Supplementary Material for this article can be found online at: https://www.frontiersin.org/articles/10.3389/fmicb.2021.751571/full#supplementary-material

Supplementary Figure 1 | Water contact angle images on PET film surface after incubating with *Bacillus* species AIIW2.

Supplementary Table 1 | Quantitative RT-PCR primers sequence.

Supplementary Table 2 | Description of high-quality read. * C1_R1, C1_R2; C2_R1, C2_R2; C3_R1, C3_R2—paired reads of control samples in triplicates. * T1 R1, T1 R2; T2 R1, T2 R2, T3 R1, T3 R2—paired reads of PET treated samples in triplicates.

Supplementary Table 3 | A detailed description of filtered reads for mRNA-seq.

Supplementary Table 4 | Up- and down-regulated genes in *Bacillus* AIIW2 growing with PET film.

Supplementary Table 5 | Genes and their annotations of *Bacillus* AIIW2 growing with and without PET film mRNA-seq profile.

Supplementary Table 6 | GO annotation and functional categorization of DEGs in *Bacillus* AIIW2 growing with PET film.

Supplementary Table 7 | RT-PCR and RNA-seq expression correlation data.

REFERENCES

Albertsson, A. C., Andersson, S. O., and Karlsson, S. (1987). The mechanism of biodegradation of polyethylene. *Polym. Degrad. Stab.* 18, 73–87. doi: 10.1016/0141-39108790084-X

Andrady, A. L., and Neal, M. A. (2009). Applications and societal benefits of plastics. *Philos. Trans. R. Soc. B Biol. Sci.* 364, 1977–1984.

Andrews, S. (2010). *FastQC: a Quality Control Tool for High Throughput Sequence Data*. Version 0.11. 2.

Arutchelvi, J., Sudhakar, M., Arkatkar, A., Doble, M., Bhaduri, S., and Uppara, P. V. (2008). Biodegradation of polyethylene and polypropylene. *Ind. J. Biotechnol.* 7, 9–22.

Austin, H. P., Allen, M. D., Donohoe, B. S., Rorrer, N. A., Kearns, F. L., Silveira, R. L., et al. (2018). Characterization and engineering of a plastic-degrading aromatic polyesterase. *Proc. Natl. Acad. Sci. U S A.* 115, E4350—-E4357.

Balasubramanian, V., Natarajan, K., Hemambika, B., Ramesh, N., Sumathi, C. S., Kottaimuthu, R., et al. (2010). High-density polyethylene (HDPE)-degrading potential bacteria from marine ecosystem of Gulf of Mannar. *India. Lett. Appl. Microbiol.* 51, 205–211. doi: 10.1111/j.1472-765X.2010.02883.x

Barth, M., Honak, A., Oeser, T., Wei, R., Belisário-Ferrari, M. R., Then, J., et al. (2016). A dual enzyme system composed of a polyester hydrolase and a carboxylesterase enhances the biocatalytic degradation of polyethylene terephthalate films. *Biotechnol. J.* 11, 1082–1087. doi: 10.1002/biot.201600008

Barth, M., Oeser, T., Wei, R., Then, J., Schmidt, J., and Zimmermann, W. (2015). Effect of hydrolysis products on the enzymatic degradation of polyethylene terephthalate nanoparticles by a polyester hydrolase from Thermobifida fusca. *Biochem. Eng. J.* 93, 222–228. doi: 10.1016/j.bej.2014.10.012

Bollinger, A., Thies, S., Knieps-Grünhagen, E., Gertzen, C., Kobus, S., Höppner, A., et al. (2020). A novel polyester hydrolase from the marine bacterium *Pseudomonas* aestusnigri – structural and functional insights. *Front. Microbiol.* 11:114. doi: 10.3389/fmicb.2020.00114

Castro-Aguirre, E., Auras, R., Selke, S., Rubino, M., and Marsh, T. (2017). Insights on the aerobic biodegradation of polymers by analysis of evolved carbon dioxide in simulated composting conditions. *Polym. Degrad. Stab.* 137, 251–271.

Chen, Z., Wang, Y., Cheng, Y., Wang, X., Tong, S., Yang, H., et al. (2020). Efficient biodegradation of highly crystallized polyethylene terephthalate through cell surface display of bacterial PETase. *Sci. Total Environ.* 709:136138. doi: 10.1016/j.scitotenv.2019.136138

Funabashi, M., Ninomiya, F., and Kunioka, M. (2009). Biodegradability evaluation of polymers by ISO 14855-2. *Int. J. Mol. Sci.* 10, 3635–3654.

Ge, S. X., Jung, D., and Yao, R. (2020). ShinyGO: a graphical gene-set enrichment tool for animals and plants. *Bioinformatics* 36, 2628–2629.

Gong, J., Kong, T., Li, Y., Li, Q., Li, Z., and Zhang, J. (2018). Biodegradation of microplastic derived from poly(ethylene terephthalate) with bacterial whole-cell biocatalysts. *Polymers (Basel)* 10:1326. doi: 10.3390/polym10121326

Gravouil, K., Ferru-Clément, R., Colas, S., Helye, R., Kadri, L., Bourdeau, L., et al. (2017). Transcriptomics and lipidomics of the environmental strain Rhodococcus ruber point out consumption pathways and potential metabolic bottlenecks for polyethylene degradation. *Environ. Sci. Technol.* 51, 5172–5181. doi: 10.1021/acs.est.7b00846

Harshvardhan, K., and Jha, B. (2013). Biodegradation of low-density polyethylene by marine bacteria from pelagic waters, Arabian Sea, India. *Mar. Pollut. Bull.* 77, 100–106. doi: 10.1016/j.marpolbul.2013.10.025

Hermanová, S., Šmejkalová, P., Merna, J., and Zarevúcka, M. (2015). Biodegradation of waste PET based copolyesters in thermophilic anaerobic sludge. *Polym. Degrad. Stab.* 111, 176–184.

ISO 14855 (2005). *Determination of the Ultimate Aerobic Biodegradability and Disintegration of Plastic Materials Under Controlled Composting Conditions—Method by Analysis of Evolved Carbon Dioxide*. Geneva: ISO.

Janczak, K., Dąbrowska, G. B., Raszkowska-Kaczor, A., Kaczor, D., and Hrynkiewicz, K. (2020). Biodegradation of the plastics PLA and PET in cultivated soil with the participation of microorganisms and plants. *Int. Biodeterior. Biodegrad.* 155:105087. doi: 10.1016/j.ibiod.2020.105087

Janczak, K., Hrynkiewicz, K., Znajewska, Z., and Dąbrowska, G. (2018). Use of rhizosphere microorganisms in the biodegradation of PLA and PET polymers in compost soil. *Int. Biodeterior. Biodegrad.* 130, 65–75. doi: 10.1016/j.ibiod.2018.03.017

Kanehisa, M., Sato, Y., Kawashima, M., Furumichi, M., and Tanabe, M. (2016). KEGG as a reference resource for gene and protein annotation. *Nucleic Acids Res.* 44, D457—-D462.

Kawai, F., Oda, M., Tamashiro, T., Waku, T., Tanaka, N., Yamamoto, M., et al. (2014). A novel Ca2+-activated, thermostabilized polyesterase capable of hydrolyzing polyethylene terephthalate from Saccharomonospora viridis AHK190. *Appl. Microbiol. Biotechnol.* 98, 10053–10064. doi: 10.1007/s00253-014-5860-y

Koshti, R., Mehta, L., and Samarth, N. (2018). Biological recycling of polyethylene terephthalate: a mini-review. *J. Polym. Environ.* 26, 3520–3529. doi: 10.1007/s10924-018-1214-7

Kumar, V., Maitra, S. S., Singh, R., and Burnwal, D. K. (2020). Acclimatization of a newly isolated bacteria in monomer tere-phthalic acid (TPA) may enable it to attack the polymer poly-ethylene tere-phthalate(PET). *J. Environ. Chem. Eng.* 8:103977. doi: 10.1016/j.jece.2020.103977

Kumari, A., Bano, N., Chaudhary, D. R., and Jha, B. (2020). Draft genome sequence of plastic degrading *Bacillus sp.* AIIW2 isolated from the Arabian ocean. *J. Basic Microbiol.* 61, 37–44.

Kumari, A., Chaudhary, D. R., and Jha, B. (2019). Destabilization of polyethylene and polyvinylchloride structure by marine bacterial strain. *Environ. Sci. Pollut. Res.* 26, 1507–1516. doi: 10.1007/s11356-018-3465-1

Langmead, B., and Salzberg, S. L. (2012). Fast gapped-read alignment with Bowtie 2. *Nat. Methods* 9:357.

Lithner, D., Larsson, Å, and Dave, G. (2011). Environmental and health hazard ranking and assessment of plastic polymers based on chemical composition. *Sci. Total Environ.* 409, 3309–3324.

Malausa, T., Gilles, A., Meglécz, E., Blanquart, H., Duthoy, S., Costedoat, C., et al. (2011). High-throughput microsatellite isolation through 454 GS-FLX Titanium pyrosequencing of enriched DNA libraries. *Mol. Ecol. Resour.* 11, 638–644.

Matsunaga, M., and Whitney, P. J. (2000). Surface changes brought about by corona discharge treatment of polyethylene film and the effect on subsequent microbial colonization. *Polym. Degrad. Stab.* 70, 325–332. doi: 10.1016/S0141-3910(00)00105-1

Mohee, R., Unmar, G. D., Mudhoo, A., and Khadoo, P. (2008). Biodegradability of biodegradable/degradable plastic materials under aerobic and anaerobic conditions. *Waste Manag.* 28, 1624–1629. doi: 10.1016/j.wasman.2007.07.003

Moriya, Y., Itoh, M., Okuda, S., Yoshizawa, A. C., and Kanehisa, M. (2007). KAAS: an automatic genome annotation and pathway reconstruction server. *Nucleic Acids Res.* 35, W182—-W185.

Mueller, R. J. (2006). Biological degradation of synthetic polyesters-Enzymes as potential catalysts for polyester recycling. *Process Biochem.* 41, 2124–2128. doi: 10.1016/j.procbio.2006.05.018

Patel, R. K., and Jain, M. (2012). NGS QC Toolkit: a toolkit for quality control of next generation sequencing data. *PLoS One* 7:e30619. doi: 10.1371/journal.pone.0030619

Perz, V., Baumschlager, A., Bleymaier, K., Zitzenbacher, S., Hromic, A., Steinkellner, G., et al. (2016). Hydrolysis of synthetic polyesters by Clostridium botulinum esterases. *Biotechnol. Bioeng.* 113, 1024–1034. doi: 10.1002/bit.25874

Radhakumary, C., Nair, P. D., Mathew, S., and Nair, C. R. (2005). Biopolymer composite of chitosan and methyl methacrylate for medical applications. *Trends Biomater. Artif. Organs* 18, 117–124.

Reid, M. F., and Fewson, C. A. (1994). Molecular characterization of microbial alcohol dehydrogenases. *Crit. Rev. Microbiol.* 20, 13–56. doi: 10.3109/10408419409113545

Ribitsch, D., Acero, E. H., Greimel, K., Dellacher, A., Zitzenbacher, S., Marold, A., et al. (2012). A new esterase from *Thermobifida halotolerans* hydrolyses polyethylene terephthalate (PET) and polylactic acid (PLA). *Polymers (Basel)* 4, 617–629. doi: 10.3390/polym4010617

Ribitsch, D., Heumann, S., Trotscha, E., Herrero, Acero, E., Greimel, K., et al. (2011). Hydrolysis of polyethyleneterephthalate by p-nitrobenzylesterase from Bacillus subtilis. *Biotechnol. Prog.* 27, 951–960. doi: 10.1002/btpr.610

Roager, L., and Sonnenschein, E. C. (2019). Bacterial candidates for colonization and degradation of marine plastic debris. *Environ. Sci. Technol.* 53, 11636–11643. doi: 10.1021/acs.est.9b02212

Sarkhel, R., Sengupta, S., Das, P., and Bhowal, A. (2020). Comparative biodegradation study of polymer from plastic bottle waste using novel isolated bacteria and fungi from marine source. *J Polym. Res.* 27, 1–8. doi: 10.1007/s10965-019-1973-4

Smoot, M. E., Ono, K., Ruscheinski, J., Wang, P. L., and Ideker, T. (2011). Cytoscape 2.8: new features for data integration and network visualization. *Bioinformatics* 27, 431–432.

Su, X., Guo, L., Ding, L., Qu, K., and Shen, C. (2016). Induction of viable but nonculturable state in Rhodococcus and transcriptome analysis using RNA-seq. *PLoS One* 11:e0147593. doi: 10.1371/journal.pone.0147593

SunilKumar, M., Francis, T., Thachil, E. T., and Sujith, A. (2012). Low density polyethylene–chitosan composites: a study based on biodegradation. *Chem. Eng. J.* 204, 114–124.

Szklarczyk, D., Franceschini, A., Kuhn, M., Simonovic, M., Roth, A., Minguez, P., et al. (2011). The STRING database in 2011: functional interaction networks of proteins, globally integrated and scored. *Nucleic Acids Res.* 39, D561–D568. doi: 10.1093/nar/gkq973

Tokiwa, Y., and Calabia, B. P. (2004). Review degradation of microbial polyesters. *Biotechnol. Lett.* 26, 1181–1189.

Trapnell, C., Roberts, A., Goff, L., Pertea, G., Kim, D., Kelley, D. R., et al. (2012). Differential gene and transcript expression analysis of RNA-seq experiments with TopHat and Cufflinks. *Nat. Protoc.* 7, 562–578.

Verma, H., Dhingra, G. G., Sharma, M., Gupta, V., Negi, R. K., Singh, Y., et al. (2020). Comparative genomics of *Sphingopyxis spp*. unravelled functional attributes. *Genomics* 112, 1956–1969. doi: 10.1016/j.ygeno.2019.11.008

Vertommen, M. A., Nierstrasz, V. A., Van, Der, V. M., and Warmoeskerken, M. M. (2005). Enzymatic surface modification of poly (ethylene terephthalate). *J. Biotechnol.* 120, 376–386. doi: 10.1016/j.jbiotec.2005.06.015

Wang, W., Ge, J., Yu, X., and Li, H. (2020). Environmental fate and impacts of microplastics in soil ecosystems: progress and perspective. *Sci. Total Environ.* 708:134841.

Yoshida, S., Hiraga, K., Takehana, T., Taniguchi, I., Yamaji, H., Maeda, Y., et al. (2016). A bacterium that degrades and assimilates poly(ethylene terephthalate). *Science* 351, 1196–1199. doi: 10.1126/science.aad6359

Zampolli, J., Zeaiter, Z., Di Canito, A., and Di Gennaro, P. (2019). Genome analysis and -omics approaches provide new insights into the biodegradation potential of Rhodococcus. *Appl. Microbiol. Biotechnol.* 103, 1069–1080. doi: 10.1007/s00253-018-9539-9537

Conflict of Interest: The authors declare that the research was conducted in the absence of any commercial or financial relationships that could be construed as a potential conflict of interest.

Publisher's Note: All claims expressed in this article are solely those of the authors and do not necessarily represent those of their affiliated organizations, or those of the publisher, the editors and the reviewers. Any product that may be evaluated in this article, or claim that may be made by its manufacturer, is not guaranteed or endorsed by the publisher.

frontiers in Microbiology

MINI REVIEW
published: 28 September 2021
doi: 10.3389/fmicb.2021.746293

Advances in Studies on Microbiota Involved in Nitrogen Removal Processes and Their Applications in Wastewater Treatment

Wenning Mai[1,2†], Jiamin Chen[1,3†], Hai Liu[4], Jiawei Liang[2], Jinfeng Tang[5] and Yongjun Wei[3,6]*

[1]School of Ecology and Environment, Zhengzhou University, Zhengzhou, China, [2]College of Public Health, Zhengzhou University, Zhengzhou, China, [3]Laboratory of Synthetic Biology, Zhengzhou University, Zhengzhou, China, [4]Henan Public Security Bureau, Zhengzhou, China, [5]Key Laboratory for Water Quality and Conservation of Pearl River Delta, Ministry of Education, School of Environmental Science and Engineering, Linköping University – Guangzhou University Research Center on Urban Sustainable Development, Guangzhou University, Guangzhou, China, [6]Key Laboratory of Advanced Drug Preparation Technologies, Ministry of Education, School of Pharmaceutical Sciences, Zhengzhou University, Zhengzhou, China

OPEN ACCESS

Edited by:
Tian Li,
Nankai University, China

Reviewed by:
Chengmei Liao,
Nankai University, China
Hui Wang,
Xi'an University of Technology, China

***Correspondence:**
Yongjun Wei
yongjunwei@zzu.edu.cn

[†]These authors have contributed equally to this work

Specialty section:
This article was submitted to Microbiotechnology, a section of the journal Frontiers in Microbiology

Received: *23 July 2021*
Accepted: *27 August 2021*
Published: *28 September 2021*

Citation:
Mai W, Chen J, Liu H, Liang J, Tang J and Wei Y (2021) Advances in Studies on Microbiota Involved in Nitrogen Removal Processes and Their Applications in Wastewater Treatment. Front. Microbiol. 12:746293. doi: 10.3389/fmicb.2021.746293

The discharge of excess nitrogenous pollutants in rivers or other water bodies often leads to serious ecological problems and results in the collapse of aquatic ecosystems. Nitrogenous pollutants are often derived from the inefficient treatment of industrial wastewater. The biological treatment of industrial wastewater for the removal of nitrogen pollution is a green and efficient strategy. In the initial stage of the nitrogen removal process, the nitrogenous pollutants are converted to ammonia. Traditionally, nitrification and denitrification processes have been used for nitrogen removal in industrial wastewater; while currently, more efficient processes, such as simultaneous nitrification-denitrification, partial nitrification-anammox, and partial denitrification-anammox processes, are used. The microorganisms participating in nitrogen pollutant removal processes are diverse, but information about them is limited. In this review, we summarize the microbiota participating in nitrogen removal processes, their pathways, and associated functional genes. We have also discussed the design of efficient industrial wastewater treatment processes for the removal of nitrogenous pollutants and the application of microbiome engineering technology and synthetic biology strategies in the modulation of the nitrogen removal process. This review thus provides insights that would help in improving the efficiency of nitrogen pollutant removal from industrial wastewater.

Keywords: nitrogen pollution removal, nitrifying bacteria, denitrifying bacteria, anammox, microbiome, wastewater

INTRODUCTION

Industrial development improves our life quality; nevertheless, the industries, such as those producing paper and pharmaceutical products, generate large amounts of industrial wastewater (Liang et al., 2021; Singh et al., 2021). Nitrogen is one of the main industrial wastewater pollutants (Sun et al., 2021), the spread of which pollutes the environment (Chen et al., 2018), damages the ecosystem, and affects human health (Liu et al., 2021). Nitrogenous pollutants

in wastewater mainly comprise inorganic nitrogen and organic nitrogen (Odedishemi Ajibade et al., 2021). The organic nitrogen pollutants can be catalyzed by microorganisms to form inorganic pollutants (Wei et al., 2015). Thus, the primary task of wastewater treatment is the removal of inorganic nitrogen. Therefore, developing green and sustainable strategies to remove inorganic nitrogen pollutants is of great interest (Deng et al., 2021).

Both physicochemical and biological methods are used for removing nitrogenous pollutants in wastewater. The physicochemical methods include stripping, wet oxidation technology, electrochemical technology (Monfet et al., 2018), ion exchange, and adsorption methods (Mook et al., 2012). While physicochemical methods require higher capital and generate solid wastes as secondary contamination, biological methods are mainly used for the efficient removal of nitrogen pollutants (Monfet et al., 2018; Wang et al., 2020c; Chen et al., 2021b). Inorganic nitrogen pollutants are mainly available in the form of ammonia nitrogen (NH_4^+-N), nitrite nitrogen (NO_2^--N), and nitrate nitrogen (NO_3^--N). Biological removal of these nitrogen pollutants in wastewater treatment plants mainly involves the process of ammonification, nitrification, denitrification, and anammox processes (Guo et al., 2020; Liu et al., 2020). These nitrogen removal processes convert nitrogen pollutants to several different oxidation states, and each process needs special running parameters (Rahimi et al., 2020). In each process, different microorganisms function and varying metabolic reactions are involved, and the efficiency of each nitrogen removal process is divergent (Zhang et al., 2021b). Hence, understanding the biological removal processes at species and molecular level is essential for the development of efficient nitrogen pollution removal strategies.

In this review, we aim to summarize the nitrogen removal processes and their microbiota used for the removal of nitrogen pollutants, their functional genes, metabolic pathways, and associated mechanisms. The application and optimization of nitrogen pollution removal process are systematically described, and their operating effectiveness is compared. Based on current nitrogen removal processes, we also discuss and propose the future application of these functional microorganisms and their engineering for industrial wastewater treatment *via* microbiota engineering and synthetic biology strategies.

BIOLOGICAL DENITRIFICATION PROCESS FOR NITROGEN POLLUTANT REMOVAL

The biological nitrogen pollutant removal process mainly involves partial nitrification (PN), nitrification, denitrification, and anammox (**Supplementary Table S1** and **Supplementary information**). The microbial processes and their associated genes involved in nitrogen removal have been identified in previous studies (**Supplementary Figure S1**; Wang et al., 2014; Rahman et al., 2018; Li et al., 2021b). The nitrification process converts ammonia nitrogen into nitrate nitrogen and involves ammonia-oxidizing bacteria (AOB) and nitrite-oxidizing bacteria (NOB). AOB and NOB are autotrophic Gram-negative aerobic bacteria that use the energy released in the nitrification process for growth. First, ammonia nitrogen is transformed into nitrite nitrogen by AOB (Mehrani et al., 2020) through the PN process (Wang et al., 2020a), a complex biochemical process that involves electron transfer, and generates energy and diverse intermediates (Xia et al., 2019; Ren et al., 2020; Qian et al., 2021). The process initiates by oxidation of NH_4^+-N to hydroxylamine (NH_2OH) by ammonia monooxygenase, which is then oxidized to nitrite nitrogen by hydroxylamine oxidoreductase. The nitrite nitrogen is further transformed into nitrate nitrogen by nitrite oxidoreductase of NOB (Staley et al., 2018).

Denitrification is an important step of the biological nitrogen cycle (Zhang et al., 2019); it involves several enzymes and generates various intermediate metabolites (Ren et al., 2020). Four key enzymes of nitrate reductase, nitrite reductase, nitric oxide reductase, and nitrous oxide reductase catalyze the transformation of the nitrate to nitrogen gas (Ding et al., 2019). Most denitrifying bacteria, being heterotrophic facultative anaerobes, carry out the reaction under anaerobic conditions in two steps using nitrate as an electron acceptor and organic matter (organic carbon) as electron donor (Semedo et al., 2018).

THE TRADITIONAL BIOLOGICAL NITROGEN REMOVAL PROCESS AND SIMULTANEOUS NITRIFICATION-DENITRIFICATION PROCESS

The traditional biological nitrogen removal (BNR) process involves sequential, full-scale nitrification and denitrification reactions to transform ammonia nitrogen into nitrogen gas as: $NH_4^+ \rightarrow NO_2^- \rightarrow NO_3^- \rightarrow NO_2^- \rightarrow N_2$. This process has been applied for effectively removing nitrogen pollutants from the wastewater (Kornaros et al., 2010; Chen et al., 2021c; Zhang et al., 2021a; **Figure 1A**). Based on the BNR process, simultaneous nitrification-denitrification (SND) process has been developed, wherein, the nitrification and denitrification reactions occur synchronously in the same reactor and convert ammonia nitrogen into nitrogen gas (Wang et al., 2006).

Compared with the traditional BNR process, the SND process reduces the investment in equipment and space occupation and is thus a cost-effective process for nitrogen pollutant removal from industrial wastewater (**Supplementary Table S2**; Xiang et al., 2020). The microorganisms involved in the SND process are mainly nitrifying bacteria and aerobic denitrifying bacteria (**Figure 1B**). The primary factors affecting the nitrogen removal efficiency include the carbon to nitrogen ratio (COD/N), dissolved oxygen (DO) concentration, sludge concentration, and pH (Chang et al., 2019). Especially, the simultaneous nitrification-denitrification process requires the simultaneous presence of aerobic and anaerobic environments within the same reactor; hence, the DO concentration directly affects the denitrification rate and efficiency (Wang et al., 2018). Moreover, the SND process had been applied for the removal of phosphorus

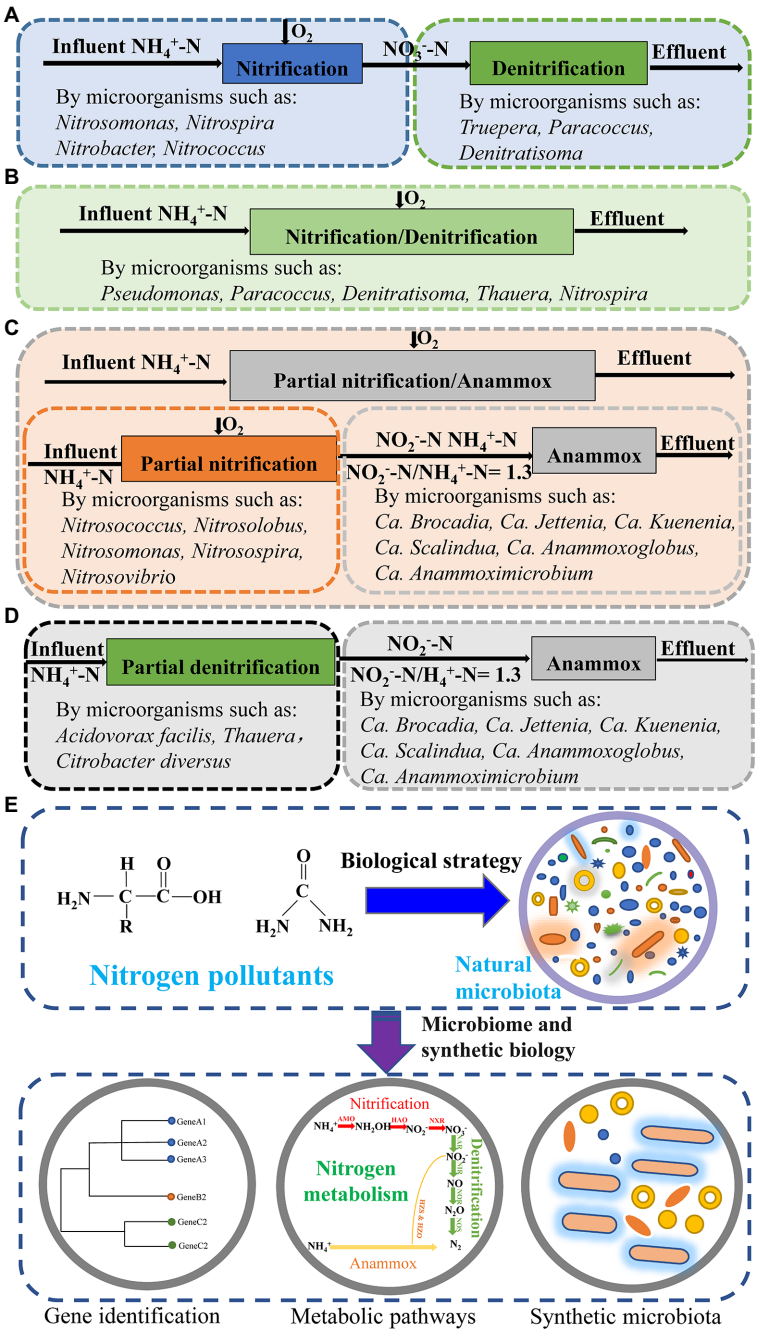

FIGURE 1 | Biological nitrogen removal processes and the microorganisms involved in these processes. **(A)** Traditional nitrification and denitrification processes. **(B)** Simultaneous nitrification-denitrification process. **(C)** Partial nitrification-anammox process. **(D)** Partial denitrification-anammox process. **(E)** Microbiome and synthetic biology strategy used for nitrogen pollutant removal process. The natural microbiota is used for nitrogen pollutant removal; with the help of microbiome and synthetic biology strategy, new nitrogen removal strains can be isolated and engineered strains can be constructed; and these strains can be engineered for synthetic microbiota with efficient nitrogen removal ability.

pollutants from municipal wastewater, showing the SND process is feasible in phosphorus removal (Salehi et al., 2019).

Due to the requirements of proper DO and COD/N, the establishment of SND process and sustaining SND process at high efficiency and a stable state for industrial wastewater treatment is difficult (Lai et al., 2020). Some novel microorganisms, including aerobic denitrifying bacteria, low DO nitrifying bacteria, heterotrophic denitrifying bacteria, and some autotrophic denitrifying bacteria, have been identified and used to improve the efficiency and robustness of SND process (Wang et al., 2017; Carneiro Fidélis Silva et al., 2019). Moreover, optimization carbon-to-nitrogen ratio, DO

concentration, carrier materials, and other strategies have been used for SND startup and stable running (Dobbeleers et al., 2017; Iannacone et al., 2019; Salcedo Moyano et al., 2021). However, the denitrification process under aerobic conditions is rarely reported, and little information about the SND microbiota is available (Liu et al., 2019; Li et al., 2021a). In the future, giving insights into the SND process and optimizing SND startup, including the design of proper wastewater treatment plant, dynamic microbiota of the running bioreactors, and recovering the association between functional microbiota and running performance, are necessary for industrial-scale nitrogen wastewater treatment with SND process.

ANAEROBIC AMMONIUM OXIDATION PROCESS FOR NITROGEN POLLUTANT REMOVAL

In 1995, anaerobic ammonium oxidation (Anammox)—a revolutionary process—was identified during a denitrification process for wastewater treatment (Mulder et al., 1995). This discovery provides an understanding of the available nitrogen processing in nature and is a novel applicable process for the removal of nitrogen pollutants (Speth et al., 2016). Anammox process can efficiently remove nitrogen pollutants in the wastewater containing high levels of ammonia nitrogen and low levels of organic pollutants. This process is being applied these days in hundreds of large-scale wastewater treatment plants (Ali and Okabe, 2015) and can potentially treat low-strength nitrogen wastewater by optimizing reactor types and operation parameters (Li et al., 2021d).

THE ANAMMOX PROCESS FOR NITROGEN REMOVAL

In the anammox process, anammox bacteria directly convert ammonia nitrogen and nitrite nitrogen into nitrogen gas, using ammonia nitrogen as the electron donor and nitrite nitrogen as the electron acceptor in anaerobic environments (Chen et al., 2021a). First, NO_2^--N is reduced to NO, which is used as the electron acceptor of NH_4^+-N to produce N_2H_4. N_2H_4 is further oxidized to form N_2 (van de Graaf et al., 1997). The anammox process is low cost because no energy input is needed (Xu et al., 2020). The bacteria involved in the anammox process are different from those in the traditional BNR process (**Supplementary Table S2**; Zhu et al., 2008; Wen et al., 2020).

The anammox process requires NO_2^- as an electron acceptor, but the wastewater often contains NH_4^+ and no NO_2^-. This NO_2^- can be provided by the PN process for initiation and continuation of the anammox process (Chen et al., 2020). The partial nitrification-anammox (PN/A) process is a short biological denitrification method that can achieve high efficiency of denitrification at a proper temperature, DO concentration, hydraulic retention time, and pH (Val Del Rio et al., 2019; Zhang et al., 2019) with the help of AOB and anammox bacteria (Lv et al., 2011; **Figure 1C**). This process can efficiently remove nitrogen pollutants without adding organic carbon sources and controlling wastewater COD concentration (Sheng et al., 2020).

The PN/A process can save about 50% oxygen with low sludge generation, and no release of CO_2 into the air (Huang et al., 2020). According to the available estimates, the PN/A process can save more than 90% of the operating cost (Zhao et al., 2021). However, the low growth rate of anammox bacteria, the low robustness of anammox bacteria to environmental changes, and the nitrogen removal rate limited the application of anammox for nitrogen pollutant removal (Weralupitiya et al., 2021; Wang et al., 2021c). The quorum sensing strategy had been proposed for improving functions of the PN/A process, which might enhance nitrogen removal efficiency through PN/A process in the future (Zhao et al., 2021).

THE PARTIAL DENITRIFICATION PROCESS USED FOR NITROGEN REMOVAL

Partial denitrification (PDN) stops the reduction of Nitrite nitrogen to nitrogen and is considered to be an alternative process for providing nitrite to anammox bacteria (Fu et al., 2019; Cui et al., 2020). By treating wastewater with high-level nitrate nitrogen and low-level ammonia nitrogen, the PDN-anammox (PDN/A) process can reduce organic carbon source input and generate less sludge (Zhang et al., 2020). The microorganisms mainly functioned in the PDN process are partial denitrifying bacteria and anammox bacteria, including *Acidovorax facilis*, *Citrobacter diversus*, and some *Thauera* species (**Figure 1D**; Wang et al., 2020d).

AOB and anammox bacteria (AnAOB) are the primary functional microorganisms in the PN process and anaerobic ammonia oxidation, and they are also essential for autotrophic denitrification (Wu et al., 2019). However, the PN/A process can produce more than 11% nitrate nitrogen using one-stage or two-stage PN/A processes, which needs to be processed further (Li et al., 2020b). The combination of denitrification PN, and anammox processes (DN-PN/A) in a self-circulating integrated plant is a promising and efficient process to remove nitrogen pollutants from wastewater (Yan et al., 2020). The primary microorganisms involved in the process are AOB, AnAOB, and denitrifying bacteria (Du et al., 2021), and the reactions involved in the DN-PN/A process are as:

Partial nitrification :

$$NH_4^+ + 1.5\,O_2 \rightarrow NO_2^- + 2H^+ + H_2O \quad (1)$$

Anammox :

$$NH_4^+ + 1.32\,NO_2^- \rightarrow 1.02N_2 + 0.26NO_3^- + 2.03H_2O \quad (2)$$

Denitrification reaction :

$$8NO_3^- + 5CH_3COOH \rightarrow 10CO_2 + 4N_2 + 8OH^- + 6H_2O \quad (3)$$

In principle, the DN-PN/A process can remove 100% of ammonia nitrogen, but it is difficult to create a balance between the growth of heterotrophic microorganisms and autotrophic microorganisms (AOB, AnAOB, and other microorganisms) in one integrated reactor (Ma et al., 2020). Thus, research needs to be conducted to develop or engineer optimized DN-PN/A microbiota (Jiang et al., 2021).

INDUSTRIAL APPLICATION OF BNR FOR WASTEWATER TREATMENT

The traditional biological denitrification process is based on three reactions, including ammonification, nitrification, and denitrification, and the associated microorganisms can be accumulated as activated sludge (**Supplementary Figure S2**). The ammoniation reaction takes place in the aeration tank and can remove organic carbon and transfer organic nitrogen to NH_4^+-N (**Supplementary Table S1**). After precipitation, the effluent from the ammoniation process enters the nitrification tank where NH_4^+-N is converted to NO_3^--N. The nitrification reaction requires an acid to decrease the pH of the reactor. The NO_3^--N is reduced to N_2 in the denitrification process, which requires organic carbon sources, such as methanol and glucose. In practice, original wastewater containing organic carbon is mixed with the nitrification effluent (Falås et al., 2016).

In addition to the described processes, the anaerobic-aerobic process (A/O) or recurring denitrification process is also used for removing nitrogen pollutants. The A/O process can efficiently use original organic compounds in wastewater, reduce air input, and in the process, the intermediate tank and reflux system are removed (Zhang et al., 2013). The A/O process significantly reduces construction and operation costs. Based on the A/O process, the anaerobic/anoxic/aerobic (A^2/O) process is optimized to carry out the denitrification and dephosphorization processes, which can be synchronously in one reactor, and simultaneously remove the phosphorus, showing that traditional biological wastewater treatment strategy is efficient and cost-friendly (Park et al., 2021).

To conduct operations for nitrogen removal, the microbiota of the nitrogen removal processes is examined. *Nitrospira*, *Thauera*, *Dechloromonas*, and *Ignavibacterium* are the most abundant microbial genera in the A^2/O sludge (Kim et al., 2013; Xiang et al., 2021). Further, *Nitrosomonas*, *Nitrospira*, and *Nitrobacter* have been identified as the key taxa for nitrite oxidation (Wang et al., 2019; Li et al., 2020a; Feng et al., 2021; Zhou et al., 2021), and *Truepera, Paracoccus*, and *Denitratisoma* were found to primarily carry out denitrification (Wang et al., 2019; Deng et al., 2020; Li et al., 2020a; Wang et al., 2020b). Recently, the autotrophic nitrogen removal systems, including PN, anammox, and the PN/A processes in two bioreactors or in a single bioreactor, were used as cost-effective ways to treat NH_4^+ rich wastewater (Dehestaniathar et al., 2021).

The anammox process for industrial wastewater treatment was developed in China more than a decade ago (Ni et al., 2010). For synthetic wastewater treatment, the primary functional anammox microbes were identified to be *Nitrosomonas*, *Stuttgartiensis*, and *Candidatus Kuenenia* (Zhang et al., 2013). The anammox process has also been used for the treatment of vitamin B_2 production wastewater, and *Ca. Kuenenia* and *Nanaocystis* were found to be the main functional microorganisms (**Table 1**; Mai et al., 2020). Besides, new anammox bacterial species and sulfate-dependent anammox bacteria, such as *Anammoxoglobus sulfate* (Liu et al., 2008) and *Bacillus benzoevorans* (Cai et al., 2010), were found to assist in removing ammonium and sulfate simultaneously during wastewater treatment (Nie et al., 2021). Currently, with the aid of molecular techniques, at least five genera of anammox bacterial have been identified, including *Ca. Brocadia* (Kartal et al., 2008), *Ca. Kuenenia* (Schmid et al., 2000), *Ca. Scalindua* (Ali et al., 2020), *Ca. Anammoxoglobus* (Kartal et al., 2007), and *Ca. Jettenia asiatica* (Ali et al., 2013). However, no pure culture of these anammox has been obtained yet. In the future, culturomics may contribute to the isolation of anammox bacteria and help unravel nitrogen metabolic pathways of anammox (Lagier et al., 2018).

THE APPLICATION OF MICROBIOME AND SYNTHETIC BIOLOGY FOR NITROGEN REMOVAL

High-throughput sequencing techniques, metagenomics, and other microbiome strategies are being applied to analyze microbiota with the ability to remove nitrogen pollutants (Xiang et al., 2021). There is a great diversity in the dominant microorganisms functioned in different nitrogen pollutant removal processes. Nevertheless, most microorganisms are assigned to the phyla of Proteobacteria, Bacteroidetes, Nitrospirae, and Chloroflexiphyla (**Table 1**), and some bacteria in the ammonification, nitrification, and denitrification processes have already been isolated (**Table 1**). Although several anammox bacteria have been identified using molecular techniques, no pure culture of the anammox bacteria has yet been obtained (**Table 1**; Zhang and Okabe, 2020).

In the future, microbiome strategies can be used to discover anammox genomes and the functional genes in the PN/A microbiota and other microbiota. Based on metabolic information inferred from the microbiome data, a proper medium can be designed for the isolation or enrichment of anammox bacteria (Wei et al., 2020). Besides, the functional genes and pathways discovered in the microorganisms that can remove nitrogen pollutants can be expressed in the model organisms, such as *Escherichia coli* (Wang et al., 2021a), *Clostridium perfringens* (Wang et al., 2011), *Klebsiella pneumoniae* (Wang et al., 2021b), and others (Wang et al., 2020c), to build genetically engineered strains for nitrogen pollutant removal (**Figure 1E**). These isolated strains, engineered strains, and enriched microbiota can be used for the construction of a series of synthetic microbiota with nitrogen removal ability, as well as those that can accomplish different nitrogen removal processes (Jiang et al., 2021;

TABLE 1 | Biological nitrogen removal processes for different wastewater types.

Wastewater types	Main process	Nitrogen removal microorganisms in the microbiota	References
Domestic wastewater	anaerobic/anoxic/aerobic (A^2/O)	*Dechloromonas; Nitrospira; Arcobacter; Dokdonella*	Xiang et al., 2021
Campus wastewater	Synchronous nitration denitrification (SND)	*Nitrospira; Thermomicrobia; Denitratisoma; Rhodocyclaceae*	Xiang et al., 2020
Synthetic wastewater	Anammox	*Candidatus* Scalindua; *Actinomarinales*	Zhang et al., 2013
Sewage	Partial denitrification-anammox (PDN/A)	*Thauera; Candidatus Brocadia*	Wang et al., 2020b
Landfill leachate	Partial nitrification-denitrification (PND)	*Nitrosomonas; Nitrospira; Ottowia; Pseudomonas; Thermomonas; Thiobacillus; Paracoccus; Thauera; Arenimonas*	Li et al., 2020a
Mature landfill leachate	Simultaneous partial nitrification, anammox and denitrification (SNAD)	*Nitrosomonas; Chloroflexi; Ignavibacteria; Candidatus Brocadia; Candidatus Jettenia*	Wang et al., 2019
Municipal wastewater	Partial nitrification-simultaneous anammox and denitrification (PN-SAD)	*Limnobacter; Ignavibacter; Thauera; Denitration; Candidatus Brocadia*	Deng et al., 2020
Piggery wastewater	Heterotrophic nitrification-anammox	*Candidatus Kuenenia; Planctomyces; Pirellula; Hyphomicrobium; Rhodobacter; Ignavibacterium*	Zhou et al., 2021
Vitamin B_2 production wastewater	Anammox	*Candidatus Kuenenia; Nanaocystis*	Mai et al., 2020
Domestic sewage	Anaerobic/Aerobic/Anoxic/Aerobic process (AOAO)	*Dechloromonas; Candidatus Competibacter*; *Nitrospira; Nitrosomonas*	Feng et al., 2021

Li et al., 2021c). Based on the nitrogen pollutant types and concentration, proper synthetic microbiota can be selected and developed for nitrogen pollutant removal (**Figure 1E**).

PERSPECTIVES

In this review, current biological denitrification processes and associated functional microorganisms have been summarized. The advantages and limitations of current mainstream denitrification processes in wastewater treatment have also been reviewed, and PN/A, PDN/A, DN-PN/A, and other anammox processes might be the main nitrogen removal strategies in the next few years. In order to enhance nitrogen removal efficiency, proposing novel integrated process for nitrogen removal and giving insight into the molecular mechanisms of each nitrogen removal process are essential for nitrogen pollutant removal in the industrial-scale wastewater. Moreover, some primary nitrogen pollutant removal bacteria have not yet been cultured in the laboratory, and microbiome should be implemented for the recovery of microorganisms functioned in the nitrogen pollutant removal process. In the future, synthetic biology strategies would help construct/synthesize microbiota for the efficient treatment of nitrogen pollutants in wastewater based on the nitrogen removal isolates and engineered microbial strains.

AUTHOR CONTRIBUTIONS

YW conceived the study. JC, YW, WM, JT, HL, and JL drafted the manuscript. JC and YW prepared the figures. HL and JT revised the manuscript. All the authors read, revised, and approved the manuscript.

FUNDING

This work was supported by the National Natural Science Foundation of China (no. 32111530179), and the Science and Technology Program of Guangzhou, China (no. 202102010401).

ACKNOWLEDGMENTS

We would like to thank TopEdit (www.topeditsci.com) for the English language editing of this manuscript.

SUPPLEMENTARY MATERIAL

The Supplementary Material for this article can be found online at: https://www.frontiersin.org/articles/10.3389/fmicb.2021.746293/full#supplementary-material

REFERENCES

Ali, M., Chai, L.-Y., Tang, C.-J., Zheng, P., Min, X.-B., Yang, Z.-H., et al. (2013). The increasing interest of ANAMMOX research in China: bacteria, process development, and application. *Biomed. Res. Int.* 2013:134914. doi: 10.1155/2013/134914

Ali, M., and Okabe, S. (2015). Anammox-based technologies for nitrogen removal: advances in process start-up and remaining issues. *Chemosphere* 141, 144–153. doi: 10.1016/j.chemosphere.2015.06.094

Ali, M., Shaw, D. R., and Saikaly, P. E. (2020). Application of an enrichment culture of the marine anammox bacterium "ca. Scalindua sp. AMX11" for nitrogen removal under moderate salinity and in the presence of organic carbon. *Water Res.* 170:115345. doi: 10.1016/j.watres.2019.115345

Cai, J., Jiang, J., and Zheng, P. (2010). Isolation and identification of bacteria responsible for simultaneous anaerobic ammonium and sulfate removal. *Sci. China Chem.* 53, 645–650. doi: 10.1007/s11426-010-0053-8

Carneiro Fidélis Silva, L., Santiago Lima, H., Antônio de Oliveira Mendes, T., Sartoratto, A., de Paula Sousa, M., Suhett de Souza, R., et al. (2019). Heterotrophic nitrifying/aerobic denitrifying bacteria: ammonium removal

under different physical-chemical conditions and molecular characterization. *J. Environ. Manag.* 248:109294. doi: 10.1016/j.jenvman.2019.109294

Chang, M., Wang, Y., Pan, Y., Zhang, K., Lyu, L., Wang, M., et al. (2019). Nitrogen removal from wastewater via simultaneous nitrification and denitrification using a biological folded non-aerated filter. *Bioresour. Technol.* 289:121696. doi: 10.1016/j.biortech.2019.121696

Chen, Z., Chen, Y., Zheng, X., Wang, X., Wang, Y., and Chen, J. (2021c). Comparison of complete nitritation–denitrification and partial nitritation–anammox for iron oxide wastewater treatment. *J. Clean. Prod.* 294:126281. doi: 10.1016/j.jclepro.2021.126281

Chen, C., Jiang, Y., Zou, X., Guo, M., Liu, H., Cui, M., et al. (2021a). Insight into the influence of particle sizes on characteristics and microbial community in the anammox granular sludge. *J. Water Process Eng.* 39:101883. doi: 10.1016/j.jwpe.2020.101883

Chen, Z., Wang, X., Chen, X., Chen, J., Feng, X., and Peng, X. (2018). Nitrogen removal via nitritation pathway for low-strength ammonium wastewater by adsorption, biological desorption and denitrification. *Bioresour. Technol.* 267, 541–549. doi: 10.1016/j.biortech.2018.07.084

Chen, G., Zhang, Y., Wang, X., Chen, F., Lin, L., Ruan, Q., et al. (2020). Optimizing of operation strategies of the single-stage partial nitrification-anammox process. *J. Clean. Prod.* 256:120667. doi: 10.1016/j.jclepro.2020.120667

Chen, Y., Zheng, R., Sui, Q., Ritigala, T., Wei, Y., Cheng, X., et al. (2021b). Coupling anammox with denitrification in a full-scale combined biological nitrogen removal process for swine wastewater treatment. *Bioresour. Technol.* 329:124906. doi: 10.1016/j.biortech.2021

Cui, B., Yang, Q., Liu, X., Wu, W., Liu, Z., and Gu, P. (2020). Achieving partial denitrification-anammox in biofilter for advanced wastewater treatment. *Environ. Int.* 138:105612. doi: 10.1016/j.envint.2020.105612

Dehestaniathar, S., Nesari, S., Borzooei, S., and Abolfathi, S. (2021). Application of natural biodegradable fiber as biofilm medium and carbon source in DEnitrifying AMmonium OXidation (DEAMOX) process for nitrogen removal from wastewater. *J. Taiwan Inst. Chem. Eng.* 119, 108–114. doi: 10.1016/j.jtice.2021.01.030

Deng, S., Peng, Y., Zhang, L., and Wu, L. (2020). Advanced nitrogen removal from municipal wastewater via two-stage partial nitrification-simultaneous anammox and denitrification (PN-SAD) process. *Bioresour. Technol.* 304:122955. doi: 10.1016/j.biortech.2020.122955

Deng, M., Zhao, X., Senbati, Y., Song, K., and He, X. (2021). Nitrogen removal by heterotrophic nitrifying and aerobic denitrifying bacterium pseudomonas sp. DM02: removal performance, mechanism and immobilized application for real aquaculture wastewater treatment. *Bioresour. Technol.* 322:124555. doi: 10.1016/j.biortech.2020.124555

Ding, X., Wei, D., Guo, W., Wang, B., Meng, Z., Feng, R., et al. (2019). Biological denitrification in an anoxic sequencing batch biofilm reactor: performance evaluation, nitrous oxide emission and microbial community. *Bioresour. Technol.* 285:121359. doi: 10.1016/j.biortech.2019.121359

Dobbeleers, T., D'aes, J., Miele, S., Caluwé, M., Akkermans, V., Daens, D., et al. (2017). Aeration control strategies to stimulate simultaneous nitrification-denitrification via nitrite during the formation of aerobic granular sludge. *Appl. Microbiol. Biotechnol.* 101, 6829–6839. doi: 10.1007/s00253-017-8415-1

Du, Y., Yu, D., Wang, X., Zhen, J., Bi, C., Gong, X., et al. (2021). Achieving simultaneous nitritation, anammox and denitrification (SNAD) in an integrated fixed-biofilm activated sludge (IFAS) reactor: quickly culturing self-generated anammox bacteria. *Sci. Total Environ.* 768:144446. doi: 10.1016/j.scitotenv.2020.144446

Falås, P., Wick, A., Castronovo, S., Habermacher, J., Ternes, T. A., and Joss, A. (2016). Tracing the limits of organic micropollutant removal in biological wastewater treatment. *Water Res.* 95, 240–249. doi: 10.1016/j.watres.2016.03.009

Feng, Y., Peng, Y., Wang, B., Liu, B., and Li, X. (2021). A continuous plug-flow anaerobic/aerobic/anoxic/aerobic (AOAO) process treating low COD/TIN domestic sewage: realization of partial nitrification and extremely advanced nitrogen removal. *Sci. Total Environ.* 771:145387. doi: 10.1016/j.scitotenv.2021.145387

Fu, J., Lin, Z., Zhao, P., Wang, Y., He, L., and Zhou, J. (2019). Establishment and efficiency analysis of a single-stage denitrifying phosphorus removal system treating secondary effluent. *Bioresour. Technol.* 288:121520. doi: 10.1016/j.biortech.2019.121520

Guo, Y., Chen, Y., Webeck, E., and Li, Y. Y. (2020). Towards more efficient nitrogen removal and phosphorus recovery from digestion effluent: latest developments in the anammox-based process from the application perspective. *Bioresour. Technol.* 299:122560. doi: 10.1016/j.biortech.2019.122560

Huang, X., Mi, W., Hong, N., Ito, H., and Kawagoshi, Y. (2020). Efficient transition from partial nitritation to partial nitritation/Anammox in a membrane bioreactor with activated sludge as the sole seed source. *Chemosphere* 253:126719. doi: 10.1016/j.chemosphere.2020.126719

Iannacone, F., Di Capua, F., Granata, F., Gargano, R., Pirozzi, F., and Esposito, G. (2019). Effect of carbon-to-nitrogen ratio on simultaneous nitrification denitrification and phosphorus removal in a microaerobic moving bed biofilm reactor. *J. Environ. Manag.* 250:109518. doi: 10.1016/j.jenvman.2019.109518

Jiang, Y., Xia, W., Zhao, R., Wang, M., Tang, J., and Wei, Y. (2021). Insight into the interaction Between microplastics and microorganisms based on a bibliometric and visualized analysis. *Bull. Environ. Contam. Toxicol.*. doi:10.1007/s00128-021-03201-y. [Epub ahead of print].

Kartal, B., Niftrik, L. V., Rattray, J., Vossenberg, J. L. C. M. V. D., and Strous, M. (2008). Candidatus 'Brocadia fulgida': an autofluorescent anaerobic ammonium oxidizing bacterium. *FEMS Microbiol. Ecol.* 63, 46–55. doi: 10.1111/j.1574-6941.2007.00408.x

Kartal, B., Rattray, J., Van Niftrik, L. A., van De Vossenberg, J., Schmid, M. C., Webb, R. I., et al. (2007). Candidatus "Anammoxoglobus propionicus" a new propionate oxidizing species of anaerobic ammonium oxidizing bacteria. *Syst. Appl. Microbiol.* 30, 39–49. doi: 10.1016/j.syapm.2006.03.004

Kim, B.-C., Kim, S., Shin, T., Kim, H., and Sang, B.-I. (2013). Comparison of the bacterial communities in anaerobic, anoxic, and Oxic chambers of a pilot A2O process using pyrosequencing analysis. *Curr. Microbiol.* 66, 555–565. doi: 10.1007/s00284-013-0311-z

Kornaros, M., Dokianakis, S. N., and Lyberatos, G. (2010). Partial nitrification/denitrification can be attributed to the slow response of nitrite oxidizing bacteria to periodic anoxic disturbances. *Environ. Sci. Technol.* 44, 7245–7253. doi: 10.1021/es100564j

Lagier, J. C., Dubourg, G., Million, M., Cadoret, F., Bilen, M., Fenollar, F., et al. (2018). Culturing the human microbiota and culturomics. *Nat. Rev. Microbiol.* 16, 540–550. doi: 10.1038/s41579-018-0041-0

Lai, C., Guo, Y., Cai, Q., and Yang, P. (2020). Enhanced nitrogen removal by simultaneous nitrification-denitrification and further denitrification (SND-DN) in a moving bed and constructed wetland (MBCW) integrated bioreactor. *Chemosphere* 261:127744. doi: 10.1016/j.chemosphere.2020.127744

Li, J., Du, Q., Peng, H., Zhang, Y., Bi, Y., Shi, Y., et al. (2020a). Optimization of biochemical oxygen demand to total nitrogen ratio for treating landfill leachate in a single-stage partial nitrification-denitrification system. *J. Clean. Prod.* 266:121809. doi: 10.1016/j.jclepro.2020.121809

Li, Y., Fu, L., Li, X., Wang, Y., and Liu, H. (2021c). Novel strains with superior degrading efficiency for lincomycin manufacturing biowaste. *Ecotoxicol. Environ. Saf.* 209:111802. doi: 10.1016/j.ecoenv.2020.111802

Li, H., Liu, Q., Yang, P., Duan, Y., Zhang, J., and Li, C. (2021a). Encapsulation of microorganisms for simultaneous nitrification and denitrification in aerobic reactors. *J. Environ. Chem. Eng.* 9:105616. doi: 10.1016/j.jece.2021.105616

Li, W., Shi, C., Yu, Y., Ruan, Y., Kong, D., Lv, X., et al. (2021b). Interrelationships between tetracyclines and nitrogen cycling processes mediated by microorganisms: a review. *Bioresour. Technol.* 319:124036. doi: 10.1016/j.biortech.2020.124036

Li, X., Tan, X.-W., Yuan, Y., Huang, Y., Li, B.-L., and Jin, R. (2020b). Highly efficient and low-energy nitrogen removal of sludge reduction liquid by coupling denitrification- partial nitrification-Anammox in an innovative auto-recycling integration device with different partitions. *Bioresour. Technol.* 302:122880. doi: 10.1016/j.biortech.2020.122880

Li, Y., Zhang, M., Xu, D., Shan, X., and Zheng, P. (2021d). Potential of anammox process towards high-efficient nitrogen removal in wastewater treatment: theoretical analysis and practical case with a SBR. *Chemosphere* 281:130729. doi: 10.1016/j.chemosphere.2021.130729

Liang, J., Mai, W., Wang, J., Li, X., Su, M., Du, J., et al. (2021). Performance and microbial communities of a novel integrated industrial-scale pulp and paper wastewater treatment plant. *J. Clean. Prod.* 278:123896. doi: 10.1016/j.jclepro.2020.123896

Liu, L., Ji, M., Wang, F., Wang, S., and Qin, G. (2020). Insight into the influence of microbial aggregate types on nitrogen removal performance and microbial

community in the anammox process - A review and meta-analysis. *Sci. Total Environ.* 714:136571. doi: 10.1016/j.scitotenv.2020.136571

Liu, Y., Ngo, H. H., Guo, W., Peng, L., Wang, D., and Ni, B. (2019). The roles of free ammonia (FA) in biological wastewater treatment processes: a review. *Environ. Int.* 123, 10–19. doi: 10.1016/j.envint.2018.11.039

Liu, J., Su, J., Ali, A., Wang, Z., Chen, C., and Xu, L. (2021). Role of porous polymer carriers and iron-carbon bioreactor combined micro-electrolysis and biological denitrification in efficient removal of nitrate from wastewater under low carbon to nitrogen ratio. *Bioresour. Technol.* 321:124447. doi: 10.1016/j.biortech.2020.124447

Liu, S., Yang, F., Gong, Z., Meng, F., Chen, H., Xue, Y., et al. (2008). Application of anaerobic ammonium-oxidizing consortium to achieve completely autotrophic ammonium and sulfate removal. *Bioresour. Technol.* 99, 6817–6825. doi: 10.1016/j.biortech.2008.01.054

Lv, Y., Wang, L., Wang, X., Yang, Y., Wang, Z., and Li, J. (2011). Macroscale and microscale analysis of Anammox in anaerobic rotating biological contactor. *J. Environ. Sci.* 23, 1679–1683. doi: 10.1016/S1001-0742(10)60564-5

Ma, H., Xue, Y., Zhang, Y., Kobayashi, T., Kubota, K., and Li, Y.-Y. (2020). Simultaneous nitrogen removal and phosphorus recovery using an anammox expanded reactor operated at 25 °C. *Water Res.* 172:115510. doi: 10.1016/j.watres.2020.115510

Mai, W., Hu, T., Li, C., Wu, R., Chen, J., Shao, Y., et al. (2020). Effective nitrogen removal of wastewater from vitamin B2 production by a potential anammox process. *J. Water Process Eng.* 37:101515. doi: 10.1016/j.jwpe.2020.101515

Mehrani, M. J., Sobotka, D., Kowal, P., Ciesielski, S., and Makinia, J. (2020). The occurrence and role of Nitrospira in nitrogen removal systems. *Bioresour. Technol.* 303:122936. doi: 10.1016/j.biortech.2020.122936

Monfet, E., Aubry, G., and Ramirez, A. (2018). Nutrient removal and recovery from digestate: a review of the technology. *Biofuels* 9, 247–262. doi: 10.1080/17597269.2017.1336348

Mook, W. T., Chakrabarti, M. H., Aroua, M. K., Khan, G. M. A., Ali, B. S., Islam, M. S., et al. (2012). Removal of total ammonia nitrogen (TAN), nitrate and total organic carbon (TOC) from aquaculture wastewater using electrochemical technology: a review. *Desalination* 285, 1–13. doi: 10.1016/j.desal.2011.09.029

Mulder, A., van De Graaf, A. A., Robertson, L. A., and Kuenen, J. G. (1995). Anaerobic ammonium oxidation discovered in a denitrifying fluidized bed reactor. *FEMS Microbiol. Ecol.* 16, 177–183. doi: 10.1111/j.1574-6941.1995.tb00281.x

Ni, B.-J., Hu, B.-L., Fang, F., Xie, W.-M., Kartal, B., Liu, X.-W., et al. (2010). Microbial and physicochemical characteristics of compact anaerobic ammonium-oxidizing granules in an Upflow anaerobic sludge blanket reactor. *Appl. Environ. Microbiol.* 76:2652. doi: 10.1128/AEM.02271-09

Nie, W.-B., Ding, J., Xie, G.-J., Tan, X., Lu, Y., Peng, L., et al. (2021). Simultaneous nitrate and sulfate dependent anaerobic oxidation of methane linking carbon, nitrogen and sulfur cycles. *Water Res.* 194:116928. doi: 10.1016/j.watres.2021.116928

Odedishemi Ajibade, F., Wang, H.-C., Guadie, A., Fausat Ajibade, T., Fang, Y.-K., Muhammad Adeel Sharif, H., et al. (2021). Total nitrogen removal in biochar amended non-aerated vertical flow constructed wetlands for secondary wastewater effluent with low C/N ratio: microbial community structure and dissolved organic carbon release conditions. *Bioresour. Technol.* 322:124430. doi: 10.1016/j.biortech.2020.124430

Park, M., Kim, J., Lee, T., Oh, Y.-K., Nguyen, V. K., and Cho, S. (2021). Correlation of microbial community with salinity and nitrogen removal in an anammox-based denitrification system. *Chemosphere* 263:128340. doi: 10.1016/j.chemosphere.2020.128340

Qian, Y., Ding, Y., Ma, H., Chi, Y., Yuan, H., Li, Y.-Y., et al. (2021). Startup and performance of a novel single-stage partial nitritation/anammox system for reject water treatment. *Bioresour. Technol.* 321:124432. doi: 10.1016/j.biortech.2020.124432

Rahimi, S., Modin, O., and Mijakovic, I. (2020). Technologies for biological removal and recovery of nitrogen from wastewater. *Biotechnol. Adv.* 43:107570. doi: 10.1016/j.biotechadv.2020.107570

Rahman, M. M., Shan, J., Yang, P., Shang, X., Xia, Y., and Yan, X. (2018). Effects of long-term pig manure application on antibiotics, abundance of antibiotic resistance genes (ARGs), anammox and denitrification rates in paddy soils. *Environ. Pollut.* 240, 368–377. doi: 10.1016/j.envpol.2018.04.135

Ren, Y., Hao Ngo, H., Guo, W., Wang, D., Peng, L., Ni, B.-J., et al. (2020). New perspectives on microbial communities and biological nitrogen removal processes in wastewater treatment systems. *Bioresour. Technol.* 297:122491. doi: 10.1016/j.biortech.2019.12249

Salcedo Moyano, A.J., Delforno, T.P., and Subtil, E.L. (2021). Simultaneous nitrification-denitrification (SND) using a thermoplastic gel as support: pollutants removal and microbial community in a pilot-scale biofilm membrane bioreactor. *Environ. Technol.*. doi:10.1080/09593330.2021.1950843. [Epub ahead of print].

Salehi, S., Cheng, K. Y., Heitz, A., and Ginige, M. P. (2019). Simultaneous nitrification, denitrification and phosphorus recovery (SNDPr) - An opportunity to facilitate full-scale recovery of phosphorus from municipal wastewater. *J. Environ. Manag.* 238, 41–48. doi: 10.1016/j.jenvman.2019.02.063

Schmid, M., Twachtmann, U., Klein, M., Strous, M., Juretschko, S., Jetten, M., et al. (2000). Molecular evidence for genus level diversity of bacteria capable of catalyzing anaerobic ammonium oxidation. *Syst. Appl. Microbiol.* 23, 93–106. doi: 10.1016/S0723-2020(00)80050-8

Semedo, M., Song, B., Sparrer, T., and Phillips, R. L. (2018). Antibiotic effects on microbial communities responsible for denitrification and N2O production in grassland soils. *Front. Microbiol.* 9:2121. doi: 10.3389/fmicb.2018.02121

Sheng, L., Lei, Z., Dzakpasu, M., Li, Y.-Y., Li, Q., and Chen, R. (2020). Application of the anammox-based process for nitrogen removal from anaerobic digestion effluent: a review of treatment performance, biochemical reactions, and impact factors. *J. Water Process Eng.* 38:101595. doi: 10.1016/j.jwpe.2020.101595

Singh, R., D'alessio, M., Meneses, Y., Bartelt-Hunt, S., and Ray, C. (2021). Nitrogen removal in vermifiltration: mechanisms, influencing factors, and future research needs. *J. Environ. Manag.* 281:111868. doi: 10.1016/j.jenvman.2020.111868

Speth, D. R., In't Zandt, M. H., Guerrero-Cruz, S., Dutilh, B. E., and Jetten, M. S. M. (2016). Genome-based microbial ecology of anammox granules in a full-scale wastewater treatment system. *Nat. Commun.* 7:11172. doi: 10.1038/ncomms11172

Staley, C., Breuillin-Sessoms, F., Wang, P., Kaiser, T., Venterea, R. T., and Sadowsky, M. J. (2018). Urea amendment decreases microbial diversity and selects for specific nitrifying strains in eight contrasting agricultural soils. *Front. Microbiol.* 9:634. doi: 10.3389/fmicb.2018.00634

Sun, Z., Li, J., Fan, Y., Meng, J., and Deng, K. (2021). Efficiency and mechanism of nitrogen removal from piggery wastewater in an improved microaerobic process. *Sci. Total Environ.* 774:144925. doi: 10.1016/j.scitotenv.2020.144925

Val Del Rio, A., Campos, J. L., da Silva, C., Pedrouso, A., and Mosquera-Corral, A. (2019). Determination of the intrinsic kinetic parameters of ammonia-oxidizing and nitrite-oxidizing bacteria in granular and flocculent sludge. *Sep. Purif. Technol.* 213, 571–577. doi: 10.1016/j.seppur.2018.12.048

van de Graaf, A. A., de Bruijn, P., Robertson, L. A., Jetten, M. S. M., and Kuenen, J. G. (1997). Metabolic pathway of anaerobic ammonium oxidation on the basis of 15N studies in a fluidized bed reactor. *Microbiology* 143, 2415–2421. doi: 10.1099/00221287-143-7-2415

Wang, Y., Ji, X. M., and Jin, R. C. (2021c). How anammox responds to the emerging contaminants: status and mechanisms. *J. Environ. Manag.* 293:112906. doi: 10.1016/j.jenvman.2021.112906

Wang, J., Liang, J., Li, Y., Tian, L., and Wei, Y. (2021a). Characterization of efficient xylanases from industrial-scale pulp and paper wastewater treatment microbiota. *AMB Express* 11:19. doi: 10.1186/s13568-020-01178-1

Wang, Y., Lin, Z., He, L., Huang, W., Zhou, J., and He, Q. (2019). Simultaneous partial nitrification, anammox and denitrification (SNAD) process for nitrogen and refractory organic compounds removal from mature landfill leachate: performance and metagenome-based microbial ecology. *Bioresour. Technol.* 294:122166. doi: 10.1016/j.biortech.2019.122166

Wang, Z.-B., Liu, X.-L., Bu, C.-N., Ni, S.-Q., and Sung, S. (2020d). Microbial diversity reveals the partial denitrification-anammox process serves as a new pathway in the first mainstream anammox plant. *Sci. Total Environ.* 764:142917. doi: 10.1016/j.scitotenv.2020.142917

Wang, H., Song, Q., Wang, J., Zhang, H., He, Q., Zhang, W., et al. (2018). Simultaneous nitrification, denitrification and phosphorus removal in an aerobic granular sludge sequencing batch reactor with high dissolved oxygen: effects of carbon to nitrogen ratios. *Sci. Total Environ.* 642, 1145–1152. doi: 10.1016/j.scitotenv.2018.06.081

Wang, J., Wang, Y., Bai, J., Liu, Z., Song, X., Yan, D., et al. (2017). High efficiency of inorganic nitrogen removal by integrating biofilm-electrode

with constructed wetland: autotrophic denitrifying bacteria analysis. *Bioresour. Technol.* 227, 7–14. doi: 10.1016/j.biortech.2016.12.046

Wang, B., Wang, Z., Wang, S., Qiao, X., Gong, X., Gong, Q., et al. (2020a). Recovering partial nitritation in a PN/A system during mainstream wastewater treatment by reviving AOB activity after thoroughly inhibiting AOB and NOB with free nitrous acid. *Environ. Int.* 139:105684. doi: 10.1016/j.envint.2020.105684

Wang, M., Wei, Y., Ji, B., and Nielsen, J. (2020c). Advances in metabolic engineering of Saccharomyces cerevisiae for cocoa butter equivalent production. *Front. Bioeng. Biotechnol.* 8:594081. doi: 10.3389/fbioe.2020.594081

Wang, X. J., Xia, S. Q., Chen, L., Zhao, J. F., Renault, N. J., and Chovelon, J. M. (2006). Nutrients removal from municipal wastewater by chemical precipitation in a moving bed biofilm reactor. *Process Biochem.* 41, 824–828. doi: 10.1016/j.procbio.2005.10.015

Wang, W., Yu, X., Wei, Y., Ledesma-Amaro, R., and Ji, X.-J. (2021b). Reprogramming the metabolism of *Klebsiella pneumoniae* for efficient 1, 3-propanediol production. *Chem. Eng. Sci.* 236:116539. doi: 10.1016/j.ces.2021.116539

Wang, C., Zhao, Y., Xie, B., Peng, Q., Hassan, M., and Wang, X. (2014). Nitrogen removal pathway of anaerobic ammonium oxidation in on-site aged refuse bioreactor. *Bioresour. Technol.* 159, 266–271. doi: 10.1016/j.biortech.2014.02.093

Wang, D., Zheng, Q., Huang, K., Springael, D., and Zhang, X.-X. (2020b). Metagenomic and metatranscriptomic insights into the complex nitrogen metabolic pathways in a single-stage bioreactor coupling partial denitrification with anammox. *Chem. Eng. J.* 398:125653. doi: 10.1016/j.cej.2020.125653

Wang, R., Zong, W., Qian, C., Wei, Y., Yu, R., and Zhou, Z. (2011). Isolation of *Clostridium perfringens* strain W11 and optimization of its biohydrogen production by genetic modification. *Int. J. Hydrog. Energy* 36, 12159–12167. doi: 10.1016/j.ijhydene.2011.06.105

Wei, Y., Wu, Y., Zhang, L., Zhou, Z., Zhou, H., and Yan, X. (2020). Genome recovery and metatranscriptomic confirmation of functional acetate-oxidizing bacteria from enriched anaerobic biogas digesters. *Environ. Pollut.* 265:114843. doi: 10.1016/j.envpol.2020.114843

Wei, Y., Zhou, H., Zhang, J., Zhang, L., Geng, A., Liu, F., et al. (2015). Insight into dominant cellulolytic bacteria from two biogas digesters and their glycoside hydrolase genes. *PLoS One* 10:e0129921. doi: 10.1371/journal.pone.0145700

Wen, R., Jin, Y., and Zhang, W. (2020). Application of the Anammox in China-A review. *Int. J. Environ. Res. Public Health* 17:1090. doi: 10.3390/ijerph17031090

Weralupitiya, C., Wanigatunge, R., Joseph, S., Athapattu, B. C. L., Lee, T. H., Kumar Biswas, J., et al. (2021). Anammox bacteria in treating ammonium rich wastewater: recent perspective and appraisal. *Bioresour. Technol.* 334:125240. doi: 10.1016/j.biortech.2021.125240

Wu, L., Shen, M., Li, J., Huang, S., Li, Z., Yan, Z., et al. (2019). Cooperation between partial-nitrification, complete ammonia oxidation (comammox), and anaerobic ammonia oxidation (anammox) in sludge digestion liquid for nitrogen removal. *Environ. Pollut.* 254:112965. doi: 10.1016/j.envpol.2019.112965

Xia, Z., Wang, Q., She, Z., Gao, M., Zhao, Y., Guo, L., et al. (2019). Nitrogen removal pathway and dynamics of microbial community with the increase of salinity in simultaneous nitrification and denitrification process. *Sci. Total Environ.* 697:134047. doi: 10.1016/j.scitotenv.2019.134047

Xiang, Y., Shao, Z., Chai, H., Ji, F., and He, Q. (2020). Functional microorganisms and enzymes related nitrogen cycle in the biofilm performing simultaneous nitrification and denitrification. *Bioresour. Technol.* 314:123697. doi: 10.1016/j.biortech.2020.123697

Xiang, J., Wang, C., Lv, W., Liu, Y., Sun, J., and Gong, T. (2021). Differences of bacterial communities in two full-scale A2/O municipal wastewater treatment plants and their effects on effluent total nitrogen removal. *Environ. Technol. Innov.* 21:101317. doi: 10.1016/j.eti.2020.101317

Xu, Y., Xu, Y., Li, T., Wang, G., and Dai, X. (2020). Two-step partial nitrification-anammox process for treating thermal-hydrolysis anaerobic digester effluent: start-up and microbial characterisation. *J. Clean. Prod.* 252:119784. doi: 10.1016/j.jclepro.2019.119784

Yan, J., Wang, S., Wu, L., Li, S., Li, H., Wang, Y., et al. (2020). Long-term ammonia gas biofiltration through simultaneous nitrification, anammox and denitrification process with limited N_2O emission and negligible leachate production. *J. Clean. Prod.* 270:122406. doi: 10.1016/j.jclepro.2020.122406

Zhang, W., Bai, Y., Ruan, X., and Yin, L. (2019). The biological denitrification coupled with chemical reduction for groundwater nitrate remediation via using SCCMs as carbon source. *Chemosphere* 234, 89–97. doi: 10.1016/j.chemosphere.2019.06.005

Zhang, X., Li, D., Liang, Y., He, Y., Zhang, Y., and Zhang, J. (2013). Autotrophic nitrogen removal from domestic sewage in MBR–CANON system and the biodiversity of functional microbes. *Bioresour. Technol.* 150, 113–120. doi: 10.1016/j.biortech.2013.09.067

Zhang, P., Liang, J., Mai, W., Wu, Y., Dai, J., and Wei, Y. (2021a). The efficiency of integrated wastewater treatment plant for pollutant removal from industrial-scale lincomycin production. *J. Water Process Eng.* 42:102133. doi: 10.1016/j.jwpe.2021.102133

Zhang, L., and Okabe, S. (2020). Ecological niche differentiation among anammox bacteria. *Water Res.* 171:115468. doi: 10.1016/j.watres.2020.115468

Zhang, X., Song, Z., Tang, Q., Wu, M., Zhou, H., Liu, L., et al. (2021b). Performance and microbial community analysis of bioaugmented activated sludge for nitrogen-containing organic pollutants removal. *J. Environ. Sci.* 101, 373–381. doi: 10.1016/j.jes.2020.09.002

Zhang, Z., Zhang, Y., and Chen, Y. (2020). Recent advances in partial denitrification in biological nitrogen removal: From enrichment to application. *Bioresour. Technol.* 298:122444. doi: 10.1016/j.biortech.2019.122444

Zhao, Z.-C., Xie, G.-J., Liu, B.-F., Xing, D.-F., Ding, J., Han, H.-J., et al. (2021). A review of quorum sensing improving partial nitritation-anammox process: functions, mechanisms and prospects. *Sci. Total Environ.* 765:142703. doi: 10.1016/j.scitotenv.2020.142703

Zhou, Z., Wang, K., Qiang, J., Pang, H., Yuan, Y., An, Y., et al. (2021). Mainstream nitrogen separation and side-stream removal to reduce discharge and footprint of wastewater treatment plants. *Water Res.* 188:116527. doi: 10.1016/j.watres.2020.116527

Zhu, G., Peng, Y., Li, B., Guo, J., Yang, Q., and Wang, S. (2008). Biological removal of nitrogen from wastewater. *Rev. Environ. Contam. Toxicol.* 192, 159–195. doi: 10.1007/978-0-387-71724-1_5

Conflict of Interest: The authors declare that the research was conducted in the absence of any commercial or financial relationships that could be construed as a potential conflict of interest.

Publisher's Note: All claims expressed in this article are solely those of the authors and do not necessarily represent those of their affiliated organizations, or those of the publisher, the editors and the reviewers. Any product that may be evaluated in this article, or claim that may be made by its manufacturer, is not guaranteed or endorsed by the publisher.

frontiers in Microbiology

ORIGINAL RESEARCH
published: 27 October 2021
doi: 10.3389/fmicb.2021.749888

Hydrodynamics Regulate Longitudinal Plankton Community Structure in an Alpine Cascade Reservoir System

Yang Liu[1,2], Chengyan Li[1], Shenglong Jian[3,4], Shiyu Miao[1], Kemao Li[3,4], Hongtao Guan[3,4], Yaqi Mao[1], Zhongyi Wang[1] and Changzhong Li[1,2]**

[1] College of Eco-Environmental Engineering, Qinghai University, Xining, China, [2] State Key Laboratory of Plateau Ecology and Agriculture, Qinghai University, Xining, China, [3] Qinghai Provincial Fishery Environmental Monitoring Center, Xining, China, [4] The Key Laboratory of Plateau Aquatic Organism and Ecological Environment in Qinghai, Qinghai Provincial Fishery Environmental Monitoring Center, Xining, China

OPEN ACCESS

Edited by:
Lean Zhou,
Changsha University of Science and Technology, China

Reviewed by:
Bin Liang,
Harbin Institute of Technology, Shenzhen, China
Yin Ye,
Northwestern Polytechnical University, China
Yang Lei,
Southern University of Science and Technology, China

***Correspondence:**
Shenglong Jian
jianshenglong@163.com
Changzhong Li
lichangzhong@qhu.edu.cn

Specialty section:
This article was submitted to Microbiotechnology, a section of the journal Frontiers in Microbiology

Received: *30 July 2021*
Accepted: *20 September 2021*
Published: *27 October 2021*

Citation:
Liu Y, Li C, Jian S, Miao S, Li K, Guan H, Mao Y, Wang Z and Li C (2021) Hydrodynamics Regulate Longitudinal Plankton Community Structure in an Alpine Cascade Reservoir System. Front. Microbiol. 12:749888. doi: 10.3389/fmicb.2021.749888

Previous studies report significant changes on biotic communities caused by cascade reservoir construction. However, factors regulating the spatial–temporal plankton patterns in alpine cascade reservoir systems have not been fully explored. The current study explored effects of environmental factors on the longitudinal plankton patterns, through a 5-year-long study on the environmental factors and communities of phytoplankton and zooplankton in an alpine cascade reservoir system located upstream of Yellow River region. The findings showed that phytoplankton and zooplankton species numbers in the studied cascade reservoir system were mainly regulated by the hydrological regime, whereas nutrient conditions did not significantly affect the number of species. Abundance and biovolume of phytoplankton in cascade reservoirs were modulated by the hydrological regime and nutrient conditions. The drainage rate, N:P ratio, and sediment content in cascade reservoirs were negatively correlated with abundance and biovolume of phytoplankton. Abundance and biovolume of zooplankton were not significantly correlated with the hydrological regime but showed a strong positive correlation with nutrient conditions in cascade reservoirs. Shannon–Wiener index (*H'*) and the Pielou index (*J*) of phytoplankton were mainly regulated by the hydrological regime factors, such as drainage rate and sediment content in cascade reservoirs. However, temperature and nutrient conditions were the main factors that regulated the Shannon–Wiener index (*H'*) and the Pielou index (*J*) of zooplankton. Species number, abundance, and biovolume of phytoplankton showed a significant positive correlation with those of zooplankton. Hydrodynamics and nutrient conditions contributed differently in regulating community structure of phytoplankton or zooplankton. These findings provide an understanding of factors that modulate longitudinal plankton community patterns in cascade reservoir systems.

Keywords: phytoplankton, zooplankton, cascade reservoirs, community pattern, damming, Qinghai-Tibetan plateau

INTRODUCTION

Several dams are built on rivers worldwide to increase the use of water resources and meet surging domestic power demand (Graf, 1999; Finer and Jenkins, 2012; Grumbine and Pandit, 2013). Dams cause longitudinal river discontinuity and convert some original river ecosystems into reservoir or lake ecosystems with low water flow, high water transparency, and raised temperature (Magilligan and Nislow, 2005; Okuku et al., 2016; Van Cappellen and Maavara, 2016). Serial constructions of dams lead to a cascade reservoir system along the river. Several studies have explored the effects of cascade reservoirs on river ecosystems (Fan et al., 2015; Algarte et al., 2016; Wang Y. et al., 2016; Kang et al., 2017; Baumgartner et al., 2020). Studies report that cascade reservoirs cause significant changes in phytoplankton (Padisák et al., 2000; Silva et al., 2005; Wang et al., 2018), zooplankton (Hart, 2004; Perbiche-Neves and Nogueira, 2010; Okuku et al., 2016), benthic animals (Callisto et al., 2005), fish (Draštík et al., 2008), water physiochemical characteristics (Jorcin and Nogueira, 2005; Karnaukhova, 2007), and hydrological regimes (Matsuno et al., 2003) in river ecosystems. The effect of the construction of cascade reservoirs on rivers is significant for rivers in high-altitude areas whose ecological environment is more fragile. However, studies on the effects of construction of cascade reservoirs on alpine river ecosystems are limited.

Plankton, including phytoplankton and zooplankton, plays an important role in material circulation and energy flow in river or aquatic ecosystems (Cury et al., 2000; Richardson and Schoeman, 2004; Frederiksen et al., 2006). Phytoplankton is the main primary producer, whereas zooplankton is a group connecting the food webs of river ecosystems and are the most sensitive species to changes (Padisák et al., 2000; Silva et al., 2005; Perbiche-Neves and Nogueira, 2010; Wang et al., 2018). Therefore, community characteristics and dynamics of plankton are often used to explore the structure and functioning of river ecosystems, help in identifying regulating factors of plankton dynamics, and in evaluating effects of human activities on natural river ecosystems (Paerl et al., 2010; Okuku et al., 2016).

Previous studies on phytoplankton or zooplankton in individual reservoir reported that hydrology, nutrient availability, and biota interactions were the main controlling factors of plankton composition and biomass in reservoirs (Rangel et al., 2012; Beaver et al., 2013; Chang et al., 2014; Silva et al., 2014; Amaral et al., 2020). However, the detailed relationship between plankton community and these environmental factors was reservoir specific and more complex since conflicting results were reported (Beaver et al., 2013; Silva et al., 2014). Previous studies on the plankton pattern formation mechanism in reservoirs that omitted either phytoplankton or zooplankton may be inaccurate owing to the predation relationship between phytoplankton and zooplankton (Chang et al., 2014). Lack of a detailed investigation on environmental variables, phytoplankton, zooplankton, and fish characteristics may partly account for the contradicting findings from previous studies (Chang et al., 2014). Although studies on phytoplankton or zooplankton community in individual reservoirs are abundant, studies on longitudinal plankton community pattern and corresponding structuring factors after cascade reservoir construction are few (Okuku et al., 2016). Most studies only explored the effects on either phytoplankton or zooplankton (Padisák et al., 2000; Hart, 2004; Silva et al., 2005; Perbiche-Neves and Nogueira, 2010; Wang et al., 2018), and studies that explored both phytoplankton and zooplankton in a continuous cascade reservoir system are limited (Silva et al., 2005; Okuku et al., 2016; Wang et al., 2018). Environmental variables, phytoplankton community characteristics, zooplankton community characteristics, and fish community characteristics should be explored together to avoid potentially conflicting conclusions among studies. However, systematic and longtime span study of both phytoplankton community and zooplankton community in cascade reservoir system have not been conducted. Longitudinal plankton community pattern and corresponding regulating factors in cascade reservoir systems are not fully understood.

In the current study, the longitudinal distribution pattern of plankton and the corresponding regulation factors were explored for the first time in a high-altitude alpine cascade reservoir system. Longitudinal variation and dynamics of both phytoplankton and zooplankton community characteristics, including species number/composition, abundance, biovolume and biodiversity index, fish community composition, and environmental factors (environmental variables–phytoplankton–zooplankton–fish) were sampled for 5 years in the 300-km alpine and oligotrophic plateau cascade reservoirs. This study sought to (1) describe the longitudinal variation of plankton community pattern along the alpine cascade reservoirs, (2) promote understanding of environmental variables–phytoplankton–zooplankton–fish interactions in cascade reservoir systems, and (3) identify factors regulating plankton community pattern in cascade reservoir systems. The findings of the current study will promote understanding of factors that modulate the longitudinal plankton community patterns in cascade reservoir systems worldwide.

MATERIALS AND METHODS

Study Area

Yellow River is the second largest river in China and the sixth largest in the world. The altitude upstream of Yellow River varies between 2,000 and 4,000 m above sea level. Twelve reservoirs have been built between Longyang Gorge (LYG) and Jishi Gorge (JSG) upstream of Yellow River, forming the largest cascade reservoir system in China. The cascade reservoir system is approximately 300-km long and 800-m drop, and has an average annual runoff of 2.8×10^{10} m^3. All reservoirs are weekly or daily regulated reservoirs except for the upstream LYG, which is an annually regulated reservoir (Miao et al., 2020). Detailed morphological characteristics of each cascade reservoir have been reported by Miao et al. (2020). The cascade reservoir system is oligotrophic with a low TP and a high N:P ratio (Miao et al., 2020). Furthermore, it comprises a broad latitudinal gradient of depth, water residence time, and nutrient levels. The drainage rate was calculated by dividing individual reservoir storage by the daily outflow.

Sample Collection and Analysis

To explore the plankton community pattern and corresponding regulating factors after cascade reservoir construction, sampling sites were established in the lacustrine zone of each reservoir in Longyang Gorge (LYG), Laxi Gorge (LXG), Lijia Gorge (LJG), Gongbo Gorge (GBG), and Suzhi Gorge (SZG) (**Figure 1**). Sampling was carried out four times yearly from March to October for 5 years from 2013 to 2017.

Sample collection, species identification, and biovolume determination of plankton were performed following the Specification for Freshwater Plankton Surveys (SC/T 9402-2010). In the current study, qualitative and quantitative samples of both phytoplankton and zooplankton were collected. Species identification and counting were performed using an optical microscope with a phytoplankton counting chamber. Plankton biovolume (wet weight) was estimated using biovolume ($mm^3\ L^{-1}$) and converted from the plankton abundance using quantitative plankton samples (Hillebrand et al., 1999; Sun and Liu, 2003). Fishes were caught with approval by the local authority using cages and gill net methods (SC/T 9102.1-2007) to evaluate predation pressure on zooplankton. Primary species identification and numbering was conducted in the field. Fishes were released back after identification, photographing, and numbering.

GPS coordinates, altitude, water temperature, and pH of the sampling points were determined on-site. Dissolved oxygen (DO) level was determined using the iodometric method (GB 7489-87) within 24 h after sampling. Total nitrogen (TN) was determined by ultraviolet spectrophotometry after digestion of samples with alkaline potassium persulfate (HJ 636-2012). Total phosphorus (TP) was determined using ammonium molybdate spectrophotometry method (GB/T 1183-1989). Chemical oxygen demand (COD_{Mn}) was evaluated using alkaline potassium permanganate titration method (GB 11892-1989). The level of suspended solid (SS) was determined using gravimetric method (GB 11901-1989). Biological oxygen demand (BOD_5) was determined by dilution and inoculation method (HJ 505-2009).

Statistical Analysis

Data on plankton abundance, biomass, and biodiversity indexes, and environmental variables were presented as means ± standard deviations (mean ± SD) to show yearly variability. Phytoplankton and zooplankton community structures were expressed as species number, abundance, biomass, Shannon–Wiener diversity indexes, and Pielou evenness indexes. The 5-year results were used to show plankton community composition in the cascade reservoir system. Plankton diversity was measured by Shannon–Wiener diversity and Pielou evenness indexes.

Remote-sensing images of sampling points were generated by Google Earth (version 7.3.3.7699). Origin software (version 8.6) was used to map the longitudinal and temporal variations of plankton characteristics. Corrplot package (version 0.84) was used for Pearson's correlation analysis between phytoplankton communities, zooplankton communities, and environmental parameters. Detrended correspondence analysis (DCA) showed that the size of the gradient was less than 3; thus, redundancy analysis (RDA) was conducted among the Hellinger transformed phytoplankton, zooplankton, and environmental factors using CANOCO 5.0. Network analysis between plankton community characteristics and environmental factors in the cascade reservoirs was performed using Cytoscape tool (Version 3.8.1). Mean values of plankton abundance, biovolume, and biodiversity index for each site over the 5 years were used for Pearson's correlation analysis, redundancy analysis, and network analysis. The values of $^{*}p < 0.05$, $^{**}p < 0.01$, and $^{***}p < 0.001$ showed significant correlation.

RESULTS

Phytoplankton Community Composition and Longitudinal Variation

Eight phyla with 102 species of phytoplankton were identified in the five cascade reservoirs over the 5 years with 39 Bacillariophyta species (38.2%) and 39 Chlorophyta species (38.2%) (**Figure 2A**). The number of phytoplankton species, especially Bacillariophyta, Chlorophyta, and Cyanophyta, determined in LYG was significantly higher compared with that in the other reservoirs (**Figures 2B,C**). *Synedra acus*, *Navicula* sp., *Cymbella* sp., *Diatoma vulgare*, *Synedra* sp., *Cyclotella* sp., and *Achnanthes* sp. in the Bacillariophyta phylum, *Chlamydomona* sp. and *Ulothrix* sp. in Chlorophyta, and *Phormidium* sp. and *Oscillatoria tenuis* in Cyanophyta and *Ceratium hirundinella* in the Pyrrophyta phylum were the widely distributed species found in all five cascade reservoirs. The findings showed that the Bacillariophyta–Chlorophyta pattern of phytoplankton composition did not change over time. The average phytoplankton abundance and biovolume were 1.8×10^5 cells/L and 66.6 μg/L, respectively, in the five cascade reservoirs over the 5 years of study. Abundance and biovolume of phytoplankton decreased longitudinally along the river from upstream LYG to downstream SZG (**Figure 2C**). The average phytoplankton Shannon–Wiener diversity index and Pielou index were 2.08 and 0.73, respectively, in the five cascade reservoirs over the 5 years (**Figure 2D**).

Zooplankton Community Composition and Longitudinal Variation

Four phyla comprising 52 zooplankton species were identified in the five cascade reservoirs over the 5 years with 30 Rotatoria species (57.7%) and 9 Protozoa species (17.3%) (**Figure 3A**). Rotatoria and Protozoa were the dominant species in the five cascade reservoirs. Although Rotatoria and Protozoa were the predominant zooplankton species in the five cascade reservoirs, the zooplankton composition in each cascade reservoir was significantly different (**Figure 3B**). Analysis showed that LYG had the maximum number of zooplankton species (**Figure 3B**). *Acanthocystis* sp. and *Tintinnopsis wangi* in the Protozoa phylum, *Synchaeta* sp., *Keratella cochlearis*, *Polyarthra trigla*, and *Asplanchna* sp. in the Rotatoria phylum, and *Bosmina*

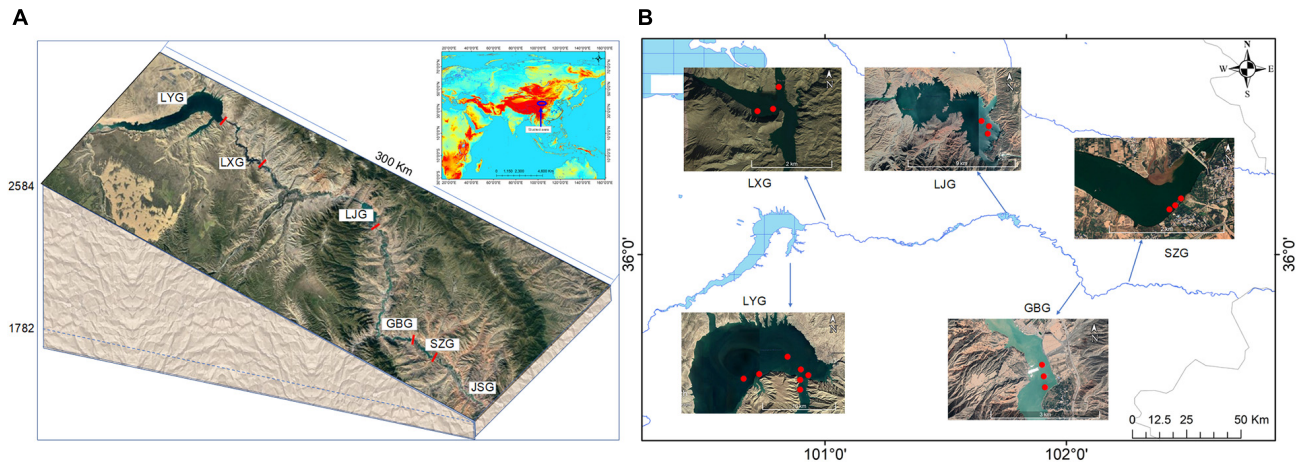

FIGURE 1 | Schematic diagram of the location of the cascade reservoirs **(A)** and sampling points in the cascade reservoirs **(B)**. Dams are shown by solid bars.

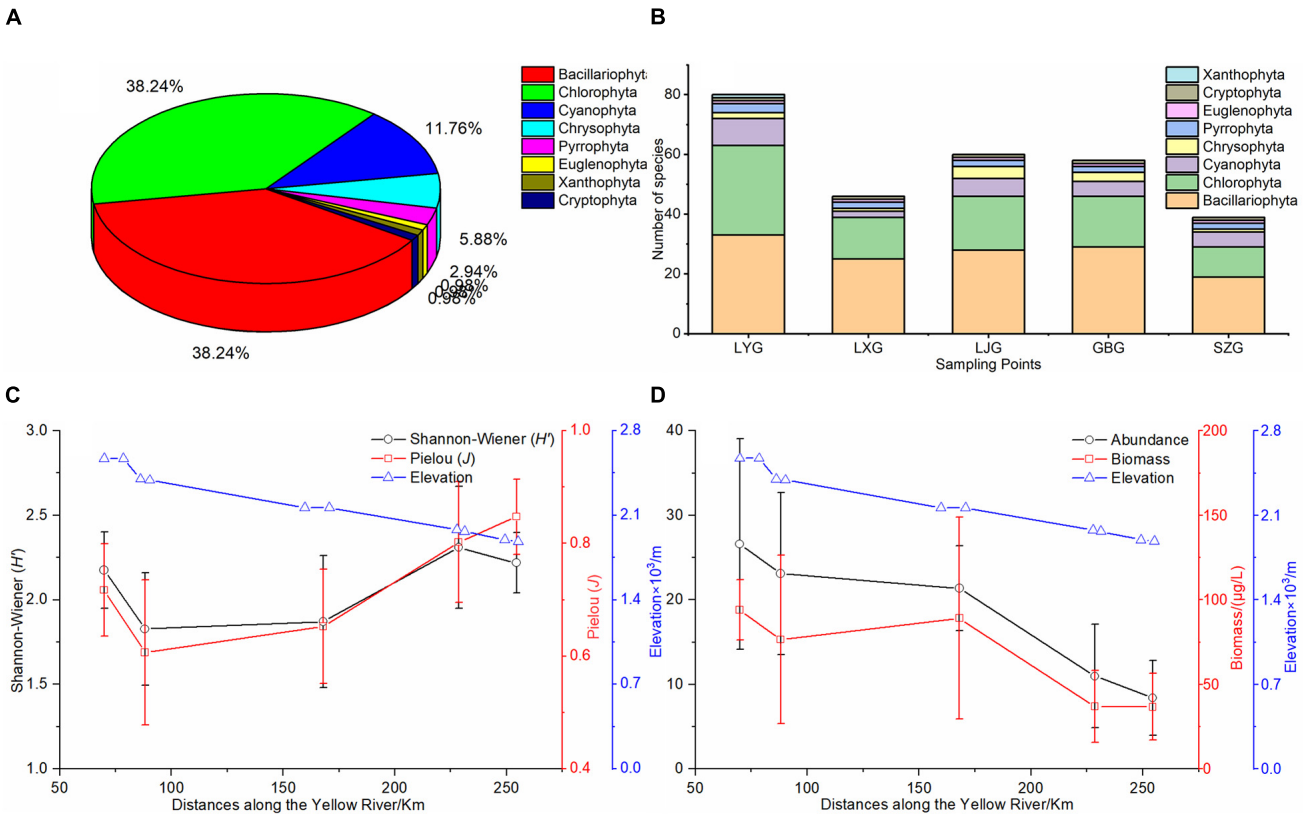

FIGURE 2 | Phytoplankton pattern in the cascade reservoirs. **(A)** Phytoplankton species composition over the 5 years of study, **(B)** phytoplankton species composition in each cascade reservoir, **(C)** longitudinal changes in the Shannon–Wiener index (*H'*) and Pielou index (*J*) of phytoplankton along the cascade reservoirs, and **(D)** longitudinal changes in phytoplankton abundance and biovolume along the cascade reservoirs. Locations of cascade reservoirs are recorded as kilometers upriver from the inlet site of the LYR.

longirostris in the Cladocera phylum were widely distributed in the reservoirs. Zooplankton species identified over the 5 years gradually decreased longitudinally from upstream LYG to downstream SZG (**Figure 3B**). Average zooplankton abundance, biovolume, Shannon–Wiener diversity index, and Pielou index were 294.44 cells/L, 402.1 μg/L, 1.56, and 0.73, respectively, in the five cascade reservoirs over the 5 years (**Figures 3C,D**).

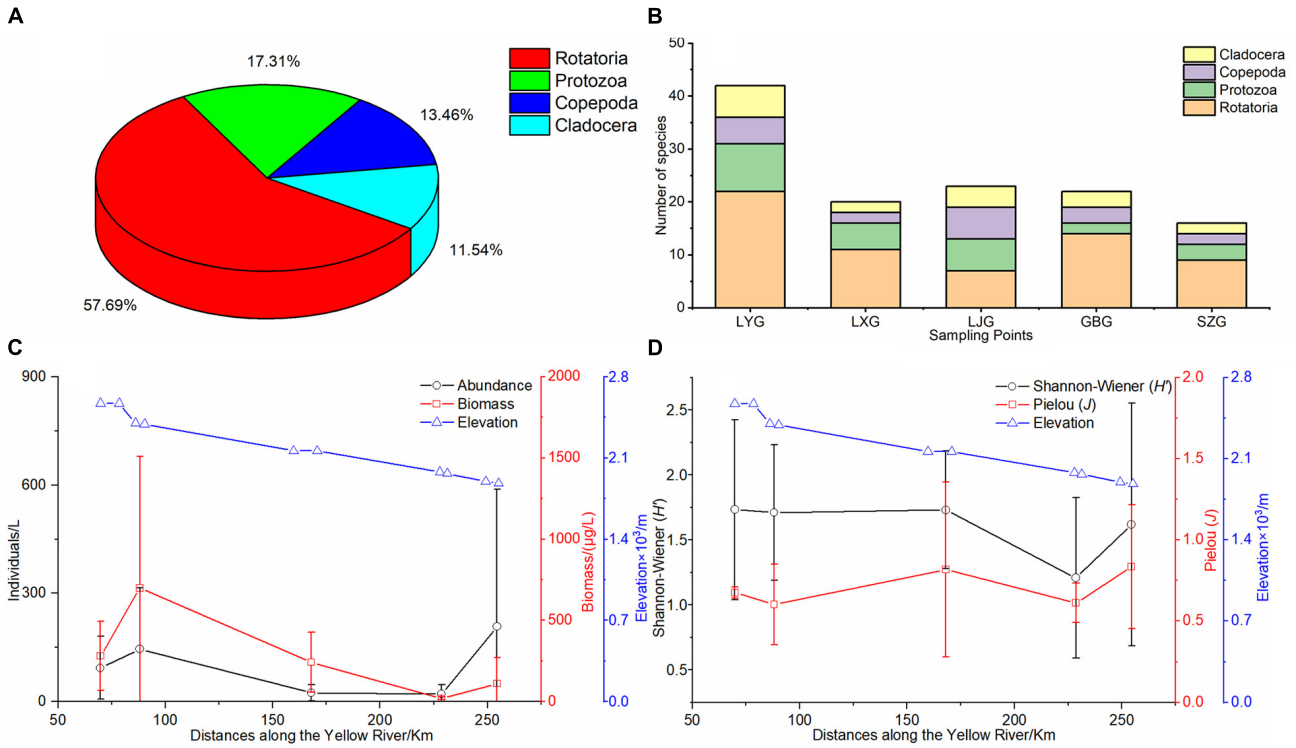

FIGURE 3 | Zooplankton pattern in the cascade reservoirs. **(A)** Zooplankton species composition over the 5 years of study, **(B)** zooplankton species composition in each cascade reservoir, **(C)** longitudinal changes in zooplankton abundance and biovolume along the cascade reservoirs, and **(D)** longitudinal changes in the Shannon–Wiener index (*H'*) and Pielou index (*J*) of zooplankton along the cascade reservoirs.

Factors Modulating the Longitudinal Phytoplankton Pattern

The findings showed that variations in phytoplankton composition among cascade reservoirs were mainly shaped by hydrological regime; however, water chemistry modulated phytoplankton composition (**Figures 4–6**). The number of phytoplankton species was mainly modulated by the hydrological regime of cascade reservoirs (**Figures 4**, **5**). Notably, volume, area, flow, drainage rate, and altitude showed significant effects on modulation of phytoplankton species (**Figures 4–6**). The drainage rate of cascade reservoirs showed significant negative effects on phytoplankton species number (**Figures 4–6**). A higher drainage rate was correlated with lower phytoplankton species number in cascade reservoirs (**Figures 4**, **5**). Decrease in drainage rate significantly increased the species number of Bacillariophyta and Chlorophyta in the alpine and oligotrophic cascade reservoirs in the upstream Yellow River (**Figures 4**, **5**). Nutrient parameters, such as COD, TN, and TP levels, were not significantly correlated with phytoplankton species number in the studied cascade reservoirs (**Figures 4**, **5**). However, abundance and biovolume of phytoplankton were synergistically affected by hydrological regime and nutrient levels (**Figures 4–6**). Drainage rate, N:P ratio, and sediment content were negatively correlated with abundance and biovolume of phytoplankton (**Figures 4**, **5**). This finding showed that phytoplankton abundance and biovolume decreased with increase in drainage rate and N:P ratio in cascade reservoirs. The Shannon–Wiener index (*H'*) and the Pielou index (*J*) of phytoplankton were modulated by water depth, drainage rate, flow and sediment content (**Figures 4**, **5**). Notably, abundance and biovolume of phytoplankton were low, whereas, the Shannon–Wiener index (*H'*) and Pielou index (*J*) of phytoplankton were high in cascade reservoirs with high sediment content and high drainage rate (**Figures 4**, **5**). The findings showed high abundance and biovolume of phytoplankton in deep cascade reservoirs, whereas the Shannon–Wiener index (H') and the Pielou index (*J*) of phytoplankton (P_H' and P_J) were low (**Figures 4**, **5**). These findings show that water depth, drainage rate, and sediment content played an important role in modulating phytoplankton community composition in cascade reservoir systems.

Factors Modulating the Longitudinal Zooplankton Pattern

Although Rotatoria and Protozoa were the most dominant species in all cascade reservoirs, the species number, abundance, biovolume, and biodiversity index of zooplankton differed along cascade reservoirs (**Figure 3B**). The species number of zooplankton was mainly modulated by hydrological regime in the studied cascade reservoir system (**Figures 4–6**). Notably, volume, area, flow, and drainage rate significantly modulated the number of zooplankton species (**Figures 4**, **5**). The drainage rate showed significant negative effects on the species number of

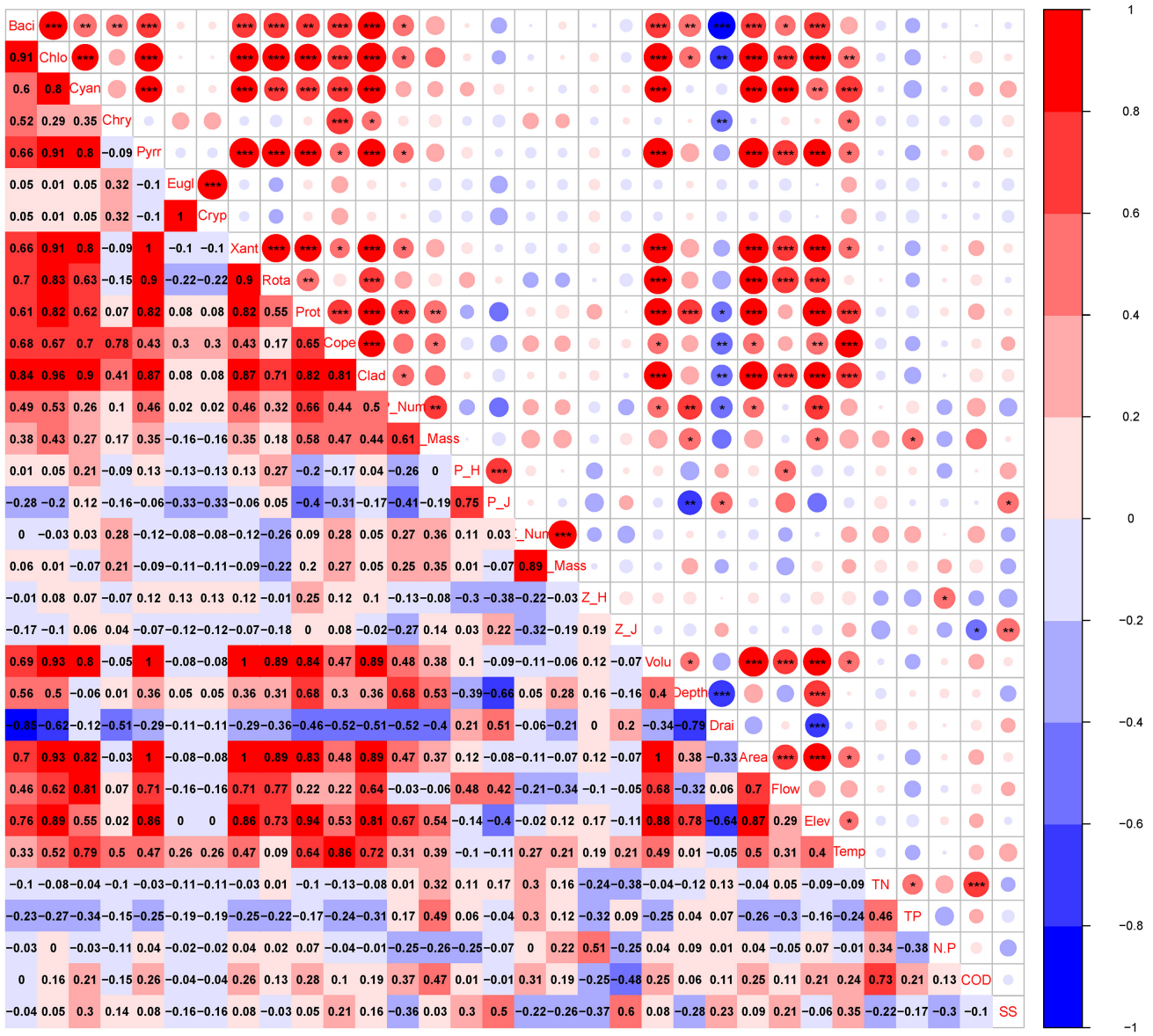

FIGURE 4 | Pearson's correlation analysis between plankton and environmental factors in the cascade reservoirs over the 5 years. Baci, Bacillariophyta; Chlo, Chlorophyta; Cyan, Cyanophyta; Chry, Chrysophyta; Pryy, Pyrrophyta; Eugl, Euglenophyta; Cryp, Cryptophyta; Xant, Xanthophyta; Rota, Rotatoria; Prot, Protozoa; Cope, Copepoda; Clad, Cladocera; P_Num, phytoplankton abundance; P_Mass, phytoplankton biovolume; P_H, phytoplankton Shannon–Wiener diversity index; P_J, phytoplankton Pielou index; Z_Num, zooplankton abundance; Z_Mass, zooplankton biovolume; Z_H, zooplankton Shannon–Wiener diversity index; Z_J, zooplankton Pielou index; Volu, volume; depth, depth; Drai, drainage rate; Area, area; Flow, runoff; Elev, altitude; Temp, temperature; TN, total nitrogen; TP, total phosphorus; N.P, N:P ratio; COD, chemical oxygen demand; SS, suspended substances. *, **, and *** in the upper part indicates significance. Numbers in the lower part indicate correlation coefficient.

zooplankton (**Figure 4**). A high drainage rate was correlated with lower zooplankton species number (**Figures 4**, **5**). Nutrients, such as COD, TN, and TP, showed insignificant effects on zooplankton species number (**Figures 4**, **5**). Notably, abundance and biovolume of zooplankton was not significantly correlated with the hydrological regime. However, a strong positive correlation with temperature, TN, TP, and COD was observed, whereas abundance and biovolume of zooplankton were negatively correlated with the sediment content (**Figure 4**). These findings indicated that abundance and biovolume of zooplankton were higher in cascade reservoirs with high water temperature, high nutrient levels, and low sediment content. Contrary to that of phytoplankton, the biodiversity of zooplankton was not significantly correlated with the hydrological regime; however, it showed a significant correlation with temperature and nutrient levels (**Figures 4**, **5**). Regulation of biodiversity of zooplankton by temperature and nutrient levels was probably through regulation of abundance and biovolume of phytoplankton.

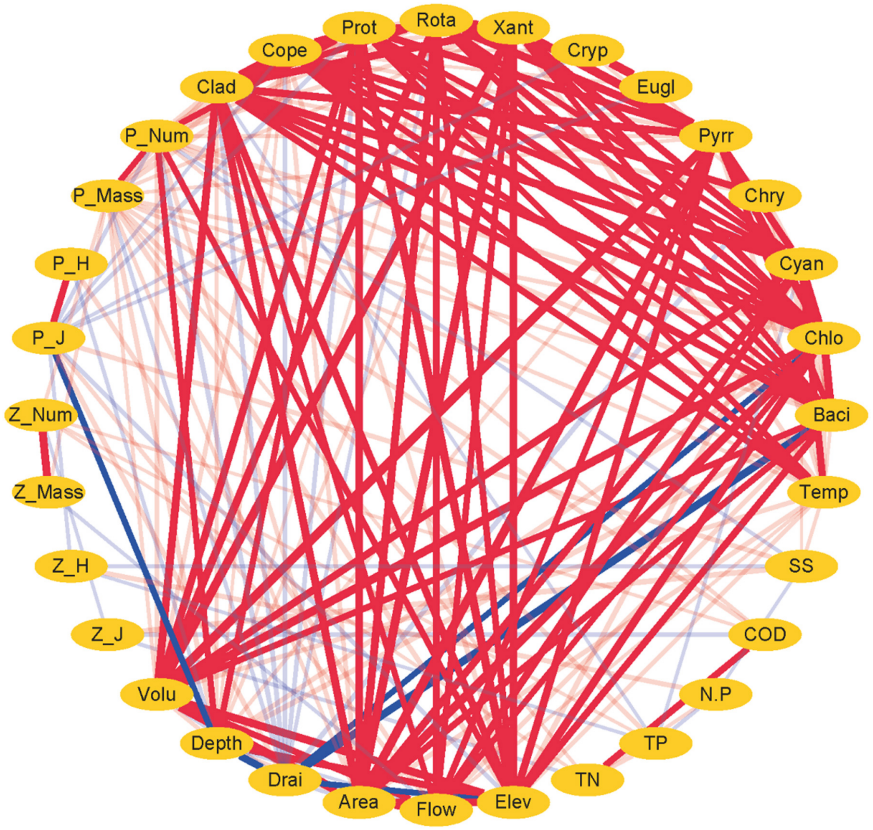

FIGURE 5 | Network analysis between plankton and environmental factors in the cascade reservoirs over the 5 years. Red lines indicate positive correlation. Blue lines indicate negative correlation. Larger width of lines indicates a stronger correlation.

Sediment content showed different effects on biodiversity of zooplankton compared with that of phytoplankton (**Figures 4–6**). Sediment content in cascade reservoirs was correlated with a low Shannon–Wiener index (*H'*), and a high Pielou index (*J*) of zooplankton (**Figure 4**). These findings show the important role of drainage rate, temperature, nutrient levels, and sediment content in regulating community pattern of zooplankton in cascade reservoir systems.

Correlation Analysis Between Phytoplankton and Zooplankton Communities

Pearson's correlation analysis (**Figure 4**) and network analysis (**Figure 5**) showed that the phytoplankton species number was positively correlated with zooplankton species number in the cascade reservoirs over the 5 years (**Figures 4**, **5**). Correlation coefficients between Chlorophyta and the four zooplankton phyla were more than 0.9 (**Figures 4**, **5**). Furthermore, abundance and biovolume of phytoplankton showed a positive correlation with abundance and biovolume of zooplankton (**Figures 4**, **5**). This finding is consistent with the predatory relationship between phytoplankton and zooplankton. The Shannon–Wiener index of phytoplankton was negatively correlated with the Shannon–Wiener index of zooplankton in the cascade reservoirs (**Figures 4**, **5**). Abundance and biovolume were negatively correlated with biodiversity for both phytoplankton and zooplankton.

DISCUSSION

Phytoplankton Community Variation Regulated by Physicochemical Factors

This study explored the effects of different factors on the plankton community patterns in an alpine and oligotrophic cascade reservoir system. Plankton samples were collected for 5 years in the cascade reservoirs, to ensure that the study data were systematic for reliable conclusions. Phytoplankton species composition in the alpine cascade reservoirs showed a dominant Bacillariophyta–Chlorophyta pattern (Qiu et al., 2019). Bacillariophyta is dominant at low temperature (Schabhüttl et al., 2013) and high turbulence (Harris and Baxter, 1996) riverine waters (Reynolds et al., 2002; Beaver et al., 2013). The cascade reservoirs in the current study are located in the upstream Yellow River in the alpine zone with low nutrient levels and dissolved organic materials. Therefore, only a few species from the genera such as *Microcystis*, *Anabaena*, and *Aphanizomenon* in the Cyanophyta phylum, which are adapted

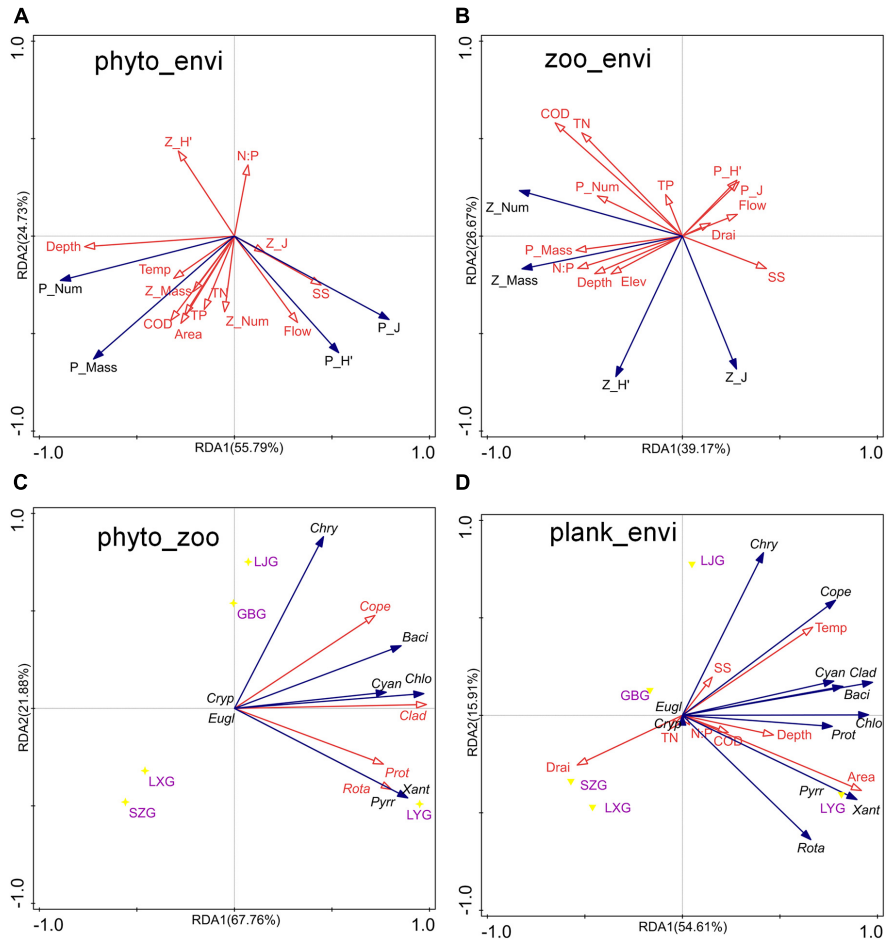

FIGURE 6 | Redundancy analysis (RDA) among phytoplankton, zooplankton, and environmental factors in the cascade reservoirs over the 5 years. **(A)** RDA of phytoplankton community composition and environmental factors, **(B)** RDA of zooplankton community composition and environmental factors, **(C)** RDA of the number of phytoplankton and zooplankton species, and **(D)** RDA of the number of plankton species and environmental factors.

to eutrophic water with relatively high water temperature, and abundant dissolved organic substances were observed in the current study (Reynolds et al., 2002; Silva and Costa, 2015). However, temperature was significantly positively correlated with numbers of Cyanophyta and Chlorophyta species. Phytoplankton community composition in the cascade reservoirs in the upstream Yellow River were similar to those reported in the upstream Yangtze River (Chen et al., 2013; Yin et al., 2017), upstream Lancang–Mekong River (Yin et al., 2017), and Qaidam River (Chen et al., 2012) in the Qinghai–Tibet plateau. These regions show characteristics of phytoplankton composition in oligotrophic waters in the alpine region of the Qinghai–Tibet plateau. The finding showed that diatoms had stronger ability to adapt to harsh environments. Nutrient-rich diatoms provide abundant food for aquatic animals in harsh alpine waters and have important ecological significance in the food chain of oligotrophic and alpine ecosystems.

Abundance (1.8×10^5 cells/L) and biovolume (66.6 μg/L) of phytoplankton species in the alpine cascade reservoirs were low. This may be because the cascade reservoirs in the upstream are located on the Qinghai–Tibet plateau, where growth and reproduction of phytoplankton are significantly inhibited by high altitude, low water temperature, and low phosphorus levels (Amaral et al., 2020). Oligotrophic aquatic systems with low species number and biovolume of phytoplankton and simple ecosystem structure are vulnerable to external factors. Low phytoplankton species number, abundance, biovolume, and diversity index observed in the current study indicate that the phytoplankton community in the alpine cascade reservoirs was less stable and less resistant to external disturbance. The findings indicated that the ecosystem of high-altitude rivers is more fragile compared with rivers in low-altitude areas. Alpine river ecosystems are more vulnerable to environmental changes and human activities; therefore, the environmental impact of human activities on alpine river should be carefully explored.

Although some phytoplankton species were present along cascade reservoirs, the phytoplankton community composition was different along cascade reservoirs. Hydrodynamic characteristics of cascade reservoir systems vary worldwide. However, hydrology characteristics are the main factors that

modulate the community structure of phytoplankton (Silva et al., 2005; Beaver et al., 2013; Qu et al., 2018). The current study explored the factors regulating the phytoplankton patterns in cascade reservoirs. The findings of this study showed that the environmental factors controlling species number, abundance, biovolume, and biodiversity of phytoplankton can be different in cascade reservoir systems. The species number and the biodiversity index (including the Shannon–Wiener index and Pielou index) of phytoplankton were mainly modulated by the hydrological regime of cascade reservoirs. Hydrological parameters, such as volume, area, and flow were correlated with the drainage rate of cascade reservoirs. Drainage rate/water residence time, and the sediment content of cascade reservoirs were the most important factors modulating the species number and biodiversity index of phytoplankton. This may be because cascade reservoirs with larger water volume, higher drainage rate, and higher sediment content provide spatial heterogeneity to more phytoplankton species (Okuku et al., 2016; Graco-Roza et al., 2020). The findings showed that the hydrological regime modulated phytoplankton species number, abundance, and biovolume of phytoplankton. However, abundance and biovolume of phytoplankton were significantly modulated by nutrient levels compared with the hydrological regime in cascade reservoirs. Higher nitrogen and phosphorus levels promote growth of phytoplankton. Previous studies report that phytoplankton biomass changes in response to nutrient availability mainly in oligotrophic conditions (Özkan et al., 2016; Wang et al., 2018; Amaral et al., 2020). However, some studies report that bioavailable nitrogen and phosphorus are weakly correlated with phytoplankton biomass (Beaver et al., 2013; Okuku et al., 2016). The relationship between nutrient levels and phytoplankton biomass is more complex in flowing cascade reservoir environments owing to multiple structuring factors (Beaver et al., 2013; Silva et al., 2014; Okuku et al., 2016). Hydrology and phosphorus concentrations were significantly correlated with phytoplankton biomass in 12 tropical hydroelectric reservoirs in Brazil (Rangel et al., 2012; Silva et al., 2014). Drainage rate and N:P ratio showed significant negative effects on phytoplankton abundance and biovolume in cascade reservoirs, which was consistent with findings reported by Silva et al. (2014). This can be attributed to the high drainage rate of the cascade reservoirs, which may cause unstable water environment, increased sediment content, and low transparency, which negatively affect the growth of phytoplankton (Silva and Costa, 2015; Okuku et al., 2016; Chen et al., 2018). Notably, high nutrients levels (COD, TN, and TP) significantly promote growth of phytoplankton. Okuku et al. (2016) reported that water retention time is not positively correlated with phytoplankton abundance in cascade reservoirs, and smaller reservoirs showed higher abundance, despite their significantly shorter retention time. However, the findings of the current study showed that LYG (with larger volume, longer water retention time, and more static water) showed the highest phytoplankton abundance and biomass compared with the other cascade reservoirs. In addition, the drainage rate of cascade reservoirs significantly modulated species composition and biovolume of phytoplankton indicating the role of hydraulic stability to phytoplankton (Beaver et al., 2013; Silva and Costa, 2015). The findings showed that increased residence time, low sediment content, and high levels of nutrients increase phytoplankton abundance and biovolume (Bowes et al., 2016; Rao et al., 2018). Furthermore, the findings indicate that sediment content reduced abundance and biovolume of phytoplankton, and increased the diversity index of phytoplankton in the studied cascade reservoirs.

Zooplankton Community Variation Regulated by Physicochemical Factors

Although previous studies report that physicochemical factors modulate zooplankton communities and dynamics (Sellami et al., 2010; Chang et al., 2014), only a few studies have explored zooplankton community patterns along cascade reservoirs and the factors that regulate these patterns. The findings showed that the composition of the zooplankton community in the studied cascade reservoir system was simple with a few large zooplankton species. A high-altitude environment with low water temperature, strong ultraviolet, and low abundance of phytoplankton and bacteria are negatively correlated with zooplankton abundance (Silva et al., 2014). Therefore, zooplankton species number, abundance, and biovolume were low in the studied alpine cascade reservoir system. High flushing environments in reservoirs favored small-sized zooplankton with short generation times, such as rotifers (Obertegger et al., 2007; Beaver et al., 2013; Silva et al., 2014). Rotifers were dominant in riverine ecosystems with low water residence time (Baranyi et al., 2002; Okuku et al., 2016), which is consistent with the findings of the current study in the flowing cascade reservoir system. However, the findings showed that the species number of rotifers was significantly correlated with the volume and the area of reservoirs, and more species number of Rotatoria was detected in low-flushing LYG compared with other high-flushing reservoirs in our study.

The findings in this 5-year study showed the importance of physicochemical factors on zooplankton communities (Anneville et al., 2007; Sellami et al., 2010; Chang et al., 2014). However, the findings showed that effects of physicochemical factors on species composition, abundance/biovolume and biodiversity index was different in the cascade reservoir system. Zooplankton species number along cascade reservoirs was mainly regulated by the hydrological regime of cascade reservoirs. However, the abundance, biovolume, and biodiversity of zooplankton showed a weak correlation with hydrological regime, and significantly positive correlation with temperature and nutrient levels (TN, TP, and COD). The finding on weak correlation between zooplankton abundance and the hydrology was not consistent with findings from previous studies that high zooplankton abundance was observed in the lentic zones or reservoirs due to reduced water speed and longer retention times (Thorp et al., 1994; Basu and Pick, 1997; Reckendorfer et al., 1999; Okuku et al., 2016). The correlation between abundance and biovolume of zooplankton and temperature, and nutrient levels was because higher temperature and nutrient levels contribute to the growth of phytoplankton through the supply of food for zooplankton (Lampert et al., 1986; Vanni, 1987;

Elser and Goldman, 1991; Tavares et al., 2019). Therefore, factors affecting abundance and biovolume of phytoplankton may also affect zooplankton abundance and biovolume. Furthermore, the findings showed that the sediment content did not significantly decrease the Shannon–Wiener index of zooplankton; however, it was significantly correlated with a high Pielou index of zooplankton. A previous study reported that turbidity decreased zooplankton taxa numbers in three tropical cascading reservoirs, which is consistent with the findings of the current study (Okuku et al., 2016).

Comparison of Effects of Physicochemical Factors on Zooplankton and Phytoplankton Community

Sampling and analysis of both zooplankton and phytoplankton were conducted in this 5-year study. A comparison of the effects of the physicochemical factors on zooplankton and phytoplankton communities showed that the effects of physicochemical factors on zooplankton and phytoplankton showed differences in the cascade reservoir system. Species numbers of phytoplankton and zooplankton along cascade reservoirs were mainly regulated by hydrological regime of cascade reservoirs. This finding indicates the importance of hydrological characteristics in shaping zooplankton and phytoplankton community species composition. However, factors regulating abundance, biovolume, and biodiversity of zooplankton were different from those regulating phytoplankton. Sediment content decreased the Shannon–Wiener index of both phytoplankton and zooplankton in the current study. However, sediment content decreased the Pielou index of phytoplankton but increased the Pielou index of zooplankton. A significant positive correlation between phytoplankton Shannon–Wiener index (*H'*) and Pielou index (*J*) was observed in the present study, which was consistent with findings from previous studies (Stirling and Wilsey, 2001; Ricotta and Avena, 2003; Okuku et al., 2016). This finding indicates that the phytoplankton Shannon–Wiener index (*H'*) was highly correlated with the Pielou index (*J*) compared with phytoplankton abundance and biomass (Okuku et al., 2016). However, insignificant positive correlation was observed between the zooplankton Shannon–Wiener index (*H'*) and the Pielou index (*J*).

Interaction Between Zooplankton and Phytoplankton Communities

Previous limited numbers of studies on plankton community in cascade reservoir systems only focused on either phytoplankton or zooplankton and seldom focused on both in one study. The findings of the current study showed a significant correlation between phytoplankton and zooplankton in species number, abundance, and biovolume in cascade reservoirs. The significant correlation between zooplankton and phytoplankton species number/composition was consistent with findings from a study by Chang et al. (2014) that explored a subtropical reservoir. Furthermore, a significant correlation was observed between zooplankton and phytoplankton biomass. Strong zooplankton–phytoplankton interactions were expected since zooplankton feeds on phytoplankton (Matveev, 2003; Hunt and Matveev, 2005; Bonecker et al., 2007). However, weak zooplankton–phytoplankton interactions based on biomass have been reported in previous studies (Crisman and Beaver, 1990; Havens et al., 2000; Wang et al., 2007; Yuan and Pollard, 2018). Lack of a detailed investigation on environmental variables–phytoplankton–zooplankton–fish characteristics is partly the reason for these contradicting findings (Chang et al., 2014). Zooplankton biomass is regulated by physicochemical factors, availability of phytoplankton, and fish predation (Yoshida et al., 2001; Hansson et al., 2007; Attayde et al., 2010). The significant correlation between zooplankton and phytoplankton biomass in the studied cascade reservoir can be attributed to a strong bottom–up regulation of phytoplankton (Yuan and Pollard, 2018) and low top–down control of planktivorous fish (Lu and Xie, 2001; Pinto-Coelho et al., 2005; Hansson et al., 2007; Havens et al., 2009; Chang et al., 2014). In the current study, the predation pressure by fish on zooplankton was explored through fish survey. The catches of the current survey and previous studies indicated a low top–down control. Previous studies report low fish species number and fish biomass with very limited planktivorous fishes in alpine cascade reservoirs (Tang and He, 2013; Wang H. et al., 2016; Qiu et al., 2019). Analysis of the biomass, abundance, and distribution of the catches showed that *Hypomesus olidus*, *Gymnocypris eckloni* Herzensten, *Triplophysa scleroptera*, and *Schizopygopsis pylzovi* Kessler were the most dominant species (Tang and He, 2013; Qiu et al., 2019). The dominant taxa, including Schizothorax and Triplophysa in the studied cascade reservoir system, were mainly omnivorous fish. *Schizopygopsis pylzovi* Kessler mainly feed on algae, *Hypomesus olidus* and *Gymnocypris eckloni* Herzensten mainly feed on zooplankton, whereas *Triplophysa scleroptera* mainly feed on benthic gammarid and aquatic insects (Tang and He, 2013). The findings did not show other planktivorous invertebrate predators apart from fish. Therefore, zooplankton biomass was not significantly regulated by fish predation in the studied alpine and oligotrophic cascade reservoirs, which may be different from those in temperate, subtropical, and tropical lakes (Yoshida et al., 2001). Although the top–down control of fish on the zooplankton biomass was low, the findings of the current study showed clear bottom–up regulation of phytoplankton species number, abundance, and biomass on zooplankton community. These findings provide an understanding on interactions between phytoplankton and zooplankton in cascade reservoir system.

Environmental Implications for Water Conservancy Facilities

The findings of the current study showed that the community structure of plankton is significantly affected by the hydrological regime of the cascade reservoir system (**Figures 5**, **6**). Therefore, plankton community structure is an ideal biomarker to reflect the impact of cascade reservoir construction on the river ecosystem (Li et al., 2013; Graco-Roza et al., 2021). Taxa composition of phytoplankton in the cascade reservoir system were mainly

modulated by hydrological conditions (**Figures 5**, **6**). On the contrary, abundance and biomass of phytoplankton were mainly modulated by hydrological conditions and nutrient levels (**Figures 5**, **6**). Drainage rate, sediment content, and nutrient conditions contributed differently in regulating composition, abundance, biovolume, and biodiversity index of both phytoplankton and zooplankton. The hydrological regime can affect material circulation and energy transfer of the cascade reservoir ecosystem by affecting the taxa composition and biomass of plankton (Bertrand et al., 2001; Dias et al., 2016). Therefore, it is the most important regulating factor of the cascade reservoir ecosystem (**Figures 5**, **6**; Li et al., 2013). The findings of the current study can be used to predict the effects of the proposed water conservancy facilities on community composition of plankton. More Chlorophyta species can be expected in a stable environment with low flow velocity and low sediment content, and more diatom species can be expected to survive in the environment of high flow velocity, high sediment content, and low water temperature. Relatively high phytoplankton biomass and abundance can be expected in cascade reservoirs with stable water environment of slow water flow, high transparency, and warm water temperature (**Figures 5**, **6**). Phytoplankton grow and reproduce rapidly and can quickly adapt to changing hydrological characteristics of the cascade reservoir system and form a new plankton community (Wang et al., 2012; Chen et al., 2020). However, benthonic invertebrates with weak mobility and fish, mainly the spawning sites and feeding sites, are much slower to adapt to hydrological changes (Moreno and Callisto, 2006; Zhang et al., 2010). Studies should explore the impact of changes in the structure of plankton community on the community structure of benthonic invertebrates and fish in the upper reaches of rivers. The discharge flow of the reservoir should be kept stable when constructing and operating cascade reservoirs in the upper reaches of the river.

CONCLUSION

The longitudinal distribution pattern of plankton and the corresponding regulation factors were systematically explored for the first time in a high-altitude alpine cascade reservoir system. Results showed that plankton community structure is sensitive to the hydrological regime and is an ideal biomarker for evaluating the effects of cascade reservoir construction on a river ecosystem. The findings of the current study also showed that Bacillariophyta and Chlorophyta were the predominant phytoplankton phyla, whereas predominant zooplankton phyla in the alpine and oligotrophic cascade reservoir system were Rotatoria and Protozoa. The phytoplankton and zooplankton species number was mainly regulated by hydrological regime. Notably, drainage rate was the most significant factor, whereas nutrient levels did not significantly have an effect on phytoplankton and zooplankton species abundance. Abundance and biovolume of phytoplankton were modulated by hydrological regime and nutrient levels, whereas abundance and biovolume of zooplankton were mainly regulated by nutrient levels and sediment content. The Shannon–Wiener index and Pielou index of phytoplankton was mainly regulated by drainage rate and sediment content. On the contrary, the Shannon–Wiener index and Pielou index of zooplankton were mainly regulated by temperature and nutrient levels and less regulated by hydrological regime. Sediment content was negatively correlated with abundance and biovolume of both phytoplankton and zooplankton. However, sediment content was positively correlated with the Shannon–Wiener index and Pielou index of phytoplankton, but was negatively correlated with the Shannon–Wiener index of zooplankton. Phytoplankton can quickly adapt to changing hydrological conditions in a cascade reservoir system, and attention should be paid to the changes in community structure of benthonic invertebrates and fish.

DATA AVAILABILITY STATEMENT

The raw data supporting the conclusions of this article will be made available by the authors, without undue reservation.

AUTHOR CONTRIBUTIONS

SJ, YL, and CZL designed the study. KL, SJ, HG, and SM collected and analyzed the samples. YL and CGL drew the figures. YL, CGL, and SJ wrote the manuscript. All authors analyzed and interpreted the data, and approved the final version of the manuscript.

FUNDING

This research was supported by National Natural Science Foundation of China (No. 31760763) and Qinghai Science and Technology Department Project (Nos. 2018-ZJ-703 and 2019-NK-A2).

ACKNOWLEDGMENTS

We are grateful to the excellent work of all those who participated in this study.

REFERENCES

Algarte, V. M., Dunck, B., Leandrini, J. A., and Rodrigues, L. (2016). Periphytic diatom ecological guilds in floodplain: ten years after dam. *Ecol. Indic.* 69, 407–414. doi: 10.1016/j.ecolind.2016.04.049

Amaral, L. M., Carolina De Almeida Castilho, M., Henry, R., and Ferragut, C. (2020). Epipelon, phytoplankton and zooplankton responses to the experimental oligotrophication in a eutrophic shallow reservoir. *Environ. Pollut.* 263(Pt A):114603. doi: 10.1016/j.envpol.2020.114603

Anneville, O., Molinero, J. C., Souissi, S., Balvay, G., and Gerdeaux, D. (2007). Long-term changes in the copepod community of Lake Geneva. *J. Plankton Res.* 29, i49–i59. doi: 10.1093/plankt/fbl066

Attayde, J. L., Van Nes, E. H., Araujo, A. I. L., Corso, G., and Scheffer, M. (2010). Omnivory by planktivores stabilizes plankton dynamics, but may either promote or reduce algal biomass. *Ecosystems* 13, 410–420. doi: 10.1007/s10021-010-9327-4

Baranyi, C., Hein, T., Holarek, C., Keckeis, S., and Schiemer, F. (2002). Zooplankton biomass and community structure in a Danube River floodplain system: effects of hydrology. *Freshw. Biol.* 47, 473–482. doi: 10.1046/j.1365-2427.2002.00822.x

Basu, B. K., and Pick, F. R. (1997). Phytoplankton and zooplankton development in a lowland, temperate river. *J. Plankton Res.* 19, 237–253. doi: 10.1093/plankt/19.2.237

Baumgartner, M. T., Piana, P. A., Baumgartner, G., and Gomes, L. C. (2020). Storage or run-of-river reservoirs: exploring the ecological effects of dam operation on stability and species interactions of fish assemblages. *Environ. Manage.* 65, 220–231. doi: 10.1007/s00267-019-01243-x

Beaver, J. R., Jensen, D. E., Casamatta, D. A., Tausz, C. E., Scotese, K. C., Buccier, K. M., et al. (2013). Response of phytoplankton and zooplankton communities in six reservoirs of the middle Missouri River (USA) to drought conditions and a major flood event. *Hydrobiologia* 705, 173–189. doi: 10.1007/s10750-012-1397-1

Bertrand, C., Siauve, V., Fayolle, S., and Cazaubon, A. (2001). Effects of hydrological regime on the drift algae in a regulated Mediterranean river (River Verdon, southeastern France). *Regulated Rivers Res. Manage.* 17, 407–416. doi: 10.1002/rrr.654

Bonecker, C. C., Nagae, M. Y., Bletller, M. C. M., Velho, L. F. M., and Lansac-to^Ha, F. A. (2007). Zooplankton biomass in tropical reservoirs in southern Brazil. *Hydrobiologia* 579, 115–123. doi: 10.1007/s10750-006-0391-x

Bowes, M. J., Loewenthal, M., Read, D. S., Hutchins, M. G., Prudhomme, C., Armstrong, L. K., et al. (2016). Identifying multiple stressor controls on phytoplankton dynamics in the River Thames (UK) using high-frequency water quality data. *Sci. Total Environ.* 569–570, 1489–1499. doi: 10.1016/j.scitotenv.2016.06.239

Callisto, M., Goulart, M., Barbosa, F. A. R., and Rocha, O. (2005). Biodiversity assessment of benthic macroinvertebrates along a reservoir cascade in the lower São Francisco river (northeastern Brazil). *Braz. J. Biol.* 65, 229–240. doi: 10.1590/S1519-69842005000200006

Chang, C. W., Shiah, F. K., Wu, J. T., Miki, T., and Hsieh, C. H. (2014). The role of food availability and phytoplankton community dynamics in the seasonal succession of zooplankton community in a subtropical reservoir. *Limnologica* 46, 131–138. doi: 10.1016/j.limno.2014.01.002

Chen, J., Wang, P., Wang, C., Wang, X., Miao, L., Liu, S., et al. (2020). Distinct assembly mechanisms underlie similar biogeographic patterns of rare and abundant bacterioplankton in cascade reservoirs of a large river. *Front. Microbiol.* 11:158. doi: 10.3389/fmicb.2020.00158

Chen, N., Mo, Q., Kuo, Y. M., Su, Y., and Zhong, Y. (2018). Hydrochemical controls on reservoir nutrient and phytoplankton dynamics under storms. *Sci. Total Environ.* 619-620, 301–310. doi: 10.1016/j.scitotenv.2017.09.216

Chen, Y. Q., Shen, Z. X., and Liu, Y. T. (2012). Study on community structure of phytoplankton in Geermu River of Chaidamu River system in autumn. *Sci. Technol. Qinghai Agric. For.* 86, 10–15.

Chen, Y. Q., Shen, Z. X., Liu, Y. T., and Li, K. M. (2013). Community structure and diversity assessment of phytoplankton from Qumalai to Yushan section in the upstream reach of the Yangtze river in spring and autum. *Res. Environ. Yangtze Basin* 22, 1325–1332.

Crisman, T. L., and Beaver, J. R. (1990). "Applicability of planktonic biomanipulation for managing eutrophication in the subtropics," in *Biomanipulation Tool for Water Management*, eds R. D. Gulati, E. H. R. R. Lammens, M. L. Meijer, and E. Van Donk (Heidelberg: Springer Netherlands), 177–185.

Cury, P., Bakun, A., Crawford, R. J. M., Jarre, A., Quiñones, R. A., Shannon, L. J., et al. (2000). Small pelagics in upwelling systems: patterns of interaction and structural changes in "wasp-waist" ecosystems. *ICES J. Mar. Sci.* 57, 603–618. doi: 10.1006/jmsc.2000.0712

Dias, J. D., Simões, N. R., Meerhoff, M., Lansac-Tôha, F. A., Velho, L. F. M., and Bonecker, C. C. (2016). Hydrological dynamics drives zooplankton metacommunity structure in a Neotropical floodplain. *Hydrobiologia* 781, 109–125. doi: 10.1007/s10750-016-2827-2

Draštík, V., Kubečka, J., Tušer, M., Čech, M., Frouzová, J., Jarolím, O., et al. (2008). The effect of hydropower on fish stocks: comparison between cascade and non-cascade reservoirs. *Hydrobiologia* 609, 25–36. doi: 10.1007/s10750-008-9393-1

Elser, J. J., and Goldman, C. R. (1991). Zooplankton effects on phytoplankton in lakes of contrasting trophic status. *Limnol. Oceanogr.* 36, 64–90. doi: 10.4319/lo.1991.36.1.0064

Fan, H., He, D., and Wang, H. (2015). Environmental consequences of damming the mainstream Lancang-Mekong River: a review. *Earth Sci. Rev.* 146, 77–91. doi: 10.1016/j.earscirev.2015.03.007

Finer, M., and Jenkins, C. N. (2012). Proliferation of hydroelectric dams in the andean amazon and implications for Andes-Amazon connectivity. *PLoS One* 7:e35126. doi: 10.1371/journal.pone.0035126

Frederiksen, M., Edwards, M., Richardson, A. J., Halliday, N. C., and Wanless, S. (2006). From plankton to top predators: bottom-up control of a marine food web across four trophic levels. *J. Anim. Ecol.* 75, 1259–1268. doi: 10.1111/j.1365-2656.2006.01148.x

Graco-Roza, C., Santos, J. B. O., Huszar, V. L. M., Domingos, P., Soininen, J., and Marinho, M. M. (2020). Downstream transport processes modulate the effects of environmental heterogeneity on riverine phytoplankton. *Sci. Total Environ.* 703:135519. doi: 10.1016/j.scitotenv.2019.135519

Graco-Roza, C., Soininen, J., Corrêa, G., Pacheco, F. S., Miranda, M., Domingos, P., et al. (2021). Functional rather than taxonomic diversity reveals changes in the phytoplankton community of a large dammed river. *Ecol. Indic.* 121:107048. doi: 10.1016/j.ecolind.2020.107048

Graf, W. L. (1999). Dam nation: a geographic census of American dams and their large-scale hydrologic impacts. *Water Resour. Res.* 35, 1305–1311. doi: 10.1029/1999WR900016

Grumbine, R. E., and Pandit, M. K. (2013). Threats from india's Himalaya Dams. *Science* 339, 36–37. doi: 10.1126/science.1227211

Hansson, L. A., Nicolle, A., Brodersen, J., Romare, P., Anders Nilsson, P., Brönmark, C., et al. (2007). Consequences of fish predation, migration, and juvenile ontogeny on zooplankton spring dynamics. *Limnol. Oceanogr.* 52, 696–706. doi: 10.4319/lo.2007.52.2.0696

Harris, G. P., and Baxter, G. (1996). Interannual variability in phytoplankton biomass and species composition in a subtropical reservoir. *Freshw. Biol.* 35, 545–560. doi: 10.1111/j.1365-2427.1996.tb01768.x

Hart, R. C. (2004). Cladoceran periodicity patterns in relation to selected environmental factors in two cascading warm-water reservoirs over a decade. *Hydrobiologia* 526, 99–117. doi: 10.1023/B:HYDR.0000041610.56021.63

Havens, K. E., East, T. L., Marcus, J., Essex, P., Bolan, B., Raymond, S., et al. (2000). Dynamics of the exotic Daphnia lumholtzii and native macro-zooplankton in a subtropical chain-of-lakes in Florida, U.S.A. *Freshw. Biol.* 45, 21–32. doi: 10.1046/j.1365-2427.2000.00614.x

Havens, K. E., Elia, A. C., Taticchi, M. I., and Fulton, R. S. (2009). Zooplankton–phytoplankton relationships in shallow subtropical versus temperate lakes Apopka (Florida, USA) and Trasimeno (Umbria, Italy). *Hydrobiologia* 628, 165–175. doi: 10.1007/s10750-009-9754-4

Hillebrand, H., Dürselen, C. D., Kirschtel, D., Pollingher, U., and Zohary, T. (1999). Biovolume calculation for pelagic and benthic microalgae. *J. Phycol.* 35, 403–424. doi: 10.1046/J.1529-8817.1999.3520403.X

Hunt, R. J., and Matveev, V. F. (2005). The effects of nutrients and zooplankton community structure on phytoplankton growth in a subtropical Australian reservoir: an enclosure study. *Limnologica* 35, 90–101. doi: 10.1016/j.limno.2005.01.004

Jorcin, A., and Nogueira, M. G. (2005). Temporal and spatial patterns based on sediment and sediment–water interface characteristics along a cascade of reservoirs (Paranapanema River, south-east Brazil). *Lakes Reserv. Manage.* 10, 1–12. doi: 10.1111/j.1440-1770.2005.00254.x

Kang, H., Jung, S. H., and Park, D. (2017). Development of an ecological impact assessment model for dam construction. *Landscape Ecol. Eng.* 13, 15–31. doi: 10.1007/s11355-015-0287-x

Karnaukhova, G. A. (2007). Lithological-geochemical differentiation of bottom deposits in the Angara cascade reservoirs. *Geochem. Int.* 45, 390–398. doi: 10.1134/S0016702907040064

Lampert, W., Fleckner, W., Rai, H., and Taylor, B. E. (1986). Phytoplankton control by grazing zooplankton: a study on the spring clear-water phase1. *Limnol. Oceanogr.* 31, 478–490. doi: 10.4319/lo.1986.31.3.0478

Li, J., Dong, S., Liu, S., Yang, Z., Peng, M., and Zhao, C. (2013). Effects of cascading hydropower dams on the composition, biomass and biological integrity of phytoplankton assemblages in the middle Lancang-Mekong River. *Ecol. Eng.* 60, 316–324. doi: 10.1016/j.ecoleng.2013.07.029

Lu, M., and Xie, P. (2001). Impacts of filter-feeding fishes on the long-term changes of crustacean zooplankton in a eutrophic subtropical chinese lake. *J. Freshw. Ecol.* 16, 219–228. doi: 10.1080/02705060.2001.9663806

Magilligan, F. J., and Nislow, K. H. (2005). Changes in hydrologic regime by dams. *Geomorphology* 71, 61–78. doi: 10.1016/j.geomorph.2004.08.017

Matsuno, Y., Tasumi, M., Van Der Hoek, W., Sakthivadivel, R., and Otsuki, K. (2003). Analysis of return flows in a tank cascade system in Sri Lanka. *Paddy Water Environ.* 1, 173–181. doi: 10.1007/s10333-003-0029-9

Matveev, V. (2003). Testing predictions of the lake food web theory on pelagic communities of Australian reservoirs. *Oikos* 100, 149–161. doi: 10.1034/j.1600-0706.2003.11651.x

Miao, S., Jian, S., Liu, Y., Li, C., Guan, H., Li, K., et al. (2020). Long-term and longitudinal nutrient stoichiometry changes in oligotrophic cascade reservoirs with trout cage aquaculture. *Sci. Rep.* 10:13483. doi: 10.1038/s41598-020-68866-7

Moreno, P., and Callisto, M. (2006). Benthic macroinvertebrates in the watershed of an urban reservoir in Southeastern Brazil. *Hydrobiologia* 560, 311–321. doi: 10.1007/s10750-005-0869-y

Obertegger, U., Flaim, G., Braioni, M. G., Sommaruga, R., Corradini, F., and Borsato, A. (2007). Water residence time as a driving force of zooplankton structure and succession. *Aquat. Sci.* 69, 575–583. doi: 10.1007/s00027-007-0924-z

Okuku, E. O., Tole, M., Kiteresi, L. I., and Bouillon, S. (2016). The response of phytoplankton and zooplankton to river damming in three cascading reservoirs of the Tana River, Kenya. *Lakes Reserv.* 21, 114–132. doi: 10.1111/lre.12127

Özkan, K., Jeppesen, E., Davidson, T. A., Bjerring, R., Johansson, L. S., Søndergaard, M., et al. (2016). Long-term trends and temporal synchrony in plankton richness, diversity and biomass driven by re-oligotrophication and climate across 17 Danish lakes. *Water* 8:427. doi: 10.3390/w8100427

Padisák, J., Barbosa, F.a.R., Borbély, G., Borics, G., Chorus, I., Espindola, E. L. G., et al. (2000). Phytoplankton composition, biodiversity and a pilot survey of toxic cyanoprokaryotes in a large cascading reservoir system (Tietê basin, Brazil). *SIL Proc.* 27, 2734–2742. doi: 10.1080/03680770.1998.11898164

Paerl, H. W., Rossignol, K. L., Hall, S. N., Peierls, B. L., and Wetz, M. S. (2010). Phytoplankton community indicators of short- and long-term ecological change in the anthropogenically and climatically impacted neuse river estuary, North Carolina, USA. *Estuaries Coasts* 33, 485–497. doi: 10.1007/s12237-009-9137-0

Perbiche-Neves, G., and Nogueira, M. G. (2010). Multi-dimensional effects on Cladoceran (Crustacea, Anomopoda) assemblages in two cascade reservoirs in Southeast Brazil. *Lakes Reserv.* 15, 139–152. doi: 10.1111/j.1440-1770.2010.00429.x

Pinto-Coelho, R., Pinel-Alloul, B., Méthot, G., and Havens, K. E. (2005). Crustacean zooplankton in lakes and reservoirs of temperate and tropical regions: variation with trophic status. *Can. J. Fish. Aquat. Sci.* 62, 348–361. doi: 10.1139/f04-178

Qiu, J., Li, T. J., and Li, F. F. (2019). Evaluation of environmental and ecological impacts of the leading large-scale reservoir on the upper reaches of the Yellow River. *Sustainability* 11:3818. doi: 10.3390/su11143818

Qu, Y., Wu, N., Guse, B., and Fohrer, N. (2018). Riverine phytoplankton shifting along a lentic-lotic continuum under hydrological, physiochemical conditions and species dispersal. *Sci. Total Environ.* 619–620, 1628–1636. doi: 10.1016/j.scitotenv.2017.10.139

Rangel, L. M., Silva, L. H. S., Rosa, P., Roland, F., and Huszar, V. L. M. (2012). Phytoplankton biomass is mainly controlled by hydrology and phosphorus concentrations in tropical hydroelectric reservoirs. *Hydrobiologia* 693, 13–28. doi: 10.1007/s10750-012-1083-3

Rao, K., Zhang, X., Yi, X. J., Li, Z. S., Wang, P., Huang, G. W., et al. (2018). Interactive effects of environmental factors on phytoplankton communities and benthic nutrient interactions in a shallow lake and adjoining rivers in China. *Sci. Total Environ.* 619–620, 1661–1672. doi: 10.1016/j.scitotenv.2017.10.135

Reckendorfer, W., Keckeis, H., Winkler, G., and Schiemer, F. (1999). Abundance in the River Danube, Austria: the significance of inshore retention. *Freshw. Biol.* 41, 583–591.

Reynolds, C. S., Huszar, V., Kruk, C., Naselli-Flores, L., and Melo, S. (2002). Towards a functional classification of the freshwater phytoplankton. *J. Plankton Res.* 24, 417–428. doi: 10.1093/plankt/24.5.417

Richardson, A. J., and Schoeman, D. S. (2004). Climate impact on Plankton ecosystems in the Northeast Atlantic. *Science* 305, 1609–1612. doi: 10.1126/science.1100958

Ricotta, C., and Avena, G. (2003).). On the relationship between Pielou's evenness and landscape dominance within the context of Hill's diversity profiles. *Ecol. Indic.* 2, 361–365. doi: 10.1016/S1470-160X(03)00005-0

Schabhüttl, S., Hingsamer, P., Weigelhofer, G., Hein, T., Weigert, A., and Striebel, M. (2013). Temperature and species richness effects in phytoplankton communities. *Oecologia* 171, 527–536. doi: 10.1007/s00442-012-2419-4

Sellami, I., Guermazi, W., Hamza, A., Aleya, L., and Ayadi, H. (2010). Seasonal dynamics of zooplankton community in four mediterranean reservoirs in humid area (Beni Mtir: north of Tunisia) and semi arid area (Lakhmes, Nabhana and Sidi Saâd: center of Tunisia). *J. Therm. Biol.* 35, 392–400. doi: 10.1016/j.jtherbio.2010.08.004

Silva, A. P. C., and Costa, I. A. S. D. (2015). Biomonitoring ecological status of two reservoirs of the Brazilian semi-arid using phytoplankton assemblages (Q index). *Acta Limnologica Brasiliensia* 27, 1–14. doi: 10.1590/S2179-975X2014

Silva, C. A. D., Train, S., and Rodrigues, L. C. (2005). Phytoplankton assemblages in a Brazilian subtropical cascading reservoir system. *Hydrobiologia* 537, 99–109. doi: 10.1007/s10750-004-2552-0

Silva, L. H. S., Huszar, V. L. M., Marinho, M. M., Rangel, L. M., Brasil, J., Domingues, C. D., et al. (2014). Drivers of phytoplankton, bacterioplankton, and zooplankton carbon biomass in tropical hydroelectric reservoirs. *Limnologica* 48, 1–10. doi: 10.1016/j.limno.2014.04.004

Stirling, G., and Wilsey, B. (2001). Empirical relationships between species richness, evenness, and proportional diversity. *Am. Nat.* 158, 286–299. doi: 10.1086/321317

Sun, J., and Liu, D. (2003). Geometric models for calculating cell biovolume and surface area for phytoplankton. *J. Plankton Res.* 25, 1331–1346. doi: 10.1093/plankt/fbg096

Tang, W., and He, D. (2013). Fish resource survey on Cihaxia to Jishixia stretches in the upper reaches of Yellow River (2005-2010). *J. Lake Sci.* 25, 600–608. doi: 10.18307/2013.0419

Tavares, D. A., Lambrecht, R. W., De Almeida Castilho, M. C., Henry, R., and Ferragut, C. (2019). Epipelon responses to N and P enrichment and the relationships with phytoplankton and zooplankton in a mesotrophic reservoir. *Aquat. Ecol.* 53, 303–314. doi: 10.1007/s10452-019-09690-8

Thorp, J. H., Black, A. R., Haag, K. H., and Wehr, J. D. (1994). Zooplankton assemblages in the Ohio river: seasonal, tributary, and navigation dam effects. *Can. J. Fish. Aquat. Sci.* 51, 1634–1643. doi: 10.1139/f94-164

Van Cappellen, P., and Maavara, T. (2016). Rivers in the anthropocene: global scale modifications of riverine nutrient fluxes by damming. *Ecohydrol. Hydrobiol.* 16, 106–111. doi: 10.1016/j.ecohyd.2016.04.001

Vanni, M. J. (1987). Effects of nutrients and zooplankton size on the structure of a phytoplankton community. *Ecology* 68, 624–635.

Wang, B., Qiu, X. L., Peng, X., and Wang, F. (2018). Phytoplankton community structure and succession in karst cascade reservoirs, SW China. *Inland Waters* 8, 229–238. doi: 10.1080/20442041.2018.1443550

Wang, H., Liu, X., and Wang, M. (2016). Investigation on aquatic organisms in yangqu section of the upper Yellow River in Qinghai province. *Hebei Fish.* 9, 17–21. doi: 10.3969/j.issn.1004-6755.2016.09.005

Wang, S., Dong, R. M., Dong, C. Z., Huang, L., Jiang, H., Wei, Y., et al. (2012). Diversity of microbial plankton across the three Gorges Dam of the Yangtze River, China. *Geosci. Front.* 3, 335–349. doi: 10.1016/j.gsf.2011.11.013

Wang, S., Xie, P., Wu, S., and Wu, A. (2007). Crustacean zooplankton distribution patterns and their biomass as related to trophic indicators of 29 shallow subtropical lakes. *Limnologica* 37, 242–249. doi: 10.1016/j.limno.2007.02.002

Wang, Y., Rhoads, B. L., and Wang, D. (2016). Assessment of the flow regime alterations in the middle reach of the Yangtze River associated with dam construction: potential ecological implications. *Hydrolog. Process.* 30, 3949–3966. doi: 10.1002/hyp.10921

Yin, D., Xu, J., Jin, Y., and Xu, Z. (2017). Characteristics of phytoplankton assemblage and distribution in the source regions of the Yangtze River and Lancang River. *J. Yangtze River Sci. Res. Inst.* 34, 61–66. doi: 10.11988/ckyyb.20150878

Yoshida, T., Kagami, M., Bahadur Gurung, T., and Urabe, J. (2001). Seasonal succession of zooplankton in the north basin of Lake Biwa. *Aquat. Ecol.* 35, 19–29. doi: 10.1023/A:1011498202050

Yuan, L. L., and Pollard, A. I. (2018). Changes in the relationship between zooplankton and phytoplankton biomasses across a eutrophication gradient. *Limnol. Oceanogr.* 63, 2493–2507. doi: 10.1002/lno.10955

Zhang, M., Shao, M., Xu, Y., and Cai, Q. (2010). Effect of hydrological regime on the macroinvertebrate community in three-gorges reservoir, China. *Quaternary International* 226, 129–135. doi: 10.1016/j.quaint.2009.12.019

Conflict of Interest: The authors declare that the research was conducted in the absence of any commercial or financial relationships that could be construed as a potential conflict of interest.

frontiers in Microbiology

ORIGINAL RESEARCH
published: 04 November 2021
doi: 10.3389/fmicb.2021.749783

An Ultrafast One-Step Quantitative Reverse Transcription–Polymerase Chain Reaction Assay for Detection of SARS-CoV-2

Jadranka Milosevic[1,2], Mengrou Lu[2], Wallace Greene[3], Hong-Zhang He[1,2] and Si-Yang Zheng[2,4]**

[1] Captis Diagnostics Inc., Pittsburgh, PA, United States, [2] Biomedical Engineering Department, Carnegie Mellon University, Pittsburgh, PA, United States, [3] Penn State Hershey Medical Center, Penn State College of Medicine, Hershey, PA, United States, [4] Electrical & Computer Engineering, Carnegie Mellon University, Pittsburgh, PA, United States

OPEN ACCESS

Edited by:
Wei Zhi, The Pennsylvania State University (PSU), United States

Reviewed by:
Jltendra Kumar, National Institute of Immunology (NII), India
Xu Yu, Huazhong University of Science and Technology, China
Yuan Wan, Binghamton University, United States
Ka Ho Leung, Clarkson University, United States

***Correspondence:**
Hong-Zhang He
simonhe@captisdx.com
Si-Yang Zheng
siyangz@andrew.cmu.edu

Specialty section:
This article was submitted to Microbiotechnology, a section of the journal Frontiers in Microbiology

Received: *29 July 2021*
Accepted: *30 September 2021*
Published: *04 November 2021*

Citation:
Milosevic J, Lu M, Greene W, He H-Z and Zheng S-Y (2021) An Ultrafast One-Step Quantitative Reverse Transcription–Polymerase Chain Reaction Assay for Detection of SARS-CoV-2. Front. Microbiol. 12:749783. doi: 10.3389/fmicb.2021.749783

We developed an ultrafast one-step RT-qPCR assay for SARS-CoV-2 detection, which can be completed in only 30 min on benchtop *Bio-Rad* CFX96. The assay significantly reduces the running time of conventional RT-qPCR: reduced RT step from 10 to 1 min, and reduced the PCR cycle of denaturation from 10 to 1 s and extension from 30 to 1 s. A cohort of 60 nasopharyngeal swab samples testing showed that the assay had a clinical sensitivity of 100% and a clinical specificity of 100%.

Keywords: ultrafast, one-step RT-qPCR assay, SARS-CoV-2 detection, COVID-19, nasopharyngeal swab

INTRODUCTION

The current highly transmissible outbreak of severe acute respiratory syndrome coronavirus (SARS-CoV-2) is the leading cause of morbidity and mortality across the globe (Andrasfay and Goldman, 2021; Cohen, 2021; Woolf et al., 2021). Researchers have intensively invested in developing innovation for cost-effective point-of-care test kits and efficient laboratory techniques for confirmation of SARS-CoV-2 infection (Carter et al., 2020; Chen et al., 2020; Shuren and Stenzel, 2020; Venter and Richter, 2020; Wiersinga et al., 2020; El Jaddaoui et al., 2021; Mardian et al., 2021; Taleghani and Taghipour, 2021; Vandenberg et al., 2021; Yüce et al., 2021). Among those technologies, real-time quantitative reverse transcription–polymerase chain reaction (qRT-PCR) of nasopharyngeal swabs is the current gold standard in the clinical setting to confirm the clinical diagnosis of coronavirus disease 2019 (COVID-19) caused by severe acute respiratory syndrome coronavirus 2 (SARS-CoV-2) (Carter et al., 2020; Ji et al., 2020; Tang et al., 2020; Kevadiya et al., 2021). Conventional qRT-PCR for SARS-CoV-2 detection usually takes approximately 2 h on benchtop qPCR instrument, with 10 min of reverse transcription, followed with initial denaturation for 1 min, and 45 PCR cycles of 10 s denaturation and 30 s extension (**Figure 1**; Vogels et al., 2020). However, the ongoing COVID-19 pandemic poses substantial challenges for health-care systems and their infrastructure. Therefore, to meet the pandemic challenges, it is important to significantly shorten the turnaround time in the race for increasing the number of diagnostic tests.

MATERIALS AND METHODS

Clinical Samples

A cohort of 60 clinical nasopharyngeal swab samples including 30 SARS-COV-2 negative and 30 SARS-CoV-2 positive sample were pre-collected and deidentified, which meets the requirement

of the Institutional Review Board (IRB) Exemption 4. Those clinical nasopharyngeal swab samples were stored in virial transport media at −80°C until future use. The nasopharyngeal swab samples have been tested by a Clinical Laboratory Improvement Amendments (CLIA)-certified diagnostic laboratory with an FDA approved diagnostic kit at Penn State Health Milton S. Hershey Medical Center.

Ultrafast One-Step Quantitative Reverse Transcription–Polymerase Chain Reaction for Severe Acute Respiratory Syndrome Coronavirus Detection

The ultrafast one-step qRT-PCR was developed using primers and probes set targeting the N1 and N2 regions in the nucleocapsid (N) gene of SARS-CoV-2 and the human RNase P gene as previously published by "United States Center for Disease Control and Prevention" (CDC) (**Table 1**; Centers for Disease Control and Prevention [CDC], 2020). The primers and probes for N1, nucleocapsid N2, and RNase P (RP) were purchased from Integrated DNA Technologies (IDT) and diluted as recommended. Synthetic SARS-CoV-2 RNA (ATCC, VT-3276T) was used as SARS-Cov-2 RNA standards in all condition optimization of ultrafast one-step qRT-PCR assay for detection of SARS-Cov-2. The ultrafast one-step qRT-PCR was performed as follows: the one-step qRT-PCR master mix (100 μL) was prepared according to the components in **Table 2**. Then, in each sample, 2 μL of SARS-CoV-2 RNA standard or extracted RNA samples were added to 8 μL of ultrafast one-step qRT-PCR master mix. Then, 10 μL of reaction solution with RNA sample and qRT-PCR master mix was loaded into 96 hard-shell PCR plates (Bio-Rad Laboratories), and the PCR plate was loaded in CFX96 Real-Time PCR detection system (Bio-Rad Laboratories). Thermal cycling conditions included 1 min reverse transcription at 50°C, 1 min at 95°C for reverse transcription deactivation and initial activation of SpeedStar HS DNA polymerase, followed by 40 cycles of 1 s denaturing at 95°C and 1 s extension at 55°C. All samples with cycle threshold (Ct) value of both N1, N2, and RP $\leq$ 38 were considered as positive according to CDC guidelines.

TABLE 1 | Primers and probes for N1, N2, and RNase P (RP) (Centers for Disease Control and Prevention [CDC], 2020).

Name	Oligonucleotide sequence (5′–3′)
2019-nCoV_N1-Forward primer	GAC CCC AAA ATC AGC GAA AT
2019-nCoV_N1-Revere primer	TCT GGT TAC TGC CAG TTG AAT CTG
2019-nCoV_N1-Probe	FAM-ACC CCG CAT TAC GTT TGG TGG ACC-BHQ1
2019-nCoV_N2- Forward primer	TTA CAA ACA TTG GCC GCA AA
2019-nCoV_N2- Revere primer	GCG CGA CAT TCC GAA GAA
2019-nCoV_N2-Probe	FAM-ACA ATT TGC CCC CAG CGC TTC AG-BHQ1
RP- Forward primer	AGA TTT GGA CCT GCG AGC G
RP- Revere primer	GAG CGG CTG TCT CCA CAA GT
RP- Probe	FAM—TTC TGA CCT GAA GGC TCT GCG CG—BHQ-1

FDA Approved Diagnostic Kit "Xpert® Xpress SARS-CoV-2"

The Xpert Xpress SARS-CoV-2 test is an automated *in vitro* diagnostic test for qualitative detection of nucleic acid from SARS-CoV-2. The Xpert Xpress SARS-CoV-2 test was performed on GeneXpert Instrument Systems according to the protocol from the manufacturer (Loeffelholz Michael et al., 2020; Food Drug Administration [FDA], 2021).

RNA Extraction From Nasopharyngeal Swab Samples

Total RNA was isolated from the heat inactivated nasopharyngeal swab samples using Direct-zol™ RNA Microprep (R2060, Zymo Research) by following the manufacturer's instruction. In brief, 300 μL of nasopharyngeal swab samples were lysed in 400 μL of Trizol. Then 700 μL of 100% ethanol was added, followed by column purification using Zymo-Spin™ Column. Direct-zol™ RNA PreWash and RNA Wash Buffer were added sequentially to wash the column. Finally, RNA was eluted in 12 μL of nuclease free water and stored in −80°C until future use.

Statistical Analysis

Continuous and categorical variables are expressed as means (SD) and number (%), respectively, analyzed with Prism 8.0.1 (GraphPad Software, La Jolla, CA). Clinical agreements were analyzed according to Clinical and Laboratory Standards Institute (CLSI) EP12-A2 as recommended in FDA Guidelines, performed with MedCalc® Statistical Software version 19.7.4 (MedCalc Software Ltd., Ostend, Belgium).

RESULTS AND DISCUSSION

Here, we described an ultrafast one-step qRT-PCR assay for the qualitative detection of SARS-CoV-2 that is fully compatible with conventional benchtop qPCR instruments. SARS-CoV-2 RNA was reverse transcribed for 1 min into cDNA and amplified with 40 PCR cycles of 1 s denaturing and 1 s extension step (**Figure 1**). This one-step qRT-qPCR assay can detect down to 25 copies of SARS-CoV-2 RNA in 10 μL reaction volume. The assay employs primers and probes developed by the United States Centers for Disease Control and Prevention (CDC) targeting N1 and N2 regions of nucleocapsid gene of SARS-CoV-2 with the internal control human RNase P gene (RP). The total ultrafast one-step qRT-PCR can be completed in 30 min on benchtop *Bio-Rad* CFX96 platform.

In developing the ultrafast one-step qRT-PCR assay, we reasoned that the enzymes in the qRT-PCR are key to significantly shortening the qRT-PCR and to keeping comparable sensitivity as conventional qRT-PCR for SARS-CoV-2 detection. We found that SpeedSTAR HS DNA Polymerase is optimized for PCR with extension time as fast as 10 s/kb. The amplicons of N1, N2, and RP are within the length of 100 bp. Therefore, we

TABLE 2 | Components of the ultrafast one-step qRT-PCR master mix.

Reverse transcription master mix			
Stock solution	**Supplier**	**Volume/μL for 10 reactions**	**Final concentration**
10 mM dNTPs	Thermo Fisher Scientific (R0191)	1.2	0.012 mM
5X SuperScript IV Reverse Transcriptase buffer	Thermo Fisher Scientific (18090010)	6	0.03X
100 mM DTT	Thermo Fisher Scientific (18090010)	1	0.11 mM
RNaseOUT inhibitor (40 U/μL)	Thermo Fisher Scientific (10777019)	1	4 U
SuperScript IV Reverse Transcriptase (200 U/μL)	Thermo Fisher Scientific (18090010)	1	20 U
Stabilizer Reagent	Sigma (PNS1010)	1	0.1 μL
qPCR master mix			
SpeedStar HS DNA polymerase (5 U/μL)	TaKaRa (RR070B)	0.8	0.4 U
Fast Buffer I (10X)	TaKaRa (RR070B)	10	0.1 X
N1 forward primer/reverse primer/probe (10 μM)	IDT	4/4/2	40 nM/40 nM/20 nM
N2 forward primer/reverse primer/probe (10 μM)	IDT		
RP forward primer/reverse primer/probe (10 μM)	IDT		
Nuclease Free H_2O		Mix reverse transcription master mix with qPCR master mix, and then add up to 100 μL for qRT-PCR Master Mix	
qRT-PCR		Aliquot 8 μL of qRT-PCR Master Mix, and then add 2 μL of RNA template per reaction	

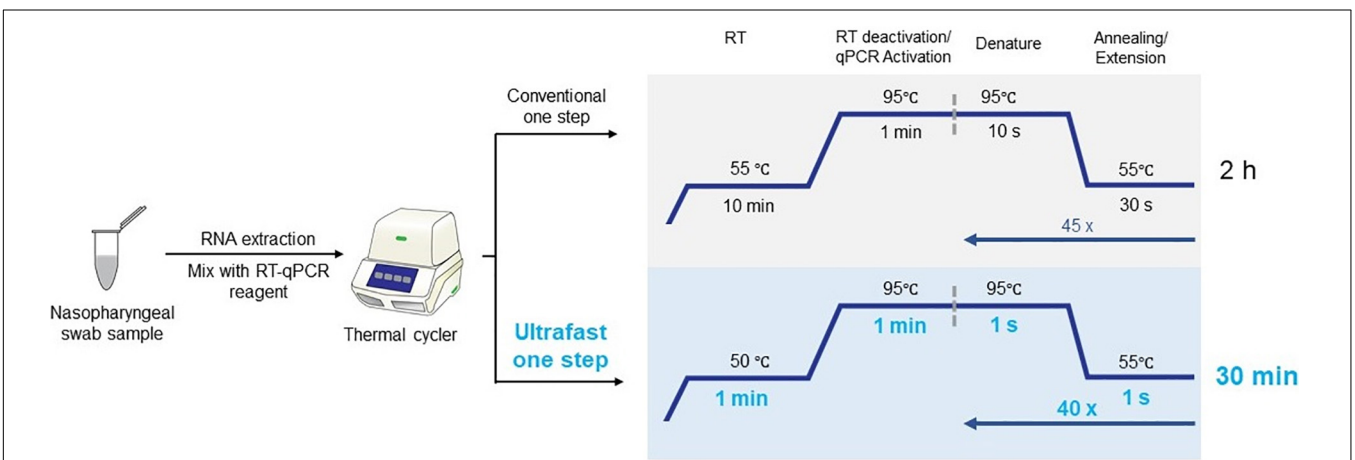

FIGURE 1 | Workflow of ultrafast one-step qRT-PCR with comparison with conventional qRT-PCR for SARS-CoV-2 detection.

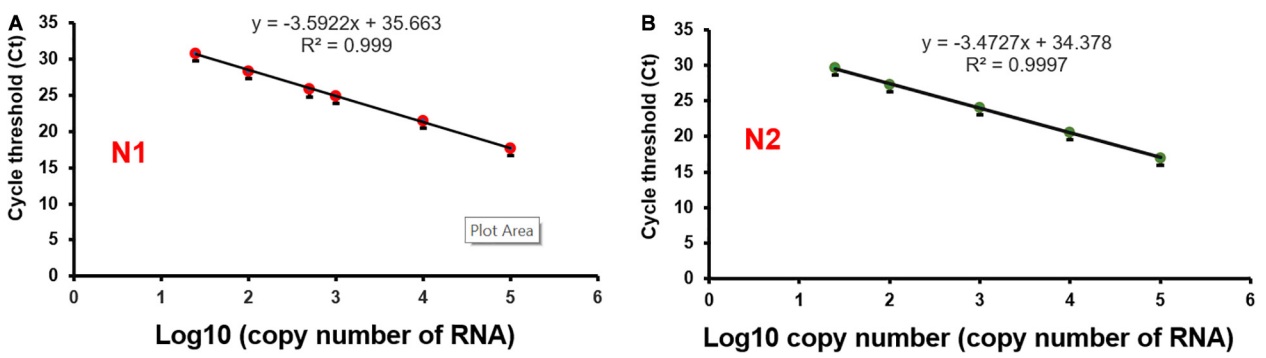

FIGURE 2 | Limit of detection of ultrafast one-step qRT-PCR assay. SARS-Cov-2 synthetic RNA genome was used as a model sample. RNA templates were series diluted in the range of 25–1 × 10^5 copies. Ultrafast one-step qRT-PCR assay detects both N1 **(A)** and N2 **(B)** regions of the nucleocapsid gene of SARS-CoV-2.

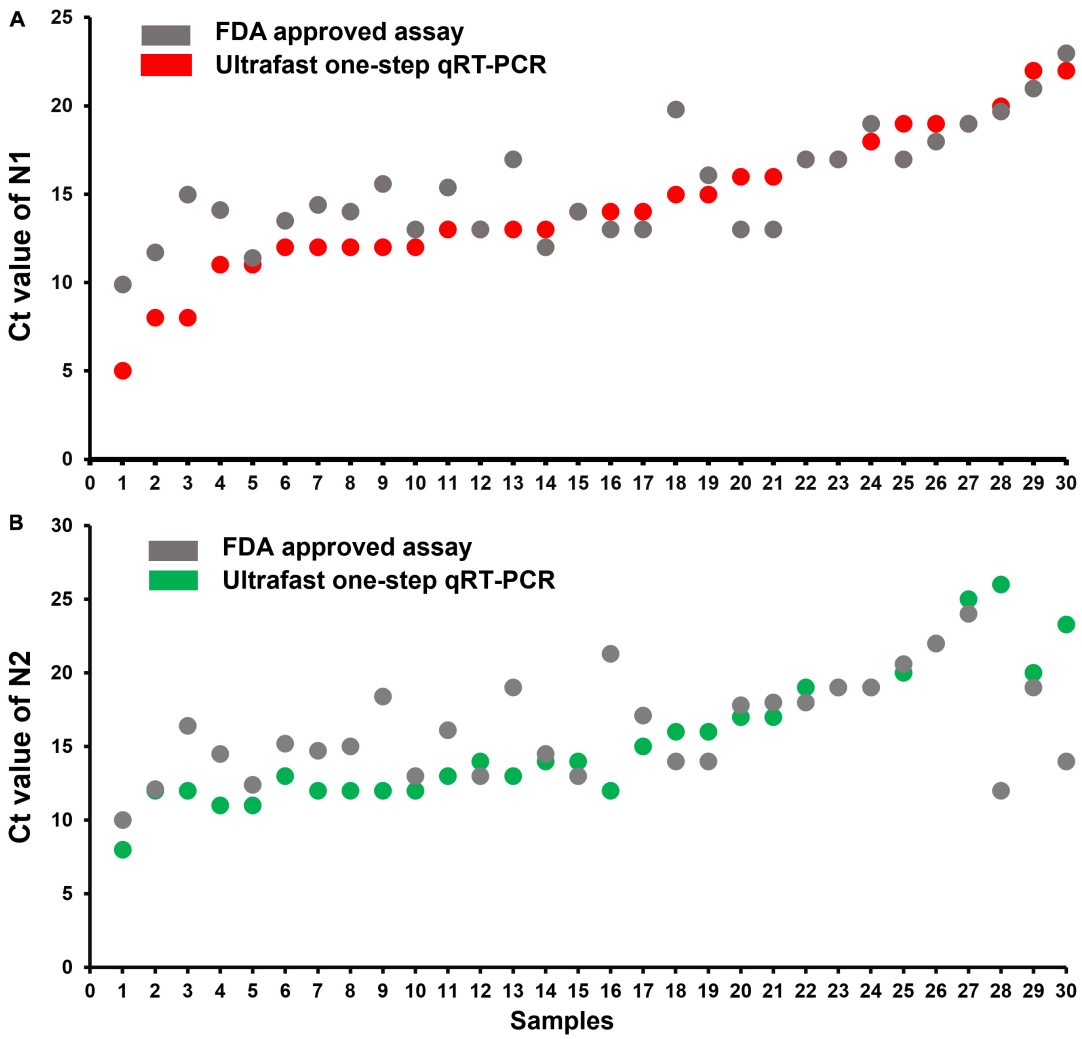

FIGURE 3 | Cycle threshold (Ct values) of N1 and N2 correlation of ultrafast one-step qRT-PCR with FDA-approved assay "Xpert® Xpress SARS-CoV-2" for SARS-CoV-2 positive samples. **(A)** Ct value of N1 and **(B)** Ct value of N2 from the 30 SARS-CoV-2 positive samples.

investigated whether the N1/N2 SARS-CoV-2 RNA could be detected with the fast PCR cycle setting of 2 s/cycle (it includes 1 s denaturing and 1 s extension step) on a conventional qPCR instrument by using SpeedSTAR HS DNA Polymerase (Giese et al., 2009). Using synthetic SARS-CoV-2 RNA from ATCC as the model, we found that 0.4 U of SpeedSTAR HS DNA Polymerase (in 10 μL of qRT-PCR reaction mixture) in the one-step qRT-qPCR assay can detect down to 25 copies of N1 and N2 of SARS-CoV-2 RNA (**Figure 2**). Furthermore, in RT step, we chose SuperScript IV Reverse Transcriptase because of its fast speed in cDNA synthesis (Martín-Alonso et al., 2021). We demonstrated that ultrafast one-step qRT-PCR can still detect down to 25 copies of N1 and N2 of SARS-CoV-2 RNA genome (**Figure 2**) by reducing the RT step from 10 min to 1 min with 20 U of SuperScript IV Reverse Transcriptase (in 10 μL of qRT-PCR reaction mixture). The limit of detection of the developed ultrafast one-step qRT-PCR is comparable to the other CDC qRT-PCR tests (Arnaout et al., 2020). During the optimization of this ultrafast one-step qRT-PCR assay, we investigated various time length of RT step (5, 2, and 1 min) and priming step (5, 2, 1, and 0 min). The result showed that there is no significant change in Ct values of N1 gene when RT step was reduced to only 1 min (**Supplementary Figure 1**). Furthermore, Ct values of the N1 gene decreased after removing the RT priming step (**Supplementary Figure 2**). Therefore, we used 1 min of RT step with any RT priming for the ultrafast one-step qRT-PCR assay. We also have investigated the various amounts of superscript IV reverse transcriptase (SSIV) in this assay. The result showed that there was no significant difference in Ct values between the SSIV concentration of 20, 50, and 80 U/10 μL reaction mixture. However, SSIV at 30 U/10 μL reaction mixture exhibited the lowest Ct for the N1 gene (**Supplementary Figure 3**). To lower the cost of this assay, we choose the SSIV at concentration of 20 U/10 μL in the formulation of the assay. We also have investigated the compatibility of this ultrafast one-step qRT-PCR assay with QuantStudio 7 Flex real-time PCR systems

TABLE 3 | Cycle threshold (Ct) value of SARS CoV-2 positive samples of ultrafast one-step qRT-PCR in comparison to an FDA approved test "Xpert® Xpress SARS-CoV-2".

	Ultrafast one-step qRT-PCR test		FDA approved test "Xpert® Xpress SARS-CoV-2"	
Positive samples	**Ct of N1**	**Ct of N2**	**Ct of N1**	**Ct of N2**
1	12.3	12.8	13.5	15.2
2	12.7	13.4	15.4	16.1
3	14.6	15.5	19.8	21.3
4	8	11.7	11.7	12.1
5	10.6	11.1	14.1	14.5
6	5.3	7.9	9.9	10
7	12.2	12.2	14.4	14.7
8	15.4	16.4	14	14.5
9	13.5	26	12	12
10	15.2	15	16.1	17.1
11	20.1	20.3	19.7	20.6
12	17.1	17	17	17.8
13	17.1	16.7	19	19
14	14.7	14.8	13	14
15	7.7	12.5	15	16.4
16	10.9	10.7	11.4	12.4
17	15.9	16.4	13	14
18	22.3	22.1	21	22
19	22.4	24.7	23	24
20	18.9	18.8	17	18
21	19.1	19.4	18	19
22	12.2	12	14	15
23	14.2	13.6	13	13
24	13.5	13.6	13	13
25	19	18.9	19	19
26	13	12.2	15.6	18.4
27	15.9	15.8	13	14
28	16.8	17	17	18
29	12.2	12.1	13	13
30	13.1	13	17	19

(Thermo Fisher Scientific, United States), which is also widely used in Clinical Laboratory Improvement Amendments (CLIA) certified laboratory. There were 10^4 RNA copies of synthetic SARS-CoV-2 used and tested with the same protocol as benchtop Bio-Rad CFX96 qPCR instrument. The result showed that all N1, N2, and RNase P (RP) genes have been detected with Ct of 20–22 (**Supplementary Figure 4**), which is consistent with the data from the Bio-Rad CFX96 qPCR instrument. However, the qRT-PCR assay running time was 38:47 min, which is a little bit longer than the Bio-Rad CFX96 qPCR instrument. We hypothesize that the time difference is due to the slower heating and cooling speed in the QuantStudio 7 instrument. We envision that boosting heating and cooling speed of the qPCR instrument will further shorten this ultrafast one-step qRT-PCR assay to even less than 10 min. The recipe of the ultrafast one-step qPCR-PCR master mix (**Table 2**) and running protocol of ultrafast one-step qPCR-PCR are detailed in the Methods section.

TABLE 4 | Cycle threshold (Ct) value of SARS CoV-2 negative samples of the ultrafast one-step qRT-PCR.

	Ultrafast one-step qRT-PCR test		
Negative samples	**Ct of N1**	**Ct of N2**	**Ct of RP**
1	NA	NA	27
2	NA	NA	24
3	NA	NA	27
4	NA	NA	23
5	NA	NA	26
6	NA	NA	25
7	NA	NA	26
8	NA	NA	26
9	NA	NA	23
10	NA	NA	28
11	NA	NA	25
12	NA	NA	18
13	NA	NA	23
14	NA	NA	29
15	NA	NA	27
16	NA	NA	28
17	NA	NA	23
18	NA	NA	29
19	NA	NA	27
20	NA	NA	29
21	NA	39	38
22	NA	37	29
23	NA	NA	28
24	NA	NA	33
25	NA	NA	28
26	NA	NA	27
27	NA	NA	29
28	NA	38	26
29	NA	NA	26
30	NA	NA	28

TABLE 5 | Positive and negative predictive values of ultrafast one-step qRT-PCR for SARS-CoV-2 detection in nasopharyngeal samples.

		Comparator Assay (FDA approved assay "Xpert® Xpress SARS-CoV-2")	
		Positive	**Negative**
Ultrafast One Step qRT-PCR	Positive	30	0
	Negative	0	30
	Total	30	30
Percent Positive Agreement (PPA)		30/30 = 100% (95% CI: 88.7–100.0%)	
Percent Negative Agreement (PNA)		30/30 = 100% (95% CI: 88.7–100.0%)	
Percent Overall Agreement (POA)		60/60 = 100% (95% CI: 94.0–100.0%)	

To evaluate the performance of the ultrafast one-step qRT-PCR in a clinical setting, we performed a blinded and randomized study with 30 SARS-CoV-2–positive and 30 SARS-CoV-2–negative nasopharyngeal swab samples obtained from patients.

Ultrafast one-step qRT-PCR testing showed that SARS-CoV-2 positive samples exhibited N1, N2, and RNase P gene, and the cycle threshold (Ct) values of N1, N2, and RP are very close to those obtained with FDA approved diagnostics kit "Xpert® Xpress SARS-CoV-2" (**Figure 3** and **Table 3**). In SARS-CoV-2 negative samples, N1 was not detected in all negative samples, Ct values of N2 in three negative samples were above 35, which still qualifies as SARS-CoV-2 negative samples according to the CDC guidelines (**Table 4**). Overall, the testing results showed that the ultrafast one-step qRT-PCR had a clinical sensitivity of 100% and a clinical specificity of 100% (**Table 5**). Furthermore, we found that the SARS-Cov-2 viral loads in clinical samples are 3, 2×10^3 – 3.0×10^4 and over 6.8×10^4 (**Supplementary Table 1**) with the standard curves for N1 (**Figure 2A**). The simplified format of ultrafast one-step qRT-PCR for detection of SARS-CoV-2 in nasopharyngeal swabs is suitable for use in clinical diagnostic laboratories. The limitation of this study includes that we have not explored other sample types. We will further validate ultrafast one-step qRT-PCR for SARS-CoV-2 detection in saliva samples without RNA extraction.

CONCLUSION

In summary, we have developed an ultrafast one-step qRT-PCR assay for COVID-19 diagnosis, which had a significantly reduced running time of RT and PCR step compared to conventional qRT-PCR. We further demonstrated that the ultrafast one-step qRT-PCR exhibits a limit of detection for SARS-CoV-2 that is comparable to other CDC qRT-PCR assays. Importantly, this ultrafast one-step qRT-PCR has been validated to have a clinical sensitivity of 100% and a clinical specificity of 100% with a cohort of 60 SARS-CoV-2 nasopharyngeal swab samples. We hypothesize that the success of this assay is due to the characteristics of the SpeedSTAR HS DNA Polymerase, which synthesizes new DNA strands with a speed of 10 s/kb. We envision that the high speed and high fidelity of DNA polymerase will result in fast and accurate pathogen diagnosis assay.

Furthermore, this ultrafast protocol is faster than most of the current SARS-CoV-2 detection. However, due to the limit of heating and cooling speed of the current benchtop qPCR instrument, the ultrafast one-step qRT-PCR assay protocol still takes around 30 min. We envision that boosting the heating and cooling speed of qPCR instrument will further shorten this ultrafast one-step qRT-PCR assay to less than 10 min, which will be much faster than the *Accula*^{TM} *System for SARS-CoV-2 test*. Additionally, the throughput of the Accula^{TM} System for SARS-CoV-2 test is limited to 2 samples per run, which is significantly less than 96 and/or 384 samples per run in this ultrafast one-step qRT-PCR assay. Compared with RT-LAMP, this ultrafast one-step qRT-PCR assay achieved 100% clinical sensitivity and specificity, which is much better than that of RT-LAMP with reported specificity (98%) and sensitivity (87%) (Baba et al., 2021). As such, we believe this work would be of interest to the general healthcare audience, especially those in the field of virus detection.

DATA AVAILABILITY STATEMENT

The original contributions presented in the study are included in the article/**Supplementary Material**, further inquiries can be directed to the corresponding author/s.

AUTHOR CONTRIBUTIONS

JM, H-ZH, and S-YZ designed the research. JM and WG performed research. JM and ML analyzed the data. JM, H-ZH, and S-YZ wrote the manuscript with input from all authors.

ACKNOWLEDGMENTS

We thank Dr. Florent Letronne from SARS-CoV-2 testing laboratory at Carnegie Mellon University for providing us access to QuantStudio 7 Flex real-time PCR systems, and Sheng Zhang from the Biomedical Engineering Department at Carnegie Mellon University for performing the validation of the ultrafast one-step qRT-PCR assay protocol. This work was financially supported National Institutes of Health (NIH/NIAID 7R01AI134911 and NIH/NIAID 1R43AI145614-01).

SUPPLEMENTARY MATERIAL

The Supplementary Material for this article can be found online at: https://www.frontiersin.org/articles/10.3389/fmicb.2021.749783/full#supplementary-material

REFERENCES

Andrasfay, T., and Goldman, N. (2021). Reductions in 2020 US life expectancy due to COVID-19 and the disproportionate impact on the Black and Latino populations. *Proc. Natl. Acad. Sci.* 118:e2014746118. doi: 10.1073/pnas.2014746118

Arnaout, R., Lee, R. A., Lee, G. R., Callahan, C., Yen, C. F., Smith, K. P., et al. (2020). SARS-CoV2 testing: the limit of detection matters. *bioRxiv* [Preprint]. doi: 10.1101/2020.06.02.131144

Baba, M. M., Bitew, M., Fokam, J., Lelo, E. A., Ahidjo, A., Asmamaw, K., et al. (2021). Diagnostic performance of a colorimetric RT -LAMP for the identification of SARS-CoV-2: a multicenter prospective clinical evaluation in sub-Saharan Africa. *EClinicalMedicine* 40:101101. doi: 10.1016/j.eclinm.2021.101101

Carter, L. J., Garner, L. V., Smoot, J. W., Li, Y., Zhou, Q., Saveson, C. J., et al. (2020). Assay Techniques and Test Development for COVID-19 Diagnosis. *ACS Central Sci.* 6, 591–605. doi: 10.1021/acscentsci.0c00501

Centers for Disease Control and Prevention [CDC] (2020). *Research Use Only 2019-Novel Coronavirus (2019-nCoV) Real-time RT-PCR Primers and Probes*. Available online at: https://www.cdc.gov/coronavirus/2019-ncov/lab/rt-pcr-panel-primer-probes.html (accessed June 6, 2020).

Chen, Q., He, Z., Mao, F., Peri, H., Cao, H., and Liu, X. (2020). Diagnostic technologies for COVID-19: a review. *RSC Adv.* 10, 35257–35264. doi: 10.1039/D0RA06445A

Cohen, J. (2021). Is India's coronavirus death 'paradox' vanishing? *Science* 372, 552–553. doi: 10.1126/science.372.6542.552

El Jaddaoui, I., Allali, M., Raoui, S., Sehli, S., Habib, N., Chaouni, B., et al. (2021). A review on current diagnostic techniques for COVID-19. *Expert Rev. Mol. Diagn.* 21, 141–160. doi: 10.1080/14737159.2021.1886927

Food Drug Administration [FDA] (2021). *Xpert® Xpress SARS-CoV-2*. Available online at: https://www.fda.gov/media/136314/download (accessed June 6, 2020).

Giese, H., Lam, R., Selden, R., and Tan, E. (2009). Fast Multiplexed Polymerase Chain Reaction for Conventional and Microfluidic Short Tandem Repeat Analysis. *J. Forens. Sci.* 54, 1287–1296. doi: 10.1111/j.1556-4029.2009.01200.x

Ji, T., Liu, Z., Wang, G., Guo, X., Akbar Khan, S., Lai, C., et al. (2020). Detection of COVID-19: a review of the current literature and future perspectives. *Biosens. Bioelectron.* 166:112455. doi: 10.1016/j.bios.2020.112455

Kevadiya, B. D., Machhi, J., Herskovitz, J., Oleynikov, M. D., Blomberg, W. R., Bajwa, N., et al. (2021). Diagnostics for SARS-CoV-2 infections. *Nat. Mater.* 20, 593–605. doi: 10.1038/s41563-020-00906-z

Loeffelholz Michael, J., Alland, D., Butler-Wu, S. M., Pandey, U., Perno, C. F., Nava, A., et al. (2020). Multicenter evaluation of the Cepheid Xpert Xpress SARS-CoV-2 test. *J. Clin. Microbiol.* 58, e00926–20. doi: 10.1128/JCM.00926-20

Mardian, Y., Kosasih, H., Karyana, M., Neal, A., and Lau, C.-Y. (2021). Review of current COVID-19 diagnostics and opportunities for further development. *Front. Med.* 8:615099. doi: 10.3389/fmed.2021.615099

Martín-Alonso, S., Frutos-Beltrán, E., and Menéndez-Arias, L. (2021). Reverse transcriptase: from transcriptomics to genome editing. *Trends Biotechnol.* 39, 194–210. doi: 10.1016/j.tibtech.2020.06.008

Shuren, J., and Stenzel, T. (2020). Covid-19 molecular diagnostic testing — lessons learned. *New Engl. J. Med.* 383:e97. doi: 10.1056/NEJMp2023830

Taleghani, N., and Taghipour, F. (2021). Diagnosis of COVID-19 for controlling the pandemic: a review of the state-of-the-art. *Biosens. Bioelectron.* 174:112830. doi: 10.1016/j.bios.2020.112830

Tang, Y.-W., Schmitz, J. E., Persing, D. H., and Stratton, C. W. (2020). Laboratory diagnosis of COVID-19: current issues and challenges. *J. Clin. Microbiol.* 58, e00512–20. doi: 10.1128/JCM.00512-20

Vandenberg, O., Martiny, D., Rochas, O., van Belkum, A., and Kozlakidis, Z. (2021). Considerations for diagnostic COVID-19 tests. *Nat. Rev. Microbiol.* 19, 171–183. doi: 10.1038/s41579-020-00461-z

Venter, M., and Richter, K. (2020). Towards effective diagnostic assays for COVID-19: a review. *J. Clin. Pathol.* 73, 370–377. doi: 10.1136/jclinpath-2020-206685

Vogels, C. B. F., Brito, A. F., Wyllie, A. L., Fauver, J. R., Ott, I. M., Kalinich, C., et al. (2020). Analytical sensitivity and efficiency comparisons of SARS-CoV-2 RT–qPCR primer–probe sets. *Nat. Microbiol.* 5, 1299–1305. doi: 10.1038/s41564-020-0761-6

Wiersinga, W. J., Rhodes, A., Cheng, A. C., Peacock, S. J., and Prescott, H. C. (2020). Pathophysiology, transmission, diagnosis, and treatment of coronavirus disease 2019 (COVID-19): a review. *JAMA* 324, 782–793. doi: 10.1001/jama.2020.12839

Woolf, S. H., Chapman, D. A., and Lee, J. H. (2021). COVID-19 as the leading cause of death in the United States. *JAMA* 325, 123–124. doi: 10.1001/jama.2020.24865

Yüce, M., Filiztekin, E., and Özkaya, K. G. (2021). COVID-19 diagnosis -a review of current methods. *Biosens. Bioelectron.* 172:112752. doi: 10.1016/j.bios.2020.112752

Conflict of Interest: There is patent pending on the ultrafast one-step qRT-PCR assay for pathogen detection (US63/178797) method used in this work. S-YZ declares a competing interest in the form of consulting for and equity ownership in Captis Diagnostics. JM and H-ZH are employed by Captis Diagnostics Inc.

The remaining authors declare that the research was conducted in the absence of any commercial or financial relationships that could be construed as a potential conflict of interest.

Publisher's Note: All claims expressed in this article are solely those of the authors and do not necessarily represent those of their affiliated organizations, or those of the publisher, the editors and the reviewers. Any product that may be evaluated in this article, or claim that may be made by its manufacturer, is not guaranteed or endorsed by the publisher.

frontiers in Microbiology

ORIGINAL RESEARCH
published: 30 November 2021
doi: 10.3389/fmicb.2021.771381

Biochemical and Physiological Responses of Harmful *Karenia mikimotoi* to Algicidal Bacterium *Paracoccus homiensis* O-4

Ning Ding, Yanbing Wang, Junfeng Chen, Siyu Man, Feng Lan, Chao Wang, Lijun Hu, Peike Gao and Renjun Wang**

College of Life Sciences, Qufu Normal University, Qufu, China

OPEN ACCESS

Edited by:
Lean Zhou,
Changsha University of Science and Technology, China

Reviewed by:
Gang Li,
South China Sea Institute of Oceanology, Chinese Academy of Sciences (CAS), China
Wenjie Xia,
Nankai University, China

***Correspondence:**
Peike Gao
gpkyll-001@163.com
Renjun Wang
wangrenjun2002@126.com

Specialty section:
This article was submitted to Microbiotechnology, a section of the journal Frontiers in Microbiology

Received: *06 September 2021*
Accepted: *01 November 2021*
Published: *30 November 2021*

Citation:
Ding N, Wang Y, Chen J, Man S, Lan F, Wang C, Hu L, Gao P and Wang R (2021) Biochemical and Physiological Responses of Harmful Karenia mikimotoi to Algicidal Bacterium Paracoccus homiensis O-4. Front. Microbiol. 12:771381. doi: 10.3389/fmicb.2021.771381

Harmful algal blooms caused by *Karenia mikimotoi* frequently occur worldwide and severely threaten the marine environment. In this study, the biochemical and physiological responses of *K. mikimotoi* to the algicidal bacterium *Paracoccus homiensis* O-4 were investigated, and the effects on the levels of reactive oxygen species (ROS), malondialdehyde content, multiple antioxidant systems and metabolites, photosynthetic pigments, and photosynthetic index were examined. The cell-free supernatant in strain O-4 significantly inhibited *K. mikimotoi* cell growth. The bacterium caused the *K. mikimotoi* cells to activate their antioxidant defenses to mitigate ROS, and this effect was accompanied by the upregulation of intracellular antioxidant enzymes and non-enzyme systems. However, the overproduction of ROS induced lipid peroxidation and oxidative damage within *K. mikimotoi* cells, ultimately leading to algal death. In addition, the photosynthetic efficiency of the algal cells was significantly inhibited by O-4 and was accompanied by a reduction in photosynthetic pigments. This study indicates that O-4 inhibits *K. mikimotoi* through excessive oxidative stress and impaired photosynthesis. This research into the biochemical and physiological responses of *K. mikimotoi* to algicidal bacteria provides insights into the prophylaxis and control of harmful algal blooms *via* interactions between harmful algae and algicidal bacteria.

Keywords: *Karenia mikimotoi*, *Paracoccus homiensis*, algicidal activity, ROS, photosynthesis

INTRODUCTION

Harmful algal blooms (HABs) are typically related to the discharge of nitrogen and phosphorus nutrients from industry and agriculture and cause considerable threats to fisheries and public health worldwide (Zhang et al., 2014; Berdalet et al., 2016). *Karenia mikimotoi* is a dominant dinoflagellate species in large-scale red tides that causes the mortality of benthic and pelagic organisms by secreting toxic substances (Mooney et al., 2010; Kurekin et al., 2014; O'Boyle et al., 2016; Aoki et al., 2017). Various approaches and techniques (including physical, chemical, and biological methods) have been developed to prevent and control HABs (Lee et al., 2013). Various organisms and their metabolites are potential suppressors of HABs, including algicidal bacteria (Wang et al., 2012), actinomycetes (Zhang et al., 2013), viruses (Cai et al., 2011), and macrophytes (Zhou et al., 2010).

Studies on the interactions between algae and bacteria have resulted in the isolation of algicidal bacteria primarily belonging to the Bacteroidetes, Firmicutes, and Proteobacteria. The representative algicidal bacteria in Bacteroidetes include *Flavobacterium* sp. (Zheng et al., 2018), *Cytophaga*, and *Cellulophaga* (Imai et al., 2006). *Bacillus* (Oh et al., 2011) is the representative algicidal bacteria in the Firmicutes. *Halomonas* (Fang et al., 2012), *Vibrio* (Iwata et al., 2003), *Alteromonas* (Iwata et al., 2003), *Pseudoalteromonas* (Imai et al., 2006), *Thalassospira* (Lu et al., 2016), *Alteromonas* sp., *Marinobacter* sp., *Idiomarina* sp., and *Paracoccus* sp. (Zheng et al., 2018) are the most reported algicidal bacteria in Proteobacteria. *Flavobacteria* sp. is widely found in a number of different environments and exhibits algicidal activity against *Prorocentrum micans* by a direct attack (Shi et al., 2012). *Pseudoalteromonas haloplanktis* AFMB-08041 could suppress the harmful dinoflagellate *Prorocentrum minimum* with an algicidal rate up to 94.5% (Kim et al., 2009). The *Micrococcus luteus* strain SY-13 can secrete an extracellular substance that causes cell lysis in the red tide dinoflagellate *Cochlodinium polykrikoides* (Kim et al., 2008). The genus *Paracoccus* sp. is used in the biodegradation of wastewater treatment and is under investigation for its ability to lyse *Prorocentrum donghaiense* (Zhang et al., 2018).

Algicidal bacteria can inhibit algal growth or lyse algae by attacking the cells directly or indirectly by secreting extracellular substances, including proteins, polypeptides, biosurfactants, amino acids, and antibiotics (Zhuang et al., 2018). The mechanisms involved in the algicide of HABs primarily involve four pathways: cell structure damage, alteration of enzymatic or non-enzymatic systems, inhibition of algal photosynthesis/respiration, and restriction of gene expression (Zhang et al., 2010; Pokrzywinski et al., 2017). To understand the mechanisms of the algicidal process, the physiological and biochemical responses in algal cells require investigation. Aquatic organisms, including algae, can boost their antioxidant defense systems to ease the degree of damage caused by harmful reactive oxygen species (ROS) and lipid peroxidation. Superoxide dismutase (SOD), catalase (CAT), peroxidase (POD), glutathione peroxidase (GPx), glutathione disulfide (GSSG), and macromolecular compounds (such as carotenoids and glutathione) form antioxidant defense systems to prevent damage from the external environment (Yang et al., 2011; Kirilovsky, 2015). Hu et al. (2015) reported that the *Bacillus* sp. Y1 and Y4 decreased photosynthetic pigment content, induced ROS production, and upregulated enzymatic antioxidant systems in HABs.

Previously, we isolated an algicidal bacterium, *Paracoccus homiensis* O-4, and investigated its algicidal activity against *K. mikimotoi*. In the present study, the physiological and biochemical responses of the alga to the algicidal substances from *P. homiensis* O-4 were further investigated particularly from the following aspects: (1) the algicidal mode of *P. homiensis* O-4 against *K. mikimotoi*; (2) the extent of oxidative damage and antioxidant systems activity of algal cells; and (3) the effects of strain O-4 on the algal photosystem in *K. mikimotoi*. Thus, the study objective was to elucidate the biochemical and physiological responses of the algal cells to the algicidal activity of the bacterium and guide the potential application of *P. homiensis* O-4 in controlling HABs dominated by *K. mikimotoi*.

MATERIALS AND METHODS

Karenia mikimotoi and Cultivation

Karenia mikimotoi was obtained from the Laboratory of Microalgae Research, Ocean University of China, Qingdao, China. The axenic algae were cultured at 25°C in sterile f/2 medium (Lananan et al., 2013) prepared with 0.45-μm filtered natural seawater, with a light intensity of approximately 80 μmol photons m^{-2} s^{-1} under a 12 h:12 h light:dark cycle. The axenic culture of *K. mikimotoi* was tested by culturing on the plates and microscopy method. Cell numbers were counted using a hemocytometer under a light microscope (CX21FS1; Olympus, Tokyo, Japan).

Algicidal Activity of Strain O-4 on *Karenia mikimotoi*

The strain *P. homiensis* O-4 was previously isolated from seawater (Zheng et al., 2018; Ding et al., 2021). The 16S rRNA gene sequence of the strain was deposited in GenBank (MG457257). Seawater was obtained from Luxun Park, Qingdao, China. The bacterial strain was cultured in 2216E agar medium (peptone 5 g, yeast extraction 1 g, ferric phosphorous acid 0.1 g, agar 10 g, pH 7.6–7.8, fixed capacity to 1 L using sterile seawater) at 25°C for 72 h. For the algicidal test, 1-, 3-, and 5-ml amounts of the bacterial solutions (with volume ratios of 1%, 3%, and 5%, respectively) were each inoculated into the 100-ml flask containing exponentially growing *K. mikimotoi* algal cultures. The algal cells were fixed with Lugol's iodine. The algicidal activity was monitored by counting the cell numbers using a microscope. Algicidal activity by O-4 was calculated according to the following equation: algicidal activity (%) = $(1-Tt/Ct) \times 100\%$, where T and C are the concentrations of algal cells in the treatment and control groups, respectively, and t is the incubation time. All experiments were performed in triplicate.

Algicidal Mode of Strain O-4

To assess the mode of action in the algae inhibition of *K. mikimotoi*, the cell-free filtrate was used: the bacterial culture after 72-h cultivation was centrifuged at 15,000 × *g* for 10 min at 4°C and passed through a 0.22-μm membrane filter (Merck Millipore, Darmstadt, Germany). The remaining cell pellets in the bottle were washed twice with a sterile 2216E medium. The cells were resuspended in f/2 medium with the same concentration (3%), shaken, and then labeled as O-4 cells. The control group comprised an algae culture supplemented with a 3% sterile 2216E medium.

Measurement of Photosynthetic Pigments and Photosynthetic Index

The contents of chlorophyll a (Chl *a*) and carotenoid (Car) were analyzed after the 3 and 5% strain O-4 treatment. Algal cells were collected *via* centrifugation (5,000 rpm, 20 min) after 0,

4, 8, 12, 24, and 48 h of culture. Algal pigments were extracted using 85% acetone solution in the dark at 4°C for 24 h, followed by centrifugation (5,000 rpm, 10 min). The absorbance of the supernatant was measured at the wavelengths of 470, 645, and 663 nm (Gan and Lian, 2021). The absorbance of 85% acetone was used as the control. The formula of photosynthetic pigment is as follows:

$$Ca(mgL^{-1}) = 12.21 \times A663nm - 2.81 \times A645nm$$

$$Cb(mgL^{-1}) = 20.13 \times A645nm - 5.03 \times A663nm$$

$$(\text{Cc (mg L}^{-1}) = \frac{(1,000 - \text{A470nm} - 3.27\text{Ca} - 104\text{Cb})}{229}$$

where Ca, Cb, and Cc represent the concentrations of chlorophyll a, chlorophyll b, and total carotenoid.

The maximum photochemical quantum yield of photosystem II is Fv/Fm, representing the maximum photosynthetic potential. The chlorophyll fluorescence parameters of the treated algae cells were measured using a water pulse amplitude modulation chlorophyll fluorescence analyzer (Walz, Germany). Algal cells were dark-adapted for 15 min before the experiment. The algal fluorescence was detected using a measuring light (0.01 μmol photons m^{-2} s^{-1}) with a saturation pulse (0.8 s, 3,500 μmol photons m^{-2} s^{-1}). The maximum photochemical quantum yield of the photosystem (Fv/Fm) was used to indicate the efficiency in light energy conversion during photosynthesis.

Measurement of Reactive Oxygen Species Content

The intracellular ROS level within *K. mikimotoi* was measured using a ROS detection kit (Biyuntian, Shanghai, China) with slight modifications. The methods were as follows: (1) after 4, 8, 12, 24, 36, and 48 h of culture, 40 ml of algal solution was centrifuged at 4°C, and the supernatant was immediately discarded to collect algal cells; (2) DCFH-DA probe dye was added, and the mixture was incubated at 37°C for 30 min; (3) the mixture was centrifuged (at 1,000 rpm, 5 min), and the algal cells were washed with PBS; (4) the mixture was centrifuged again to settle the solution, and the supernatant was discarded to obtain the algal cells; (5) after resuspending the cells using PBS, the fluorescence intensity was measured with an excitation wavelength of 488 nm and an emission wavelength of 525 nm using a flow cytometer (Novocyte 2040R, ACEA, United States).

Measurement of Malondialdehyde Content and Superoxide Dismutase, Catalase, Peroxidase, and Glutathione Peroxidase Activity

Bacterial filtrates of O-4 were inoculated in the exponential phase axenic *K. mikimotoi* cultures until the concentration of the bacterial solution reached 3 and 5%. An axenic 2216E medium of the same volume was added separately to act as a control. After co-culture for 0, 6, 12, 24, and 48 h, algal cells were collected using centrifugation (10,000 rpm, 20 min), followed by washing with PBS (50 mM, pH 7.4). The cell disruption was assessed using an ultrasonic cell disruption system (200 W, 5 s; 10 s, five times at less than below 4°C). The extracting solution was centrifuged for 15 min at 10,000 × *g*, and the supernatant was used in the cell membrane permeability analysis. Lipid peroxidation levels were measured by assessing the malondialdehyde level following the methods by Dogru et al. (2008).

The crude protease solution was also obtained as described previously (Ding et al., 2018). After co-culture for 0, 6, 12, 24, and 48 h, the algal cell suspension was centrifuged at 4°C for 20 min (10,000 rpm min^{-1}). The supernatants were discharged, and the algal cells were collected. The algal cells were washed with PBS (0.05 mol L^{-1}, pH 7.8) and transferred to a test tube. Under ice-bath conditions, the algal cells were crushed by ultrasound for 5 min (5 s, interval of 10 s, 200 W). An amount of 1.5 ml of supernatant was absorbed into the Eppendorf tube and centrifuged again at 4°C for 15 min. The supernatants obtained after centrifugation comprised the crude protease solution to be measured. The SOD, CAT, and POD activities in the algal cells were measured following the manufacturer's instructions (Jiancheng, Nanjing, China). Glutathione peroxidase was measured using a GPx assay kit (Biyuntian, Shanghai, China).

Measurement of Glutathione, Glutathione Disulfide, Ascorbic Acid, and Dehydroascorbic Acid

Glutathione (GSH) was determined following the instructions in a GSH assay kit (Jiancheng, Nanjing, China). Glutathione oxidized (GSSG) was measured using a GSSG assay kit (Solarbio, Beijing, China). Ascorbic acid (AsA) and dehydroascorbic acid (DHA) were determined *via* the method described in Ding et al. (2018) as follows. Supernatants of 200 μl were prepared (as described above), then 200 μl of dithiothreitol (5 mmol L^{-1}) and 500 μl of potassium phosphate of buffer solution (100 mmol L^{-1}, pH 7.4) were added to the test tube, and the mixture was incubated at 25°C for 10 min. Then, 100 μl of *N*-ethylmaleimide, 400 μl of trichloroacetic acid (0.61 mol L^{-1}), 400 μl of phosphoric acid (0.8 mol L^{-1}), 400 μl of 2,2'-bipyridine (0.5 mol L^{-1}), and 200 μl of ferric chloride (3 mol L^{-1}) were added to the mixture. They were set in the water bath and incubated at 55°C for 10 min. The absorbance of each tube was measured at a wavelength of 525 nm. The total ascorbic acid content could then be calculated. In the above process, the dithiothreitol and *N*-ethylmaleimide were not added, and alternatively, the double steaming water and the reduced ascorbic acid content could be measured. The DHA content was the difference between total AsA and AsA content.

Data Analysis

The data were presented as means, and their standard errors were analyzed using SPSS 20.0 (SPSS Inc., Chicago, IL, United States).

RESULTS

Algicidal Activity and Mode of Strain O-4

The effects of O-4 on the growth of *K. mikimotoi* are presented in **Figure 1**. The results indicate that the algicidal activity by strain O-4 against *K. mikimotoi* cells was concentration-dependent. When compared to the control group, the addition of 1% O-4 exhibited no algicidal activity ($p > 0.05$), and within 120 h, the growth of *K. mikimotoi* slightly increased. In the treatment groups receiving 3 and 5% O-4 bacterial culture, there was significant growth inhibition ($p < 0.05$). The 3% O-4 caused 83% of the cells to be lysed after the treatment duration of 48 h. In the 3% O-4 treatments, 94% of the cells were lysed after 120 h. The 5% bacterial concentration of O-4 exhibited the strongest algicidal activity, leaving no visible intact algal cells after 120 h. The results suggest that the algicidal effects are enhanced with an increased bacterial concentration and treatment duration. Due to the strong algicidal activity in the 3 and 5% O-4 bacterial cultures, they were used in the subsequent stages of our evolving research program.

The bacterial cells and cell-free filtrate were separated and inoculated into *K. mikimotoi* cultures to explore the action of the algicidal mode of O-4. The results are provided in **Figure 2**. The additional bacterial cells did not significantly inhibit the growth of *K. mikimotoi*. However, both the cell-free filtrate and bacterial culture caused a significant inhibitory effect on *K. mikimotoi* ($p < 0.05$). The cell-free filtrate of O-4 reduced the algal cell density, and the algicidal activity against *K. mikimotoi* was 88.6% after 60 h. These results imply that the algicidal activity by O-4 is indirect.

Effects of Strain O-4 on the Algal Photosystem in *Karenia mikimotoi*

To investigate the stress caused by O-4 on the algae, we determined the Chl *a*, carotenoid content, and maximum quantum yield of photosystem (PS) II [variable fluorescence (Fv)/maximum fluorescence (Fm)]. **Figures 3A,B** demonstrate that the pigment contents of the algal cells treated with O-4 were significantly lower than that in the control group after 48 h ($p < 0.01$). After 12 h, the contents of both Chl *a* and carotenoids in the 3% O-4 treatment groups decreased to 32% (Chl *a*) and 57% (carotenoids), respectively, compared to the control. After 48 h, the pigment content was reduced by approximately 86% (Chl *a*) and 60% (carotenoid) compared to the control. Moreover, after 48 h, the reduction in Chl *a* and carotenoid contents in the 5% O-4 treatment groups was approximately 90% (Chl *a*) and 91% (carotenoids) with respect to the control. These results indicate that O-4 is capable of damaging pigments in algal cells.

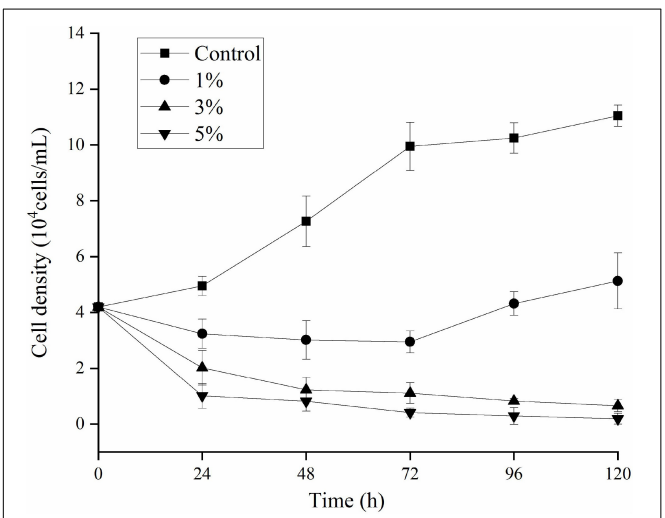

FIGURE 1 | Algicidal activity levels using different doses of *Paracoccus homiensis* O-4 against *Karenia mikimotoi*. Error bars represent the standard deviation of the triplicates.

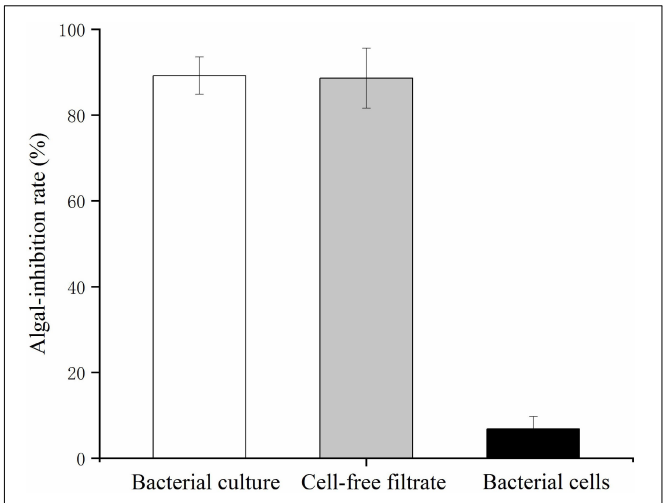

FIGURE 2 | Algicidal activities against *Karenia mikimotoi* by *Paracoccus homiensis* O-4 treatment groups (bacterial culture, cell-free filtrate, and bacterial cells). Error bars represent the standard deviation of the triplicates.

The Fv/Fm ratio was evaluated to determine the photosynthetic status of the algal cells after the 3 and 5% O-4 treatments (**Figure 4**). The Fv/Fm values decreased significantly relative to untreated cells after 12 h ($p < 0.05$). As the treatment duration progressed, the Fv/Fm values continued to decrease. At 48 h, when compared to the Fv/Fm values of the control group, the 3% treatment group was 3.1-fold lower ($p < 0.05$), and the 5% treatment group was 6.2-fold lower ($p < 0.01$. These results demonstrate that the photosynthetic capacity was inhibited in the treated cells (**Figure 4**).

Reactive Oxygen Species Levels and Lipid Peroxidation of *Karenia mikimotoi* Under Algicidal Activity

An ROS level analysis explored the oxidative stress caused by O-4 in *K. mikimotoi* cells. **Figure 5** shows a slight increase in DCF fluorescence intensity in the control group. Conversely, the DCF fluorescence intensity was significantly increased in algal cells treated with O-4 ($p < 0.05$,

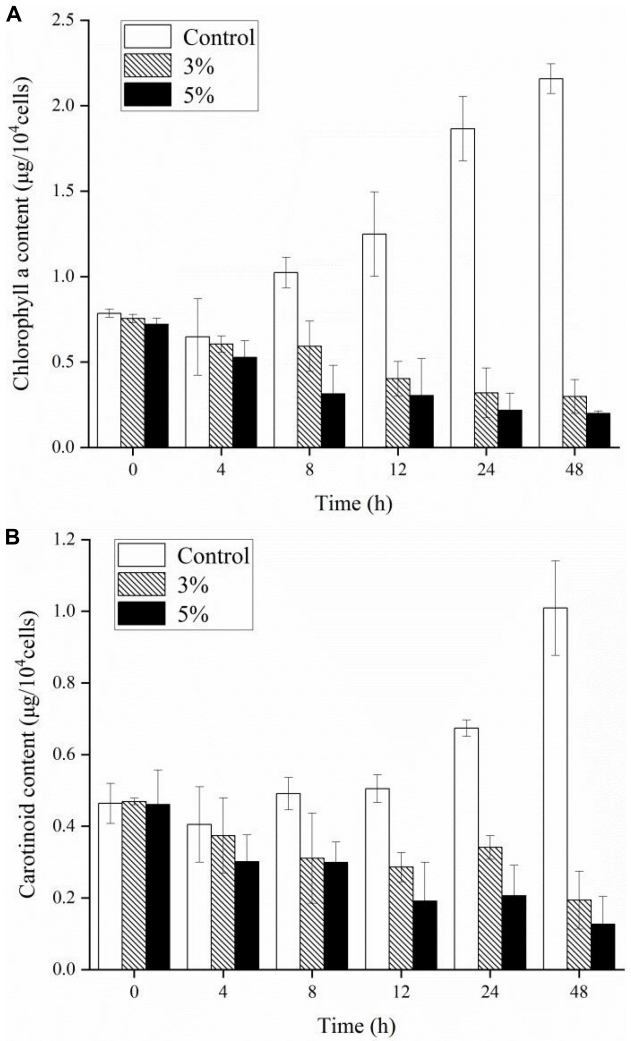

FIGURE 3 | Effects of different doses of *Paracoccus homiensis* O-4 on the Chl *a* **(A)** and carotenoid contents **(B)** in *K. mikimotoi*. Error bars represent the standard deviation of the triplicates.

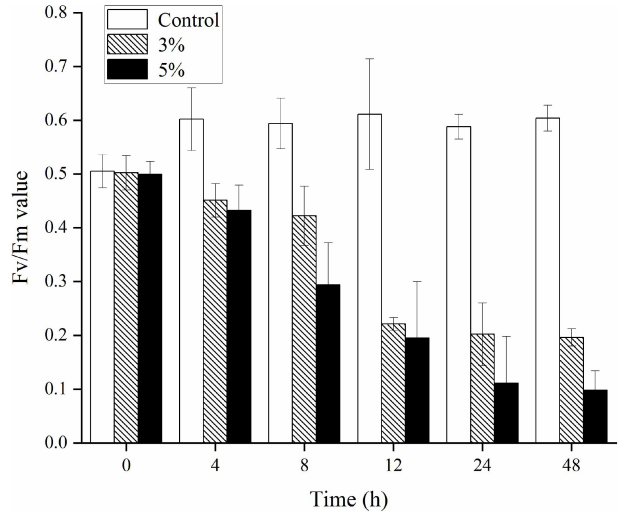

FIGURE 4 | Effects of photosynthetic efficiency (Fv/Fm) within *Karenia mikimotoi* treated with varying doses of *Paracoccus homiensis* O-4. Error bars represent the standard deviation of the triplicates.

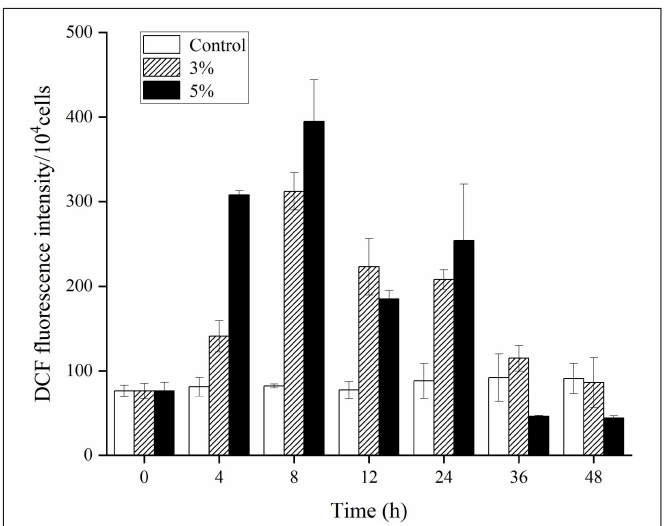

FIGURE 5 | Effects of ROS levels within *Karenia mikimotoi* after exposure to different doses of *Paracoccus homiensis* O-4. Error bars represent the standard deviation of the triplicates.

Figure 5). The ROS levels were significantly increased after 8 h of exposure in both treatment groups containing O-4, with ROS levels 3.8-fold (3% O-4) and 4.8-fold (5% O-4) higher than the control group. However, the ROS levels in both treatment groups began decreasing after 12 h of exposure, and at 48 h, the ROS content of algal cells in both treatment groups was maintained at a low level compared to the control.

Figure 6 illustrates the effects of O-4 on lipid peroxidation in the algal cells. Algae cells exposed to O-4 exhibited a pronounced increase in MDA content. The MDA levels in all the treated groups were higher than those in the controls ($p < 0.05$), and MDA content increased with exposure duration and increased concentrations of O-4. At 48 h, the MDA levels were 2.4 (3% O-4 group) and 3.5 (5% O-4 group) times higher than the control group.

Responses of Antioxidative Enzymes to Strain O-4 Treatment

We investigated the physiological defense responses induced by exposure to the algicidal O-4 by determining the representative enzymatic activities within cells, including SOD, CAT, POD, and GPx (**Figures 7A–D**). **Figure 7A** demonstrates that SOD activity increased as the exposure duration increased relative to the control in all treatment groups ($p < 0.05$). The SOD activity initially decreased slightly until 48 h of exposure in the 5% group. The CAT values were significantly higher in the 3% O-4 treatment groups when compared to the control (**Figure 7B**); the values

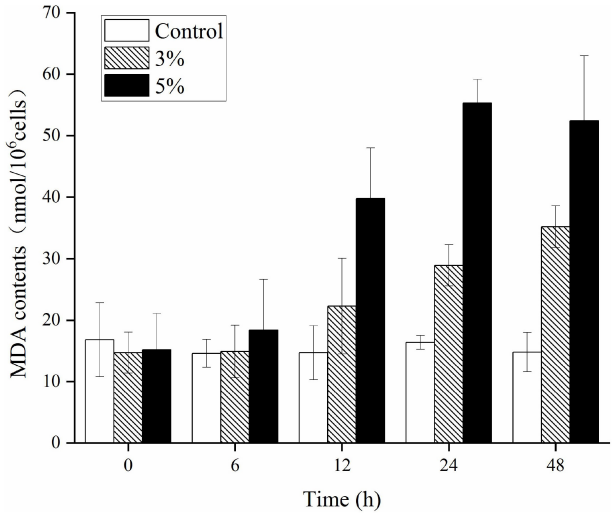

FIGURE 6 | Effects of MDA contents in *Karenia mikimotoi* after exposure to different volumes of *Paracoccus homiensis* O-4. Error bars represent the standard deviation of the triplicates.

were 1.2-fold higher after 12 h, 1.78-fold after 24 h, and 6.36-fold after 48 h ($p < 0.05$). The CAT values were significantly higher in the 5% O-4 treatment groups when compared to the control; the values were 1.51-fold higher ($p < 0.05$) after 12 h, 4.82-fold ($p < 0.05$) after 24 h, and 17.0-fold after 48 h ($p < 0.01$). The POD values of 3% O-4 treatment group were slightly lower than the control groups after 6-h and 12-h exposure but increased significantly with exposure duration and additional ratios (**Figure 7C**), reaching a peak at 48 h ($p < 0.05$). The GPx activity had similar results to the POD activity (**Figure 7D**). When algal cells were exposed to 3 and 5% O-4 bacterial cultures for 48 h, the activity values were 2.79 and 3.67 times higher than the control, respectively ($p < 0.05$).

Responses of Antioxidative Non-enzymes to Strain O-4 Treatment

Antioxidant non-enzymatic activities (including GSH, GSSG, AsA, and DHA) were assayed to analyze the algal cell protective responses against O-4 (**Figures 8A–D**). **Figure 8A** shows that GSH was stimulated by O-4 ($p < 0.05$). The only exception was the 3% treatment group after 12 h. The GSH content in the treatment groups compared to the control groups increased from 498 to 634 μmol L^{-1} (3%) and 511 to 909 μmol L^{-1} (5%) within 48 h. The GSSG contents of the algae in both treatment groups increased significantly with increasing O-4 concentrations and treatment duration and remained higher than the control group over 48 h ($p < 0.05$, **Figure 8B**). The AsA levels in *K. mikimotoi* cells were similar to the GSSG results (**Figure 8C**). At 48 h, the AsA levels were 1.5-fold (3% O-4) and 1.66-fold (5% O-4) higher than the control group. **Figure 8D** graphically demonstrates the effects of the strain O-4 on DHA in *K. mikimotoi* cells. After 12 h, the 3% O-4 group exhibited a stimulatory effect on DHA. Within 48 h, there was a significant inhibitory effect on the DHA in the 5% O-4 treatment group ($p < 0.05$).

DISCUSSION

Over the past decades, HABs have frequently occurred in eutrophic coastal areas of Europe and China, and *K. mikimotoi* is a dominant HAB species (Qian et al., 2009; Kurekin et al., 2014). Some marine bacteria can promote or reduce algal blooms (Teeling et al., 2012). Algicidal bacteria can act as potential biological controllers in the degradation and termination of HAB species (Schoemann et al., 2005). In this study, we evaluated the algicidal activity and inhibitory mechanisms of the *P. homiensis* strain O-4 against the harmful *K. mikimotoi*. The algicidal activity of O-4 was time- and concentration-dependent, using 3 and 5% ratios of bacterial culture in approximately 90 and 95% algal lysis over 96 h, respectively. The density of algal cells in high concentrations of the bacterial culture (3 and 5%) decreased significantly compared to the control and 1% concentration groups, which suggested that strain O-4 had an effective algicidal activity on *K. mikimotoi*, and the higher concentrations were even more efficient. Thus, the results suggest that this strain is a viable algal-lysing agent for regulating *K. mikimotoi*. A similar study revealed a marine algicidal bacterium *Mangrovimonas yunxiaonensis* strain LY01 caused 87% inhibition of toxic *Alexandrium tamarense* after 60 h of exposure (Li et al., 2014).

We explored the biochemical and physiological responses of *K. mikimotoi* induced by the algicidal bacterium *P. homiensis* O-4. A direct attack requires direct contact between the bacteria and algal cells, whereas an indirect attack occurs when algicidal bacteria produce algicidal substances to inhibit algal cells and does not require cell-to-cell contact. The addition of cell-free filtrate and bacterial culture showed algicidal activity. Conversely, the washed bacterial cells exhibited no significant algicidal effect on *K. mikimotoi*. Therefore, the O-4 algicidal mode was indirect, as the algicidal activity was likely to be expressed through the excretion of extracellular algicidal substances. Our results were consistent with a previous study that found that the algicidal bacteria *Hahella* sp. KA22 can lyse the toxic dinoflagellate *Heterosigma akashiwo* by producing the extracellular compound prodigiosin (Zhang et al., 2020).

Direct and indirect external stress can induce algal cells to trigger excessive ROS levels, which cause severe oxidative damage or cellular death (Apel and Hirt, 2004). ROS, including O^{-2}, O_2, HO_2, H_2O_2, RO, OH, ROO, and ROOH, are relatively reactive in live cells and are continuously generated as the by-products of diverse metabolic pathways in various cellular organelles, such as the mitochondria, chloroplasts, and peroxisomes. Consequently, the proteins, DNA, lipids, and carbohydrates of cells are damaged by excessive ROS, eventually leading to cell death (Gill and Tuteja, 2010). In the present study, O-4 caused an ROS explosion in *K. mikimotoi* cells compared to the controls within a short exposure (8 h in all treatment groups).

These results imply that the stress caused by O-4 induced algal cells to produce excess ROS, ultimately causing cell death. The ROS caused oxidative damage to *K. mikimotoi* cells, as evidenced

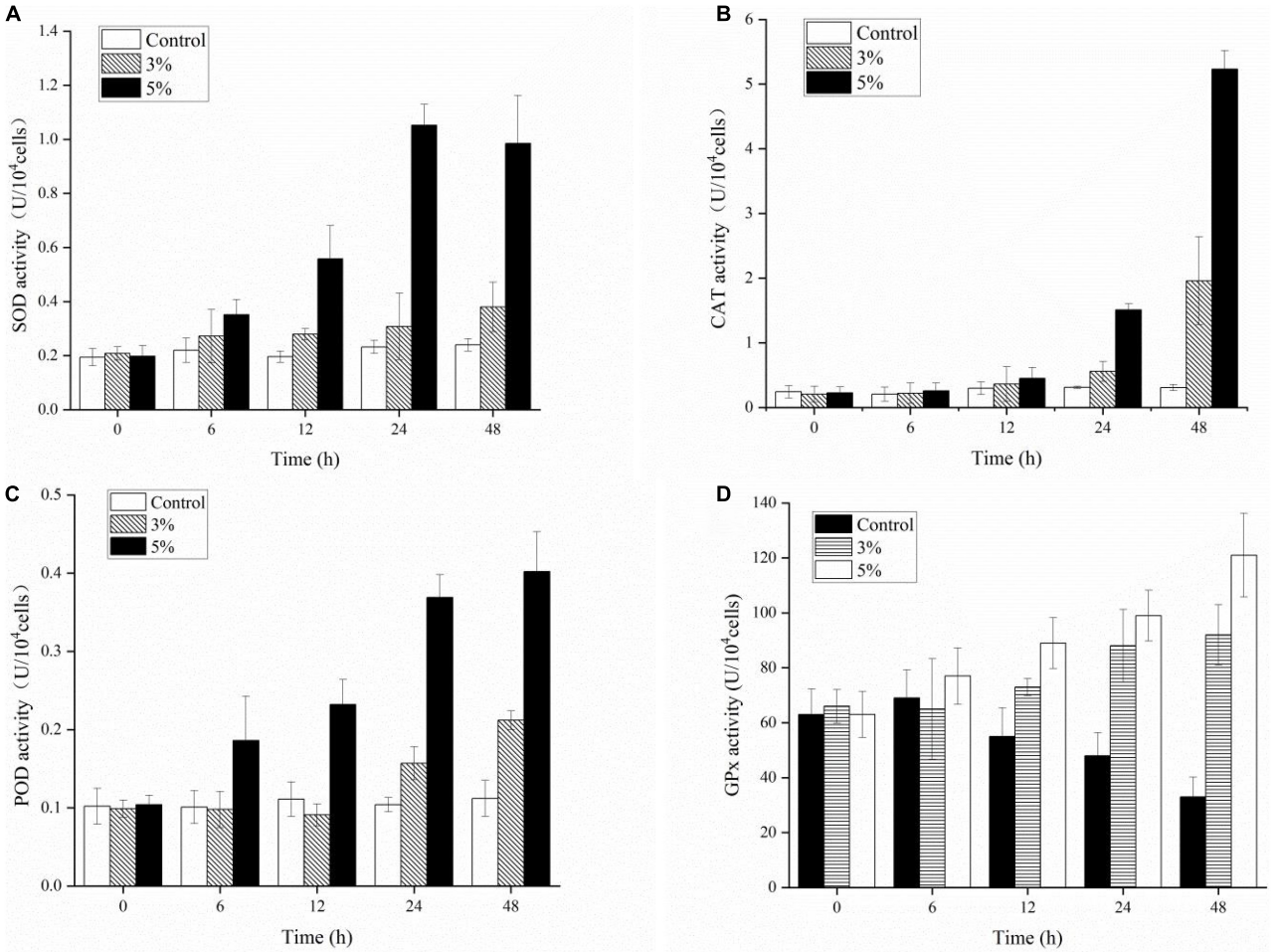

FIGURE 7 | Effects of enzymic antioxidants including SOD **(A)**, CAT **(B)**, POD **(C)**, and GPx **(D)** activities in *Karenia mikimotoi* after exposure to varying levels of *Paracoccus homiensis* O-4.

by the upregulation of the MDA content within cells upon exposure to O-4. Malondialdehyde is considered an indicator of lipid peroxidation and is a major peroxidation product that reflects the degree of cellular oxidative damage (Yamauchi et al., 2008). Cell membranes consist of primarily unsaturated phospholipids and are sensitive to oxidative attack; therefore, additional ROS results in excess accumulation of MDA (Qian et al., 2008). The increase in MDA levels within algal cells after exposure to O-4 indicated that the O-4 induced membrane lipid peroxidation and caused oxidative damage to the cell membrane systems of *K. mikimotoi*. This phenomenon has previously been observed, resulting in the MDA content being upregulated after a short exposure to an allelochemical (Qian et al., 2009).

To protect living cells from oxidative damage and environmental stress, important enzymatic antioxidants are engaged, including superoxide dismutase (SOD), catalase (CAT), peroxidase (POD), and glutathione peroxidase. Superoxide dismutase and POD can catalyze the dismutation of O^{-2} to H_2O_2 and O_2, and degradation converts them into H_2O and O_2 under the promotion of CAT and GPx, easing the impact of oxidative stress and initiating cell repair (Valentine et al., 1998; Kwok et al., 2012). Additionally, to reduce oxidative stress induced by algicidal compounds, a series of non-enzymatic antioxidants (including AsA, GSH, and GSSG) is also activated to scavenge the excess intracellular ROS. The O^{-2} and H_2O_2 can also be removed by AsA to reduce the damage from lipid peroxidation (Deutsch, 1998). As antioxidants, GSH and GSSG play many important roles in modulating the redox environment of the membrane and cell-wall-related proteins and maintain the sulfur status to protect cells from various stresses (Aziz et al., 1996). Our results suggest that antioxidant enzymes and non-enzyme systems were initiated at varying levels after exposure to O-4. The algicidal compounds generated by O-4 were toxic to the *K. mikimotoi* cells and caused them to produce excessive ROS. The antioxidant systems may be responsible for the algicidal activity in O-4 by strengthening the activities of both antioxidant enzymes and non-enzyme systems. However, high doses of O-4 were fatal to *K. mikimotoi* cells because the high ROS levels surpassed the capacity of the cells to defend

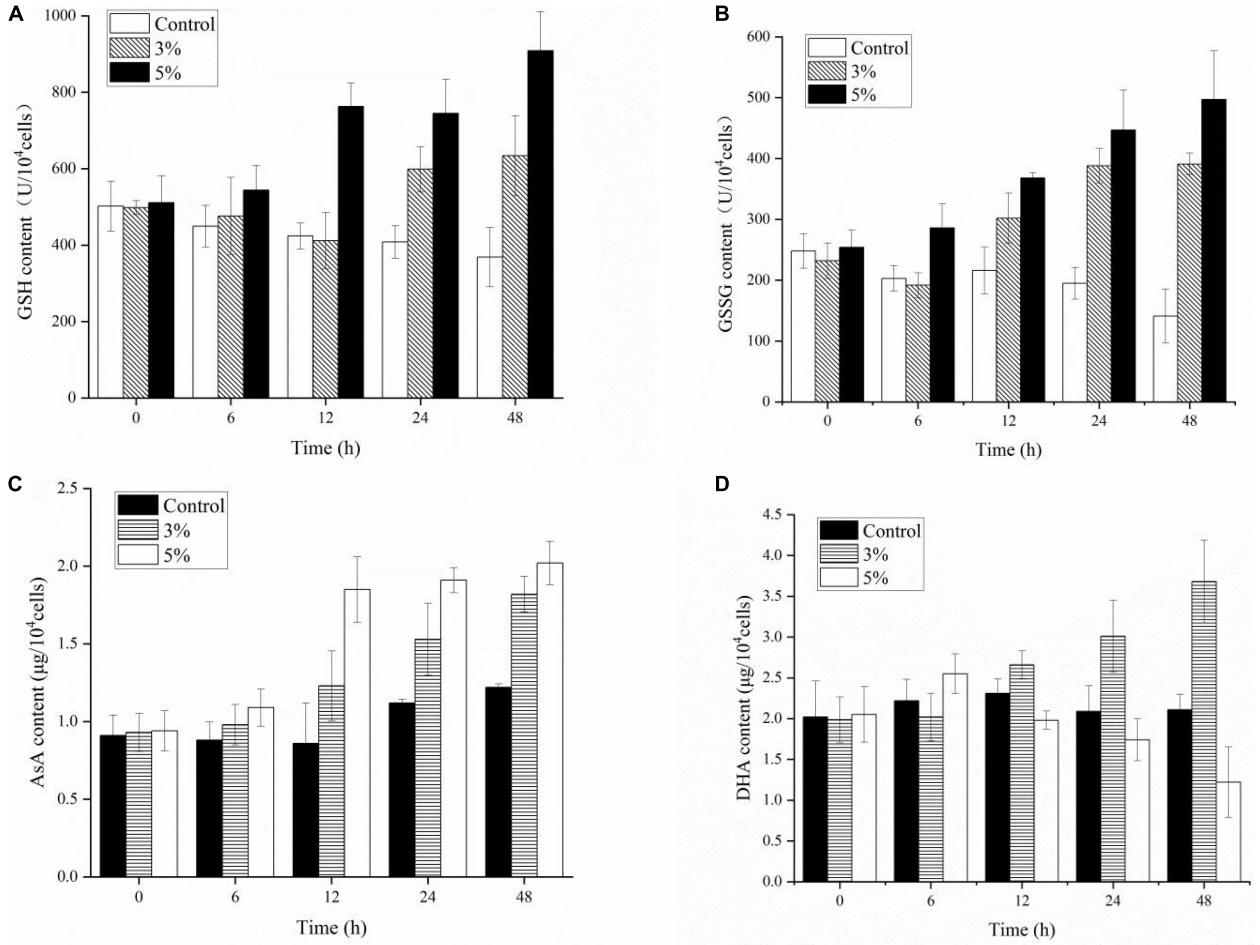

FIGURE 8 | Effects of non-enzymic antioxidants including GSH **(A)**, GSSG **(B)**, AsA **(C)**, and DHA **(D)** activities in *Karenia mikimotoi* after exposure to *Paracoccus homiensis* O-4 at different doses.

themselves, ultimately causing cell death. Our results showed that a significant inhibitory effect on DHA occurred when the cells were treated with O-4. Dehydroascorbic acid acts as an important oxidoreductase during metabolic processes, and is relatively sensitive to environmental stress and noxious substances (Zhang et al., 2016). In this study, the algal cell viability was closely associated with DHA. The downregulation of DHA levels, when exposed to O-4, demonstrated that the regular metabolism in *K. mikimotoi* cells was disrupted and crucial enzyme activity was suppressed.

K. mikimotoi is a dominant species in marine photoautotrophic phytoplankton, and photosynthesis in algal cells plays a key role in global primary production. The PSII system acts as a major pigment–protein complex that can catalyze photosynthesis and is sensitive to adverse environmental conditions (Nymark et al., 2009). Photosynthetic pigments primarily include Chl *a* and carotenoids in the thylakoid membrane, which harvest light and energy for conversion in the photosynthetic process. The significant declines in Chl *a* and carotenoid contents after exposure to O-4 may be caused by their impacts on electron flow and the regular operation of the PSII system. Another photosynthesis index, Fv/Fm, represents the maximum efficiency of PSII. However, external environmental factors, including light intensity, temperature, and biotic stress, typically decrease the Fv/Fm values (Kumar et al., 2014). The inhibition of Fv/Fm values after treatment with O-4 suggests that the photosynthetic efficiency was seriously impeded and that dysfunction occurred in the PSII system. Overall, the reductions in pigment content and Fv/Fm values, and the transferring of excitation energy to ROS as singlet oxygen, eventually caused a decline in the interference capacity of ROS generation.

In conclusion, the algicidal bacterium *P. homiensis* O-4 exerted an efficient inhibitory effect on *K. mikimotoi* cells. O-4 caused the algae to produce excessive ROS, and the antioxidant enzyme systems increased. The antioxidant non-enzymic substances played a synergistic role in reducing the damage caused by ROS. Meanwhile, membrane lipid oxidation increased, and cell membrane integrity was lost. Photosynthetic systems, including photosynthetic pigments and photosynthetic efficiency, were seriously damaged. Superfluous ROS overloaded

the antioxidant defense systems, and damage to critical systems and functions ultimately caused algal cell death.

DATA AVAILABILITY STATEMENT

Publicly available datasets were analyzed in this study. This data can be found here: GenBank (MG457257).

AUTHOR CONTRIBUTIONS

PG and RW conceived and proposed the idea. ND, YW, JC, SM, FL, CW, and LH carried out the experiments and conducted data analysis. ND and PG drafted the manuscript. All authors have read and approved the final manuscript.

FUNDING

This work was supported by the Shandong Provincial Agricultural Fine Species Project (2019LZGC020), the National Natural Science Foundation of China (31971503 and 31901188), the Shandong Jining Key Research and Development Project (2019ZDGH019), the Shandong Provincial Natural Science Foundation (ZR2020QC048 and ZR2019BB040), and the Postdoctoral Science Foundation of China (2021M691850).

ACKNOWLEDGMENTS

We would like to thank Editage (www.editage.cn) for English language editing.

REFERENCES

Aoki, K., Kameda, T., Yamatogi, T., Ishida, N., Hirae, S., Kawaguchi, M., et al. (2017). Spatio-temporal variations in bloom of the redtide dinoflagellate *Karenia mikimotoi* in Imari Bay, Japan, in 2014: factors controlling horizontal and vertical distribution. *Mar. Pollut. Bull.* 43, 1–10. doi: 10.1016/j.marpolbul.2017.07.019

Apel, K., and Hirt, H. (2004). Reactive oxygen species: metabolism, oxidative stress, and signal transduction. *Annu. Rev. Plant Biol.* 55, 373–399. doi: 10.1146/annurev.arplant.55.031903.141701

Aziz, J., Roberto, T., Enrico, M., and Serge, D. (1996). Characterization of glutathione uptake in broad bean leaf protoplasts. *Plant Physiol.* 111, 1145–1152. doi: 10.1104/pp.111.4.1145

Berdalet, E., Fleming, L. E., Gowen, R., Davidson, K., Hess, P., Backer, L. C., et al. (2016). Marine harmful algal blooms, human health and wellbeing: challenges and opportunities in the 21st century. *J. Mar. Biol. Assoc. U. K.* 96, 61–91. doi: 10.1017/S0025315415001733

Cai, W. W., Wang, H., Tian, Y., Chen, F., and Zheng, T. L. (2011). Bacteriophage influences algal bloom decline by modulating algicidal bacteria population dynamics. *Appl. Environ. Microbiol.* 77, 7837–7840.

Deutsch, J. C. (1998). Ascorbic acid oxidation by hydrogen peroxide. *Anal. Biochem.* 255, 1–7. doi: 10.1006/abio.1997.2293

Ding, N., Du, W. J., Feng, Y. L., Song, Y. H., Wang, C., Li, C., et al. (2021). Algicidal activity of a novel indigenous bacterial strain of *Paracoccus homiensis* against the harmful algal bloom species, *Karenia mikimotoi*. *Arch. Microbiol.* 203, 4821–4828. doi: 10.1007/S00203-021-02468-3

Ding, N., Wang, R. J., Gao, P. K., Chen, J. L., Han, M. A. X., Wang, J. G., et al. (2018). Allelopathic effects of linolenic acid secreted by macroalgae on *Prorocentrum donghaiense*. *China J. Ecol.* 37, 1410–1416. doi: 10.13292/j.1000-4890.201805.003

Dogru, M. I., Dogru, A. K., Gul, M., Esrefoglu, M., Yurekli, M., Erdogan, S., et al. (2008). The effect of adrenomedullin on rats exposed to lead. *J. Appl. Toxicol.* 28, 140–146. doi: 10.1002/jat.1259

Fang, J. I., Zhu, Y., Hao, R., Cheng, H. C., and Dong, R. J. (2012). Isolation, identification and characterization of algicidal bacteria against *Spirulina platensis*. *Sci. Technol. Food Ind.* 33, 221–320. doi: 10.13386/j.issn1002-0306.2012.12.010

Gan, Y. H., and Lian, J. J. (2021). Effect of various extracts on extracting of chlorophyll from *Anoectochilus roxburghii*. *Chin. J. Trop. Agric.* 41, 86–91. doi: 10.12008/j.issn.1009-2196.2021.03.014

Gill, S. S., and Tuteja, N. (2010). Reactive oxygen species and antioxidant machinery in abiotic stress tolerance in crop plants. *Plant Physiol. Biochem.* 48, 909–930. doi: 10.1016/j.plaphy.2010.08.016

Hu, X. L., Yin, P. H., Zhao, L., and Yu, Q. M. (2015). Characterization of cell viability in *Phaeocystis globosa* cultures exposed to marine algicidal bacteria. *Biotechnol. Bioprocess Eng.* 20, 58–66. doi: 10.1007/s12257-014-0437-2

Imai, I., Fujimaru, D., Nishigaki, T., Kurosaki, M., and Sugita, H. (2006). Algicidal bacteria isolated from the surface of seaweeds from the coast of Osaka Bay in the Seto Inland Sea, Japan. *Afr. J. Mar. Sci.* 28, 319–323. doi: 10.2989/18142320609504170

Iwata, Y., Sugahara, I., Kimura, T., Khohashi, K., Noritake, K., and Kowa, H. (2003). Algicidal activity of a *Karenia mikimotoi*-killing bacterium isolated from Gokasho Bay, Japan. *Jpn. Soc. Aquacult. Sci.* 51, 451–458. doi: 10.11233/aquaculturesci1953.51.451

Kim, J. D., Kim, J. Y., Park, J. K., and Lee, C. G. (2009). Selective control of the *Prorocentrum minimum* harmful algal blooms by a novel algal-lytic bacterium *Pseudoalteromonas haloplanktis* AFMB-008041. *Mar. Biotechnol.* 11, 463–472. doi: 10.1007/s10126-008-9167-9

Kim, M., Jeong, S., and Lee, S. (2008). Isolation, identification, and algicidal activity of marine bacteria against *Cochlodinium polykrikoides*. *J. Appl. Phycol.* 20, 1069–1078.

Kirilovsky, D. (2015). Photosynthesis: dissipating energy by carotenoids. *Nat. Chem. Biol.* 11, 242–243. doi: 10.1038/nchembio.1771

Kumar, K. S., Dahms, H. U., Lee, J. S., Kim, H. C., Lee, W. C., and Shin, K. H. (2014). Algal photosynthetic responses to toxic metals and herbicides assessed, by chlorophyll a fluorescence. *Ecotoxicol. Environ. Safe* 104, 51–71. doi: 10.1016/j.ecoenv.2014.01.042

Kurekin, A. A., Miller, P. I., and Vander, W. H. J. (2014). Satellite discrimination of *Karenia mikimotoi* and *Phaeocystis* harmful algal blooms in European coastal waters: merged classification of ocean colour data. *Harmful Algae* 31, 163–176. doi: 10.1016/j.hal.2013.11.003

Kwok, C. T., Merwe, J. P., Chiu, J. M. Y., and Wu, R. S. S. (2012). Antioxidant responses and lipid peroxidation in gills and hepatopancreas of the mussel *Perna viridis* upon exposure to the red-tide organism *Chattonella marina* and hydrogen peroxide. *Harmful Algae* 13, 40–46. doi: 10.1016/j.hal.2011.10.001

Lananan, F., Jusoh, A., Ali, N., Lam, S. S., and Endut, A. (2013). Effect of Conway medium and f/2 medium on the growth of six genera of South China Sea marine microalgae. *Bioresour. Technol.* 141, 75–82.

Lee, Y. C., Jin, E., Jung, S. W., Kim, Y. M., Chang, K. S., Yang, J. W., et al. (2013). Utilizing the algicidal activity of aminoclay as a practical treatment for toxic red tides. *Sci. Rep.* 3:1292. doi: 10.1038/srep01292

Li, Y., Zhu, H., Guan, C., Zhang, H., Guo, J., Chen, Z., et al. (2014). Towards molecular, physiological, and biochemical understanding of photosynthetic inhibition and oxidative stress in the toxic *Alexandrium tamarense* induced by a marine bacterium. *Appl. Microbiol. Biotechnol.* 98, 4637–4652. doi: 10.1007/s00253-014-5578-x

Lu, X., Zhou, B., Xu, L., Liu, L., Wang, G., Liu, X., et al. (2016). A marine algicidal *Thalassospira* and its active substance against the harmful algal bloom species *Karenia mikimotoi*. *Appl. Microbiol. Biotechnol.* 100, 5131–5139. doi: 10.1007/s00253-016-7352-8

Mooney, B. D., Hallegraeff, G. M., and Place, A. R. (2010). Ichthyotoxicity of four species of gymnodinioid dinoflagellates (*Kareniaceae*, *Dinophyta*) and purified

karlotoxins to larval sheepshead minnow. *Harmful Algae* 9, 557–562. doi: 10.1016/j.hal.2010.04.005

Nymark, M., Valle, K. C., Brembu, T., Hancke, K., Winge, P., Andresen, K., et al. (2009). An integrated analysis of molecular acclimation to high light in the marine diatom *Phaeodactylum tricornutum*. *PLoS One* 4:e7743. doi: 10.1371/journal.pone.0007743

O'Boyle, S., Mcdermott, G., Silke, J., and Cusack, C. (2016). Potential impact of an exceptional bloom of *Karenia mikimotoi* on dissolved oxygen levels in waters off western Ireland. *Harmful Algae* 53, 77–85. doi: 10.1016/j.hal.2015.11.014

Oh, J. I., Kim, M. J., Lee, J. Y., Ko, I. J., Kim, W., and Si, W. K. (2011). Isolation and characterization of algicidal bacteria from *Cochlodinium polykrikoides* culture. *Biotechnol. Bioprocess Eng.* 16, 1124–1133. doi: 10.1007/s12257-011-0232-2

Pokrzywinski, K. L., Tilney, C. L., Warner, M. E., and Coyne, K. J. (2017). Cell cycle arrest and biochemical changes accompanying cell death in harmful dinoflagellates following exposure to bacterial algicide IRI-160AA. *Sci. Rep.* 7:45102. doi: 10.1038/srep45102

Qian, H. F., Chen, W., Sheng, G. D., Xu, X. Y., Liu, W. P., and Fu, Z. W. (2008). Effects of glufosinate on antioxidant enzymes, subcellular structure, and gene expression in the unicellular green alga *Chlorella vulgaris*. *Aquat. Toxicol.* 88, 301–307. doi: 10.1016/j.aquatox.2008.05.009

Qian, H., Xu, X., Chen, W., Jiang, H., Jin, Y., Liu, W., et al. (2009). Allelochemical stress causes oxidative damage and inhibition of photosynthesis in *Chlorella vulgaris*. *Chemosphere* 75, 368–375. doi: 10.1016/j.chemosphere.2008.12.040

Schoemann, V., Becquevort, S., Stefels, J., Rousseau, W., and Lancelot, C. (2005). *Phaeocystis* blooms in the global ocean and their controlling mechanisms: a review. *J. Sea Res.* 53, 43–66. doi: 10.1016/j.seares.2004.01.008

Shi, R., Huang, H., Zhanhui, Q. I., Weian, H. U., and Tian, Z. (2012). Algicidal activity against *Prorocentrum micans* by a marine bacterium isolated from a HABs area, *South China. Acta Ecol. Sin.* 32, 4993–5001.

Teeling, H., Fuchs, B. M., Becher, K., Klockow, C., Gardebrecht, A., and Bennke, C. M. (2012). Substrate-controller succession of marine bacterioplankton populations induced by a phytoplankton bloom. *Science* 336, 608–611. doi: 10.1126/science.1218344

Valentine, J. S., Wertz, D. L., Lyons, T. J., Liou, L. L., Goto, J. J., and Gralla, E. B. (1998). The dark side of dioxygen biochemistry. *Curr. Opin. Chem. Biol.* 2, 253–262. doi: 10.1016/S1367-5931(98)80067-7

Wang, B. X., Yang, X. R., Zhou, Y. Y., Lv, J. L., Su, J. Q., Tian, Y., et al. (2012). An algicidal protein produced by bacterium isolated from the Donghai Sea, China. *Harmful Algae* 13:83.

Yamauchi, Y., Furutera, A., Seki, K., Toyoda, Y., Tanaka, K., and Sugimoto, Y. (2008). Malondialdehyde generated from peroxidized linolenic acid causes protein modification in heat-stressed plants. *Plant Physiol. Biochem.* 46, 786–793. doi: 10.1016/j.plaphy.2008.04.018

Yang, C. Y., Liu, S. J., Zhou, S. W., Wu, H. F., Yu, J. B., and Xia, C. H. (2011). Allelochemical ethyl 2-methyl acetoacetate (EMA) induces oxidative damage and antioxidant responses in *Phaeodactylum tricornutum*. *Pestic. Biochem. Phys.* 100, 93–103. doi: 10.1016/j.pestbp.2011.02.014

Zhang, B., Cai, G., Wang, H., Li, D., Yang, X., An, X., et al. (2014). Streptomyces alboflavus RPS and its novel and high algicidal activity against harmful algal bloom species *Phaeocystis globosa*. *PLoS One* 9:e92907. doi: 10.1371/journal.pone.0092907

Zhang, F. X., Ye, Q., Chen, Q. L., Yang, K., Zhang, D. Y., Chen, Z., et al. (2018). Algicidal activity of novel marine bacterium *Paracoccus* sp. strain Y42 against a harmful algal-bloom-causing dinoflagellate, *Prorocentrum donghaiense*. *Appl. Environ. Microb.* 84, e1015–e1018. doi: 10.1128/AEM.01015-18

Zhang, H. J., An, X. L., Zhou, Y. Y., Zhang, B. Z., Li, D., Chen, Z. R., et al. (2013). Effect of oxidative stress induced by *Brevibacterium* sp. BS01 on a HAB causing species-*Alexandrium tamarense*. *PLoS One* 5:e63018. doi: 10.1371/journal.pone.0063018

Zhang, S., Zheng, W., and Wang, H. (2020). Physiological response and morphological changes of *Heterosigma akashiwo* to an algicidal compound prodigiosin. *J. Hazard. Mater.* 385:121530. doi: 10.1016/j.jhazmat.2019.121530

Zhang, T. T., Zheng, C. Y., Hu, W., Xu, W. W., and Wang, H. F. (2010). The allelopathy and allelopathic mechanism of phenolic acids on toxic *Microcystis aeruginosa*. *J. Appl. Phycol.* 22, 71–77. doi: 10.1007/s10811-009-9429-6

Zhang, X., Song, T., Ma, H., and Li, L. (2016). Physiological response of *Microcystis aeruginosa* to the extracellular substances from an *Aeromonas* sp. *RSC Adv.* 6, 103662–103667. doi: 10.1039/c6ra17917g

Zheng, N. N., Ding, N., Gao, P. K., Han, M. A. X., Liu, X. X., Wang, J. G., et al. (2018). Diverse algicidal bacteria associated with harmful bloom-forming *Karenia mikimotoi* in estuarine soil and seawater. *Sci. Tol. Environ.* 631–632, 1415–1420. doi: 10.1016/j.scitotenv.2018.03.035

Zhou, L. H., Chen, X. H., and Zheng, T. L. (2010). Study on the ecological safety of algacides: a comprehensive strategy for their screening. *J. Appl. Phycol.* 22, 803–811. doi: 10.1007/s10811-010-9522-x

Zhuang, L., Zhao, L., and Yin, P. (2018). Combined algicidal effect of urocanic acid, N-acetylhistamine and l-histidine to harmful alga *Phaeocystis globosa*. *RSC Adv.* 8, 12760–12766. doi: 10.1039/c8ra00749g

Conflict of Interest: The authors declare that the research was conducted in the absence of any commercial or financial relationships that could be construed as a potential conflict of interest.

Publisher's Note: All claims expressed in this article are solely those of the authors and do not necessarily represent those of their affiliated organizations, or those of the publisher, the editors and the reviewers. Any product that may be evaluated in this article, or claim that may be made by its manufacturer, is not guaranteed or endorsed by the publisher.

frontiers in Microbiology

ORIGINAL RESEARCH
published: 02 December 2021
doi: 10.3389/fmicb.2021.791227

One-Step and Colorimetric Detection of Fish Freshness Indicator Hypoxanthine Based on the Peroxidase Activity of Xanthine Oxidase Grade I Ammonium Sulfate Suspension

Chen Guo[1], Shuhan You[1], Changmei Li[1], Tiantian Chen[2] and Xiudan Wang[1]**

[1] Shandong Provincial Key Laboratory of Biochemical Engineering, College of Marine Science and Biological Engineering, Qingdao University of Science and Technology, Qingdao, China, [2] CAS Key Laboratory of Marine Ecology and Environmental Sciences, Institute of Oceanology, Chinese Academy of Sciences, Qingdao, China

The global food waste problem, especially aquatic product spoilage, stimulates the accurate freshness analysis of food products. However, it still remains a great challenge to realize in-field determination of fish freshness at the time of use. In the present study, a colorimetric enzyme biosensor was developed for one-step detection of hypoxanthine (Hx), which is an important intermediate of adenosine triphosphate decomposition during fish storage. We demonstrate that xanthine oxidase grade I ammonium sulfate suspension (XOD-ASS) possesses peroxidase activity. It can oxidize different peroxidase substrates, including 3,3′,5,5′-tetramethylbenzidine, 2,2′-azino-bis(3-ethylbenzothiazoline-6-sulfonic acid) diammonium salt, and o-phenylenediamine in the presence of H_2O_2, producing visible color reactions. Further experiments indicate that XOD-ASS displayed effective peroxidase activity and could be used for H_2O_2 detection. Based on this, a one-step Hx detection method was established using only XOD-ASS as the catalyst. The method displays a good linear relationship in the range from 20 to 100 μM with a detection limit of 6.93 μM. Additionally, we successfully applied this method in testing Hx accumulation in sea bass fish samples of different storage times. The recovery values range from 97.44 to 102.56%. It is exciting to note that, compared with other methods, our proposed method provides a robust advantage on the economic reaction system, ease of preparation, short time consumption, and moderate reaction temperature. We believe that this method shows good application prospects for on-site fish freshness determination.

Keywords: hypoxanthine, fish freshness, colorimetric, one-step detection, XOD-ASS

OPEN ACCESS

Edited by:
Tian Li,
Nankai University, China

Reviewed by:
Sun Haixin,
Qingdao University, China
Xiaojia He,
Emory University, United States

****Correspondence:***
Xiudan Wang
wangxiudan@qust.edu.cn
Tiantian Chen
chentian0819@163.com

Specialty section:
This article was submitted to Microbiotechnology, a section of the journal Frontiers in Microbiology

Received: *08 October 2021*
Accepted: *28 October 2021*
Published: *02 December 2021*

Citation:
Guo C, You S, Li C, Chen T and Wang X (2021) One-Step and Colorimetric Detection of Fish Freshness Indicator Hypoxanthine Based on the Peroxidase Activity of Xanthine Oxidase Grade I Ammonium Sulfate Suspension. Front. Microbiol. 12:791227. doi: 10.3389/fmicb.2021.791227

INTRODUCTION

Nowadays, there are increasing requirements and regulations in the fields of biotechnology control, environmental protection, and food/water quality certification (Flachsbarth et al., 2015). A rising number of clinical diagnoses and veterinary tests are required regarding human and animal health (Görgülü et al., 2013). Therefore, developing rapid, easy, economic, and accurate analysis methods may aid in these processes and general laboratory tasks.

In the food industry, especially aquatic products, which are highly perishable with a limited shelf-life after slaughter, the global waste problem stimulates the accurate freshness analysis of food products (Prabhakar et al., 2020). Traditionally, to meet the freshness standard, consumers mainly rely on a sensory approach to discriminate fresh fish products, and it is highly dependent on consumers' level of perception and experience. Fishing factories try to record the capture or slaughter date of the products, but different storage or processing methods can greatly affect fish freshness. These methods are rapid and easy to carry out, but they are unreliable to assess fish freshness especially before the initial stages of spoilage.

Recently, estimating fish freshness has been widely investigated at the chemical, biochemical, and microbiological levels (Gil et al., 2011; Prabhakar et al., 2020). Various biomarkers, such as trimethylamine (TMA) and total volatile basic nitrogen (TVB-N), metabolites of adenosine triphosphate (ATP) degradation, and microbial count and activity were established as indicators of fish freshness (Cela-Pérez et al., 2015; Cheng and Sun, 2015; Peleg, 2016). TMA and TVB-N are widely preferred for assessment of fish quality and shelf life, but they lag behind as great indicators because they mainly indicate the later stages of fish spoilage (Sykes et al., 2009). Nucleotide and nucleoside metabolites produced by ATP decomposition has been demonstrated as one of the most important reasons that affect the freshness and quality of fish products (Shen et al., 1996; Carsol et al., 1997; Albelda et al., 2017). Compared with other indicators, hypoxanthine (Hx), which is an important intermediate of ATP metabolism, accumulates right after the fish is slaughtered (Cela-Pérez et al., 2015; Albelda et al., 2017). Therefore, the evaluation of Hx has the potential to determine the early stages of fish spoilage.

Hypoxanthine determination can be achieved using classic methods, such as high performance liquid chromatography (Fukuuchi et al., 2013; Qu et al., 2017) and spectrophotometric measurements (Amigo et al., 2005; Weeranantanaphan et al., 2011). These methods, in general, require expensive equipment and skilled technicians, which confines them to specialized laboratories. The emerging use of biosensors has the potential to provide simple and rapid determination platforms to overcome these challenges. The majority of developed biosensors involve a reaction that xanthine oxidase (XOD) could catalyze the oxidization of Hx and xanthine in the presence of oxygen to generate hydrogen peroxide (H_2O_2) and uric acid (UA) (Kelley et al., 2010). Then, the Hx or xanthine concentration can be determined by measuring the produced H_2O_2, UA or consumed O_2, producing an electrochemical, fluorescent, or colorimetric signal (Görgülü et al., 2013; Wu et al., 2018; Chen et al., 2020). Electrochemical biosensors can achieve fast and easy detection, but they require a potentiostat to measure the voltammetric current (Görgülü et al., 2013; Albelda et al., 2017). Fluorescent and colorimetric sensors have been widely developed by combining XOD with peroxidase or nanoenzymes with peroxidase-like activity. For example, Li et al. (2008) develop a spectrophotometric quantitation method to detect xanthine by conjugating XOD with horseradish peroxidase. A series of colorimetric or fluorescent biosensors based on the production of H_2O_2 by XOD and peroxidase-like catalytic activity of nanoenzymes, including platinum nanoparticles (Chen et al., 2020), selenium-doped graphite carbon nitride (Qiao et al., 2015), and amino-functionalized metal organic framework (Hu et al., 2018) are also established, contributing to the rapid freshness evaluation of aquatic products. In these reactions, a two-step catalytic reaction is adopted: First, XOD catalyzes the reaction of Hx or xanthine with oxygen, yielding H_2O_2; second, H_2O_2 participates in the peroxide reaction catalyzed by a peroxidase or peroxidase mimic enzyme.

In the present study, we find that XOD grade I ammonium sulfate suspension (XOD-ASS) possesses peroxidase activity; it can not only catalyze the oxidization of Hx or xanthine to produce H_2O_2, but catalyze the oxidization of 3,3′,5,5′-tetramethylbenzidine (TMB) (colorless) by H_2O_2 to produce oxidized TMB (blue). Based on this, we further propose an easy, one-step, colorimetric method for Hx detection using only XOD-ASS as the catalyst. We demonstrate the utility of our method in fish samples and realize on-site, quantitative detection of Hx, providing a cheap, easy fish-freshness evaluation method.

MATERIALS AND METHODS

Materials

Xanthine oxidase grade I ammonium sulfate suspension was purchased from Sigma-Aldrich (St. Louis, MO, United States) and used as received. Hx standard of chromatographically pure was obtained from Solarbio (Beijing, China). UA, 30% H_2O_2, glucose, glycine, ascorbic acid, cysteine, and inosine were provided by Aladdin Reagents (Shanghai, China). TMB, 2,2′-azino-bis(3-ethylbenzothiazoline-6-sulfonic acid) diammonium salt (ABTS), and o-phenylenediamine (OPD) were bought from Macklin Biochemical (Shanghai, China). Other chemicals were of analytical grade, and all compounds used in this work were prepared without any further purification. All solutions were prepared with distilled deionized water purified by a Milli-Q Purification System (Millipore, MA, United States).

The Oxidation of 3,3′,5,5′-Tetramethylbenzidine Catalyzed by Xanthine Oxidase Grade I Ammonium Sulfate Suspension

3,3′,5,5′-tetramethylbenzidine and H_2O_2 were used to examine the peroxidase activity of XOD-ASS. The reaction was performed in a 100-μL system (20 mM sodium citric buffer, pH = 5.0) containing 0.1 U/mL XOD-ASS (one unit converts 1.0 μmole of xanthine to UA per min at pH 7.5 at 25°C), 1 mM TMB, and 1 mM H_2O_2 and incubated at room temperature for 10 min. Then, the UV-vis spectrum of 400 to 800 nm was recorded with a microplate reader (Tecan i-control, Infinite M1000 PRO, Switzerland). The steady-state kinetics of XOD was recorded at 652 nm using a time-scan model of the microplate reader. Reactions without XOD-ASS or H_2O_2 were set as controls. The peroxidase activity of XOD-ASS was further verified using two other peroxidase substrates, OPD and ABTS, and the reaction system used for OPD and ABTS was the same as that for TMB. To obtain the optimal reaction conditions, the reaction

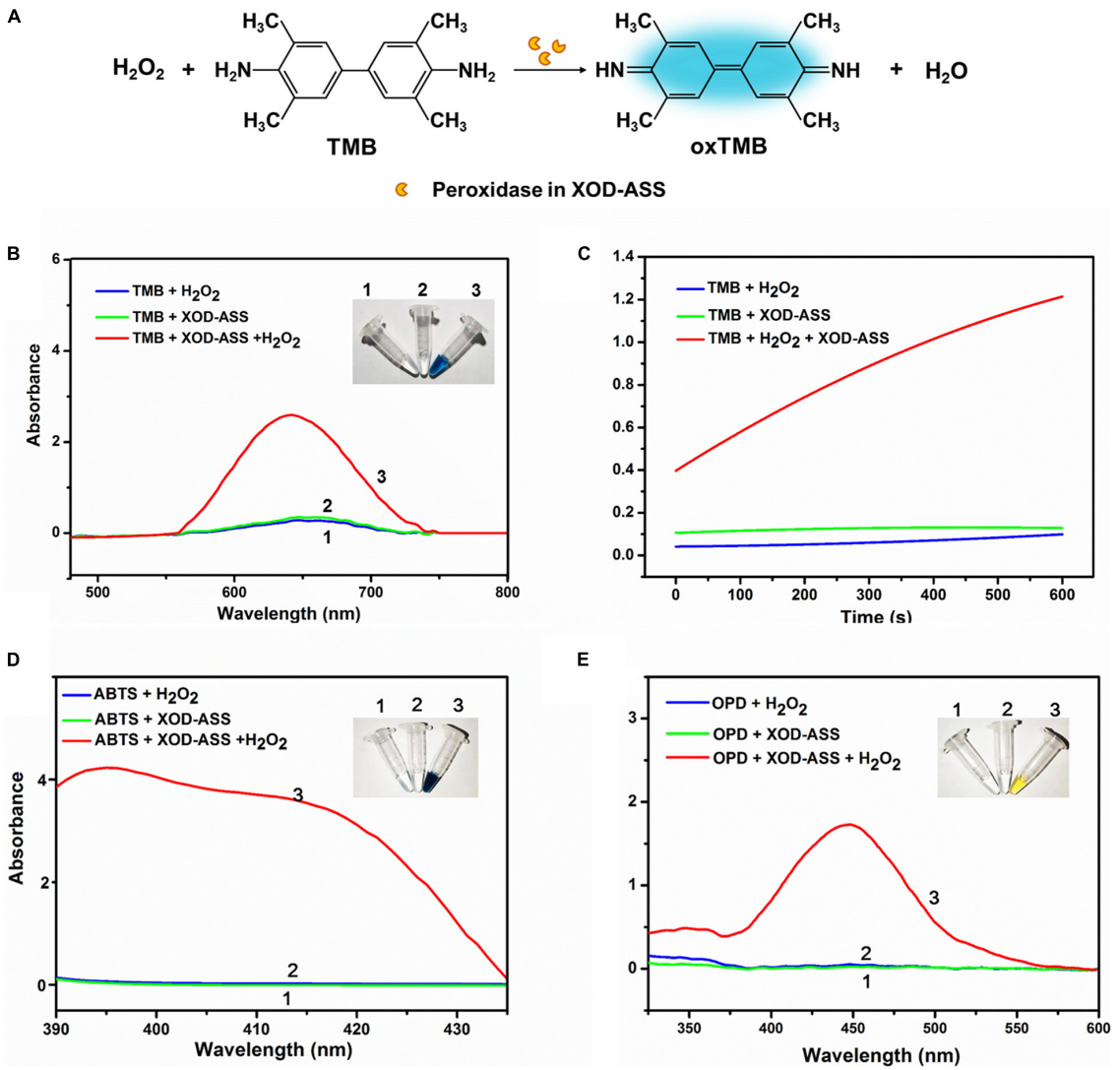

FIGURE 1 | XOD-ASS shows peroxidase activity. **(A)** Scheme illustration of oxidation of TMB into oxidized TMB by XOD-ASS. **(B)** The absorbance spectrum of XOD-ASS catalyzing the oxidation of TMB in the presence of H_2O_2. Inset represents the corresponding colorimetric result of the reactions. **(C)** The time-dependent absorbance curve at 652 nm of the reactions. **(D)** The absorbance spectrum of XOD-ASS catalyzing the oxidation of ABTS in the presence of H_2O_2. Inset represents the corresponding colorimetric result of the reactions. **(E)** The absorbance spectrum of XOD-ASS catalyzing the oxidation of OPD in the presence of H_2O_2. Inset represents the corresponding colorimetric result of the reactions.

was first incubated at a temperature from 20°C to 65°C and then in different buffer solutions with pH values from 3 to 10. Standard reaction conditions were then adopted with varying concentrations of TMB (0.1-2 mM) at a fixed concentration of H_2O_2 (1 mM) or varying concentrations of H_2O_2 (0.2-10 mM) at a fixed concentration of TMB (1 mM).

Hypoxanthine Detection Using Xanthine Oxidase Grade I Ammonium Sulfate Suspension and Selectivity Study

For Hx detection, the concentration of XOD-ASS was optimized from 0.0125 to 0.2 U/mL (concentrations of XOD), and the concentration of TMB was optimized from 0.0125 to 1.0 mM. The reaction temperature was optimized at 25°C, 37°C, and 50°C. At the optimal reaction condition, Hx detection was performed in a 100-μL system (20 mM sodium citric buffer, pH = 5.0) with variable concentrations of Hx from 0.02 to 1.0 mM. After incubation at room temperature for 10 min, the absorbance signal at 652 nm was recorded by the microplate reader.

To determine the selectivity of the detection method, a series of common substrates, including glucose, glycine, ascorbic acid, UA, cystine, and inosine with concentrations of 1 mM were adopted as interferences.

Detection of Hypoxanthine in Fish Samples

Live sea bass was bought from the local market and slaughtered to obtain fresh fish filets. In total, 24 pieces of fish filet (about 10 g/each) were randomly divided into eight groups and were left to decay for 0, 1, 3, 6, 12, 24, 36, and 48 h at room temperature,

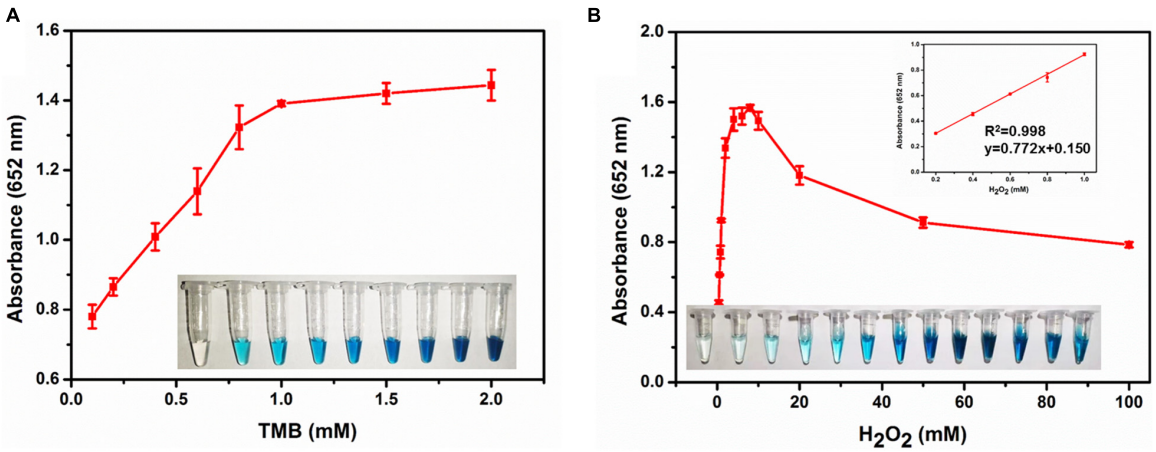

FIGURE 2 | (A) The absorbance at 652 nm in different concentrations of TMB. Inset represents the corresponding colorimetric result of the reactions. **(B)** The absorbance at 652 nm in different concentrations of H_2O_2. Inset represents the corresponding colorimetric result of the reactions and the linear calibration plot for H_2O_2.

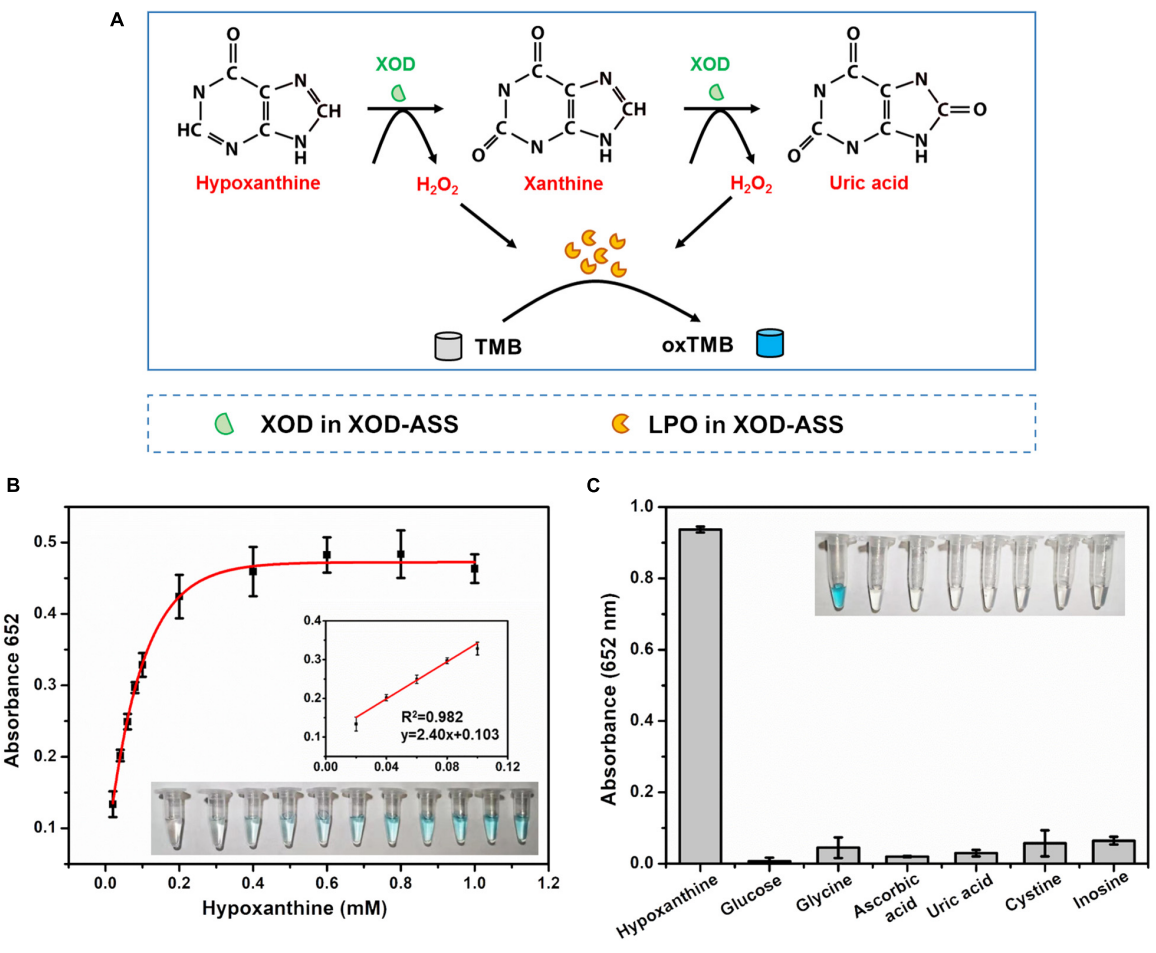

FIGURE 3 | (A) Schematic illustration of one-step and colorimetric detection of Hx catalyzed by XOD-ASS. **(B)** The absorbance at 652 nm in different concentrations of Hx. Inset represents the corresponding colorimetric result of the reactions and the linear calibration plot for Hx. **(C)** Selectivity of the established one-step Hx detection method.

respectively. At each time point, three replicates of fish filet were, respectively, minced with a mortar and pestle and stored at −20°C until analysis. For analysis, a fish meat sample of 1 g was mixed with 10 mL distilled water and homogenized using an ultrasonic homogenizer for 15 min. The homogenous mixture was centrifuged at 12,000 rpm for 10 min at 4°C, and the obtained supernatant was diluted three times with distilled water. Two samples of fish extract (3 and 6 h) were spiked with standard Hx solutions with final concentration of 10, 15, and 25 μM. To perform Hx analysis, 20 μL of the fish extract (or spiked fish extract) was mixed with 80 μL sodium citric buffer system (the final mixture contained 0.025 U/mL XOD-ASS, 0.2 mM TMB, and 20 mM sodium citric). The mixture was incubated at room temperature for 10 min, and the absorbance signal at 652 nm was recorded by the microplate reader.

Statistical Analysis

All experiments were performed at least in triplicate, and the results were presented as mean ± standard deviation and analyzed by SPSS 16.0. Significant differences among groups were evaluated by one-way analysis of variance (ANOVA) and linear regression analysis was performed. It was considered significantly different at $p < 0.05$. Origin Pro 7.5 software was used to prepare the figures.

RESULTS AND DISCUSSION

Xanthine Oxidase Grade I Ammonium Sulfate Suspension Catalyzes the Oxidation of Peroxidase Substrates

Typically, peroxidase catalyzes the oxidation of TMB and displays a significant color change from colorless to blue in the presence of H_2O_2 (Gao et al., 2007). First, we investigated the peroxidase activity of XOD-ASS using the typical peroxidase substrate TMB (**Figure 1A**). The result demonstrates that XOD-ASS catalyzed the reaction of substrate TMB in the presence of H_2O_2, producing oxidized TMB with a blue color (**Figure 1B**, inset). No color signal was observed for the reactions without XOD-ASS or H_2O_2, indicating XOD-ASS and H_2O_2 were both necessary for the oxidation of TMB. Spectroscopic analysis revealed the maximum absorption wavelength at 652 nm (**Figure 1B**), which corresponded with previous research (Gao et al., 2007; Yang et al., 2019). At the same time, the time course curves of the reactions were monitored at 652 nm (**Figure 1C**) within 600 s, confirming that the catalysis of the reaction was time-dependent, and a minimal signal was observed in the absence of XOD-ASS or H_2O_2. The peroxidase activity of XOD-ASS was further characterized by replacing TMB with other substrates ABTS and OPD. **Figures 1D,E** shows that XOD-ASS could not only catalyze the oxidation of TMB, but also ABTS to produce a color change from colorless to dark green and OPD to produce a yellow color. These results confirm that XOD-ASS possesses peroxidase activity toward three different peroxidase substrates.

Based on the spectroscopic and colorimetric results, we deduce that XOD-ASS might contain lactoperoxidase (LPO) from milk. To verify our deduction, sodium dodecyl sulfate-polyacrylamide gel electrophoresis (SDS-PAGE) was performed to detect the protein components of XOD-ASS. As shown in **Supplementary Figure 1**, multiple bands were identified in the SDS-PAGE result, demonstrating that XOD-ASS is a crude extract of bovine milk. Particularly, the two bands with the largest quantity are about 150 and 75 kDa, corresponding to the molecular weight of XOD (Enroth et al., 2000) and LPO (Atasever et al., 2013), respectively. LPO is the second most abundant enzyme in bovine milk after XOD, and the concentration can be as high as 1–19 U/mL milk (de Wit and van Hooydonk, 1996). They act together *in vivo* to generate reactive oxygen species and reactive nitrogen species, which is referred to as the "XOD-LPO" system (Al-Shehri et al., 2020). Therefore, it is reasonable that XOD-ASS contains LPO. Considering the lower cost and easier preservation, XOD-ASS might have the potential to develop a one-step Hx detection method using only XOD-ASS as the catalyst without conjugating XOD with other peroxidases or peroxidase mimic enzymes.

Steady-State Kinetics Assay

On the basis of the peroxidase catalytic activity of XOD-ASS, we investigated the optimal reaction condition of the oxidation of TMB catalyzed by XOD-ASS. As shown in

TABLE 1 | Analytical results of Hx and spiked Hx in fish extracts.

Sample	Original (μM)	Spiked (μM)	Found (μM)	Recovery (%)	RSD (%)
Sample 1 (3 h)	19.04	10	28.91	98.72	4.44
		15	33.65	97.44	5.13
		20	39.29	101.28	2.94
Sample 2 (6 h)	27.37	10	37.63	102.56	2.22
		15	41.99	97.44	2.56
		20	46.99	98.08	3.33

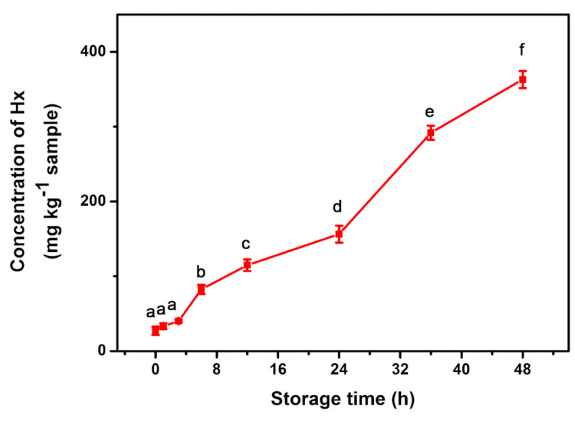

FIGURE 4 | Detection of Hx in sea bass fish sample during storage for 48 h at room temperature. Different lowercase letters indicate Hx concentrations in fish samples of different storage time are significantly different ($p < 0.05$).

TABLE 2 | Comparison of different Hx detection methods.

Catalysts	Steps	Target	Reaction temperature and time	Result readout	LOD	References
XOD + HRP	2	Hx	37°C, 8 min	A508	0.05 mM	Li et al., 2008
XOD + Selenium dopedgraphitic carbon nitride nanosheets	2	Hx	(1) 25°C, 60 min (2) 25°C, immediately	A652	0.016 μM	Qiao et al., 2015
XOD + Amino-functionalized metal organic framework	2	Hx	(1) 25°C, 40 min (2) 25°C, 10 min	Fluorescence intensity	3.93 μM	Hu et al., 2018
XOD + Platinum nanoparticles	2	Hx	(1) 37°C, 30 min (2) 37°C, 30 min	Fluorescence intensity	2.88 μM	Chen et al., 2020
XOD + BSA-stabilized Au clusters	2	Xanthine	(1) 37°C, 15 min (2) 40°C, 10 min	A652	0.5 μM	Wang et al., 2011
XOD + $MoSe_2$ nanosheets	2	Xanthine	(1) 25°C, 20 min (2) 25°C, immediately	A652	1.96 μM	Wu et al., 2018
XOD-ASS	1	Hx	25°C, 10 min	A652	6.93 μM	This work

Supplementary Figure 2, the relative activity reached the maximum at 50°C and pH 5.0, respectively. Then, substrate-dependent kinetic analysis was carried out by changing the concentration of one substrate while the concentration of another one was kept constant. As shown in **Figure 2A**, the absorbance value at 652 nm increased with substrate TMB ranging from 0.1 to 1 mM, and the value came to a plateau at higher concentrations. The color variation for the TMB response could be seen with the naked eye (**Figure 2A** inset). The color and the absorbance value were positively correlated with substrate H_2O_2 ranging from 0.2 to 8 mM, but a higher concentration could inhibit the oxidation reaction (**Figure 2B**). The absorbance value at 652 nm was linear with H_2O_2 concentration in the range from 0.2 to 1.0 mM with a correlation coefficient (R^2) of 0.998. The linear equation was calculated to be $y = 0.772x + 0.150$ (y represents absorbance 652 nm, and x represents the concentration of H_2O_2). Our results demonstrate that XOD-ASS contains effective peroxidase activity and could be used for H_2O_2 detection.

Sensitivity and Specificity for Detection Hypoxanthine

We further develop a one-step Hx detection method using the XOD-ASS mixture as the catalyst. XOD-ASS could not only catalyze the oxidization of Hx or xanthine to produce H_2O_2 (XOD functions in this reaction), but catalyzes the oxidization of TMB (colorless) by H_2O_2 to produce oxidized TMB (blue) (LPO might function in this reaction) (**Figure 3A**). The parameters that might affect the performance of the detection were optimized (**Supplementary Figure 3**), and the optimal conditions were adopted to detect Hx. As shown in **Figure 3B**, the color variation of TMB oxidation was dependent on the concentration of Hx, and the absorbance at 652 nm was regularly enhanced with increasing Hx concentration. The corresponding calibration curve (**Figure 3B** inset) displayed the linear relationship between the absorbance value and Hx concentration in the range from 20 to 100 μM ($R^2 = 0.998$, $p = 0.00091 < 0.05$). The detection limit was calculated based on a triple standard deviation of blank samples (S/N = 3, S represents sensitivity and N represents noise), and it was determined to be 6.93 μM, which is much lower than the threshold of Hx concentration in fresh aquatic products and could satisfy the application in evaluating fish freshness (Chen et al., 2020). According to a previous study, Hx concentration is lower than 529 μM in fresh aquatic products (Chen et al., 2020), so the analytical sensitivity of our method is sufficient for aquatic product freshness evaluation. The selectivity performance of our established one-step Hx detection method was further investigated by determining the effect of potentially coexisting substances, including glucose, glycine, ascorbic acid, UA, cysteine, and inosine (**Figure 3C**). The results indicate that no absorbance was obtained for these substances except Hx, demonstrating good selectivity of our XOD-ASS–based, one-step Hx detection method.

Method Validation and Detection of Hypoxanthine in the Fish Products

A standard addition method was further applied to evaluate the effectiveness of our method. Different concentrations of Hx (10, 15, and 25 μM) were added to diluted fish extracts. As shown in **Table 1**, our results show good recoveries from 97.44% to 102.56%, demonstrating satisfactory applicability of the method in real sample detection.

To explore the practical application of the developed method, sea bass fish samples at various times ranging from 1 to 48 h after death were tested for Hx accumulation. It is known that Hx starts to accumulate immediately following ATP degradation after the fish is slaughtered (Cela-Pérez et al., 2015). Our assay exhibited a gradually increasing trend during the storage process of the sea bass fish sample (**Figure 4**). Similar trends of Hx were also observed in fish such as tilapia and shrimp in previous reports (Chen et al., 2020; Mustafa et al., 2021), indicating the high efficiency and potential application of the method in real sample extracts. The obtained concentration of Hx can be related to fish-freshness monitoring. Previous studies give suggested levels of Hx in subfresh and decayed fish. For example, Qiong et al. (1998) suggest that, for *Mylopharyngodon piceus*, an Hx concentration (C_{Hx}) of ≤72 mg/kg indicates fresh; 72 mg/kg < C_{Hx} ≤ 118 mg/kg indicates subfresh; >118 mg/kg indicates spoiled. According to the national standard of China, aquatic products are considered to be fresh

when the concentration of Hx is lower than 529 μM (Chen et al., 2020). Based on these suggestions and standards, sea bass fish samples were considered fresh during 0–6 h (C_{Hx} lower than 82 mg/kg) storage at room temperature, started to deteriorate during 6–12 h (C_{Hx} of 82–115 mg/kg, subfresh, edible), and became spoiled after 12 h (no longer dietary is suggested), but these levels need further validation with TVB-N levels, and they may vary in other types of fish. Therefore, it is essential to establish a database of Hx concentrations for different kinds of fish, and this method will just meet future need as a general platform for freshness screening.

We compare our one-step Hx detection method with previously reported biosensors, which conjugate XOD with peroxidase or peroxidase-mimic nanoenzymes (**Table 2**). Compared with these methods, our proposed method requires a one-step reaction and 10 min room temperature incubation to realize the colorimetric detection of Hx. Besides this, the method involves only one catalyst XOD-ASS, which is less expensive than other forms of XOD as revealed by the Sigma official website. Based on the price of XOD-ASS and the reagents used, a cost estimate of the XOD-ASS–based solution assay per sample is about ¥0.2 ($0.03), and the cost of nanoenzyme/XOD biosensor per sample is about $0.11 and $3.4 per test for a commercial assay (Mustafa et al., 2021). Therefore, the established one-step Hx detection method provides a robust advantage on economic reaction system, short time consumption, and moderate reaction temperature, providing a simple choice for on-site fish freshness determination.

CONCLUSION

In this work, we first report that XOD-ASS contains effective peroxidase (LPO) and can be used for H_2O_2 detection. Based on this, a simple, inexpensive, and one-step Hx detection method using only XOD-ASS as the catalyst is established. The quantification of Hx displays a linear range of 20–100 μM with a detection limit of 6.93 μM. Besides this, the method has a good selectivity and shows satisfactory applicability in fish sample evaluation with good recoveries. Considering the low cost, ease of preparation, and visual detection, this method shows good application prospects for on-site fish-freshness determination.

DATA AVAILABILITY STATEMENT

The original contributions presented in the study are included in the article/**Supplementary Material**, further inquiries can be directed to the corresponding author/s.

AUTHOR CONTRIBUTIONS

CG, SY, and CL designed and conducted the experiments. TC and XW conceived and supervised the project. XW managed the funding acquisition. CG and SY compiled and analyzed the output data, and designed and wrote the first version of the manuscript. All authors edited and approved the final version of the manuscript.

FUNDING

This study was supported by the National Key Research and Development Program of China (No. 2019YFD0901705) from the Ministry of Science and Technology of the People's Republic of China.

SUPPLEMENTARY MATERIAL

The Supplementary Material for this article can be found online at: https://www.frontiersin.org/articles/10.3389/fmicb.2021.791227/full#supplementary-material

REFERENCES

Albelda, J. A. V., Uzunoglu, A., Santos, G. N. C., and Stanciu, L. A. (2017). Graphene/titianium dioxide nanocomposite-based hypoxanthine sensor for assessment of meat freshness. *Biosens. Bioelectron.* 89, 518–524. doi: 10.1016/j.bios.2016.03.041

Al-Shehri, S. S., Duley, J. A., and Bansal, N. (2020). Xanthine oxidase-lactoperoxidase system and innate immunity: biochemical actions and physiological roles. *Redox Biol.* 34:101524. doi: 10.1016/j.redox.2020.101524

Amigo, J. M., Coello, J., and Maspoch, S. (2005). Three-way partial least-squares regression for the simultaneous kinetic-enzymatic determination of xanthine and hypoxanthine in human urine. *Anal. Bioanal. Chem.* 382, 1380–1388. doi: 10.1007/s00216-005-3275-4

Atasever, A., Ozdemir, H., Gulcin, I., and Kufrevioglu, O. I. (2013). One-step purification of lactoperoxidase from bovine milk by affinity chromatography. *Food Chem.* 136, 864–870. doi: 10.1016/j.foodchem.2012.08.072

Carsol, M.-A., Volpe, G., and Mascini, M. (1997). Amperometric detection of uric acid and hypoxanthine with xanthine oxidase immobilized and carbon based screen-printed electrode. Application for fish freshness determination. *Talanta* 44, 2151–2159. doi: 10.1016/S0039-9140(97)00098-2

Cela-Pérez, M. C., Barbosa-Pereira, L., Vecino, X., Pérez-Ameneiro, M., Latorre, A. L., López-Vilariño, J. M., et al. (2015). Selective removal of ATP degradation products from food matrices II: rapid screening of hypoxanthine and inosine by molecularly imprinted matrix solid-phase dispersion for evaluation of fish freshness. *Talanta* 135, 58–66. doi: 10.1016/j.talanta.2014.12.037

Chen, J., Lu, Y., Yan, F., Wu, Y., Huang, D., and Weng, Z. (2020). A fluorescent biosensor based on catalytic activity of platinum nanoparticles for freshness evaluation of aquatic products. *Food Chem.* 310:125922. doi: 10.1016/j.foodchem.2019.125922

Cheng, J. H., and Sun, D. W. (2015). Rapid quantification analysis and visualization of *Escherichia coli* loads in grass carp fish flesh by hyperspectral imaging method. *Food Bioprocess Technol.* 8, 951–959. doi: 10.1007/s11947-014-1457-9

de Wit, J. N., and van Hooydonk, A. C. M. (1996). Structure, functions and applications of lactoperoxidase in natural antimicrobial systems. *Neth. Milk Dairy J.* 50, 227–244.

Enroth, C., Eger, B. T., Okamoto, K., Nishino, T., Nishino, T., and Pai, E. F. (2000). Crystal structures of bovine milk xanthine dehydrogenase and xanthine oxidase: structure-based mechanism of conversion. *Proc. Natl. Acad. Sci. U.S.A.* 97, 10723–10728. doi: 10.1073/pnas.97.20.10723

Flachsbarth, I., Willaarts, B., Xie, H., Pitois, G., Mueller, N. D., Ringler, C., et al. (2015). The role of Latin America's land and water resources for global food security: environmental trade-offs of future food production pathways. *PLoS One* 10:e0116733. doi: 10.1371/journal.pone.0116733

Fukuuchi, T., Yasuda, M., Inazawa, K., Ota, T., Yamaoka, N., Mawatari, K. I., et al. (2013). A simple HPLC method for determining the purine content of beer and beer-like alcoholic beverages. *Anal. Sci.* 29, 511–517. doi: 10.2116/analsci.29.511

Gao, L., Zhuang, J., Nie, L., Zhang, J., Zhang, Y., Gu, N., et al. (2007). Intrinsic peroxidase-like activity of ferromagnetic nanoparticles. *Nat. Nanotechnol.* 2, 577–583. doi: 10.1038/nnano.2007.260

Gil, L., Barat, J. M., Baigts, D., Martinez-Manez, R., Soto, J., Garcia-Breijo, E., et al. (2011). Monitoring of physical–chemical and microbiological changes in fresh pork meat under cold storage by means of a potentiometric electronic tongue. *Food Chem.* 126, 1261–1268. doi: 10.1016/j.foodchem.2010.11.054

Görgülü, M., Çete, S., Arslan, H., and Yaşar, A. (2013). Preparing a new biosensor for hypoxanthine determination by immobilization of xanthine oxidase and uricase in polypyrrole-polyvinyl sulphonate film. *Artif. Cells Blood Substit. Biotechnol.* 41, 327–331. doi: 10.3109/21691401.2012.744993

Hu, S., Yan, J., Huang, X., Guo, L., Lin, Z., Luo, F., et al. (2018). A sensing platform for hypoxanthine detection based on amino-functionalized metal organic framework nanosheet with peroxidase mimic and fluorescence properties. *Sens. Actuators B* 267, 312–319. doi: 10.1016/j.snb.2018.04.055

Kelley, E. E., Khoo, N., Hundley, N. J., Malik, U. Z., Freeman, B. A., and Tarpey, M. M. (2010). Hydrogen peroxide is the major oxidant product of xanthine oxidase. *Free Radic. Biol. Med.* 48, 493–498. doi: 10.1016/j.freeradbiomed.2009.11.012

Li, Z., Wu, M., Xu, X., and Wang, W. (2008). Catalytic spectrophotometric quantitation for hypoxanthine by conjugating xanthine oxidase with horseradish peroxidase. *Spectrosc. Spectr. Anal.* 28, 2169–2172. doi: 10.1080/10286600801908949

Mustafa, F., Othman, A., and Andreescu, S. (2021). Cerium oxide-based hypoxanthine biosensor for fish spoilage monitoring. *Sens. Actuators B* 332:129435. doi: 10.1016/j.snb.2021.129435

Peleg, M. (2016). A kinetic model and endpoints method for volatiles formation in stored fresh fish. *Food Res. Int.* 86, 156–161. doi: 10.1016/j.foodres.2016.06.004

Prabhakar, P. K., Vatsa, S., Srivastav, P. P., and Pathak, S. S. (2020). A comprehensive review on freshness of fish and assessment: analytical methods and recent innovations. *Food Res. Int.* 133:109157. doi: 10.1016/j.foodres.2020.109157

Qiao, F., Wang, J., Ai, S., and Li, L. (2015). As a new peroxidase mimetics: the synthesis of selenium doped graphitic carbon nitride nanosheets and applications on colorimetric detection of H_2O_2 and xanthine. *Sens. Actuators B* 216, 418–427. doi: 10.1016/j.snb.2015.04.074

Qiong, C., Tuzhi, P., and Liju, Y. (1998). Silk fibroin/cellulose acetate membrane electrodes incorporating xanthine oxidase for the determination of fish freshness. *Anal. Chim. Acta* 369, 245–251. doi: 10.1016/S0003-2670(98)00213-X

Qu, X., Sui, J., Mi, N., and Lin, H. (2017). Determination of four different purines and their content change in seafood by high-performance liquid chromatography. *J. Sci. Food Agric.* 97, 520–525. doi: 10.1002/jsfa.7755

Shen, L., Yang, L., and Peng, T. (1996). Amperometric determination of fish freshness by a hypoxanthine biosensor. *J. Sci. Food Agric.* 70, 298–302. doi: 10.1002/(SICI)1097-0010(199603)70:3<298::AID-JSFA499<3.0.CO;2-1

Sykes, A. V., Oliveira, A. R., Domingues, P. M., Cardoso, C. M., Andrade, J. P., and Nunes, M. L. (2009). Assessment of European cuttlefish (*Sepia officinalis*, L.) nutritional value and freshness under ice storage using a developed Quality Index Method (QIM) and biochemical methods. *Food Sci. Technol.* 42, 424–432. doi: 10.1016/j.lwt.2008.05.010

Wang, X. X., Wu, Q., Shan, Z., and Huang, Q. M. (2011). BSA-stabilized Au clusters as peroxidase mimetics for use in xanthine detection. *Biosens. Bioelectron.* 26, 3614–3619. doi: 10.1016/j.bios.2011.02.014

Weeranantanaphan, J., Downey, G., Allen, P., and Sun, D. W. (2011). A review of near infrared spectroscopy in muscle food analysis: 2005-2010. *J. Near Infrared Spectrosc.* 19, 61–104. doi: 10.1255/jnirs.924

Wu, X., Chen, T., Wang, J., and Yang, G. (2018). Few-layered $MoSe_2$ nanosheets as an efficient peroxidase nanozyme for highly sensitive colorimetric detection of H_2O_2 and xanthine. *J. Mater. Chem. B* 6, 105–111. doi: 10.1039/c7tb02434g

Yang, W., Li, J., Liu, M., Ng, D. H. L., Liu, Y., Sun, X., et al. (2019). Bioinspired hierarchical CoAl-LDH/MFe_2O_4(Ni, Zn, Co) as peroxidase mimics for colorimetric detection of glucose. *Appl. Clay Sci.* 181:105238. doi: 10.1016/j.clay.2019.105238

Conflict of Interest: The authors declare that the research was conducted in the absence of any commercial or financial relationships that could be construed as a potential conflict of interest.

Publisher's Note: All claims expressed in this article are solely those of the authors and do not necessarily represent those of their affiliated organizations, or those of the publisher, the editors and the reviewers. Any product that may be evaluated in this article, or claim that may be made by its manufacturer, is not guaranteed or endorsed by the publisher.

frontiers in Microbiology

ORIGINAL RESEARCH
published: 08 December 2021
doi: 10.3389/fmicb.2021.771463

Bioaugmentation of Atrazine-Contaminated Soil With *Paenarthrobacter* sp. Strain AT-5 and Its Effect on the Soil Microbiome

Weibin Jia, Ning Li, Tunan Yang, Weixian Dai, Jiandong Jiang, Kai Chen and Xihui Xu**

Department of Microbiology, Key Laboratory of Environmental Microbiology for Agriculture, Ministry of Agriculture, College of Life Sciences, Nanjing Agricultural University, Nanjing, China

OPEN ACCESS

Edited by:
Xiaojing Li, Agro-Environmental Protection Institute, Chinese Academy of Agricultural Sciences (CAAS), China

Reviewed by:
Wei Wang, Zhejiang University, China
Liliana Pardo Lopez, National Autonomous University of Mexico, Mexico
Mohammad Mehdizadeh, University of Mohaghegh Ardabili, Iran

***Correspondence:**
Kai Chen
chenkai@njau.edu.cn
Xihui Xu
xuxihui@njau.edu.cn

Specialty section:
This article was submitted to Microbiotechnology, a section of the journal Frontiers in Microbiology

Received: *06 September 2021*
Accepted: *12 November 2021*
Published: *08 December 2021*

Citation:
Jia W, Li N, Yang T, Dai W, Jiang J, Chen K and Xu X (2021) Bioaugmentation of Atrazine-Contaminated Soil With Paenarthrobacter sp. Strain AT-5 and Its Effect on the Soil Microbiome. Front. Microbiol. 12:771463. doi: 10.3389/fmicb.2021.771463

Atrazine, a triazine herbicide, is widely used around the world. The residue of atrazine due to its application in the fore-rotating crop maize has caused phytotoxicity to the following crop sweet potato in China. Bioaugmentation of atrazine-contaminated soil with atrazine-degrading strains is considered as the most potential method to remove atrazine from soil. Nevertheless, the feasibility of bioaugmentation and its effect on soil microbiome still need investigation. In this study, *Paenarthrobacter* sp. AT-5, an atrazine-degrading strain, was inoculated into agricultural soils contaminated with atrazine to investigate the bioaugmentation process and the reassembly of the soil microbiome. It was found that 95.9% of 5 mg kg^{-1} atrazine was removed from the soils when inoculated with strain AT-5 with 7 days, and the phytotoxicity of sweet potato caused by atrazine was significantly alleviated. qRT-PCR analysis revealed that the inoculated strain AT-5 survived well in the soils and maintained a relatively high abundance. The inoculation of strain AT-5 significantly affected the community structure of the soil microbiome, and the abundances of bacteria associated with atrazine degradation were improved.

Keywords: atrazine, bioaugmentation, phytotoxicity, *Paenarthrobacter* sp. AT-5, soil microbiome

INTRODUCTION

Atrazine is one of the photosystem-II (PSII)-inhibiting herbicides, which destroy the chloroplast light systems of plants, causing the plants to become chlorotic and finally wither and die. Atrazine is widely used in the prevention and control of broad-leaved weeds in maize, pineapple, sorghum, and sugar cane (Strong et al., 2000). Since atrazine was first put on the market in the 1950s, it has become the second largest applied pesticide in the world because of its high efficiency and low cost (Singh et al., 2018; Cao et al., 2021). Atrazine has a long half-life in soils, varying from approximately 60 days to over 1 year (Smith et al., 2005). With the wide application of atrazine, the residue of atrazine in the soil has caused great concern. Atrazine has been frequently detected in environments with concentrations as high as 250 mg kg^{-1} in soil (Chiaia-Hernandez et al., 2017), 30 μg L^{-1} in groundwater (Cerejeira et al., 2003), and 5 μg L^{-1} in surface water (Ge et al., 2010). As a potent endocrine disruptor, atrazine shows potential risk for endocrine health and immune disruption (Brodkin et al., 2007), nervous system damage (Rusiecki et al., 2004), and reproductive cancers in laboratory rodents and humans (Fan et al., 2007). Furthermore, the

residual atrazine in soils also causes phytotoxicity to subsequent crops, such as soybean (Soltani et al., 2011; Zhang et al., 2021), sorghum, oat, wheat, and sweet potato (Lima et al., 2020). Therefore, effective removal of atrazine residues from soil is of great importance.

Atrazine in environments can be dissipated by the following methods: oxidative degradation by zero-valent metals (Diao et al., 2020), photolysis (Souza et al., 2014), advanced oxidation processes (Morales-Perez et al., 2016), or bioremediation. As an eco-friendly, efficient, and low-cost method, bioremediation has been proposed as the most promising method to remove atrazine from contaminated-sites. Microorganisms capable of degrading atrazine have been reported since 1995, such as *Pseudomonas* sp. strain ADP, which is the first isolated atrazine-mineralizing strain (de Souza et al., 1998). Subsequently, more and more atrazine-degrading strains have been isolated, including *Nocardioides* sp. SP12 (Piutti et al., 2003), *Arthrobacter* sp. GZK-1 (Getenga et al., 2009), *Arthrobacter* sp. AK-YN10 (Sagarkar et al., 2016) and so on (Huang et al., 2017). To date, two types of atrazine-degrading bacteria have been described: (i) capable of completely mineralizing atrazine, harboring the genes of *atzA*/*trzN*, *atzB*, *atzC*, *atzD*, *atzE*, and *atzF* (Piutti et al., 2003), and (ii) capable of transforming atrazine into cyanuric acid, harboring the genes of *trzN*, *atzB* and *atzC* (Hernandez et al., 2011). Generally, gram-positive bacteria initiate the atrazine degradation *via* the hydrolysis reaction catalyzed by TrzN, while gram-negative bacteria catalyze the reaction by AtzA (Omotayo et al., 2011; Huang et al., 2017).

In previous studies, bioaugmentation has been proposed for atrazine degradation by inoculating atrazine-degrading bacteria to soils (Fadullon et al., 1998). Successful bioaugmentation requires the survival of the inoculated strains and keeping metabolic activity (Gomes et al., 2005). To date, the quantitative analysis of specific gene based on real-time PCR has been used for evaluating the genetic stability and survival of inoculated strains in soil samples (Chi et al., 2013). However, the interactions between the contaminants, inoculated strains, and the soil indigenous microbial communities remain largely unknown. In addition, the soil microbiome largely affects the productivity and stability of agroecosystems (van der Heijen, 2008). High-throughput sequencing has been successful in exploring the complex dynamic changes of microbial communities (Liu et al., 2020). Therefore, revealing the microbial community in soils responding to atrazine and its degrading strains will help to understand the underlying mechanism of bioaugmentation and improve the bioremediation efficiency.

In this study, an atrazine-degrading strain, *Paenarthrobacter* sp. AT-5 (formerly *Arthrobacter* sp. strain AT-5; Busse, 2016) was inoculated to evaluate the bioaugmentation processes in agricultural soils contaminated with atrazine (Xu et al., 2019). Real-time quantitative PCR (qRT-PCR) was used for calculating initial functional gene (*trzN*) to evaluate the stability and fate of strain AT-5 during the bioaugmentation process. At the same time, the alleviation of phytotoxicity of sweet potato by strain AT-5 was also investigated. More importantly, our study also aims to explore the dynamic changing process of soil microbiome during bioaugmentation. This study is helpful to understand the change of community structure of microbiome during bioaugmentation and provides a theoretical guidance for development of enhanced bioremediation strategies for atrazine-contaminated soils.

MATERIALS AND METHODS

Soil Characteristics and Preparation of Inoculum

Soil samples were collected from a maize field (0–10 cm depth) in Jiangsu Province, China, after maize was harvested. Mixed and homogenized soil samples were passed through a 2-mm sieve and then stored at 4°C before further use. The chemical and physical properties of the soil were determined by standard methods (Nelson and Sommers, 1996) and summarized in **Supplementary Table S1**.

Paenarthrobacter sp. strain AT-5, an atrazine-degrading strain isolated previously in our lab (Liu et al., 2019; Xu et al., 2019), was used for bioaugmentation. Strain AT-5 was cultured in Luria-Bertani (LB) medium at 30°C and pH 7.0 until the exponential phase. Then, the cells were harvested through centrifugation (6,000 *g* for 6 min) and washed with sterilized minimal salt medium for three times.

Phytotoxicity of Sweet Potato Seedlings Caused by Atrazine Residues in Soil

To study the phytotoxicity of subsequent crop caused by atrazine residues in soil, the "Su 22" sweet potato seedlings (obtained from Jiangsu Academy of Agricultural Sciences, China) were selected. Soils with atrazine residues were prepared by supplementing atrazine (dissolved in methanol, Sigma-Aldrich, Shanghai, China; 98% purity) to soils at five different final concentrations (10 mg kg^{-1}, 5 mg kg^{-1}, 1 mg kg^{-1}, 0.5 mg kg^{-1}, and 0.2 mg kg^{-1}, dry soil weight). The atrazine-spiked soils (250 g, dry weight) were transferred to three pots, respectively. The "Su 22" sweet potato seedlings were planted into pots and put in a growth chamber (Jiangnan, Ningbo, China) at 28/25°C with an 18-h light/6-h dark cycle. During the incubation, water was added every other day to keep the soil moisture content at 40%. The growth status of sweet potato seedlings was observed and recorded at 0, 1, 3, 7, 14, and 21 days, and three replicates were set for each treatment.

Bioaugmentation of Atrazine-Contaminated Soil With Strain AT-5

Atrazine-spiked soils were prepared as described above at a final atrazine concentration of 5 mg kg^{-1} (dry soil weight), and the carrier solvent methanol was removed through evaporation. The microcosm treatments were set as follows: (i) Control: equivalent amount of methanol and ddH_2O were added into native soil, (ii) Atr: native soil spiked with atrazine, (iii) Atr-Bio: atrazine-spiked soil with inoculation of strain AT-5 (1.0×10^7 CFU/g dry soil), (iv) Bio: native soil with inoculation of strain AT-5 (1.0×10^7 CFU/g dry soil), and (v) Sterilized soil: atrazine-spiked soil autoclaved three times (121°C, 20 min). The treated soils were sorted into plastic pots (700 g dry soil per pot) and then incubated at 28/25°C with an 18-h light/6-h

dark cycle in a growth chamber for 14 days. The soil moisture content was kept at 30% of the soil water holding capacity (WHC), and the lost water was replenished by weighing samples every day. Soils (20 g per pot) were non-destructively sampled at 0, 1, 3, 5, 7, and 14 days for atrazine detection and bacterial community analysis. Three replicates were set for each treatment.

The remaining soils of the atrazine-spiked soil (Atr) and atrazine-spiked soil with inoculation of strain AT-5 (Atr-Bio) at 14 d were planted with sweet potato seedlings to verify whether the phytotoxicity caused by atrazine was alleviated by bioaugmentation with strain AT-5. The growth status of sweet potato seedlings was measured as described in section "Phytotoxicity of Sweet Potato Caused by Atrazine and Its Alleviation by Bioaugmentation".

Extraction and Analysis of Atrazine in Soil

At each sampling time, 20 g soil (dry weight) was collected and extracted three times with 60 ml dichloromethane by horizontally mixing for 2 h at 30°C and ultra-sonication for 30 min. The extracts were concentrated by rotary evaporation, dried with nitrogen, and then resolved in 1 ml of methanol. Using this method, the extraction efficiency of atrazine in soil was 79.9%. The impurities in the extracts were removed by filtering through a 0.22-μm membrane. Atrazine was detected through high-performance liquid chromatography (HPLC; UltiMate 3,000 RSLC; Thermo Fisher Scientific, United States) using a reversed-phase C_{18} separation column (250 mm × 4.6 mm × 5μm; Thermo Fisher Scientific, Waltham, MA, United States). The mobile phase consisted of 20% water and 80% methanol (vol/vol), and the flow rate was 0.8 ml min^{-1}. The column temperature was 30°C, and the injection volume was 20 μl. Atrazine was detected at 220 nm. Under these conditions, the retention time (Rt) for atrazine was 5.97 min.

DNA Extraction, Sequencing, and Quantitative Real-Time PCR

Soil total DNA was extracted from the soil sample (0.5 g, dry weight) using a Fast DNA SPIN Kit for Soil (MP Biomedicals, United States). The V4 region of the 16S rRNA gene was amplified using the primer set 515F and 806R as described previously (Jia et al., 2021a). The amplified 16S rRNA genes were sequenced by Biozeron Biological Technology Co. Ltd. (Shanghai, China) on an Illumina HiSeq 2,500 platform.

The numbers of the inoculated strain AT-5 in soil were estimated by quantifying the copy numbers of *trzN* gene (encoding the initial hydrolase for atrazine degradation) through quantitative real-time PCR (qRT-PCR) with primers (RT-trzNF: GCAGCGTTTCACGGACAA, RT-trzNR: AGGAGCGACTGG AGGAGGAC; 235 bp; Sajjaphan et al., 2004). The *trzN* fragment was amplified from the DNA of strain AT-5 with primers (trzN-F: ATGATCCTGATCCGCGGACT, trzN-R: CTACAAG TTCTTGGGAATGA; 1383 bp) and cloned into pMD™19-T Vectors (TaKaRa, Dalian, China). The recombinant plasmid was used as the standard for quantitative analysis. The concentrations of the recombinant plasmid were detected on a NanoDrop ND-2000 spectrophotometer (ND2000, Thermo Scientific, DE, United States), and then the copy numbers of inserted *trzN* gene were calculated. Tenfold serial dilutions of the concentration-known recombinant plasmid (in triplicate) were used in the qRT-PCR assay to generate an external standard curve. The qRT-PCR was performed on the Applied Biosystems 7500 Fast real-time PCR system (Applied Biosystems, USA) with SYBR Premix Ex Taq II (Tli RNase H Plus; TaKaRa).

Sequence Analysis of 16S rRNA Gene

After sequencing, the raw reads were merged using FLASH (Magoc and Salzberg, 2011). The merged reads were quality-filtered using QIIME, and then, effective tags were clustered into operational taxonomic units (OTUs) with a 97% similarity cutoff (Caporaso et al., 2010; Edgar, 2013). The species richness and diversity, including Chao1, Shannon, and Simpson index (1-lambda), were estimated through α-diversity analysis, using QIIME (Caporaso et al., 2010). β-diversity analysis was used to evaluate the similarity of bacterial communities in different treatments (Caporaso et al., 2010). The weighted UniFrac distances were calculated using the QIIME pipeline, and principal coordinates analysis (PCoA) was performed with R using the library "vegan." Potential biomarkers were identified through linear discriminant analysis (LDA) with effect size (LEfSe; Segata et al., 2011). The Molecular Ecological Network Analysis (MENA) pipeline was used to construct the co-occurrence patterns of bacterial communities (Das and Mukherjee, 2007).

Data Availability

The sequencing data involved in this manuscript are available at NCBI under BioProject ID PRJNA765205.

RESULTS

Removal of Atrazine by Inoculation of Strain AT-5 and Its Dynamic Abundance in the Soil

In the sterilized soil, only 14.5% of atrazine disappeared at the end of incubation (14 days), showing that abiotic factors have limited contributions to atrazine dissipation (**Figure 1**). Compared to that in the sterilized soil, the concentration of atrazine in bioaugmentation treatment (Atr-Bio) was significantly reduced. The removal rates of atrazine in the atrazine treatment (Atr) and bioaugmentation treatment (Atr-Bio) were 28.3 and 97.9% at 14 days, respectively. In addition, the DT_{50} and DT_{90} values of atrazine in Atr-Bio treatment were 1.2 and 3.9 days, respectively. These results showed that indigenous microorganisms contributed a little to atrazine removal and strain AT-5 dominated the atrazine removal in the soil ($p < 0.01$).

The abundance of the inoculated strain AT-5 in the soil was calculated by quantifying the copy numbers of the initial hydrolase gene *trzN* by qRT-PCR (**Figure 1**). The amplification efficiency of PCR threshold standard curve was 98.4%. In the bioaugmentation treatment, the copy numbers of *trzN* gene decreased within the first 7 days and then kept relatively stable (the same order of magnitude at 10^6 copies g^{-1} dry soil) till

14 days, while the *trzN* gene could not be amplified with the DNA template extracted from the original soil without any treatments. These results indicated that the inoculated strain AT-5 could survive well in the soil for a period of time (14 days).

Phytotoxicity of Sweet Potato Caused by Atrazine and Its Alleviation by Bioaugmentation

Both high and low concentrations of atrazine in the soil caused phytotoxicity to sweet potato seedlings (**Supplementary Figure S2**). With a low concentration of atrazine (0.2 mg kg^{-1}) in the soil, the sweet potato seedlings survived within the 21-day cultivation period, but phytotoxicity phenomena, such as leaf yellowing, were still observed. These results suggested that sweet potato seedlings were sensitive to atrazine, and even low concentrations of atrazine in the soil would affect the planting of subsequent crops. Therefore, the remaining soils of the atrazine-spiked soil (Atr) and atrazine-spiked soil with inoculation of strain AT-5 (Atr-Bio) at 14 d were again planted with sweet potato seedlings. The concentrations of atrazine remaining in Atr and Atr-Bio soils were 3.36 ± 0.62 and 0.09 ± 0.002 mg kg^{-1}, respectively. The atrazine-spiked soil (Atr) caused serious phytotoxicity to sweet potato seedlings, and sweet potato seedlings died at 21 days. However, the sweet potato seedlings grew well in the atrazine-spiked soil with inoculation of strain AT-5 (Atr-Bio; **Figure 2**). These results further showed that bioaugmentation with strain AT-5 was effective in the removal of atrazine from soil and could prevent the damage of atrazine residues to subsequent crops.

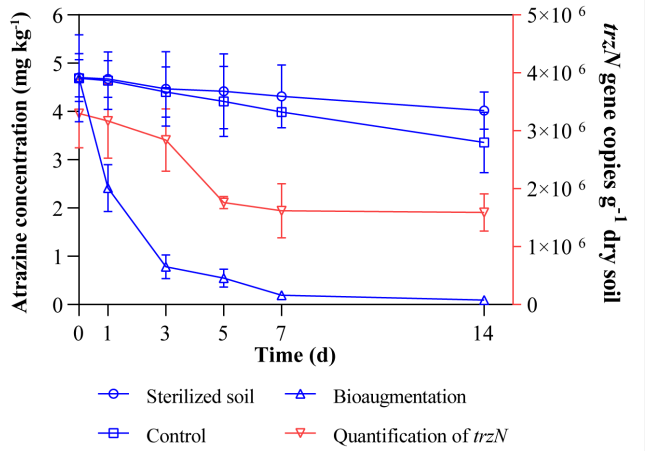

FIGURE 1 | Dissipation of atrazine in various soil samples with time and qRT-PCR quantification of *trzN* in inoculated soil microcosms. Control: native soil spiked with atrazine; Sterilized soil: sterilized soil spiked with atrazine; Bioaugmentation: atrazine-spiked soil with inoculation of strain AT-5; Quantification of *trzN*: *trzN* gene copies (g^{-1} dry soil).

Effects of Bioaugmentation and Atrazine Application on Soil Microbiome

The changes of the soil bacterial community at 0, 1, 3, 7, and 14 days in different treatment were investigated by sequencing of the 16S rRNA-amplicons. For α-diversities, the control treatment (methanol and ddH_2O application) presented higher community richness (represented by higher Chao1 indices and observed OTU numbers) and diversity (indicated by Shannon and Simpson indices) than the Atr-Bio treatment (atrazine-spiked soil with inoculation of strain AT-5) and the Bio treatment (native soil with inoculation of strain AT-5; **Figure 3**). In addition, the application of atrazine without inoculation (Atr treatment) reduced the community richness, while had little effect on community diversity (**Figure 3**). These results indicated that the inoculation of degrading strain AT-5 significantly affected the bacterial community richness and diversity in soil.

Principal coordinates analysis (PCoA) and hierarchical cluster analysis were used to investigate the influences of inoculation of strain AT-5 and atrazine application on soil bacterial communities. The soil samples were grouped into two distinct clusters based on different treatments and time: inoculation treatments (Atr-Bio and Bio) and non-inoculation treatments (Control and Atr; **Figure 4A**). In addition, the hierarchical cluster analysis also reflected the sample separation, presenting a greater distance between the inoculation treatments and other treatments (**Supplementary Figure S5**). These results showed that inoculation of strain AT-5 dominated the changes of bacterial community diversity and structure in the soil, while atrazine application nearly had no effect on bacterial community.

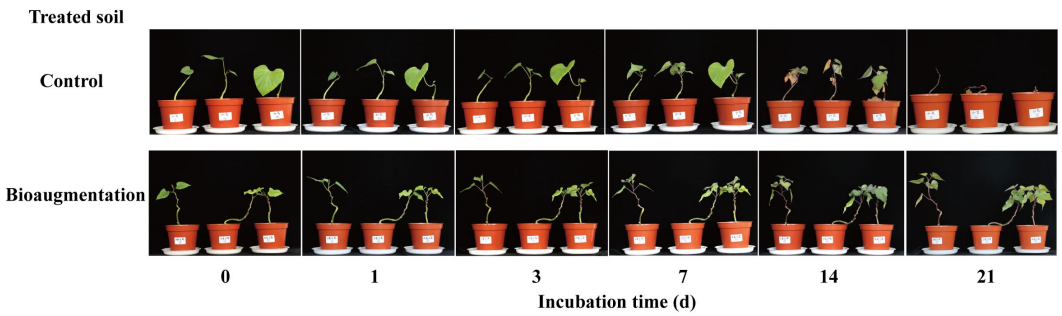

FIGURE 2 | The phytotoxicity of atrazine on sweet potato seedlings alleviated by bioaugmentation. Control: native soil spiked with atrazine after incubated 14 days, and the concentration of atrazine remaining in the control soil was 3.36 ± 0.62 mg kg^{-1}. Bioaugmentation: atrazine-spiked soil with inoculation of strain AT-5 after incubated 14 days, and the concentration of atrazine remaining in the bioaugmentation soil was 0.09 ± 0.002 mg kg^{-1}. Three replicates were set for each treatment.

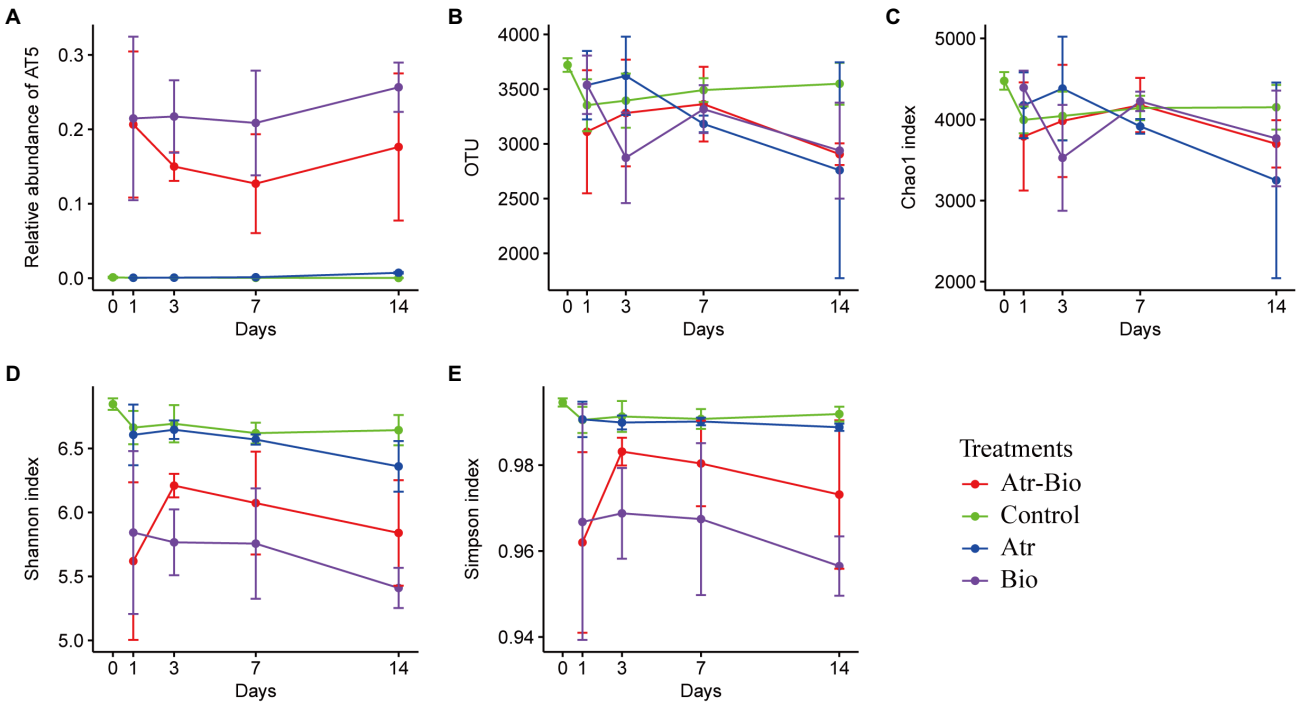

FIGURE 3 | Richness estimators and diversity indices of bacterial communities. **(A)** relative abundance of strain AT-5; **(B)** observed OTU numbers; **(C)** Chao1 indices; **(D)** Shannon indices; **(E)** Simpson indices (1-lambda). Control: equivalent amount of methanol and ddH_2O were added into native soil; Atr: native soil spiked with atrazine; Atr-Bio: atrazine-spiked soil with inoculation of strain AT-5; Bio: native soil with inoculation of strain AT-5.

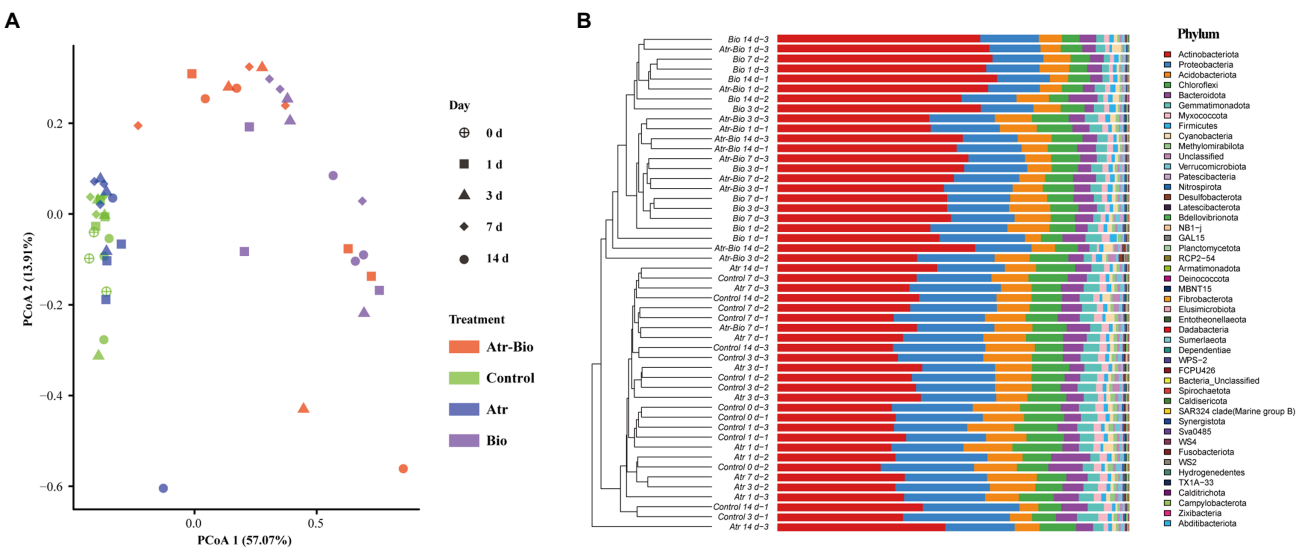

FIGURE 4 | Effects of the different treatments on the bacterial community structure. **(A)** principal coordinates analysis (PCoA) with Bray–Curtis distances of bacterial communities; **(B)** Hierarchical clustering based on relative abundances of bacterial phylum in the soil samples. Control: equivalent amount of methanol and ddH_2O were added into native soil; Atr: native soil spiked with atrazine; Atr-Bio: atrazine-spiked soil with inoculation of strain AT-5; Bio: native soil with inoculation of strain AT-5.

Bacterial Abundance and Composition

In all treatments, the bacterial phyla with higher abundances were Actinobacteriota, Proteobacteria, Acidobacteriota, Chloroflexi, and Bacteroidota (**Figure 4B**) and specifically the bacterial genera were *Paenarthrobacter*, *Pseudarthrobacter* and *Nocardioides* (**Supplementary Figure S6**). The genus *Paenarthrobacter* was

the dominant genus in inoculation treatments, and the relative abundances of *Paenarthrobacter* in the Atr-Bio treatment kept relatively stable (21.1, 15.3, 13.0, and 17.9% at 1, 3, 7, and 14 days, respectively). These results combined with the qRT-PCR data showed that the inoculated *Paenarthrobacter* sp. strain AT-5 stably survived in the soil (**Figures 1**, **3A**; **Supplementary Figure S6**).

To identify the biomarkers distinguishing different treatments, LEfSe analysis was used (**Supplementary Figure S7**). There were 58 potential biomarkers detected at all levels. At the genus level (**Figure 5A**), the potential biomarkers *Paenarthrobacter* and *Bacillus* were noted in both Bio and Atr-Bio treatments (inoculation treatment). Furthermore, the abundance of *Bacillus* was significantly increased in the inoculation treatment, indicating that inoculation of *Paenarthrobacter* sp. strain AT-5 enriched the genus *Bacillus* in the indigenous microbiome. Meanwhile, the relative abundances of 17 other potential biomarkers including *Marmoricola*, *Nocardioides*, *Agromyces*, and *Solirubrobacter*, decreased in inoculation treatment as compared to that in other treatments. These results indicated that inoculation treatment negatively selected these genera in the indigenous microbiome. It is worth noting that the positively selected biomarkers, including *Marmoricola*, *Nocardioides*, *Agromyces*, and *Solirubrobacter*, were only detected in the atrazine-spiked soil treatment (Atr) at 14 days. They increased markedly in Atr treatment at 14 days as compared to that in 1, 3, and 7 days. These four genera might be the positive biomarkers for atrazine degradation in non-inoculation treatments.

Bacterial Co-occurrence Networks

The co-occurrence patterns of bacterial communities in different treatments (Control, Atr, Bio, and Atr-Bio) were identified through constructing bacterial co-occurrence networks. The topological properties of the co-occurrence patterns varied significantly between the Atr-Bio and Atr networks (**Figure 6**). The Atr network exhibited more nodes and edges, a higher average degree and average clustering coefficient, as well as higher density and connectedness than other treatment networks, suggesting a much greater complexity and connectedness in the Atr network than that in the Atr-Bio network (**Supplementary Figure S8**). In addition, positive correlations occupied a dominant position in the all networks, regardless of the different treatments. However, compared to Atr treatments (10.2%), the negative correlations remarkably decreased in the Bio (5.9%) and Atr-Bio (3.5%) treatments, respectively. The higher negative correlations in the Atr network may be attributed to the filter of non-adaptive bacteria by atrazine application. In the Atr-Bio network, the lower negative correlations may be attributed to the removal of atrazine by bioaugmentation, leading to the recovery of the bacterial community.

DISCUSSION

Microbial communities in natural environments usually do not have the capacity to degrade organic pollutants. Bioaugmentation, a strategy of inoculating specific functional microorganisms for degradation of pollutants, has been proposed as the most potential method to clean up pollutant-contaminated sites (Huang et al., 2019; Yang et al., 2021). Though some previous studies have investigated the bioaugmentation of atrazine-contaminated sites with atrazine-degrading strains, there are few studies about the effect of bioaugmentation on indigenous soil microbial communities (Wang et al., 2013). Nevertheless, the inoculation

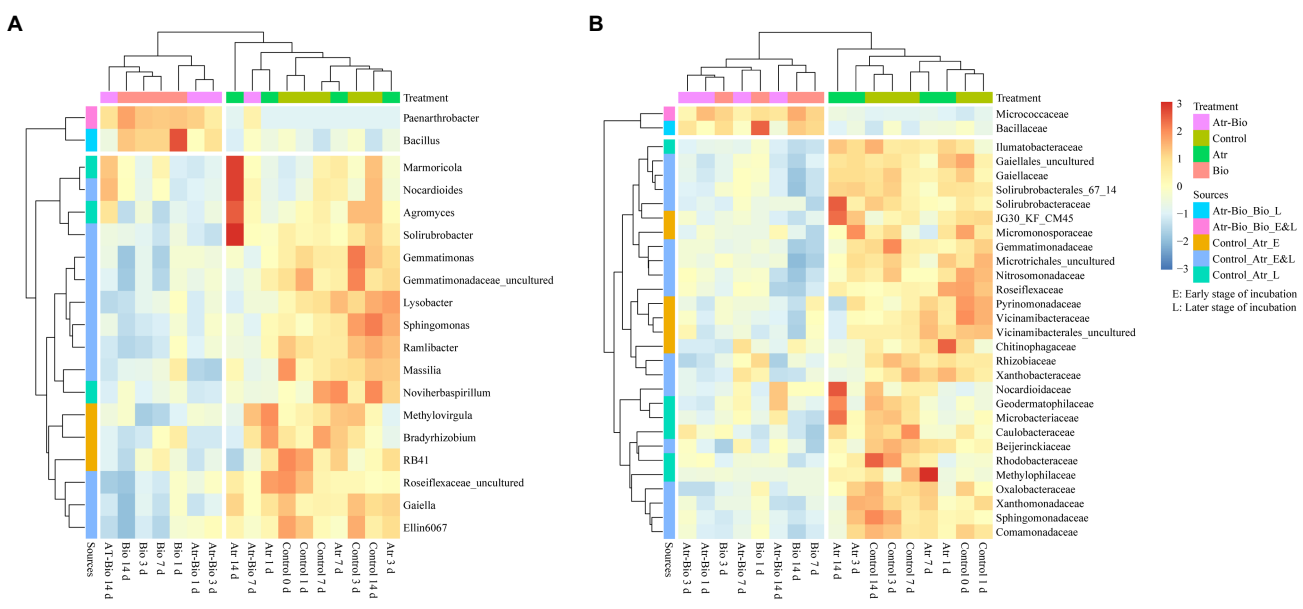

FIGURE 5 | Heatmaps showing relative abundances of differentially abundant genera **(A)** and families **(B)** identified by LEfSe analysis. Control: equivalent amount of methanol and ddH_2O were added into native soil; Atr: native soil spiked with atrazine; Atr-Bio: atrazine-spiked soil with inoculation of strain AT-5; Bio: native soil with inoculation of strain AT-5. Atr-Bio_Bio, comparison of Atr-Bio treatment vs. Bio treatment, Control_Atr, comparison of Control treatment vs. Atr treatment. Early stage, 0–5 days; late stage, 7–14 days.

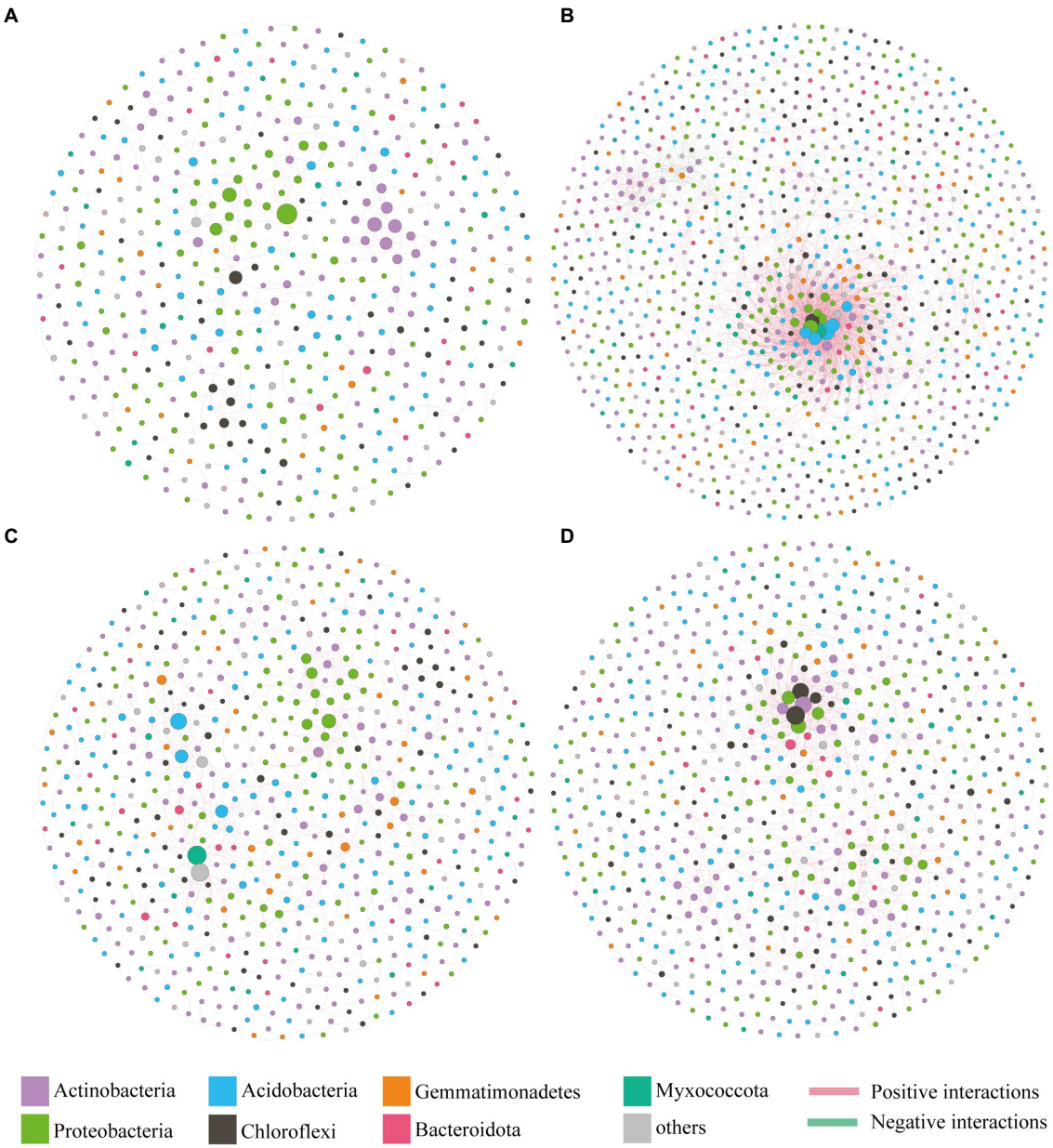

FIGURE 6 | Bacterial co-occurrence networks under different treatments. **(A)** Control; **(B)** Atr; **(C)** Bio; **(D)** Atr-Bio. Control: equivalent amount of methanol and ddH_2O were added into native soil; Atr: native soil spiked with atrazine; Atr-Bio: atrazine-spiked soil with inoculation of strain AT-5; Bio: native soil with inoculation of strain AT-5.

of exogenous strains may significantly change the structure of soil microbiome and affect its potential function (Yang et al., 2021). To determine whether bioaugmentation has negative environmental effects or not, the interactions between the inoculated exogenous strains, pollutants, and soil microbial consortia were required to be investigated. In this study, *Paenarthrobacter* sp. AT-5 was inoculated for atrazine removal to investigate the effects of bioaugmentation on the soil microbiome and the reconstructing process of microbial community.

In this study, the removal rate of atrazine by bioaugmentation of strain AT-5 was 95.9% at 7 days, Gao et al. (2018) found the half-life of atrazine in soil treated with *Arthrobacter* sp. strain HB-5 was significantly reduced to 6.3 days (Gao et al., 2018), showing that strain AT-5 has an excellent potential for atrazine degradation in soils. In addition, successful bioaugmentation relies not only on the degradability of the inoculum but also on its ability to survive in the environment (Singer et al., 2005; Chi et al., 2013). Some studies have demonstrated that the persistence of inoculum in the environment is a key factor of bioaugmentation (Chi et al., 2013; Yang et al., 2021). Our previous study showed the inoculated exogenous degrading strain could not survive well in soil, resulting in the decrease of chlorpyrifos mineralization rate (Jia et al., 2021a). By qRT-PCR and 16S rRNA-amplicon sequencing, we found that the inoculated strain AT-5 survived

well in the soil and remained relatively stable during the incubation period of 14 days, which ensured its remediation efficiency for atrazine-contaminated soils. In addition, bioremediation is often subject to environmental constraints, such as soil type (Jia et al., 2021a). However, strain AT-5 showed good remediation effects in three different soils collected from Jining, Langfang, and Xuzhou, China (**Supplementary Figures S3**, **S4**), indicating that strain AT-5 has great potentials for the remediation of atrazine-contaminated different types of soil.

Actinobacteriota and Proteobacteria were the most abundant bacterial phyla in all treatments in our study. Previous studies found that Proteobacteria are the dominant microorganisms in various pesticide-contaminated soils due to their good tolerance to pollutants (Vaishampayan et al., 2007; Jia et al., 2021b). In addition, several atrazine-degrading bacteria have been identified in Actinobacteriota and Proteobacteria, such as *Arthrobacter/Paenarthrobacter* (Vaishampayan et al., 2007), *Pseudomonas* (de Souza et al., 1998), and *Nocardioides* (Piutti et al., 2003). Compared with the control treatment, the abundance of *Bacillus* significantly increased in the inoculation treatment, indicating that the potential indigenous *Bacillus* may be directly or indirectly involved in the degradation of atrazine. Up to now, several *Bacillus*, such as *Bacillus licheniformis* ATLJ-5 (Zhu et al., 2019), *Bacillus megaterium* ATLJ-11 (Zhu et al., 2019) and *Bacillus subtilis* HB-6 (Wang et al., 2014) have been reported to be capable of degrading atrazine and its metabolites. Hence, the addition of atrazine increased the relative abundance of potential biomarkers such as *Bacillus*, which may be involved in the biodegradation of atrazine or its metabolites.

Bacterial richness and diversity significantly decreased in the inoculation treatments, which were also observed during the bioaugmentation of acetamiprid-contaminated soil with *Pigmentiphaga* sp. strain D-2 (Yang et al., 2021). This phenomenon observed in our study could be attributed to the persistence and niche occupation of strain of AT-5. Moreover, inoculation of strain AT-5 enhanced atrazine degradation, intermediate production, and nutrient consumption in soil. These changes in the microenvironment may also lead to a significant reduction in bacterial richness and diversity (Yang et al., 2021). However, there was no significant difference in richness and diversity index between the control treatment (methanol and ddH_2O application) and Atr treatment (atrazine application). These results indicated that the main driving factor for the change of bacterial community structure in the inoculation treatments is the addition of strain AT-5. It has been reported that the abundance of inoculum decreased after elimination of pollutants in soils (Cunliffe and Kertesz, 2006; Niu et al., 2009; Chi et al., 2013). Considering the influence of complex environmental factors in soils and the competition between inoculum and indigenous microorganisms, we speculate that strain AT-5 might not be able to maintain high abundance in *in-situ* soils after elimination of atrazine. Unfortunately, we did not collect soil samples from the Atr-Bio treatment on a longer time scale. Therefore, it is needed to clarify the final fate of strain AT-5 in soils in future studies.

DATA AVAILABILITY STATEMENT

The original contributions presented in the study are included in the article/**Supplementary Material**, further inquiries can be directed to the corresponding authors.

AUTHOR CONTRIBUTIONS

KC and XX conceived and designed the experiments. WJ and TY performed the experiments. XX and WJ analyzed the data. WJ, NL, and WD prepared the manuscript. JJ, KC, and XX revised the manuscript. All authors contributed to the article and approved the submitted version.

FUNDING

This work was financially supported by the grant of National Key R&D Program of China (2018YFA0901200), the National Natural Science Foundation of China (31870095 and 41977120), and the China Agriculture Research System of MOF and MARA.

SUPPLEMENTARY MATERIAL

The Supplementary Material for this article can be found online at: https://www.frontiersin.org/articles/10.3389/fmicb.2021.771463/full#supplementary-material

REFERENCES

Brodkin, M. A., Madhoun, H., Rameswaran, M., and Vatnick, I. (2007). Atrazine is an immune disruptor in adult northern leopard frogs (*Rana pipiens*). *Environ. Toxicol. Chem.* 26, 80–84. doi: 10.1897/05-469.1

Busse, H.-J. (2016). Review of the taxonomy of the genus *Arthrobacter*, emendation of the genus *Arthrobacter* sensu lato, proposal to reclassify selected species of the genus *Arthrobacter* in the novel genera *Glutamicibacter* gen. Nov., *Paeniglutamicibacter* gen. Nov., *Pseudoglutamicibacter* gen. Nov., *Paenarthrobacter* gen. Nov and *Pseudarthrobacter* gen. Nov., and emended description of *Arthrobacter* roseus. *Int. J. Syst. Evol. Microbiol.* 66, 9–37. doi: 10.1099/ijsem.0.000702

Cao, D., He, S., Li, X., Shi, L., Wang, F., Yu, S., et al. (2021). Characterization, genome functional analysis, and detoxification of atrazine by *Arthrobacter* sp. C2. *Chemosphere* 264:128514. doi: 10.1016/j.chemosphere.2020.128514

Caporaso, J. G., Kuczynski, J., Stombaugh, J., Bittinger, K., Bushman, F. D., Costello, E. K., et al. (2010). QIIME allows analysis of high-throughput community sequencing data. *Nat. Methods* 7, 335–336. doi: 10.1038/nmeth.f.303

Cerejeira, M. J., Viana, P., Batista, S., Pereira, T., Silva, E., Valerio, M. J., et al. (2003). Pesticides in Portuguese surface and ground waters. *Water Res.* 37, 1055–1063. doi: 10.1016/S0043-1354(01)00462-6

Chi, X.-Q., Zhang, J.-J., Zhao, S., and Zhou, N.-Y. (2013). Bioaugmentation with a consortium of bacterial nitrophenol-degraders for remediation of soil contaminated with three nitrophenol isomers. *Environ. Pollut.* 172, 33–41. doi: 10.1016/j.envpol.2012.08.002

Chiaia-Hernandez, A. C., Keller, A., Wachter, D., Steinlin, C., Camenzuli, L., Hollender, J., et al. (2017). Long-term persistence of pesticides and TPs in archived agricultural soil samples and comparison with pesticide application. *Environ. Sci. Technol.* 51, 10642–10651. doi: 10.1021/acs.est.7b02529

Cunliffe, M., and Kertesz, M. A. (2006). Effect of *Sphingobium yanoikuyae* B1 inoculation on bacterial community dynamics and polycyclic aromatic hydrocarbon degradation in aged and freshly PAH-contaminated soils. *Environ. Pollut.* 144, 228–237. doi: 10.1016/j.envpol.2005.12.026

Das, K., and Mukherjee, A. K. (2007). Crude petroleum-oil biodegradation efficiency of *Bacillus* subtilis and *Pseudomonas* aeruginosa strains isolated from a petroleum-oil contaminated soil from north-East India. *Bioresour. Technol.* 98, 1339–1345. doi: 10.1016/j.biortech.2006.05.032

de Souza, M. L., Wackett, L. P., and Sadowsky, M. J. (1998). The *atzABC* genes encoding atrazine catabolism are located on a self-transmissible plasmid in *pseudomonas* sp. strain ADP. *Appl. Environ. Microbiol.* 64, 2323–2326. doi: 10.1128/AEM.64.6.2323-2326.1998

Diao, Z.-H., Qian, W., Zhang, Z.-W., Jin, J.-C., Chen, Z.-L., Guo, P.-R., et al. (2020). Removals of Cr(VI) and cd(II) by a novel nanoscale zero valent iron/peroxydisulfate process and its Fenton-like oxidation of pesticide atrazine: coexisting effect, products and mechanism. *Chem. Eng. J.* 397:125382. doi: 10.1016/j.cej.2020.125382

Edgar, R. C. (2013). UPARSE: highly accurate OTU sequences from microbial amplicon reads. *Nat. Methods* 10, 996–998. doi: 10.1038/nmeth.2604

Fadullon, F. S., Karns, J. S., and Torrents, A. (1998). Degradation of atrazine in soil by Streptomyces. *J. Environ. Sci. Health Part B* 33, 37–49. doi: 10.1080/03601239809373128

Fan, W., Yanase, T., Morinaga, H., Gondo, S., Okabe, T., Nomura, M., et al. (2007). Atrazine-induced aromatase expression is SF-1 dependent: implications for endocrine disruption in wildlife and reproductive cancers in humans. *Environ. Health Perspect.* 115, 720–727. doi: 10.1289/ehp.9758

Gao, J., Song, P., Wang, G., Wang, J., Zhu, L., and Wang, J. (2018). Responses of atrazine degradation and native bacterial community in soil to *Arthrobacter* sp strain HB-5. *Ecotoxicol. Environ. Saf.* 159, 317–323. doi: 10.1016/j.ecoenv.2018.05.017

Ge, J., Cong, J., Sun, Y., Li, G., Zhou, Z., Qian, C., et al. (2010). Determination of endocrine disrupting chemicals in surface water and industrial wastewater from Beijing, China. *Bull. Environ. Contam. Toxicol.* 84, 401–405. doi: 10.1007/s00128-010-9958-3

Getenga, Z., Doerfler, U., Iwobi, A., Schmid, M., and Schroll, R. (2009). Atrazine and terbuthylazine mineralization by an *Arthrobacter* sp isolated from a sugarcane-cultivated soil in Kenya. *Chemosphere* 77, 534–539. doi: 10.1016/j.chemosphere.2009.07.031

Gomes, N. C. M., Kosheleva, I. A., Abraham, W. R., and Smalla, K. (2005). Effects of the inoculant strain *pseudomonas* putida KT2442 (pNF142) and of naphthalene contamination on the soil bacterial community. *FEMS Microbiol. Ecol.* 54, 21–33. doi: 10.1016/j.femsec.2005.02.005

Hernandez, M., Jia, Z., Conrad, R., and Seeger, M. (2011). Simazine application inhibits nitrification and changes the ammonia-oxidizing bacterial communities in a fertilized agricultural soil. *FEMS Microbiol. Ecol.* 78, 511–519. doi: 10.1111/j.1574-6941.2011.01180.x

Huang, X., He, J., Yan, X., Hong, Q., Chen, K., He, Q., et al. (2017). Microbial catabolism of chemical herbicides: microbial resources, metabolic pathways and catabolic genes. *Pestic. Biochem. Physiol.* 143, 272–297. doi: 10.1016/j.pestbp.2016.11.010

Huang, Y., Zhan, H., Bhatt, P., and Chen, S. (2019). Paraquat degradation From contaminated environments: current achievements and perspectives. *Front. Microbiol.* 10:1754. doi: 10.3389/fmicb.2019.01754

Jia, W., Shen, D., Yu, K., Zhong, J., Li, Z., Ye, Q., et al. (2021a). Reducing the environmental risk of Chlorpyrifos application through appropriate agricultural management: evidence from Carbon-14 tracking. *J. Agric. Food Chem.* 69, 7324–7333. doi: 10.1021/acs.jafc.1c02753

Jia, W., Ye, Q., Shen, D., Yu, K., Zheng, Y., Liu, M., et al. (2021b). Enhanced mineralization of chlorpyrifos bound residues in soil through inoculation of two synergistic degrading strains. *J. Hazard. Mater.* 412:125116. doi: 10.1016/j.jhazmat.2021.125116

Lima, D., Goncalves, R. C., Campos, L. J. M., Erasmo, E. A. L., Silveira, M. A., Sagio, S. A., et al. (2020). Evaluation of the selectivity of pre-emergence herbicides and their influence on the physiological and agronomic parameters of sweet potato. *Eur. J. Hortic. Sci.* 85, 401–410. doi: 10.17660/eJHS.2020/85.6.4

Liu, X., Chen, K., Chuang, S., Xu, X., and Jiang, J. (2019). Shift in bacterial community structure drives different atrazine-degrading efficiencies. *Front. Microbiol.* 10:3082. doi: 10.3389/fmicb.2019.03082

Liu, C. J., Gong, X. W., Dang, K., Li, J., Yang, P., Gao, X. L., et al. (2020). Linkages between nutrient ratio and the microbial community in rhizosphere soil following fertilizer management. *Environ. Res.* 184:109261. doi: 10.1016/j.envres.2020.109261

Magoc, T., and Salzberg, S. L. (2011). FLASH: fast length adjustment of short reads to improve genome assemblies. *Bioinformatics* 27, 2957–2963. doi: 10.1093/bioinformatics/btr507

Morales-Perez, A. A., Arias, C., and Ramirez-Zamora, R.-M. (2016). Removal of atrazine from water using an iron photo catalyst supported on activated carbon. *Adsorption* 22, 49–58. doi: 10.1007/s10450-015-9739-8

Nelson, D. W., and Sommers, L. E. (1996). "Total carbon, organic carbon, and organic matter," in *Methods of Soil Analysis. Vol. 5*. ed. J. M. Bigham (Madison, WI: SSSA Press), 961–1010.

Niu, G.-L., Zhang, J.-J., Zhao, S., Liu, H., Boon, N., and Zhou, N.-Y. (2009). Bioaugmentation of a 4-chloronitrobenzene contaminated soil with *pseudomonas putida* ZWL73. *Environ. Pollut.* 157, 763–771. doi: 10.1016/j.envpol.2008.11.024

Omotayo, A. E., Ilori, M. O., Amund, O. O., Ghosh, D., Roy, K., and Radosevich, M. (2011). Establishment and characterization of atrazine degrading cultures from Nigerian agricultural soil using traditional and bio-Sep bead enrichment techniques. *Appl. Soil Ecol.* 48, 63–70. doi: 10.1016/j.apsoil.2011.01.006

Piutti, S., Semon, E., Landry, D., Hartmann, A., Dousset, S., Lichtfouse, E., et al. (2003). Isolation and characterisation of *Nocardioides* SP SP12, an atrazine-degrading bacterial strain possessing the gene *trzN* from bulk- and maize rhizosphere soil. *FEMS Microbiol. Lett.* 221, 111–117. doi: 10.1016/S0378-1097(03)00168-X

Rusiecki, J. A., De Roos, A., Lee, W. J., Dosemeci, M., Lubin, J. H., Hoppin, J. A., et al. (2004). Cancer incidence among pesticide applicators exposed to atrazine in the agricultural health study. *J. Natl. Cancer Inst.* 96, 1375–1382. doi: 10.1093/jnci/djh264

Sagarkar, S., Bhardwaj, P., Storck, V., Devers-Lamrani, M., Martin-Laurent, F., and Kapley, A. (2016). S-triazine degrading bacterial isolate *Arthrobacter* sp AK-YN10, a candidate for bioaugmentation of atrazine contaminated soil. *Appl. Microbiol. Biotechnol.* 100, 903–913. doi: 10.1007/s00253-015-6975-5

Sajjaphan, K., Shapir, N., Wackett, L. P., Palmer, M., Blackmon, B., Tomkins, J., et al. (2004). *Arthrobacter* aurescens TC1 atrazine catabolism genes *trzN*, *atzB*, and *atzC* are linked on a 160-kilobase region and are functional in Escherichia coli. *Appl. Environ. Microbiol.* 70, 4402–4407. doi: 10.1128/AEM.70.7.4402-4407.2004

Segata, N., Izard, J., Waldron, L., Gevers, D., Miropolsky, L., Garrett, W. S., et al. (2011). Metagenomic biomarker discovery and explanation. *Genome Biol.* 12:R60. doi: 10.1186/gb-2011-12-6-r60

Singer, A. C., van der Gast, C. J., and Thompson, I. P. (2005). Perspectives and vision for strain selection in bioaugmentation. *Trends Biotechnol.* 23, 74–77. doi: 10.1016/j.tibtech.2004.12.012

Singh, S., Kumar, V., Chauhan, A., Datta, S., Wani, A. B., Singh, N., et al. (2018). Toxicity, degradation and analysis of the herbicide atrazine. *Environ. Chem. Lett.* 16, 211–237. doi: 10.1007/s10311-017-0665-8

Smith, D., Alvey, S., and Crowley, D. E. (2005). Cooperative catabolic pathways within an atrazine-degrading enrichment culture isolated from soil. *FEMS Microbiol. Ecol.* 53, 265–273. doi: 10.1016/j.femsec.2004.12.011

Soltani, N., Mashhadi, H. R., Mesgaran, M. B., Cowbrough, M., Tardif, F. J., Chandler, K., et al. (2011). The effect of residual corn herbicides on injury and yield of soybean seeded in the same season. *Can. J. Plant Sci.* 91, 571–576. doi: 10.4141/cjps10110

Souza, B. S., Dantas, R. F., Cruz, A., Sans, C., Esplugas, S., and Dezotti, M. (2014). Photochemical oxidation of municipal secondary effluents at low H_2O_2 dosage: study of hydroxyl radical scavenging and process performance. *Chem. Eng. J.* 237, 268–276. doi: 10.1016/j.cej.2013.10.025

Strong, L. C., McTavish, H., Sadowsky, M. J., and Wackett, L. P. (2000). Field-scale remediation of atrazine-contaminated soil using recombinant Escherichia coli expressing atrazine chlorohydrolase. *Environ. Microbiol.* 2, 91–98. doi: 10.1046/j.1462-2920.2000.00079.x

Vaishampayan, P. A., Kanekar, P. P., and Dhakephalkar, P. K. (2007). Isolation and characterization of *Arthrobacter* sp strain MCM B-436, an atrazine-degrading bacterium, from rhizospheric soil. *Int. Biodeterior. Biodegrad.* 60, 273–278. doi: 10.1016/j.ibiod.2007.05.001

van der Heijen, M. G. A. (2008). The unseen majority: soil microbes as drivers of plant diversity and productivity in terrestrial ecosystems (vol 11, pg 296, 2008). *Ecol. Lett.* 11:651. doi: 10.1111/j.1461-0248.2007.01139.x

Wang, Q., Xie, S., and Hu, R. (2013). Bioaugmentation with *Arthrobacter* sp strain DAT1 for remediation of heavily atrazine-contaminated soil. *Int. Biodeterior. Biodegrad.* 77, 63–67. doi: 10.1016/j.ibiod.2012.11.003

Wang, J., Zhu, L., Wang, Q., Wang, J., and Xie, H. (2014). Isolation and characterization of atrazine mineralizing *Bacillus* subtilis strain HB-6. *PLoS One* 9:e107270. doi: 10.1371/journal.pone.0116382

Xu, X., Zarecki, R., Medina, S., Ofaim, S., Liu, X., Chen, C., et al. (2019). Modeling microbial communities from atrazine contaminated soils promotes the development of biostimulation solutions. *ISME J.* 13, 494–508. doi: 10.1038/s41396-018-0288-5

Yang, H., Zhang, Y., Chuang, S., Cao, W., Ruan, Z., Xu, X., et al. (2021). Bioaugmentation of acetamiprid-contaminated soil with *Pigmentiphaga* sp. strain D-2 and its effect on the soil microbial community. *Ecotoxicology* 30, 1559–1571. doi: 10.1007/s10646-020-02336-8

Zhang, Y., Yang, C., Zheng, Z., Cao, B., You, F., Liu, Y., et al. (2021). Mechanism for various phytotoxicity of atrazine in soils to soybean: insights from soil sorption abilities and dissolved organic matter properties. *J. Environ. Manag.* 297:113220. doi: 10.1016/j.jenvman.2021.113220

Zhu, J., Fu, L., Jin, C., Meng, Z., and Yang, N. (2019). Study on the isolation of two atrazine-degrading bacteria and the development of a microbial agent. *Microorganisms* 7:80. doi: 10.3390/microorganisms7030080

Conflict of Interest: The authors declare that the research was conducted in the absence of any commercial or financial relationships that could be construed as a potential conflict of interest.

frontiers in Environmental Science

ORIGINAL RESEARCH
published: 21 December 2021
doi: 10.3389/fenvs.2021.799264

Removal Study of Crystal Violet and Methylene Blue From Aqueous Solution by Activated Carbon Embedded Zero-Valent Iron: Effect of Reduction Methods

Yongmei Wang[1], Tiantian Chen[2], Xiaolin Zhang[3] and Teza Mwamulima[3]*

[1]College of Safety and Environmental Engineering, Shandong University of Science and Technology, Qingdao, China, [2]CAS Key Laboratory of Marine Ecology and Environmental Sciences, Institute of Oceanology, Chinese Academy of Sciences, Qingdao, China, [3]College of Environmental Science and Engineering, Ocean University of China, Qingdao, China

OPEN ACCESS

Edited by:
Lean Zhou,
Changsha University of Science and Technology, China

Reviewed by:
Rui Hou,
South China Sea Institute of Oceanology (CAS), China
Hongliang Li,
Taiyuan University of Technology, China
Jingju Cai,
Central South University of Forestry and Technology, China

***Correspondence:**
Tiantian Chen
chentian0819@163.com

Specialty section:
This article was submitted to Water and Wastewater Management, a section of the journal Frontiers in Environmental Science

Received: *21 October 2021*
Accepted: *25 November 2021*
Published: *21 December 2021*

Citation:
Wang Y, Chen T, Zhang X and Mwamulima T (2021) Removal Study of Crystal Violet and Methylene Blue From Aqueous Solution by Activated Carbon Embedded Zero-Valent Iron: Effect of Reduction Methods. Front. Environ. Sci. 9:799264. doi: 10.3389/fenvs.2021.799264

Zero valent iron (ZVI) particles were embedded into porous materials to avoid aggregation and separation problems in the controlled synthesis process. To investigate the adsorption mechanism of crystal violet and methylene blue, activated carbon (AC) and AC-based ZVI extraction by solid-phase and liquid-phase reduced approaches was conducted. Characterization methods of specific surface area, scanning electron microscopy (SEM), and x-ray diffractograms (XRD) were used to elucidate the structure of adsorbents, and the adsorption capacities of crystal violet and methylene blue were obtained under experimental conditions of various pH values (2.0–10.0), adsorption times (0–72 h), and temperatures (30–50°C). The adsorption of crystal violet/methylene blue was controlled by both chemisorption and reduction. The adsorption processes were fitted to a pseudo-second-order kinetic model, and that of reduction kinetics was suitable to pseudo-first-order kinetic model. The thermodynamic study revealed that the adsorption of crystal violet and methylene blue was endothermic and spontaneous, and the adsorption isotherms fitted well to the Langmuir model. Different adsorption capacities of crystal violet and methylene blue on various adsorbents were found, indicating that both the properties of adsorbents (pore size, specific surface area, and chemical functional groups) and the structures of adsorbates had significant effect on the removal of dye molecules.

Keywords: water pollution, activated carbon, zero valent iron, crystal violet, methylene blue

INTRODUCTION

Water pollution, a known universal crisis, might cause a reduction in the population, or extinction, of living things; reduce the value of environmental resources; and pose a threat to ecological balance (Iqbal et al., 2019; Efimov et al., 2019; Li et al., 2020). The release of dye in wastewater generated from different industries has been considered to be an important source of water pollution (Bilal et al., 2016a; Nouren et al., 2017). These dyes pose a serious threat to the ecological environment since they are extremely stable and non-biodegradable, and their accumulation always leads to poor oxygenation of the water environment by preventing the photosynthesis of photosynthetic

organisms (Spadaro et al., 1992; Xu et al., 2018). Moreover, most dyes are toxic, mutagenic, and carcinogenic, leading to serious harm for aquatic animals and human health (Bilal et al., 2016a; Bilal et al., 2016b; Ramamoorthy et al., 2020). Therefore, it is quite significant to carry out the remediation of dyes in wastewater to clean the water environment and safeguard human health (Abbas et al., 2018; Amin et al., 2020).

To impede the discharge and pollution of dye in wastewater, plenty of treatment methods have been continuously improved to remove these dyes from wastewater (Chen et al., 2017; Saber-Samandari et al., 2017). Considering economics, applicability, and removal efficacy, adsorption is suggested as the most popular technique (Fernandes et al., 2010; Xu et al., 2014; Rasalingam et al., 2015), in which the selection of adsorbents is the key factor affecting removal efficiency (Fernandes et al., 2010; Zhang et al., 2020b; Liu et al., 2014). Activated carbon (AC) is known as the most effective adsorbent; however, the expensive cost of AC restricts its wide utilization. Recently, a variety of bio-based activated carbons derived from agricultural wastes such as fruit peel, crop straw, coconut shell, and vegetable residues have been synthesized to make the adsorption process more feasible and cost-effective (Mishra et al., 2021). Moreover, iron-based porous materials have been developed to be effective adsorbents for toxic dye removal from wastewater (Zhang et al., 2010; Wang et al., 2012), mainly because of the unique redox potential of zero valent iron (ZVI) combined with the high surface area and large reaction sites of porous adsorbents (Kerkez et al., 2014). Previous studies demonstrated that iron-modified montmorillonite could effectively adsorb crystal violet (CV) (Guz et al., 2014), and iron nanoparticles decorated onto three-dimensional graphene could rapidly and efficiently degrade azo dye (Wang et al., 2015).

However, the application of ZVI in actual water treatment is subject to certain restrictions, because it tends to agglomerate and is easily oxidized (Liu et al., 2007; Fan et al., 2016). Therefore, many studies have been initiated to search for different matrices to overcome the iron particle aggregation, such as adding iron on montmorillonite for the adsorption of toxic cationic dyes (Wang et al., 2017; Liu et al., 2018) and adding iron nanoparticles onto three-dimensional graphene to degrade azo dyes (Liu et al., 2018). It could be found that two different approaches, namely, solid-phase and liquid-phase iron direct reduction technology (Liu et al., 2007; Wang et al., 2017; Liu et al., 2018), are the main approaches to prepare ZVI covered on adsorbents for effectively removing toxic dyes in wastewater. Using liquid-phase iron direct reduction technology, many materials were used as matrices to fix nZVI including kaolinite (Liu et al., 2007), activated carbon (Liu et al., 2018), graphene (Wang et al., 2017), and palygorskite (Ngulube et al., 2019), which exhibited an excellent dye removal efficiency. Based on solid-phase iron direct reduction technology, different kinds of iron-based adsorbents with the ZVI particles embedded into matrixes could be prepared, overcoming the lack of instability of ZVI synthesized in the liquid-phase direct reduction approach (Wang et al., 2017; Zheng et al., 2019).

In order to research the removal efficiency and purification mechanism of dyes onto AC embedded with ZVI extracted by solid/liquid-phase direct reduction approach, a series of AC supported ZVI adsorbents were synthesized and used to remove CV and methylene blue (MB) at various pH values, adsorption times, and temperatures. CV and MB were chosen as the representation of dyes because of the wide area of applications and similar molecular weights/different molecular structures. In this study, palm kernel shells as agricultural wastes were used to prepare AC adsorbents owing to their low ash content, high in carbon and volatile content (Ajeng et al., 2021). The higher heating value of palm kernel shells was beneficial for the solid-phase iron direct reduction technology (Wang et al., 2017; Bazargan et al., 2018). Thus, AC adsorbents were used as reductants to prepare the ZVI in the solid-phase iron direct reduction process and as matrices to fix nZVI in the liquid-phase iron direct reduction process. Adsorption data were interpreted by using adsorption kinetics, adsorption isotherms, and thermodynamic models to calculate the adsorption capacities and thermodynamic parameters.

MATERIALS AND METHODS

Materials and Chemicals

Palm kernel shell (C 50.2%, H 6.2%, O 40.8%, and N 0.3%), and iron ore tailings (Fe_2O_3 27.47%, Al_2O_3 6.44%, SiO_2 22.44%, CaO 1.95%, MgO 3.07%, and S_2O_3 4.61%) were sieved through 500-mesh screens and dried in an oven at 80°C for 24 h. Analytical grade dye molecules (CV and MB), iron chloride ($FeCl_3{\cdot}6H_2O$), ethanol, sodium borohydride ($NaBH_4$), and sodium hydroxide (NaOH) were purchased from Beijing Chemical Reagents Company (Beijing, China). Water used in this experiment was deionized water.

Preparation of Adsorbents

AC from palm kernel shell (PAC, 1#) and ZVI adsorbents produced through the solid-phase direct reduction approach (PAC-mZVI, 2#) were prepared as shown in **Figure 1**. In the preparation of PAC, palm kernel shell was heated in the absence of oxygen at a heating rate of 10°C min^{-1}, a heating temperature of 800°C, and a calcining time of 40 min, to maintain its weight and produce a loose porous structure. Schematic of the preparation steps is shown in **Figure 1**.

The solid-phase direct reduction approach was chosen to produce ZVI to prepare PAC-mZVI (2#), in which iron ore tailings were reduced by palm kernel shell to ZVI during the sintering process at high temperature, as shown in the chemical reaction below:

$$C + Fe_xO_y \rightarrow Fe_xO_{y-1} + CO\uparrow$$
$$CO + Fe_xO_y \rightarrow Fe_xO_{y-1} + CO_2\uparrow$$
$$H_2 + Fe_xO_y \rightarrow Fe_xO_{y-1} + H_2O$$

According to a previous study (Wang et al., 2017), the liquid-phase direct reduction approach was chosen to produce nanoscale ZVI to prepare PAC-nZVI (3#) adsorbents, in

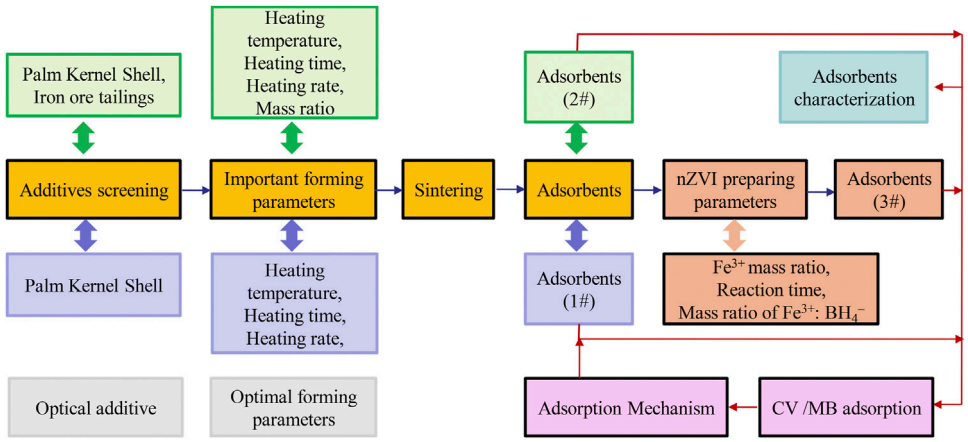

FIGURE 1 | Schematic of the preparation of the adsorbents.

which Fe^{3+} was reduced by $NaBH_4$ to ZVI on the surface of PAC as shown in the chemical reaction below:

$$2FeCl_3 + 6NaBH_4 + 18H_2O \rightarrow 2Fe^0 + 6NaCl + 6B(OH)_3 + 21H_2\uparrow$$

Iron chloride solution ($FeCl_3$) saturated PAC adsorbents and sodium borohydride solution ($NaBH_4$) were shaken at 120 r min^{-1} under a temperature of 30°C to reduce Fe^{3+} to ZVI. The optimal experimental factors influencing the amount of ZVI covered on the surface of PAC were selected at a shaking time of 1 h, a molar ratio of Fe^{3+}:BH_4^-at 1:3, and a mass ratio of Fe^{3+}:PAC adsorbent at 1:5.

Characterization

The surface area and pore size were detected according to nitrogen adsorption–desorption isotherms using the Autsorb-1 (Quantachrome, United States). The morphological characteristics and chemical components of these adsorbents were determined using scanning electron microscopy (SEM, JSM-6610 LV, Jeol, Japan) and x-ray diffractograms (XRD, 08 Advance Davinci, Bruker, Germany), respectively. Zeta potentials were determined by a Zeta Probe apparatus (Colloidal-Dynamics, United States).

Adsorption Experiments

Dye solution (100 ml) with an initial concentration of 50–1,000 mg L^{-1} and an adsorbent dose of 0.6 g were added into glass conical flasks to carry out the adsorption experiments at the constant speed of 120 rpm. The desired pH value was adjusted at the range of 2–10. Adsorption kinetic studies were carried out at various adsorption times (0–72 h). The removal efficiencies (R) and adsorption capacities (Q_t) were calculated by **Eqs 1**, **2** (Mwamulima et al., 2018). Adsorption isotherm studies were conducted with different initial concentrations of dye solution (50, 100, 200, 400, 600, 800, and 1,000 mg L^{-1}) at temperatures of 30, 40, and 50°C. The concentrations of residual CV and MB in aqueous solution were detected by UV spectrophotometry.

TABLE 1 | Textural features of palm kernel shell, PAC, PAC-mZVI, and PAC-nZVI adsorbents.

Sample	Palm kernel shell	PAC	PAC-mZVI	PAC-nZVI
S_{BET} (m^2/g)	125.12	1,075.23	445.39	725.94
S_{Micro} (m^2/g)	70.22	899.82	221.33	382.28
R_p (Å)	1,512.72	990.45	810.25	928.22

$$R = \frac{C_0 - C_t}{C_0} \times 100\% \quad (1)$$

$$Q_t = \frac{(C_0 - C_t)V}{m} \quad (2)$$

where C_0 (mg L^{-1}) is the initial concentration, C_t (mg L^{-1}) is the concentration at time t, V (L) is the volume of the solution, and m (g) is the adsorbent weight.

RESULTS AND DISCUSSION

Adsorbents Characterization

Nitrogen adsorption method was used to determine the pore diameter, pore volume, and surface area of adsorbents in **Table 1**. Compared with palm kernel shell, PAC, PAC-mZVI, and PAC-nZVI had a much larger surface area and micropore area, which might lead to the deduction that abundant micropores were generated in the process of biomass pyrolysis chemical reaction of palm kernel shell at high temperature (Guo et al., 2016). Moreover, the calcining temperature in the preparation of PAC-mZVI adsorbents had a significant impact on the reduction process, which largely determined the micropore area and pore size. The surface area of PAC-nZVI adsorbents was higher than the other three adsorbents, showing that the adsorbents prepared by the liquid-phase reduction approach had the largest BET surface area.

SEM and EDX images of PAC, PAC-mZVI, and PAC-nZVI are shown in **Figure 2**. It could be clearly found that the

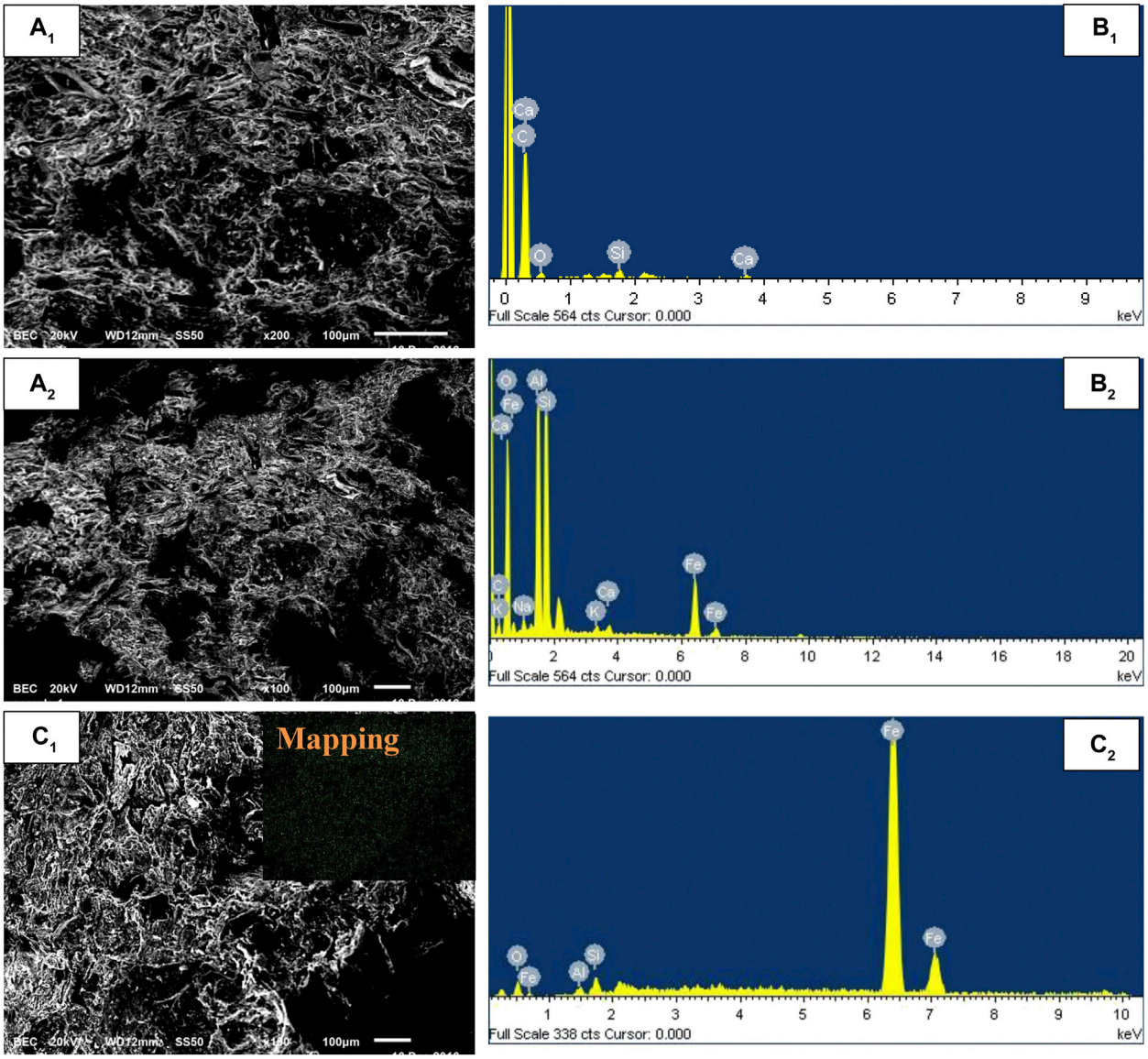

FIGURE 2 | SEM images of **(A_1)** PAC, **(B_1)** PAC-mZVI, and **(C_1)** PAC-nZVI and EDX images of **(A_2)** PAC, **(B_2)** PAC-mZVI, and **(C_2)** PAC-nZVI.

surface of these adsorbents was rough; meanwhile, numerous pores existed in these adsorbents. This could be attributed to the fact that the organic matter in palm kernel shell generated volatile CO, CO_2, and hydrogen during the sintering process (Guo et al., 2016). These volatile gases escaped from the inside of adsorbents; then, the pores were formed in this process. Moreover, PAC-nZVI adsorbents contained more pores compared with PAC-mZVI adsorbents, which might be attributed to the cementation effect of ZVI particle in the solid-phase reduction process (Wang et al., 2017). Combined with EDX analysis, it could be found that ZVI was generated in the solid-phase reduction reaction with the reductants of palm kernel shell and liquid-phase reduction reaction process in aqueous solution. As shown in **Figure 2C**, newly formed ZVI particles in the liquid-phase reduction reaction process were uniformly dispersed throughout the matrix, owing to the advantages of the liquid-phase iron reduction approach.

XRD analyses were chosen to identify various phases and phase transformations for PAC, PAC-mZVI, and PAC-nZVI adsorbents. As depicted in **Figure 3A**, the main component of PAC adsorbents was carbon. As for PAC-mZVI in **Figure 3B**, hematite (Fe_2O_3) and ZVI were found as well as the carbon that PAC contained, indicating that palm kernel shells were translated to PAC, and iron ore tailings were partly reduced to ZVI in the solid reduction process with palm kernel shell as reductants (Man et al., 2014; Wang et al., 2017). As shown in **Figure 3C**, PAC-nZVI adsorbents mainly contained carbon and ZVI. Compared with PAC-mZVI adsorbents, ZVI was the unique form of iron element in PFB-nZVI adsorbents, confirming that Fe^{3+} was directly reduced to ZVI covered on porous adsorbents in

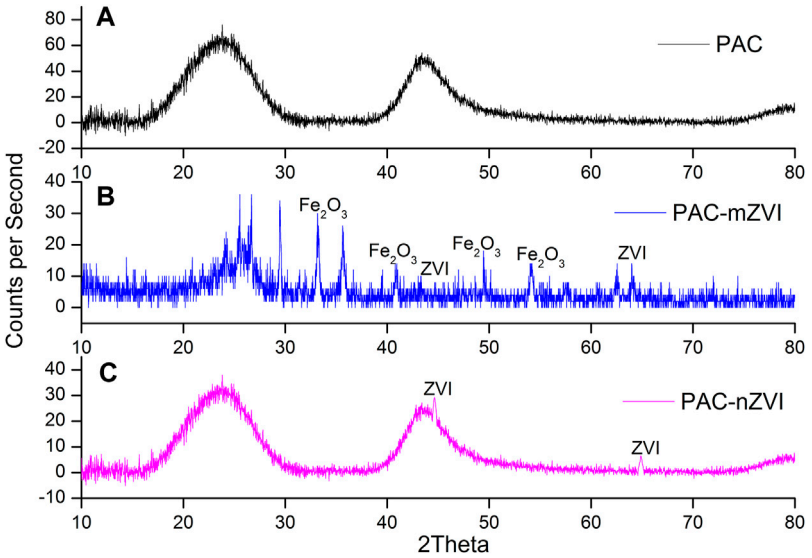

FIGURE 3 | X-ray diffractograms of three different adsorbents. **(A)** PAC, **(B)** PAC-mZVI, and **(C)** PAC-nZVI.

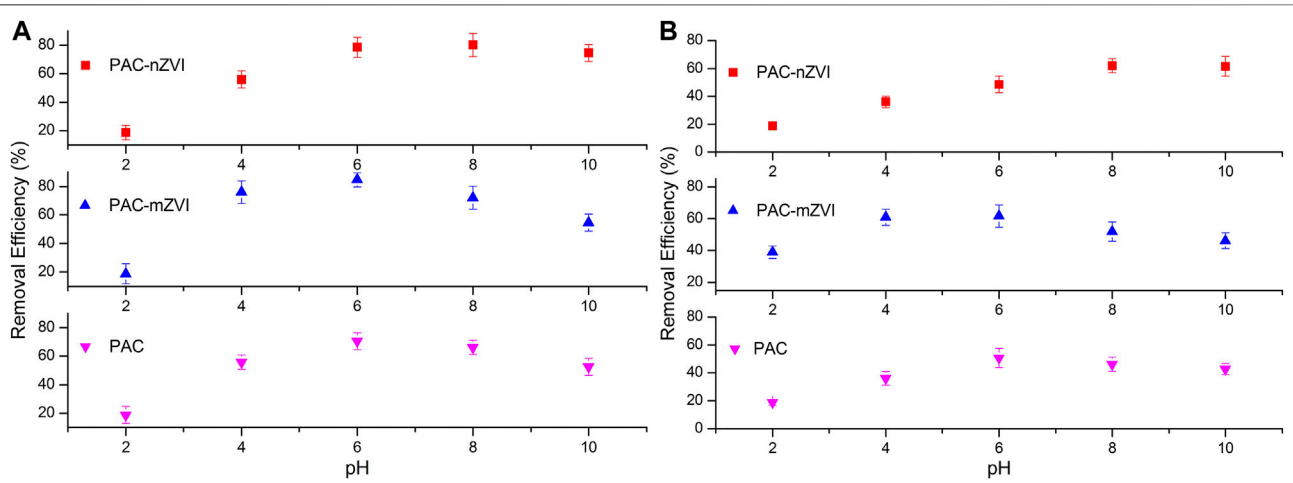

FIGURE 4 | Effects of pH on the removal of CV **(A)** and MB **(B)** by PAC, PAC-mZVI, and PAC-nZVI adsorbents.

liquid-phase reduction approach (Liu et al., 2018; Mwamulima et al., 2018).

Effects of pH on Crystal Violet and Methylene Blue Removal

Removal efficiencies of CV and MB by PAC, PAC-mZVI, and PAC-nZVI adsorbents were researched at different pH values, and effects of pH value on adsorption capacity are shown in **Figure 4**. The adsorption process was significantly affected by the changing of pH value, mainly because the existence forms of functional groups on the adsorbents were changed under different acid and alkali conditions (Wang et al., 2017; Liu et al., 2018; Mwamulima et al., 2018). As shown in **Figure 4**, removal efficiencies of dye molecules increased with the increase of pH value at the initial stage, then gradually decreased after the maximum. Meanwhile, we could find that removal efficiencies of CV by these three different adsorbents reached the maximum when pH value was approximately at 6.0, 6.0 and 8.0, respectively.

This phenomenon could be attributed to the influence of structure characteristics and the point of zero charge (pH_{pzc}) of adsorbents. As reported in previous literature, the surface of adsorbent had a positive charge at $pH < pH_{pzc}$, negative charge at $pH > pH_{pzc}$, and net zero charge at $pH = pH_{pzc}$, respectively (Hammed et al., 2016). In this study, pH_{pzc} of PAC, PAC-mZVI, and PAC-nZVI adsorbents was approximately 5.5, 7.0, and 8.0, respectively. At lower pH, excess H^+ might compete with CV/MB molecule for adsorption sites, inhibiting the adsorption process of

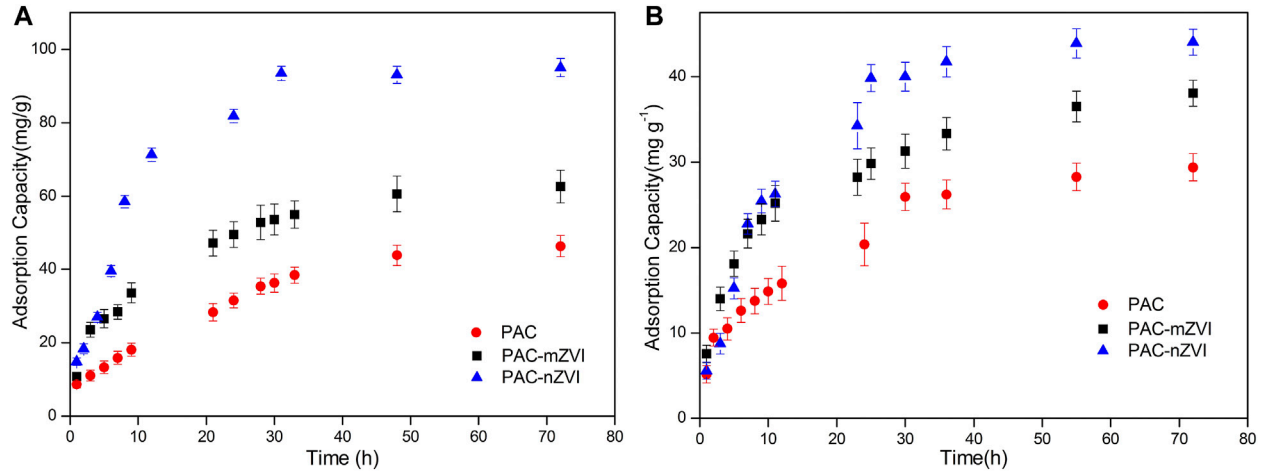

FIGURE 5 | Effects of contact time on the removal of CV **(A)** and MB **(B)** by PAC, PAC-mZVI, and PAC-nZVI adsorbents.

CV and MB onto adsorbents. Moreover, electrostatic repulsion existed between adsorbents and dye molecules, which would be also largely adverse to the adsorption of CV/MB onto adsorbents. Generally, cationic dyes were quite easily absorbed onto adsorbents with negative charges owing to the attraction of positive and negative charges. It could be concluded that excess OH^- at higher pH promoted the formation of iron hydroxide, which could occupy the reactive sites on adsorbents to decrease the reduction reaction of CV/MB in this experiment (Chen et al., 2013).

Effects of Contact Time on Crystal Violet and Methylene Blue Removal

The adsorption capacities of CV and MB at 30°C are shown in **Figure 5**. The adsorption processes of CV/MB were generally fast at the initial stage and then leveled off with time, which was attributed to the fact that huge amounts of active vacant sites on these adsorbents were gradually occupied. As depicted in **Figures 5A,B**, the adsorption of CV and MB on PAC-nZVI reached equilibrium at approximately 50 h, which was slightly longer than other adsorbents. The reason was that the specific surface area of PAC-nZVI adsorbents was larger than that of other adsorbents and a large number of pores existed in the interior of the adsorbents. Moreover, the adsorption capacity of PAC-nZVI adsorbents for CV and MB arrived at 97 mg g^{-1} and 43 mg g^{-1}, which was higher than that of other adsorbents. This could be attributed to the fact that both adsorption and reduction reactions were included in the removal processes of CV and MB by these three different adsorbents. PAC-nZVI adsorbents contained higher concentration of ZVI compared with that of other adsorbents, generating more active sites to promote the increase in adsorption capacity. Besides, it could be found that the absorption of MB reached the equilibrium faster than that of CV, which could be attributed to the fact that the triangular shape of CV was not beneficial when entering smaller pores compared with the chain shape of MB.

Effects of Temperature on Crystal Violet and Methylene Blue Removal

Changes in adsorption capacity of CV and MB under different temperatures are depicted in **Figure 6**. It could be found that the adsorption capacity of CV/MB increased with the increase of temperature, indicating that the adsorption processes of dye molecules were endothermic reaction. Moreover, the phenomenon could also be explained by the fact that high temperature could promote the increase in pore size and surface area to enlarge the adsorption capacity (Liu et al., 2018). When the temperature arrived at 50°C, the adsorption capacity of PAC-nZVI for CV and MB arrived at approximately 110 and 73 mg g^{-1}, respectively. Moreover, the change rate of adsorption capacity with time increased as the reaction temperature increased. It might be attributed to the increase in the mobility of dye molecules in aqueous solution and the formation of reactive sites on the interface of adsorbents under higher temperature (Liu et al., 2018; Mwamulima et al., 2018).

Kinetic Study

Adsorption Kinetics

Lagergren pseudo-first-order rate (**Eq. 3**) (Lagergren, 1898), pseudo-second-order rate (**Eq. 4**) (Ho and McKay, 1999), and Weber-Morris diffusion model (**Eq. 5**) (Weber and Morris, 1963) were chosen to explain the kinetics of CV and MB onto these three adsorbents, which could be described as:

$$\log(q_e - q_t) = \log q_e - \frac{k_1}{2.303}t \tag{3}$$

$$\frac{t}{q_t} = \frac{1}{k_2 q_e^2} + \frac{1}{q_e}t \tag{4}$$

$$q_t = k_{\text{int}} t^{0.5} + b \tag{5}$$

where q_e (mg g^{-1}) and qt (mg g^{-1}) are the adsorption capacities at equilibrium and time t, respectively. k_1 (1/h), k_2 (1/h), k_{int}, and b are the constants in pseudo-first-order, pseudo-second-order, and intraparticle diffusion, respectively.

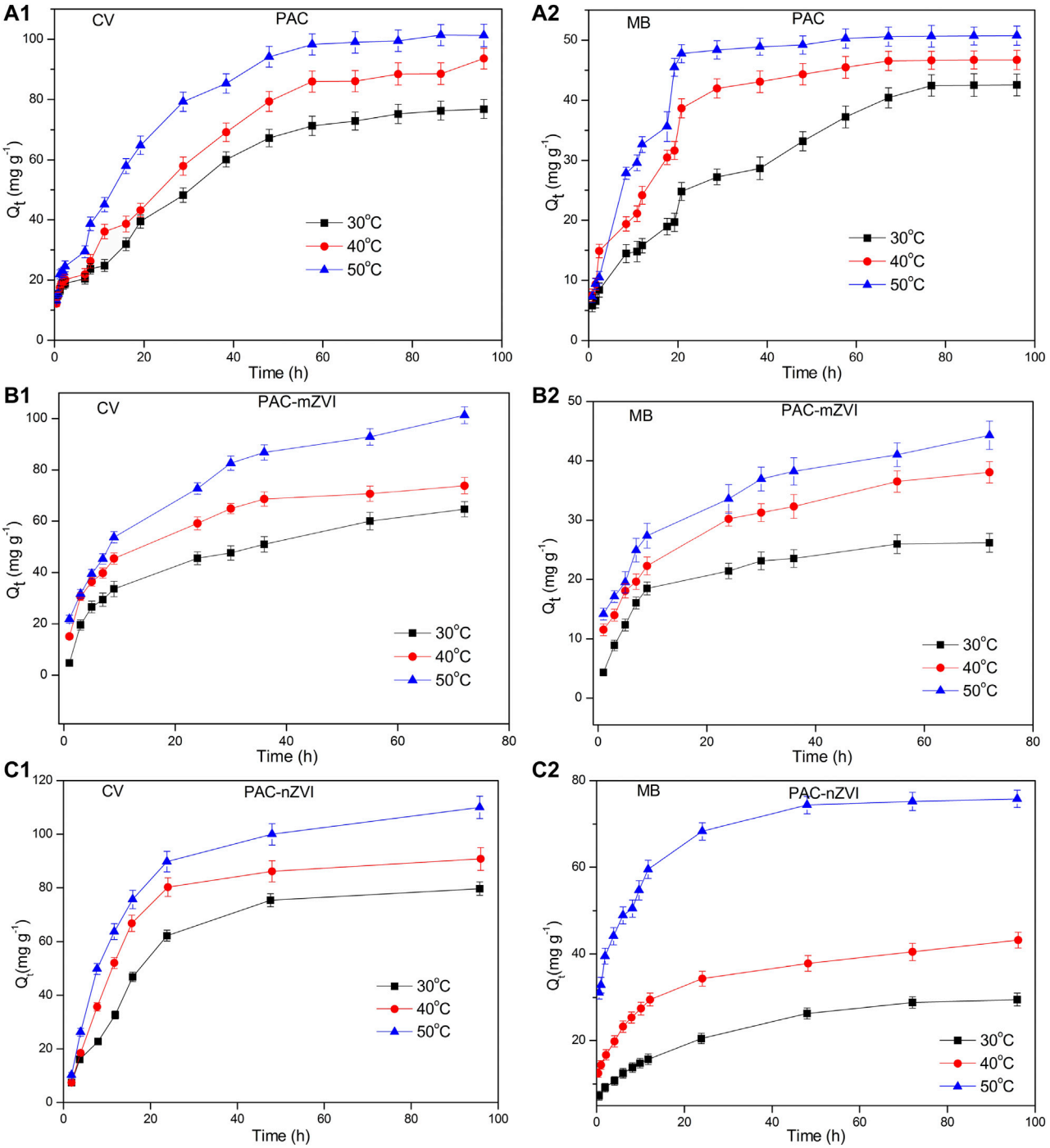

FIGURE 6 | Effects of temperature on the removal of CV and MB by PAC, PAC-mZVI, and PAC-nZVI adsorbents.

The kinetic parameters (r^2, Q_e, K_1, and K_2 values) are shown in **Table 2**. According to the previous literature, the optimal fitting model could be selected based on the parameter of r^2 value (Wang et al., 2017). Thus, it could be found that adsorption of CV/MB onto these three adsorbents fitted the pseudo-second-order rate equations well due to the relatively better r^2 values compared with that of the pseudo-first-order kinetic model. Based on the q_e values calculated from the pseudo-second-order kinetics model, PAC-nZVI adsorbent showed the highest adsorption capacities at equilibrium compared with other adsorbents. These values of q_e had quite good agreement with experimental results. Thus, we could deduce that chemisorption was the rate-controlling step in the removal process of CV/MB onto PAC and PAC-based ZVI adsorbents (Liu et al., 2018; Mwamulima et al., 2018).

TABLE 2 | Kinetic parameters for the adsorption of CV and MB dye on PAC and PAC-based ZVI adsorbents.

Adsorbents	T	Pseudo-first-order kinetic model						Pseudo-second-order kinetic equation					
		CV			MB			CV			MB		
		r^2	q_e	K_1	r^2	Q_e	K_1	r^2	q_e	K_2	r^2	q_e	K_2
PAC	30	0.9779	66	0.012	0.9536	48	0.0244	0.9862	76	0.00014	0.9666	54	0.0003
	40	0.9701	84	0.015	0.9740	53	0.0244	0.9633	91	8.1e-5	0.9770	54	0.0003
	50	0.9703	87	0.013	0.9110	66	0.025	0.9869	95	7.57e-5	0.9734	60	0.0002
	30	0.9446	58	0.104	0.8973	25	0.151	0.9963	69	0.0018	0.9919	31	0.0043
PAC-mZVI	40	0.9299	66	0.160	0.9108	33	0.142	0.9936	76	0.0025	0.9939	41	0.0036
	50	0.8687	75	0.113	0.8955	35	0.142	0.9906	100	0.0014	0.9934	53	0.0035
	30	0.8324	63	0.0035	0.9546	27	0.0005	0.9963	72	0.0039	0.9924	32	0.0022
PAC-nZVI	40	0.8531	79	0.0058	0.9668	38	0.0005	0.9926	84	0.0095	0.9652	42	0.0015
	50	0.8176	92	0.0051	0.9689	63	0.0010	0.9982	102	0.0183	0.9948	69	0.0044

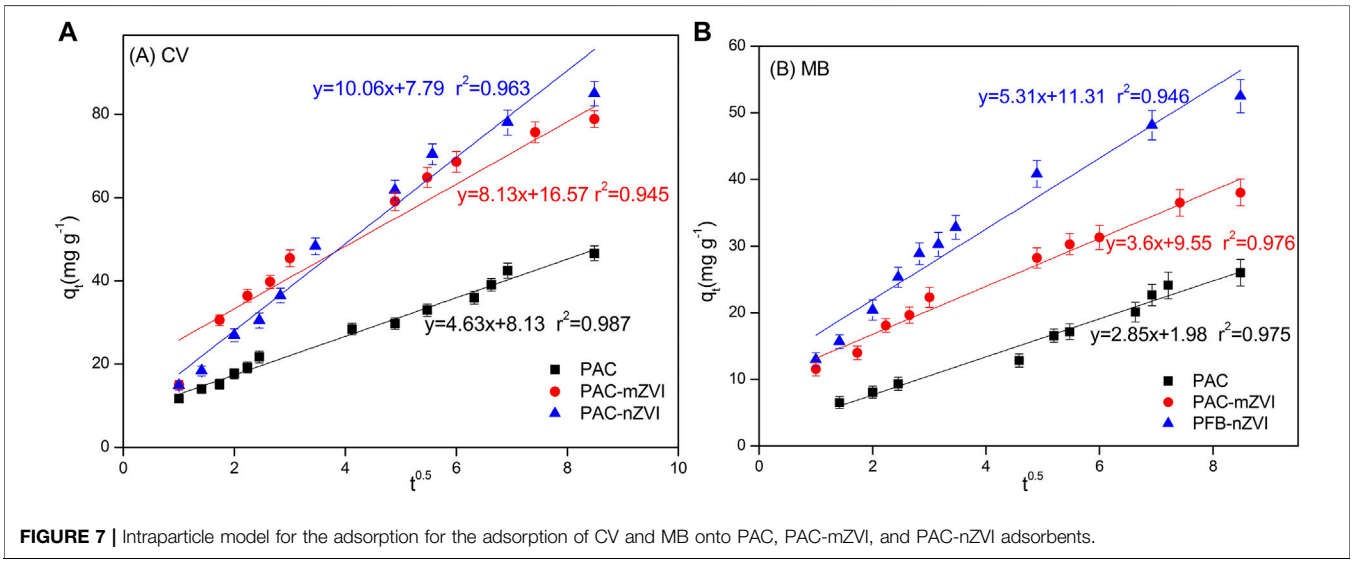

FIGURE 7 | Intraparticle model for the adsorption for the adsorption of CV and MB onto PAC, PAC-mZVI, and PAC-nZVI adsorbents.

TABLE 3 | Reduction kinetic parameters of CV and MB dyes on PAC and PAC-based ZVI adsorbents.

Adsorbents	T	Pseudo-first-order kinetic model				Pseudo-second-order kinetic equation			
		CV		MB		CV		MB	
		r^2	K_{obs}	r^2	K_{obs}	r^2	K	r^2	K
PAC	30	0.9569	0.003	0.9512	0.0001	0.9121	0.0093	0.9452	0.0002
	40	0.9715	0.0055	0.9621	0.0002	0.9352	0.0135	0.9522	0.0003
	50	0.9828	0.0063	0.9788	0.0008	0.9352	0.0135	0.9624	0.0006
	30	0.9919	0.0716	0.9967	0.0164	0.9638	0.00041	0.9968	0.00005
PAC-mZVI	40	0.9914	0.0756	0.9961	0.0348	0.8834	0.00042	0.9760	0.00012
	50	0.9918	0.0827	0.9932	0.0627	0.8835	0.0005	0.9485	0.00022
	30	0.9853	0.0029	0.9575	6e-5	0.9539	0.0060	0.8721	0.0004
PAC-nZVI	40	0.9520	0.0040	0.9608	8e-5	0.7635	0.0060	0.8093	0.0005
	50	0.8454	0.0042	0.9243	0.0002	0.6879	0.0060	0.8540	0.0005

In order to further analyze the adsorption process, the Weber-Morris diffusion model was chosen to discuss the relationship between q_t and $t^{0.5}$ based on the intraparticle diffusion theory. If the intraparticle diffusion was a rate-limiting step, the plot of q_t against $t^{0.5}$ would yield a straight line with a slope of k_{int}. As depicted in **Figures 7A, B**, the linear plot of q_t vs. $t^{0.5}$ yielded a straight line, indicating that intraparticle diffusion was a rate-limiting step. Moreover, the linear plot did not pass

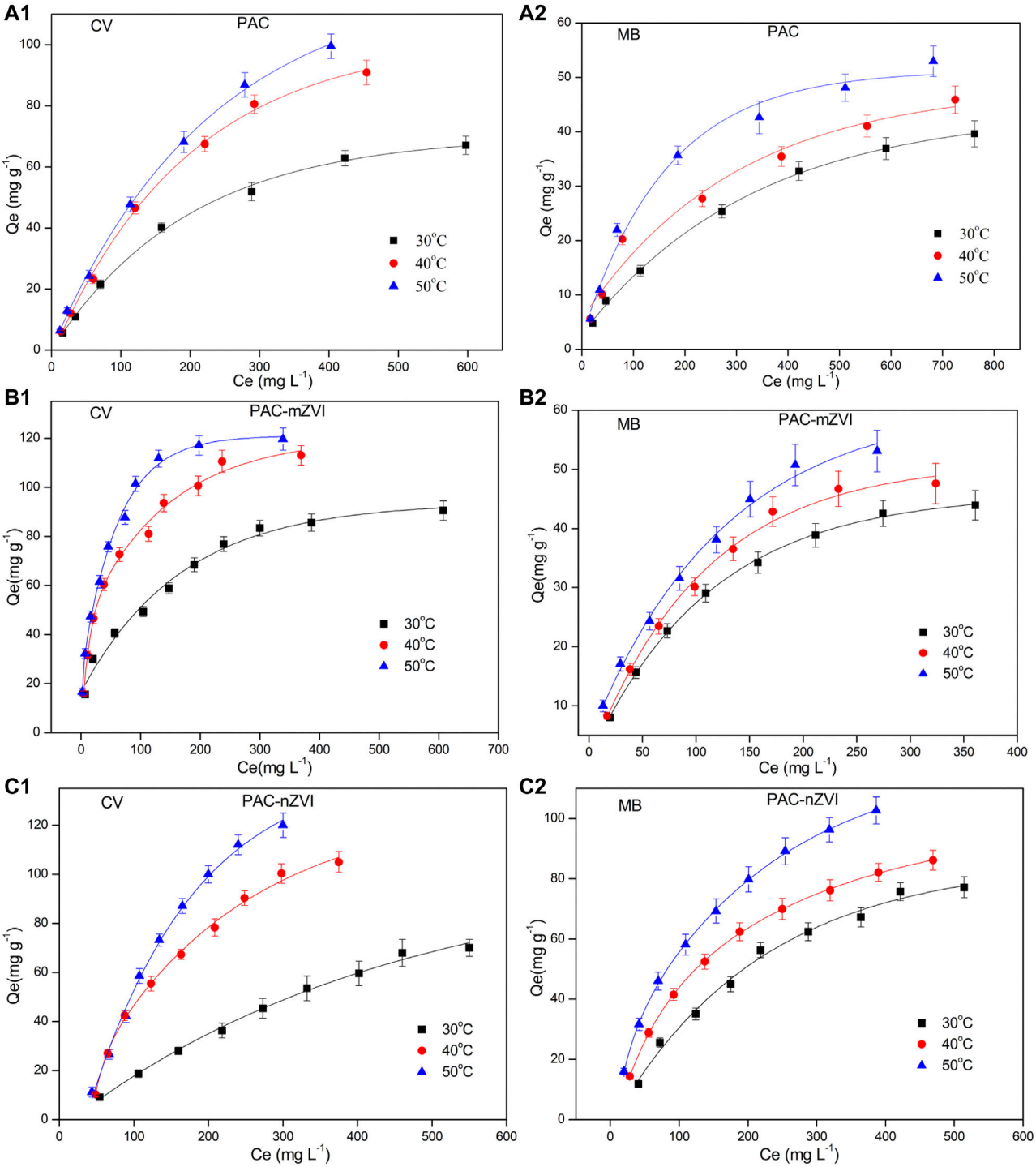

FIGURE 8 | Adsorption isotherms of CV and MB adsorbed onto PAC and PAC-based ZVI adsorbents, **(A_1)** CV by PAC; **(A_2)** MB by PAC; **(B_1)** CV by PAC-mZVI; **(B_2)** MB by PAC-mZVI; **(C_1)** CV by PAC-nZVI; **(C_2)** MB by PAC-nZVI.

through the origin, illustrating that the molecular diffusion controlled the adsorption reaction rate to some extent. Thus, it could be concluded that two processes, namely, chemisorption and diffusion, affected the removal process of these dye molecules.

Reduction Kinetics

Based on the above research results, adsorption reaction of CV/MB by PAC and PAC-based ZVI adsorbents included adsorption and chemical reduction (Chen et al., 2013; Wang et al., 2017; Ezzatahmadi et al., 2017). Pseudo-first-order and -second-order

TABLE 4 | Parameters for the adsorption isotherms of CV and MB on PAC and PAC-based ZVI adsorbents.

Adsorbents	T	Langmuir						Freundlich					
		CV			MB			CV			MB		
		r^2	q_m	b	r^2	q_m	b	r^2	K_f	1/*n*	r^2	K_f	1/*n*
PAC	30	0.9684	98	0.015	0.9968	60	0.0083	0.9862	7.6	0.414	0.9633	1.6	0.587
	40	0.9872	120	0.027	0.9879	68	0.0085	0.9633	10.1	0.451	0.9678	1.7	0.612
	50	0.9879	132	0.037	0.9823	74	0.0099	0.9869	13.2	0.439	0.9908	2.4	0.576
PAC-mZVI	30	0.9992	110	0.002	0.9935	38	0.0038	0.9632	2.2	0.545	0.9959	1.0	0.554
	40	0.9991	159	0.0023	0.9906	67	0.0045	0.9402	2.8	0.584	0.9797	2.2	0.463
	50	0.9961	204	0.0027	0.9968	84	0.0051	0.9715	1.7	0.672	0.9571	2.9	0.450
PAC-nZVI	30	0.9772	95	0.017	0.7728	68	0.0012	0.9456	2.8	0.710	0.9946	0.7	0.767
	40	0.9325	163	0.012	0.8732	79	0.0043	0.8840	21.3	0.221	0.9255	1.8	0.683
	50	0.9947	344	0.086	0.6039	99	0.0005	0.8568	55.1	0.382	0.9956	0.5	0.938

TABLE 5 | Thermodynamic parameters for the adsorption of CV and MB on PAC and PAC-based ZVI adsorbents.

Adsorbents	Temp	CV			MB		
		ΔG	ΔH	ΔS	ΔG	ΔH	ΔS
PAC	30	−4.49	38.01	140.65	−2.45	29.30	60.65
	40	−6.25			−2.61		
	50	−7.29			−3.10		
PAC-mZVI	30	−16.89	12.21	95.98	−17.89	12.12	99.08
	40	−17.81			−18.92		
	50	−18.81			−19.86		
PAC-nZVI	30	−22.06	80.40	334.05	−14.99	100.76	382.01
	40	−23.02			−18.81		
	50	−24.04			−22.78		

reduction kinetic models in **Eqs 6**, **7** were selected to study the reduction process (Kerkez et al., 2014).

$$\ln \frac{C_t}{C_0} = -k_{obs}t \tag{6}$$

$$\ln\left(\frac{1}{C_t} - \frac{1}{C_0}\right) = k_2 t \tag{7}$$

where C_0 (mg g^{-1}) and C_t (mg g^{-1}) are the concentration at the initial time and at time *t*; k_{obs} (h^{-1}) and k_2 (h^{-1}) are the rate constant of pseudo-first-order and second-order reaction, respectively.

Reduction kinetics parameters are shown in **Table 3**. Based on the reduction kinetics parameters, the pseudo-first-order kinetics model provided a better match of the experiment results of CV/MB dye, because of the relatively better r^2 values compared with that of the pseudo-second-order kinetic model. This indicated that CV/MB reacted with ZVI in the interface of the adsorbents through a solid–liquid reaction (Wang et al., 2017; Liu et al., 2018). Moreover, the reduction processes of CV/MB by these three adsorbents were endothermic, considering the reduction kinetic rate (k_{obs}) increased with the increase of temperature from 30 to 50°C. This was due to the fact that higher temperature could promote dye molecule transfer from aqueous solution to the surface of adsorbents (Adesemuyi et al., 2020).

Taking PAC-mZVI adsorbent for example, k_{obs} increased from 0.0716 to 0.0827 h^{-1} when the temperature increased from 30 to 50°C. It was depicted that the K_{obs} value of PAC-mZVI adsorbents was slightly higher, indicating that the chemical reduction reaction happened faster than that of the other two adsorbents. Based on the parameter values shown in **Tables 2**, **3**, it could be deduced that both physical adsorption and chemical reaction might handle the removal processes of CV/MB onto these adsorbents. Meanwhile, we could also find that the adsorption process of CV/MB dye was slightly faster than the reduction process by the comparison of the parameters of K_1 and K_{obs} (Chen et al., 2013).

Adsorption Isotherms

Adsorption isotherms could reveal the relationship of adsorption capacity of adsorbents and the concentration of adsorbates in aqueous solution, when the adsorption process reached equilibrium at a certain temperature. In this study, the Langmuir equation in **Eq. 8** (Langmuir, 1918) and the Freundlich equation in **Eq. 9** (Freundlich, 1906) were chosen to study the adsorption isotherms. The Langmuir equation supposed that adsorption was limited to monolayer coverage, while Freundlich isotherms assumed that the adsorption surface was heterogeneous and multilayer adsorption might be possible.

$$\frac{1}{q_e} = \frac{1}{q_{\max} C_e} + \frac{1}{q_{\max}} \tag{8}$$

$$\log q_e = \log K_F + \frac{1}{n}\log C_e \tag{9}$$

where C_e (mg L^{-1}) is the concentration of adsorbates at equilibrium, $q_{\max}$ (mg g^{-1}) is the maximum adsorption capacity, and K_F and *n* are constants related to adsorption capacity and intensity, respectively. Based on **Eqs 8**, **9**, it could be found that the near-perfect linear fitting of $1/q_e$ vs. $1/C_e$ belonged to the Langmuir model, while that of $\log q_e$ versus $\log C_e$ obeyed the Freundlich model. If the value of 1/*n* was less than 1, it might be attributed to the favorability of adsorption (Inbaraj and Chen., 2011; Fan et al., 2017).

The adsorption isotherms are depicted in **Figure 8**, and relevant adsorption isotherm parameters (b, Q_m, 1/*n*, K_f) are shown in **Table 4**. Considering the relatively better r^2 values, we could find that adsorption isotherms of CV/MB matched well with the Langmuir model. Consequently, adsorption processes of CV/MB onto PAC and PAC-based ZVI adsorbents were homogeneous and

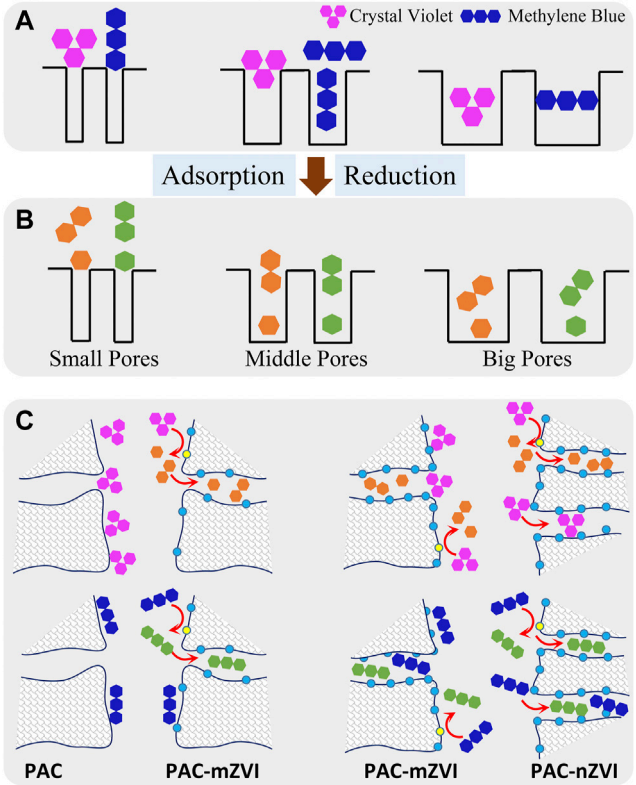

FIGURE 9 | A model of dye molecule (CV, MB) removal process by PAC and PAC-based ZVI adsorbents.

occurred at a monolayer region on the adsorbents. For the adsorption of CV dye, the Q_m value of PAC-nZVI adsorbents was the greatest compared with other adsorbents. As for MB, the Q_m value of PAC-nZVI adsorbents was 68, 79, and 99 mg g^{-1} at 30, 40, and 50°C, depicting the greatest adsorption capacity. Moreover, R_L values of CV and MB were less than 1, confirming that it was favorable for CV and MB adsorbed onto these adsorbents under this reaction condition (Inbaraj and Chen., 2011).

Thermodynamic Study

To analyze the effects of temperature on the adsorption, thermodynamic parameters including ΔH, ΔS, and ΔG were calculated based on the adsorption isotherms. The specific calculation method is shown as **Eqs 10**, **11**, respectively.

$$\Delta G = -RT \ln K \tag{10}$$

$$\ln K = \frac{\Delta S}{R} - \frac{\Delta H}{RT} \tag{11}$$

The parameter values of ΔH, ΔS, and ΔG are shown in **Table 5**. As noted, ΔG values of three different adsorbents decreased with the increase in temperature, indicating that the adsorption of CV/MB happened spontaneously. Meanwhile, ΔH values were all greater than zero, attributing to the fact that CV/MB adsorbed on adsorbents showed endothermic reactions. Moreover, values of ΔS in the adsorption processes were positive, which could further reveal the increasing randomness at the interface of solid/solution (Zhang et al., 2020a).

Mechanisms of Crystal Violet and Methylene Blue Removal by Adsorbents

CV and MB in water solution were firstly adsorbed on the surface of adsorbents, and then transported into the interior pores of adsorbents through pore diffusion. During the diffusion process, both the structural features of adsorbents and adsorbates had significant effects on the adsorption of dye molecules. When the molecular size of adsorbents was smaller than pore size, adsorbates could enter the internal pores for further adsorption action. Since the molecular structures of MB (line-shaped) and CV (fork-shaped) were different, the co-influence of the pore size of adsorbents and the structure of adsorbates on the removal processes is exhibited in **Figure 9A**.

CV and MB in the internal pores of adsorbents were finally adsorbed on the active sites of adsorbents, in which CV/MB was partly reduced by ZVI on the adsorbents. According to our previous research (Wang et al., 2017; Liu et al., 2018), CV was cleaved to two parts to generate new products *via* electrochemical reduction; however, MB reacted to its reduction state. The adsorption capacities of CV on these adsorbents were largely higher than that of MB as demonstrated in the experimental results, which might be attributed to the new products reduced from CV with smaller molecular size. Moreover, it could be deduced that specific surface area was also an important factor in the adsorption processes. The adsorption sites on the adsorbents increased with the increase in specific surface area. Based on the above discussion, the possible removal mechanisms of CV/MB from aqueous solutions on PAC and PAC-based ZVI adsorbents are proposed in **Figure 9**.

CONCLUSION

Adsorption of CV/MB on PAC and PAC-based ZVI adsorbents indicated that ZVI could efficiently remove cationic dyes from aqueous solution. The removal processes of CV/MB on adsorbents were significantly affected by the changing pH value, reaction time, and temperature. The adsorption capacities of CV/MB were fast in the initial stages and finally leveled off with time. The adsorption capacity increased with the increase in temperature. The adsorption processes of CV and MB onto these adsorbents all fitted well with the pseudo-second-order rate equations, and chemisorption was the rate-controlling step. The pseudo-first-order reduction kinetic model provided a better match of the adsorption process, indicating that dye molecules reacted with ZVI in the interface of adsorbents through a solid–liquid reaction, and the reduction process was endothermic. The adsorption isotherms obeyed the Langmuir model, indicating that CV/MB onto these adsorbents were homogeneous and occurred within a monolayer region on the surface of adsorbents. Compared with solid-phase iron direct reduction technology, PAC-nZVI adsorbents prepared by liquid-phase iron direct reduction technology showed higher adsorption capacity owing to the larger BET surface area and more ZVI particles. Furthermore, it was found that the properties of

adsorbents (pore size, specific surface area, and chemical functional groups) and the structure characteristics of adsorbates had significant effects on the adsorption efficiency of dye molecules.

DATA AVAILABILITY STATEMENT

The original contributions presented in the study are included in the article/supplementary material. Further inquiries can be directed to the corresponding author.

AUTHOR CONTRIBUTIONS

YW compiled and analyzed output data, and designed and wrote the first version of the manuscript. TC designed the study and managed the funding acquisition. XZ and TM conducted the experiments. All authors edited and approved the final version of this manuscript.

FUNDING

This study was financially supported by China Postdoctoral Science Foundation (grant number 2017M622301).

ACKNOWLEDGMENTS

The authors would like to thank Gang Zhou's team at Shandong University of Science and Technology who helped with the sampling and analysis.

REFERENCES

Abbas, M., Adil, M., Ehtisham-ul-Haque, S., Munir, B., Yameen, M., Ghaffar, A., et al. (2018). Vibrio Fischeri Bioluminescence Inhibition Assay for Ecotoxicity Assessment: A Review. *Sci. Total Environ.* 626, 1295–1309. doi:10.1016/j.scitotenv.2018.01.066

Adesemuyi, M. F., Adebayo, M. A., Akinola, A. O., Olasehinde, E. F., Adewole, K. A., and Lajide, L. (2020). Preparation and Characterisation of Biochars from Elephant Grass and Their Utilisation for Aqueous Nitrate Removal: Effect of Pyrolysis Temperature. *J. Environ. Chem. Eng.* 8, 104507. doi:10.1016/j.jece.2020.104507

Ajeng, A. A., Abdullah, R., Junia, A., Lau, B. F., Ling, T. C., and Ismail, S. (2021). Evaluation of palm Kernel Shell Biochar for the Adsorption of Bacillus Cereus. *Phys. Scr.* 96, 105004. doi:10.1088/1402-4896/ac0f3b

Amin, M., Chetpattananondh, P., and Khan, M. N. (2020). Ultrasound Assisted Adsorption of Reactive Dye-145 by Biochars from marine Chlorella Sp. Extracted Solid Waste Pyrolyzed at Various Temperatures. *J. Environ. Chem. Eng.* 8, 104403. doi:10.1016/j.jece.2020.104403

Bazargan, A., Rough, S. L., and McKay, G. (2018). Fine Tuning of Process Parameters for Improving Briquette Production from palm Kernel Shell Gasification Waste. *Environ. Tech.* 39, 931–938. doi:10.1080/09593330.2017.1317835

Bilal, M., Iqbal, M., Hu, H., and Zhang, X. (2016a). Mutagenicity and Cytotoxicity Assessment of Biodegraded Textile Effluent by Ca-Alginate Encapsulated Manganese Peroxidase. *Biochem. Eng. J.* 109, 153–161. doi:10.1016/j.bej.2016.01.020

Bilal, M., Iqbal, M., Hu, H., and Zhang, X. (2016b). Mutagenicity, Cytotoxicity and Phytotoxicity Evaluation of Biodegraded Textile Effluent by Fungal Ligninolytic Enzymes. *Water Sci. Technol.* 73, 2332–2344. doi:10.2166/wst.2016.082

Chen, J., Leng, J., Yang, X., Liao, L., Liu, L., and Xiao, A. (2017). Enhanced Performance of Magnetic Graphene Oxide-Immobilized Laccase and its Application for the Decolorization of Dyes. *Molecules* 22, 221. doi:10.3390/molecules22020221

Chen, Z., Wang, T., Jin, X., Chen, Z., Megharaj, M., and Naidu, R. (2013). Multifunctional Kaolinite-Supported Nanoscale Zero-Valent Iron Used for the Adsorption and Degradation of crystal Violet in Aqueous Solution. *J. Colloid Interf. Sci.* 398, 59–66. doi:10.1016/j.jcis.2013.02.020

Efimov, M. N., Vasilev, A. A., Muratov, D. G., Baranchikov, A. E., and Karpacheva, G. P. (2019). IR Radiation Assisted Preparation of KOH-Activated Polymer-Derived Carbon for Methylene Blue Adsorption. *J. Environ. Chem. Eng.* 7, 103514. doi:10.1016/j.jece.2019.103514

Ezzatahmadi, N., Ayoko, G. A., Millar, G. J., Speight, R., Yan, C., Li, J., et al. (2017). Clay-supported Nanoscale Zero-Valent Iron Composite Materials for the Remediation of Contaminated Aqueous Solutions: a Review. *Chem. Eng. J.* 312, 336–350. doi:10.1016/j.cej.2016.11.154

Fan, M., Li, T., Hu, J., Cao, R., Wu, Q., Wei, X., et al. (2016). Synthesis and Characterization of Reduced Graphene Oxide-Supported Nanoscale Zero-Valent Iron (nZVI/rGO) Composites Used for Pb(II) Removal. *Materials* 9, 687. doi:10.3390/ma9080687

Fan, S., Wang, Y., Wang, Z., Tang, J., Tang, J., and Li, X. (2017). Removal of Methylene Blue from Aqueous Solution by Sewage Sludge-Derived Biochar: Adsorption Kinetics, Equilibrium, Thermodynamics and Mechanism. *J. Environ. Chem. Eng.* 5, 601–611. doi:10.1016/j.jece.2016.12.019

Fernandes, A. N., Almeida, C. A. P., Debacher, N. A., and Sierra, M. M. D. S. (2010). Isotherm and Thermodynamic Data of Adsorption of Methylene Blue from Aqueous Solution onto Peat. *J. Mol. Struct.* 982, 62–65. doi:10.1016/j.molstruc.2010.08.006

Freundlich, H. (1907). Über die Adsorption in Lösungen. *Z. Phys. Chem.* 57U, 385–470. doi:10.1515/zpch-1907-5723

Guo, D., Zhu, L., Guo, S., Cui, B., Luo, S., Laghari, M., et al. (2016). Direct Reduction of Oxidized Iron Ore Pellets Using Biomass Syngas as the Reducer. *Fuel Process. Tech.* 148, 276–281. doi:10.1016/j.fuproc.2016.03.009

Guz, L., Curutchet, G., Torres Sánchez, R. M., and Candal, R. (2014). Adsorption of crystal Violet on Montmorillonite (Or Iron Modified Montmorillonite) Followed by Degradation through Fenton or Photo-Fenton Type Reactions. *J. Environ. Chem. Eng.* 2, 2344–2351. doi:10.1016/j.jece.2014.02.007

Hammed, A. K., Dewayanto, N., Du, D., Ab Rahim, M. H., and Nordin, M. R. (2016). Novel Modified ZSM-5 as an Efficient Adsorbent for Methylene Blue Removal. *J. Environ. Chem. Eng.* 4, 2607–2616. doi:10.1016/j.jece.2016.05.008

Ho, Y. S., and McKay, G. (1999). Pseudo-second Order Model for Sorption Processes. *Process Biochem.* 34, 451–465. doi:10.1016/S0032-9592(98)00112-5

Int, C., Iqbal, M., Nisar, J., Nazir, A., and Qamar, A. Z. (2019). Bioassays Based on Higher Plants as Excellent Dosimeters for Ecotoxicity Monitoring: a Review. *Chem. Int.* 5, 1–80. doi:10.31221/osf.io/z2ynm

Kerkez, D. V., Tomašević, D. D., Kozma, G., Bečelić-Tomin, M. R., Prica, M. D., Rončević, S. D., et al. (2014). Three Different clay-supported Nanoscale Zero-Valent Iron Materials for Industrial Azo Dye Degradation: a Comparative Study. *J. Taiwan Inst. Chem. Eng.* 45, 2451–2461. doi:10.1016/j.jtice.2014.04.019

Lagergren, S. (1898). Zur theorie der sogenannten adsorption gelöster stoffe, Kungliga Svenska Vetenskapsakademiens. *Handl* 24, 1–39.

Langmuir, I. (1918). The Adsorption of Gases on Plane Surfaces of Glass, Mica and Platinum. *J. Am. Chem. Soc.* 40, 1361–1403. doi:10.1021/ja02242a004

Li, Z., Chen, Z., Zhu, Q., Song, J., Li, S., and Liu, X. (2020). Improved Performance of Immobilized Laccase on Fe3O4@C-Cu2+ Nanoparticles and its Application for Biodegradation of Dyes. *J. Hazard. Mater.* 399, 123088. doi:10.1016/j.jhazmat.2020.123088

Liu, J., Wang, Y., Fang, Y., Mwamulima, T., Song, S., and Peng, C. (2018). Removal of crystal Violet and Methylene Blue from Aqueous Solutions Using the Fly Ash-Based Adsorbent Material-Supported Zero-Valent Iron. *J. Mol. Liquids* 250, 468–476. doi:10.1016/j.molliq.2017.12.003

Liu, S., Lim, M., and Amal, R. (2014). TiO2-coated Natural Zeolite: Rapid Humic Acid Adsorption and Effective Photocatalytic Regeneration. *Chem. Eng. Sci.* 105, 46–52. doi:10.1016/j.ces.2013.10.041

Liu, Y., Phenrat, T., and Lowry, G. V. (2007). Effect of TCE Concentration and Dissolved Groundwater Solutes on NZVI-Promoted TCE Dechlorination and H2 Evolution. *Environ. Sci. Technol.* 41, 7881–7887. doi:10.1021/es0711967

Man, Y., Feng, J. X., Li, F. J., Ge, Q., Chen, Y. M., and Zhou, J. Z. (2014). Influence of Temperature and Time on Reduction Behavior in Iron Ore-Coal Composite Pellets. *Powder Tech.* 256, 361–366. doi:10.1016/j.powtec.2014.02.039

Mishra, P., Singh, K., and Dixit, U. (2021). Adsorption, Kinetics and Thermodynamics of Phenol Removal by Ultrasound-Assisted Sulfuric Acid-Treated Pea (Pisum Sativum) Shells. *Sust. Chem. Pharm.* 22, 100491. doi:10.1016/j.scp.2021.100491

Mwamulima, T., Zhang, X., Wang, Y., Song, S., and Peng, C. (2018). Novel Approach to Control Adsorbent Aggregation: Iron Fixed Bentonite-Fly Ash for Lead (Pb) and Cadmium (Cd) Removal from Aqueous media. *Front. Environ. Sci. Eng.* 12, 2. doi:10.1007/s11783-017-0979-6

Ngulube, T., Gumbo, J. R., Masindi, V., and Maity, A. (2019). Preparation and Characterisation of High Performing Magnesite-Halloysite Nanocomposite and its Application in the Removal of Methylene Blue Dye. *J. Mol. Struct.* 1184, 389–399. doi:10.1016/j.molstruc.2019.02.043

Nourein, S., Bhatti, H., Iqbal, M., Bibi, I., Zafar, N., Iqbal, D., et al. (2017). Redox Mediators Assisted-Degradation of Direct Yellow 4. *Pol. J. Environ. Stud.* 26, 2885–2890. doi:10.15244/pjoes/68564

Ramamoorthy, M., Ragupathy, S., Sakthi, D., Arun, V., and Kannadasan, N. (2020). Synthesis of SnO2 Loaded on Corn Cob Activated Carbon for Enhancing the Photodegradation of Methylene Blue under Sunlight Irradiation. *J. Environ. Chem. Eng.* 8, 104331. doi:10.1016/j.jece.2020.104331

Rasalingam, S., Peng, R., and Koodali, R. T. (2015). An Insight into the Adsorption and Photocatalytic Degradation of Rhodamine B in Periodic Mesoporous Materials. *Appl. Catal. B: Environ.* 174-175, 49–59. doi:10.1016/j.apcatb.2015.02.040

Saber-Samandari, S., Saber-Samandari, S., Joneidi-Yekta, H., and Mohseni, M. (2017). Adsorption of Anionic and Cationic Dyes from Aqueous Solution Using Gelatin-Based Magnetic Nanocomposite Beads Comprising Carboxylic Acid Functionalized Carbon Nanotube. *Chem. Eng. J.* 308, 1133–1144. doi:10.1016/j.cej.2016.10.017

Spadaro, J. T., Gold, M. H., and Renganathan, V. (1992). Degradation of Azo Dyes by the Lignin-Degrading Fungus Phanerochaete Chrysosporium. *Appl. Environ. Microbiol.* 58, 2397–2401. doi:10.1016/1050-1738(93)90025-210.1128/aem.58.8.2397-2401.1992

Stephen Inbaraj, B., and Chen, B. H. (2011). Dye Adsorption Characteristics of Magnetite Nanoparticles Coated with a Biopolymer Poly(γ-Glutamic Acid). *Bioresour. Tech.* 102, 8868–8876. doi:10.1016/j.biortech.2011.06.079

Wang, J.-Q., Liu, Y.-H., Chen, M.-W., Xie, G.-Q., Louzguine-Luzgin, D. V., Inoue, A., et al. (2012). Rapid Degradation of Azo Dye by Fe-Based Metallic Glass Powder. *Adv. Funct. Mater.* 22, 2567–2570. doi:10.1002/adfm.201103015

Wang, W., Cheng, Y., Kong, T., and Cheng, G. (2015). Iron Nanoparticles Decoration onto Three-Dimensional Graphene for Rapid and Efficient Degradation of Azo Dye. *J. Hazard. Mater.* 299, 50–58. doi:10.1016/j.jhazmat.2015.06.010

Wang, Y., López-Valdivieso, A., Zhang, T., Mwamulima, T., Zhang, X., Song, S., et al. (2017). Preparation of Microscale Zero-Valent Iron-Fly Ash-Bentonite Composite and Evaluation of its Adsorption Performance of crystal Violet and Methylene Blue Dyes. *Environ. Sci. Pollut. Res.* 24, 20050–20062. doi:10.1007/s11356-017-9426-2

Weber, W. J., and Morris, J. C. (1963). Kinetics of Adsorption on Carbon from Solution. *J. Sanit. Engrg. Div.* 89, 31–59. doi:10.1061/JSEDAI.0000430

Xu, C.-H., Zhu, L.-j., Wang, X.-H., Lin, S., and Chen, Y.-m. (2014). Fast and Highly Efficient Removal of Chromate from Aqueous Solution Using Nanoscale Zero-Valent Iron/activated Carbon (nZVI/AC). *Water Air Soil Pollut.* 225, 1845. doi:10.1007/s11270-013-1845-1

Xu, H.-M., Sun, X.-F., Wang, S.-Y., Song, C., and Wang, S.-G. (2018). Development of Laccase/graphene Oxide Membrane for Enhanced Synthetic Dyes Separation and Degradation. *Sep. Purif. Tech.* 204, 255–260. doi:10.1016/j.seppur.2018.04.036

Zhang, J., Zhang, T., Liang, X., Wang, Y., Shi, Y., Guan, W., et al. (2020a). Efficient Photocatalysis of CrVI and Methylene Blue by Dispersive Palygorskite-Loaded Zero-Valent Iron/carbon Nitride. *Appl. Clay Sci.* 198, 105817. doi:10.1016/j.clay.2020.105817

Zhang, L., Yao, L., Ye, L., Long, B., Dai, Y., and Ding, Y. (2020b). Benzimidazole-based Hyper-Cross-Linked Polymers for Effective Adsorption of Chlortetracycline from Aqueous Solution. *J. Environ. Chem. Eng.* 8, 104562. doi:10.1016/j.jece.2020.104562

Zhang, X., Lin, S., Lu, X.-Q., and Chen, Z.-l. (2010). Removal of Pb(II) from Water Using Synthesized Kaolin Supported Nanoscale Zero-Valent Iron. *Chem. Eng. J.* 163, 243–248. doi:10.1016/j.cej.2010.07.056

Zheng, Q., Zhang, Z. R., Du, J., Lin, L. L., Xia, W. X., Zhang, J., et al. (2019). A Novel Direct Reduction Method to Synthesize Ordered Fe-Pt alloy Nanoparticles. *J. Mater. Sci. Tech.* 35, 560–567. doi:10.1016/j.jmst.2018.09.036

Conflict of Interest: The authors declare that the research was conducted in the absence of any commercial or financial relationships that could be construed as a potential conflict of interest.

Publisher's Note: All claims expressed in this article are solely those of the authors and do not necessarily represent those of their affiliated organizations, or those of the publisher, the editors, and the reviewers. Any product that may be evaluated in this article, or claim that may be made by its manufacturer, is not guaranteed or endorsed by the publisher.

frontiers in Microbiology

ORIGINAL RESEARCH
published: 11 January 2022
doi: 10.3389/fmicb.2021.824319

Effects of Salinity on the Biodegradation of Polycyclic Aromatic Hydrocarbons in Oilfield Soils Emphasizing Degradation Genes and Soil Enzymes

Yang Li, Wenjing Li, Lei Ji, Fanyong Song, Tianyuan Li, Xiaowen Fu, Qi Li, Yingna Xing, Qiang Zhang and Jianing Wang*

Shandong Provincial Key Laboratory of Applied Microbiology, Ecology Institute, Qilu University of Technology (Shandong Academy of Sciences), Jinan, China

OPEN ACCESS

Edited by:
Tian Li,
Nankai University, China

Reviewed by:
Shaoping Kuang,
Qingdao University of Science and Technology, China
Xiaojing Li,
Agro-Environmental Protection Institute, Chinese Academy of Agricultural Sciences (CAAS), China

***Correspondence:**
Xiaowen Fu
seanfv@163.com

Specialty section:
This article was submitted to Microbiotechnology, a section of the journal Frontiers in Microbiology

Received: *29 November 2021*
Accepted: *21 December 2021*
Published: *11 January 2022*

Citation:
Li Y, Li W, Ji L, Song F, Li T, Fu X, Li Q, Xing Y, Zhang Q and Wang J (2022) Effects of Salinity on the Biodegradation of Polycyclic Aromatic Hydrocarbons in Oilfield Soils Emphasizing Degradation Genes and Soil Enzymes. Front. Microbiol. 12:824319. doi: 10.3389/fmicb.2021.824319

The biodegradation of organic pollutants is the main pathway for the natural dissipation and anthropogenic remediation of polycyclic aromatic hydrocarbons (PAHs) in the environment. However, in the saline soils, the PAH biodegradation could be influenced by soil salts through altering the structures of microbial communities and physiological metabolism of degradation bacteria. In the worldwide, soils from oilfields are commonly threated by both soil salinity and PAH contamination, while the influence mechanism of soil salinity on PAH biodegradation were still unclear, especially the shifts of degradation genes and soil enzyme activities. In order to explain the responses of soils and bacterial communities, analysis was conducted including soil properties, structures of bacterial community, PAH degradation genes and soil enzyme activities during a biodegradation process of PAHs in oilfield soils. The results showed that, though low soil salinity (1% NaCl, *w/w*) could slightly increase PAH degradation rate, the biodegradation in high salt condition (3% NaCl, *w/w*) were restrained significantly. The higher the soil salinity, the lower the bacterial community diversity, copy number of degradation gene and soil enzyme activity, which could be the reason for reductions of degradation rates in saline soils. Analysis of bacterial community structure showed that, the additions of NaCl increase the abundance of salt-tolerant and halophilic genera, especially in high salt treatments where the halophilic genera dominant, such as *Acinetobacter* and *Halomonas*. Picrust2 and redundancy analysis (RDA) both revealed suppression of PAH degradation genes by soil salts, which meant the decrease of degradation microbes and should be the primary cause of reduction of PAH removal. The soil enzyme activities could be indicators for microorganisms when they are facing adverse environmental conditions.

Keywords: bacterial community composition, soil salinity, phenanthrene and pyrene, degradation genes, soil enzymes activity

INTRODUCTION

Polycyclic aromatic hydrocarbons (PAHs) are organic molecules consisting of two or more benzene or heterocyclic rings (Patel et al., 2020), which are mainly discharged from the process of thermal decomposition and recombination of organic materials such as coal, petroleum, petroleum gas and wood in nature. Due to the recalcitrance and hydrophobicity of PAHs, a great majority are eventually deposited in soil after transformation and migration (Sun et al., 2018), leading to a serious threat to human health and ecosystem security (Tsibart and Gennadiev, 2013; Sushkova et al., 2017; Zhang et al., 2018). Among the remediation processes of PAH pollution in soils (Rivas, 2006; Ghosal et al., 2016; Kuppusamy et al., 2016, 2017; Li et al., 2020; Zhang et al., 2021), the bio-augment remediation method is considered the most suitable choice because of its low economic cost, high efficiency and sustainability (Haritash and Kaushik, 2009; Ghosal et al., 2016).

Polycyclic aromatic hydrocarbon (PAH)-degrading genes in soils are valuable biomarkers for measuring the PAH degradation potentials of bacterial communities (Wang et al., 2016). The aerobic biodegradation process of PAHs by bacteria usually dominates by dioxygenases which incorporate both atoms of oxygen molecules into the substrates (Chikere and Fenibo, 2018). Dioxygenase, a multicomponent enzyme generally consisting of reductase, ferredoxin, and terminal oxygenase subunits (Ghosal et al., 2016), is categorized into ring-hydroxylating dioxygenases (RHDs) and ring cleaving dioxygenases (RCDs) (Chikere and Fenibo, 2018). PAH-RHDα are functional genes that encode the RHD enzymes responsible for the catalysis of PAH biodegradation under aerobic conditions (Song et al., 2015). Ring-hydroxylating dioxygenase genes include the classical genes like *nah* (Habe and Omori, 2003), *phd*, *nag* (Muangchinda et al., 2015), *nid*, *pdo*, *dfn/fln,* and *nar* (Xia et al., 2015; Chikere and Fenibo, 2018). C12O, encoding catechol 1, 2-dioxygenase, associates with cleavage of the last aromatic ring in the degradation pathway of PAHs (Han et al., 2014). The quantity and expression of these genes are very important during the biodegradation of PAHs (Ghosal et al., 2016; Liao et al., 2021).

Soil enzymes are also common representations of soil biochemical characteristics, which are produced by soil microorganisms (Cortés-Lorenzo et al., 2012; Singh, 2015; Azadi and Raiesi, 2021). Soil catalase (S-CAT) can decompose hydrogen peroxide in soil and reduce the damage of excessive accumulation of hydrogen peroxide to soil microorganisms (Sun et al., 2021). Soil polyphenol oxidase (S-PPO) is an oxidoreductase that can oxidize aromatic compounds into quinones (Sullivan, 2014). Besides, soil dehydrogenase (S-DHA), reflecting the amount of active microorganisms and their degradation ability of organic matter, can be used to evaluate the degradation performance (Lu et al., 2017). The activities of these enzymes in soils are usually the most sensitive indicators to environmental changes, and their activities are always affected by soil conditions through shifting the synthesis and structure of local microorganisms (Teng and Chen, 2019; Azadi and Raiesi, 2021).

Soils in onshore oilfields are commonly suffered by multiple environmental stresses including PAHs contamination and soil salinization (Nie et al., 2009; Cheng et al., 2017). Actually, soil salts are vital factors for microorganisms during their physiological metabolic activities and important substances to maintain cells' osmotic equilibrium (Lozupone and Knight, 2007; Rath and Rousk, 2015; Rath et al., 2019; Yang et al., 2020; Zhao et al., 2020). However, high salinity can result in dehydration or lysis of cells for microbes, then decrease microbial functions in soils (Singh, 2015; Yang et al., 2020). For microbes with salt tolerance, osmotic substances will accumulate in cells and thereby enhance the adaptation of microorganisms to salts (Hagemann, 2011; Asghar et al., 2012).

Although former studies have reported effects of the salinity on PAH degradation in soils, it is still unclear how microbial communities relate to changes of degradation genes and soil enzymes with increasing salinity. In this study, a 30-day soil remediation of PAHs under 3 salinity gradients (addition of 0, 1%, and 3% of NaCl, *w/w*) was conducted. The goals were to provide a better understanding of effect mechanisms of soil salinity on the degradation rate during a bio-augmented remediation of PAHs under salinity changes. The objectives are as follows: (1) to reveal the influence of salinity on composition and diversity of the bacterial community, and (2) to elucidate the response characteristic of functional genes and soil enzymes related to PAH degradation. The results reveal the effect extent of soil salinity on bioremediation of PAH and provide a new perspective for the assessment and remediation of PAHs in extreme environment including but not limited to oilfield soils.

MATERIALS AND METHODS

Experimental Design

In this study, bacteria colonies were isolated and enriched directly from oil-contaminated soil in the Shengli oilfield, China. The bacteria consortium, passed on NCBI database by Yang Li (Qilu University of Technology Shandong Academy of Sciences, Jinan, China), had been proven to have a synergistic biodegradation ability for PAHs in a former experiment. The soils used in this study were collected from the Shengli Oilfield of China. The sampling site was not obviously polluted by crude oil, but had beared long-term oil exploitation since the 1960s. After air dried and ground through a 10-mesh sieve, the soils were spiked with phenanthrene (PHE) and pyrene (PYR) thoroughly to make their concentrations to 200 mg/kg and 50 mg/kg in soils, respectively. Then appropriate sterilized water was added to make the soil moisture to approximately 20%. One portion of the soil was subjected to the measurement of the basic physicochemical properties of the soil, and another was prepared for the PAH degradation experiment.

After a month of aging process, the soil was divided into three parts, named LS treatment, S1 treatment and S3 treatment, respectively. Approximately 1% sodium chloride (NaCl, *w/w*) was added to S1 treatment, and 3% NaCl (*w/w*) was added to S3 treatment. The mixture was placed in a plastic sterilized box. Each box was equipped several 0.22μm filters on the cover, in order to ensure the normal respiration of soil, and prevent the influence of microorganisms from the air. Soil samples were cultured at

25°C for 30 days. All treatments were set with 3 replicates. And during each sample collection, triplicate samples were collected for chemical and biological analysis.

Determinations of Physico-Chemical Properties and Polycyclic Aromatic Hydrocarbons in Soils

The pH of the soil and the electrical conductivity (EC) method were used to evaluate soil salinity (Bañón et al., 2021), The percentage of weight loss of organic matter on ignition (W_{SOI}%) method was used to determine the soil organic matter (OM) content (Nakhli et al., 2019). The obtained samples were air-dried in the shade and passed through a 60-mesh standard sieve before analysis. Ultrasonic solvent extraction technology was used to extract PAHs from soil (Pan et al., 2013; Liao et al., 2021). A high-performance liquid chromatography (HPLC) system (Agilent, United States) equipped with a fluorescence detector (RF-10AXL) was utilized to analyze PAH concentrations (Geng et al., 2022). The soil enzymes activities of S-CAT, S-PPO and S-DHA were determined as follows: enzymes were extracted from prepared soil samples by enzyme kits and the activities were determined via a microplate reader (iMark, BIO-RAD, United States) (Li et al., 2019a).

Analysis of Microbial Community and Degradation Genes

Genomic DNA was extracted from the fresh soil samples using the Mag-Bind® Soil DNA Kit M5635-02 (Omega Bio-Tek, United States). A Nanodrop 2000 spectrophotometer (Thermo, United States) was used to check the quality and concentration of the extracted DNA. The two genes (C12O and PAH-RHDα) were amplified in a triplicate and quantified using an MA-6000 real-time fluorescence quantitative PCR instrument. The primers were synthesized following former studies (Muangchinda et al., 2015; Wang et al., 2020). The reaction system was an 8 μl template dilution sample and 8 μl mixture A. The thermal cycle reaction procedure of qPCR was as follows: 5min at 95°C for stage 1, 15 s at 95°C and 30 s at 60°C for stage 2. The whole process was conducted for 40 cycles.

Shanghai Personal Biotechnology Co., Ltd was commissioned to accomplish the composition spectrum analysis of microbial community diversity. In brief, the V3–V4 region of the bacterial 16S rRNA genes was amplified with the forward primer 338F (5′-ACTCCTACGGGAGGCAGCA-3′) and the reverse primer 806R (5′-GGACTACHVGGGTWTCTAAT-3′) (Xu et al., 2021). Agencourt AMPure Beads (Beckman Coulter, Indianapolis, IN) were used for the purification of PCR amplicons, and the PicoGreen dsDNA Assay Kit (Invitrogen, Carlsbad, CA, United States) was used for quantitative measurement. After the above stages, amplicons were pooled in equal amounts, and sequencing was performed on the Illumina MiSeq platform with MiSeq Reagent Kit v3.

Data Statistical Analysis

Before statistical analysis, Kolmogorov-Smirnov and Levene's tests were carried out to test the normality and homogeneity of differences (Liu et al., 2021). Excel 2020 (Microsoft, United States) was used for preliminary data statistics and processing. Origin (Version 2020) (Origin Laboratories, Ltd, United States) was mainly used to draw statistical graphs. All data are derived from the mean value in triplicate. SPSS Software (International Business Machines Corp, United States) was used to analyze the differences with one-way analysis of variance (ANOVA) or a non-parametric test. Picrust2 software[1] was used to predict the function of soil bacteria (KEGG).[2] The community structure of bacteria was analyzed via QIIME2 and R language. To comprehensively evaluate the characteristics of microbial community diversity, alpha diversity was utilized. The Chao1 index was used to represent richness, the Shannon and Simpson indices represented diversity, and Pielou's evenness index represented evenness.

RESULTS AND DISCUSSION

The Removal Percentage of Polycyclic Aromatic Hydrocarbons in Soil

Figure 1 demonstrates the percentage removal of PHE and PHY from soil samples at different time points. After 30 days of incubation, significant differences ($P < 0.05$) in the removal of PAHs were obtained from soils treated with different salinities. On the 7th day (**Figure 1A**), there was no significant difference of removal rates of PHE and PYR among the three treatments ($P > 0.05$), though values of degradation rate were higher in lower salinity soils than in the higher. However, on the 30th day (**Figure 1B**), the removal percentages of PHE and PYR in the LS treatment reached 64.52% and 57.83%, respectively, and the S1 treatment had the highest removal percentages of 81.85% and 60.33%, respectively. This indicated that appropriate salinity could probably promote the removal rate of PHE in soils (Wang et al., 2020). Compared with LS and S1, the addition of 3% NaCl (*w/w*) significantly decreased the degradation of PAHs, leading to removal of 39.95% and 35.54% for PHE and PYR, respectively. Many previous studies have revealed a similar result: decreased PAHs removal was caused by salinity stress (Ibekwe et al., 2018; Wang et al., 2019).

Changes of Soil Properties Under Salt Stress

Soil enzymes, pH, EC and W_{SOI}% were selected to reflect processes of biochemical reactions in the soils. As shown in **Supplementary Table 1**, pH values remained stable among different treatments of S1, S3 and LS and different sampling times. Soil conductivity and contents of organic matter were significantly influenced by the gradient salinities ($P < 0.05$).

Soil enzymes as catalysts of biochemical conversion and the biodegradation of PAHs have been studied intensively (Lipińska et al., 2015). In this study, the activities of three common soil enzymes (S-CAT, S-PPO and S-DHA) under different soil salinities and sampling times were analyzed to evaluate the

[1]https://github.com/picrust/picrust2/wiki

[2]https://www.kegg.jp/

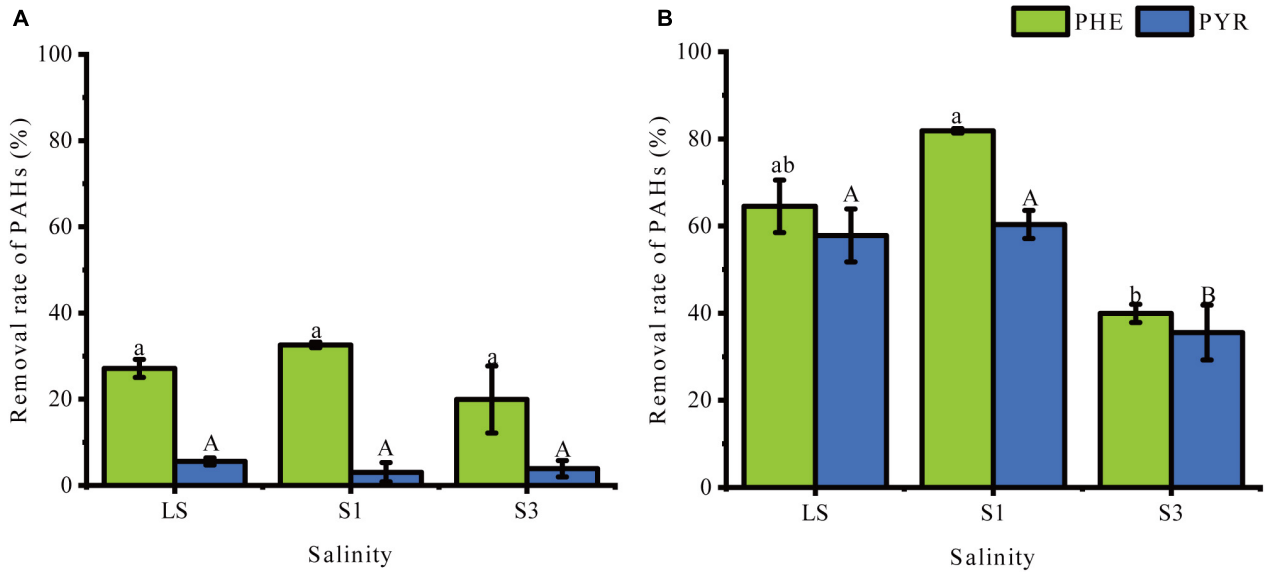

FIGURE 1 | Percent removal of PHE and PYR in treatments under different salinities. **(A)** the 7th day, **(B)** the 30th day. Error bars represent standard deviations of triplicate samples. Different letters indicate significant differences between the different salinity treatments at $P < 0.05$.

changes in the microbial community and metabolic processes (**Figure 2**). **Supplementary Table 2** showed the results of the difference analysis of enzyme activities between samples from the 7th day and 30th day. The results showed that the activities of these enzymes significantly decreased with increasing soil salinity ($P < 0.05$). All of the highest activities were found in the treatment with the lowest salinity (LS treatment).

Soil catalase (S-CAT), a common antioxidant enzyme in soil (Sun et al., 2021), can be used as an indicator of soil biomass to some extent, and soils with high biomass usually have higher catalase activity (Chabot et al., 2020). The results in **Figure 1** show that the highest S-CAT activity was observed in the LS treatment, indicating that the addition of sodium chloride reduced the S-CAT activity. On the 7th day, there was no significant difference in S-CAT activity between S1 and S3 treatments, but the difference became more pronounced in the two treatments as the incubation time progressed. The reduction of catalase activity in the high salt state leaded to a lower antioxidant capacity of soil microorganisms, which results in higher residual PAHs than in the low salt state.

Activities of S-PPO and S-DHA are both important enzymes for the breakdown of cyclic organic matter and represent the bioremediation capacity (Lu et al., 2017). In this study, these two enzyme activities were significantly decreased by the addition of salt ($P < 0.05$). This was the result of a significant inhibitory effect of the soil salinity on microbial degradation abilities of organic matters. Comparing the change in enzyme activity from the 7th day to the 30th day, the LS treatment showed the greatest change in S-DHA activity with a significant decrease of 67.89%. This may be because activity of S-DHA is an indicator of total biological activity, and bacteria without PAH-degrading abilities or that are less adapted to the environment undergo apoptosis. Li et al. (2019b) also pointed out that the increase in S-DHA activity was due to an increase in the total number of microorganisms. However, this change was absent in the treatments with relatively high salinity (S1 and S3). The reason was probably that salinity has a filter function of eliminating poorly adapted bacteria. Then the halophilic bacteria remained and were well adapted to their environment.

Abundance of Polycyclic Aromatic Hydrocarbon-Degrading Genes in Contaminated Soil

The biodegradation of PAHs in soil depends on a variety of functional genes, which are valuable biomarkers for evaluating the potential of PAH degradation (Yang et al., 2015). Real-time quantification PCR(RT-qPCR) was applied to quantify the absolute abundance of the PHA-RHDα and C12O genes (**Figure 3**). In general, the salt in soils gave a prominent stress to bacteria and mainly decreased the total abundance of PAH-degrading genes with salinity. The copy number of degradation genes was an indicator of PAH-degrading microbial abundance, the decrease of which signified a decrease of PAH-degrading microorganisms. All values of gene copies of PAH-RHDα in the lower salinity treatment were higher than those in higher soils. The copy numbers of the C12O gene showed an upward trend from S1 to S3 on the 30th day, which meant that several PAH-degrading bacteria in the S3 treatment were halophilic and thrived under high salinity conditions. Previous studies have also reported the growth and metabolism of *Halobacillus* (Li et al., 2012), a halophilic microorganism containing the C12O gene, under high salinity (Delgado-García et al., 2018). However, there was no significant difference in the gene copies between

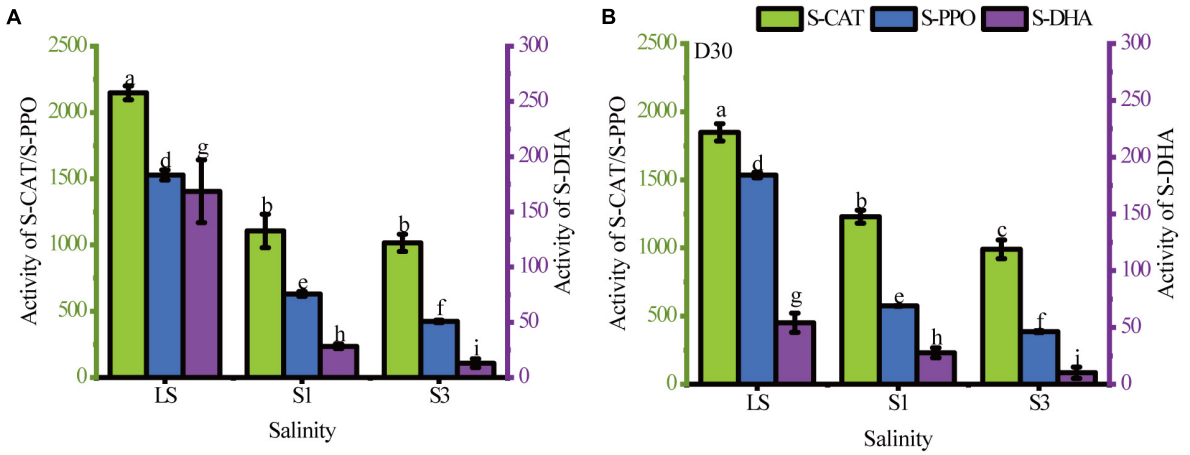

FIGURE 2 | Soil enzyme activities in the LS, S1 and S3 treatments. **(A)** the 7th day, **(B)** the 30th day. Different letters over columns represent significant differences among treatments at the $p < 0.05$ level of LSD *post hoc* comparison tests.

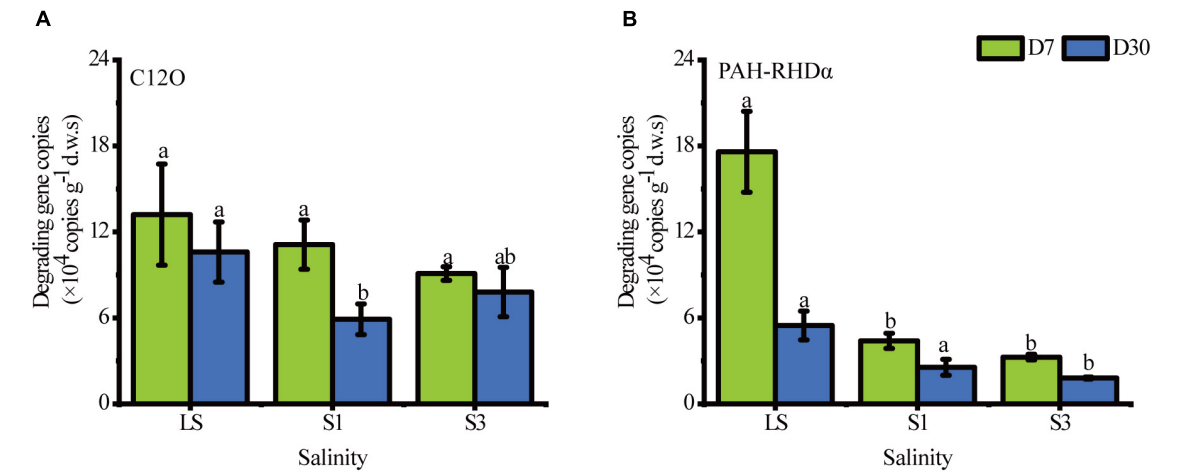

FIGURE 3 | Absolute abundance of the C12O gene and PAH-RHDα gene under the different salinity treatments. **(A)** the gene of C12O, **(B)** the gene of PAH-RHDα. Different letters over columns represent significant differences among treatments at the $p < 0.05$ level of LSD *post hoc* comparison tests.

S1 and S3 ($P = 0.254$), which could be explained by the same role played by the mildly halophilic bacteria in both the S1 and S3 treatments.

Picrust2 analysis was also conducted to predict the functional genes in relative quantity of each soil treatment. Eight genes associated with the PAH degradation (Li et al., 2019b) were selected to show significant variations among different treatments (**Figure 4**). From the 7th day to the 30th day, all numbers of these functional genes decreased. On the 7th day, the average percentages of all genes showed the lowest values in S3 treatment and the highest in the LS. The results were associated with the bacterial genera carrying PAH degradation genes (Wang et al., 2021a). On the 30th day, the average proportions of genes like k00452, k04101and k04100, increased in S1 treatment, which may be due to the abundance of bacteria containing these genes increased, and they were tolerant to the salt stress extent in the treatment of S1 (Liao et al., 2021). For the other genes, the highest abundances were only found in the LS treatment, which meant most PAH degradation bacteria were not salt-tolerant and leaded to a restrained degradation rate in high salinity soils.

Responses of Soil Microbial Community Structure to Salt Stress

Bacteria in soils usually dominate microbial communities (Pesce et al., 2018) and play a key role in the dissipation of PAHs in soils (Li et al., 2019b). In order to discuss the effect of salt stress on the microorganisms in soils, 16S rRNA sequence was conducted to analyze the structure and diversity of bacterial communities. The results showed that salt stress caused significant differences in the formation of microbial community structure from the control treatment.

Alpha diversity analysis was used to evaluate the bacterial diversity and richness during incubation (Liao et al., 2021).

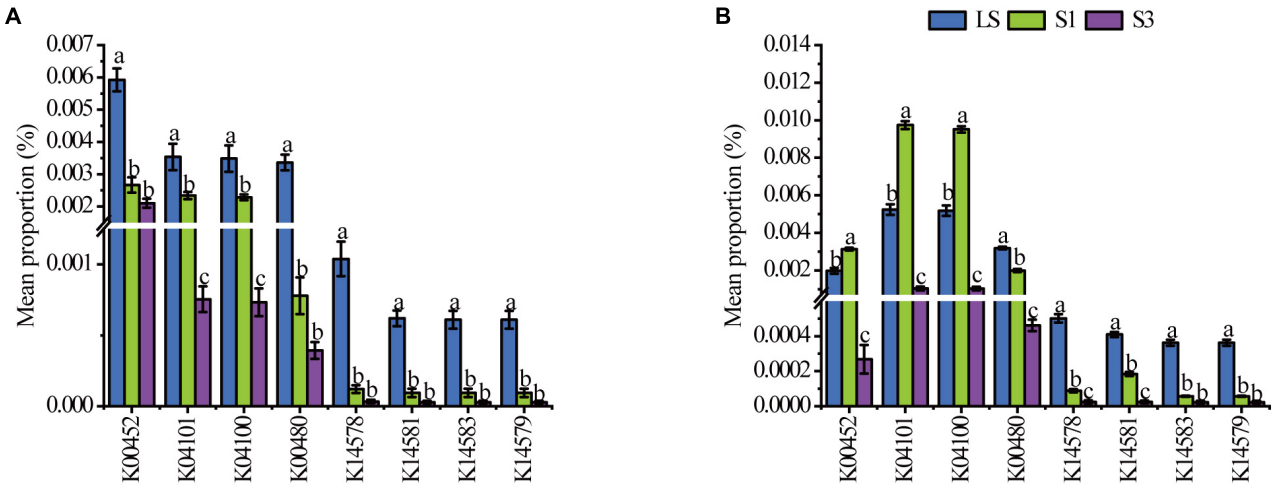

FIGURE 4 | Mean proportions of the functional genes associated with the degradation of PAHs in soil after 7 days **(A)** and 30 **(B)** days of incubation. K00452 HAAO; 3-hydroxyanthranilate 3,4-dioxygenase [EC:1.13.11.6]; K04101 ligB; protocatechuate 4,5-dioxygenase, beta chain [EC:1.13.11.8]; K04100 ligA; protocatechuate 4,5-dioxygenase, alpha chain [EC:1.13.11.8]; K00480 salicylate hydroxylase [EC:1.14.13.1]; K14578 nahAb, nagAb, ndoA, nbzAb, dntAb; naphthalene 1,2-dioxygenase ferredoxin component; K14581 nahAa, nagAa, ndoR, nbzAa, dntAa; naphthalene 1,2-dioxygenase ferredoxin reductase component [EC:1.18.1.7]; K14583 nahC; 1,2-dihydroxynaphthalene dioxygenase [EC:1.13.11.56]; K14579 nahAc, ndoB, nbzAc, dntAc; naphthalene 1,2-dioxygenase subunit alpha [EC:1.14.12.12 1.14.12.23 1.14.12.24].

A rarefaction curve (**Supplementary Figure 1**) was exhibited to show the sequenced quantities of all soil samples could effectively and accurately cover and estimate all microbial communities (Xu et al., 2021). The four commonly used alpha diversity indices were shown in **Figure 5**, which indicates that all the mean values of alpha diversity indices followed the trend of LS > S1 > S3. That is, the higher the salinity of soils from each treatment, the lower the value of the alpha diversity index, and then the more uneven the distribution of the soil bacterial community. Considering that salinity was the only factor that varied among the treatments, the results of alpha diversity analysis further proved that salinity had an appreciable impact on soil microbial diversity, richness and evenness.

Principal coordinates analysis (PCoA) based on Bray-Curtis distances was applied to analyze the overall structural variations of microbial structure (**Figure 6**). The components of PCoA1 and PCoA2 could explain 69.60% and 11.20% of the variance along their axes, respectively. The loading values of PCo1 were greatly affected by salinity and increased with the soil salinity of the treatment. In the plot, samples from different treatments separated well, which suggested significant differences among different soil salinities ($P < 0.05$). This result was consistent with the findings of alpha diversity analysis.

The statistics of taxon number under different treatments (**Supplementary Figure 2**) also revealed an increase in species richness over time and a decrease with salinity. The relative abundance and taxonomic analysis of soil microbial communities (**Supplementary Table 3**) demonstrated that *Proteobacteria* was the dominant phylum in all treatments (Cycil et al., 2020), accounting for the highest proportion of 89.20%-98.31%. Among the different treatments, the abundance was in accordance with the trend of LS < S1 < S3. The relative abundances of other phyla, including *Bacteroidetes* (0.26%–4.36%), *Firmicutes* (0.92%–3.20%), *Actinobacteria* (0.31%–3.55%), and *Chloroflexi* (0.01%–0.06%), decreased with the increase of soil salinity (De León-Lorenzana et al., 2018). *Proteobacteria, Bacteroidetes, Firmicutes, Actinobacteria,* and *Chloroflexi* have been reported to contain many genera associated with the degradation of aromatic hydrocarbons (Muangchinda et al., 2015) and to predominate in PAH-contaminated soils (Ma et al., 2016; Li et al., 2019b). The abundance of *Proteobacteria* usually increased with soil salinity (Wang et al., 2021b), and dominated the microbe communities under salt stress (Li et al., 2019a).

Furthermore, the genus in salt-stress associated with PAH degradation deserve increasing attentions (Xu et al., 2019; Wang et al., 2020; Zhang et al., 2021). **Figure 7** shows the bacterial composition at the genus level. The most frequently observed bacterial genus was *Acinetobacter*, accounting for 36.05%–81.07%, which was reported to be easier to adapt to salinity (Zhang et al., 2021). *Halomonas*, accounting for 0.28%–18.08%, showed a similar distribution characteristic to *Acinetobacter* with higher relative abundance in high salt treatment (Wang et al., 2020). In addition, the genera *Marinobacter*, *Croceicoccus*, *Stenotrophomonas*, *Pseudomonas*, and *Georgenia* were negatively affected by salinity and restrained the relative abundance. The relative abundance of other low-abundance bacteria, such as *Salinimicrobium* and *Clostridiisalibacter*, increased over time and decreased with increasing salinity (**Figure 7**).

Among the top 20 bacterial genera, 10 bacterial genera have been previously reported as PAH-degrading bacteria (Fernández-Luqueño et al., 2011; Kappell et al., 2014; Huang et al., 2015; Muangchinda et al., 2015; Ghosal et al., 2016; Sun et al., 2018), including *Acinetobacter*, *Marinobacter*,

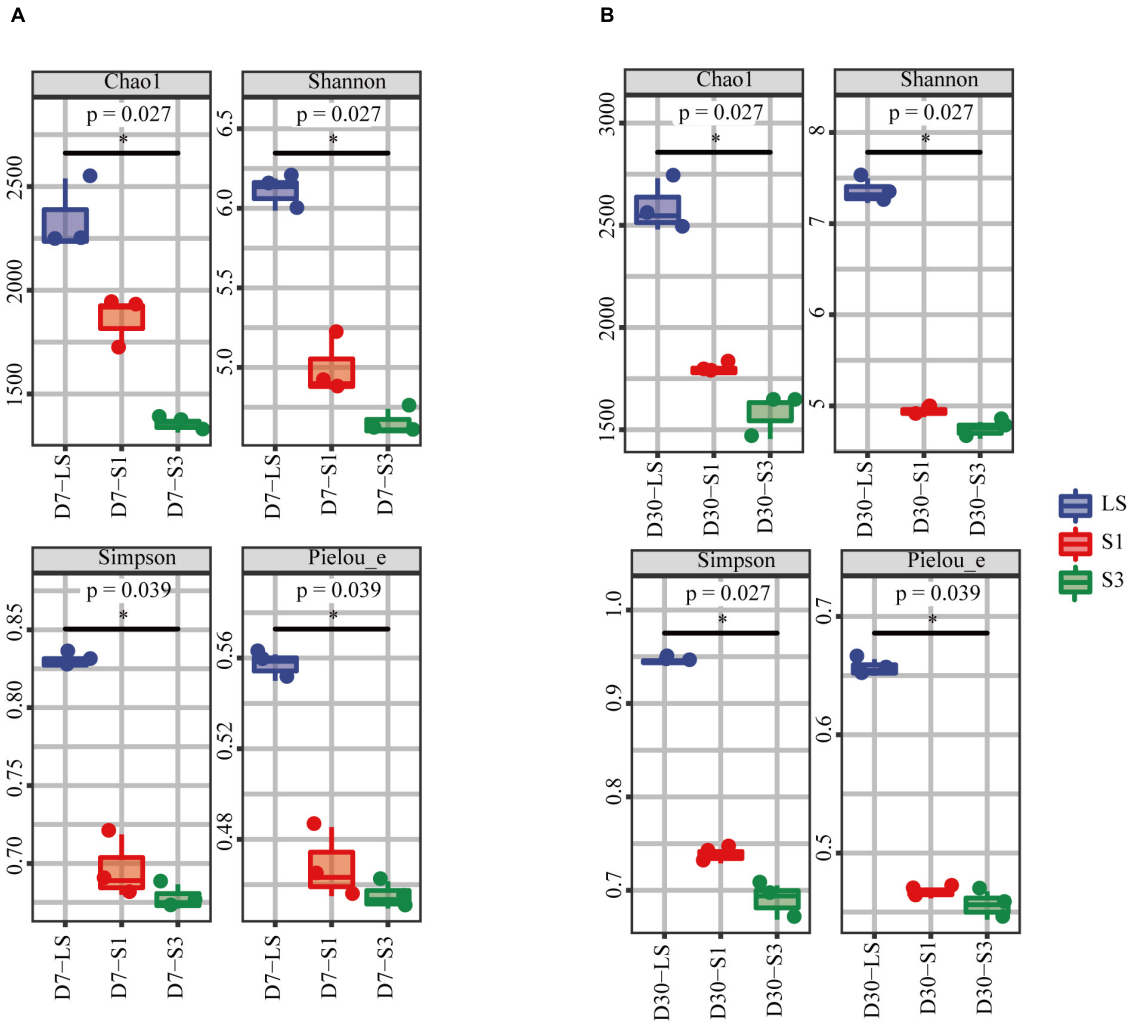

FIGURE 5 | Alpha diversity index of bacterial communities in soils from the different salinity treatments. **(A)** the 7th day, **(B)** the 30th day.

Halomonas, *Croceicoccus*, *Stenotrophomonas*, *Pseudomonas*, *Clostridiisalibacter*, *Ochrobactrum*, *Methylophaga*, and *Altererythrobacter*. As shown in **Figure 8**, the addition of salinity significantly decreased the relative abundance of some targeted genera in the treatment such as *Marinobacter*, *Salinimicrobium* etc., while others were enriched. Compared with the treatment of S1 and S3. LS treatment showed higher relative abundances of *Marinobacter*, *Salinimicrobium*, *Croceicoccus*, *Stenotrophomonas Pseudomonas*, *Orchrobactrum*, *Methylophaga,* and *Altererythrobacter* which were reported to be positively correlated with the removal percent of PAHs (Li et al., 2019b; Wang et al., 2020). *Caminicella*, *Sedimentibacter*, *Caenispirillum,* and *Gerogenia* were enriched only in the low salinity treatments, which may participate in the enhanced degradation of PAHs. In addition, salinity promoted an increase in some genera, including *Acinetobacter*, *Halomonas,* and *Clostridiisalibacter*. Moreover, the highest abundance of *Acinetobacter* and *Halomonas* appeared in the S3 treatments (Wang et al., 2020; Zhang et al., 2021). It suggested that salt application led to a decrease in soil microbial diversity, which was consistent with the results of alpha diversity. Besides, some low abundance genera associated with PAH degradation are also worth of interest and future attention,

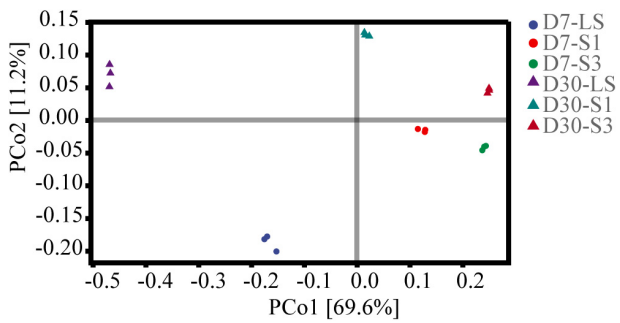

FIGURE 6 | Principal coordinates analysis (PCoA) of bacterial communities in soils from the different salinity treatments.

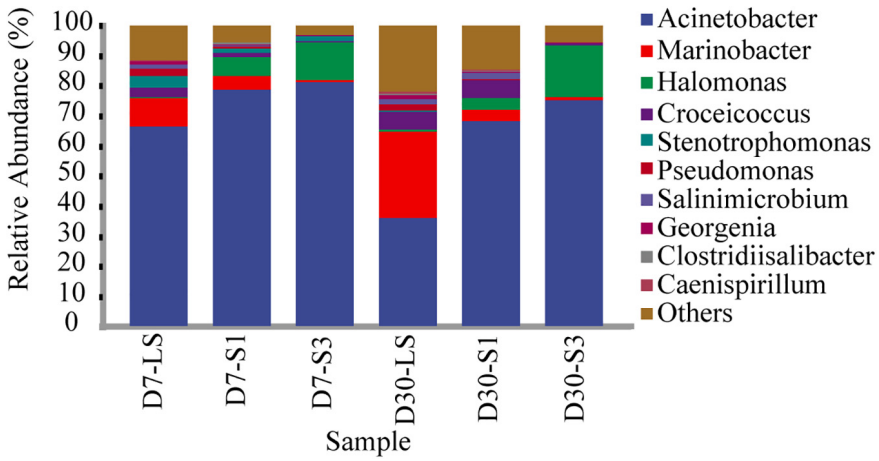

FIGURE 7 | Relative abundance of different bacteria at the genus level in soils from different treatments.

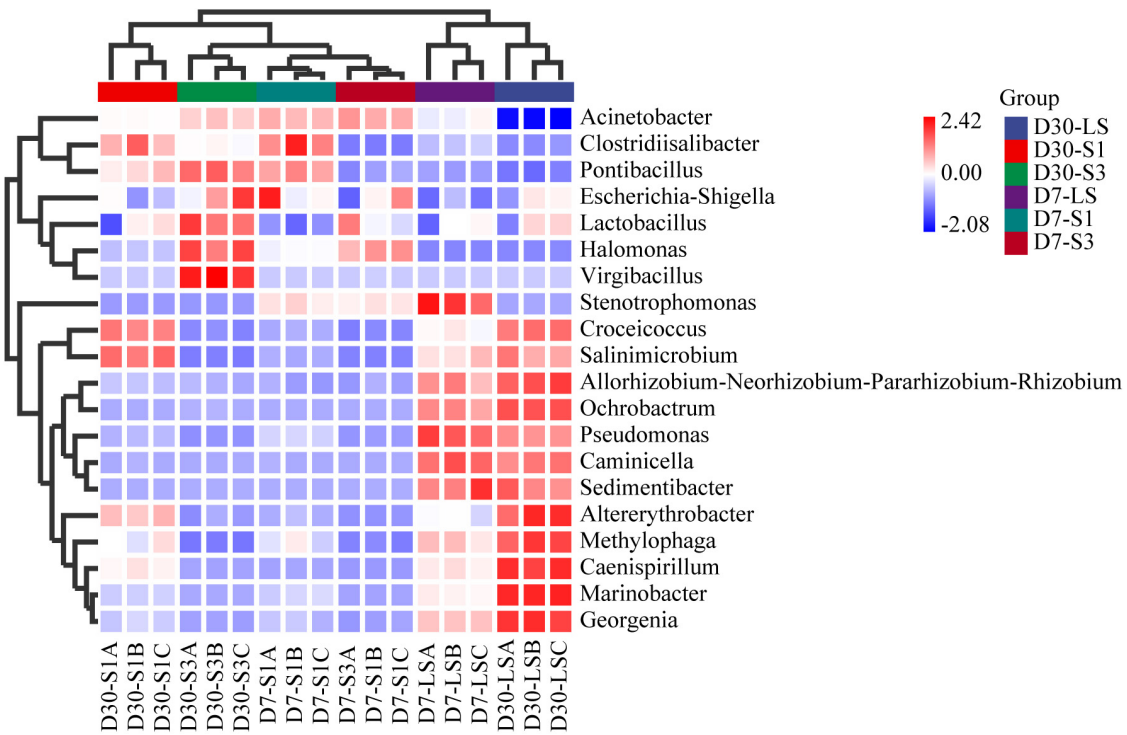

FIGURE 8 | Heatmap of the top 20 genera in soils from each treatment.

as biodegradation in complex soils occurs through synergistic interactions between bacteria (Adam et al., 2017).

Correlation Analysis of Soil Physical and Chemical Properties, Degradation Genes, Soil Enzyme Activities and Soil Microorganisms

Redundancy analysis (RDA) was conducted based on the correlation between pH, EC, W_{SOI}%, degradation genes, soil enzyme activities and the top 10 bacterial genera in relative abundance (**Figure 9**). The results showed that soil physico-chemical properties had a significant effect on the composition and function of the microbial community ($P = 0.001$). Electrical Conductivity value was the most important factor affecting the structure of soil flora and the relative abundance of species, followed by soil enzyme activity and organic matter content. The soil conductivities were positively correlated with the organic matter and some halophilic bacteria, such as *Halomonasas* and *Acinetobacter*, while negatively correlated

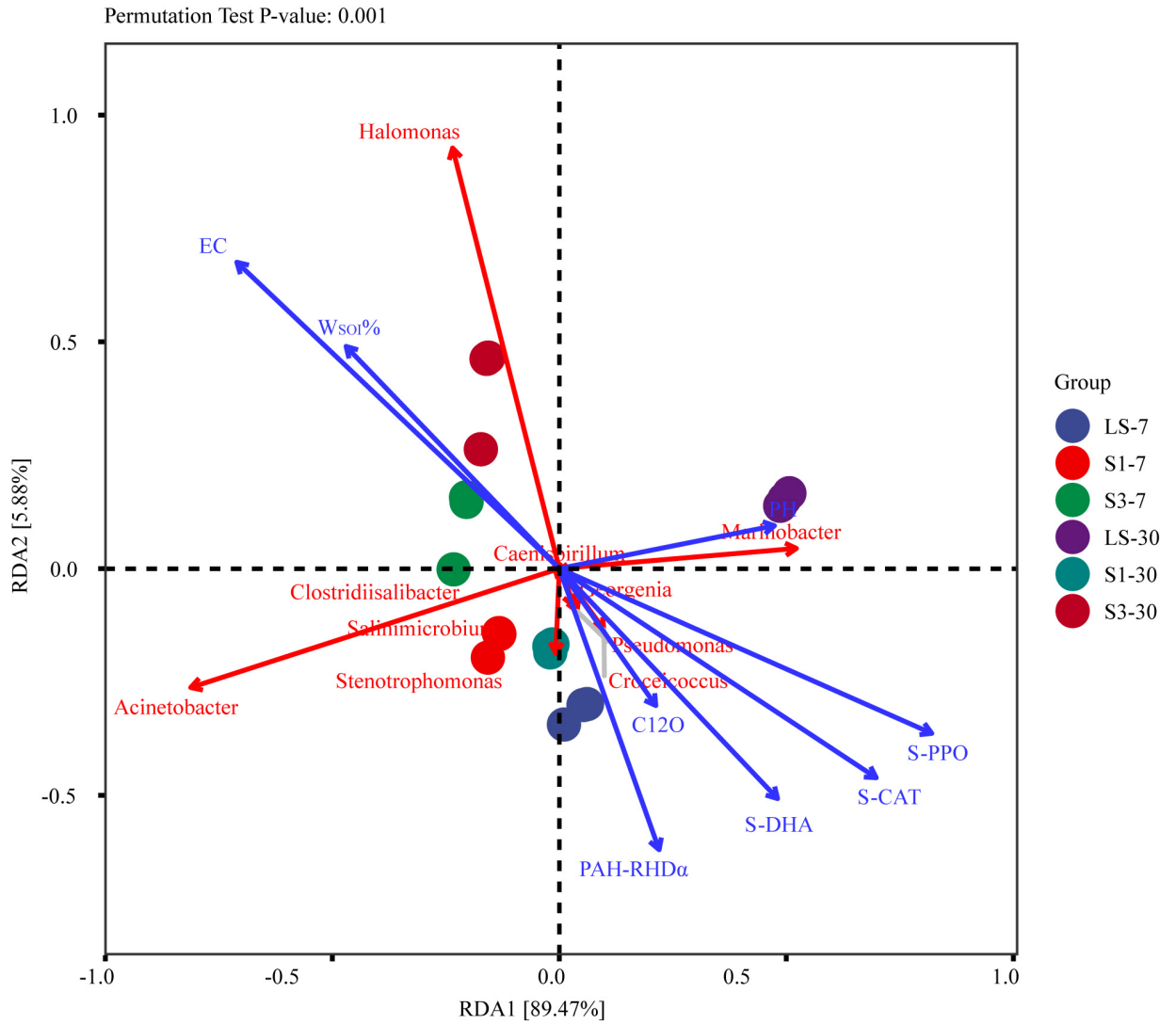

FIGURE 9 | Redundancy analysis (RDA) ordination plot to show the relationships among the soil physicochemical parameters, degradation genes, enzyme activities and the relative abundance of top 10 bacterial genera. The red arrow represents the species, and the length of the arrow represents the variability of species in the sorting space. The blue arrow line represents the influencing factor, and the length represents the influence of the factor on the composition and function of the flora.

with soil enzyme activities, PAH degradation, and pH. That is to say, in higher salinity treatments, the PAH degradation rate, soil enzyme and degradation genes will be lower. This is in accordance with other results discussed above in this paper.

Halomonasas, *Acinetobacter,* and *Marinobacter* are the three largest variants of the different species in the sorting space. The relative abundances of *Halomonas* and *Acinetobacter* were positively correlated with the soil salinity, indicating that these genera were important participants in the degradation process of PAHs during a relatively high saline environment (Czarny et al., 2020; Wright et al., 2020). However, there was a significant negative correlation between these two genera and the PAH degradation genes, indicating that these bacteria may not participate in PAH degradation directly. Wang et al. (2020) has proved that *Halomonas* cannot degrade PHE directly in experiments. The relative abundances of *Marinobacter* and other genera, including *Croceicoccus*, *Stenotrophomonas*, *Pseudomonas*, and *Salinimicrobium*, were all negatively correlated with the soil salinity, while positively correlated with pH, PAHs degradation genes and soil enzyme activities. These genera were reported to be the main force of PAH degradation in low salinity treatment (Wang et al., 2020). *Marinobacter* proved to require the cooperation of other bacteria during the biodegradation of PAHs (Cui et al., 2014), which led to a relatively low degradation rate of PAHs in high salinity soils. Soils with lower salinities had higher community diversity and richness, which led to a higher cooperation rate between different bacteria and then a higher PAH removal rate.

CONCLUSION

This study illuminated the effects of salinity on the PAH removal rate, soil enzyme activities, degradation gene abundance, and the structural changes of the soil bacterial community.

(1) The PAH degradation rate increased slightly in low saline soils, while were restrained significantly in high salt conditions.
(2) With increasing of soil salinity, not only the bacterial community diversity decreased, but also abundance of degradation gene and soil enzymes. This result could be responsible for the reduction of degradation rate in saline soils.
(3) The microbial community was filtered in high salt treatments and dominated by salt-tolerant and halophilic genera, such as *Acinetobacter* and *Halomonas*.
(4) Correlation analysis confirmed that, soil salinity was negatively related with PAH degradation, abundance of functional genes and soil enzyme activities, while positively related with some halophilic genera.

DATA AVAILABILITY STATEMENT

The original contributions presented in the study are publicly available. This data can be found here: https://www.ncbi.nlm.nih.gov/bioproject/, PRJNA788045.

AUTHOR CONTRIBUTIONS

YL, XF, and QZ designed the study. YL, WL, and LJ performed the experiment. FS, TL, QL, and YX analyzed the data. YL, XF, and JW wrote the manuscript. All authors contributed to the article and approved the submitted version.

FUNDING

This study was supported by programs of National Natural Science Foundation of China (Grant Numbers 41807111 and U1906222) and Natural Science Foundation of Shandong Province, China (Grant Number ZR2019PD018).

ACKNOWLEDGMENTS

We appreciate Xinran Hou for assistance during the soil sampling.

SUPPLEMENTARY MATERIAL

The Supplementary Material for this article can be found online at: https://www.frontiersin.org/articles/10.3389/fmicb.2021.824319/full#supplementary-material

REFERENCES

Adam, I. K. U., Duarte, M., Pathmanathan, J., Miltner, A., Brüls, T., and Kästner, M. (2017). Microbial communities in pyrene amended soil–compost mixture and fertilized soil. *AMB Exp.* 7:7. doi: 10.1186/s13568-016-0306-9

Asghar, H. N., Setia, R., and Marschner, P. (2012). Community composition and activity of microbes from saline soils and non-saline soils respond similarly to changes in salinity. *Soil Biol. Biochem.* 47, 175–178. doi: 10.1016/j.soilbio.2012.01.002

Azadi, N., and Raiesi, F. (2021). Sugarcane bagasse biochar modulates metal and salinity stresses on microbial functions and enzyme activities in saline co-contaminated soils. *Appl. Soil Ecol.* 167:104043. doi: 10.1016/j.apsoil.2021.104043

Bañón, S., Álvarez, S., Bañón, D., Ortuño, M. F., and Sánchez-Blanco, M. J. (2021). Assessment of soil salinity indexes using electrical conductivity sensors. *Sci. Hortic.* 285:110171. doi: 10.1016/j.scienta.2021.110171

Chabot, M., Morales, E., Cummings, J., Rios, N., Giatpaiboon, S., and Mogul, R. (2020). Simple kinetics, assay, and trends for soil microbial catalases. *Anal. Biochem.* 610:113901. doi: 10.1016/j.ab.2020.113901

Cheng, L., Wang, Y., Cai, Z., Liu, J., Yu, B., and Zhou, Q. (2017). Phytoremediation of petroleum hydrocarbon-contaminated saline-alkali soil by wild ornamental Iridaceae species. *Int. J. Phytoremed.* 19, 300–308. doi: 10.1080/15226514.2016.1225282

Chikere, C. B., and Fenibo, E. O. (2018). Distribution of PAH-ring hydroxylating dioxygenase genes in bacteria isolated from two illegal oil refining sites in the Niger Delta, Nigeria. *Sci. Afr.* 1:e00003. doi: 10.1016/j.sciaf.2018.e00003

Cortés-Lorenzo, C., Rodríguez-Díaz, M., López-Lopez, C., Sánchez-Peinado, M., Rodelas, B., and González-López, J. (2012). Effect of salinity on enzymatic activities in a submerged fixed bed biofilm reactor for municipal sewage treatment [article]. *Bioresour. Technol.* 121, 312–319. doi: 10.1016/j.biortech.2012.06.083

Cui, Z., Xu, G., Gao, W., Li, Q., Yang, B., Yang, G., et al. (2014). Isolation and characterization of *Cycloclasticus* strains from Yellow Sea sediments and biodegradation of pyrene and fluoranthene by their syntrophic association with *Marinobacter* strains [article]. *Int. Biodeterior. Biodegradation.* 91, 45–51. doi: 10.1016/j.ibiod.2014.03.005

Cycil, L. M., Dassarma, S., Pecher, W., Mcdonald, R., Abdulsalam, M., and Hasan, F. (2020). Metagenomic insights into the diversity of halophilic microorganisms indigenous to the Karak Salt Mine, Pakistan [original research]. *Front. Microbiol.* 11:1567. doi: 10.3389/fmicb.2020.01567

Czarny, J., Staninska-Pięta, J., Piotrowska-Cyplik, A., Juzwa, W., Wolniewicz, A., Marecik, R., et al. (2020). Acinetobacter sp. as the key player in diesel oil degrading community exposed to PAHs and heavy metals. *J. Hazard. Mater.* 383:121168. doi: 10.1016/j.jhazmat.2019.121168

De León-Lorenzana, A. S., Delgado-Balbuena, L., Domínguez-Mendoza, C. A., Navarro-Noya, Y. E., Luna-Guido, M., and Dendooven, L. (2018). Soil salinity controls relative abundance of specific bacterial groups involved in the decomposition of maize plant residues [original research]. *Front. Ecol. Evol.* 6:51. doi: 10.3389/fevo.2018.00051

Delgado-García, M., Contreras-Ramos, S. M., Rodríguez, J. A., Mateos-Díaz, J. C., Aguilar, C. N., and Camacho-Ruíz, R. M. (2018). Isolation of halophilic bacteria associated with saline and alkaline-sodic soils by culture dependent approach. *Heliyon* 4:e00954. doi: 10.1016/j.heliyon.2018.e00954

Fernández-Luqueño, F., Valenzuela-Encinas, C., Marsch, R., Martínez-Suárez, C., Vázquez-Núñez, E., and Dendooven, L. (2011). Microbial communities to mitigate contamination of PAHs in soil-possibilities and challenges: a review [review]. *Environ. Sci. Pollut. Res.* 18, 12–30. doi: 10.1007/s11356-010-0371-6

Geng, S., Qin, W., Cao, W., Wang, Y., Ding, A., Zhu, Y., et al. (2022). Pilot-scale bioaugmentation of polycyclic aromatic hydrocarbon (PAH)-contaminated soil using an indigenous bacterial consortium in soil-slurry bioreactors. *Chemosphere* 287:132183. doi: 10.1016/j.chemosphere.2021.132183

Ghosal, D., Ghosh, S., Dutta, T. K., and Ahn, Y. (2016). Current State of knowledge in microbial degradation of polycyclic aromatic hydrocarbons (PAHs): a review. *Front. Microbiol.* 7:1369. doi: 10.3389/fmicb.2016.01369

Habe, H., and Omori, T. (2003). Genetics of polycyclic aromatic hydrocarbon metabolism in diverse aerobic bacteria [article]. *Biosci. Biotechnol. Biochem.* 67, 225–243. doi: 10.1271/bbb.67.225

Hagemann, M. (2011). Molecular biology of cyanobacterial salt acclimation. *FEMS Microbiol. Rev.* 35, 87–123. doi: 10.1111/j.1574-6976.2010.00234.x

Han, X. M., Liu, Y. R., Zheng, Y. M., Zhang, X. X., and He, J. Z. (2014). Response of bacterial pdo1, nah, and C12O genes to aged soil PAH pollution in a coke factory area [article]. *Environ. Sci. Pollut. Res.* 21, 9754–9763. doi: 10.1007/s11356-014-2928-2

Haritash, A. K., and Kaushik, C. P. (2009). Biodegradation aspects of polycyclic aromatic hydrocarbons (PAHs): a review. *J. Hazard. Mater.* 169, 1–15. doi: 10.1016/j.jhazmat.2009.03.137

Huang, Y., Zeng, Y., Feng, H., Wu, Y., and Xu, X. (2015). Croceicoccus naphthovorans sp. nov., a polycyclic aromatic hydrocarbons-degrading and acylhomoserine-lactone-producing bacterium isolated from marine biofilm, and emended description of the genus *Croceicoccus*. *Int. J. Syst. Evol. Microbiol.* 65(Pt 5), 1531–1536. doi: 10.1099/ijs.0.000132

Ibekwe, A. M., Gonzalez-Rubio, A., and Suarez, D. L. (2018). Impact of treated wastewater for irrigation on soil microbial communities [article]. *Sci. Total Environ.* 62, 1603–1610. doi: 10.1016/j.scitotenv.2017.10.039

Kappell, A. D., Wei, Y., Newton, R. J., Van Nostrand, J. D., Zhou, J., Mclellan, S. L., et al. (2014). The polycyclic aromatic hydrocarbon degradation potential of Gulf of Mexico native coastal microbial communities after the deepwater horizon oil spill [original research]. *Front. Microbiol.* 5:205. doi: 10.3389/fmicb.2014.00205

Kuppusamy, S., Palanisami, T., Megharaj, M., Venkateswarlu, K., and Naidu, R. (2016). Ex-situ remediation technologies for environmental pollutants: a critical perspective. *Rev. Environ. Contam. Toxicol.* 236, 117–192.

Kuppusamy, S., Thavamani, P., Venkateswarlu, K., Lee, Y. B., Naidu, R., and Megharaj, M. (2017). Remediation approaches for polycyclic aromatic hydrocarbons (PAHs) contaminated soils: technological constraints, emerging trends and future directions. *Chemosphere* 168, 944–968. doi: 10.1016/j.chemosphere.2016.10.115

Li, H., Zhang, Q., Wang, X.-L., Ma, X.-Y., Lin, K.-F., Liu, Y.-D., et al. (2012). Biodegradation of benzene homologues in contaminated sediment of the East China Sea. *Bioresour. Technol.* 124, 129–136. doi: 10.1016/j.biortech.2012.08.033

Li, X., Qu, C., Bian, Y., Gu, C., Jiang, X., and Song, Y. (2019a). New insights into the responses of soil microorganisms to polycyclic aromatic hydrocarbon stress by combining enzyme activity and sequencing analysis with metabolomics. *Environ. Pollut.* 255(Pt 2):113312. doi: 10.1016/j.envpol.2019.113312

Li, X., Song, Y., Wang, F., Bian, Y., and Jiang, X. (2019b). Combined effects of maize straw biochar and oxalic acid on the dissipation of polycyclic aromatic hydrocarbons and microbial community structures in soil: a mechanistic study. *J. Hazard. Mater.* 364, 325–331. doi: 10.1016/j.jhazmat.2018.10.041

Li, X., Yao, S., Bian, Y., Jiang, X., and Song, Y. (2020). The combination of biochar and plant roots improves soil bacterial adaptation to PAH stress: insights from soil enzymes, microbiome, and metabolome. *J. Hazard. Mater.* 400:123227. doi: 10.1016/j.jhazmat.2020.123227

Liao, Q., Liu, H., Lu, C., Liu, J., Waigi, M. G., and Ling, W. (2021). Root exudates enhance the PAH degradation and degrading gene abundance in soils. *Sci. Total Environ.* 764:144436. doi: 10.1016/j.scitotenv.2020.144436

Lipińska, A., Wyszkowska, J., and Kucharski, J. (2015). Diversity of organotrophic bacteria, activity of dehydrogenases and urease as well as seed germination and root growth *Lepidium sativum*, *Sorghum saccharatum* and *Sinapis alba* under the influence of polycyclic aromatic hydrocarbons [article]. *Environ. Sci. Pollut. Res.* 22, 18519–18530. doi: 10.1007/s11356-015-5329-2

Liu, M., Zhao, X., Li, X., Wu, X., Zhou, H., Gao, Y., et al. (2021). Antagonistic effects of *Delia antiqua* (Diptera: Anthomyiidae)-associated bacteria against four phytopathogens. *J. Econo. Entomol.* 114, 597–610. doi: 10.1093/jee/toab002

Lozupone, C. A., and Knight, R. (2007). Global patterns in bacterial diversity [article]. *Proc. Natl. Acad. Sci.U.S.A.* 104, 11436–11440. doi: 10.1073/pnas.0611525104

Lu, H., Sun, J., and Zhu, L. (2017). The role of artificial root exudate components in facilitating the degradation of pyrene in soil [article]. *Sci. Rep.* 7:7130. doi: 10.1038/s41598-017-07413-3

Ma, J., Zhang, W., Chen, Y., Zhang, S., Feng, Q., Hou, H., et al. (2016). Spatial variability of PAHs and microbial community structure in surrounding surficial soil of coal-fired power plants in Xuzhou, China [article]. *Int. J. Environ. Res. Public Health* 13:878. doi: 10.3390/ijerph13090878

Muangchinda, C., Chavanich, S., Viyakarn, V., Watanabe, K., Imura, S., Vangnai, A. S., et al. (2015). Abundance and diversity of functional genes involved in the degradation of aromatic hydrocarbons in Antarctic soils and sediments around Syowa Station. *Environ. Sci. Pollut. Res. Int.* 22, 4725–4735. doi: 10.1007/s11356-014-3721-y

Nakhli, S. A. A., Panta, S., Brown, J. D., Tian, J., and Imhoff, P. T. (2019). Quantifying biochar content in a field soil with varying organic matter content using a two-temperature loss on ignition method. *Sci. Total Environ.* 658, 1106–1116. doi: 10.1016/j.scitotenv.2018.12.174

Nie, M., Zhang, X., Wang, J.-Q., Jiang, L.-F., Yang, J., Quan, Z., et al. (2009). Rhizosphere effects on soil bacterial abundance and diversity in the Yellow River deltaic ecosystem as influenced by petroleum contamination and soil salinization. *Soil Biol. Biochem.* 41, 2535–2542. doi: 10.1016/j.soilbio.2009.09.012

Pan, D., Wang, J., Chen, C., Huang, C. A., Cai, Q., and Yao, S. (2013). Ultrasonic assisted extraction combined with titanium-plate based solid phase extraction for the analysis of PAHs in soil samples by HPLC-FLD. *Talanta* 108, 117–122. doi: 10.1016/j.talanta.2013.02.066

Patel, A. B., Shaikh, S., Jain, K. R., Desai, C., and Madamwar, D. (2020). Polycyclic aromatic hydrocarbons: sources, toxicity, and remediation approaches [review]. *Front. Microbiol.* 11:2675. doi: 10.3389/fmicb.2020.562813

Pesce, S., Perceval, O., Bonnineau, C., Casado-Martinez, C., Dabrin, A., Lyautey, E., et al. (2018). Looking at biological community level to improve ecotoxicological assessment of freshwater sediments: report on a first French-Swiss workshop. *Environ. Sci. Pollut. Res.* 25, 970–974. doi: 10.1007/s11356-017-0620-z

Rath, K. M., Fierer, N., Murphy, D. V., and Rousk, J. (2019). Linking bacterial community composition to soil salinity along environmental gradients. *ISME J.* 13, 836–846. doi: 10.1038/s41396-018-0313-8

Rath, K. M., and Rousk, J. (2015). Salt effects on the soil microbial decomposer community and their role in organic carbon cycling: a review. *Soil Biol. Biochem.* 81, 108–123. doi: 10.1016/j.soilbio.2014.11.001

Rivas, F. J. (2006). Polycyclic aromatic hydrocarbons sorbed on soils: a short review of chemical oxidation based treatments [review]. *J. Hazard. Mater.* 138, 234–251. doi: 10.1016/j.jhazmat.2006.07.048

Singh, K. (2015). Microbial and enzyme activities of saline and sodic soils. *Land Degrad. Dev.* 27, 706–718. doi: 10.1002/ldr.2385

Song, M., Luo, C., Jiang, L., Zhang, D., Wang, Y., Zhang, G., et al. (2015). Identification of Benzo[a]pyrene-metabolizing bacteria in forest soils by using DNA-based stable-isotope probing. *Appl. Environ. Microbiol.* 81, 7368–7376. doi: 10.1128/aem.01983-15

Sullivan, M. L. (2014). Beyond brown: polyphenol oxidases as enzymes of plant specialized metabolism. *Front. Plant Sci.* 5:783. doi: 10.3389/fpls.2014.00783

Sun, J., Pan, L., Tsang, D. C. W., Zhan, Y., Zhu, L., and Li, X. (2018). Organic contamination and remediation in the agricultural soils of China: a critical review. *Sci. Total Environ.* 615, 724–740. doi: 10.1016/j.scitotenv.2017.09.271

Sun, N., Li, M., Liu, G., Jing, M., He, F., Cao, Z., et al. (2021). Toxic mechanism of pyrene to catalase and protective effects of vitamin C: studies at the molecular and cell levels. *Int. J. Biol. Macromol.* 171, 225–233. doi: 10.1016/j.ijbiomac.2020.12.169

Sushkova, S. N., Minkina, T., Deryabkina, I., Mandzhieva, S., Zamulina, I., Bauer, T., et al. (2017). Influence of PAH contamination on soil ecological status. *J. Soils Sediments* 18, 2368–2378. doi: 10.1007/s11368-017-1755-8

Teng, Y., and Chen, W. (2019). Soil microbiomes—a promising strategy for contaminated soil remediation: a review. *Pedosphere* 29, 283–297. doi: 10.1016/s1002-0160(18)60061-x

Tsibart, A. S., and Gennadiev, A. N. (2013). Polycyclic aromatic hydrocarbons in soils: sources, behavior, and indication significance (a review). *Eur. Soil Sci.* 46, 728–741. doi: 10.1134/S1064229313070090

Wang, C., Huang, Y., Zhang, Z., Hao, H., and Wang, H. (2020). Absence of the nahG-like gene caused the syntrophic interaction between Marinobacter and other microbes in PAH-degrading process. *J. Hazard. Mater.* 384:121387. doi: 10.1016/j.jhazmat.2019.121387

Wang, M., Chen, S., Chen, L., and Wang, D. (2019). Responses of soil microbial communities and their network interactions to saline-alkaline stress in Cd-contaminated soils [article]. *Environ. Pollut.* 252, 1609–1621. doi: 10.1016/j.envpol.2019.06.082

Wang, M., Wang, L., Shi, H., Liu, Y., and Chen, S. (2021a). Soil bacteria, genes, and metabolites stimulated during sulfur cycling and cadmium mobilization under sodium sulfate stress. *Environ. Res.* 201:111599. doi: 10.1016/j.envres.2021.111599

Wang, M., Zhao, S., Wang, L., Chen, S., Li, S., Lei, X., et al. (2021b). Salt stress-induced changes in microbial community structures and metabolic processes result in increased soil cadmium availability. *Sci. Total Environ.* 782:147125. doi: 10.1016/j.scitotenv.2021.147125

Wang, Q., Liu, X., Zhang, X., Hou, Y., Hu, X., Liang, X., et al. (2016). Influence of tea saponin on enhancing accessibility of pyrene and cadmium phytoremediated with *Lolium multiflorum* in co-contaminated soils [article]. *Environ. Sci. Pollut. Res.* 23, 5705–5711. doi: 10.1007/s11356-015-5784-9

Wright, M. H., Bentley, S. R., and Greene, A. C. (2020). Draft genome sequence of *Halomonas* sp. Strain ML-15, a haloalkaliphilic, polycyclic aromatic hydrocarbon-degrading bacterium. *Microbiol. Resour. Announc.* 9, e01175–20.

Xia, Y., Debolt, S., Dreyer, J., Scott, D., and Williams, M. A. (2015). Characterization of culturable bacterial endophytes and their capacity to promote plant growth from plants grown using organic or conventional practices [article]. *Front. Plant Sci.* 6:490. doi: 10.3389/fpls.2015.00490

Xu, X., Liu, W., Wang, W., Tian, S., Jiang, P., Qi, Q., et al. (2019). Potential biodegradation of phenanthrene by isolated halotolerant bacterial strains from petroleum oil polluted soil in Yellow River Delta. *Sci. Total Environ.* 664, 1030–1038. doi: 10.1016/j.scitotenv.2019.02.080

Xu, Z., Yang, Z., Zhu, T., Shu, W., and Geng, L. (2021). Ecological improvement of antimony and cadmium contaminated soil by earthworm *Eisenia fetida*: soil enzyme and microorganism diversity. *Chemosphere* 273:129496. doi: 10.1016/j.chemosphere.2020.129496

Yang, C., Wang, X., Miao, F., Li, Z., Tang, W., and Sun, J. (2020). Assessing the effect of soil salinization on soil microbial respiration and diversities under incubation conditions. *Appl. Soil Ecol.* 155:103671. doi: 10.1016/j.apsoil.2020.103671

Yang, Y., Wang, J., Liao, J., Xie, S., and Huang, Y. (2015). Abundance and diversity of soil petroleum hydrocarbon-degrading microbial communities in oil exploring areas [article]. *Appl. Microbiol. Biotechnol.* 99, 1935–1946. doi: 10.1007/s00253-014-6074-z

Zhang, X., Kong, D., Liu, X., Xie, H., Lou, X., and Zeng, C. (2021). Combined microbial degradation of crude oil under alkaline conditions by *Acinetobacter baumannii* and *Talaromyces* sp. *Chemosphere* 273:129666. doi: 10.1016/j.chemosphere.2021.129666

Zhang, Y., Hou, D., Xiong, G., Duan, Y., Cai, C., Wang, X., et al. (2018). Structural equation modeling of PAHs in ambient air, dust fall, soil, and cabbage in vegetable bases of Northern China [article]. *Environ. Pollut.* 239, 13–20. doi: 10.1016/j.envpol.2018.03.084

Zhao, Q., Bai, J., Gao, Y., Zhao, H., Zhang, G., and Cui, B. (2020). Shifts in the soil bacterial community along a salinity gradient in the Yellow River Delta [article]. *Land Degrad. Dev.* 31, 2255–2267. doi: 10.1002/ldr.3594

Conflict of Interest: The authors declare that the research was conducted in the absence of any commercial or financial relationships that could be construed as a potential conflict of interest.

Publisher's Note: All claims expressed in this article are solely those of the authors and do not necessarily represent those of their affiliated organizations, or those of the publisher, the editors and the reviewers. Any product that may be evaluated in this article, or claim that may be made by its manufacturer, is not guaranteed or endorsed by the publisher.

frontiers in Microbiology

ORIGINAL RESEARCH
published: 26 January 2022
doi: 10.3389/fmicb.2021.811697

Nitrogen Advanced Treatment of Urban Sewage by Denitrification Deep-Bed Filter: Removal Performance and Metabolic Pathway

Xiao Huang[1,2], Yixiao Xing[1], Hongjie Wang[2,3], Zhongyi Dai[4] and Tiantian Chen[5]**

[1] Jiangsu Key Laboratory of Atmospheric Environment Monitoring and Pollution Control, Collaborative Innovation Center of Atmospheric Environment and Equipment Technology, School of Environmental Science and Engineering, Nanjing University of Information Science and Technology, Nanjing, China, [2] Shenzhen Key Laboratory of Water Resource Utilization and Environmental Pollution Control, School of Civil and Environmental Engineering, Harbin Institute of Technology, Shenzhen, China, [3] State Key Laboratory of Urban Water Resource and Environment, School of Environment, Harbin Institute of Technology, Harbin, China, [4] China Municipal Engineering Central South Design and Research Institute Co., Ltd., Wuhan, China, [5] CAS Key Laboratory of Marine Ecology and Environmental Sciences, Institute of Oceanology, Chinese Academy of Sciences, Qingdao, China

OPEN ACCESS

Edited by:
Tian Li,
Nankai University, China

Reviewed by:
Junfeng Chen,
Qufu Normal University, China
Wentao Shang,
The University of Hong Kong, Hong Kong SAR, China

***Correspondence:**
Hongjie Wang
whj1533@qq.com
Tiantian Chen
chentian0819@163.com

Specialty section:
This article was submitted to Microbiotechnology, a section of the journal Frontiers in Microbiology

Received: *09 November 2021*
Accepted: *10 December 2021*
Published: *26 January 2022*

Citation:
Huang X, Xing Y, Wang H, Dai Z and Chen T (2022) Nitrogen Advanced Treatment of Urban Sewage by Denitrification Deep-Bed Filter: Removal Performance and Metabolic Pathway. Front. Microbiol. 12:811697. doi: 10.3389/fmicb.2021.811697

This study aimed to explore the performance of denitrification deep-bed filter (DN-DBF) to treat municipal sewage for meeting a more stringent discharge standard of total nitrogen (TN) (10.0 mg L^{-1}). A lab-scale DN-DBF was conducted to optimize operation parameters and reveal the microbiological mechanism for TN removal. The results showed that more than 12.7% TN removal was obtained by adding methanol compared with sodium acetate. The effluent TN concentration reached 6.0–7.0 mg L^{-1} with the optimal influent carbon and nitrogen ratio (C/N) and hydraulic retention time (HRT) (3:1 and 0.25 h). For the nitrogen removal mechanism, *Blastocatellaceae_Subgroup_4 and norank_o_JG30-KF-CM45* were dominant denitrification floras with an abundance of 6–10%. Though large TN was removed at the top layer of DN-DBF, microbial richness and diversity at the middle layer were higher than both ends. However, the relative abundance of nitrite reductase enzymes (EC1.7.2.1) gradually increases as the depth increases; conversely, the relative abundance of nitrous oxide reductase gradually decreased.

Keywords: advanced treatment, denitrification deep-bed filter, conditions optimization, total nitrogen, metabolic pathway

INTRODUCTION

Eutrophication, caused by excessive discharged nutrients (nitrogen and phosphorus) from wastewater treatment plants, has become one of the most urgent problems and gained significant attention in recent years (Piao and Kim, 2016). In some regions with sensitive aquatic ecology in China, the total nitrogen (TN) concentration is limited to less than 10.0 mg L^{-1}, which is superior to Chinese integrated wastewater discharge standard first-A (TN $\leq$ 15 mg L^{-1}). However, the traditional secondary biological treatment was difficult to meet due to the strict TN discharge standard (Li et al., 2014). Hence, more and more advanced treatment technologies are needed to control TN discharge and protect the limited water sources.

Tertiary denitrification was required to further remove the nitrate nitrogen (NO_3^--N) so as to achieve a high TN discharging standard since NO_3^--N is the major component of TN in a secondary effluent. Denitrification deep-bed filter (DN-DBF) could transform NO_3^--N to N_2 and be considered to be an effective means to improve TN removal efficiency (Husband et al., 2014; Löwenberg et al., 2016; Shi et al., 2016). However, previous studies on DN-DBF just to meet one-class A discharge standard, for the parameters [such as carbon source type, chemical oxygen demand (COD) and TN (C/N) ratio, and hydraulic retention time (HRT)] of further advanced treatment were not yet clear (Cao et al., 2016; Xu et al., 2016).

Carbon source type and dosage play important roles that need to be optimized during the tertiary denitrification process for meeting a higher discharge standard. Many materials could be utilized as carbon sources, such as waste paper (Bao et al., 2016; Haske-Cornelius et al., 2021), biodegradable polymer (Wang et al., 2021), and wheat straw (Khokhar et al., 2014; Liu et al., 2021). Readily biodegradable organic matters are the optimal electron donors compared with refractory organic and other electron donors (Cao et al., 2016; Luo et al., 2020). Meanwhile, an insufficient dose would result in a low denitrification rate, while COD concentration would not meet the discharge standard when excessive dosage carbon sources are added (Ge et al., 2012). On the other hand, a conflict exists between TN removal efficiency and construction cost, which results from too long or too short HRT. Hence, appropriate C/N ratios and HRT should be optimized to achieve the optimum denitrification effect.

Meanwhile, microbial action in DN-DBF restricts the performance of TN removal, which indicates that it is necessary to analyze the characteristics of the microbial community in DN-DBF to reveal the mechanism of TN removal. Microbial communities and functional microorganisms in wastewater treatment are closely related to environmental and operational conditions (Adrados et al., 2014; Feng and Tong, 2015). Previous studies reported that the dominant denitrifying bacterial genera were *Dechloromonas*, *Acidovorax*, *Bosea*, *Polaromonas*, and *Chryseobacterium*, and particle sizes and packing type affected the community composition diversity (Tian and Wang, 2021; Yang et al., 2021). However, current studies only focused on the changes of microbial communities, but few on metabolic pathways.

Therefore, this study optimized operating parameters (carbon source type, C/N, and HRT) and investigated the performance of DN-DBF to ensure effluent compliance with the TN discharge standard (10.0 mg L^{-1}). Besides, high-throughput sequencing technology was applied to reveal the degradation mechanism of pollutants.

MATERIALS AND METHODS

Experimental Systems

The tertiary DN-DBF (**Figure 1**) was made from a plexiglass column with a diameter of 100 mm and a height of 1.8 m, and packed with 2–3 mm sizes of quartz sand. The packed height was 1.1 m, and a 0.3 m support gravel stone layer was set under that. The porosity and bulk density were 0.42 and 1.18 kg m^3, respectively. The effluent of micro-coagulated was pumped to the top of DN-DBF and the effluent was discharged at the bottom. Besides, the sampling points and piezometers were installed on both sides of the DN-DBF and the intervals were 100 and 200 mm, respectively. The filtering media were backwashed every 24 h for 16 min by combined air and water for 8 min and water backwashing for 8 min. During backwashing, the air flow rate was 95.5 m h^{-1} and the water flow rate was 31.8 m h^{-1}.

The secondary effluent was collected from an anaerobic-multistage anaerobic/oxic (A-MAO) process to a micro-flocculation tank, in which phosphorus was removed by polyaluminium chloride (PAC). The flocs were subsided in the settling tank, and the effluent was pumped into DN-DBF with external organic carbon. The main characteristics of the secondary effluent from the A-MAO process and the influent of DN-DBF are summarized in **Table 1**.

System Performance and Batch Experiments

Operating conditions of the DN-DBF are shown in **Table 2**. Carbon source type [methanol (CH_3OH) and sodium acetate (NaAC)], C/N (7.0–8.0, 5.0–6.0, 4.0–5.0, 3.0–4.0, and 1.5–3.0), and HRT (0.5, 0.25, and 0.1 h) were investigated by long-time batch experiments at different periods. Under steady state, samples were taken at 0, 10, 30, 50, 70, 90, and 110 cm along the DN-DBF depth, and TN and COD concentrations were tested so as to investigate denitrification performance. Besides, the biomass attached on quartz sand samples and suspended biofilm were taken and measured from the DN-DBF regularly.

Chemical Analysis Methods

Samples were collected from the micro-flocculation setting tank and effluent of DN-DBF once a day. Besides, samples in different depths were collected when the system was in stable operation. COD, TN, ammonia nitrogen (NH_4^+-N), NO_3^--N, and total phosphorus (TP) were analyzed according to standard methods (APHA, 2005). Biofilm biomass was determined using the weighted method. pH and temperature were monitored online by using WTW pH/Oxi 340i meter with dissolved oxygen (DO) and pH probes (WTW, Germany).

Microbiological Analysis Methods

In order to evaluate the diversity of microbial community structure of the DN-DBF system, three biofilm samples were collected at the 95th day from three parts (10, 50, and 100 cm). The total DNA was extracted with the Fast DNA Spin Kit for Soil (MP Biomedicals, Santa Ana, CA, United States). The purified DNA was applied in polymerase chain reaction (PCR) analysis by PCR instrument (9700, GeneAmp® ABI, Foster City, CA, United States) with the primer set of 338F (50-ACTCCTACGGGAGGCAGCA-30) and 806R (50-GGACTACCAGGGTATCTAAT-30). Besides, the PCR programs were as follows: initial denaturation at 95°C for 3 min; followed by 30 cycles of denaturation at 95°C for 30 s, annealing at 45°C for 30 s, elongation at 72°C for 45 s; and finally at 72°C for 10 min

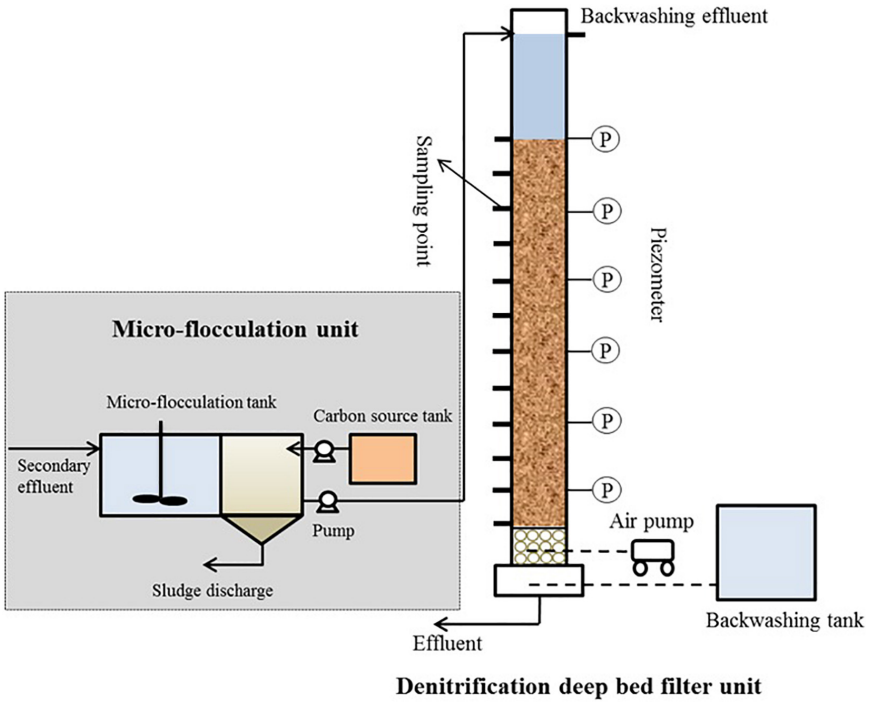

FIGURE 1 | Schematic diagram of the denitrification deep bed filter.

and 10°C until halted by user. The amplicons were sequenced on an Illumina MiSeq platform by Majorbio company (Shanghai, China). The original image data files were transformed into original sequencing sequence by CASAVA base recognition analysis, and the results were stored in FASTQ file format.

Paired-end reads of the original DNA fragments were merged using Trimmomatic and FLASH softwares (V1.2.7[1]) (Magoc and Salzberg, 2011), and sequencing reads were assigned to each sample based on a unique barcode. Mothur version v.1.30.1 was used to calculate microbial richness and diversity (ACE index, Chao 1 index, Simpson index, and Shannon index) (Schloss et al., 2011). The operational taxonomic units (OTUs) were assigned with Usearch software (version 7.1[2]), and all sequence column similarities within a stationary threshold (>97%) were combined together to be considered as one of the OTUs. Microbial abundance at the phylum and genus levels was counted depending on taxonomic data.

PICRUSt software[3] was used to remove the 16S marker gene, and Non-supervised Orthologous Groups (eggNOG)[4] databases and Kyoto Encyclopedia of Genes and Genomes (KEGG)[5] were used to conduct the 16S rRNA functional prediction.

[1]http://ccb.jhu.edu/software/FLASH/

[2]http://drive5.com/uparse/

TABLE 1 | Main characteristics of influent wastewater.

Parameter	Secondary effluent		Influent of DN-DBF	
	Range	Average	Range	Average
COD/(mg L^{-1})	15–40	28.6	40–100	–
NH_4^+-N/(mg L^{-1})	0–2	1.41	0–1.5	0.76
NO_3^--N/(mg L^{-1})	7–11	8.51	7–11	8.62
TN/(mg L^{-1})	9–14	13.42	8–14	13.14
TP/(mg L^{-1})	0.30–0.50	0.43	0.10–0.30	0.18
pH	6.50–7.20	6.80	6.10–6.90	6.70
T/°C	22–30	27	22–30	27

RESULTS AND DISCUSSION

Optimization of Denitrification Deep-Bed Filter Operating Conditions

Carbon Source Types

CH_3OH and NaAC were added to DN-DBF. The effect of carbon source types on denitrification was compared, as shown in **Figure 2A**. The average TN removal efficiency was 41.11 and 51.04% with an effluent concentration of 8.09 and 6.80 mg L^{-1}, respectively, when equal COD was dosed by CH_3OH and NaAC. More 10% removal efficiency and 1.29 mg L^{-1} TN were removed by CH_3OH than NaAC with 0.598 and 0.750 kg (m^3 $d)^{-1}$ TN translated into N_2, respectively. Therefore, CH_3OH was the optimal carbon source for denitrification of DN-DBF. The denitrification rate of using CH_3OH as carbon source was

[3]http://huttenhower.sph.harvard.edu/galaxy/root?tool_id=PICRUSt_normalize/

[4]http://eggnog.embl.de/

[5]http://www.genome.jp/kegg/

TABLE 2 | Operation parameters of different stages.

Stages	Periods (day)	Operation parameters				
		Carbon source type	TN (mg L^{-1})	COD (mg L^{-1})	C/N	HRT (h)
I	1–10	Methanol (CH_3OH)	13.15–14.78	39.87–45.93	3.0–3.5	0.25
II	10–20	Sodium acetate (NaAC)	13.05–14.61	39.56–42.95	3.0–3.5	0.25
III	20–29	CH_3OH	12.42–15.04	99.0–110.98	7.0–8.0	0.5
IV	29–37	CH_3OH	12.84–14.99	74.25–85.10	5.0–6.0	0.5
V	37–46	CH_3OH	12.97–15.06	60.62–67.76	4.0–5.0	0.5
VI	49–55	CH_3OH	13.15–14.78	39.87–46.32	3.0–4.0	0.5
VII	55–65	CH_3OH	13.39–15.39	24.62–30.52	1.5–3.0	0.5
VIII	65–75	CH_3OH	11.66–14.81	38.54–44.52	3.0–4.0	0.5
IX	75–85	CH_3OH	11.72–14.52	39.41–45.29	3.0–4.0	0.25
X	85–95	CH_3OH	12.65–15.62	40.12–46.55	3.0–4.0	0.1

higher than NaAC, even compared to previous studies in other bioreactor configurations (**Table 3**).

Due to the low cost and high efficiency of CH_3OH and NaAC, they have been widely used by many sorts of denitrification process (Wei et al., 2016). CH_3OH and NaAC requirement correlated with the removal of NO_3^--N could be estimated by Eqs 1, 2; 2.47 g CH_3OH (about 3.7 g COD) and 5.60 g CH_3OONa (about 4.37 g COD) were consumed to transform 1 g NO_3^- to N_2. Therefore, more NaAC was consumed to achieve the denitrification process. Previous studies have shown that carbon source switchover resulted to the change of microbial community structure (Liang et al., 2014). Therefore, the difference in denitrification efficiency between methanol and sodium acetate may be caused by the difference in microbial community structure.

$$NO_3^- + 1.08\ CH_3OH + 0.24H_2CO_3 \rightarrow 0.06C_5H_7NO_2 + 0.47\ N_2 + 1.68\ H_2O + HCO_3^- \quad (1)$$

$$NO_3^- + 1.06\ CH_3OO^- + 0.70\ H_2CO_3 \rightarrow 0.15C_5H_7NO_2 + 0.42\ N_2 + 0.73\ H_2O + 2.06\ HCO_3^- \quad (2)$$

C/N Ratio

Five C/N ratios (7.0–8.0, 5.0–6.0, 4.0–5.0, 3.0–4.0, and 1.5–3.0) were examined to study the effect of their nitrogen removing performance on DN-DBF. As shown in **Figure 2B**, TN removal efficiency gradually decreased and the concentration in effluent rose as the C/N radio reduced. The removal efficiency of TN maintained stable vibration that ranged from 72.05 to 88.89% and effluent concentration was 1.38–3.54 mg L^{-1} when C/N ratio exceeded 4. With further reduction of C/N, stable TN removal performance was destroyed and the efficiency dropped to 13.65–25.33% with high TN concentration (10.20–15.39 mg L^{-1}) in the effluent.

In addition, it should be noted that large-dosage carbon sources resulted in less TN concentration in the effluent, and excessive COD concentration would not meet the discharge standard, while an insufficient dose would lead to a low denitrification rate. COD in effluent was 21.36–46.32 mg L^{-1} at the first three periods (C/N was 7.0–8.0, 5.0–6.0, and 4.0–5.0). Though the COD value was inferior to discharge standard, the utilization of carbon source was low and more COD was wasted (**Figure 2B**). However, TN was over 10 mg L^{-1} with a low-concentration COD (15.51–18.32 mg L^{-1}) when C/N was below 3.0. Hence, the optimal and economical influent C/N was 3.0–4.0, which could meet the TN discharge standard (10.0 mg L^{-1}).

The theoretical demand of COD and actual consumption value is demonstrated in **Figure 2C**. The theoretical demand of COD was correlated by Eq. 1 and its less than actual consumption was due to the fact that partial carbon source was consumed or degraded by other processes instead of denitrification. Meanwhile, part of NO_3^--N was absorbed for assimilation in the biological reactor (Constantin and Fick, 1997; Zhang et al., 2021). Cheng and Lin (1993) utilized methanol as a carbon source for denitrification and established the theoretical C/N ratio of 0.71. Wang et al. (2009) found that low C/N (C/N = 1) was not sufficient for the denitrification bacteria to grow. Nevertheless, Gómez et al. (2000), Fan et al. (2001), and Wei et al. (2016) concluded that the optimal C/N ratio was 1.25, 1.1, and 2.2 for denitrification with methanol as the electron donor, which was inconsistent with this study.

Hydraulic Retention Time

Hydraulic retention time, as another important parameter for DN-DBF, restricts the denitrification performance and the occupied area of structure. **Figure 2D** showed the effect of different HRT (0.5, 0.25, and 0.1 h) on TN removal. TN removal efficiency decreased and effluent concentration increased with the tightening of HRT, and the average TN removal efficiency was 63.37 and 49.47% with the effluent concentration of 4.75 and 6.59 mg L^{-1} when HRT was 0.5 and 0.25 h, respectively, while the steep increase of TN concentration in the effluent (average concentration was 10.08 mg L^{-1}) reflected the fact that 0.1 h could not meet the discharge standard and the optimal and economical HRT was 0.25 h.

Denitrification is a rapid process of nitrogen conversion compared with the ammonia oxidation process. Farabegoli et al. (2003) drew a conclusion that 55% TN removal efficiency was obtained when influent TN concentration was 15 mg L^{-1} and

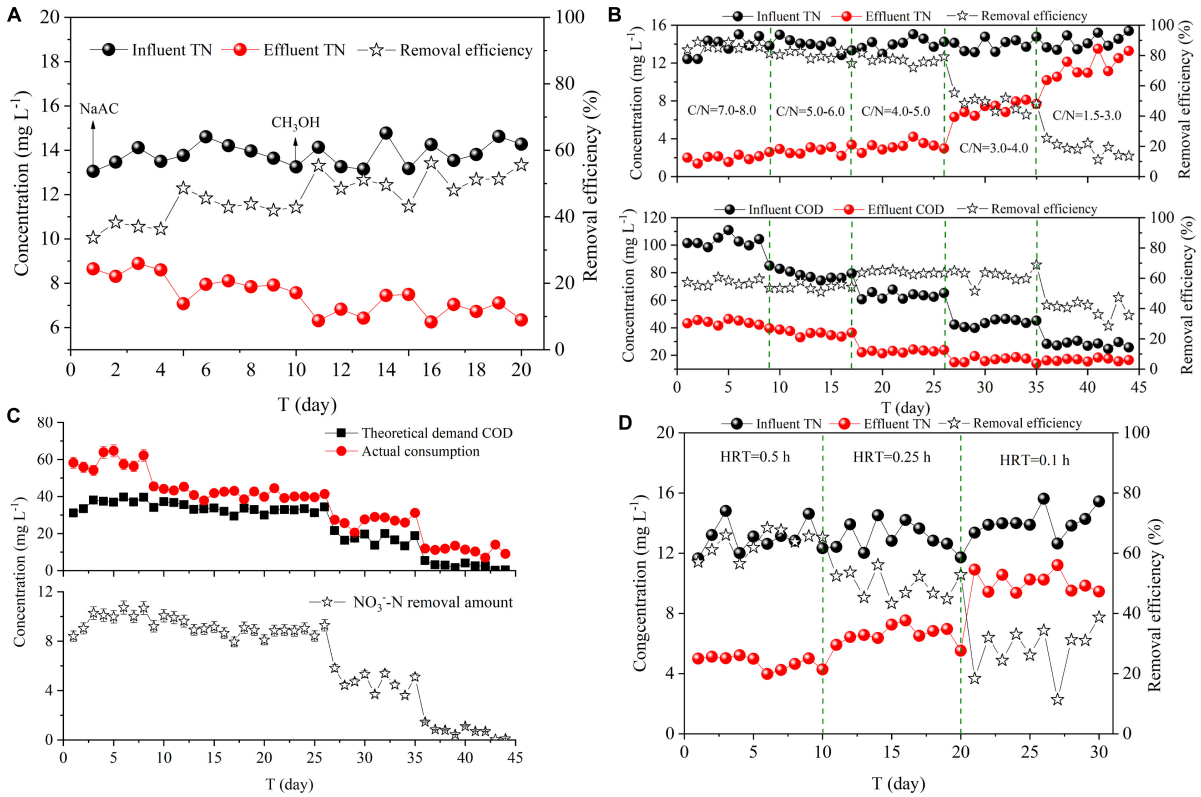

FIGURE 2 | Effect of operating conditions on TN removal **(A)** Carbon source types, **(B,C)** C/N ratios, **(D)** HRT.

HRT was 7 min. The above conclusion was similar to this study. Nevertheless, Shen and Wang (2011) used cross-linked starch/polycaprolactone blends as solid carbon source and concluded that the 26.86 mg NO_3^--N $(L\ h)^{-1}$ and 90% NO_3^--N were removed at HRT 1 h, which was obviously more than those in this study. The phenomenon was inferred that carbon source style was the main factor that restricted HRT.

TABLE 3 | Performance comparisons with other bioreactor configurations.

Carbon source	C/N ratio	Influent NO_3^--N (mg L^{-1})	Denitrification rate [kg NO_3^--N $(m^3\ d)^{-1}$]	References
Sugar	6.25	40	3.21	Karanasios et al., 2016
Ethanol	1.5	9.8	0.001	Shi et al., 2016
No mention	10	1.5–2.0	0.082	Wang et al., 2016
Sodium acetate	3	14.5–19	0.343	Wu and Li, 2017
Brewery wastewater	5.2	30	1.11	Dong et al., 2012
Bakery wastewater	5.2	30	1.24	Dong et al., 2012
Methanol	5.2	30	1.44	Dong et al., 2012
Methanol	3.0–3.5	12–13	0.750	This study
Sodium acetate	3.0–3.5	12–13	0.598	This study

Nutrient Removal and Head Loss Along the Filter Depth

Nutrient removal along the filter depth reflected the pollutants' removal features of DN-DBF (**Figure 3**), the concentration of TN and COD in the influent were 14.14 and 42.37 mg L^{-1}, and 55.37 and 64.81% removal efficiency were achieved with effluent concentration of 6.31 and 14.91 mg L^{-1}. It is interesting that the denitrification rates of both pollutants were higher at the top of

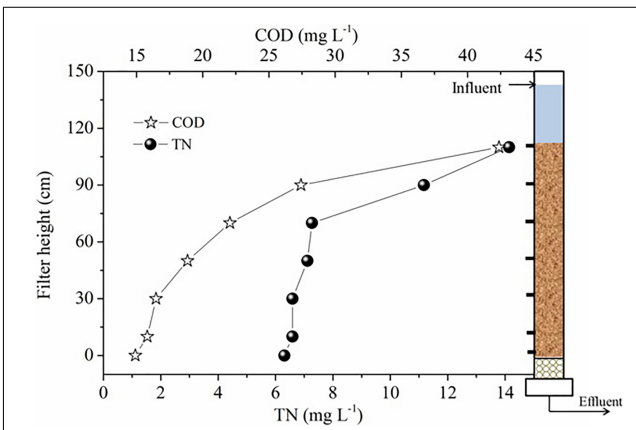

FIGURE 3 | Concentration profiles of TN and COD along the DN-DBF depth.

TABLE 4 | Head loss along DN-DBF (m H_2O).

Filter depth (cm)	*T* (h)							
	0	1	2	4	8	12	16	20
10	0.000	0.005	0.022	0.032	0.065	0.084	0.123	0.152
30	0.005	0.011	0.035	0.046	0.087	0.113	0.248	0.296
50	0.008	0.015	0.044	0.057	0.095	0.124	0.269	0.314
70	0.011	0.025	0.051	0.068	0.106	0.135	0.287	0.383
90	0.022	0.036	0.066	0.079	0.125	0.147	0.317	0.394

the filter than the bottom part; 48.85% TN and 47.93% COD were removed at the top 40 cm, while 5.52% TN and 16.87% COD were removed at the bottom 70 cm. The study of Dong et al. (2012) found that the specific denitrification rate along the biofilter depth was 3.80, 1.21, 0.66, and 0.09 kg NO_3^--N $(m^3\ d)^{-1}$, respectively, and the highest specific denitrification rate appeared at 0–20 cm. It might be because more biomass accumulated on top of head loss; this is another standard to evaluate the performance of DN-DBF, and its change along the filter depth is shown in **Table 4**. As the increase of filter depth and operation time is extending, the head loss presented a significant increasing trend. The head loss changed by low increasing rates before the 12th hour, but the stable station was broken and the head loss jumped from 0.083–0.147 to 0.152–0.394 mH_2O after the 12th hour. The specific incremental rate of head loss before the 12th hour along the filter depth was 0.007, 0.009, 0.010, 0.011, and 0.012 mH_2O, respectively. However, the specific incremental rate after the 12th hour was 0.009–0.031 mH_2O. Thus, the optimal backwash time was 12 h. Simate (2015) found that the head loss of the granular filter bed ran up suddenly at the 18th hour, which is similar to this study.

Biofilm Biomass Along the Filter Depth

Biomass yield is an important indicator to be taken into account for explaining the denitrification performance of DN-DBF. Biomass yields in different filter depths are summarized in **Figure 4**; the total biomass and attached biomass increased at the first 30 cm of DN-DBF, and reduced as filter depth continued to increase. However, the suspended biomass was reduced along with the filter depth. The maximum quality of attached biomass, suspended biomass, and total biomass was 21.03, 20.01, and 33.10 mg SS (g quartz sand)$^{-1}$, respectively, and appeared at 30, 10, and 30 cm. On the other hand, a similar rule was discovered for volatile suspended solids (VSS). The ratio of suspended solids (SS) and VSS was about 1.5–2.0, which indicated that approximately 40–50% inorganic particles exited and contributed to the head loss of DN-DBF.

TABLE 5 | Bacterial richness and diversity along DN-DBF.

0	ACE	Chao	Shannon	Simpson
10	1060	1059	50589	0.01017
50	1089	1094	5.707	0.00894
100	1064	1065	5.633	0.00886

At the top layer of this filter, the suspended biomass was more than the attached biomass, but it was opposite the other sampling point. The reason for this phenomenon may be that the SS was intercepted on the first 10 cm and hydraulic scour affected the formation of biofilms (Li et al., 2011; Wu et al., 2016). This result is consistent with Dong et al. (2012). There was a high correlation between biofilm biomass and effluent quality. Large TN and COD were removed at the top of the filter due to the accumulation of biofilm biomass. Meanwhile, the higher the biomass yield rates resulted from more COD and NO_3^--N that were needed for complete denitrification and cell growth (Christensson et al., 1994).

Microbial Mechanism of Nitrogen Removal

Microbial Richness and Diversity

The microbial biochemistry processes play an important role in the treatment of wastewater by DN-DBF. Therefore, analysis of the microbial process could help to characterize the mechanism and approach. In this section, 16S rRNA gene high-throughput sequencing technology was utilized to analyze the microbial

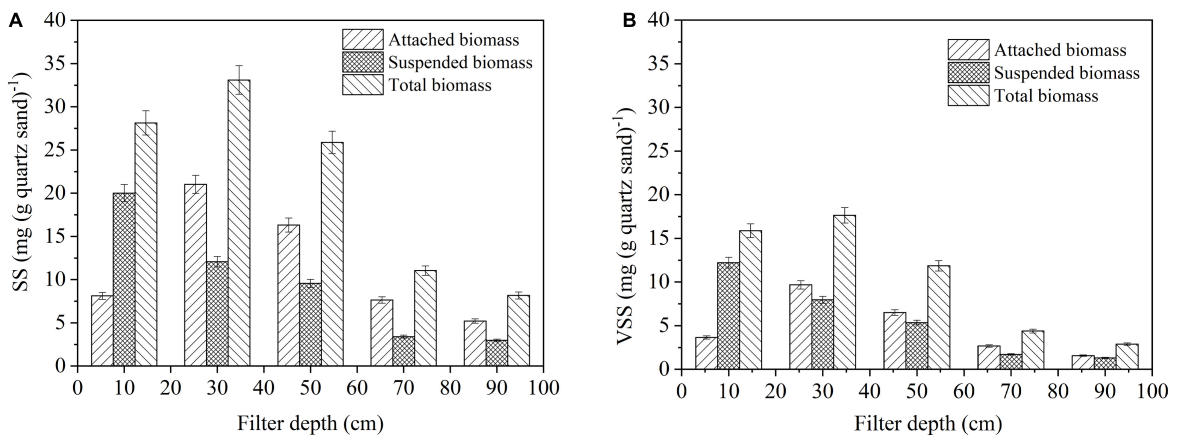

FIGURE 4 | Change of biofilm biomass along the DN-DBF depth **(A)** SS and **(B)** VSS.

community of the samples and assess the diversity and richness of the bacterial community, which was utilized to explain the denitrification mechanism of DN-DBF.

From 10 to 100 cm, the ACE and Chao index showed a tendency to rise and then fall, which indicated that the system owned the maximum microbial abundance when the filter depth was 50 cm (**Table 5**). Meanwhile, the variation of Shannon and Simpson diversity index from 10 to 100 cm illustrated that the diversity of microbial community also reached peak value at 50 cm. Community diversity was directly determined by species richness and species evenness. This phenomenon reflected that the backwashing process led to impacting on the stability of microorganisms and contributed to the lower diversity of microbial community than the middle part. Sun et al. (2016) and Huang et al. (2020) reported the maximal diversity index appeared at the middle part in the denitrification filler by comparing the diversity index (Shannon) along a denitrification filler, which was consistent with this study.

Microbial Community Composition

During the process of operation, the bacteria with higher relative abundance of microbial community mainly affiliated to four phyla, i.e., Proteobacteria, Chloroflexi, Actinobacteria, and Saccharibacteria. All of them were substantiated to be the dominant denitrifying bacteria (**Figure 5A**). The results explained that the relative abundance of dominant denitrifying bacteria directly affected the denitrification efficiency. Previous researches have indicated that multiple types of Proteobacteria microorganisms were in several wastewater treatment bioreactors, which was in accord with the study of Ma et al. (2015). When the depth of filter was between 10 and 50 cm, Blastobacter was dominant and abundant, which was affiliated to α-Proteobacteria; it was a crucial participant in nitrogen removal and COD degradation in wastewater treatment.

Figure 5B demonstrates the dominant microbial flora abundance at family level. The abundance of microbial communities was evenly distributed, except for the *Blastocatellaceae_Subgroup_4* and *norank_o_JG30-KF-CM45* abundance of 6–10%, and the remaining flora abundance fluctuates between 2 and 5%. Chang et al. (2019) used a denitrification filter to remove polluted river, and results showed that *Blastocatellaceae* was the dominant heterotrophic denitrifying bacteria with a proportion of 2.3%. *JG30-KF-CM45* was also a typical denitrifying bacterium and proportional to the organic load in an urban sewage treatment process (Remmas et al., 2017). Meanwhile, the *norank_p_Saccharibacteria* under the Spirulina was reported as a denitrification group participating in organic matter removal (Sun et al., 2018). *Caldilineaceae* was with an abundance of about 4%, which was similar to previous reports such as Wu et al. (2018) who found that its share in short-range denitrification was 3.72%. Besides, *Xanthomonadales_Incertal_Sidis*, *Hyphomicrobiaceae*, and *norank_p_Parcubacteria* are typical heterotrophic anti-nitrifying bacteria. *norank_c_Acidobacteria*, *Lactobacilliaceae*, and *norank_o_Acidimicrobiales* were organic degradation bacteria belonging to Acidobacteria, which was related to the addition of carbon sources in the influent. *Nitrosomonadaceae* and *norank_c_Nitrospira* are nitrifying bacteria, whose appearance indicated that nitrification occurred at the upper and end of this filter.

Pathway of Nitrogen Metabolism

Figure 6 and **Table 6** demonstrate the abundance of key enzymes related to nitrogen cycle depending on functional prediction. Specific enzymes, such as nitrate reductase (EC1.7.2.1), chlorophyllide reductase iron protein subunit X (EC1.18.6.1), nitronate monooxygenase (EC1.13.12.16), and nitrilase (EC3.5.5.1), are involved in the denitrification process of DN-DBF. With the augmentation of the depth of the filter, the reduction of chlorophyllide reductase iron protein subunit X (EC1.18.6.1), nitrilase (EC3.5.5.1), nitrate reductase 2 (EC1.7.99.4), nitric oxide reductase (EC1.7.2.5), and chlorophyllide reductase iron protein subunit X (EC1.18.6.1) took on an upward and then downward tendency. Huang et al. (2020) discussed the abundance of key enzymes related to nitrogen cycle in an iron carbon-based constructed wetland (CW), and chlorophyllide reductase iron protein subunit X (EC1.18.6.1) in CW with Fe^0-C filter demonstrated the lowest abundance at the middle layer and the highest value appeared in CW with ceramsite filler, which was consistent with this study.

At the filter depth of 50 cm, the abundance of relative enzyme reached the maximum, and the number and denitrifying activity

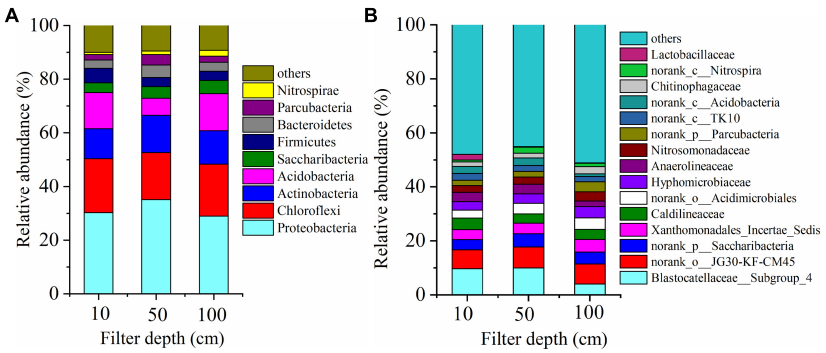

FIGURE 5 | Change of microbial community composition along the DN-DBF depth **(A)** at phylum level and **(B)** at genus level.

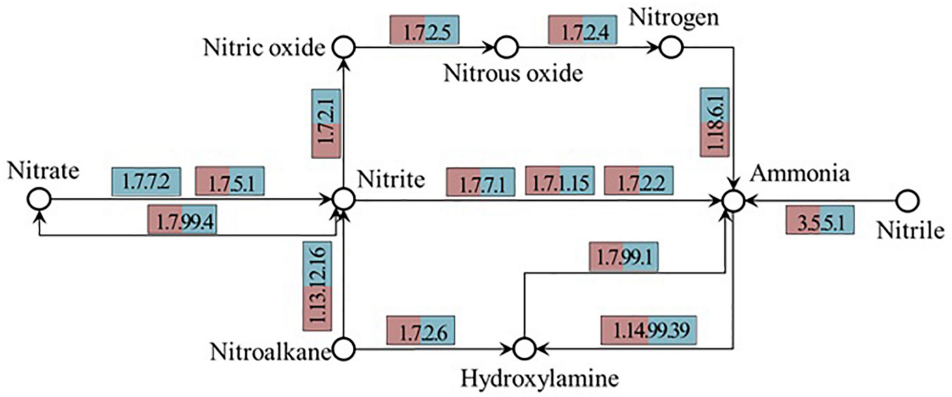

FIGURE 6 | Nitrogen cycle related key enzymes along the DN-DBF depth.

TABLE 6 | Abundance of nitrogen cycle-related key enzymes along DN-DBF (10^{-3} %).

Enzyme	10 cm	50 cm	100 cm	Function description
EC1.7.99.4	58.47	66.99	66.51	Nitrate reductase 2, delta subunit
EC1.7.2.1	4.06	5.18	5.92	Nitrite reductase (NO-forming)
EC1.7.2.5	5.50	5.97	4.94	Nitric oxide reductase, cytochrome *b*-containing subunit I
EC1.7.2.4	17.83	16.88	15.74	Nitrous-oxide reductase
EC1.7.7.1	13.00	10.56	13.50	Ferredoxin-nitrite reductase
EC1.7.2.2	7.88	7.49	8.94	Formate-dependent nitrite reductase, periplasmic cytochrome c552 subunit
EC1.18.6.1	86.08	105.08	96.97	Chlorophyllide reductase iron protein subunit X
EC3.5.5.1	41.60	48.91	40.71	Nitrilase
EC1.7.99.1	1.31	1.37	1.32	Hydroxylamine reductase
EC1.13.12.16	25.52	23.59	24.32	Nitronate monooxygenase

of corresponding denitrifying bacteria was the highest; therefore, the denitrification was the strongest with the highest nitrogen removal rate in this part. The results coincided with the changes of microbial community composition and diversity. During the denitrification process, nitrite reductase controlled the reduction of NO_3^--N and the production of N_2O, and the process of transforming N_2O to NO was commanded by nitrous oxide reductase. The relative abundance of nitrite reductase gradually increases as the depth increases, and conversely, the relative abundance of nitrous oxide reductase gradually decreased. It indicated that more N_2O is converted to NO with the deepening of the filter. It is worth noting that the relative abundance of nitronate monooxygenase demonstrated a decrease first and then ascended. In view of the effect of influent and backwashing, DO was enriched on both ends of the filter. Hence, the abundance of aerobic bacteria was relatively large and resulted in high nitronate monooxygenase abundance in the center of this filter.

CONCLUSION

The DN-DBF parameters were optimized for the advanced treatment of TN from the secondary effluent. More than 12.7% of TN removal efficiency was obtained by adding methanol compared with sodium acetate, and the optimal influent C/N ratio and HRT were 3:1 and 0.25 h, respectively. The backwash time was 12 h, and the total and attached biomass reached the maximum at 30 cm of DN-DBF, where the diversity and richness of microbial community was higher than that in both ends. High-throughput sequencing technology showed that Proteobacteria, Chloroflexi, Actinobacteria, and Saccharibacteria were dominant flora at phylum level, and *Blastocatellaceae_Subgroup_4 and norank_o_JG30-KF-CM45* were dominant denitrification floras with an abundance of 6–10%. Meanwhile, the abundance of nitrite reductase enzymes (EC1.7.2.1) reached the maximum at 50 cm.

DATA AVAILABILITY STATEMENT

The original contributions presented in the study are included in the article/supplementary material, further inquiries can be directed to the corresponding authors.

AUTHOR CONTRIBUTIONS

ZD and TC made substantial contributions to the conception or design of the work and the acquisition, analysis, or interpretation of data for the work, drafted the work or revised it critically for important intellectual content, gave final approval of the version to be published, and agreed to be accountable for all aspects of the work in ensuring that questions related to the accuracy or integrity of any part of the work are appropriately investigated

and resolved. All authors listed have made a substantial, direct, and intellectual contribution to the work, and approved it for publication.

FUNDING

This work was supported by a project grant from the National Natural Science Foundation of China (421078064), Project of Shenzhen Science and Technology Plan (Grant Nos. KCXFZ202001011006362, KJYY20180718094802190, and JCYJ20200109113006046), Project of China Municipal Engineering Central South Design and Research Institute (Theory and Application: High Efficiency, Energy Saving and Intelligent Biological Enhanced Denitrification Process), and Doctor Program of Entrepreneurship and Innovation in Jiangsu Province (Grant No. R2020SCB10).

REFERENCES

Adrados, B., Sanchez, O., Arias, C. A., Becares, E., Garrido, L., Mas, J., et al. (2014). Microbial communities from different types of natural wastewater treatment systems: vertical and horizontal flow constructed wet-lands and biofilters. *Water Res.* 55, 304–312. doi: 10.1016/j.watres.2014.02.011

APHA (2005). *Standard Methods for the Examination of Water and Wastewater, 21th Edn*. Washington, DC: American Public Health Association.

Bao, T., Chen, T., Wille, M. L., Chen, D., Yu, S., Bian, J., et al. (2016). Production of zeolite composite filters using waste paper pulp as slow release carbon source and performance investigation in a biological aerated filter. *J. Water Process Eng.* 9, 38–46. doi: 10.1016/j.jwpe.2015.11.009

Cao, X., Li, Y., Jiang, X., Zhou, P., Zhang, J., and Zheng, Z. (2016). Treatment of artificial secondary effluent for effective nitrogen removal using a combination of corncob carbon source and bamboo charcoal filter. *Int. Biodeter. Biodegr.* 115, 164–170. doi: 10.1016/j.ibiod.2016.08.018

Chang, J., Mei, J., Jia, W., Chen, J., Li, X., Ji, B., et al. (2019). Treatment of heavily polluted river water by tidal-operated biofilters with organic/inorganic media: evaluation of performance and bacterial community. *Bioresour. Technol.* 279, 34–42. doi: 10.1016/j.biortech.2019.01.060

Cheng, K. C., and Lin, Y. F. (1993). Relationship between denitrifying bacteria and methanogenic bacteria in a mixed culture system of acclimated sludges. *Water Res.* 27, 1749–1759. doi: 10.1016/0043-1354(93)90113-V

Christensson, M., Lie, E., and Welander, T. (1994). A comparison between ethanol and methanol as carbon sources for denitrification. *Water Sci. Technol.* 30, 83–90. doi: 10.2166/wst.1994.0255

Constantin, H., and Fick, M. (1997). Influence of c-sources on the denitrification rate of a high-nitrate concentrated industrial wastewater. *Water Res.* 31, 583–589. doi: 10.1016/S0043-1354(96)00268-0

Dong, W. Y., Zhang, X. B., Wang, H. J., Sun, F. Y., and Liu, T. Z. (2012). Enhanced denitrification with external carbon sources in a biological anoxic filter. *Water Sci. Technol.* 66, 2243–2250. doi: 10.2166/wst.2012.460

Fan, B., Qu, J. H., Lei, P. J., and Li, D. P. (2001). Studies on nitrate removal by a combined heterotrophy electrode biofilm reactor. *Acta Sci. Circum.* 21, 257–262. doi: 10.1016/j.jhazmat.2011.06.008

Farabegoli, G., Gavasci, R., Lombardi, F., and Romani, F. (2003). Denitrification in tertiary filtration: application of an up-flow filter. *J. Environ. Sci. Health Part A* 38, 2169–2177. doi: 10.1081/ese-120023349

Feng, J., and Tong, Z. (2015). Bacterial assembly and temporal dynamics in activated sludge of a full-scale municipal wastewater treatment plant. *ISME J.* 9:683. doi: 10.1038/ismej.2014.162

Ge, S., Peng, Y., Wang, S., Lu, C., Cao, X., and Zhu, Y. (2012). Nitrite accumulation under constant temperature in anoxic denitrification process: the effects of carbon sources and COD/NO3–N. *Bioresour. Technol.* 114, 137–143. doi: 10.1016/j.biortech.2012.03.016

Gómez, M. A., González-López, J., and Hontoria-Garc ′ıa, E. (2000). Influence of carbon source on nitrate removal of contaminated groundwater in a denitrifying submerged filter. *Hazard Mater. J.* 80, 69–80. doi: 10.1016/S0304-3894(00)00282-X

Haske-Cornelius, O., Gierlinger, S., Vielnascher, R., Gabauer, W., Prall, K., Pellis, A., et al. (2021). Cultivation of heterotrophic algae on paper waste material and digestate. *Algal. Res.* 54:102193. doi: 10.1016/j.algal.2021.102193

Huang, X., Yang, X. M., Zhu, J., and Yu, J. H. (2020). Microbial interspecific interaction and nitrogen metabolism pathway for the treatment of municipal wastewater by iron carbon based constructed wetland. *Bioresour. Technol.* 315:123814. doi: 10.1016/j.biortech.2020.123814

Husband, J. A., Slattery, L., Corsoro, F., and Antwi, J. (2014). Full-scale operating experience of deep bed denitrification filter achieving <1.5 mg/l total nitrogen and <0.05 mg/l total phosphorus. *Proc.Water Environ. Fed.* 12, 3185–3197. doi: 10.2166/wst.2012.874

Karanasios, K. A., Vasiliadou, I. A., Tekerlekopoulou, A. G., Akratos, C. S., Pavlou, S., and Vayenas, D. V. (2016). Effect of C/N ratio and support material on heterotrophic denitrification of potable water in bio-filters using sugar as carbon source. *Int. Biodeter. Biodegr.* 111, 62–73. doi: 10.1016/j.ibiod.2016.04.020

Khokhar, Z., Syed, Q., Nadeem, M., Irfan, M., Wu, J., Samra, Z., et al. (2014). Enhanced production of cellulase by *Trichoderma reesei* using wheat straw as a carbon source. *World Appl. Sci. J.* 30, 1095–1104. doi: 10.5829/idosi.wasj.2014.30.09.14138

Li, W. W., Sheng, G. P., Wang, Y. K., Liu, X. W., Xu, J., and Yu, H. Q. (2011). Filtration behaviors and biocake formation mechanism of mesh filters used in membrane bioreactors. *Sep. Purif. Technol.* 81, 472–479. doi: 10.1016/j.seppur.2011.08.026

Li, Y., Wang, Q., Wu, Y., Li, W., and Liu, Z. (2014). Application of micro-flocculation and sand filtration as advanced wastewater treatment technique. *Desalin. Water Treat.* 52, 1299–1306. doi: 10.1080/19443994.2013.787029

Liang, B., Cheng, H., Van Nostrand, J. D., Ma, J., Yu, H., Kong, D., et al. (2014). Microbial community structure and function of nitrobenzene reduction biocathode in response to carbon source switchover. *Water Res.* 54, 137–148. doi: 10.1016/j.watres.2014.01.052

Liu, C., Wang, X., Yang, H., Liu, C., Zhang, Z., and Chen, G. (2021). Biodegradable polyhydroxyalkanoates production from wheat straw by recombinant *Halomonas elongata* A1. *Int. J. Biol. Macromol.* 187, 675–682. doi: 10.1016/j.ijbiomac.2021.07.137

Löwenberg, J., Zenker, A., Krahnstover, T., Boehler, M., Baggenstos, M., Koch, G., et al. (2016). Upgrade of deep bed filtration with activated carbon dosage for compact micropollutant removal from wastewater in technical scale. *Water Res.* 94, 246–256. doi: 10.1016/j.watres.2016.02.033

Luo, G., Hou, Z., Tian, L., and Tan, H. (2020). Comparison of nitrate-removal efficiency and bacterial properties using PCL and PHBV polymers as a carbon source to treat aquaculture water. *Aquac. Fish.* 5, 92–98. doi: 10.1016/j.aaf.2019.04.002

Ma, Q., Qu, Y., Shen, W., Zhang, Z., Wang, J., Liu, Z., et al. (2015). Bacterial community compositions of coking wastewater treatment plants in steel industry revealed by Illumina high-throughput sequencing. *Bioresour. Technol.* 179, 436–443. doi: 10.1016/j.biortech.2014.12.041

Magoc, T. J., and Salzberg, S. L. (2011). FLASH: fast length adjustment of short reads to improve genome assemblies. *Bioinformatics* 27, 2957–2963. doi: 10.1093/bioinformatics/btr507

Piao, W., and Kim, Y. (2016). Evaluation of monthly environmental loads from municipal wastewater treatment plants operation using life cycle assessment. *Environ. Eng. Res.* 21, 284–290. doi: 10.4491/eer.2015.124

Remmas, N., Melidis, P., Zerva, I., Kristoffersen, J. B., Nikolaki, S., Tsiamis, G., et al. (2017). Dominance of candidate Saccharibacteria in a membrane bioreactor treating medium age landfill leachate: effects of organic load on microbial communities, hydrolytic potential and extracellular polymeric substances. *Bioresour. Technol.* 238, 48–56. doi: 10.1016/j.biortech.2017.04.019

Schloss, P. D., Gevers, D., and Westcott, S. L. (2011). Reducing the effects of PCR amplification and sequencing artifacts on 16S rRNA-based studies. *PLoS One* 12:e27310. doi: 10.1371/journal.pone.0027310

Shen, Z., and Wang, J. (2011). Biological denitrification using cross-linked starch/PCL blends as solid carbon source and biofilm carrier. *Bioresour. Technol.* 102, 8835–8838. doi: 10.1016/j.biortech.2011.06.090

Shi, Y., Wei, N., and Wu, G. (2016). Tertiary denitrification of the secondary effluent in biofilters packed with composite carriers under different carbon to nitrogen ratios. *Environ. Eng. Res.* 21, 311–317. doi: 10.4491/eer.2015.134

Simate, G. S. (2015). The treatment of brewery wastewater for reuse by integration of coagulation/flocculation and sedimentation with carbon nanotubes 'sandwiched' in a granular filter bed. *J. Ind. Eng. Chem.* 21, 1277–1285. doi: 10.1016/j.jiec.2014.06.001

Sun, Y. X., Shen, D., Zhou, X., Shi, N., and Tian, Y. (2016). Microbial diversity and community structure of denitrifying biological filters operated with different carbon sources. *SpringerPlus* 5:1752. doi: 10.1186/s40064-016-3451-3

Sun, Z., Xie, D. G., Jiang, X. R., Fu, G. H., Xiao, D. X., and Zheng, L. (2018). Effect of eco-remediation and microbial community using multilayer solar planted floating island (MS-PFI) in the drainage channel. *bioRxiv* [Preprint] bioRxiv: 327965, doi: 10.1101/327965

Tian, L., and Wang, L. (2021). Multi-omics analysis reveals structure and function of biofilm microbial communities in a pre-denitrification biofilter. *Sci. Total Environ.* 757:143908. doi: 10.1016/j.scitotenv.2020.143908

Wang, H., Chen, N., Feng, C., and Deng, Y. (2021). Insights into heterotrophic denitrification diversity in wastewater treatment systems: progress and future prospects based on different carbon sources. *Sci. Total Environ.* 780:146521. doi: 10.1016/j.scitotenv.2021.146521

Wang, Q., Feng, C., Zhao, Y., and Hao, C. (2009). Denitrification of nitrate contaminated groundwater with a fiber-based biofilm reactor. *Bioresour. Technol.* 100, 2223–2227. doi: 10.1016/j.biortech.2008.07.057

Wang, Z., Fei, X., He, S., Huang, J., and Zhou, W. (2016). Application of light-weight filtration media in an anoxic biofilter for nitrate removal from micro-polluted surface water. *Water Sci. Technol.* 74, 1016–1024. doi: 10.2166/wst.2016.299

Wei, N., Shi, Y., Wu, G., Hu, H., Guo, Y., Wu, Y., et al. (2016). Removal of nitrogen and phosphorus from the secondary effluent in tertiary denitrifying biofilters combined with micro-coagulation. *Water Sci. Technol.* 73, 2754–2760. doi: 10.2166/wst.2016.130

Wu, C., Wang, Y., Zhou, Y., and Zhu, C. (2016). Pretreatment of petrochemical secondary effluent by micro-flocculation and dynasand filtration: performance and DOM removal characteristics. *Water Air Soil Pollut.* 227:415. doi: 10.1007/s11270-016-3118-2

Wu, L., Li, Z., Zhao, C., Liang, D., and Peng, Y. (2018). A novel partial-denitrification strategy for post-anammox to effectively remove nitrogen from landfill leachate. *Sci. Total Environ.* 633, 745–751. doi: 10.1016/j.scitotenv.2018.03.213

Wu, X. H., and Li, Y. M. (2017). Effect of C/N ratio on denitrification of denitrification filters with different filter materials. *Chinese J. Environ. Eng.* 11, 55–62.

Xu, J. H., He, S. B., Wu, S. Q., Huang, J. C., Zhou, W. L., and Chen, X. C. (2016). Effects of HRT and water temperature on nitrogen removal in autotrophic gravel filter. *Chemosphere* 147, 203–209. doi: 10.1016/j.chemosphere.2015.12.136

Yang, L., Guo, L. K., Ren, Y. X., Dou, J. W., Zhu, P. T., Cui, S., et al. (2021). Denitrification performance, biofilm formation and microbial diversity during startup of slow sand filter using powdery polycaprolactone as solid carbon source. *J. Environ. Chem. Eng.* 9:105561. doi: 10.1016/j.jece.2021.105561

Zhang, F., Peng, Y., Wang, Z., Jiang, H., Ren, S., and Qiu, J. (2021). New insights into co-treatment of mature landfill leachate with municipal sewage via integrated partial nitrification, Anammox and denitratation. *J. Hazard Mater.* 415:125506. doi: 10.1016/j.jhazmat.2021.125506

Conflict of Interest: The authors declare that the research was conducted in the absence of any commercial or financial relationships that could be construed as a potential conflict of interest.

Publisher's Note: All claims expressed in this article are solely those of the authors and do not necessarily represent those of their affiliated organizations, or those of the publisher, the editors and the reviewers. Any product that may be evaluated in this article, or claim that may be made by its manufacturer, is not guaranteed or endorsed by the publisher.

frontiers in Microbiology

ORIGINAL RESEARCH
published: 02 February 2022
doi: 10.3389/fmicb.2022.836052

Comparative Analysis of Selective Bacterial Colonization by Polyethylene and Polyethylene Terephthalate Microplastics

Yuhao Song, Baoxin Zhang, Lianwei Zou, Feng Xu, Yaqi Wang, Shaoqi Xin, Yang Wang, Hongyuan Zhang, Ning Ding and Renjun Wang**

College of Life Sciences, Qufu Normal University, Qufu, China

In this study, we report the biodiversity and functional characteristics of microplastic-attached biofilms originating from two freshwater bacterial communities. Even though the microplastic-biofilm (MPB) diversities are mostly determined by original bacteria instead of microplastic types, the results from 16S rRNA amplicon sequencing still showed that the dynamic biofilm successions on different microplastics were highly dissimilar. Furthermore, the analysis of biomarkers indicated distinct bacterial species with significant dissimilarities between different MPBs, which further determined the associated functions. The co-occurrence networks showed distinct interconnective characteristics in different MPBs: The structure of MPB incubated in the lake water sample was more robust under environmental stresses, and bacteria in the tap water MPB interacted more cooperatively. Regarding this cooperative interaction, the analysis of functional prediction, in this study, also showed that more symbionts and parasites colonized on microplastics in the tap water than in the lake water. Moreover, it was suggested that MPBs were more easily formed in the tap water sample. The overall results revealed significant dissimilarities in bacterial diversity, succession, and associated functions between MPBs, in which bacterial species with specific functions should be taken seriously.

Keywords: polyethylene, polyethylene terephthalate, microplastic-attached biofilm, freshwater, biodiversity

OPEN ACCESS

Edited by:
Lean Zhou,
Changsha University of Science and Technology, China

Reviewed by:
Xiaomei Liu,
Nankai University, China
Weiwe Cai,
Beijing Jiaotong University, China

****Correspondence:***
Yuhao Song
sdsyuhao@163.com
Renjun Wang
wangrenjun2002@126.com

Specialty section:
This article was submitted to Microbiotechnology, a section of the journal Frontiers in Microbiology

Received: *15 December 2021*
Accepted: *10 January 2022*
Published: *02 February 2022*

Citation:
Song Y, Zhang B, Zou L, Xu F, Wang Y, Xin S, Wang Y, Zhang H, Ding N and Wang R (2022) Comparative Analysis of Selective Bacterial Colonization by Polyethylene and Polyethylene Terephthalate Microplastics. Front. Microbiol. 13:836052. doi: 10.3389/fmicb.2022.836052

INTRODUCTION

Plastic is a common polymeric material worldwide owing to its excellent performance (e.g., durability, anticorrosion, and plasticity) and relatively low cost, and it has already played indispensable roles in all walks of life. With an increasing demand for diverse types of plastic, its global production increased continuously from 1.7 to almost 360 million tons during the last 70 years (PlasticsEurope, 2019), consequently leading to a large amount of plastic waste that has been disposed into the environment. Among these disposed plastics, plastic components of polyethylene (PE), polyethylene terephthalate (PET), and polypropylene (PP) are commonly produced and used, and they account for 90% of plastic production, along with polystyrene (PS) and polyvinyl chloride (PVC; Andrady and Neal, 2009; Alimi et al., 2018). Generally,

these disposed plastics exhibit poor degradability in natural environments, primarily resulting in the formation of microplastics of different sizes (<5 mm) and shapes (e.g., fibers and fragments) by physical (e.g., mechanical wear), chemical (e.g., photooxidation), and biological processes (Hidalgo-Ruz et al., 2012; De Sa et al., 2018; Rachman, 2018; Shabbir et al., 2020).

Regarding aquatic ecosystems, microplastics are extensively distributed in most types of marine and freshwater environments (Klein et al., 2015; Ivleva et al., 2017; Di and Wang, 2018), and they have even been detected in preserved areas and polar regions in recent years (Claessens et al., 2013; De Sa et al., 2018). A number of studies have indicated that these microplastics exhibit toxicological effects on various aquatic organisms through uptake and accumulation; further, they pose a potential threat to human health by transmission along the food web (Cole et al., 2015; Sussarellu et al., 2016; Connors et al., 2017; Chapron et al., 2018; Ogonowski et al., 2018). In addition, microplastics have been revealed to be indirect harmful factors, which may serve as vectors that selectively enrich aquatic pathogens to new environments compared with natural substrates (e.g., rock and leaf) and could provide footholds for pathogens to invade aquatic organisms (e.g., coral; Lamb et al., 2018; Wu et al., 2019). Through long-term exposure and migration by water flow in aquatic environments, microplastics can be potential carbon sources that gradually release organic compounds into the water phase, thus contributing to the prolonged survival and growth of surrounding bacterial communities and the selective colonization of microplastic-attached biofilms that are distinct from other natural substrates (Tomboulian et al., 2004; Stern and Lagos, 2008; De Tender et al., 2015; Rummel et al., 2017).

When microplastics were disposed into the aquatic environments, the microplastic-attached biofilms were rapidly assembled and could be observed within 2 weeks, and their community structures are generally much different from that of the planktonic bacterial assemblages (McCormick et al., 2014, 2016; De Tender et al., 2017). Therefore, it has been suggested that microplastics are unique niches that colonize bacteria containing specific structural and functional patterns (Zettler et al., 2013; Miao et al., 2019). For example, recent studies have identified polymeric materials as potential vectors that carry aquatic (opportunistic) pathogens and harmful algae to remote environments (Viršek et al., 2017; Arias-Andres et al., 2018). More importantly, horizontal gene transfer may occur between biofilm and planktonic bacteria that mediates the transformation of several important genes such as antibiotic resistant genes (Bengtsson-Palme and Larsson, 2015; Li et al., 2015; Martinez et al., 2015; Arias-Andres et al., 2018). Until now, most studies have focused on two perspectives in terms of the comparison of microplastic-attached vs. planktonic bacteria and bacteria on natural vs. microplastic substrates (De Tender et al., 2015, 2017; Chae and An, 2017; Jiang et al., 2018; Miao et al., 2019; Wu et al., 2019), but the knowledge of biodiversity and functional characteristics of microplastic-attached biofilms exposed to different freshwater sources is still insufficient.

Thus, in this study, two commonly used plastic components, PE and PET materials were chosen as the microplastics tested for bacterial colonization, and two freshwater bacterial communities, one from lake water and one from tap water, were selected as the bacterial source of biofilms. 16S rRNA gene amplicon sequencing was performed to determine the bacterial diversities of biofilms, and bioinformatic tools were adopted to investigate the potential functions of each biofilm on microplastics. This study aims to decipher microplastic-attached biofilms with respect to (i) bacterial diversities of microplastic-biofilms (MPBs) in freshwater habitats and (ii) the associated functional patterns.

MATERIALS AND METHODS

Sample Collection and Preparation of Microplastics

In order to culture the MPBs in this study, two freshwater bacterial communities, one originating from tap water and the other from lake water, were, respectively, collected from the in-house plumbing system (keep the water flowing for 5 min before sampling) of the drinking water distribution network at Qufu Normal University and Nansi Lake, Shandong Province, East China. Nansi Lake is the largest freshwater lake in northern China and its branch rivers flow through many cities as crucial drinking water sources. Here, each sample in triplicate was placed in pretreated carbon-free glass bottles (the method of carbon-free glassware preparation is described in the **Supplementary Material**) and then stored at 4°C during transportation and processed within 24 h. The main water quality parameters of two freshwater samples were determined and are listed in **Supplementary Table 1**. Prior to the related experiments, samples were prefiltered through 10-μm membrane filters to remove large organisms and particles.

Polyethylene and PET were chosen as the microplastics tested in this study. The PET material was purchased from Sigma-Aldrich Co., Ltd. (Shanghai, China) with a columned form (diameter: ~3.5 mm, length: ~4.5 mm), and the PE material was processed from a drinking water pipe (poly-ethylene silane cross-linked, PE-Xb) with a lamellar form (length: ~4.0 mm, width: ~3.5 mm, and thickness: ~1.5 mm). The selection of millimeter-sized PE and PET materials aims to provide sufficient surface area for the bacterial colonization that could reflect the biodiversity and interconnections of MPBs more comprehensively. Prior to the test, the microplastic particles used in the subsequent experiment were washed three times with ultrapure water and then autoclaved (120°C for 30 min) to avoid any contamination.

Experiment of Biofilm Incubation on Microplastics

To investigate the bacterial growth and diversity of biofilms originating from two freshwater types on microplastics, 30 particles of each microplastic (~750 mg) in triplicate were, respectively, added into 1-L carbon-free glass bottles (Schott

Duran, Germany) containing 500 ml freshwater samples. Subsequently, the biofilms on microplastic particles were incubated at 25°C for 30 days. Meanwhile, the original lake and tap water samples without the addition of microplastics (i.e., the planktonic bacteria in the freshwater samples) in triplicate were set, respectively, as the experimental controls. During this experiment, all samples for the biofilm incubation were supplemented with equivalent volume of their sterile sampling water regularly to maintain stable abiotic conditions. Three particles of PE and PET microplastics were taken at regular intervals (every 10 days) for further DNA extraction.

DNA Extraction, 16S rRNA Amplicon Sequencing, and Sequence Processing

The PE and PET microplastics for biofilm-DNA extraction were firstly rinsed three times with sterilized phosphate buffer solution to remove the free-living bacteria. The DNA extraction of biofilms on microplastics was then processed using the PowerBiofilm® DNA isolation Kit (MoBio Laboratories, Carlsbad, CA, United States) in accordance with the manufacturer's protocol. The biofilm-DNA obtained was inspected through 2.0% agarose gel electrophoresis and quantified with a Qubit® 2.0 Fluorometer (Invitrogen, Life technologies, Thermo Fisher Scientific Inc., United States) using a Qubit® dsDNA BR Assay kit (Invitrogen, Life technologies, Thermo Fisher Scientific Inc., United States). Prior to 16S rRNA amplicon sequencing, biofilm samples and biofilm sample groups were classified and named according to the freshwater source, types of microplastic, and incubation time (e.g., "L-PE-10" represents a biofilm sample originating from lake water on PE particles after incubation for 10 days; "L-PE" represents the biofilm sample group that includes samples "L-PE-10," "L-PE-20," and "L-PE-30"; and "L-PE/PET-0" and "T-PE/PET-0" represent the planktonic lake and tap water bacteria).

Gene amplification and sequencing were conducted using an Illumina platform with HiSeq2500 paired-end 250 bp mode as described previously (Liu et al., 2014). Primer pairs of 341 F (5′-CCTACGGGNGGCWGCAG-3′) and 806 R (5′-GGACTACHVGGGTATCTAAT-3′) were chosen to amplify the V3–V4 hypervariable region of bacterial and archaeal 16S rRNA genes. The raw sequence data were carried out using the QIIME pipeline (version 1.9.0; Caporaso et al., 2010). The quality of raw reads was controlled by excluding high-nitrogen (>20% of total reads) and low-quality (quality score ≥ 20) reads. Then, the two pair-end sequencing data were merged *via* FLASH v1.2.11 and quality filtered (Bokulich et al., 2013). The ultimate sequences were obtained by removing chimeras through comparison with the Gold database r20110519 using the UCHIME algorithm (Edgar et al., 2011). For clustering analysis, these sequences were clustered into operational taxonomic units (OTUs) by 97% similarity in USEARCH v7.0.1090 (Edgar, 2013), and taxonomy assignments were conducted using the SILVA database as the reference (Quast et al., 2013). OTUs with no annotation or archaea-related annotation were excluded. The Ribosomal Database Program classifier was used for species annotation to all OTUs at a confidence limit of 0.8–1.

Statistical Analysis and Functional Gene Prediction

Non-metric multidimensional scaling (NMDS) was performed for visualization of biofilm bacterial community similarities based on the Bray–Curtis dissimilarity using the Vegan package in R (Philip, 2003).

The linear discriminant analysis (LDA) effect size (LEfSe) analysis was performed for visualization of specifically major biofilm bacterial clusters between different sample groups using LEfSe v1.0 software (Nicola et al., 2011). Kruskal–Wallis and Wilcoxon sum tests between sample groups were used for the selection of specifically major biofilm bacterial clusters in each sample group, and the relative importance of each bacterial cluster was then evaluated through LDA. In this study, bacterial clusters with an LDA score ≥ 4 were selected, because they have strong relative importance in each biofilm sample group.

Two aspects of the potential functions of each biofilm sample group were predicted using corresponding bioinformatic tools. The metabolic functions based on the Kyoto Encyclopedia of Genes and Genomes (KEGG) pathway were analyzed using Tax4Fun (Aßhauer et al., 2015), and ecological functions were assessed using the functional annotation of prokaryotic taxa (FAPROTAX; Louca et al., 2016).

Correlation analysis between variables was performed through linear pairwise Pearson correlation in the SPSS software, and the dissimilarities of alpha diversity indexes and relative abundance of functional genes between sample groups were evaluated using a paired-sample *t*-test in the SPSS software.

RESULTS AND DISCUSSION

Phylogenetic Diversity of Bacterial Communities in MPBs

16S rRNA amplicon sequencing was performed for the comparative analysis of MPB diversities originating from lake and tap water samples. All of the MPB DNA samples reached sufficient sequencing depths (Good's coverage values > 0.99) to ensure the accurate results (**Supplementary Table 2**).

Biofilm samples at $t = 10$, 20, and 30 days were drawn for the evaluation of changes in bacterial community during incubation. Along with increasing incubation time, the overlapped bacterial OTUs between lake and tap water MPBs were relatively constant (no more than 30%), whereas the intrinsic bacterial OTUs showed distinct patterns (**Figures 1A**,**B**; **Supplementary Table 3**). Regarding the PE material, the intrinsic OTU number of lake water PE-biofilms gradually decreased, which was the converse of that of tap water PE-biofilms. However, the changes in intrinsic OTUs of L-PET and T-PET were irregular (**Figures 1A**,**B**; **Supplementary Table 3**). Moreover, the overall OTU number of lake water MPBs was much higher than that of tap water MPBs, regardless of PE and PET materials (**Figures 1C**,**D**). These results suggested that different microplastics serve as new vectors for different species sorting during biofilm growth and succession, thus resulting in diverse bacterial survival strategies of MPBs and varying degrees of

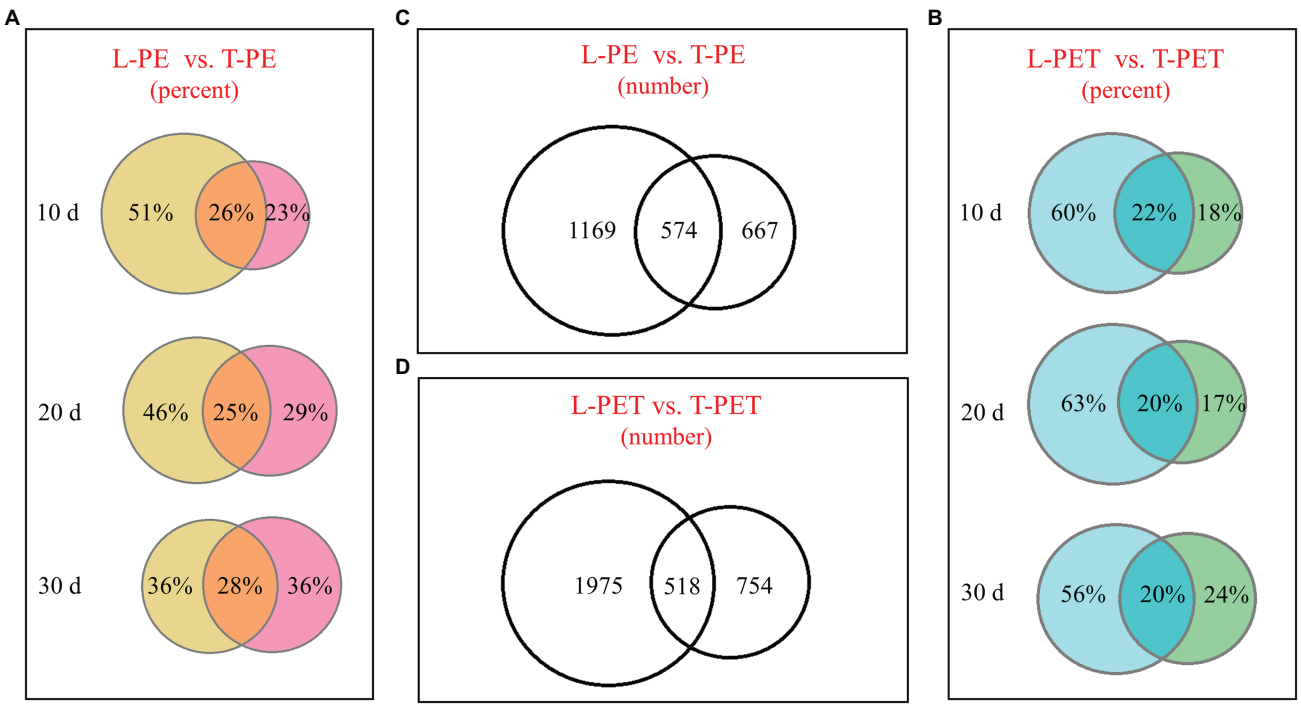

FIGURE 1 | Venn diagrams showing the operational taxonomic units (OTUs) number or percentage of microplastic-biofilms (MPBs). **(A,B)** The OTUs percentage of polyethylene (PE) and polyethylene terephthalate (PET) biofilms incubated with lake and tap water at $t = 10$, 20, and 30 days; **(C,D)** the OTU number of MPB sample groups.

reduced ability to withstand external stresses and maintain their fundamental activities compared to the original bacterial communities (Girvan et al., 2005; Philippot et al., 2013; Miao et al., 2019).

In this study, the alpha diversity indices (Chao, Ace, Shannon, and Simpson) were applied for the evaluation of biofilm bacterial richness and evenness on PE and PET materials (**Figures 2A-H**; **Supplementary Table 4**). As mentioned above, it can also be demonstrated that there were fewer diverse bacterial species of MPBs from tap water than lake water through the comparison of Chao and Ace indices, in which the values of T-PE and T-PET were lower than those of L-PE and L-PET (**Figures 2A,B,E**; **Supplementary Table 4**), suggesting that MPBs have stronger resistance and resilience to perturbation in lake water than in tap water (Girvan et al., 2005; Philippot et al., 2013). More importantly, the Chao and Ace indices exhibited significant dissimilarities ($p < 0.01$ and $p < 0.05$) between L-PET and T-PET (**Figures 2E,F**), indicating that the changes in bacterial richness for lake and tap water biofilms were significantly different on PET material over the course of 30 days. Considering the Shannon and Simpson indices, the bacterial evenness of lake water MPBs was higher than that of tap water MPBs, and yet there were no statistical dissimilarities.

In addition, the NMDS analysis was performed to compare the bacterial community structure in MPBs. Firstly, as shown in **Figure 3**, the bacterial community structure of MPBs was much different from that of the planktonic bacterial communities (i.e., the experimental controls; **Supplementary Figure 1**), especially for the lake water samples. This suggested that more bacterial species in tap water were selectively attached to microplastics, and consequently the bacterial community structures of MPBs were more closely related to the original bacterial communities than lake water. Secondly, there were no dramatic differences in biofilm bacterial community structure between PE and PET materials in the same water sample (**Figure 3**), indicating that in this study, the original bacterial communities in freshwater habitats, instead of microplastic types, undoubtedly determined the associated MPBs; this result is consistent with those of previous studies (Miao et al., 2019; Wu et al., 2019; Wang et al., 2020). However, the alpha diversity indices, including Ace, Chao, and Shannon values, were significantly dissimilar between L-PE and L-PET, which suggested distinct bacterial successions of MPBs in PE and PET materials in lake water during the 30 days of incubation (**Supplementary Figure 2**).

Interestingly, the phylum-level analysis of MPBs revealed that the relative abundance of predominant biofilm bacteria was dependent on microplastic types, of which the phyla Proteobacteria and Planctomycetes were the most abundant bacteria on PE and PET materials, respectively (**Supplementary Figure 3**; **Supplementary Table 5**). These two phyla of biofilm bacteria commonly attach to diverse types of polymeric materials (Miao et al., 2019; Wu et al., 2019; Li et al., 2020; Wang et al., 2020). Proteobacteria are critical for the community stability of MPBs and gene transfer among the biofilm bacterial species (Wu et al., 2019; Wang et al., 2020), and Planctomycetes was reported to be closely related

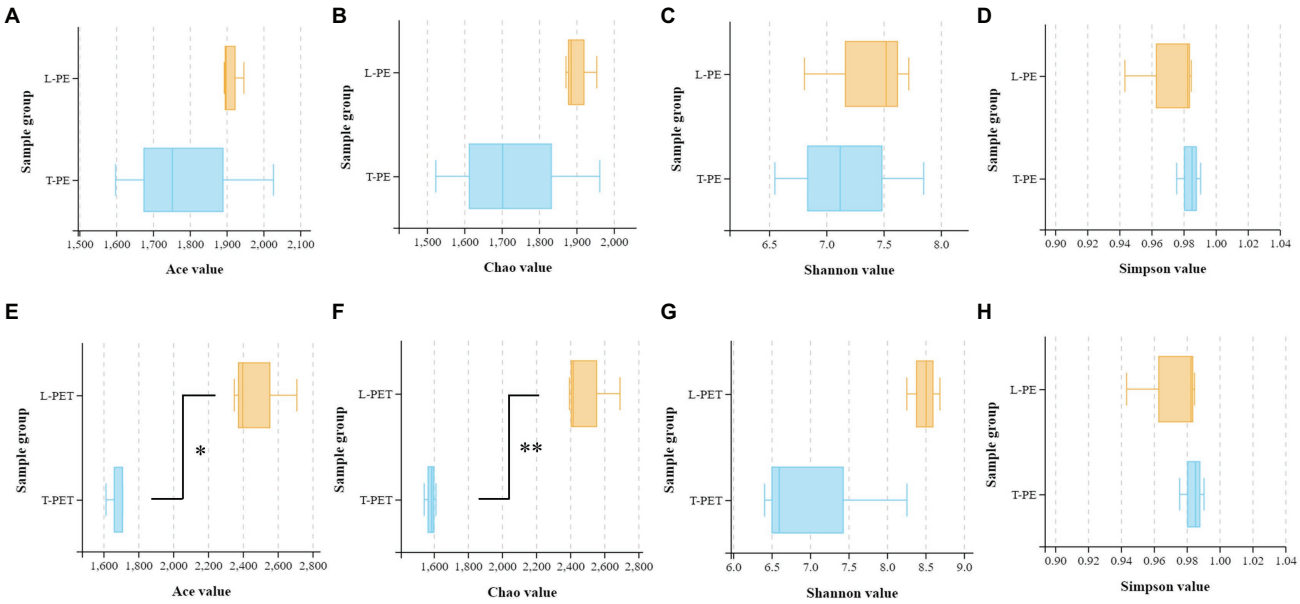

FIGURE 2 | Box plots showing the Ace **(A,E)**, Chao **(B,F)**, Shannon **(C,G)**, and Simpson **(D,H)** indexes related to alpha diversity of different biofilm sample groups (**A-D**: L-PE vs. T-PE; E-H: L-PET vs. T-PET). The asterisks (* and **) represent significant ($p < 0.05$ and $p < 0.01$) dissimilarities between two MPB sample groups.

to ammonium oxidation (Mohamed et al., 2010). However, this "microplastic-dependent" pattern was not applicable to the predominant biofilm bacteria at the class and genus levels. Of the subclasses of Proteobacteria, *Gammaproteobacteria*, which are repeatedly reported to be the predominant bacterial class in MPBs in both freshwater and seawater environments (Wu et al., 2019; Wang et al., 2020), accounted for the highest proportion of MPB bacteria in this study, followed by *Alphaproteobacteria* (except for L-PE; **Supplementary Figure 3**; **Supplementary Table 5**). In addition, *Aquabacterium* (Proteobacteria), *Fimbriiglobus* (Planctomycetes), and *Gemmata* (Planctomycetes) were major bacterial genera of tap water MPBs, whereas *Pirellula* (Planctomycetes) and *Chthoniobacter* (Verrucomicrobia) were generally predominant bacterial general of lake water MPBs (**Supplementary Figure 3**; **Supplementary Table 5**).

The comparison of biomarkers in MPBs with significant dissimilarities between lake and tap water samples was conducted using LEfSe analysis. For the biofilms on PE material, as shown by **Figure 4A**, tap water MPBs contain more biomarkers (i.e., *Alphaproteobacteria*, *Gemmatales*, and *Chitinophagales*) than lake water MPBs (i.e., Virrucomicrobia, OM190, *Pirellulales*, and *Rubinisphaeraceae*). Furthermore, the genera *SWB02*, *Apolymeric materialshiplicatus*, *Gemmata*, and *Fimbriiglobus* in tap water MPBs and the family *Chthoniobacteraceae* in lake water MPBs were the most important biomarkers, which contributed to the continuous significant dissimilarities for at least three taxonomic levels (i.e., from phylum to genus levels) between L-PE and T-PE (**Figure 4A**). Moreover, the relative abundance of the bacterial genus *Mycobacterium* showed a significant correlation ($p < 0.05$, Pearson's $r = 0.999$) between L-PE and T-PE along with the incubation time (**Supplementary Table 6**). Conversely, concerning the biofilms on PET material, more biomarkers belonged to the MPBs in lake water than in tap water; the families *Solibacteraceae subgroup_3*, *Pedosphaeraceae*, *Chthoniobacteraceae*, and *Phycisphaeraceae* in lake water MPBs, and the family *Ruminococcaceae*, the genera *Gemmata* and *Fimbriiglobus* in tap water MPBs were the most important (**Figure 4B**). These biomarkers further influenced the functional diversities of MPB communities, of which the genera *Gemmata* and *Pirellula* were reported to be crucial bacteria in nitrogen removal (Xia et al., 2019) and the families *Chthoniobacteraceae* and *Pirellulaceae* are commonly dominant bacteria that play key roles in the interconnection within bacterial communities in lake water (Zhu et al., 2019).

Co-occurrence Networks Between Bacterial OTUs in Lake and Tap Water MPBs

The results presented above identified distinct bacterial diversities (i.e., dynamic succession, structure, and abundance) between MPBs originating from lake and tap water samples, suggesting an underlying discrepancy in the interactions within their complex bacterial communities. Thus, an examination of the co-occurrence networks was carried out to evaluate the bacterial community complexity of different MPBs. Based on the Pearson correlation coefficient, paired bacterial OTUs that were significantly correlated ($p < 0.05$; Pearson's $|r| > 0.9$) were chosen for further topology analysis using Gephi v 0.9.2 software. In the co-occurrence network, nodes and edges represent taxonomic OTUs at the phylum level and significant correlations between paired OTUs, respectively. Furthermore, colors were used for

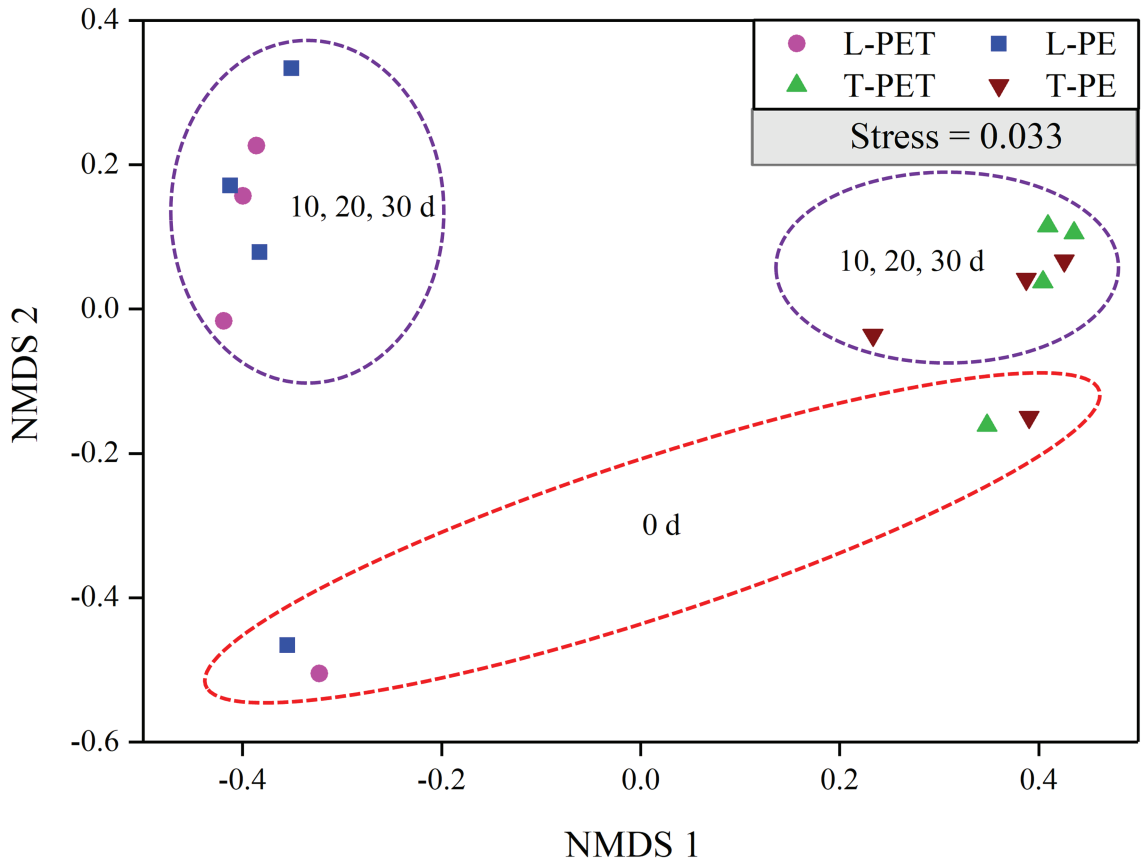

FIGURE 3 | Non-metric multidimensional scaling (NMDS) of biofilm bacterial communities originating from lake and tap water on microplastics (represented by OTUs) calculated with Bray–Curtis dissimilarity between samples. In this plot, points that are closer together represent more similar bacterial communities to each other than those further away. A low stress value indicates a robust diagram.

the classification of different bacterial phyla (for nodes) and positive/negative correlations (for edges), and sizes of nodes are proportional to the degree that characterizes the number of edges. In **Figure 5**, it can be clearly observed that the number of nodes and edges was dramatically higher for biofilms in the tap water sample (99 and 127 nodes; 685 and 1,575 edges) than for those in the lake water sample (84 and 76 nodes; 287 and 253 edges) irrespective of PE or PET materials, indicating that the bacterial intercorrelations of MPBs in tap water were more complicated. Furthermore, the values of average degree (i.e., the number of edges per node) were higher for T-PE/T-PET (13.838/24.803) than for L-PE/L-PET (6.714/6.658), which may also characterize the complex interconnectivity of the whole tap water MPB networks (**Supplementary Table 7**). Interestingly, the number of nodes and edges was more likely to be positively correlated with bacterial richness and diversity, which has been proposed in previous studies (Wu et al., 2019; Wang et al., 2020). However, this study's results showed a lower bacterial OTU number and richness (i.e., Ace and Chao values) for tap water MPBs than for those in lake water.

The modularity parameter was used to determine whether a network had a modular structure, in which case the values should generally exceed 0.4 (Newman, 2006; Barberan et al., 2012). In this study, the modularity parameters of all MPBs (0.656 for L-PE; 0.568 for T-PE; 0.72 for L-PET; and 0.407 for T-PET) indicated that the networks within each biofilm bacterial community had modular structures (**Supplementary Table 7**). The modularity values of tap water MPBs were lower than those of lake water MPBs, which are generally characterized by low independence among different modular groups. Moreover, the characteristic of the modularity parameter, combined with the average path length and the clustering coefficient, have commonly been used to estimate the degree of interconnection among different members within a network (Zhou et al., 2010; Deng et al., 2012; Wang et al., 2020). Within a biofilm bacterial community, the short average path length and high clustering coefficient meant that the effects of external disturbances could immediately reach to the whole community network, which would be further amplified if different modular groups were highly interdependent (i.e., low modularity; Faust and Raes, 2012; Wu et al., 2019; Wang et al., 2020). Of the MPBs examined in this study, L-PE and L-PET had low clustering coefficients and longer average path lengths compared to those of T-PE and T-PET (**Supplementary Table 7**), suggesting that the structure and function of lake water MPBs were more stable than tap water MPBs under environmental perturbations. Furthermore, bacterial nodes with a high degree

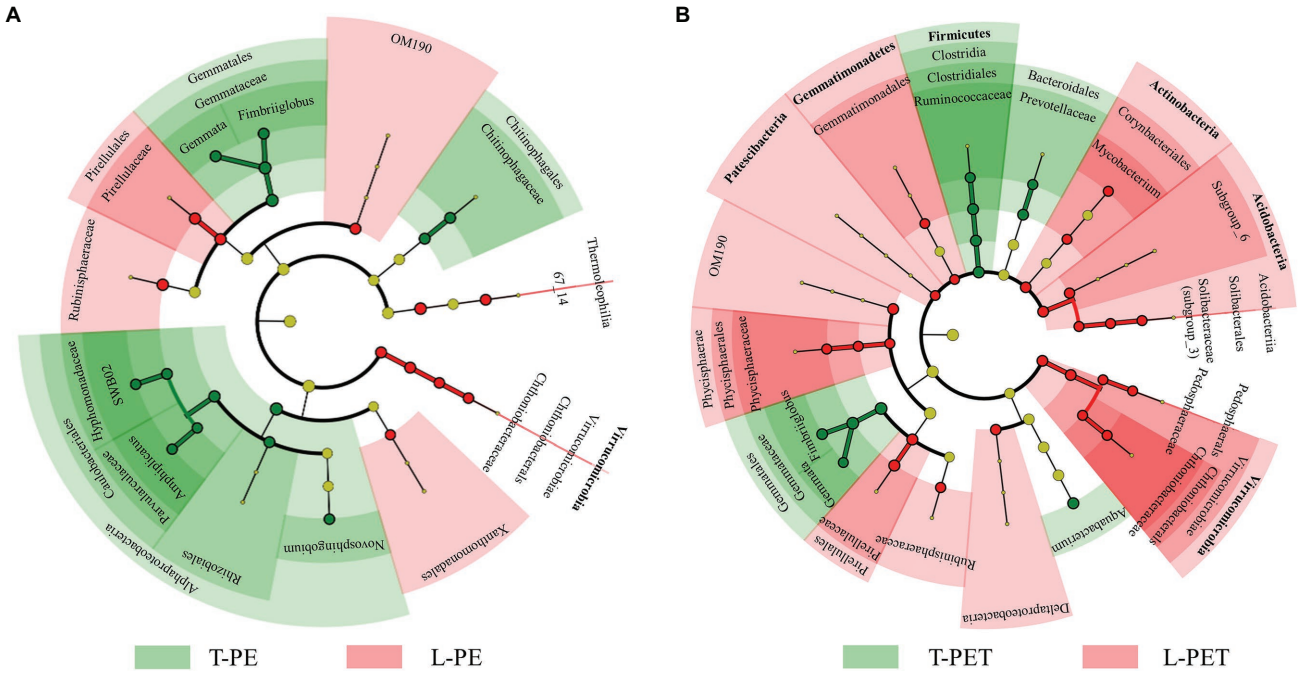

FIGURE 4 | The cladogram of biofilm bacterial clusters with significant dissimilarities ($p < 0.05$) between lake and tap water samples on PE **(A)** and PET **(B)** materials using linear discriminant analysis (LDA) effect size (LEfSe) analysis. The green and red regions (including circles) represent the respective biofilm bacterial clusters originating from tap and lake water, and the yellow circles represent bacterial clusters without significant dissimilarities. Each chart inside out represents biofilm bacterial taxonomies from phylum to genus levels. Bacterial clusters with ≥4 of LDA values are labeled.

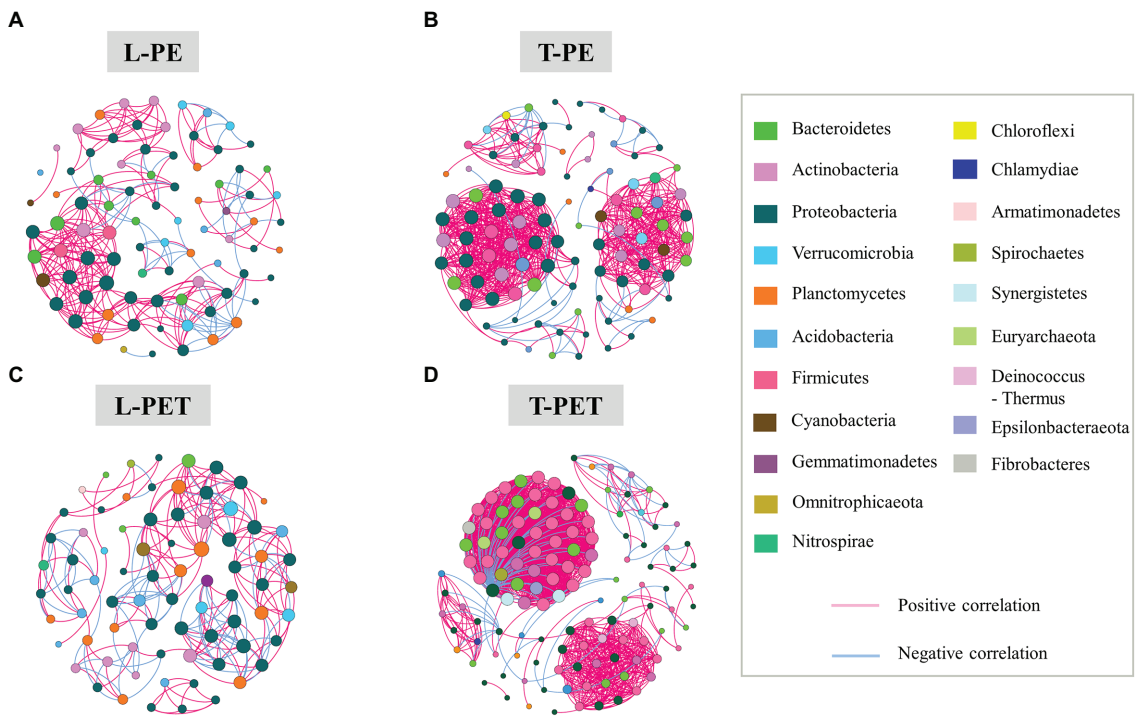

FIGURE 5 | Co-occurrence networks of MPB bacterial communities in L-PE **(A)**, T-PE **(B)**, L-PET **(C)**, and T-PET **(D)** sample groups based on correlation analysis. Each node represents one OTU, of which the size is proportional to the number of connections (i.e., degree) and the color represents bacterial taxonomy at the phylum level. An edge represents significantly strong ($p < 0.05$; Pearson's correlation coefficient $r > 0.9$) correlation (purple for positive correlation and blue for negative correlation) between bacterial OTUs.

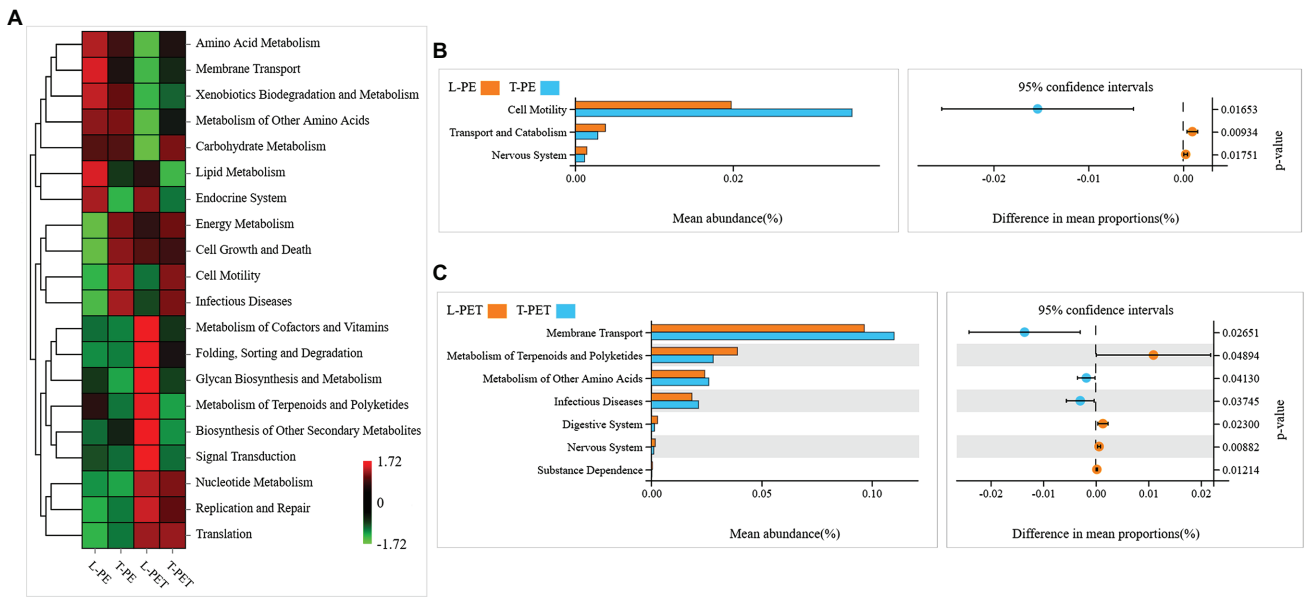

FIGURE 6 | Potential metabolic functions of biofilm bacterial communities on PE and PET materials according to Kyoto Encyclopedia of Genes and Genomes (KEGG) metabolic pathway (level 2). The correlations between each sample group and top 20 metabolic functions in KEGG pathway are shown in heatmap **(A)**. The column and dot plots **(B,C)** show the mean abundance and difference in mean proportions of metabolic functions, which are significantly dissimilar ($p < 0.05$) between two biofilm sample groups using Welch's *t*-test.

(i.e., connectivity) were generally considered to be critical species sustaining the stability of the entire bacterial community (Berry and Widder, 2014; Shi et al., 2016). Previous studies have frequently identified the phylum Proteobacteria as keystone bacteria in natural MPBs (Wu et al., 2019; Wang et al., 2020), which is consistent with this study's results for all of the MPBs except T-PET (keystone bacteria: Firmicutes). Moreover, in contrast to lake water MPBs, most of the correlations between paired bacterial OTUs in tap water MPBs were positive, revealing cooperative interrelations among bacterial species in tap water MPBs (**Figure 5**; **Supplementary Table 8**).

Potential Functions of Lake and Tap Water MPBs

The differences in potential functions of MPBs originating from lake and tap water sample were predicted using bioinformatic tools. In this study, the top 20 metabolic functions based on level 2 of the KEGG metabolic pathway were selected. It was clearly evident that the metabolic functions of T-PE and T-PET were similar, whereas those of L-PE and L-PET were mostly opposite (**Figure 6A**). Furthermore, the metabolic function of membrane transport was significantly ($p < 0.05$) higher in T-PET than in L-PET (**Figure 6C**), indicating that the fundamental metabolic activities of PET-biofilm in the tap water sample could be better maintained than those of PET-biofilm in the lake water sample. Moreover, the significantly higher degree of cell motility and membrane transport (**Figures 6B**,**C**), which are essential functions for biofilm formation and maturation (Bryant et al., 2016; Jiang et al., 2018), indicated that the MPBs examined in this study were more easily formed in tap water than in lake water.

In addition, distinct ecological functions were observed in MPBs from lake and tap water samples, which were attributed to dominant and exclusive bacterial groups. Similarly, the highest relative abundance for PE- and PET-biofilms in ecological functions was chemoheterotrophy, followed by symbiotic and parasitic functions (**Figure 7**). The enrichment of symbionts and parasites on polymeric materials is not surprising and is attributable to the fact that tight cooperations among bacterial species are ever-present within these microecosystems (Wu et al., 2019; Li et al., 2020; Wang et al., 2020). Moreover, different ecological functions at low abundance in PE and PET biofilms (e.g., cyanobacteria, aromatic compound degradation, human pathogens, and sulfur and nitrogen cycle) were mainly attributed to one or several exclusive bacterial taxa as mentioned above, thereby exhibiting distinct ecological functions in different biofilms. Nevertheless, according to the statistical analysis, none of these ecological functions exhibited significant dissimilarities between MPBs from lake and tap water samples, suggesting similar ecological functions of MPBs exposed to different freshwater habitats.

CONCLUSION

Microplastics could serve as vectors that selectively enrich distinct bacterial assemblages and associated functions from different freshwater environments. Herein, the dynamic changes of bacterial communities in MPBs reveal that the successions of biofilm communities on different microplastic particles are dissimilar over a long period of incubation in the same freshwater environment, especially in lake water. Furthermore,

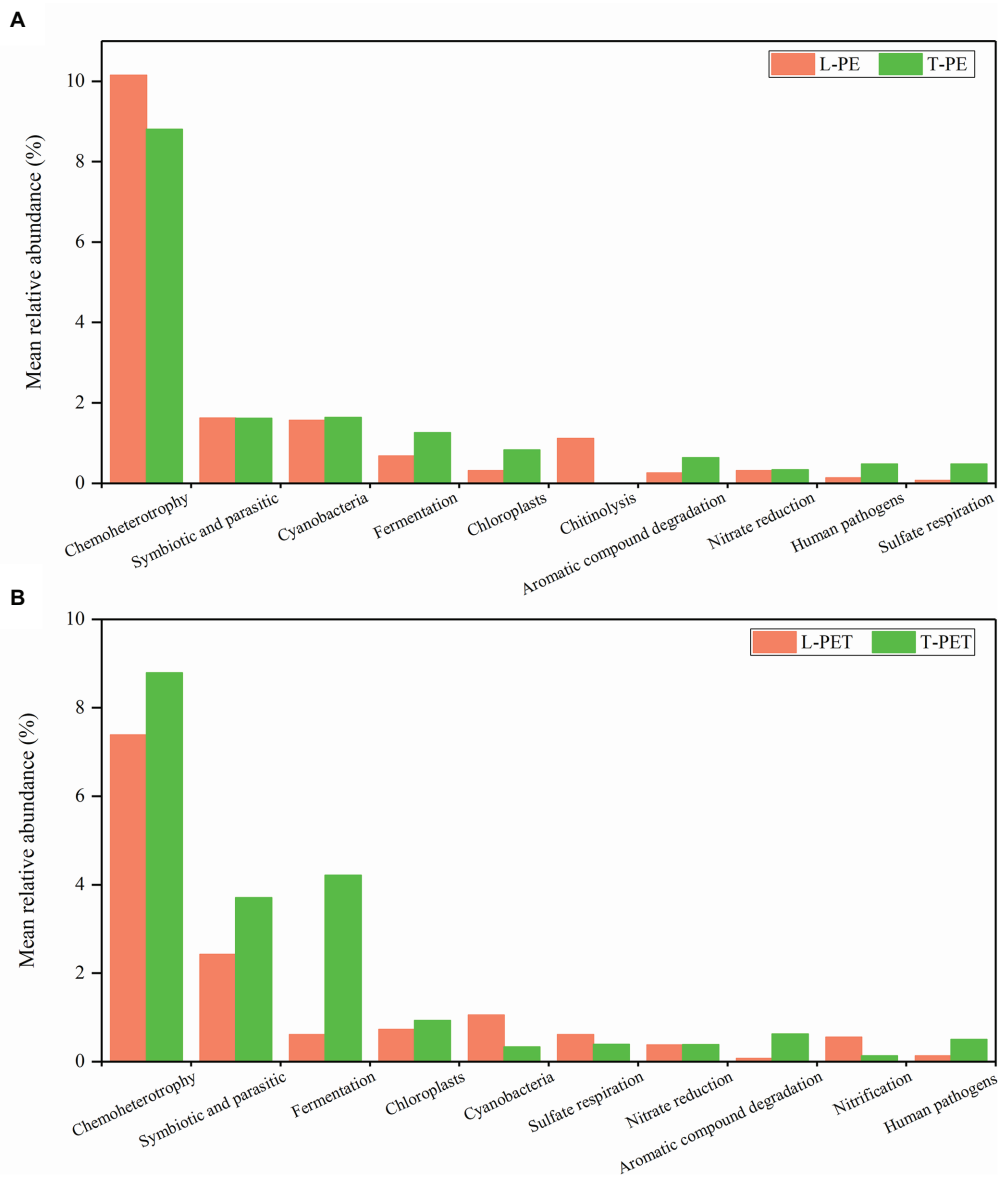

FIGURE 7 | Mean relative abundance of dominant ecological functions in each biofilm sample group. The top 10 ecological functions of biofilm samples on PE **(A)** and PET **(B)** materials are selected, respectively.

the MPB communities exhibit distinct interconnective characteristics; that is, the structures of lake water MPBs are more stable under external stresses, and the bacterial species interact more cooperatively in tap water MPBs. Thus, microplastics are likely to be gathering habitats for several symbionts and parasites. More importantly, indispensable functions in biofilm formation and maturation are more significantly encoded in tap water MPBs.

DATA AVAILABILITY STATEMENT

The original contributions presented in the study are publicly available. This data can be found here: The datasets generated during or analyzed during the current study are available from the corresponding author on reasonable request. The 16S amplicon sequences were available at National Center for Biotechnology Information (NCBI) Sequence Read Archive with the accession numbers from SRR11911199 to 11911214.

AUTHOR CONTRIBUTIONS

YS contributed to the study conception and design. Material preparation, data collection and analysis were performed by all authors. The first draft of the manuscript was written by YS and BZ, and all authors commented on previous

versions of the manuscript. All authors read and approved the final manuscript.

FUNDING

This work was supported by the National Natural Science Foundation of China (no. 32001193 to YS and no. 31971503 to RW) and Shandong Provincial Agricultural Fine Species Project (2019LZGC020 to RW).

SUPPLEMENTARY MATERIAL

The Supplementary Material for this article can be found online at: https://www.frontiersin.org/articles/10.3389/fmicb.2022.836052/full#supplementary-material

REFERENCES

Alimi, O. S., Budarz, J. F., Hernandez, L. M., and Tufenkji, N. (2018). Microplastics and nanoplastics in aquatic environments: aggregation, deposition, and enhanced contaminant transport. *Environ. Sci. Technol.* 52, 1704–1724. doi: 10.1021/acs.est.7b05559

Andrady, A. L., and Neal, M. A. (2009). Applications and societal benefits of plastics. *Philos. Trans. R. Soc. Lond. Ser. B Biol. Sci.* 364, 1977–1984. doi: 10.1098/rstb.2008.0304

Arias-Andres, M., Klumper, U., Rojas-Jimenez, K., and Grossart, H. P. (2018). Microplastic pollution increases gene exchange in aquatic ecosystems. *Environ. Pollut.* 237, 253–261. doi: 10.1016/j.envpol.2018.02.058

Aßhauer, K. P., Wemheuer, B., Daniel, R., and Meinicke, P. (2015). Tax4Fun: predicting functional profiles from metagenomic 16S rRNA data. *Bioinformatics* 31, 2882–2884. doi: 10.1093/bioinformatics/btv287

Barberan, A., Bates, S. T., Casamayor, E. O., and Fierer, N. (2012). Using network analysis to explore co-occurrence patterns in soil microbial communities. *ISME J.* 6, 343–351. doi: 10.1038/ismej.2011.119

Bengtsson-Palme, J., and Larsson, D. G. J. (2015). Antibiotic resistance genes in the environment: prioritizing risks. *Nat. Rev. Microbiol.* 13:396. doi: 10.1038/nrmicro3399-c1

Berry, D., and Widder, S. (2014). Deciphering microbial interactions and detecting keystone species with co-occurrence networks. *Front. Microbiol.* 5:219. doi: 10.3389/fmicb.2014.00219

Bokulich, N. A., Subramanian, S., Faith, J. J., Gevers, D., Gordon, J. I., Knight, R., et al. (2013). Quality-filtering vastly improves diversity estimates from Illumina amplicon sequencing. *Nat. Methods* 10, 57–59. doi: 10.1038/nmeth.2276

Bryant, J. A., Clemente, T. M., Viviani, D. A., Fong, A. A., Thomas, K. A., Kemp, P., et al. (2016). Diversity and activity of communities inhabiting plastic debris in the North Pacific gyre. *mSystems* 1, e00024–e00016. doi: 10.1128/mSystems

Caporaso, J. G., Kuczynski, J., Stombaugh, J., Bittinger, K., Bushman, F. D., Costello, E. K., et al. (2010). QIIME allows analysis of high-throughput community sequencing data. *Nat. Methods* 7, 335–336. doi: 10.1038/nmeth.f.303

Chae, Y., and An, Y. J. (2017). Effects of micro- and nanoplastics on aquatic ecosystems: current research trends and perspectives. *Mar. Pollut. Bull.* 124, 624–632. doi: 10.1016/j.marpolbul.2017.01.070

Chapron, L., Peru, E., Engler, A., Ghiglione, J. F., Meistertzheim, A. L., Pruski, A. M., et al. (2018). Macro- and microplastics affect cold-water corals growth, feeding and behaviour. *Sci. Rep.* 8:15299. doi: 10.1038/s41598-018-33683-6

Claessens, M., van Cauwenberghe, L., Vandegehuchte, M. B., and Janssen, C. R. (2013). New techniques for the detection of microplastics in sediments and field collected organisms. *Mar. Pollut. Bull.* 70, 227–233. doi: 10.1016/j.marpolbul.2013.03.009

Cole, M., Lindeque, P., Fileman, E., Halsband, C., and Galloway, T. S. (2015). The impact of polystyrene microplastics on feeding, function and fecundity in the marine copepod Calanus helgolandicus. *Environ. Sci. Technol.* 49, 1130–1137. doi: 10.1021/es504525u

Connors, K. A., Dyer, S. D., and Belanger, S. E. (2017). Advancing the quality of environmental microplastic research. *Environ. Toxicol. Chem.* 36, 1697–1703. doi: 10.1002/etc.3829

De Sa, L. C., Oliveira, M., Ribeiro, F., Rocha, T. L., and Futter, M. N. (2018). Studies of the effects of microplastics on aquatic organisms: what do we know and where should we focus our efforts in the future? *Sci. Total Environ.* 645, 1029–1039. doi: 10.1016/j.scitotenv.2018.07.207

De Tender, C. A., Devriese, L. I., Haegeman, A., Maes, S., Ruttink, T., and Dawyndt, P. (2015). Bacterial community profiling of plastic litter in the Belgian part of the North Sea. *Environ. Sci. Technol.* 49, 9629–9638. doi: 10.1021/acs.est.5b01093

De Tender, C., Devriese, L. I., Haegeman, A., Maes, S., Vangeyte, J., Cattrijsse, A., et al. (2017). Temporal dynamics of bacterial and fungal colonization on plastic debris in the North Sea. *Environ. Sci. Technol.* 51, 7350–7360. doi: 10.1021/acs.est.7b00697

Deng, Y., Jiang, Y. H., Yang, Y., He, Z., Luo, F., and Zhou, J. (2012). Molecular ecological network analyses. *BMC Bioinform.* 13:113. doi: 10.1186/1471-2105-13-113

Di, M. X., and Wang, J. (2018). Microplastics in surface waters and sediments of the three gorges reservoir, China. *Sci. Total Environ.* 616-617, 1620–1627. doi: 10.1016/j.scitotenv.2017.10.150

Edgar, R. C. (2013). UPARSE: highly accurate OTU sequences from microbial amplicon reads. *Nat. Methods* 10, 996–998. doi: 10.1038/nmeth.2604

Edgar, R. C., Haas, B. J., Clemente, J. C., Quince, C., and Knight, R. (2011). UCHIME improves sensitivity and speed of chimera detection. *Bioinformatics* 27:2194. doi: 10.1093/bioinformatics/btr381

Faust, K., and Raes, J. (2012). Microbial interactions: from networks to models. *Nat. Rev. Microbiol.* 10, 538–550. doi: 10.1038/nrmicro2832

Girvan, M. S., Campbell, C. D., Killham, K., Prosser, J. I., and Glover, L. A. (2005). Bacterial diversity promotes community stability and functional resilience after perturbation. *Environ. Microbiol.* 7, 301–313. doi: 10.1111/j.1462-2920.2005.00695.x

Hidalgo-Ruz, V., Gutow, L., Thompson, R. C., and Thiel, M. (2012). Microplastics in the marine environment: a review of the methods used for identification and quantification. *Environ. Sci. Technol.* 46, 3060–3075. doi: 10.1021/es2031505

Ivleva, N. P., Wiesheu, A. C., and Niessner, R. (2017). Microplastic in aquatic ecosystems. *Angew. Chem. Int. Edit.* 56, 1720–1739. doi: 10.1002/anie.201606957

Jiang, P. L., Zhao, S. Y., Zhu, L. X., and Li, D. J. (2018). Microplastic-associated bacterial assemblages in the intertidal zone of the Yangtze estuary. *Sci. Total Environ.* 624, 48–54. doi: 10.1016/j.scitotenv.2017.12.105

Klein, S., Worch, E., and Knepper, T. P. (2015). Occurrence and spatial distribution of microplastics in river shore sediments of the Rhine-Main area in Germany. *Environ. Sci. Technol.* 49, 6070–6076. doi: 10.1021/acs.est.5b00492

Lamb, J. B., Willis, B. L., Fiorenza, E. A., Couch, C. S., Howard, R., Rader, D. N., et al. (2018). Plastic waste associated with disease on coral reefs. *Science* 359, 460–462. doi: 10.1126/science.aar3320

Li, J., Huang, W., Jiang, R., Han, X., Zhang, D., and Zhang, C. (2020). Are bacterial communities associated with microplastics influenced by marine habitats? *Sci. Total Environ.* 733:139400. doi: 10.1016/j.scitotenv.2020.139400

Li, B., Yang, Y., Ma, L., Ju, F., Guo, F., Tiedje, J. M., et al. (2015). Metagenomic and network analysis reveal wide distribution and co-occurrence of environmental antibiotic resistance genes. *ISME J.* 9, 2490–2502. doi: 10.1038/ismej.2015.59

Liu, J., Hua, Z. S., Chen, L. X., Kuang, J. L., Li, S. J., Shu, W. S., et al. (2014). Correlating microbial diversity patterns with geochemistry in an extreme and heterogeneous environment of mine tailings. *Appl. Environ. Microbiol.* 80, 3677–3686. doi: 10.1128/AEM.00294-14

Louca, S., Parfrey, L. W., and Doebeli, M. (2016). Decoupling function and taxonomy in the global ocean microbiome. *Science* 353, 1272–1277. doi: 10.1126/science.aaf4507

Martinez, J. L., Coque, T. M., and Baquero, F. (2015). What is a resistance gene? Ranking risk in resistomes. *Nat. Rev. Microbiol.* 13, 116–123. doi: 10.1038/nrmicro3399

McCormick, A. R., Hoellein, T. J., London, M. G., Hittie, J., Scott, J. W., and Kelly, J. J. (2016). Microplastic in surface waters of urban rivers: concentration, sources, and associated bacterial assemblages. *Ecosphere* 7:e01556. doi: 10.1002/ecs2.1556

McCormick, A., Hoellein, T. J., Mason, S. A., Schluep, J., and Kelly, J. J. (2014). Microplastic is an abundant and distinct microbial habitat in an urban river. *Environ. Sci. Technol.* 48, 11863–11872. doi: 10.1021/es503610r

Miao, L., Wang, P., Hou, J., Yao, Y., Liu, Z., Liu, S., et al. (2019). Distinct community structure and microbial functions of biofilms colonizing microplastics. *Sci. Total Environ.* 650, 2395–2402. doi: 10.1016/j.scitotenv.2018.09.378

Mohamed, N. M., Saito, K., Tal, Y., and Hill, R. T. (2010). Diversity of aerobic and anaerobic ammonia-oxidizing bacteria in marine sponges. *ISME J.* 4, 38–48. doi: 10.1038/ismej.2009.84

Newman, M. E. J. (2006). Modularity and community structure in networks. *Proc. Natl. Acad. Sci. U. S. A.* 103, 8577–8582. doi: 10.1073/pnas.0601602103

Nicola, S., Jacques, I., Levi, W., Dirk, G., Larisa, M., Wendy, S. G., et al. (2011). Metagenomic biomarker discovery and explanation. *Genome Biol.* 12:R60. doi: 10.1186/gb-2011-12-6-r60

Ogonowski, M., Motiei, A., Ininbergs, K., Hell, E., Gerdes, Z., Udekwu, K. I., et al. (2018). Evidence for selective bacterial community structuring on microplastics. *Environ. Microbiol.* 8, 2796–2808. doi: 10.1111/1462-2920.14120

Philip, D. (2003). VEGAN, a package of R functions for community ecology. *J. Veg. Sci.* 14:930, 927. doi: 10.1111/j.1654-1103.2003.tb02228.x

Philippot, L., Spor, A., Henault, C., Bru, D., Bizouard, F., Jones, C. M., et al. (2013). Loss in microbial diversity affects nitrogen cycling in soil. *ISME J.* 7, 1609–1619. doi: 10.1038/ismej.2013.34

PlasticsEurope (2019). Plastics—the facts-2019. Available at: https://www.plasticseurope.org/en/resources/publications/1804-plastics-facts-2019 (Accessed April 6, 2020).

Quast, C., Pruesse, E., Yilmaz, P., Gerken, J., Schweer, T., Yarza, P., et al. (2013). The SILVA ribosomal RNA gene database project: improved data processing and web-based tools. *Nucleic Acids Res.* 41, 590–596. doi: 10.1093/nar/gks1219

Rachman, C. M. (2018). Microplastics research—from sink to source. *Science* 360, 28–29. doi: 10.1126/science.aar7734

Rummel, C. D., Jahnke, A., Gorokhova, E., Kühnel, D., and Schmitt-Jansen, M. (2017). Impacts of biofilm formation on the fate and potential effects of microplastic in the aquatic environment. *Environ. Sci. Technol. Lett.* 4, 258–267. doi: 10.1021/acs.estlett.7b00164

Shabbir, S., Faheem, M., Ali, N., Kerr, P. G., Wang, L. F., Kuppusamy, S., et al. (2020). Periphytic biofilm: an innovative approach for biodegradation of microplastics. *Sci. Total Environ.* 717:137064. doi: 10.1016/j.scitotenv.2020.137064

Shi, S., Nuccio, E. E., Shi, Z. J., He, Z., Zhou, J., and Firestone, M. K. (2016). The interconnected rhizosphere: high network complexity dominates rhizosphere assemblages. *Ecol. Lett.* 19, 926–936. doi: 10.1111/ele.12630

Stern, B. R., and Lagos, G. (2008). Are there health risks from the migration of chemical substances from plastic pipes into drinking water? A review. *Hum. Ecol. Risk Assess.* 14, 753–779. doi: 10.1080/10807030802235219

Sussarellu, R., Suquet, M., Thomas, Y., Lambert, C., Fabioux, C., Pernet, M. E. J., et al. (2016). Oyster reproduction is affected by exposure to polystyrene microplastics. *Proc. Natl. Acad. Sci. U. S. A.* 113, 2430–2435. doi: 10.1073/pnas.1519019113

Tomboulian, P., Schweitzer, L., Mullin, K., Wilson, J., and Khiari, D. (2004). Materials used in drinking water distribution systems: contribution to taste and odor. *Water Sci. Technol.* 49, 219–226. doi: 10.2166/wst.2004.0575

Viršek, M. K., Lovšin, M. N., Koren, S., Kržan, A., and Peterlin, M. (2017). Microplastics as a vector for the transport of the bacterial fish pathogen species *Aeromonas salmonicida*. *Mar. Pollut. Bull.* 125, 301–309. doi: 10.1016/j.marpolbul.2017.08.024

Wang, J., Qin, X., Guo, J., Jia, W., Wang, Q., Zhang, M., et al. (2020). Evidence of selective enrichment of bacterial assemblages and antibiotic resistant genes by microplastics in urban rivers. *Water Res.* 183:116113. doi: 10.1016/j.watres.2020.116113

Wu, X., Pan, J., Li, M., Li, Y., Bartlam, M., and Wang, Y. (2019). Selective enrichment of bacterial pathogens by microplastic biofilm. *Water Res.* 165:114979. doi: 10.1016/j.watres.2019.114979

Xia, Z., Wang, Q., She, Z., Gao, M., and Jin, C. (2019). Nitrogen removal pathway and dynamics of microbial community with the increase of salinity in simultaneous nitrification and denitrification process. *Sci. Total Environ.* 697:134047. doi: 10.1016/j.scitotenv.2019.134047

Zettler, E. R., Mincer, T. J., and Amaral-Zettler, L. A. (2013). Life in the "plastisphere": microbial communities on plastic marine debris. *Environ. Sci. Technol.* 47, 7137–7146. doi: 10.1021/es401288x

Zhou, J., Deng, Y., Luo, F., He, Z., Tu, Q., and Zhi, X. (2010). Functional molecular ecological networks. *MBio* 1, e00169–e00010. doi: 10.1128/mBio.00169-10

Zhu, C., Zhang, J., Nawaz, M. Z., Mahboob, S., Al-Ghanim, K. A., Khan, I. A., et al. (2019). Seasonal succession and spatial distribution of bacterial community structure in a eutrophic freshwater Lake, Lake Taihu. *Sci. Total Environ.* 669, 29–40. doi: 10.1016/j.scitotenv.2019.03.087

Conflict of Interest: The authors declare that the research was conducted in the absence of any commercial or financial relationships that could be construed as a potential conflict of interest.

Publisher's Note: All claims expressed in this article are solely those of the authors and do not necessarily represent those of their affiliated organizations, or those of the publisher, the editors and the reviewers. Any product that may be evaluated in this article, or claim that may be made by its manufacturer, is not guaranteed or endorsed by the publisher.

frontiers in Microbiology

ORIGINAL RESEARCH
published: 14 February 2022
doi: 10.3389/fmicb.2022.844432

Variation of High and Low Nucleic Acid-Content Bacteria in Tibetan Ice Cores and Their Relationship to Black Carbon

Guannan Mao[1], Mukan Ji[2], Baiqing Xu[1,3,4], Yongqin Liu[1,2,3,4] and Nianzhi Jiao[5]*

[1]Key Laboratory of Tibetan Environment Changes and Land Surface Processes, Institute of Tibetan Plateau Research, Chinese Academy of Sciences, Beijing, China, [2]Center for the Pan-Third Pole Environment, Lanzhou University, Lanzhou, China, [3]CAS Center for Excellence in Tibetan Plateau Earth Sciences, Chinese Academy of Sciences, Beijing, China, [4]College of Resources and Environment, University of Chinese Academy of Sciences, Beijing, China, [5]State Key Laboratory of Marine Environmental Science, Xiamen University, Xiamen, China

Nutrient enrichment caused by black carbon (BC) is a major ecological crisis in glacial ecosystems. The microbiological effects of BC were assessed in this study by using fluorescent fingerprinting assay based on flow cytometry (FCM) of bacterial communities with low (LNA) and high (HNA) nucleic acid-content bacteria. Here, we investigated a high-resolution temporal variation of bacterial abundance and LNA/HNA ratio in Tibetan ice cores. Our results revealed that bacterial abundance was proportional to the atmospheric BC on the glaciers. The shift of LNA functional groups to HNA functional groups in glaciers suggested BC emissions increased the proportion of highly active cells. In addition, distinct number of LNA and HNA functional groups was identified between the monsoon and non-monsoon seasons. Westerly winds with high amounts of BC accounted for high ratio of HNA functional groups during the non-monsoon season. In comparison, high moisture during the monsoon season decreased atmospheric BC loading, which increases the ratio of LNA functional groups. Correlations between BC and functional groups were very strong, showing that two functional groups may serve as early-warning indicators of microbiological effects of BC at low trophic level. Our approach provides a potential early-warning framework to study the influences of atmospheric BC on the glaciological community.

Keywords: black carbon, bacteria functional groups, early-warning indicators, Tibetan Plateau, temporal variation, ice cores

OPEN ACCESS

Edited by:
Lean Zhou,
Changsha University of Science and Technology, China

Reviewed by:
Zongqiang Zhu,
Guilin University of Technology, China
Wenwen Kong,
Hebei University of Technology, China

****Correspondence:***
Yongqin Liu
yqliu@itpcas.ac.cn

Specialty section:
This article was submitted to Microbiotechnology, a section of the journal Frontiers in Microbiology

Received: *28 December 2021*
Accepted: *24 January 2022*
Published: *14 February 2022*

Citation:
Mao G, Ji M, Xu B, Liu Y and Jiao N (2022) Variation of High and Low Nucleic Acid-Content Bacteria in Tibetan Ice Cores and Their Relationship to Black Carbon. Front. Microbiol. 13:844432. doi: 10.3389/fmicb.2022.844432

INTRODUCTION

Probing the bioavailability of black carbon (BC) released into the atmosphere is pivotal to understanding their impacts on the climate and environment. BC could impact the local and regional environment by absorbing solar radiation (Reid et al., 2005) and deteriorating trophic status (Odhiambo and Routh, 2016) when they deposited onto the surface of glaciers. BC is considered highly chemically recalcitrant; however, some studies exhibited that the microbes in oligotrophic environments could use BC as a nutritional and carbon source (Cheng and Foght, 2007;

Stubbins et al., 2012). Bacteria not only are living in extremely cold and oligotrophic environments (Liu et al., 2016b), but also participate in the regional environmental variability, such as nutrient migration and transformation of organic carbon (Falkowski et al., 2008; Madsen, 2011). Despite of the crucial roles of bacteria in geochemical processes, there are still limited data on specific bacteria endpoints responses to long-term environmental and climatic changes. Glacial ice cores could record soluble chemical substance and bacteria in chronologically deposited archives (Legrand and Mayewski, 1997; Xiang et al., 2009), which present historical data on a range of climate changes and anthropogenic activity to occur (Liu et al., 2016b; Santibanez et al., 2016).

The ecosystem of Tibetan Plateau is sensitive to global climate change (Xu et al., 2009a; Liu et al., 2016b). The Tibetan Plateau lies in the immediate vicinity of two developing countries, China and India, and thus is subjected to influence of anthropogenic activities (Xu et al., 2009b; Yao et al., 2012; Li et al., 2016). Tibetan ice cores provide a medium to understand the long-term microbial responses relative to climate changes and anthropogenic activities. The relationship between bacterial abundance and the atmospheric circulation was observed in samples of Tibetan ice cores (Zhang et al., 2007). Specifically, dust carried by the westerly winds leaded to a higher bacterial abundance (Yao et al., 2008; Chen et al., 2016), while wet scavenging of Indian monsoon decreased bacterial abundance (Zhang et al., 2007). In addition to atmospheric circulation, the anthropogenic activities also increased bacterial abundance. Previous studies showed that increasing of bacterial abundance was associated with the deterioration of trophic status, such as increasing industrial production activities, desertification of grasslands, and deposition of BC from southern Asia (Miteva et al., 2009; Hara and Zhang, 2012; Liu et al., 2016b). Thus, bacteria in the ice cores could be a sensitive biomarker of climate and environmental changes.

The flow cytometry (FCM) combined with fluorescent staining technique has been widely used to quantify and visualize bacteria in environmental samples (Liu et al., 2016a; Sharuddin et al., 2018). Bacteria can be broadly divided into LNA and HNA functional groups (i.e., FCM's fingerprints; Besmer et al., 2017), based on the observed correlation between fluorescence intensity and cellular nucleic acid content (Gasol et al., 1999; Lebaron et al., 2002; Bouvier et al., 2007; Proctor et al., 2018). Moreover, the composition and proportion of HNA and LNA functional groups could vary, depending on their adaptation to environmental conditions, that is, the HNA functional groups were sensitive to changes in nutrient and carbon availability in the environment (Kaartokallio et al., 2013; Santos et al., 2019), whereas the LNA functional groups were commonly linked to oligotrophic ecosystems (Mary et al., 2006; Wang et al., 2009). Thereby, the shift between HNA and LNA functional groups may be a potential biological indicator for environmental and climate changes. Unfortunately, there is still a lack of information on the distribution and shift of LNA and HNA functional groups in the Tibetan Plateau.

The objective of this study was to elucidate that the influences of regional anthropogenic BC on LNA and HNA functional groups assessed using FCM technology. Atmospheric BC has been shown an impact on regional carbon budget (Wang et al., 2019), therefore, we hypothesize that increasing deposition of BC could transform ecological status and microbiol structure. To achieve this, two glacier ice cores from Tibetan Plateau were investigated for temporal variation of LNA and HNA functional groups during the past half-century. In particular, we combined microbiological studies with BC analysis of the glacier ice cores to infer the relationship between the LNA-to-HNA ratio and anthropogenic activity.

MATERIALS AND METHODS

Sampling Sites

Two ice cores were drilled at accumulation zones of two glaciers on the south of Tibetan Plateau (**Supplementary Figure 1**). The Zuoqiupu Glacier ice core [ZQP, 96.92°E,29.21°N, 5600 m above sea level (m.a.s.l.)] was retrieved from Mt. Gangrigabusupply. The Noijinkangsang Glacier ice core (NJKS; 90.20°E, 29.04°N, 5950 m.a.s.l.) was taken from Mt. Noijin Kangsang. Data from meteorological stations located Mt. Gangrigabusupply and Mt. Noijin Kangsang showed that average annual air precipitation was 392 mm (from 1960 to 2006) and 797 mm (from 1960 to 2006), and annual air temperature was 2.8°C (from 1960 to 2006) and 12.1°C (from 1960 to 2006). NJKS and ZQP are influenced by distinct prevailing weather patterns. NJKS is strongly influenced by the monsoon in summer and by the westerly jet stream in winter (Tian et al., 2001). ZQP is heavily marine influenced, with oceanic moisture directly transported from the Bay of Bengal along the Brahmaputra River valley (Tian et al., 2001). In addition, the two glaciers should receive BC both from the south *via* the Indian monsoon during summer and from the west *via* westerly winds (Xu et al., 2009a).

Ice Core Drilling and Sampling

On 2006, 97 and 33 m length ice cores (12 cm diameter) were drilled from ZQP and NJKS, respectively, and then transported frozen and processed in a cold room at −20°C. The samples were processed as described in Liu et al. (2016b). Half of ice core was used for microbial analyses, and the remaining half was used for physicochemical analysis. In the sterile environment, the ice cores were cut into 10–20 cm long segments and outer ring was sawed off 1 cm to decontaminate. After decontamination, samples were placed in the sterile containers and melted at 4°C (Christner et al., 2005).

Chemical Analysis and Dating

The concentration of water-insoluble organic, elemental, and total carbon of BC samples was carried out as described in Xu et al. (2009b). Briefly, ice cores were cut lengthways into four columns. Every column was cut at intervals 10–20 cm into segments and used for chemical measurements. After melting, the liquid sample was filtered through a quartz fiber filter, ensuring the uniform particles were distributed on the surface of filter paper, then oven-dried at 40°C for 6 h. The oven-dried

samples were then transferred to a glass vacuum desiccator. Organic carbon and elemental carbon were carried out based on the Interagency Monitoring of Protected Visual Environments (IMPROVE) thermal/optical reflectance protocol. Oxygen isotope ratios, BC, and organic carbon concentrations were used to date the ice cores as described by Xu et al. (2009b).

ZQP Glacier was selected to compare the seasonal variations. Annual precipitation of samples was measured at the nearest meteorological station. The annual water equivalent precipitation from 1960 to 2006 averaged 797 mm at the drill site. Glaciers in this region were reported as "spring accumulation," and the largest precipitation happens in the April as meteorological station recorded. Consider the glacier accumulation and monsoon occurrence time, a three-season approach was used based on the annual accumulation regime, with the pre-monsoon season from January to May, monsoon season from June through September, and the post-monsoon season from October through December.

Flow Cytometry and Measuring LNA (HNA) Functional Groups

Staining and FCM were carried out to quantify total cell concentration and abundance of LNA (HNA) functional groups based on the methods described previously (Hammes et al., 2008; Prest et al., 2013). The basic principle of FCM measurements is that bacteria are stained with fluorescent dyes in order to distinguish them from background (e.g., BC and other particles; Prest et al., 2013). Ice core melt water was fixed with 1% glutaraldehyde incubated for 10 min and analyzed within 8 h. Sample volumes of 1 ml were stained with 10 µl SYBR® Green I [1:100 dilution in .20-µm-filtered dimethyl sulfoxide (DMSO), Invitrogen]. The samples and dye were mixed by a brief vortex and then incubated for 10 min in the dark at 37°C before measurement.

Measurements were performed using an EPICS ALTRA II flow cytometer (Beckman Coulter, United States) equipped with a 100-mW water-cooled argon-ion laser, emitting at a fixed wavelength of 488 nm. Bacterial signals were triggered on green fluorescence. The multi-parameter data were analyzed as follows. First, bacterial cells were selected using fixed gating on the two-parameter dot plots of green fluorescence (FL1-H; 530 nm) versus red fluorescence (FL3-H; >670 nm). Next, two fixed gates were applied to separate LNA from HNA functional groups using the same two-parameter dot plots as described by Prest et al. (2013). Triplicate samples were measured. Total cell concentration and abundance of LNA (HNA) functional groups were averaged over the three replicates. The corresponding optical signals are converted into electronic signals. The output data were processed using the CytoWin 4.1 software.[1]

Statistical Analysis

The correlation between HNA and LNA functional groups was tested by running ordinary least squares regression (Rubbens et al., 2019). To explore the time trends of LNA/HNA ratio, Poisson generalized additive models (GAMs) were used to model (Liu et al., 2016b). The GAMs accounts for the Poisson distribution of cell counts, the detected over-dispersion of the response, and the autocorrelation expected in time series. The GAMs allow exploration of non-linearities between the responses and explanatory variables and allow specification of the distribution of the response variable (bacterial abundance) by a function (Marra and Wood, 2011). Differences in non-monsoon and monsoon samples data were analyzed using parametric tests. Permutational multivariate analysis of variance (PERMANOVA) was used to investigate differences in abiotic and biotic variables between two season samples. Correlations were performed to test the associations LNA/HNA ratio and bacteria abundance with environmental variables and BC factors using vegan package. Procrustes test and Mantel test (Dixon, 2003) were used to explore the relationships between BC factors and proportion of LNA and HNA functional groups in different seasons with R package vegan. Monte Carlo value of p for rotational agreement significance testing was determined from 999 permutations. Variation partition analysis (VPA) was used to delineate the effects of environmental and BC components on variation of LNA/HNA ratio. The above-mentioned statistical analyses were performed using R (v3.4.3).

RESULTS AND DISCUSSION

Dominance of LNA Functional Groups in Ice Cores

Fluorescent fingerprinting based on FCM data is a robust and standardized approach to identify LNA and HNA functional groups (Prest et al., 2013; Proctor et al., 2018; Santos et al., 2019). The reproducible staining methods and the fixed FCM gate were applied for all samples to ensure comparable results. Both the LNA and HNA functional groups were identified in Tibetan ice cores (**Supplementary Figure 2**), consistent with other ecosystems (Bouvier et al., 2007; Bowman et al., 2017; Proctor et al., 2018). The abundance of LNA functional groups and HNA functional groups was significantly correlated in both the NJKS and ZQP glaciers (ordinary least squares regression, adjusted $R^2 = .67$, $p < .001$). This suggests that the bimodal distribution of fluorescence intensity could be ubiquitous in Tibetan glaciers. Furthermore, the mean proportion of LNA functional groups to total cell counts was 62.4% ± 7.2% (**Supplementary Figure 3**), which is a typical value for oligotrophic ecosystems (Wang et al., 2009; Kaartokallio et al., 2013). LNA functional groups could survive and withstand limited nutrient environments due to their high affinity and binding-protein dependent uptake system (Salcher et al., 2011). In addition, LNA functional groups can adopt a dormancy strategy to withstand limited nutrient concentration (La Ferla et al., 2014). LNA functional groups have small microbial cell sizes (Proctor et al., 2018). The abundant microbial population in Greenland glacier ice core was dominated by small cells (Miteva and Brenchley, 2005). Small cell size is advantageous for more efficient nutrient uptake in oligotrophic conditions due to a larger surface-to-volume ratio, protection against predators, and occupation of microenvironments (Miteva and Brenchley, 2005).

[1]http://www.sb-roscoff.fr/phyto/cyto.html

Consistently, Santos et al. (2019) pointed out that LNA functional groups are biomarkers of nutrient-limited environments.

Total Cell Concentration Was Proportional to the BC

TCC as a proxy has often been used to assess bioavailable carbon in the environment (Elhadidy et al., 2016), and it also reflected the level of nutrients (Sharuddin et al., 2018; Qi et al., 2021). In the temporal scale, TCC and BC displayed a similar increasing trend in NJKS and ZQP, respectively. BC and TCC remained relatively stable or slightly increased in 1960–1980; however, a rapid ascending pattern was observed after 1980 until 2006 (**Figures 1A,B**). We also found a positive relationship between the BC and TCC in both the NJKS and ZQP glaciers (ordinary least squares regression, adjusted $R^2 = .63$, $p < .001$; **Figure 1C**). There might be two reasons for the

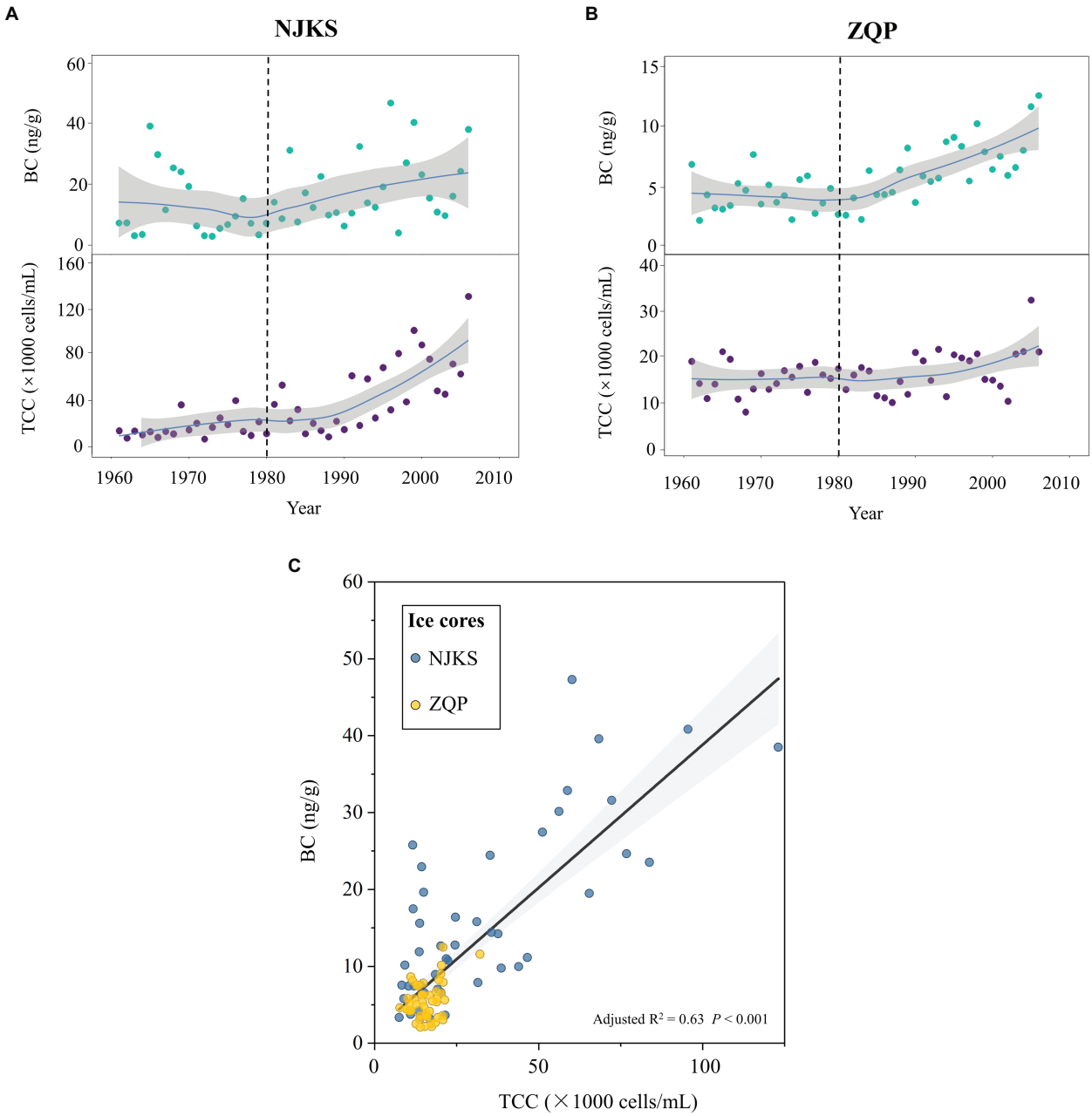

FIGURE 1 | Temporal variation of total cells concentration (TCC) and black carbon (BC) concentration from 1960 to 2006 in Noijinkangsang (NJKS) and Zuoqiupu (ZQP) glacier ice cores and their correlation. Time trends (solid lines) of TCC and BC in NJKS **(A)** and ZQP **(B)**. All trends were estimated using GAMs. The gray-shaded areas in the graphs represent the 95% CIs. **(C)** Correlation between TCC and BC across the two glacier ice cores. The gray-shaded areas in the graphs represent the 95% CIs.

increasing of TCC: (i) bacteria were brought onto the glacier by a carrier of BC. This finding was consistent with previous studies (Zhang et al., 2007; Yao et al., 2008; Liu et al., 2016b), which demonstrated atmospheric deposition was responsible for transporting bacteria and (ii) dissolved BC boosted accumulation of nutrient concentration on the glaciers and was available for bacterial reproduction during post-depositional process (Santibanez et al., 2018). Previously BC was considered recalcitrant and inaccessible for bacteria; however, BC is very reactive and oligotrophic bacteria can consume as a carbon source for their growth (Hartnett and Hamilton, 2016). It has been reported that UV light could stimulate chemical changes in BC and making it easier for degradation by microorganisms (Malits et al., 2015). Since most glacial regions receive maximum light all year round (Zheng et al., 2000; Shen et al., 2015), the levels of BC degradation will thereby increase resulting in increment of bacteria abundance.

Temporal and Seasonal Variation of LNA (HNA) Functional Groups

Temporal Variation

The abundance ratio of LNA-to-HNA functional groups decreased for the period examined (**Figure 2**), and the generalized additive model (GAM) analysis showed that the reduction was statistically significant ($p < .05$). Typically, the ratio of LNA functional groups

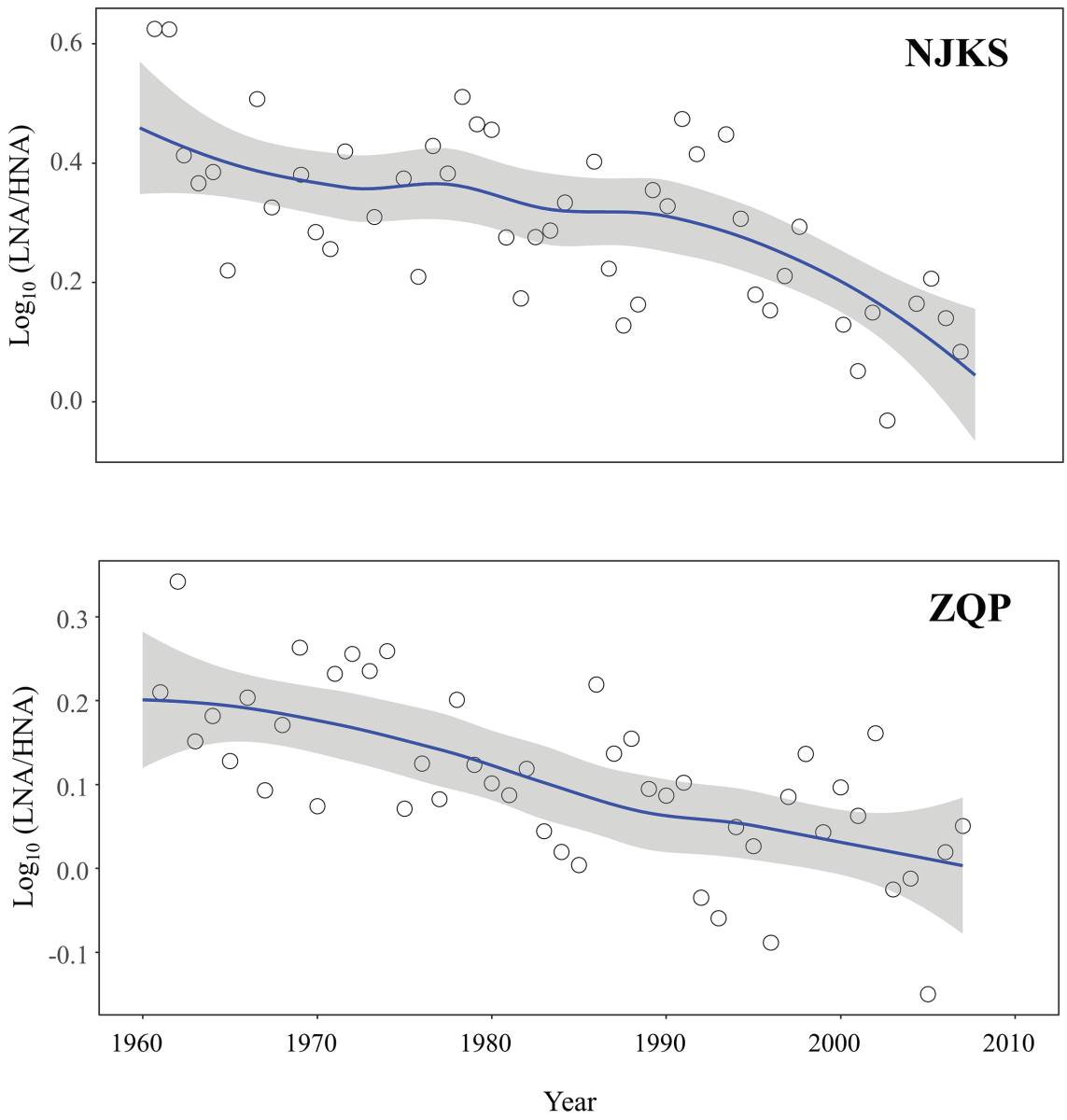

FIGURE 2 | Time trends (solid lines) of Log_{10} (LNA/HNA) in NJKS (edf = 8.19) and ZQP (edf = 5.49) glacier ice cores. All trends were estimated using GAMs. The gray-shaded areas in the graphs represent the 95% CIs.

was higher than HNA functional groups in oligotrophic conditions with minimum contamination (Servais et al., 2003; Salcher et al., 2011). On the other hand, compared with LNA functional groups, HNA functional groups are more sensitive to changes in nutritional environment (Santos et al., 2019). In other words, HNA functional groups highly related to increment of nutrients (Sharuddin et al., 2018). It should be noted that BC ($p < .001$) significantly and negatively correlated with the LNA-to-HNA ratio in both glaciers (**Figure 3**), which suggested that a dissolved fraction of BC could be responsible for the reduced LNA-to-HNA ratio. It is worth noting that a given bacterium can be sometimes categorized as LNA functional groups and sometimes HNA functional groups depending on environmental conditions (Wang et al., 2009; Martinez-Garcia et al., 2012). This classification inconsistency is mainly since LNA functional groups should be dormant under oligotrophic conditions, but then switch to an active condition following organic loading (Sharuddin et al., 2018; Santos et al., 2019). In fact, this feature can better explain the bioindicator value of LNA-to-HNA ratio since they sensitively respond to fluctuations in environmental conditions rather than they are only dependent on the community taxon composition.

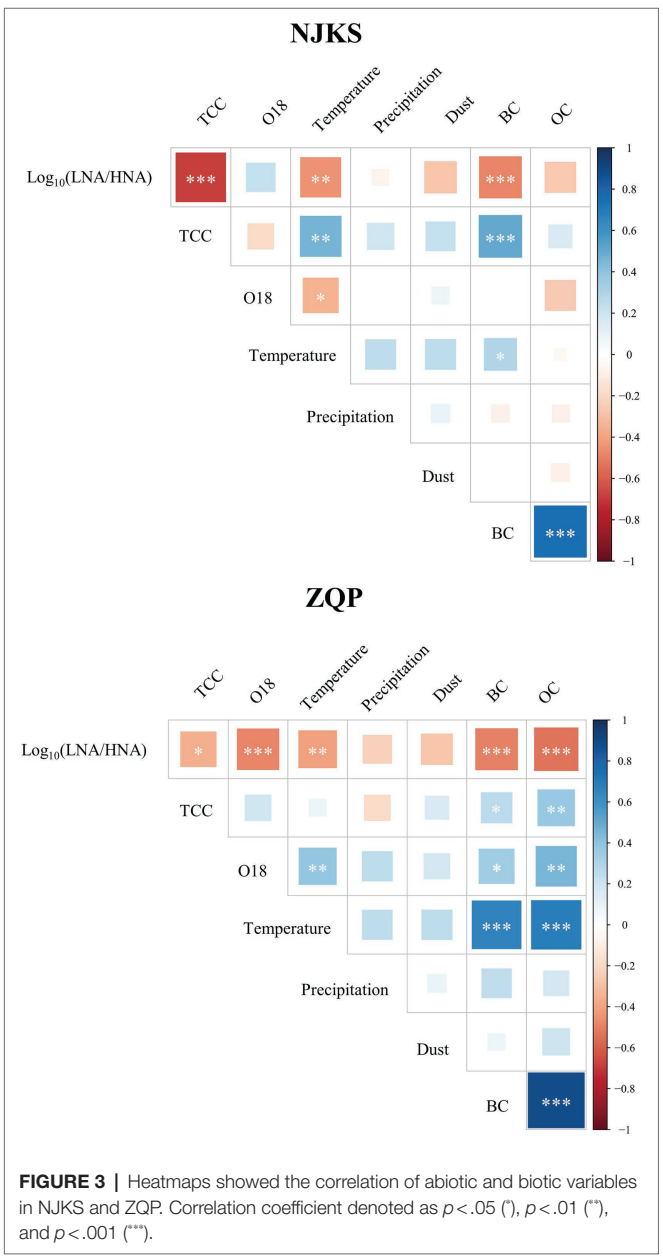

FIGURE 3 | Heatmaps showed the correlation of abiotic and biotic variables in NJKS and ZQP. Correlation coefficient denoted as $p < .05$ (*), $p < .01$ (**), and $p < .001$ (***).

Seasonal Variation

Seasonal fluctuation in the LNA-to-HNA ratio was also observed in the ZQP Glacier. O18 isotopic ratio, an Indian monsoon precipitation proxies (Yu et al., 2021), exhibited a negative correlation with the LNA-to-HNA ratio significantly ($p < .001$, **Figure 3**). As shown in **Figure 4**, LNA functional groups were more prevalent in the monsoon samples with an average LNA-to-HNA ratio of $.14 \pm .11$ (**Figure 4**). Bacteria deposited during the monsoon period are partly originated from the Indian Ocean, which is dominated by LNA functional groups numerically (Zubkov et al., 2006). This could explain the higher LNA ratio during the monsoon season. The TCC also showed seasonal variation. TCC in monsoon samples ($12.9 \pm 4.7 \times 10^3$ cells/ml) was significantly lower ($p < .01$ or $p < .001$) than those in the pre-monsoon ($18.4 \pm 7.5 \times 10^3$ cells/ml) and post-monsoon samples ($16.5 \pm 9.3 \times 10^3$ cells/ml), while no significant difference was found between pre-monsoon and post-monsoon samples. This seasonal variation in the distribution of bacteria is related to the atmospheric circulation on the Tibetan Plateau (Yao et al., 2008). Specifically, a higher TCC was observed during the non-monsoon season, consistent with the higher atmospheric deposition loading brought by the westerlies (Kang et al., 2000).

Increasing BC on the Tibetan Plateau could influence bacterial distribution. BC variation exhibited an opposite trend of a lower concentration during the monsoon season (3.41 ± 2.47 ng/g) and higher during the pre-monsoon (7.38 ± 3.46 ng/g) and post-monsoon periods (6.39 ± 3.87 ng/g; **Figure 4**). There was no significant different between pre-monsoon and post-monsoon. Environmental factors can also affect the LNA-to-HNA ratio. Temperature exhibited a negative correlation with the LNA-to-HNA ratio significantly ($p < .01$; **Figure 3**). The temperature dependence of metabolic rates of bacteria in deep glacier ice was for survival of imprisoned bacteria (Price and Sowers, 2004). High temperature leaded to more activity bacteria, as recorded in the ice core. With principal coordinate analysis (PCoA), the pre-monsoon and post-monsoon samples were clearly clustered into one group and separated from the monsoon samples (**Supplementary Figure 4**), which was confirmed by dissimilarity test (PERMANOVA, $p < .001$).

Correlation Between BC and LNA and HNA Functional Groups

We applied Procrustes analysis to test for functional groups and BC factors across seasonal samples. Our analysis showed that BC variations correlated with functional groups using Euclidean distances in the non-monsoon season (**Figure 5A**, Procrustes, Monte Carlo $p < .01$, 999 permutations). This was consistent with the Mantel test results ($r = .22$, $p = .003$). Interestingly, we did not find a similar correspondence between

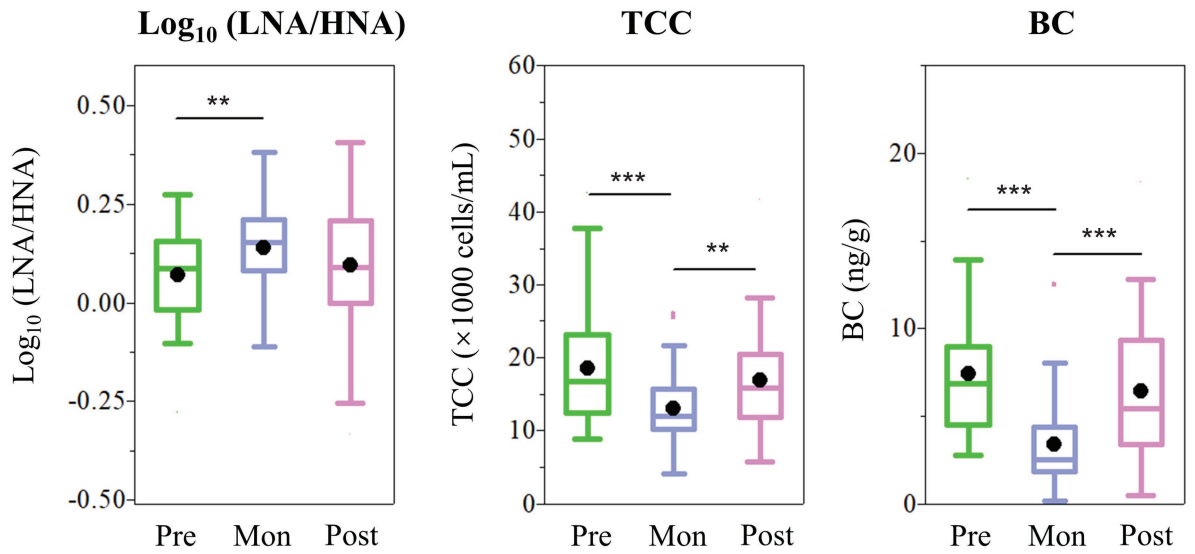

FIGURE 4 | Seasonal variation of Log_{10} (LNA/HNA), TCC and BC concentration in ZQP. Correlation coefficient denoted as $p < .05$ (*), $p < .01$ (**), and $p < .001$ (***).

BC variations and functional groups during the monsoon period (**Figure 5A**, Procrustes, Monte Carlo $p = .36$, 999 permutations). Variation partitioning analysis (VPA) further differentiated the contributions of BC factors and environmental factors on functional groups' variations (**Figure 5B**). The BC (49.78%) showed a greater contribution to functional groups' variations in non-monsoon. In comparison, BC only explained 4.44% for the functional groups' variations in the monsoon season. The joint effects of multiple factors explained 2.26% and 16.45%, leaving 44.15% and 73.78% of functional groups' variations in the non-monsoon and monsoon seasons, respectively. Both the Procrustes analysis and VPA results demonstrated that potential causal relationships may occur between LNA (HNA) functional groups and BC factors in the non-monsoon season.

A scheme illustrating how two functional groups respond to BC under influence of westerly winds and Indian Monsoon was proposed to explain the pattern observed (**Figure 5C**). During non-monsoon seasons, BC deposited onto the southeastern Tibetan Plateau by the westerly winds (Xu et al., 2009a). UV light could stimulate chemical changes in BC, leaching of dissolved BC boosts accumulation of nutrient concentration on the glaciers (Malits et al., 2015). The diverse characteristics of BC and high reactivity have the potential to alter microbial biomass growth, community structure, and activity in many ways. Bacteria transition from death or a dormant state (primarily LNA functional groups) to active growth (primarily HNA functional groups) in the nutrient-rich condition (Bouvier et al., 2007; Wang et al., 2009). Previous results have indicated that an immediate increase in bacterial abundance and metabolically activity in glaciers after BC deposition (Liu et al., 2016b; Santibanez et al., 2018). BC could adsorb organic matter and nutrients and serve as a nutrient reservoir for microorganisms (Busscher et al., 2008; Weinbauer et al., 2012).

In comparison, BC was lower during the monsoon seasons (**Figure 4**). This could be due to the high atmospheric moisture of the Indian monsoon that enhanced precipitation of BC before it reached glaciers (Xu et al., 2009a; Yang et al., 2021). LNA functional groups are dominant in nutrient-limited environments on account of their high nutrient acquisition efficiency (Sharuddin et al., 2018; Santos et al., 2019). Thereby, organic loads are crucial factors influencing the LNA-to-HNA ratio. This has been proposed previously that trophic statuses of the growth conditions were associated with LNA/HNA ratio (Santos et al., 2019). In this study, the higher proportion of HNA functional groups during the non-monsoon season could be related to their eutrophic status (Servais et al., 2003). This finding aligns with the microbial biogeography study of the same glacier that Actinobacteria, which is categorized as "overlapped" HNA (i.e., sometimes categorized as HNA and sometimes LNA; Vila-Costa et al., 2012; Proctor et al., 2018), was the dominant phylum with increasing BC concentrations (Liu et al., 2016b). The "overlapped" functional groups depend on environmental condition. The hypotheses of Bouvier et al. (2007) could explain "overlapped" functional groups: (i) that LNA functional groups consist of dormant groups that move to HNA when they become active in the optimal condition and (ii) that HNA functional groups consist of active groups that move into the LNA fraction after inactivation.

CONCLUSION

In this study, high-resolution temporal variations of bacterial abundance and functional groups in ice cores from the Tibetan Plateau were investigated. A variation of the LNA/HNA ratio was detected, which is a measure of the transition of bacterial community from a dormancy to an actively growth. Our data identified an accumulation of nutrient concentration on the glaciers

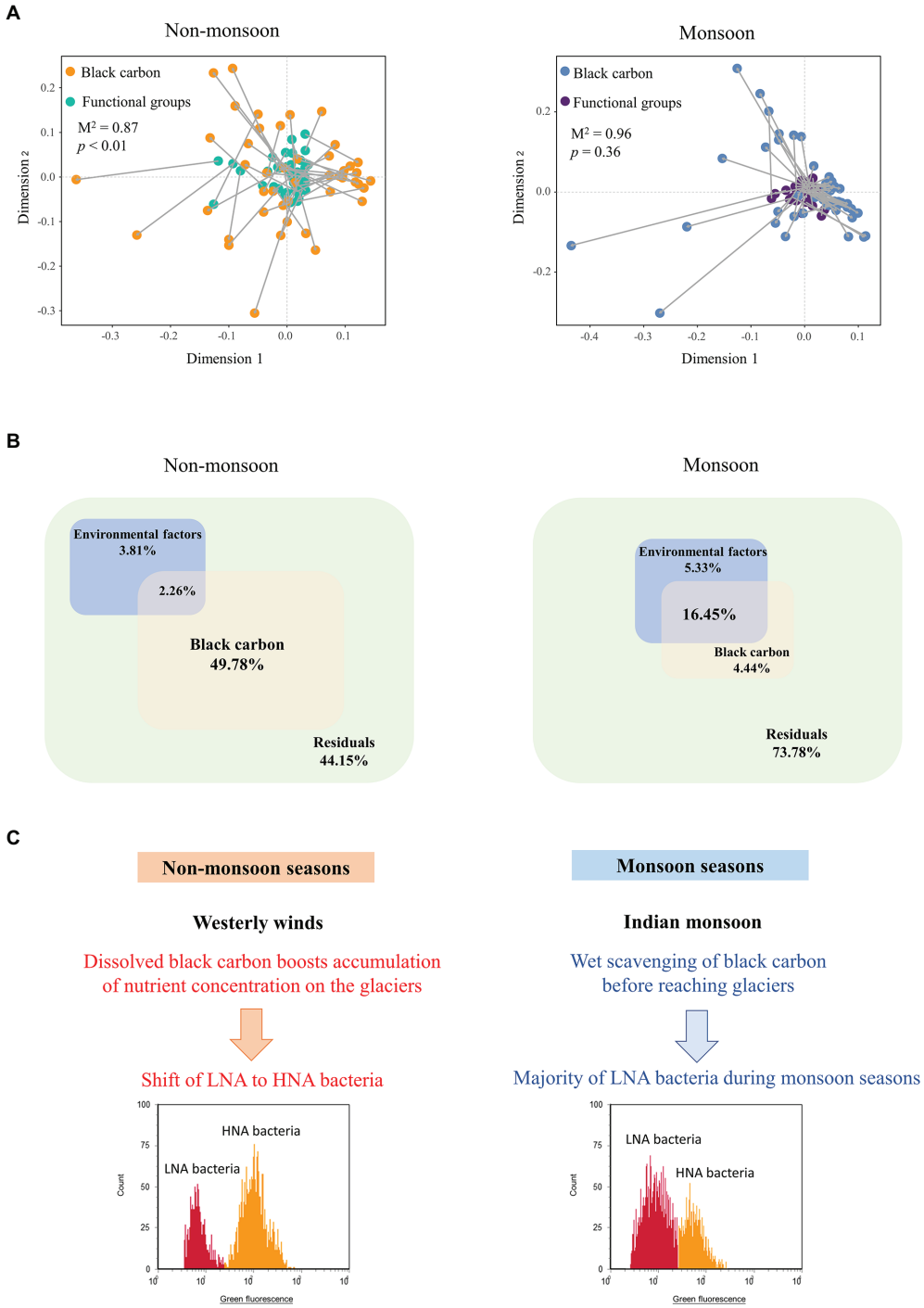

FIGURE 5 | Relationships between BC and LNA and HNA functional groups. **(A)** Procrustes analyses of the correlations between BC and functional groups during non-monsoon and monsoon. M^2 values represent the Procrustes sum of squares. Value of p represents the significance under 999 permutations test. **(B)** Variation partitioning analysis (VPA) differentiating the effect (%) of environmental factors and BC on proportion of LNA and HNA. **(C)** Schematic representation of HNA and LNA functional groups respond to BC under influence of Indian Monsoon.

over the last half-century and demonstrated the rapid deterioration of trophic status on the sensitive ecosystem due to increment of BC. The responses of bacteria endpoints to nutritional environment caused by anthropogenic activity indicated that endless BC emissions could result in serious and irreversible impacts on trophic statuses of the Tibetan Plateau. The fluorescent fingerprinting had considerable potential application for bacterial monitoring and early-warning detection of microbiological effects of BC.

DATA AVAILABILITY STATEMENT

The original contributions presented in the study are included in the article/**Supplementary Material**, further inquiries can be directed to the corresponding author.

AUTHOR CONTRIBUTIONS

GM and YL contributed to the study conception and design. Material preparation, data collection, and analysis were performed by GM, MJ, BX, YL, and NJ. The first draft of the manuscript was written by GM and MJ. GM, MJ, BX, YL, and NJ commented on previous versions of the manuscript. All authors read and approved the final manuscript.

FUNDING

This work was supported by the National Research and Development Program of China (grant no. 2019YFC1509103), the National Natural Science Foundation of China (grant nos. 91851207, 42101128, and 41988101), and the China Postdoctoral Science Foundation (2021M693254).

SUPPLEMENTARY MATERIAL

The Supplementary Material for this article can be found online at: https://www.frontiersin.org/articles/10.3389/fmicb.2022.844432/full#supplementary-material

REFERENCES

Besmer, M. D., Sigrist, J. A., Props, R., Buysschaert, B., Mao, G. N., Boon, N., et al. (2017). Laboratory-scale simulation and real-time tracking of a microbial contamination event and subsequent shock-chlorination in drinking water. *Front. Microbiol.* 8:1900. doi: 10.3389/fmicb.2017.01900

Bouvier, T., del Giorgio, P. A., and Gasol, J. M. (2007). A comparative study of the cytometric characteristics of high and low nucleic-acid bacterioplankton cells from different aquatic ecosystems. *Environ. Microbiol.* 9, 2050–2066. doi: 10.1111/j.1462-2920.2007.01321.x

Bowman, J. S., Amaral-Zettler, L. A., Rich, J. J., Luria, C. M., and Ducklow, H. W. (2017). Bacterial community segmentation facilitates the prediction of ecosystem function along the coast of the western Antarctic peninsula. *ISME J.* 11, 1460–1471. doi: 10.1038/ismej.2016.204

Busscher, H. J., Dijkstra, R. J. B., Langworthy, D. E., Collias, D. I., Bjorkquist, D. W., Mitchell, M. D., et al. (2008). Interaction forces between waterborne bacteria and activated carbon particles. *J. Colloid Interface Sci.* 322, 351–357. doi: 10.1016/j.jcis.2008.03.018

Chen, Y., Li, X. K., Si, J., Wu, G. J., Tian, L. D., and Xiang, S. R. (2016). Changes of the bacterial abundance and communities in shallow ice cores from Dunde and Muztagata glaciers, Western China. *Front. Microbiol.* 7:1716. doi: 10.3389/fmicb.2016.01716

Cheng, S. M., and Foght, J. M. (2007). Cultivation-independent and -dependent characterization of bacteria resident beneath John Evans glacier. *FEMS Microbiol. Ecol.* 59, 318–330. doi: 10.1111/j.1574-6941.2006.00267.x

Christner, B. C., Mikucki, J. A., Foreman, C. M., Denson, J., and Priscu, J. C. (2005). Glacial ice cores: a model system for developing extraterrestrial decontamination protocols. *Icarus* 174, 572–584. doi: 10.1016/j.icarus.2004.10.027

Dixon, P. (2003). VEGAN, a package of R functions for community ecology. *J. Veg. Sci.* 14, 927–930. doi: 10.1111/j.1654-1103.2003.tb02228.x

Elhadidy, A. M., Van Dyke, M. I., Peldszus, S., and Huck, P. M. (2016). Application of flow cytometry to monitor assimilable organic carbon (AOC) and microbial community changes in water. *J. Microbiol. Methods* 130, 154–163. doi: 10.1016/j.mimet.2016.09.009

Falkowski, P. G., Fenchel, T., and Delong, E. F. (2008). The microbial engines that drive Earth's biogeochemical cycles. *Science* 320, 1034–1039. doi: 10.1126/science.1153213

Gasol, J. M., Zweifel, U. L., Peters, F., Fuhrman, J. A., and Hagstrom, A. (1999). Significance of size and nucleic acid content heterogeneity as measured by flow cytometry in natural planktonic bacteria. *Appl. Environ. Microbiol.* 65, 4475–4483. doi: 10.1128/AEM.65.10.4475-4483.1999

Hammes, F., Berney, M., Wang, Y. Y., Vital, M., Koster, O., and Egli, T. (2008). Flow-cytometric total bacterial cell counts as a descriptive microbiological parameter for drinking water treatment processes. *Water Res.* 42, 269–277. doi: 10.1016/j.watres.2007.07.009

Hara, K., and Zhang, D. (2012). Bacterial abundance and viability in long-range transported dust. *Atmos. Environ.* 47, 20–25. doi: 10.1016/j.atmosenv.2011.11.050

Hartnett, H. E., and Hamilton, G. (2016). Urban Soot Black Carbon Biodegradation Rates. American Geophysical Union, Fall Meeting 2016, abstract: B22C-08.

Kaartokallio, H., Sogaard, D. H., Norman, L., Rysgaard, S., Tison, J. L., Delille, B., et al. (2013). Short-term variability in bacterial abundance, cell properties, and incorporation of leucine and thymidine in subarctic sea ice. *Aquat. Microb. Ecol.* 71, 57–73. doi: 10.3354/ame01667

Kang, S. C., Wake, C. P., Qin, D. H., Mayewski, P. A., and Yao, T. D. (2000). Monsoon and dust signals recorded in Dasuopu glacier, Tibetan Plateau. *J. Glaciol.* 46, 222–226. doi: 10.3189/172756500781832864

La Ferla, R., Maimone, G., Caruso, G., Azzaro, F., Azzaro, M., Decembrini, F., et al. (2014). Are prokaryotic cell shape and size suitable to ecosystem characterization? *Hydrobiologia* 726, 65–80. doi: 10.1007/s10750-013-1752-x

Lebaron, P., Servais, P., Baudoux, A. C., Bourrain, M., Courties, C., and Parthuisot, N. (2002). Variations of bacterial-specific activity with cell size and nucleic acid content assessed by flow cytometry. *Aquat. Microb. Ecol.* 28, 131–140. doi: 10.3354/ame028131

Legrand, M., and Mayewski, P. (1997). Glaciochemistry of polar ice cores: a review. *Rev. Geophys.* 35, 219–243. doi: 10.1029/96RG03527

Li, Z. Q., Lau, W. K. M., Ramanathan, V., Wu, G., Ding, Y., Manoj, M. G., et al. (2016). Aerosol and monsoon climate interactions over Asia. *Rev. Geophys.* 54, 866–929. doi: 10.1002/2015RG000500

Liu, J., Hao, Z., Ma, L., Ji, Y., Bartlam, M., and Wang, Y. (2016a). Spatio-temporal variations of high and low nucleic acid content bacteria in an Exorheic River. *PLoS One* 11:e0153678. doi: 10.1371/journal.pone.0153678

Liu, Y., Priscu, J. C., Yao, T., Vick-Majors, T. J., Xu, B., Jiao, N., et al. (2016b). Bacterial responses to environmental change on the Tibetan plateau over the past half century. *Environ. Microbiol.* 18, 1930–1941. doi: 10.1111/1462-2920.13115

Madsen, E. L. (2011). Microorganisms and their roles in fundamental biogeochemical cycles. *Curr. Opin. Biotechnol.* 22, 456–464. doi: 10.1016/j.copbio.2011.01.008

Malits, A., Cattaneo, R., Sintes, E., Gasol, J. M., Herndl, G. J., and Weinbauer, M. G. (2015). Potential impacts of black carbon on the marine microbial community. *Aquat. Microb. Ecol.* 75, 27–42. doi: 10.3354/ame01742

Marra, G., and Wood, S. N. (2011). Practical variable selection for generalized additive models. *Comput. Stat. Data Anal.* 55, 2372–2387. doi: 10.1016/j.csda.2011.02.004

Martinez-Garcia, M., Swan, B. K., Poulton, N. J., Gomez, M. L., Masland, D., Sieracki, M. E., et al. (2012). High-throughput single-cell sequencing identifies photoheterotrophs and chemoautotrophs in freshwater bacterioplankton. *ISME J.* 6, 113–123. doi: 10.1038/ismej.2011.84

Mary, I., Heywood, J. L., Fuchs, B. M., Amann, R., Tarran, G. A., Burkill, P. H., et al. (2006). SAR11 dominance among metabolically active low nucleic acid bacterioplankton in surface waters along an Atlantic meridional transect. *Aquat. Microb. Ecol.* 45, 107–113. doi: 10.3354/ame045107

Miteva, V. I., and Brenchley, J. E. (2005). Detection and isolation of ultrasmall microorganisms from a 120,000-year-old Greenland glacier ice core. *Appl. Environ. Microbiol.* 71, 7806–7818. doi: 10.1128/AEM.71.12.7806-7818.2005

Miteva, V., Teacher, C., Sowers, T., and Brenchley, J. (2009). Comparison of the microbial diversity at different depths of the GISP2 Greenland ice core

in relationship to deposition climates. *Environ. Microbiol.* 11, 640–656. doi: 10.1111/j.1462-2920.2008.01835.x

Odhiambo, M., and Routh, J. (2016). Does black carbon contribute to eutrophication in large lakes? *Curr. Pollut. Rep.* 2, 236–238. doi: 10.1007/s40726-016-0042-4

Prest, E. I., Hammes, F., Kotzsch, S., van Loosdrecht, M. C. M., and Vrouwenvelder, J. S. (2013). Monitoring microbiological changes in drinking water systems using a fast and reproducible flow cytometric method. *Water Res.* 47, 7131–7142. doi: 10.1016/j.watres.2013.07.051

Price, P. B., and Sowers, T. (2004). Temperature dependence of metabolic rates for microbial growth, maintenance, and survival. *Proc. Natl. Acad. Sci. U. S. A.* 101, 4631–4636. doi: 10.1073/pnas.0400522101

Proctor, C. R., Besmer, M. D., Langenegger, T., Beck, K., Walser, J. C., Ackermann, M., et al. (2018). Phylogenetic clustering of small low nucleic acid-content bacteria across diverse freshwater ecosystems. *ISME J.* 12, 1344–1359. doi: 10.1038/s41396-018-0070-8

Qi, J., Huang, Z., Maki, T., Kang, S., Guo, J., Liu, K., et al. (2021). Airborne bacterial communities over the Tibetan and Mongolian Plateaus: variations and their possible sources. *Atmos. Res.* 247:105215. doi: 10.1016/j.atmosres.2020.105215

Reid, J. S., Koppmann, R., Eck, T. F., and Eleuterio, D. P. (2005). A review of biomass burning emissions part II: intensive physical properties of biomass burning particles. *Atmos. Chem. Phys.* 5, 799–825. doi: 10.5194/acp-5-799-2005

Rubbens, P., Schmidt, M. L., Props, R., Biddanda, B. A., Boon, N., Waegeman, W., et al. (2019). Randomized lasso links microbial taxa with aquatic functional groups inferred from flow cytometry. *mSystems* 4, e00093–e00119. doi: 10.1128/mSystems.00093-19

Salcher, M. M., Pernthaler, J., and Posch, T. (2011). Seasonal bloom dynamics and ecophysiology of the freshwater sister clade of SAR11 bacteria 'that rule the waves' (LD12). *ISME J.* 5, 1242–1252. doi: 10.1038/ismej.2011.8

Santibanez, P. A., Maselli, O. J., Greenwood, M. C., Grieman, M. M., Saltzman, E. S., McConnell, J. R., et al. (2018). Prokaryotes in the WAIS divide ice core reflect source and transport changes between last glacial maximum and the early Holocene. *Glob. Chang. Biol.* 24, 2182–2197. doi: 10.1111/gcb.14042

Santibanez, P. A., McConnell, J. R., and Priscu, J. C. (2016). A flow cytometric method to measure prokaryotic records in ice cores: an example from the West Antarctic ice sheet divide drilling site. *J. Glaciol.* 62, 655–673. doi: 10.1017/jog.2016.50

Santos, M., Oliveira, H., Pereira, J. L., Pereira, M. J., Goncalves, F. J. M., and Vidal, T. (2019). Flow cytometry analysis of low/high DNA content (LNA/HNA) bacteria as bioindicator of water quality evaluation. *Ecol. Indic.* 103, 774–781. doi: 10.1016/j.ecolind.2019.03.033

Servais, P., Casamayor, E. O., Courties, C., Catala, P., Parthuisot, N., and Lebaron, P. (2003). Activity and diversity of bacterial cells with high and low nucleic acid content. *Aquat. Microb. Ecol.* 33, 41–51. doi: 10.3354/ame033041

Sharuddin, S. S., Ramli, N., Mohd-Nor, D., Hassan, M. A., Maeda, T., Shirai, Y., et al. (2018). Shift of low to high nucleic acid bacteria as a potential bioindicator for the screening of anthropogenic effects in a receiving river due to palm oil mill effluent final discharge. *Ecol. Indic.* 85, 79–84. doi: 10.1016/j.ecolind.2017.10.020

Shen, M. G., Piao, S. L., Jeong, S. J., Zhou, L. M., Zeng, Z. Z., Ciais, P., et al. (2015). Evaporative cooling over the Tibetan Plateau induced by vegetation growth. *Proc. Natl. Acad. Sci. U. S. A.* 112, 9299–9304. doi: 10.1073/pnas.1504418112

Stubbins, A., Niggemann, J., and Dittmar, T. (2012). Photo-lability of deep ocean dissolved black carbon. *Biogeosciences* 9, 1661–1670. doi: 10.5194/bg-9-1661-2012

Tian, L., Masson-Delmotte, V., Stievenard, M., Yao, T. D., and Jouzel, J. (2001). Tibetan Plateau summer monsoon northward extent revealed by measurements of water stable isotopes. *J. Geophys. Res.-Atmos* 106, 28081–28088. doi: 10.1029/2001JD900186

Vila-Costa, M., Gasol, J. M., Sharma, S., and Moran, M. A. (2012). Community analysis of high- and low-nucleic acid-containing bacteria in NW Mediterranean coastal waters using 16S rDNA pyrosequencing. *Environ. Microbiol.* 14, 1390–1402. doi: 10.1111/j.1462-2920.2012.02720.x

Wang, T. J., Gao, T. C., Zhang, H. S., Ge, M. F., Lei, H. C., Zhang, P. C., et al. (2019). Review of Chinese atmospheric science research over the past 70 years: atmospheric physics and atmospheric environment. *Sci. China Earth Sci.* 62, 1903–1945. doi: 10.1007/s11430-019-9536-1

Wang, Y. Y., Hammes, F., Boon, N., Chami, M., and Egli, T. (2009). Isolation and characterization of low nucleic acid (LNA)-content bacteria. *ISME J.* 3, 889–902. doi: 10.1038/ismej.2009.46

Weinbauer, M., Cattaneo, R., Malits, A., Motegi, C., Gasol, J., Herndl, G., et al. (2012). "Black carbon and microorganisms in aquatic systems," in *Advances in Environmental Research. Vol. 25*. ed. J. A. Daniels (Nova Science Publishers), 1–37.

Xiang, S. R., Shang, T. C., Chen, Y., and Yao, T. D. (2009). Deposition and postdeposition mechanisms as possible drivers of microbial population variability in glacier ice. *FEMS Microbiol. Ecol.* 70, 165–176. doi: 10.1111/j.1574-6941.2009.00759.x

Xu, B., Cao, J., Hansen, J., Yao, T., Joswia, D. R., Wang, N., et al. (2009a). Black soot and the survival of Tibetan glaciers. *Proc. Natl. Acad. Sci. U. S. A.* 106, 22114–22118. doi: 10.1073/pnas.0910444106

Xu, B. Q., Wang, M., Joswiak, D. R., Cao, J. J., Yao, T. D., Wu, G. J., et al. (2009b). Deposition of anthropogenic aerosols in a southeastern Tibetan glacier. *J. Geophys. Res.-Atmos.* 114:17209. doi: 10.1029/2008JD011510

Yang, J., Ji, Z., Kang, S., and Tripathee, L. (2021). Contribution of south Asian biomass burning to black carbon over the Tibetan Plateau and its climatic impact. *Environ. Pollut.* 270:116195. doi: 10.1016/j.envpol.2020.116195

Yao, T., Liu, Y., Kang, S., Jiao, N., Zeng, Y., Liu, X., et al. (2008). Bacteria variabilities in a Tibetan ice core and their relations with climate change. *Glob. Biogeochem. Cycles* 22:GB4017. doi: 10.1029/2007GB003140

Yao, T., Thompson, L., Yang, W., Yu, W., Gao, Y., Guo, X., et al. (2012). Different glacier status with atmospheric circulations in Tibetan Plateau and surroundings. *Nat. Clim. Chang.* 2, 663–667. doi: 10.1038/NCLIMATE1580

Yu, W., Yao, T., Thompson, L. G., Jouzel, J., Zhao, H., Xu, B., et al. (2021). Temperature signals of ice core and speleothem isotopic records from Asian monsoon region as indicated by precipitation delta O-18. *Earth Planet. Sci. Lett.* 554:116665. doi: 10.1016/j.epsl.2020.116665

Zhang, S., Hou, S., Ma, X., Qin, D., and Chen, T. (2007). Culturable bacteria in Himalayan glacial ice in response to atmospheric circulation. *Biogeosciences* 4, 1–9. doi: 10.5194/bg-4-1-2007

Zheng, D., Zhang, Q., and Wu, S. (2000). Mountain geoecology and sustainable development of the Tibetan plateau. *Geoj. Libr.* 57, 181–202. doi: 10.1007/978-94-010-0965-2

Zubkov, M. V., Tarran, G. A., and Burkill, P. H. (2006). Bacterioplankton of low and high DNA content in the suboxic waters of the Arabian Sea and the Gulf of Oman: abundance and amino acid uptake. *Aquat. Microb. Ecol.* 43, 23–32. doi: 10.3354/ame043023

Conflict of Interest: The authors declare that the research was conducted in the absence of any commercial or financial relationships that could be construed as a potential conflict of interest.

Publisher's Note: All claims expressed in this article are solely those of the authors and do not necessarily represent those of their affiliated organizations, or those of the publisher, the editors and the reviewers. Any product that may be evaluated in this article, or claim that may be made by its manufacturer, is not guaranteed or endorsed by the publisher.

frontiers in Microbiology

ORIGINAL RESEARCH
published: 02 March 2022
doi: 10.3389/fmicb.2022.838836

Immobilization of *Ochrobactrum* sp. on Biochar/Clay Composite Particle: Optimization of Preparation and Performance for Nitrogen Removal

Pengfei Sun[1,2,3], Xiao Huang[4], Yixiao Xing[4], Wenlong Dong[5], Jianghua Yu[4], Jie Bai[6] and Weiyan Duan[7]**

[1] Ministry of Natural Resources, Fourth Institute of Oceanography, Beihai, China, [2] Key Laboratory of Tropical Marine Ecosystem and Bioresource, Ministry of Natural Resources, Beihai, China, [3] Guangxi Beibu Gulf Key Laboratory of Marine Resources, Environment and Sustainable Development, Beihai, China, [4] Jiangsu Key Laboratory of Atmospheric Environment Monitoring and Pollution Control, Collaborative Innovation Center of Atmospheric Environment and Equipment Technology, School of Environmental Science and Engineering, Nanjing University of Information Science and Technology, Nanjing, China, [5] Shandong Marine Forecast and Hazard Mitigation Service, Qingdao, China, [6] College of Environmental Science and Engineering, Ocean University of China, Qingdao, China, [7] Ocean College of Hebei Agricultural University, Qinhuangdao, China

OPEN ACCESS

Edited by:
Tian Li,
Nankai University, China

Reviewed by:
Peidong Su,
Research Center for Eco-Environmental Sciences (CAS), China
Hanxiang Li,
Chongqing University, China

***Correspondence:**
Xiao Huang
huangxiao901231@126.com
Weiyan Duan
duanweiyan@hebau.edu.cn

Specialty section:
This article was submitted to Microbiotechnology, a section of the journal Frontiers in Microbiology

Received: 18 December 2021
Accepted: 26 January 2022
Published: 02 March 2022

Citation:
Sun P, Huang X, Xing Y, Dong W, Yu J, Bai J and Duan W (2022) Immobilization of Ochrobactrum sp. on Biochar/Clay Composite Particle: Optimization of Preparation and Performance for Nitrogen Removal. Front. Microbiol. 13:838836. doi: 10.3389/fmicb.2022.838836

The objective of this study was to prepare biochar/clay composite particle (BCCP) as carrier to immobilize *Ochrobactrum* sp. to degrade ammonia nitrogen (NH_4^+-N), and the effects of calcined program and immobilizing material were investigated. Results reflected that the parameters were as follows: calcined temperature 400°C, heating rate 20°C min^{-1}, and holding time 2 h, and the adsorption capacity could reach 0.492 mg g^{-1}. Sodium alginate/polyvinyl alcohol, as embedding material, jointed with NH_4^+-N adsorption process and then degraded by *Ochrobactrum* sp. with 79.39% degradation efficiency at 168 h. Immobilizing *Ochrobactrum* sp. could protect strain from high salt concentration to achieve the exceeding degradation efficiency than free bacteria, but could not block the impact of low temperature.

Keywords: biochar/clay composite particle, calcined temperature, ammonia-oxidizing bacteria, immobilization, *Ochrobactrum* sp.

INTRODUCTION

Liaohe Estuary Wetland (LEW) owned the functions of regulating climate, alleviating flood peak, providing habitat for wildlife, and protecting biodiversity, and crab farming is the main industry there (Lin et al., 2016). Hence, serious ammonia nitrogen (NH_4^+-N) pollution was caused by excessive crab feed and contributed to the eutrophication in LEW (Hina et al., 2015).

A kind of biochar/clay composite particle (BCCP) absorbing NH_4^+-N was prepared with waste biochar and clay in LEW by previous studies and demonstrated that its removal effectively related to the ratio of materials, and the dosage of crosslinking agent and pore-forming agent (Huang et al., 2020). In fact, the calcined temperature and program of BCCP are also the key parameters restricting and affecting its adsorption performance and adsorption capacity depending on the changing of adsorption site quantity and adsorption material structures (Mandal and Mayadevi, 2008; Feng et al., 2013; Sun et al., 2015). Lin et al. (2009) found that the phenol adsorption capacity by nano-hydroxyapatite powder from aqueous solution reduced obviously when it was calcined at

high temperature. For TiO_2, the organic moieties were destroyed by high calcination temperature and affected the adsorption performance (Feng et al., 2020). On the contrary, Yan et al. (2018) prepared porous diatomite microspheres with different calcined temperatures, and concluded that the production was amorphous at 800°C and crystallized into crystobalite at 1,000°C. Nevertheless, whether a relationship between calcined temperature and NH_4^+-N adsorption capacity of BCCP exists or not needs to be further researched.

NH_4^+-N adsorption process is only the transfer of NH_4^+-N without complete conversion by ammonia-oxidizing bacteria (AOB). For LEW, the harsh environmental conditions of low temperature in winter and high salinity reduced the biological removal efficiency for NH_4^+-N. Therefore, screening high-efficiency degradation bacteria is a necessary method, and a previous study confirmed that an effective conversion process for NH_4^+-N could be achieved by salt- and cold-tolerant AOB under high-salt and low-temperature condition (Huang et al., 2017). Nevertheless, the application of high-effectivity degrading strains in a large-scale watershed faces an inevitable problem, i.e., the dilution of tide for using highly efficient AOB, which results in more difficult and inefficient application of traditional adsorption materials and biotechnology.

The immobilization technology of high-efficiency degradation bacteria is to fix the bacteria on a carrier, so as to solve the problem that the free high-efficiency degradation bacteria are washed away in the dynamic river. Hence, this technology is a potential application for wetland environmental restoration. Some previous studies have shown that immobilized strains could effectively remove reactive dyes, mineralize Ca^{2+} and Mg^{2+}, and remove manganese (Reddy and Osborne, 2020; Yan et al., 2020; Atcharaporn et al., 2020). Meanwhile, whether this technology can maintain the degradation performance for salt- and cold-tolerant AOB converting NH_4^+-N and resist low temperature and high salt environment is worth discussing.

Therefore, the purpose of this study is to propose a method that can be applied to remove NH_4^+-N in LEW. Based on the previous research, BCCP was prepared and the influence of calcined temperature and program on its adsorption performance was discussed. Then, immobilized AOB was explored to investigate the contribution of different immobilization methods on NH_4^+-N degradation. Finally, salt- and cold-resistance characteristics of immobilization were further studied to deepen the application value of immobilization technology.

MATERIALS AND METHODS

Biochar, Clay, and Ammonia-Oxidizing Bacteria

The reed straw selected was washed with deionized water and dried at 105°C for 24 h in an open crucible to remove the surface magazine. Then it was crushed with a micro plant crusher (Beijing Weiye, Z102), screened to obtain 0.85 mm reed powder, and placed in a quartz tube inside a tube furnace to produce the biochar through slow pyrolysis in a N_2 environment at 600°C for 3 h, respectively. The biochar samples were washed with deionized water several times to remove impurities, and then grinded into 0.15 mm powder and sealed in a container for further testing. The detailed information of the biochar characteristics is shown in Huang et al. (2020), and the composition of C, H, O, and N were 72.5, 4.18, 18.32, and 0.67%, respectively. The proportion of ash was 12.31%.

The clay was placed in an open crucible at 105°C for 24 h. Then it was crushed with a micro plant crusher (Beijing Weiye, Z102) and screened to obtain 0.15 mm clay powder.

The AOB was isolated from LEW with the characteristics of cold and salt tolerance and similar to the branch *Ochrobactrum* sp. The obtained 16S rDNA sequence of HXN-1 strain was registered in GenBank under accession numbers KP276672, and the characteristics of *Ochrobactrum* sp. and phylogenetic tree are listed in Huang et al. (2017). The details were as follows: catalase test (−), starch hydrolyzing enzyme test (+), citrate utilization test (+), MR test (−), glucose fermentation test (−), VP test (−), and indole test (−). The NH_4^+-N removal rate by *Ochrobactrum* sp. exceeds 60% at 15°C and 20‰ condition.

Preparation of Biochar/Clay Composite Particle

The optimum preparation formulation of BCCP and the proportion of raw material obtained in a previous study are demonstrated as follows: 15% biochar, 79% clay, 3% Na_2SiO_3, and 3% $NaHCO_3$ (v/v) (Huang et al., 2020). These materials were mixed, placed in a disc-type ball-making machine (BY-300; TianZhuo, Zhengzhou) to produce BCCP with a particle size of 8∼10 mm, and dried at 45°C for 6 h in a constant temperature drying oven. The calcined process was slow pyrolysis in a N_2 environment at 400, 450, 500, 550, 600, and 700°C for 3 h, respectively. Besides, the heating rate and holding time were optimized and their optimization scope was 5∼20 °C min^{-1} and 1∼4 h, respectively. The firing process is shown in **Figure 1**. The calcined process orthogonal test level of BCCP is demonstrated in **Table 1**.

Adsorption Experiment of Biochar/Clay Composite Particles for Ammonia Nitrogen

Adsorption Batch Experiment

BCCP (1.0 g) calcined with six different temperatures were put into a 50-ml flask with pure NH_4^+-N solution and shaken at 150 r min^{-1} for 300 min at 25°C. Samples were collected at 5, 10, 20, 40, 60, 90, 120, 150, 180, 240, and 300 min. The samples were filtrated by 0.45-μm RC membrane to determine NH_4^+-N concentration.

The adsorption capacity during the adsorption period was calculated by Equation (1):

$$q_t = (C_0 - C_t)\frac{V}{m} \quad (1)$$

where q_t is the amount of NH_4^+-N during the adsorption time (mg kg^{-1}); C_0 and C_t (mg L^{-1}) are the initial NH_4^+-N concentrations and different time residual concentration,

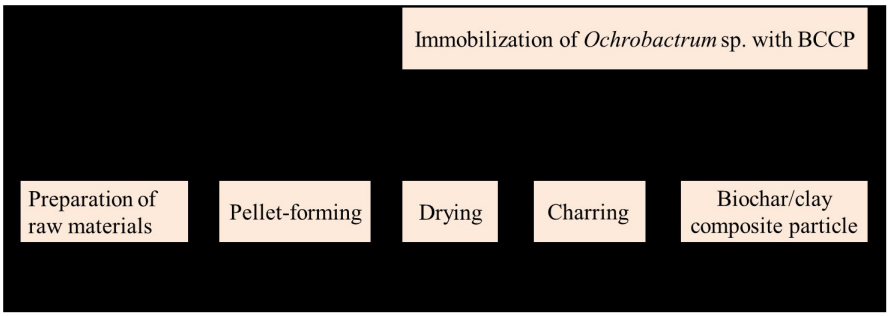

FIGURE 1 | Calcined program of BCCP and immobilization of *Ochrobactrum* sp.

respectively. V is the volume of reaction system (L), and m is the mass of adsorbent (g).

Adsorption Kinetics

The data coming from adsorption batch experiment were fitted with pseudo-first- and pseudo-second-order models and intraparticle model, the expressions as following Equations (2)–(4):

$$q_t = q_e\left(1 - e^{-K_1 t}\right) \quad \text{(Firstorder)} \tag{2}$$

$$\frac{t}{q_t} = \frac{1}{K_2 q_e^{\,2}} + \frac{t}{q_e} \quad \text{(Secondorder)} \tag{3}$$

$$q_t = K_p\sqrt{t} + C \quad \text{(Intraparticlemodel)} \tag{4}$$

where q_e ($mg{\cdot}g^{-1}$) is the adsorbed amounts of NH_4^+-N by the BCCP at equilibrium time, and q_t is the adsorbed amount at a given time interval (t). K_1 and K_2 are the rate constants for the pseudo-first- and pseudo-second-order models, respectively. Kp is the intraparticle diffusion rate constant ($mg{\cdot}g^{-1}\ min^{1/2}$), and C ($mg\ g^{-1}$) is a constant that reflects the boundary layer effect. A plot of q_t against $t^{1/2}$ gave a linear relationship from which the Kp value was determined from the slope and C as the intercept.

TABLE 1 | Calcined process orthogonal test level of BCCP.

Levels	Calcined temperature (°C)	Heating rate (°C min^{-1})	Holding time (h)	Empty column
1	400	5	1	1
2	400	10	2	2
3	400	15	3	3
4	400	20	4	4
5	500	5	2	3
7	500	10	1	4
7	500	15	4	1
8	600	20	3	2
9	600	5	3	4
10	600	10	4	3
11	600	15	1	2
12	600	20	2	1
13	700	5	4	2
14	700	10	3	1
15	700	15	2	4
16	700	20	1	3

Adsorption Isotherms

Freundlich and Langmuir equations were used to fit the adsorption isotherms of BCCP with different calcined temperatures, and the equation is given by

$$\log q_e = \log K_F + \frac{1}{n}\,logC_e \quad \text{(Freundlichequation)} \tag{5}$$

$$q_e = \frac{q_{max} K_L C_e}{1 + K_L C_e} \quad \text{(Langmuirequation)} \tag{6}$$

where q_e ($mg{\cdot}g^{-1}$) is the amount of NH_4^+-N adsorbed by the BCCP at equilibrium time, and q_{max} ($mg\ g^{-1}$) and K_L ($L\ mg^{-1}$) are Langmuir constants that indicate the maximum adsorption and relative binding energy of BCCP, respectively. K_F and n are Freundlich constants that measure the relative NH_4^+-N adsorption capacity and adsorption intensity of BCCP, respectively, while C_e ($mg\ L^{-1}$) denotes the equilibrium concentration of NH_4^+-N remaining in solution after adsorption is complete.

Immobilization of *Ochrobactrum* sp. With Biochar/Clay Composite Particle

The AOB strain HXN-1 (*Ochrobactrum* sp.) used in this study was enriched with culture medium to OD_{600} = 0.6. The prepared BCCPs were soaked into high-efficiency degrading bacteria (OD_{600}) for 24 h and afterward were transferred into the embedding solution for immobilization.

Two immobilization groups were set with sodium alginate (SA) and polyvinyl alcohol (PVA). (1) SA immobilization group: 2% SA aqueous solution and 2% $CaCl_2$ aqueous solution were mixed and autoclaved at 121°C for 30 min. (2) SA/PVA immobilization group: 2% SA and 12% PVA aqueous solutions were prepared according to the aforementioned method. For the BCCP adhesive, two kinds of embedding liquid were transferred into 2% $CaCl_2$ solution and saturated boric acid–2% $CaCl_2$ solution, respectively, and afterward placed in a 4°C refrigerator for 24 h.

Batch Experiment of Ammonia Nitrogen Degradation by *Ochrobactrum* sp.

Influence of Immobilization Material and Bacteria on Ammonia Nitrogen Degradation

HXN-1was made into gel particles by the method of 2.4 and named SA-B and SA/PVA-B and the blank gel particles were named SA-C and SA/PVA-C. SA and PVA as base material to immobilize *Ochrobactrum* sp. was named SA/PVA-B, and as control group without adding *Ochrobactrum* sp. was named SA/PVA-C. The aforementioned gel particles were put into 100 ml of 50 mg L^{-1} NH_4^+-N medium, placed in a shaking incubator at 25°C, 180 r min^{-1} for 7 days, and NH_4^+-N concentration was measured daily. The medium characteristics were demonstrated in Huang et al. (2017). Free bacteria (FB) were used as a control group.

Influence of Salinity and Temperature on Ammonia Nitrogen Degradation

Six kinds of gel particles were, respectively, put into 100 ml of 50 mg L^{-1} NH_4^+-N solution with different salinities (0, 5, 15, 25, and 35‰) under 25°C condition. Also, the same six kinds of gel particles were with different temperatures (15, 20, 25, 30, and 35°C) with 5‰ salinity. All of these were placed in a shaking incubator and shocked with 180 r min^{-1} for 10 days and NH_4^+-N concentration was measured daily. Free bacteria were used as a control group.

Analytical Method

Fourier-transform infrared spectroscopy (FTIR) spectra were recorded between 400 and 4000 cm^{-1} on a Nicolet 6,700 Fourier transform spectrometer. Clay, biochar, and BCCP were pelletized from a mixture of 1.5 mg dried sample with 200 mg KBr.

The water sample was filtered with a 0.45-μm filter membrane (Minisart RC 15), and the NH_4^+-N concentration was measured with a Nessler reagent. Each sample was measured in triplicate, and their average value was analyzed.

Statistical Analysis

All experiment groups were set in three replicates, and the average values of each sample were calculated and showed in charts. Origin 8.6 software was used for drawing figures.

RESULTS AND DISCUSSION

Effect of Calcined Program on Ammonia Nitrogen Adsorption by Biochar/Clay Composite Particle

To a certain extent, the control of calcined program (calcined temperature, heating rate, holding time) changes the surface structure of BCCP and then affects the adsorption performance for NH_4^+-N. Previous studies have shown that the adsorption performance of biochar was affected by calcined temperature and heating rate (Yakkala et al., 2013; Mahdi et al., 2018). Therefore, orthogonal experiment was used in this study to discuss the effect of calcined program on NH_4^+-N adsorption by BCCP, and the results are demonstrated in **Table 2**. Different BCCPs prepared by calcined temperature, holding time, and heating rate resulted in unequal NH_4^+-N adsorption capacity. The minimum adsorption capacity was 0.394 mg g^{-1}, the maximum value was 0.454 mg g^{-1}, and the average adsorption capacity was 0.424 mg g^{-1}. The adsorption capacity of BCCP fluctuated with the increase of calcined temperature, and the best adsorption capacity appeared at 400°C; the adsorption capacity was 0.446 mg g^{-1}, and the lowest was 500°C with the adsorption capacity reducing to 0.402 mg g^{-1}.

Heating rate has a significant impact on the adsorption properties of BCCP and the adsorption capacity of BCCP decreased first and then increased with the increase of heating rate. The maximum adsorption capacity appeared at 20°C min^{-1}. It can be interpreted that the increase of flexural strength decreased the loss tangent tan α when the temperature rose slowly. Meanwhile, the material was uniform with low porosity. However, too fast temperature rising would make it difficult to discharge the gas in BCCP and inhibited the reduction of porosity. Therefore, the adsorption capacity increased when the heating rate was from 10 to 20°C min^{-1}.

The increase of holding time also promoted the adsorption capacity of BCCP first and then decreased. The maximum value appeared at 2 h with 0.437 mg g^{-1} adsorption capacity. The influence of holding time on adsorption properties of BCCPs mainly included two aspects, i.e., one was to stabilize the physical and chemical changes of materials, and the other was

TABLE 2 | NH_4^+-N adsorption by BCCP with different calcined programs.

Levels	Calcined temperature (°C)	Heating rate (°C min^{-1})	Holding time (h)	Empty column	Result (mg g^{-1})
1	400	5	1	1	0.454
2	400	10	2	2	0.451
3	400	15	3	3	0.444
4	400	20	4	4	0.435
5	500	5	2	3	0.412
7	500	10	1	4	0.397
7	500	15	4	1	0.401
8	500	20	3	2	0.396
9	600	5	3	4	0.421
10	600	10	4	3	0.415
11	600	15	1	2	0.409
12	600	20	2	1	0.492
13	700	5	4	2	0.415
14	700	10	3	1	0.418
15	700	15	2	4	0.394
16	700	20	1	3	0.426
Average value 1	0.446	0.426	0.421	0.441	0.424
Average value 2	0.402	0.420	0.437	0.418	
Average value 3	0.434	0.421	0.420	0.424	
Average value 4	0.413	0.437	0.417	0.412	
Range analysis	0.044	0.017	0.020	0.029	
Primary relation	ACB				
Optimal scheme	A1B4C2 (calcined temperature: 400°C, heating rate: 20°C min^{-1}, holding time: 2 h)				

to homogenize the tissue structure. Too long holding time was not conducive to the formation of a strong skeleton, reduced mechanical properties, and caused glaze crack (Yang and Chow, 2019). Therefore, the holding time needed to be moderate, and the best holding time was 2 h in this study.

The primary relation of calcined temperature, heating rate, and holding time on NH_4^+-N adsorption was judged according to the magnitude of extreme difference; the primary and secondary sequences of the three ingredients were ACB, which proved that calcined temperature occupied the most prominent position, and then holding time and heating rate owned the least impact. Besides, it was concluded that A1B4C2 was the best preparation condition for BCCP, and the parameters were as follows: calcined temperature 400°C, heating rate 20°C/min, and holding time 2 h.

Effect of Calcined Temperature on Ammonia Nitrogen Adsorption by Biochar/Clay Composite Particle

Ammonia Nitrogen Removal Performance

NH_4^+-N adsorption performances from aqueous solution by six BCCPs with different temperatures were conducted, and the results are shown in **Figure 2**. The adsorption equilibrium time among six experimental groups was 180 min, and the NH_4^+-N removal efficiency by BCCP adsorption was about 29.4∼34.5%. The removal efficiency at 400°C group was better than that of the other four groups with the adsorption capacity of 0.473 mg g^{-1}. However, the value decreased first and then increased with the increase of calcined temperature. The same phenomenon existed in the research of Chen et al. (2018) who found that the surface area and pore volume of bentonite increased to 56.09 and 0.0611 cm^3 g^{-1} when the calcined temperature was 400°C, respectively, but sharply declined to 30.53 and 0.051 cm^3 g^{-1} at 800°C. Yan et al. (2018) prepared a kind of porous diatomite microsphere by spray drying method and the methylene blue adsorption capacity and removal efficiency demonstrated the maximum values when the calcined temperature was 600°C, and decreased when the temperature rose. Ojeda-López et al. (2021) found that adsorbent/adsorbate interactions for CO_2, CH_4, and N_2 were inversely proportional to calcined temperature (CMF-600 > CMF-700 > CMF-800) by the mean of the isosteric enthalpy of adsorption measurements.

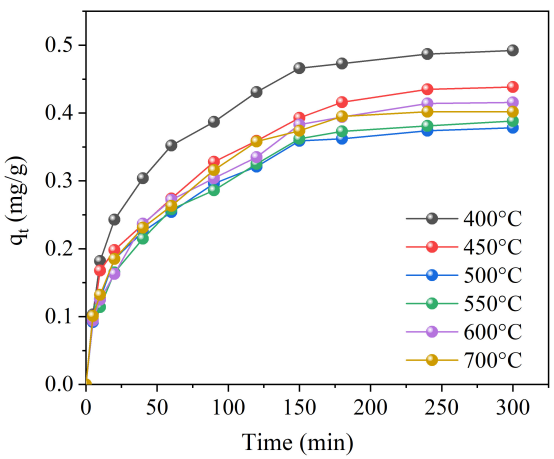

FIGURE 2 | Adsorption capacity at different calcined temperatures.

This was because the pore volume and Brunauer–Emmett–Teller (BET) surface area reached maximum at some temperature and decreased further with the increase of calcined temperature (Kar and Equeenuddin, 2019). The organic compounds presenting in biochar or clay would condense on the surface of the particles, and clog the pores to decrease specific surface area after cooling with the increase of calcined temperature (Atkinson et al., 2010). Also, four forms of water existed in clay minerals (i.e., surface adsorbed water, pore adsorbed water, crystalline water combined with octahedral cations at the edge of pore, and cationic structural water combined with octahedral layer), and high temperature led to the adsorbed water, pore water, and bound water in the material lost when the temperature was less than 600°C, and the carbon in biochar and clay was oxidized. Meanwhile, the decomposition of $NaHCO_3$ increased the pores and adsorption in the green body. The decrease of adsorption capacity from 500°C might be due to the fission of C400 biochar fired at 400°C with the temperature rising to 500°C, and the forming of ash adsorbed in the pores of BCCP and reduced its adsorption performance for NH_4^+-N. When the temperature exceeded 600°C, the water in BCCP evaporated and decomposed violently, and the pore structure was deformed, the porosity decreased, and the adsorption capacity decreased.

Many materials were reported to adsorb NH_4^+-N, such as slag, biochar, and coal slag balls. The NH_4^+-N adsorption behavior of slag was found in either neutral or alkaline conditions with 3.1 mg g^{-1} sorption capacity (Zhang et al., 2013). Vu et al. (2017) prepared biochar using corncob and the highest adsorption capacity was 22.6 mg g^{-1}. However, Kong et al. (2021) reported that the biochar prepared from distilled spirit achieved lees adsorption capacity (5.92 mg g^{-1}). Wang et al. (2016) prepared coal slag balls using modified coal slag and organic binder (PVA) and the NH_4^+-N adsorption capacity was only 0.09 mg g^{-1}. The higher adsorption capacity of biochar depends on the large specific surface area and abundant adsorption sites (Li et al., 2018, 2019), and composition was also a key factor affecting the adsorption capacity. In this study, the high proportion of inorganic clay in BCCP resulted in small adsorption capacity.

Adsorption Kinetics and Isotherm

Adsorption kinetics could be fitted by first-order kinetic model, second-order kinetic model, and intraparticle model, and all of them could well fit the NH_4^+-N adsorption process by BCCPs with different calcined temperature (**Table 3**). Comparing with first-order kinetic and intraparticle diffusion models, the second-order kinetic model was more suitable for describing the NH_4^+-N adsorption process by BCCPs, which was reflected by chemical adsorption processes including ion exchange among chemical bonds and adsorption process. Si–O–Si, –OH functional group on BCCP was involved in the reaction between chemical bonds during NH_4^+-N adsorption process (**Figure 3**). Yan et al. (2018)

TABLE 3 | The adsorption kinetic parameters of BCCP under different calcined temperatures.

		Pseudo-first-order			Pseudo-second-order			Intraparticle diffusion	
T	q_e	K_1	q_{eq}	R^2	K_2	q_{eq}	R^2	k_p	R^2
(°C)	(mg g^{-1})	(min^{-1})	(mg g^{-1})		[g (mg min)$^{-1}$]	(mg g^{-1})		[g (mg $min^{0.5}$)$^{-1}$]	
400	0.492	0.031	0.462	0.925	0.077	0.525	0.980	0.025	0.900
450	0.438	0.024	0.409	0.871	0.070	0.468	0.940	0.023	0.949
500	0.378	0.028	0.356	0.908	0.092	0.405	0.968	0.019	0.923
550	0.388	0.023	0.369	0.923	0.069	0.428	0.967	0.021	0.939
600	0.416	0.022	0.395	0.926	0.061	0.460	0.970	0.023	0.946
700	0.402	0.025	0.386	0.914	0.075	0.442	0.964	0.021	0.926

used porous diatomite microsphere to adsorb methylene blue and also found that the adsorption process followed the pseudo-second-order kinetic model.

The adsorption equilibrium isotherm could reflect the distribution of adsorbate molecules in liquid and solid phases under an equilibrium state (Huang et al., 2020). Both Langmuir isotherm and Freundlich isotherm models could better fit NH_4^+-N adsorption by BCCP prepared with different temperatures (**Table 4**). However, Freundlich model with $R^2 = 0.941 \sim 0.988$ was more suitable than Langmuir model ($R^2 = 0.880 \sim 0.946$), and the conclusion was coincident with Yan et al. (2018). Adsorption site energy distribution characteristic and curvature in the isotherm could be responded by n in Freundlich model (Huang et al., 2020). The value of n was between 1 and 10 in this study, which proved that all adsorption processes of BCCPs with different calcined temperatures were preferential adsorption.

Fourier-Transform Infrared Spectroscopy Spectra of Biochar/Clay Composite Particles Under Different Temperatures

The FTIR is an essential technique to qualitatively determine characteristic functional groups of the adsorbents (**Figure 3**).

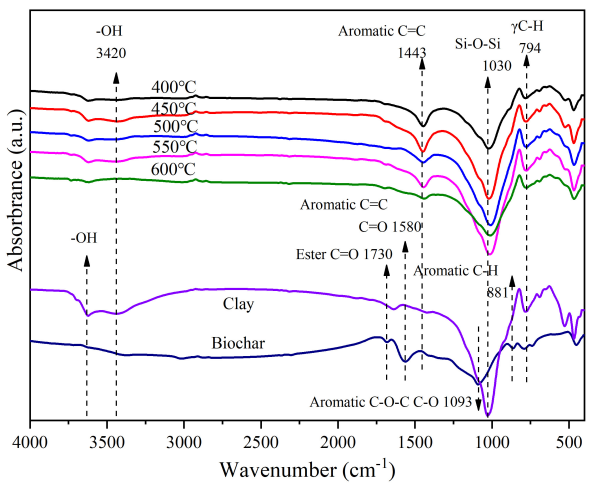

FIGURE 3 | FTIR of raw materials and biochar/clay at different calcined temperatures.

The peak of IR curved at 1,030 cm^{-1} exhibited the introducing of Si–O–Si bonds on the BCCPs (Liu et al., 2012). The bands appearing below 1,100 cm^{-1} might be attributed to Si–O stretching, Si–O–Si bending, Si–O–Al bending, and Si–O–Mg bending vibrations (Chen et al., 2017). For the otherwise typical bands, the intensity of the OH stretch at approximately 3,420 cm^{-1} in the spectrum of clay was considerably larger than in the FTIR spectrum of the BCCP. The intensity of the CO_3^{2-} stretch at approximately 1,440 cm^{-1} in the spectrum of BCCPs appeared depending on the addition of $NaHCO_3$.

Ammonia Nitrogen Degradation Performance by Immobilizing *Ochrobactrum* sp. on Biochar/Clay Composite Particle

Comparison of Immobilization Methods for Ammonia Nitrogen Degradation

BCCP, as a carrier for microbial immobilization, is an effective method to ensure that the efficient flora continue its degradation efficiency in natural water and avoid the risk of free bacteria being dispersed to reduce its pollutant degradation performance (Huang et al., 2020). For maintaining its degradation efficiency, immobilization method becomes the main control factor restricting pollutant transformation in microbial immobilization process. In this study, immobilization method was studied first and the results are shown in **Figure 4A**. The immobilization

TABLE 4 | The Langmuir and Freundlich adsorption isotherm constant of BCCP under different calcined temperatures.

T (°C)	Langmuir isotherm constants			Freundlich isotherm constants		
	q_m	K_L	R^2	1/n	KF	R^2
	(mg g^{-1})	(L mg^{-1})			(mg g^{-1}) (L mg^{-1})^n	
400	0.946	0.029	0.895	0.303	0.155	0.988
450	0.907	0.031	0.910	0.304	0.149	0.984
500	0.900	0.027	0.934	0.319	0.132	0.980
550	0.737	0.026	0.880	0.320	0.107	0.975
600	0.891	0.012	0.946	0.394	0.072	0.956
700	0.854	0.015	0.945	0.376	0.080	0.941

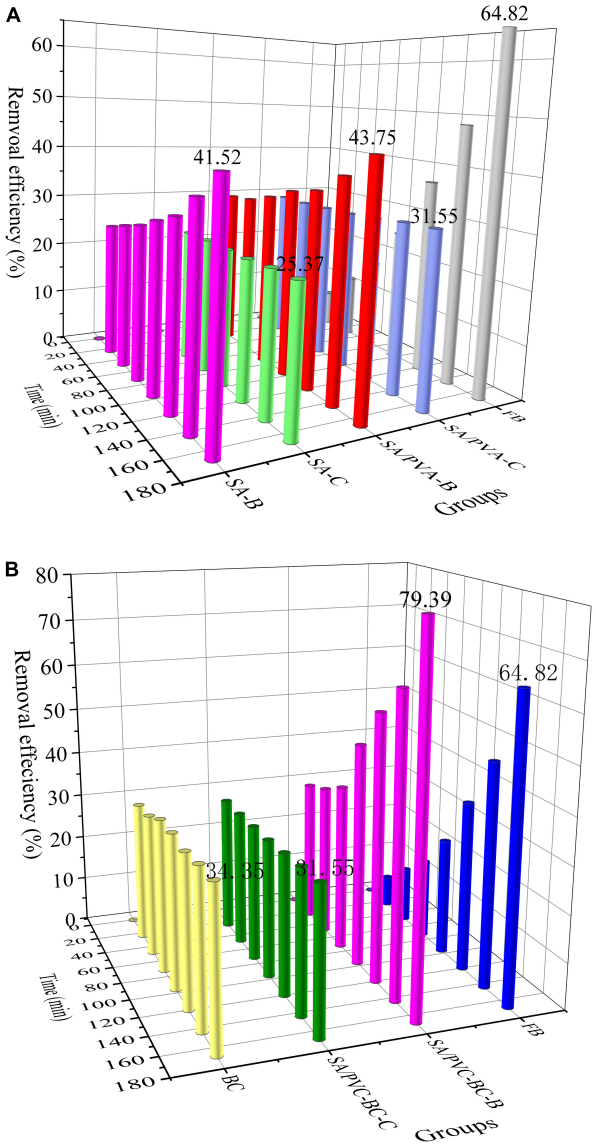

FIGURE 4 | NH_4^+-N removal efficiency by immobilized *Ochrobactrum* sp. **(A)** Comparison of immobilization methods and **(B)** NH_4^+-N removal efficiency by immobilization of *Ochrobactrum* sp. on BCCP. FB, free *Ochrobactrum* sp. without any immobilization methods; SA-B, SA as base material to immobilize *Ochrobactrum* sp.; SA-C, SA as control group without adding *Ochrobactrum* sp.; SA/PVA-B, SA and PVA as base material to immobilize *Ochrobactrum* sp.; SA/PVA-C, SA and PVA as control group without adding *Ochrobactrum* sp.; BC, BCCP alone for adsorption as control group.

of *Ochrobactrum* sp. exhibited preferable nitrogen removal capacities when ammonium chloride was used as the sole nitrogen source. During the initial stage of the experiment (the first 24 h), the gel particles (SA-C and SA/PVA-C groups) adsorbed NH_4^+-N from solution with high efficiency and their adsorption efficiencies were 22.59 and 29.59%, respectively, which were 10∼19% higher than that of the conclusion of Yan et al. (2020). Compared with two immobilization methods, on the contrary, the biodegradation performance of free *Ochrobactrum* sp. (FB group) at initial stage was very low (only 6.87% NH_4^+-N was transformed in 24 h) and NH_4^+-N removal efficiency reached 64.82% after 168 h. However, the value was 41.52 and 43.75% in SA-B and SA/PVA-B group, respectively, and they did not beat the FB group. Although the removal efficiency decreased, it could also be concluded that SA/PVA as immobilized material was more appropriate.

The fact that more nitrogen source and oxygen were obtained by free bacteria than immobilized bacteria prolonged the removal time by gel particle–immobilized bacteria (Yan et al., 2020). However, gel particles could provide stable micropores and protect cells from environmental changes and toxic substances (Hsieh et al., 2008; Hou et al., 2013). Zhang et al. (2021) prepared magnetic PVA–SA–diatomite composite carriers for immobilized microorganism and the highest NH_4^+-N removal rate reached 72.5% at 12 h. It was found that the adsorptions of NH_4^+-N by non-magnetic ingredients and Fe_3O_4 contributed 21.2 and 25.5%, respectively, and microorganism metabolism contributed 53.2%. Immobilized degrading bacteria in PVA–SA hydrogel bead was also reported to remove polycyclic aromatic hydrocarbons (PAHs) and the removal efficiency was around 77% in 96 h (Chen et al., 2021). Liu et al. (2019) investigated the effect of PVA–SA–cell cryogel bead–immobilized *Bacillus* sp. on the degradation of phenanthrene. The results indicated that the use of gel beads increased the number of adsorption sites to accelerate phenanthrene degradation.

The Improvement of Ammonia Nitrogen Degradation With Biochar/Clay Composite Particle as Carrier

On the basis of optimizing the immobilization method, BCCP was proposed as a carrier for *Ochrobactrum* sp. immobilization and the NH_4^+-N removal efficiency is demonstrated in **Figure 4B**. The strong adsorption of BCCP and gel made NH_4^+-N removal rate reach a high value on the first day. The efficiency of BC group (BCCP alone for adsorption as control group, 30.95%) was higher than that of SA/PVA-C group (29.94%), which reflected that the adsorption performance of gel particle was lower than BCCP and gel hindered the adsorption process of BCCP. Until 168 h, the removal efficiency was 34.35 and 31.55%, respectively, and little change was discovered during the process. On the contrary, the degradation efficiency of free *Ochrobactrum* sp. was dilatory and only 6.87% was achieved at the first 24 h, and increased to 84.82% at 168 h. This phenomenon reflected that biodegradation played its advantages. For SA/PVA-BC-B group, the degradation efficiency of NH_4^+-N kept higher than free *Ochrobactrum* sp. during the reaction process and it was up to 79.39% at 168 h, which exceeded 14.57% than free *Ochrobactrum* sp. group.

Compared with SA/PVA for microbial immobilization without adding BCCP, the results showed that BCCP as carrier to immobilize *Ochrobactrum* sp. could improve its degradation efficiency for NH_4^+-N. Because the porous structure of BCCP provided a larger surface area and a greater number of holes, it could store more substrate and promote microbial growth. The porous structure of BCCPs provides larger specific surface area and more pores, and can store more matrix and promote microbial growth (Chen et al., 2016).

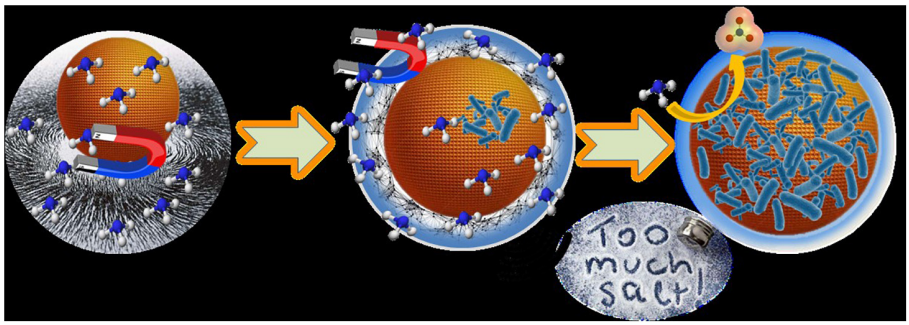

FIGURE 5 | NH_4^+-N removal mechanism by immobilization of *Ochrobactrum* sp. on BCCP.

Ammonia Nitrogen Degradation Mechanism of Immobilizing *Ochrobactrum* sp. With Biochar/Clay Composite Particle

Based on the aforementioned research results, the NH_4^+-N degradation mechanism of immobilizing *Ochrobactrum* sp. with BCCP is demonstrated in **Figure 5**. The potential mechanisms were summarized as follows: the physical adsorption of gel and BCCP promoted NH_4^+-N accumulation rapidly on the surface of BCCP, and provided more appropriate condition for microbial degradation. However, the gel covering on BCCP had a certain resistance for BCCP adsorption. Besides, the *Ochrobactrum* sp. embedded in gel could degrade the high concentration of NH_4^+-N adsorbed on BCCP surface. The porosity of BCCP provides a necessary place for *Ochrobactrum* sp. growth and reproduction, and the adsorption driving force from BCCP promoted the biotransformation of *Ochrobactrum* sp.

Effect of Salinity and Temperature on Nitrogen Removal

Effect of Salinity

Microbial immobilization can resist the adverse environment. Salinity, as an important factor, affected the growth of microorganisms and osmotic pressure of cell membrane. In high-salinity environment, the growth of microorganisms was inhibited (Wang et al., 2017). The effect results of salinity on NH_4^+-N degradation are demonstrated in **Figure 6A**. For low salinity (lower than 5‰), free *Ochrobactrum* sp. group kept high NH_4^+-N removal efficiency (89.37–90.43%) and the degradation performance decreased to 36.24% when the salinity was up to 35‰. The phenomenon reflected that the nitrification process of *Ochrobactrum* sp. was inhabited under high salinity condition. However, the NH_4^+-N degradation efficiency was 69.32∼72.31% in 0 and 5‰ experiment groups, and the immobilization with BCCP produced a marked enhancement performance that displayed 12.47% higher than free *Ochrobactrum* sp. when the salinity increased to 35‰. Gao et al. (2020) found that immobilized materials owned a protective effect on bacteria in environments with high salinity and bacterial growth was inhibited when the salinity was higher than 15‰. Bacteria needed to obtain additional energy from the substrate to maintain cell activity in a high-salinity environment, and they could gradually adapt to high salinity environments over time (Moussa et al., 2005; Ge et al., 2019).

Effect of Temperature

Temperature is another key factor affecting microbial growth and enzyme activity, and the low temperature resistance for

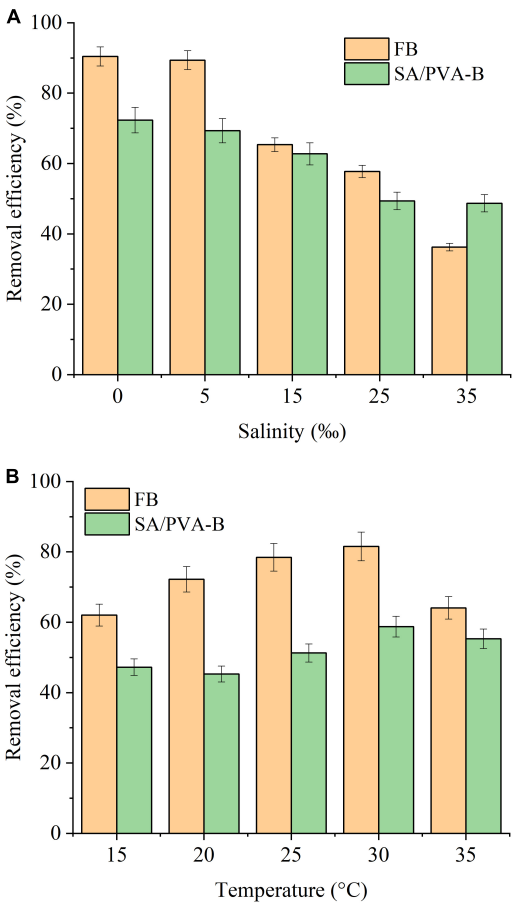

FIGURE 6 | Effects of **(A)** salinity and **(B)** temperature on different immobilized biomaterials. FB, free *Ochrobactrum* sp. without any immobilization methods; SA/PVA-B, SA and PVA as base material to immobilize *Ochrobactrum* sp.

immobilized microorganisms is shown in **Figure 6B**. The NH_4^+-N removal efficiency of free or immobilized *Ochrobactrum* sp. groups increased with the temperature increasing from 15 to 30°C, while the efficiency decreased rapidly at 35°C. Compared with free bacteria group, microbial immobilization did not show its advantages, and its degradation efficiency was inferior to free *Ochrobactrum* sp. under different temperature conditions. For free bacteria group, 81% degradation efficiency was achieved at 30°C, which was 20% more than immobilized *Ochrobactrum* sp. group. For AOB, the optimal temperature is 30°C and bacteria grow perfectly at this temperature (Huang et al., 2017). When the temperature was lower than the optimal temperature, it affected the enzymatic reaction of cells and limited the growth rate of bacteria (Serra-Maia et al., 2016; Binnal and Babu, 2017; Huang et al., 2017; Manhaeghe et al., 2019). On the contrary, higher temperature could inactivate certain proteins in cell, reduced the activity of the microorganism, and even led to cell death (Ras et al., 2013; Serra-Maia et al., 2016; Nwoba et al., 2019). In this study, immobilized *Ochrobactrum* sp. did not play an effective role in resisting low temperature, but protected the *Ochrobactrum* sp. from the changes in salinity. The reason might be that as SA and PVA are the embedding materials of immobilized *Ochrobactrum* sp., the dense protective layer formed by them could buffer the salt concentration of microbial layer on the surface of BCCP, but could not block the impact of low temperature.

CONCLUSION

The optimum calcined parameters of CBBP were calcined temperature 400°C, heating rate 20°C min^{-1}, and holding time 2 h, and the composite particle owned better adsorption performance with 38.75% NH_4^+-N removal efficiency and 0.492 mg g^{-1} adsorption capacity. SA/PVA was more suitable as embedding material and jointed with BCCP (carrier) adsorbing NH_4^+-N, which was then degraded by *Ochrobactrum* sp. with the degradation efficiency of 79.39% at 168 h. Immobilizing *Ochrobactrum* sp. could protect the strain from high salt concentration to achieve the exceeding degradation efficiency than free bacteria; however, it could not block the impact of low temperature.

DATA AVAILABILITY STATEMENT

The original contributions presented in the study are included in the article/supplementary material, further inquiries can be directed to the corresponding author/s.

AUTHOR CONTRIBUTIONS

PS contributed to the data curation, methodology, and writing–original draft, review, and editing. XH designed all the experiments, and revised and examined the manuscript. YX reviewed and edited the manuscript. WLD, JY, and JB contributed to the data curation and investigation. WYD interpreted the data and provided the resources. All authors read and approved the final manuscript.

FUNDING

This work was supported by the Special Project of Guangxi Science and Technology Base and Talent (GUIKE AD20297065), and the National Natural Science Foundation of China (U20A20103).

REFERENCES

Atcharaporn, Y., Pinit, K., Nichada, J., Jitrin, C., Nontipa, S., and Andrew, J. (2020). Simultaneous manganese adsorption and biotransformation by *Streptomyces violarus strain* SBP_1 cell-immobilized biochar. *Sci. Total. Environ.* 713:136708. doi: 10.1016/j.scitotenv.2020.136708

Atkinson, C. J., Fitzgerald, J. D., and Hipps, N. A. (2010). Potential mechanisms for achieving agricultural benefits from biochar application to temperate soils: a review. *Plant. Soil.* 337, 1–18. doi: 10.1007/s11104-010-0464-5

Binnal, P., and Babu, P. N. (2017). Optimization of environmental factors affecting tertiary treatment of municipal wastewater by chlorella protothecoides in a lab scale photobioreactor. *J. Water Process. Eng.* 17, 290–298. doi: 10.1016/j.jwpe.2017.05.003

Chen, L., Chen, X. L., Zhou, C. H., Yang, H. M., Ji, S. F., Tong, D. S., et al. (2017). Environmental-friendly montmorillonite-biochar composites: Facile production and tunable adsorption-release of ammonium and phosphate. *J. Clean. Prod.* 156, 648–659. doi: 10.1016/j.jclepro.2017.04.050

Chen, W., Zhang, H., Zhang, M., Shen, X., Zhang, X., Wu, F., et al. (2021). Removal of PAHs at high concentrations in a soil washing solution containing TX-100 *via* simultaneous sorption and biodegradation processes by immobilized degrading bacteria in PVA-SA hydrogel beads. *J. Hazard. Mater.* 410:124533. doi: 10.1016/j.jhazmat.2020.124533

Chen, X., Wu, L., Liu, F., Luo, P., Zhuang, X., Wu, J., et al. (2018). Performance and mechanisms of thermally treated bentonite for enhanced phosphate removal from wastewater. *Environ. Sci. Pollut. R.* 25, 15980–15989. doi: 10.1007/s11356-018-1794-8

Chen, Y., Yu, B., Lin, J., Naidu, R., and Chen, Z. (2016). Simultaneous adsorption and biodegradation (SAB) of diesel oil using immobilized acinetobacter venetianus on porous material. *Chem. Eng. J.* 289, 463–470. doi: 10.1016/j.cej.2016.01.010

Feng, J., Ding, Y., Guo, Y., Li, X., and Li, W. (2013). Calcination temperature effect on the adsorption and hydrogenated dissociation of CO_2 over the NiO/MgO catalyst. *Fuel.* 109, 110–115. doi: 10.1016/j.fuel.2012.08.028

Feng, J., Liu, Y., Zhang, L., Zhu, J., Chen, J., Xu, H., et al. (2020). Effects of calcination temperature on organic functional groups of TiO_2 and the adsorption performance of the TiO_2 for methylene blue. *Sep. Sci. Technol.* 55, 672–683. doi: 10.1080/01496395.2019.1574822

Gao, Y., Wang, X., Li, J., Lee, C. T., Ong, P. Y., Zhang, Z., et al. (2020). Effect of aquaculture salinity on nitrification and microbial community in moving bed bioreactors with immobilized microbial granules. *Bioresour. Technol.* 297:122427. doi: 10.1016/j.biortech.2019.122427

Ge, C. H., Dong, Y., Li, H., Li, Q., Ni, S. Q., Gao, B., et al. (2019). Nitritation-anammox process-A realizable and satisfactory way to remove nitrogen from high saline wastewater. *Bioresour. Technol.* 275, 86–93. doi: 10.1016/j.biortech.2018.12.032

Hina, K., Hedley, M., Camps-Arbestain, M., and Hanly, J. (2015). Comparison of pine bark, biochar and zeolite as sorbents for NH_4^+-N removal from Water. *Clean Soil Air Water.* 43, 86–91. doi: 10.1002/clen.201300682

Hou, D., Shen, X., Luo, Q., He, Y., Wang, Q., and Liu, Q. (2013). Enhancement of the diesel oil degradation ability of a marine bacterial strain by immobilization on a novel compound carrier material. *Mar. Pollut. Bull.* 67, 146–151. doi: 10.1016/j.marpolbul.2012.11.021

Hsieh, F. M., Huang, C., Lin, T. F., Chen, Y. M., and Lin, J. C. (2008). Study of sodium tripolyphosphate-crosslinked chitosan beads entrapped with *pseudomonas* putida for phenol degradation. *Process. Biochem.* 43, 83–92. doi: 10.1016/j.procbio.2007.10.016

Huang, X., Bai, J., Li, K., Zhao, Y., Tian, W., and Hu, C. (2020). Preparation of clay/biochar composite adsorption particle and performance for ammonia nitrogen removal from aqueous solution. *J. Ocean. U. China.* 19, 729–739. doi: 10.1007/s11802-020-4150-9

Huang, X., Bai, J., Li, K. R., Zhao, Y. G., Tian, W. J., and Dang, J. J. (2017). Characteristics of two novel cold- and salt-tolerant ammonia-oxidizing bacteria from Liaohe Estuarine Wetland. *Mar. Pollut. Bull.* 114, 192–200. doi: 10.1016/j.marpolbul.2016.08.077

Kar, S., and Equeenuddin, S. M. (2019). Adsorption of chromium (VI) onto natural mesoporous goethite: Effect of calcination temperature. *Groundwater Sustain. Devel.* 2019:100250. doi: 10.1016/j.gsd.2019.100250

Kong, W., Zhang, M., Liu, Y., Gou, J., Wei, Q., and Shen, B. (2021). Physico-chemical characteristics and the adsorption of ammonium of biochar pyrolyzed from distilled spirit lees, tobacco fine and Chinese medicine residues. *J. Anal. Appl. Pyrolysis.* 156:105148. doi: 10.1016/j.jaap.2021.105148

Li, R., Wang, J. J., Gaston, L. A., Zhou, B., Li, M., Xiao, R., et al. (2018). An overview of carbothermal synthesis of metal–biochar composites for the removal of oxyanion contaminants from aqueous solution. *Carbon.* 129, 674–687. doi: 10.1016/j.carbon.2017.12.070

Li, S., Harris, S., Anandhi, A., and Chen, G. (2019). Predicting biochar properties and functions based on feedstock and pyrolysis temperature: A review and data syntheses. *J. Clean. Prod.* 215, 890–902. doi: 10.1016/j.jclepro.2019.01.106

Lin, K., Pan, J., Chen, Y., Cheng, R., and Xu, X. (2009). Study the adsorption of phenol from aqueous solution on hydroxyapatite nanopowders. *J. Hazard. Mater.* 161, 231–240. doi: 10.1016/j.jhazmat.2008.03.076

Lin, Q., Ishikawa, T., Akoh, R., Yang, F., and Zhang, S. (2016). Soil salinity reduction by river water irrigation in a reed field: A case study in Shuangtai Estuary Wetland. *Northeast China. Ecol. Eng.* 89, 32–39. doi: 10.1016/j.ecoleng.2016.01.003

Liu, Q., Yao, X., Cheng, H., and Frost, R. L. (2012). An infrared spectroscopic comparison of four chinese palygorskites. *Spectrochim. Acta A.* 96, 784–789. doi: 10.1016/j.saa.2012.07.025

Liu, S.-H., Zeng, Z.-T., Niu, Q.-Y., Xiao, R., Zeng, G.-M., Liu, Y., et al. (2019). Influence of immobilization on phenanthrene degradation by Bacillus sp. *P1 presence Cd (II). Sci. Total. Environ.* 655, 1279–1287. doi: 10.1016/j.scitotenv.2018.11.272

Mahdi, Z., Qiming, J. Y., and El Hanandeh, A. (2018). Removal of lead(II) from aqueous solution using date seed-derived biochar: batch and column studies. *Appl. Water. Sci.* 8:181. doi: 10.1007/s13201-018-0829-0

Mandal, S., and Mayadevi, S. (2008). Adsorption of fluoride ions by Zn-Al layered double hydroxides. *Appl. Clay Sci.* 40, 54–62. doi: 10.1016/j.clay.2007.07.004

Manhaeghe, D., Michels, S., Rousseau, D. P., and Van Hulle, S. W. (2019). A semi-mechanistic model describing the influence of light and temperature on the respiration and photosynthetic growth of Chlorella vulgaris. *Bioresour. Technol.* 274, 361–370. doi: 10.1016/j.biortech.2018.11.097

Moussa, M. S., Hooijmans, C. M., Lubberding, H. J., Gijzen, H. J., and Van Loosdrecht, M. C. M. (2005). Modelling nitrification, heterotrophic growth and predation in activated sludge. *Water Res.* 39, 5080–5098. doi: 10.1016/j.watres.2005.09.038

Nwoba, E. G., Parlevliet, D. A., Laird, D. W., Alameh, K., and Moheimani, N. R. (2019). Moheimani. *Light management technologies for increasing algal photobioreactor efficiency. Algal Res.* 39:101433. doi: 10.1016/j.algal.2019.101433

Ojeda-López, R., Ramos-Sánchez, G., García-Mendoza, C., Cs Azevedo, D., Guzmán-Vargas, A., and Felipe, C. (2021). Effect of calcination temperature and chemical composition of pan-derived carbon microfibers on N_2. *CO_2, and CH_4 adsorption. Materials.* 14:3914. doi: 10.3390/ma14143914

Ras, M., Steyer, J. P., and Bernard, O. (2013). Temperature effect on microalgae: a crucial factor for outdoor production. *Rev. Environ. Sci. Biotechnol.* 12, 153–164. doi: 10.1007/s11157-013-9310-6

Reddy, S., and Osborne, J. W. (2020). Biodegradation and biosorption of reactive red 120 dye by immobilized *pseudomonas* guariconensis: Kinetic and toxicity study. *Water Environ. Res.* 92, 1230–1241. doi: 10.1002/wer.1319

Serra-Maia, R., Bernard, O., Gonçalves, A., Bensalem, S., and Lopes, F. (2016). Influence of temperature on chlorella vulgaris growth and mortality rates in a photobioreactor. *Algal Res.* 18, 352–359. doi: 10.1016/j.algal.2016.06.016

Sun, Q., Hu, X., Zheng, S., Sun, Z., Liu, S., and Li, H. (2015). Influence of calcination temperature on the structural, adsorption and photocatalytic properties of TiO_2 nanoparticles supported on natural zeolite. *Powder Technol.* 274, 88–97. doi: 10.1016/j.powtec.2014.12.052

Vu, T. M., Doan, D. P., Van, H. T., Nguyen, T. V., Vigneswaran, S., and Ngo, H. H. (2017). Removing ammonium from water using modified corncob-biochar. *Sci. Total. Environ.* 579, 612–619. doi: 10.1016/j.scitotenv.2016.11.050

Wang, Y., Chen, J., Zhou, S., Wang, X., Chen, Y., Lin, X., et al. (2017). 16S rRNA gene high-throughput sequencing reveals shift in nitrogen conversion related microorganisms in a CANON system in response to salt stress. *Chem. Eng. J.* 317, 512–521. doi: 10.1016/j.cej.2017.02.096

Wang, Y., Tian, W., Wu, C., Bai, J., and Zhao, Y. (2016). Synthesis of coal cinder balls and its application for CODCr and ammonia nitrogen removal from aqueous solution. *Desalin. Water. Treat.* 57, 21781–21793. doi: 10.1080/19443994.2015.1130653

Yakkala, K., Yu, M. R., Roh, H., Yang, J. K., and Chang, Y. Y. (2013). Buffalo weed (Ambrosia trifida L. var. trifida) biochar for cadmium (II) and lead (II) adsorption in single and mixed system. *Desalin. Water. Treat.* 51, 7732–7745. doi: 10.1080/19443994.2013.792546

Yan, H., Han, Z., Zhao, H., Pan, J., Zhao, Y., Tucker, M. E., et al. (2020). The bio-precipitation of calcium and magnesium ions by free and immobilized *Lysinibacillus fusiformis* DB1-3 in the wastewater. *J. Clean. Prod.* 252:119826. doi: 10.1016/j.jclepro.2019.119826

Yan, S., Huo, W., Yang, J., Zhang, X., Wang, Q., Wang, L., et al. (2018). Green synthesis and influence of calcined temperature on the formation of novel porous diatomite microspheres for efficient adsorption of dyes. *Powder Technol.* 2018, 260–269. doi: 10.1016/j.powtec.2018.01.090

Yang, Y., and Chow, C. L. (2019). Tal cracking prediction of frameless glazing exposed to radiant fluxes increasing with height. *Fire. Mater.* 43, 747–756. doi: 10.1002/fam.2734

Zhang, L., Zhang, H., Guo, W., and Tian, Y. (2013). Sorption characteristics and mechanisms of ammonium by coal by-products: slag, honeycomb-cinder and coal gangue. *Int. J. Environ. Sci. Technol.* 10, 1309–1318. doi: 10.1007/s13762-012-0168-x

Zhang, Y., Yu, Z., Hu, Y., Song, C., Li, F., He, W., et al. (2021). Immobilization of nitrifying bacteria in magnetic PVA–SA-diatomite carrier for efficient removal of NH4+-N from effluents. *Environ. Technol. Inno.* 22:101407. doi: 10.1016/j.eti.2021.101407

Conflict of Interest: The authors declare that the research was conducted in the absence of any commercial or financial relationships that could be construed as a potential conflict of interest.

Publisher's Note: All claims expressed in this article are solely those of the authors and do not necessarily represent those of their affiliated organizations, or those of the publisher, the editors and the reviewers. Any product that may be evaluated in this article, or claim that may be made by its manufacturer, is not guaranteed or endorsed by the publisher.

frontiers in Microbiology

ORIGINAL RESEARCH
published: 14 March 2022
doi: 10.3389/fmicb.2022.846228

Biochar-Mediated Degradation of Roxarsone by *Shewanella oneidensis* MR-1

Li Wengang[1,2,3†], *Chen Fang*[2†], *Zhong Rong*[1] *and Chen Cuihong*[1*]

[1] Key Laboratory of Pollution Processes and Environmental Criteria (Ministry of Education)/Tianjin Engineering Center of Environmental Diagnosis and Contamination Remediation, College of Environmental Science and Engineering, Nankai University, Tianjin, China, [2] School of Resources and Materials, Northeastern University at Qinhuangdao, Qinhuangdao, China, [3] Tangshan Ecological Environmental Bureau, Tangshan, China

It is widely believed that biochar plays an essential role in sequestrating pollutants. The impacts of biochar on microbial growth, and consequently on the environmental fate of pollutants, however, remains poorly understood. In this study, wheat-straw-derived biochar was used to investigate how biochar amendment affected *Shewanella oneidensis* MR-1 growth and roxarsone transformation in water under anaerobic conditions. Three biochar with different physicochemical properties were used to mediate the roxarsone degradation. The results showed that the degradation rate of roxarsone could be accelerated by the increase of biochar pyrolysis temperature. From the characterization of biochar, the total specific surface area, micropore surface area and micropore volume of biochar increase, but the average pore diameter decreases as the pyrolysis temperature increases. Through infrared spectroscopy analysis, it was found that as the pyrolysis temperature increases, the degree of condensation of biochar increases, thereby increasing the pollutant removal rate. From the changes of the relative concentration of MR-1 and its secreted extracellular polymer content, the growth promotion ability of biochar also increases as the pyrolysis temperature increases. These results suggest that wheat-straw-derived biochar may be an important agent for activating microbial growth and can be used to accelerate the transformation of roxarsone, which could be a novel strategy for roxarsone remediation.

Keywords: kinetics, biochar, *Shewanella oneidensis* MR-1, roxarsone, transformation

OPEN ACCESS

Edited by:
Tian Li,
Nankai University, China

Reviewed by:
Jing Lu,
North University of China, China
Gao Yang,
Changsha University of Science and Technology, China

***Correspondence:**
Chen Cuihong
chencuih@nankai.edu.cn

†These authors share first authorship

Specialty section:
This article was submitted to Microbiotechnology, a section of the journal Frontiers in Microbiology

Received: *30 December 2021*
Accepted: *08 February 2022*
Published: *14 March 2022*

Citation:
Wengang L, Fang C, Rong Z and Cuihong C (2022) Biochar-Mediated Degradation of Roxarsone by Shewanella oneidensis MR-1. Front. Microbiol. 13:846228. doi: 10.3389/fmicb.2022.846228

INTRODUCTION

As human demand for meat continues to increase, the poultry industry has gradually become one of the fastest-growing agricultural sectors in decades. Through the extensive application of veterinary drugs and feed additives, production efficiency and product quality have been improved (Sarmah et al., 2006). Roxarsone (3-nitro-4-hydroxyphenylarsine) was first produced 70 years ago, which was used as feed additives to control coccidial intestinal parasites and prevent parasitic infections and improve the pigmentation of meat (Silbergeld and Nachman, 2008; Nachman et al., 2013). The use of roxarsone in the poultry industry has been banned in most developed countries, including China, but long-term extensive usage has resulted in a massive accumulation of roxarsone in the environment (Huang et al., 2019; Wang G. et al., 2020). Roxarsone is barely decomposed within the animal body, and is usually excreted as its initial form along with the animal

waste (Makris et al., 2008). Along with the storage or field application of animal waste or direct discharge into the environment, roxarsone can easily enter into the surface- or ground-water and soil due to its water-soluble capacity (Silbergeld and Nachman, 2008; Huang et al., 2019). Roxarsone can be oxidized, reduced, methylated or demethylated through numerous physical, chemical and biological interactions, and eventually produce a variety of arsenic compounds (Garbarino et al., 2003; Chen et al., 2016; Han et al., 2017; Oyewumi and Schreiber, 2017).

Shewanella species are widely distributed in freshwater, marine, soil and sedimentary, environments (Heidelberg et al., 2002; Harris et al., 2010). Many strains of *Shewanella* species can couple anaerobic growth with the respiratory reduction of minerals and other high-redox potential contaminants (Aulenta et al., 2013; Shi et al., 2016; Wang H. F. et al., 2020). To accomplish this coupling, *Shewanella* strains usually metabolize substrates to generate electrons and transport them to the outer surface of the membrane, where contaminants are reduced directly or indirectly (Kato et al., 2012; Shi et al., 2016; Wang H. F. et al., 2020). Some organic matter, such as biochar and humic substances, can mediate electron transfer at the interface between microbes and acceptors, thus accelerating the biochemical transformation (Klüpfel et al., 2014b; Pignatello et al., 2017; Stern et al., 2018; Wang H. F. et al., 2020).

Natural organic matter (NOM)-mediated microbial redox reactions are important for the biogeochemical cycles of carbon and redox-active compounds. Biochar, a significant fraction of natural organic matter, is produced by incomplete combustion and usually has the advantages of eco-friendly properties, reusability and cost-effectiveness (Kappler et al., 2014; Hemavathy et al., 2020; Gayathri et al., 2021). Biochar usually have a highly porous structure, multiple surface functional groups, and condensed aromatic structures, these properties confer biochar with great potential for many environmental and ecological application (Ahmad et al., 2014; Xu et al., 2019; Wang H. F. et al., 2020). Biochar not only could accept or release electrons (Klüpfel et al., 2014a). It also could act as an electron mediator (i.e., electron shuttle) to accelerate redox reactions (Saquing et al., 2016). Previous studies have shown that biochar can facilitate the biochemical degradation of toxic organic compounds (Zhang et al., 2019; Wang H. F. et al., 2020). The surface functional groups and condensed aromatic structures constitute the electroactive components in biochar (Sun et al., 2017). However, limited knowledge is available for the role of biochar in the redox reaction for roxarsone.

Therefore, the central goal of this work is to compare roxarsone removal by *Shewanella oneidensis* MR-1 in the presence and absence of biochar, and to elucidate the influence of biochar on the biotransformation of roxarsone.

MATERIALS AND METHODS

Materials

The raw material for preparing biochar in this experiment was wheat straw (from Hebei Province, China). The preparation method of biochar adopts the method in references (Zuriaga-Agustí et al., 2013; Lyu et al., 2016). Briefly, the dried wheat straw powder was heated at 300, 500, and 600°C for 2 h in a stainless-steel reactor in a Muffle Furnace under the O_2-limited condition. After it was cooled to room temperature, and then passed through a 100-mesh sieve and washed with deionized water until the biochar was neutral. Keep it in a sealed bag and place it in a desiccator for later use. Biochar prepared at 300, 500, and 600°C were termed 300BC, 500BC and 600BC.

Shewanella oneidensis MR-1 was cultivated in LB medium at 30°C. After incubation for 16 h, 50 mL of the culture was centrifuged (6,000 *g* for 5 min), and the cell pellet was washed twice with anoxic bicarbonate buffer (*pH* 7) and suspended in the same buffer.

Methods

Microbial degradation experiments were conducted in 50 mL anaerobic bottles. The experiments were designed into 5 groups, divided into biochar combined with MR-1 group (called 300BC biotic, 500BC biotic, and 600BC biotic), MR-1 alone group (called only MR-1), and blank group. Each group has three parallel samples. The initial concentration of roxarsone was 1.0 mmol/L, the initial concentration of MR-1 (OD600) was 0.8, and 5 mmol/L of sodium lactate was added as an exogenous carbon source. The N_2/CO_2 (80:20) mixed gas was purged into the butyl-stopper glass bottles for 15 min to remove oxygen. The anaerobic flask was placed in a constant temperature shaker under dark conditions. The parameters of the shaker were set to 100 rpm and 30°C. When the reaction time was 12, 24, 36, 48, 84, 132, 168, and 192 h, the concentration of roxarsone in the sample was analyzed. When the reaction time was 0, 48, 72, and 100 h, the extracellular polymer was extracted, and the protein and polysaccharide content were determined.

In this experiment, the concentration of roxarsone was determined by a high-performance liquid chromatograph (Flexar, PerkinElmer, United States), and the wavelength was 264 nm. The chromatographic column used in the determination was a C18 column (4.6 mm × 150 mm). The mobile phase was composed of 0.05 mol/L potassium dihydrogen phosphate (KH_2PO_4), methanol, and 10% glacial acetic acid (V/V). The volume ratio was 95:5:0.1, and the mobile phase flow rate was set to 1.0 mL/min. The column temperature was 30°C.

Extracellular polymeric substances (EPS) was extracted by an improved cation exchange resin method (Liang Z. W. et al., 2010; Zuriaga-Agustí et al., 2013). 10 mL of bacterial suspension was placed in a centrifuge tube, centrifuged at 2,000 *g* for 15 min at 4°C, and the supernatant was discarded. Resuspend the pellet with 10 mL PBS buffer. Add 1 g of sodium type 732 type cation exchange resin (20–50 mesh) to the suspension, which was shaken at 40 rpm for 6 h at 4°C, and then centrifuged for 15 min with a high-speed centrifuge. The centrifuge parameters were set to 4°C and 10,000 *g*. After centrifugation, the supernatant was filtered with a 0.22-μm polyethersulfone filter, and stored at −20°C for testing. The sulfuric acid-anthrone method was used to determine the polysaccharides in EPS (Yuan et al., 2011). The BCA protein concentration determination kit was used to detect the protein content. To determine the relative concentration of

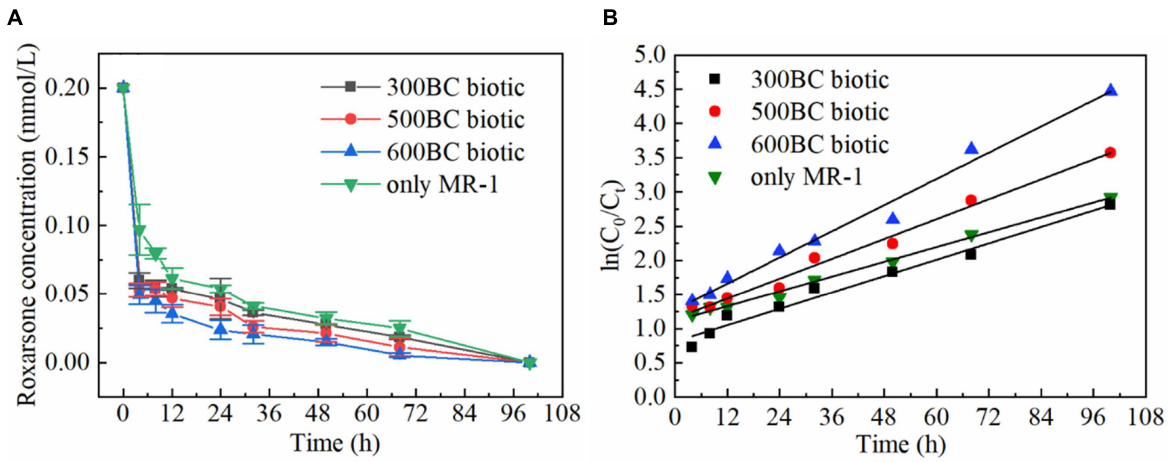

FIGURE 1 | Biotransformation of roxarsone by MR-1 in the presence and absence of biochar. **(A)** The concentration of roxarsone within reaction time. **(B)** The change of $\ln(C_0/C_t)$ with reaction time.

TABLE 1 | Degradation rates of roxarsone by MR-1 in the presence and absence of biochar.

Time/h	300BC biotic	500BC biotic	600BC biotic	only MR-1
4 h	70.04% d	73.53% c	75.29% b	51.61% a
68 h	90.76% b	94.37% c	97.32% d	87.53% a

Different small letters in the same time refer to the difference at significance level $p < 0.05$.

TABLE 2 | Kinetic parameters of roxarsone removal by MR-1 in the presence and absence of biochar.

	Rate constant K (h^{-1})	R^2
Only MR-1	0.017 ± 0.0006	0.98
300BC biotic	0.020 ± 0.0011	0.99
500BC biotic	0.024 ± 0.0016	0.98
600BC biotic	0.032 ± 0.0012	0.99

MR-1 in different groups, 5 mL samples were taken from the treatment groups at 24, 48, and 84 h, the OD600 value was measured with a microplate reader.

The physical and chemical properties of biochar samples (300BC, 500BC, and 600BC) were analyzed by JOEL JSM-7800F field emission scanning electron microscope (FE-SEM), American Mike ASAP 2460 multi-station extended automatic rapid surface area analyzer, the Nicolet iS50 Fourier transform infrared spectrometer. The surface group in biochar samples are analyzed by solid-state ^{13}C nuclear magnetic resonance (NMR) spectroscopy on a 400 MHz NMR spectrometer (Advance III WB 400, Bruker, Germany).

The degradation rates of roxarsone by MR-1 in the presence and absence of biochar were analyzed by one-way analysis of variance (ANOVA) followed by Duncan test using SPSS 27.0 software. The results were considered significant when the *p* value was less than 0.05.

RESULTS AND DISCUSSION

Roxarsone Transformation Kinetics in the Presence of Biochar and MR-1

The biotransformation of roxarsone in the presence and absence of biochar was shown in **Figure 1**. According to the results in **Table 1**, roxarsone was almost completely degraded in all groups within 68 h. It was found that the degradation rates of roxarsone at 68 h were: 600BC biotic > 500BC biotic > 300BC biotic > only MR-1, and the degradation rates were increased by 9.79, 6.84, and 3.23% with the addition of 600BC, 500BC and 300BC. Therefore, biochar had a promoting effect on removing roxarsone by MR-1. The ability of biochar to promote the degradation of roxarsone by MR-1 was followed as: 600BC > 500BC > 300BC. It was found that the change of $\ln(C_0/C_t)$ with time (t) showed a good linear relationship (C_0 is the initial concentration of roxarsone, C_t is the concentration of roxarsone remaining in the reaction when the reaction time is t), in line with the first-order kinetic reaction fitting equation. The kinetic curves of the removal of roxarsone by MR-1 in the presence and absence of biochar were shown in **Figure 1B**. The average rate constant fitted by the first-order kinetic equation was 0.017 h^{-1} in the only MR-1 group, and the removal rates of roxarsone by MR-1 combined with biochar group were greater than that of only MR-1 group. According to the results in **Table 2** the average rate constants in MR-1 combined with 300BC, 500BC, and 600BC groups were 0.020, 0.024, and 0.032 h^{-1}, which showed the order: 600BC biotic > 500BC biotic > 300BC biotic. It can be seen that when the pyrolysis temperature is in the range of 300–600°C, the higher the pyrolysis temperature of biochar, the greater the promotion effect of biochar on the removal of roxarsone by MR-1. Lehmann et al. (2011) summarized a large amount of literature and found that the addition of biochar in most studies can increase the biomass of microorganisms. On the other hand, Klüpfel et al. (2014b) found that in the process of biochar combined with MR-1 for oxidation-reduction, the biochar produced at the medium

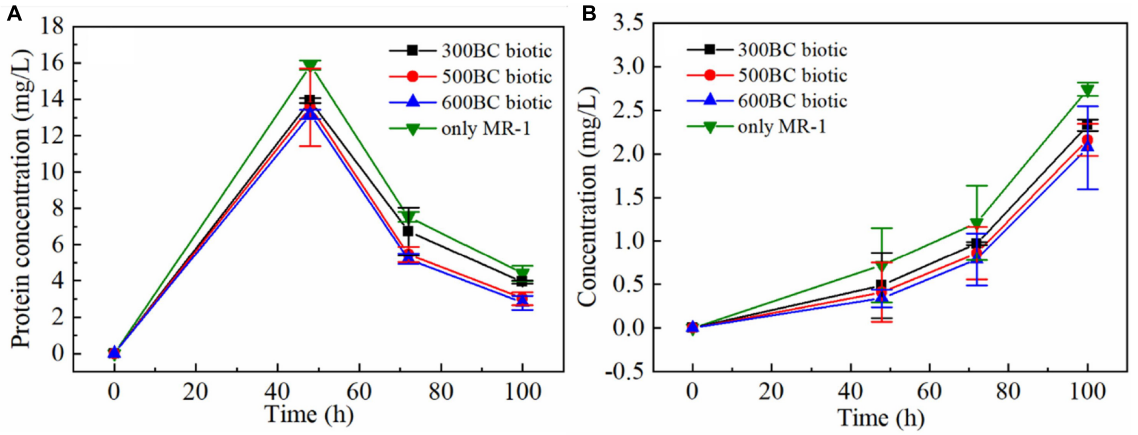

FIGURE 2 | Changes of protein **(A)** and polysaccharides **(B)** of MR-1 in the presence and absence of biochar.

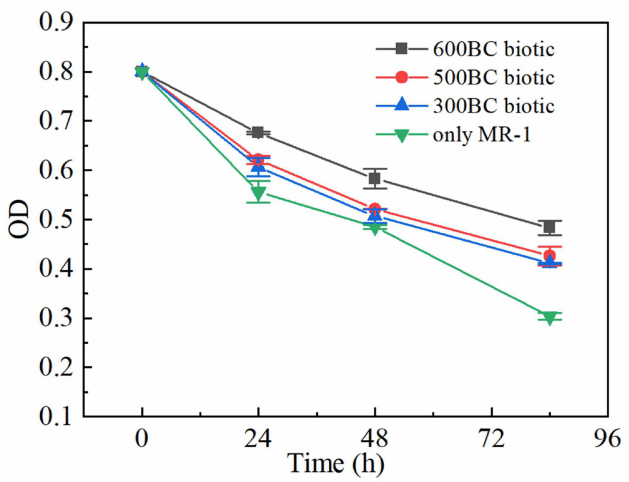

FIGURE 3 | Changes of OD in the presence and absence of biochars.

to high temperature pyrolysis temperature (400∼600°C) showed the highest ability to accept and supply electrons, while the low-temperature pyrolysis temperature (300°C) biochar has the worst effect. Because the pyrolysis temperature of biochar was related to its transfer rate of electrons, it affected the speed of MR-1's reaction to remove roxarsone. Zhang et al. (2019) found that with the increase of pyrolysis temperature, the conversion ability of biochar was gradually changing from the supply of electrons to the dominance of electrons. The surface functional groups and condensed aromatic structure play an important role in the reaction.

Extracellular Polymeric Substances Changes of MR-1 Under Different Biochar

In order to explore the effect of biochar on the secretion of the extracellular polymer by MR-1, the content of protein and polysaccharides at 48, 72, and 100 h in different treatments were measured, as shown in the **Figure 2**. It can be seen that the changing trend of the protein concentration and polysaccharides concentration was the same in the presence and absence of biochar. At the same time, the polysaccharides and protein content in the only MR-1 group was higher than that of biochar combined with MR-1 group. And in the presence of biochar, the polysaccharide and protein content in the 300BC biotic group was the highest, and that in the 600BC biotic group was the lowest. Therefore, the higher the pyrolysis temperature of the biochar, the lower the content of polysaccharides and proteins produced by MR-1 during the reaction. Because the poorer the living environment of MR-1 was, the more extracellular polymers were secreted, MR-1 can adapt to the surrounding environment to ensure survival (Vu et al., 2009). The results showed that MR-1 survives well in the presence of biochar, and the growth environment of 600BC was the best, followed by the growth environment of 500BC, and the growth

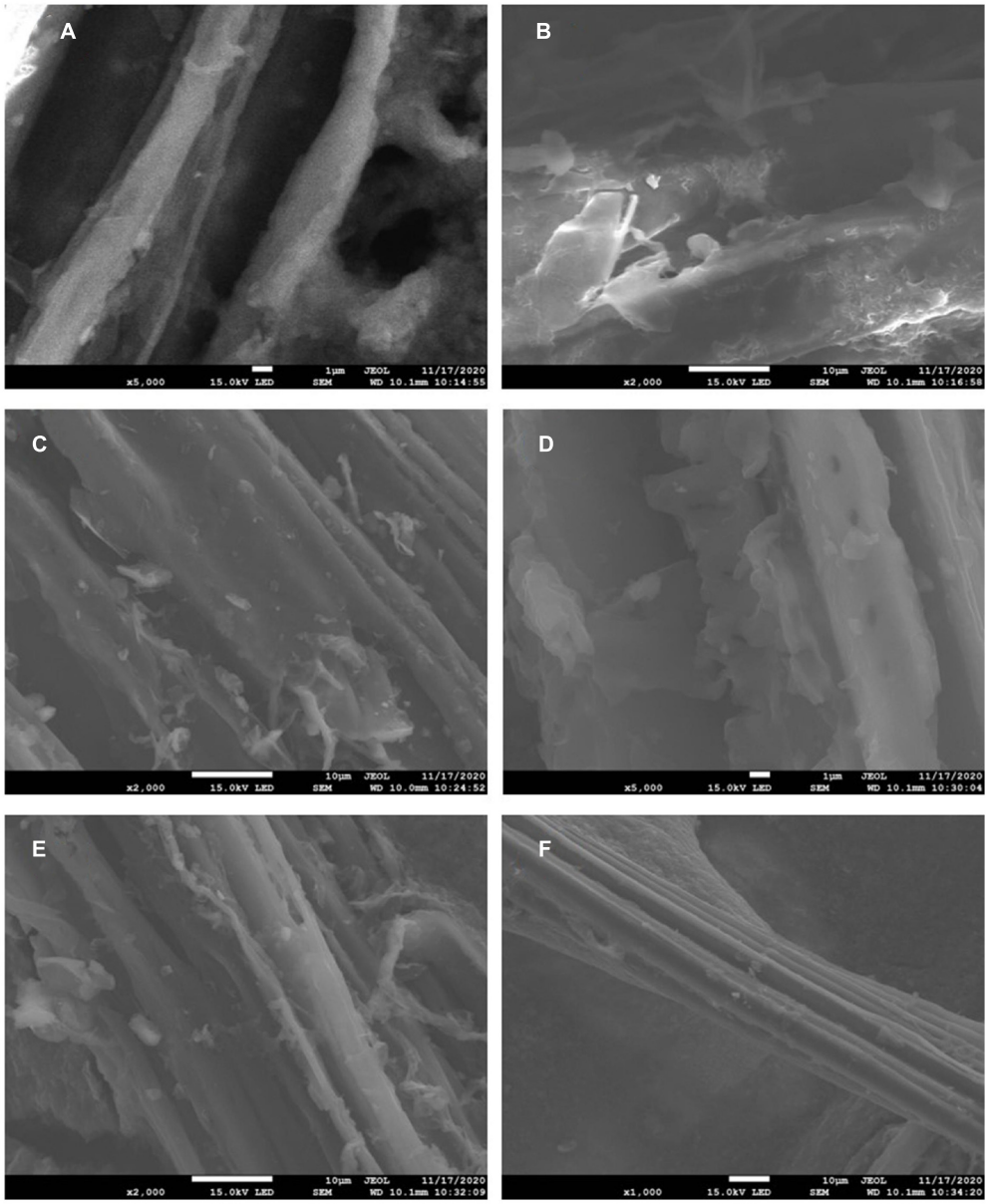

FIGURE 4 | Electron micrographs of biochar at different pyrolysis temperatures before the reaction [panels **(A,B)** are 300BC; panels **(C,D)** are 500BC; panels **(E,F)** are 600BC].

TABLE 3 | Specific surface area, pore volume, and pore diameter of biochar.

Sample	Total specific surface area (m^2/g)	Micropore surface area (m^2/g)	Outer surface area (m^2/g)	Micropore volume (cm^3/g)	BET average pore diameter (nm)
BC300	2.08	1.32	0.76	0.0004	7.22
BC500	41.27	32.99	8.28	0.0132	3.17
BC600	162.04	128.53	33.51	0.0511	2.13

environment of 300BC was the worst. This was because, on the one hand, biochar can provide nutrients for microorganisms; on the other hand, because of its large surface area, porous structure, and strong affinity for microorganisms, biochar can be used as a habitat for microorganisms (Lehmann et al., 2011; Wahla et al., 2020).

The Relative Concentration Changes of MR-1 Under Different Biochar

As shown in **Figure 3**, the OD values in the presence and absence of biochar decreased as the reaction time lasted, which inferred that the MR-1 is in the stationary and decline phase and the proliferation slowed down as the degradation of roxarsone. The OD values in the only MR-1 group decreased fastest. In the presence of biochar, the OD value of MR-1 in the whole reaction process was sorted: 600BC biotic group > 500BC biotic group > 300BC biotic group. Moreover, when the reaction reached 84 h, the OD values in the presence of biochar were much greater than that of only MR-1 group, especially the OD value of the 600BC biotic group was the largest. The living or dead states of MR-1 in the presence and absence of biochar was determined by Live/Dead assay using a laser scanning confocal microscope when the reaction reached 55 h (**Supplementary Figure S1**). In 600BC biotic group, most of the MR-1 exhibit green fluorescence, which indicated that the number of live MR-1 was much larger than the dead MR-1, and the growth activity is the best compared to other groups. The addition of biochar made the bacteria grow better, and the activity was better. The addition of biochar benefited to the MR-1 growth, which was consistent with previous research results. Liang B. Q. et al. (2010) studied the effect of biochar on microorganisms in soil, and found that the biomass of microorganisms in soils with high biochar content was 125% higher than that in adjacent soils with low biochar content.

The Physical and Chemical Properties of Biochar

Microscopic Morphology of Biochar

Figure 4 was a scanning electron micrograph of biochar prepared under the conditions of pyrolysis temperature of 300, 500, and 600°C. It can be seen from the figure that there were wrinkles, micropores, different pore structures and morphologies on the surface of biochar. When the pyrolysis temperature was 300°C, there were fewer particles and massive debris on the surface of biochar. When the pyrolysis temperature rose to 500 and 600°C, cellulose, lignin, and other components in biomass were decomposed gradually with the increase of pyrolysis temperature, and the surface of biochar became more wrinkled at 600°C. Therefore, the pyrolysis temperature had a great influence on the surface microstructure of biochar.

Analysis of Specific Surface Area and Pore Structure

In order to further understand the difference in morphology of biochar at different pyrolysis temperatures, the specific surface area and pore structure of the biochar were analyzed by the BET specific surface area analyzer. The specific surface area, pore volume, and pore size of the biochar at different pyrolysis temperatures were measured, which was shown in **Table 3**. Compared with 300BC, when the pyrolysis temperature was increased to 600°C, the specific surface area of biochar increased significantly. The total specific surface area increased from 2.08 to 162.04 m^2/g. The micropore surface area occupied 79.3% of the total specific surface area, indicating the existence of a large number of internal pores. And the average pore diameter

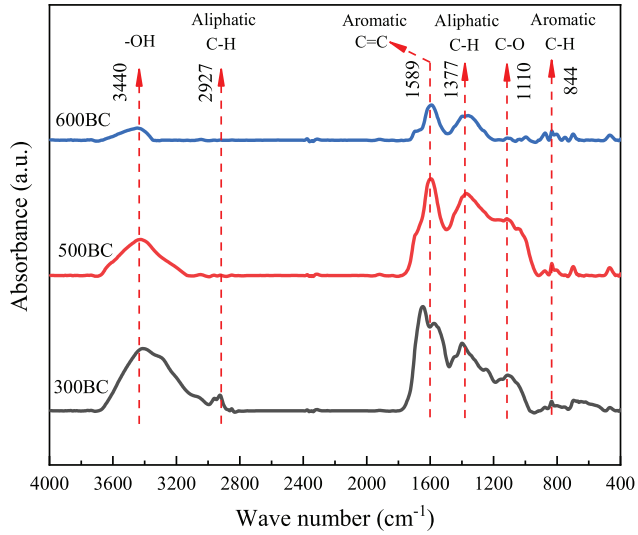

FIGURE 5 | Infrared spectra of biochar prepared at different pyrolysis temperatures.

decreased with the increase of pyrolysis temperature. When the pyrolysis temperature increased from 300 to 500°C, the pore volume of micropores increased significantly, from 0.0004 to 0.0132 cm^3/g, an increase of more than 30 times. In the pyrolysis temperature range of 500–600°C, the specific surface area and pore volume of biochar increased, which may be due to the decomposition of cellulose and fat of wheat straw. Chang et al. (2017) found that the higher the temperature in the biochar preparation process, the larger the internal pore volume. when the pyrolysis temperature rose from 200 to 600°C, the number of micropores in the prepared biochar also increased significantly.

When biochar was applied to the soil, its pore size may have an extremely important effect on the growth of MR-1. Researchers have speculated that both bacteria and fungi can better defend against competitors by exploring the pore environment in biochar. Although there is currently no quantifiable evidence to prove that the pores of biochar have a protective effect on microorganisms, the pore size distribution of biochar and microorganisms, as well as the visually detectable results, provide a basis for this hypothesis. There has been some evidence that pore size has a significant influence on the retention of microorganisms (Saito and Marumoto, 2002; Lehmann et al., 2011).

Infrared Spectroscopy Analysis of Biochar

The Fourier infrared transform spectra of 300BC, 500BC, and 600BC were shown in **Figure 5**, respectively. First, the peak at 3,430 cm^{-1} was considered to be caused by the stretching vibration of OH. The 2,924–2,927 cm^{-1} and 1,377 cm^{-1} represented the aliphatic C-H stretching vibration absorption peaks on the biopolymer (Such as cellulose, hemicellulose, and lignin), 1589 cm^{-1} was aromatic C = C absorption peak, and 1,110 cm^{-1} was the CO stretching vibration absorption peak of hydrocarbons (Schwanninger et al., 2004; Tatzber et al., 2009).

Finally, at 788–881 cm^{-1} was the plane vibration of C-H on aromatic carbon. With the increase of pyrolysis temperature, the aliphatic C and O-containing functional groups in the hemicellulose, cellulose, and lignin in the biomass gradually disappear. The absorption peak of -OH at 3,440 cm^{-1} gradually decreased, and that of C=C and C-H on aromatic carbon increased. Further, the NMR spectroscopy also reveal an enhancement of aromatic C=C and ketone groups (C=O) with increasing pyrolysis temperature (**Supplementary Figure S2**). Both aromatic C=C and C=O are necessary for high-performance electron exchange capacity (Wang H. F. et al., 2020). The temperature was positively related to the aromatic cluster size (Cao et al., 2012). Based on these, it can be inferred that as the degree of condensation of biochar increased, the ability of the electron shuttle may increase, thereby increasing the pollutant removal rate. However, the "mediator mechanism" of biochar need further study.

CONCLUSION

In this paper, roxarsone biotransformation was promoted by the biochar. The higher the pyrolysis temperature of biochar, the higher the biotransformation rate. When the pyrolysis temperature increases, the pore volume and specific surface area of biochar increase, and MR-1 grows better. Through infrared spectroscopy and NMR analysis, it can be seen that as the pyrolysis temperature increases, the degree of condensation of biochar increases, thereby increasing the removal rate of pollutants. However, the mechanism of biochar mediating the biochemical transformation of roxarsone needs more attention. The transformation mechanism of roxarsone was not studied in this paper, which was important in the arsenic geochemical cycle.

DATA AVAILABILITY STATEMENT

The original contributions presented in the study are included in the article/**Supplementary Material**, further inquiries can be directed to the corresponding author.

AUTHOR CONTRIBUTIONS

L-WG and C-CH designed the research. L-WG and Z-R performed the research. L-WG, C-CH, and C-F analyzed the data, and wrote the manuscript with input from all authors.

FUNDING

This work was financially supported by the National Key Research and Development Program of China (2019YFC1804105) and the Tianjin Natural Science Foundation of China (17JCQNJC08400).

ACKNOWLEDGMENTS

The authors thank Wangxin for providing the *Shewanella oneidensis* MR-1 and Cui Yuxiao, Wang Yannan, and Lu Yuan for assistant with the experiment in characterizing the biochar.

SUPPLEMENTARY MATERIAL

The Supplementary Material for this article can be found online at: https://www.frontiersin.org/articles/10.3389/fmicb.2022.846228/full#supplementary-material

REFERENCES

Ahmad, M., Rajapaksha, A. U., Lim, J. E., Zhang, M., Bolan, N., Mohan, D., et al. (2014). Biochar as a sorbent for contaminant management in soil and water: a review. *Chemosphere* 99, 19–33. doi: 10.1016/j.chemosphere.2013.10.071

Aulenta, F., Rossetti, S., Amalfitano, S., Majone, M., and Tandoi, V. (2013). Conductive magnetite nanoparticles accelerate the microbial reductive dechlorination of trichloroethene by promoting interspecies electron transfer processes. *ChemSusChem* 6, 433–436. doi: 10.1002/cssc.201200748

Cao, X. Y., Pignatello, J. J., Li, Y., Lattao, C., Chappell, M. A., Chen, N., et al. (2012). Characterization of wood chars produced at different temperatures using advanced solid-state 13C NMR spectroscopic techniques. *Energy Fuels* 26, 5983–5991. doi: 10.1021/ef300947s

Chang, X. L., Hu, X. F., Jiang, Y. F., Sun, H., and Mu, Z. F. (2017). Biochar made from wheat straw: preparation and characterization. *Environ. Sci. Technol.* 40, 24–29.

Chen, G., Ke, Z., Liang, T., Liu, L., and Wang, G. (2016). *Shewanella oneidensis* MR-induced Fe(III) reduction facilitates roxarsone transformation. *PLoS One* 11:e0154017. doi: 10.1371/journal.pone.0154017

Garbarino, J. R., Bednar, A. J., Rutherford, D. W., Beyer, R. S., and Wershaw, R. L. (2003). Environmental fate of roxarsone in poultry litter. I. Degradation of roxarsone during composting. *Environ. Sci. Technol.* 37, 1509–1514. doi: 10.1021/es026219q

Gayathri, R., Gopinath, K. P., and Kumar, P. S. (2021). Adsorptive separation of toxic metals from aquatic environment using agro waste biochar: application in electroplating industrial wastewater. *Chemosphere* 262:128031. doi: 10.1016/j.chemosphere.2020.128031

Han, J.-C., Zhang, F., Cheng, L., Mu, Y., Liu, D.-F., Li, W.-W., et al. (2017). Rapid release of arsenite from roxarsone bioreduction by exoelectrogenic bacteria. *Environ. Sci. Technol. Lett.* 4, 350–355. doi: 10.1021/acs.estlett.7b00227

Harris, H. W., El-Naggar, M. Y., Bretschger, O., Ward, M. J., Romine, M. F., Obraztsova, A. Y., et al. (2010). Electrokinesis is a microbial behavior that requires extracellular electron transport. *Proc. Natl. Acad. Sci. U.S.A.* 107, 326–331. doi: 10.1073/pnas.0907468107

Heidelberg, J. F., Paulsen, I. T., Nelson, K. E., Gaidos, E. J., Nelson, W. C., Read, T. D., et al. (2002). Genome sequence of the dissimilatory metal ion-reducing bacterium *Shewanella oneidensis*. *Nat. Biotechnol.* 20, 1118–1123. doi: 10.1038/nbt749

Hemavathy, R. V., Kumar, P. S., Kanmani, K., and Jahnavi, N. (2020). Adsorptive separation of Cu(II) ions from aqueous medium using thermally/chemically treated *Cassia fistula* based biochar. *J. Clean. Prod.* 249:119390. doi: 10.1016/j.jclepro.2019.119390

Huang, K., Peng, H., Gao, F., Liu, Q. Q., Lu, X., Shen, Q., et al. (2019). Biotransformation of arsenic-containing roxarsone by an aerobic soil bacterium *Enterobacter* sp. CZ-1. *Environ. Pollut.* 247, 482–487. doi: 10.1016/j.envpol.2019.01.076

Kappler, A., Wuestner, M., Ruecker, A., Harter, J., Halama, M., and Behrens, S. (2014). Biochar as an electron shuttle between bacteria and Fe(III) minerals. *Environ. Sci. Technol. Lett.* 1, 339–344. doi: 10.1021/ez5002209

Kato, S., Hashimoto, K., and Watanabe, K. (2012). Microbial interspecies electron transfer via electric currents through conductive minerals. *Proc. Natl. Acad. Sci. U.S.A.* 109, 10042–10046. doi: 10.1073/pnas.1117592109

Klüpfel, L., Piepenbrock, A., Kappler, A., and Sander, M. (2014b). Humic substances as fully regenerable electron acceptors in recurrently anoxic environments. *Nat. Geosci.* 7, 195–200. doi: 10.1038/ngeo2084

Klüpfel, L., Keiluweit, M., Kleber, M., and Sander, M. (2014a). Redox properties of plant biomass-derived black carbon (biochar). *Environ. Sci. Technol.* 48, 5601–5611. doi: 10.1021/es500906d

Lehmann, J., Rillig, M. C., Thies, J., Masiello, C. A., Hockaday, W. C., and Crowley, D. (2011). Biochar effects on soil biota – A review. *Soil. biol. Biochem.* 43, 1812–1836. doi: 10.1016/j.soilbio.2011.04.022

Liang, B. Q., Lehmann, J., Sohi, S. P., Thies, J. E., O'neill, B., Trujillo, L., et al. (2010). Black carbon affects the cycling of non-black carbon in soil. *Org. Geochem.* 41, 206–213. doi: 10.1016/j.orggeochem.2009.09.007

Liang, Z. W., Li, W. H., Yang, S. Y., and Du, P. (2010). Extraction and structural characteristics of extracellular polymeric substances (EPS), pellets in autotrophic nitrifying biofilm and activated sludge. *Chemosphere* 81, 626–632. doi: 10.1016/j.chemosphere.2010.03.043

Lyu, H., Gong, Y., Tang, J., Huang, Y., and Wang, Q. (2016). Immobilization of heavy metals in electroplating sludge by biochar and iron sulfide. *Environ. Sci. Pollut. Res. Int.* 23, 14472–14488. doi: 10.1007/s11356-016-6621-5

Makris, K. C., Quazi, S., Punamiya, P., Sarkar, D., and Datta, R. (2008). Fate of arsenic in swine waste from concentrated animal feeding operations. *J. Environ. Qual.* 37, 1626–1633. doi: 10.2134/jeq2007.0479

Nachman, K. E., Baron, P. A., Raber, G., Francesconi, K. A., Navas-Acien, A., and Love, D. C. (2013). Roxarsone, inorganic arsenic, and other arsenic species in chicken: a U.S.-based market basket sample. *Environ. Health Perspect.* 121, 818–824. doi: 10.1289/ehp.1206245

Oyewumi, O., and Schreiber, M. (2017). Using column experiments to examine transport of as and other trace elements released from poultry litter: implications for trace element mobility in agricultural watersheds. *Environ. Pollut.* 227, 223–233. doi: 10.1016/j.envpol.2017.04.063

Pignatello, J. J., Mitch, W. A., and Xu, W. (2017). Activity and reactivity of pyrogen carbonaceous matter toward organic compounds. *Environ. Sci. Technol.* 51, 8893–8908. doi: 10.1021/acs.est.7b01088

Saito, M., and Marumoto, T. (2002). Inoculation with arbuscular mycorrhizal fungi: the status quo in Japan and the future prospects. *Plant Soil* 244, 273–279. doi: 10.1007/978-94-017-1284-2_27

Saquing, J. M., Yu, Y.-H., and Chiu, P. C. (2016). Wood-derived black carbon (biochar) as a microbial electron donor and acceptor. *Environ. Sci. Technol. Lett.* 3, 62–66. doi: 10.1016/j.chemosphere.2018.10.080

Sarmah, A. K., Meyer, M. T., and Boxall, A. B. A. (2006). A global perspective on the use, sales, exposure pathways, occurrence, fate and effects of veterinary antibiotics (VAs) in the environment. *Chemosphere* 65, 725–759. doi: 10.1016/j.chemosphere.2006.03.026

Schwanninger, M., Rodrigues, J. C., Pereira, H., and Hinterstoisser, B. (2004). Effects of short-time vibratory ball milling on the shape of FT-IR spectra of wood and cellulose. *Vib. Spectrosc.* 36, 23–40. doi: 10.1016/j.vibspec.2004.02.003

Shi, L., Dong, H., Reguera, G., Beyenal, H., Lu, A., Liu, J., et al. (2016). Extracellular electron transfer mechanisms between microorganisms and minerals. *Nat. Rev. Microbiol.* 14, 651–662. doi: 10.1038/nrmicro.2016.93

Silbergeld, E. K., and Nachman, K. (2008). The environmental and public health risks associated with arsenical use in animal feeds. *Ann. N. Y. Acad. Sci.* 1140, 346–357. doi: 10.1196/annals.1454.049

Stern, N., Mejia, J., He, S., Yang, Y., Ginder-Vogel, M., and Roden, E. E. (2018). Dual role of humic substances as electron donor and shuttle for dissimilatory iron reduction. *Environ. Sci. Technol.* 52, 5691–5699. doi: 10.1021/acs.est.7b06574

Sun, T., Levin, B. D. A., Guzman, J. J. L., Enders, A., Muller, D. A., Angenent, L. T., et al. (2017). Rapid electron transfer by the carbon matrix in natural pyrogenic carbon. *Nat. Commun.* 8:14873. doi: 10.1038/ncomms14873

Tatzber, M., Stemmer, M., Spiegel, H., Katzlberger, C., Zehetner, F., Haberhauer, G., et al. (2009). Spectroscopic behaviour of 14C-labeled humic acids in a long-term field experiment with three cropping systems. *Aust. J. Soil Res.* 47, 459–469. doi: 10.1071/SR08231

Vu, B., Chen, M., Crawford, R. J., and Ivanova, E. P. (2009). Bacterial extracellular polysaccharides involved in biofilm formation. *Molecules* 14, 2535–2554. doi: 10.3390/molecules14072535

Wahla, A. Q., Anwar, S., Mueller, J. A., Arslan, M., and Iqbal, S. (2020). Immobilization of metribuzin degrading bacterial consortium MB3R on biochar enhances bioremediation of potato vegetated soil and restores bacterial community structure. *J. Hazard. Mater.* 390:121493. doi: 10.1016/j.jhazmat.2019.121493

Wang, G., Han, N., Liu, L., Ke, Z. C., Li, B. G., and Chen, G. W. (2020). Molecular density regulating electron transfer efficiency of S. oneidensis MR-1 mediated roxarsone biotransformation. *Environ. Pollut.* 262:114370. doi: 10.1016/j.envpol.2020.114370

Wang, H. F., Zhao, H.-P., and Zhu, L. Z. (2020). Role of pyrogenic role of pyrogenic carbon in parallel microbial reduction of nitrobenzene in the liquid and sorbed phases. *Environ. Sci. Technol.* 54, 8760–8769. doi: 10.1021/acs.est.0c01061

Xu, X., Huang, H., Zhang, Y., Xu, Z., and Cao, X. (2019). Biochar as both electron donor and electron shuttle for the reduction transformation of Cr(VI) during its sorption. *Environ. Pollut.* 244, 423–430. doi: 10.1016/j.envpol.2018.10.068

Yuan, S. J., Sun, M., Sheng, G. P., Li, Y., Li, W. W., Yao, R. S., et al. (2011). Identification of key constituents and structure of the extracellular polymeric substances excreted by bacillus megaterium TF10 for their flocculation capacity. *Environ. Sci. Technol.* 45, 1152–1157. doi: 10.1021/es1030905

Zhang, Y., Xu, X. Y., Zhang, P. Y., Zhao, L., Qiu, H., and Cao, X. D. (2019). Pyrolysis-temperature depended quinone and carbonyl groups as the electron accepting sites in barley grass derived biochar. *Chemosphere* 232, 273–280. doi: 10.1016/j.chemosphere.2019.05.225

Zuriaga-Agustí, E., Bes-Piá, A., Mendoza-Roca, J. A., and Alonso-Molina, J. L. (2013). Influence of extraction methods on proteins and carbohydrates analysis from MBR activated sludge flocs in view of improving EPS determination. *Sep. Purif. Technol.* 112, 1–10. doi: 10.1016/j.seppur.2013.03.048

Conflict of Interest: The authors declare that the research was conducted in the absence of any commercial or financial relationships that could be construed as a potential conflict of interest.

Publisher's Note: All claims expressed in this article are solely those of the authors and do not necessarily represent those of their affiliated organizations, or those of the publisher, the editors and the reviewers. Any product that may be evaluated in this article, or claim that may be made by its manufacturer, is not guaranteed or endorsed by the publisher.

frontiers in Microbiology

ORIGINAL RESEARCH
published: 22 March 2022
doi: 10.3389/fmicb.2022.814323

Effects of Antimony on Rice Growth and Its Existing Forms in Rice Under Arbuscular Mycorrhizal Fungi Environment

Min Zhou[1,2†], Xinru Li[2†], Xuesong Liu[2], Yidong Mi[1,2], Zhiyou Fu[2], Ruiqing Zhang[3], Hailei Su[2], Yuan Wei[2], Huifang Liu[2] and Fanfan Wang[2*]*

[1] College of Environment, Hohai University, Nanjing, China, [2] State Key Laboratory of Environmental Criteria and Risk Assessment, Chinese Research Academy of Environmental Sciences, Beijing, China, [3] School of Ecology and Environment, Inner Mongolla University, Hohhot, China

Arbuscular mycorrhizal fungi (AMF) can form symbiotic relationships with most terrestrial plants and regulate the uptake and distribution of antimony (Sb) in rice. The effect of AMF on the uptake and transport of Sb in rice was observed using pot experiments in the greenhouse. The results showed that AMF inoculation increased the contact area between roots and metals by forming mycelium, and changed the pH and Eh of the root soil, leading to more Sb entering various parts of the rice, especially at an Sb concentration of 1,200 mg/kg. The increase in metal toxicity further led to a decrease in the rice chlorophyll content, which directly resulted in a 22.7% decrease in aboveground biomass, 21.7% in underground biomass, and 11.3% in grain biomass. In addition, the antioxidant enzyme results showed that inoculation of AMF decreased 22.3% in superoxide dismutase, 9.9% in catalase, and 20.7% in peroxidase compared to the non-inoculation groups, further verifying the negative synergistic effect of AMF inoculation on the uptake of Sb in rice. The present study demonstrated the effect of AMF on the uptake and transport of Sb in the soil–rice system, facilitating future research on the related mechanism in the soil–rice system under Sb stress.

Keywords: arbuscular mycorrhizal fungi, rice, antimony, uptake, transformation, biomass, antioxidant enzyme

HIGHLIGHTS

- AMF should reduce the plant physiological character like decrease in chlorophyll and biomass under different concentration of Sb in the soil-rice system.
- AMF inoculation leading to more Sb entering various parts of the rice.
- Inoculation of AMF increased metal toxicity further led to a decrease in rice biomass.
- The activity of antioxidant enzyme decreased further verifying the negative synergistic effect of AMF inoculation on the uptake of Sb in rice.

OPEN ACCESS

Edited by:
Xiaojing Li,
Agro-Environmental Protection Institute (CAAS), China

Reviewed by:
Jinjin Wang,
South China Agricultural University, China
Jianxu Wang,
State Key Laboratory of Environmental Geochemistry, Institute of Geochemistry (CAS), China
Qing Zhao,
Guangdong Institute of Eco-environmental and Soil Sciences (CAS), China

***Correspondence:**
Yuan Wei
rbq-wy@163.com
Fanfan Wang
wwffaannaza@126.com

† These authors have contributed equally to this work and share first authorship

Specialty section:
This article was submitted to Microbiotechnology, a section of the journal Frontiers in Microbiology

Received: *13 November 2021*
Accepted: *07 February 2022*
Published: *22 March 2022*

Citation:
Zhou M, Li X, Liu X, Mi Y, Fu Z, Zhang R, Su H, Wei Y, Liu H and Wang F (2022) Effects of Antimony on Rice Growth and Its Existing Forms in Rice Under Arbuscular Mycorrhizal Fungi Environment. Front. Microbiol. 13:814323. doi: 10.3389/fmicb.2022.814323

INTRODUCTION

Antimony (Sb) is a carcinogenic element. Excessive Sb exposure leads to serious health consequences for humans, causing damage to the respiratory, cardiovascular, and urinary systems (Schnorr et al., 1995). Therefore, Sb was listed as a priority pollutant by the European Union (Filella et al., 2002) and the Environmental Protection Agency (Wei et al., 2015). Moreover, the antimony compound was listed as group 2B by the International Agency for Research on Cancer (IARC) (Saerens et al., 2019), and a restrictive pollutant by China. At present, the main sources of Sb pollution are anthropogenic activities, such as mining, metallurgy, alloy, fireproof materials, and medicines (Fan et al., 2016). In China, Sb concentrations in the soil can reach 3,365–5,949.2 mg/kg in the surrounding area of Sb mines at LengShuiJiang, Hunan province (Li et al., 2018; Zhang Q.M. et al., 2020; Zhang Y.X. et al., 2020), and the Sb content in paddy soil surrounding Xikuangshan was over 1,500 mg/kg (Okkenhaug et al., 2012). Although Sb is a non-essential element to plants, Sb in the soil can readily accumulate in plants and enter the food chain. Rice is a staple food crop, providing for 3 billion people in the world (Ren et al., 2014). Therefore, rice safety is crucial to the global population. The World Health Organization (WHO) reported that rice is the major pathway for Sb to enter the food chain, accounting for 33% of the intake of Sb in the human body. Wu et al. (2011) reported that the Sb concentration of rice can reach up to 0.93 mg/kg near the XiKuangShan mine. The tolerable daily intake (TDI) of Sb near the XiKuangShan mine is 1.54-fold higher than the WHO recommended value (Wu et al., 2011). Therefore, research on rice uptake and transport of Sb in soil–rice systems for food safety has become particularly important.

Microorganisms are essential components in soil–plant systems. The interaction between microorganisms and plant is important component in ecosystem, and was considered as an important partner that regulate local and systemic mechanisms in plant (Meena et al., 2017). Therefore, it is inevitable to consider the effect of microorganisms on the uptake and transport of Sb in soil–rice systems. AMF are a category of beneficial microorganisms in which all species identified belong to *Glomeromycota* (Redecker et al., 2013), and AMF can form symbiotic relationships with more than 80% of terrestrial plants (Wang and Shi, 2008). A large number of papers have reported AMF can form symbiosis with rice (Chen et al., 2017; Parvin et al., 2019). For example, Parvin et al. (2019) used high throughput Illumina sequencing found that there were 77 operational taxonomic units (OTUs, based on a sequence similarity threshold of 97%) from eight AMF families from 45 rice fields. In addition, AMF can form symbioses with plants when the plants are exposed to excessive Sb (Wei et al., 2015; Pierart et al., 2018; Xi et al., 2021). AMF accelerate the growth of plants by improving essential mineral element uptake, changing the root structure of host plants, and increasing heavy metal resistance (Solís-Domínguez et al., 2011; Hernández-Ortega et al., 2012). For instance, He et al. (2014) observed that inoculation with *Glomeraceae* had a significantly positive effect on plant growth, especially at high concentrations of heavy metals, compared to plants not inoculated with *Glomeraceae*. Furthermore, there are numerous reports on the effect of AMF on the uptake of Sb in plants. For example, under Sb exposure, AMF improved Sb absorption in carrots (Pierart et al., 2018) and *Cynodon dactylon* (Wei et al., 2016), whereas the opposite result was observed in maize (Shen et al., 2017). However, only a few studies have reported the effect of resistant bacteria on the uptake of Sb from soil–rice systems. For instance, Long et al. (2020) reported that an Sb-resistant bacterium can alter the iron plaque distribution of rice roots thus affect the uptake of Sb by rice, and Sun et al. (2019) found that when rice was exposed to antimony, different flooding conditions resulted in different microbial community structures. Therefore, based on above analysis, we speculated that AMF may be formed symbiotic relationship with rice, and, affect rice on Sb uptake and distribution.

To investigate the effect of AMF on the uptake of Sb in rice, we designed a comparative experiment of AMF inoculation with non-inoculated tests and measured chlorophyll, antioxidant enzymes, and Sb adsorption in different parts of rice plants using inductively coupled plasma mass spectrometry (ICP-MS, Agilent 7500, Agilent Technology, United States), the chlorophyll meter (SPAD-502 Plus, Tuo Pu, China), and ultraviolet and visible spectrophotometer technology (Agilent 8453, Agilent Technology, United States). The aim of this study was to: (1) measure biomass and chlorophyll to elucidate the effect of AMF on growth and physiology; (2) determine the effect of AMF on the chemical properties of rhizosphere soil by measuring pH and redox potential (Eh); (3) determine the effect of AMF on the uptake of Sb by measuring the Sb concentration of different plant parts and Sb speciation; and (4) further analyze the activities of several typical antioxidant enzymes to evaluate the effects of AMF on the accumulation of Sb in rice. These results will further reveal the distribution and morphology of Sb in rice under the presence of AMF, which will help us better understand the migration and transformation of Sb in soil-rice system after AMF inoculation and the related effects on food crops.

MATERIALS AND METHODS

Soil, Fungi, and Plants

Soil was collected from Hunan Agricultural University in Hunan Province, China (113°5′23″E, 28°11′24″N). It was air dried and passed through a 2-mm sieve. The soil was then sterilized by autoclave steam for 2 h at 121°C under 0.1 MPa pressure. Four soil Sb concentrations (0, 300, 600, and 1,200 mg Sb/kg) were prepared by adding an appropriate volume of potassium pyroantimonate [$KSb(OH)_6$] stock solutions (0, 300, 600, and 1,200 mg Sb/kg as $K_2H_2Sb_2O_7{\cdot}4H_2O$ in ultrapure water) to the soil and then adding ultrapure water (Millipore-Q water, 18 Ω·cm) to maintain field capacity. The soil was aged for 4 weeks before being used in the experiment.

AMF (*Glomus mosseae*, BGC NM01A) was obtained from the Beijing Academy of Agriculture and Forestry Sciences, which contained the spores and hyphae of AMF and the rhizosphere soil of cultivated AMF.

Rice seeds (*Oryza sativa* L., Xiangwanxian No. 12) were purchased from the Hunan Rice Research Institute. They were

surface-sterilized by soaking in 10% H_2O_2 solution for 20 min and then rinsed with ultrapure water five times to clear the residual H_2O_2. The seeds were wrapped in aseptic wet gauze placed in the FPQ multi-stage artificial climate box for 3 days in the dark for germination. The wet gauze was changed every 6 h. The germinated seeds were transferred to a 5.4-L polyvinyl chloride plate with 32-orifices containing aseptic soil substrate in the FPQ multi-stage artificial climate box and were cultured for 3 weeks. For 1 week, 10 mL 0.5-strength Hoagland nutrient solution was added to the orifices at the three leaf stage; thereafter, full strength Hoagland nutrient solution was used (Ren et al., 2014). The ratio of the light-to-dark cycle was 14–10 h with 180–240 μmol/(m^2·s) sodium light. The temperature of the light period and that of the dark period were kept at 27 ± 1 and 20 ± 1°C, respectively. The relative humidity was maintained at 65–70%.

Pot Experiment Design

In the pot cultural experiment, rice was selected as the host plant, and *Glomus mosseae* was used as the inoculum. Two series of soil, which had four Sb concentrations (0, 300, 600, and 1,200 mg/kg) in each series, were prepared and used for rice growth. For each Sb concentration, three parallel pots, with each pot containing 5 kg of soil, were employed. The first series was inoculated with inactive AMF (M−); the second series was inoculated with active AMF (M+). The AMF in the first series was inactivated by autoclaved steam for 2 h at 121°C under 0.1 MPa pressure and then put into each pot. The rice seedlings at the four-leaf stage of a similar size and shape from culturing were selected and planted in each pot. Three seedlings were planted in each experimental pot. The base fertilizer was composted of $CO(NH_2)_2$, $Ca(H_2PO_4)_2$, and KCl, and the respective rates were 1, 1, and 1.5 g/kg soil (He and Yang, 1999). The experiments were conducted in the greenhouse of the Chinese Research Academy of Environmental Sciences in Beijing. After 120 days, the rice plants were harvested.

Infection of Rice by Arbuscular Mycorrhizal Fungi

AMF infection of rice root was determined after 30 days of transplanting. The method of infection was measured according to Vierheilig et al. (2005) with some modifications. The fresh roots were cleared with deionized water, and then cut into 2-cm root segments. Cleared roots were added into stationary liquid for 24 h which contained formaldehyde, acetic acid and 50% ethanol, and the volume of rates were 13, 5, and 200, respectively. After cleaned, the root segments were transferred to the 50-mL beaker which contained 10% KOH. Then the beaker was in water bath at 90°C for root segments transparent. 5% acetic acid were added to root segments for acidification. The root segments were stained with 5% ink-vinegar for 5 min and cleared with tap water which contained several drops acetic acid. The root segments were then transferred to glass slide and added 2 drops of lactic acetic acid. The root segments were observed under a microscope (LIOO JS-750T, Germany).

Biomass of Rice and Chlorophyll Content of Rice Leaves

After harvesting, rice plants were rinsed with deionized water five times. The plants were cut into roots, stems, leaves, and grain by ceramic scissors and then dried in an oven for 72 h at 65°C. All parts of the rice plant were weighed with an electronic balance. Each part was weighed three times, and the average was taken.

The middle of the sixth top leaf was used to measure the chlorophyll content with a chlorophyll meter. Each part was measured three times, and the average was taken.

Antimony Concentration in Rice and Antimony Speciation in Rice Plants

The roots, stems, leaves, and grain of rice were freeze dried with a FD5-series freeze dryer (SIM, United States), and 100 mg of each sample was transferred to a digestion vessel containing 2 mL HNO_3. The digestion vessel was sealed and digested in a microwave instrument (CEM, United States) for 2 h according to the digestion procedure (**Supplementary Table 1**), after cooling to room temperature. The digestion tubes were opened and transferred to a water bath (90°C) until the digestion solution became clear. Then, it was cooled to an ambient temperature. The solution was diluted with 1% HNO_3 to 50 mL and filtered through a 0.45-μm polyether sulfone membrane before being analyzed by ICP-MS. The certified reference material, tomato leaves (ESP-1, China National Environmental Monitoring Center reference material), was used for quality control.

The method for measuring Sb speciation in rice plants was done according to Okkenhaug et al. (2012) with some modifications. After being frozen and dried, the rice roots were cut into fragments with ceramic scissors. Plant samples (0.3000 g) were weighed into a 5-mL centrifuge tube containing 3 mL of 100 mM citric acid. The solutions were oscillated for 30 min at 50°C with a vortex centrifuge and centrifuged at 1,033 × g for 10 min. The supernatants were extracted once again with the above method. The extraction solutions of the two supernatants were filtered with a 0.45-μm polyether sulfone membrane and stabilized with 10 mL of citric acid. The solutions were measured by ICP-MS.

Soil pH and Redox Potential

The soil samples were air-dried, ground to a power with a quartz mortar, and filtered through a 2-mm sieve. The soil pH was determined based on a soil-to-deionized water ratio of 1:2.5. The soil–water mixture was stirred for 5 min and settled for 30 min. The supernatant was then measured with a calibrated pH meter (PHBJ-260, Lei Ci, China). The results were replicated three times.

The Eh value for rhizosphere soil was measured following the method previously described by Chen et al. (1997) with a platinum electrode. Briefly, the platinum electrode (0.5-mm diameter) was inserted to a depth of 5 cm within the rhizosphere soil to measure the Eh value at different positions in each pot. Each pot was measured three times, and the average was calculated.

Activity of Antioxidant Enzymes and Malondialdehyde Content

To prepare the enzyme solution, 3 g fresh rice leaves were added to a glass mortar containing 30 mL phosphate buffer (pH 7.8) at 4°C. The mixture was homogenized and transferred into a 50-mL centrifuge tube. This was followed by centrifuging for 15 min at 1,837 × g. The supernatant was collected and transferred to a 150-mL volumetric flask. The centrifugation process was then repeated once. Ultrapure water was used to obtain a solution volume of 150 mL in the volumetric flask. This solution was used to determine enzyme activities (superoxide dismutase, SOD; peroxidase, POD; catalase, CAT) and the content of malondialdehyde (MDA).

Superoxide Dismutase Assay

The SOD assay was performed according to Giannopolitis and Ries (1977). Briefly, 3 mL of SOD test solution were prepared by mixing 1.5 mL 0.05 mol/L phosphate buffer, 0.3 mL 130 mmol/L methionine (Met) solution, 0.3 mL 0.75 mmol/L nitroblue tetrazolium (NBT) solution, 0.3 mL 0.1 mmol/L disodium edetate dihydrate (EDTA-Na_2) solution, 0.3 mL 0.02 mmol/L riboflavin, 0.05 mL enzyme solution, and 0.25 mL of deionized water. Phosphate buffer was used instead of enzyme solution for the control group. The solutions were kept in the dark and irradiated under 4,000 xl fluorescent lamps for 20 min. The absorbance was determined at 560 nm with an ultraviolet and visible spectrophotometer.

Catalase Assay

The CAT assay was performed using the method of Knörzer et al. (1996). In brief, 2.5 mL enzyme solution and 2.5 mL 0.1 mol/L H_2O_2 were mixed in 50-mL triangular flasks. The solution was then heated in a water bath for 10 min at 30°C. After heating, 2.5 mL 10% H_2SO_4 was immediately added to the triangular flask. $KMnO_4$ (0.1 mol/L) was used to titrate the solution in the triangular flask after the solution became colorless, and the number of burettes was recorded. The enzyme solution of the control group was inactivated. CAT was measured at a wavelength of 240 nm by an ultraviolet and visible spectrophotometer.

Peroxidase Assay

To measure the activity of POD, 2.9 mL 0.05 mol/L phosphate buffer, 1.0 mL 2% H_2O_2, 1.0 mL 0.05 mol/L guaiacol, and 0.1 mL enzyme solution were added to a 10-mL test tube and immediately heated in a water bath for 15 min at 37°C. Then the test tube was immediately transferred to an ice bath, and 2.0 mL of 20% trichloroacetic acid (TCA) was added to terminate the reaction. This was followed by centrifuging at 2,871 × g for 10 min. The supernatant was collected and diluted with phosphate buffer to 20 mL. The activity of POD was measured at an absorbance of 470 nm by an ultraviolet and visible spectrophotometer. A control group was also prepared in the same procedure, except the enzyme solution was inactivated.

Malondialdehyde Content

The MDA content was assayed using Chakraborty et al. (2013). Enzyme solution (0.5 mL) was added to the centrifuge tube containing 1 mL 20% trichloroacetic acid (TCA) and 0.5% thiobarbituric acid (TBA). The mixture was incubated for 30 min at 95°C and then stopped by placing the tubes in an ice bath. The mixture was centrifuged for 10 min at 11,487 × g (GTR21-1, China). The absorbance of the supernatant, measured by an ultraviolet and visible spectrophotometer at 600 nm, was subtracted from the absorbance at 532 nm.

Statistical Analyses

The biomass, chlorophyll content, MDA content, Sb concentration in different parts, antioxidant enzymes, pH, and Eh data in rhizosphere soil were shown as the mean ± standard deviations (n = 3), except for the speciation of Sb in rice roots. All data were examined with one-way analysis of variance (ANOVA) combined with Student's t-test ($P < 0.05$). The experimental data were analyzed with SPSS® 21.0 (SPSS, United States) software. The graphs were plotted with Origin 9.1 (OriginLab, United States).

RESULTS AND DISCUSSION

Effects of Arbuscular Mycorrhizal Fungi Inoculation on Biomass and Chlorophyll Content of Rice

In the same concentration of Sb polluted environment, the reduction of aboveground and underground biomass of rice in the AMF inoculated group was significantly enhanced compared with that in the AMF non-inoculated group (**Figures 1A,B** and **Supplementary Table 2**). As shown in **Figure 1**, AMF had little effect on both aboveground rice biomass and underground rice biomass without Sb contamination (concentration of Sb was 0 mg/kg). With the increase in Sb concentration, the negative effect of AMF on rice biomass gradually appeared and became more and more obvious, the same phenomenon can also be seen intuitively in **Supplementary Figure 1**. The degree of biomass reduction resulting from AMF inoculation was similar in both the aboveground and underground parts of rice. For example, AMF inoculated rice treated with a series dose (300, 600, and 1,200 mg/kg) of Sb resulted in a 5.63–22.78% reduction in aboveground biomass relative to that inoculated with inactive AMF, while the M+ group treated with Sb at the same concentration resulted in a 6.14–22.56% reduction in underground biomass relative to the M− group. In addition, significant linear correlations were observed between the concentration of Sb and biomass values of the M+ and M− groups (**Figures 1C,D**). The linear slope showed that, for both aboveground and underground biomass, the slope of the M+ group was significantly greater than that of the M− group. These results indicated that the heavy metal exposure levels in rice was the direct influencing factor leading to biomass reduction, and the addition of AMF could significantly aggravate this phenomenon. This is likely because AMF inoculation could

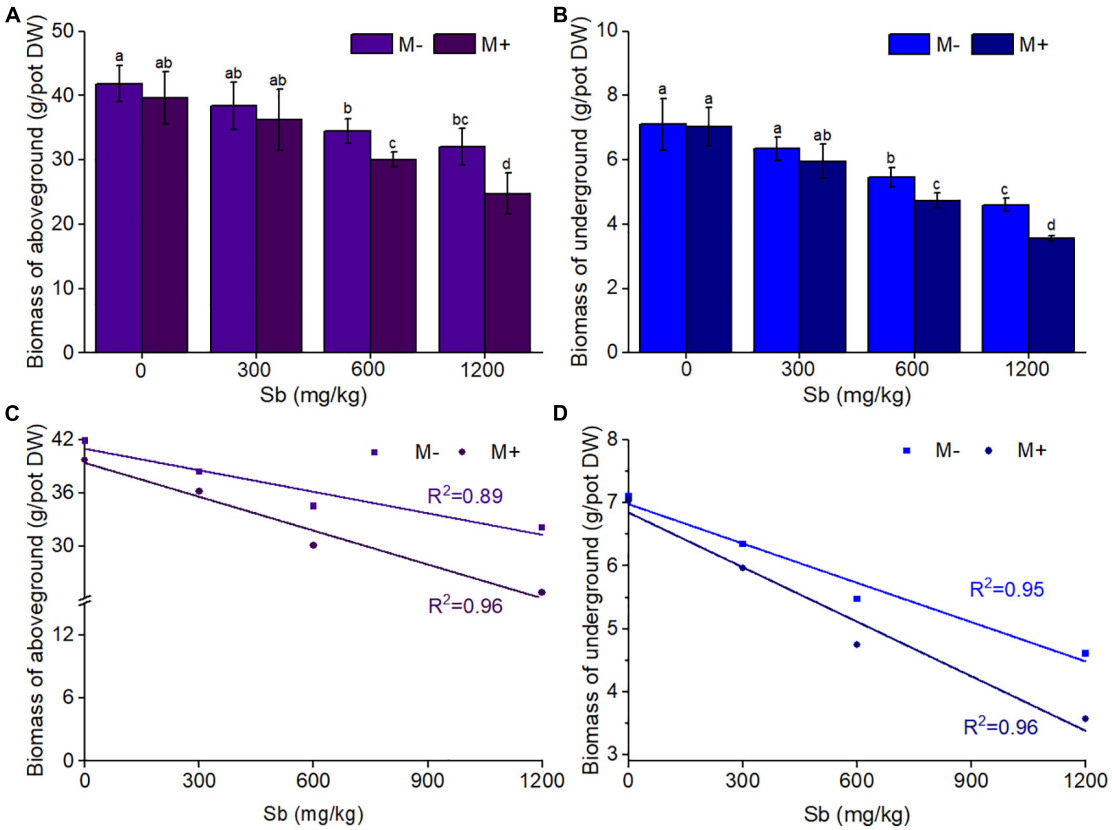

FIGURE 1 | Effects of AMF on rice biomass of aboveground and underground. **(A)** Biomass of aboveground, **(B)** biomass of underground, **(C)** the liner relationship between biomass of aboveground and concentrations of Sb, **(D)** the liner relationship between biomass of underground and concentrations of Sb. DW represents dry weight. Error bar was calculated from three parallel samples. Error bars sharing no common letter indicate that biomass are significantly different at $P < 0.05$ level for treatments. The data are means ± standard deviations (SDs) ($n = 3$).

make more Sb transfer from soil to the root of rice through mycelia, thus inhibiting the biomass of rice (Guo et al., 1996; Chen et al., 2003). This was observed in the microstructures of AMF infection on rice roots through the ink–vinegar staining method (**Figure 2**). In addition, our results found that inoculation with AMF inhibited plant growth in comparison with non-inoculated groups, the another possible reason may be that the cost of organic carbon obtained by AMF from plants was greater than that of other nutrients provided by AMF (Johnson et al., 1997; Liao et al., 2003; Citterio et al., 2005).

AMF inoculation of rice significantly reduced chlorophyll content, and the chlorophyll content decreased with increasing concentrations of Sb (**Figure 3** and **Supplementary Table 3**). **Figure 3A** showed that the chlorophyll content of the M+ groups was significantly lower than that of the M− groups at the same Sb concentration. Without heavy metal pollution, the chlorophyll content of the inoculated group was reduced by 1.17% compared with that of the non-inoculated group. When treated with a series dose (300, 600, and 1,200 mg/kg) of Sb, chlorophyll content was reduced 2.68–9.01% relative to those inoculated with inactive AMF rice (M− group). Chlorophyll is an important factor in plant photosynthesis, and its content directly affects the plant biomass (Felip and Catalan, 2000). Therefore, the effect of AMF inoculation on chlorophyll content in rice was consistent with that on biomass (**Figure 1**). This indicated that the growth of rice plants treated with Sb was further inhibited by AMF inoculation according to the decrease in chlorophyll content.

We further measured membrane lipid peroxidation (MDA), and the results were shown in **Figure 3B** and **Supplementary Table 3**. The MDA content in the M+ groups was higher than that in the M− groups (**Figure 3B**), which demonstrated that the inoculation of AMF accelerated the degree of membrane lipid peroxidation and increased chloroplast membrane breakage, resulting in chloroplast leakage. MDA is one of the final products of membrane lipid peroxidation caused by membrane structure breakage, which increases the content and further reflects the degree of membrane structure breakage, such as in the cell and chloroplast membranes (Sun et al., 2013; Wu et al., 2019).

Effects of Arbuscular Mycorrhizal Fungi Inoculation on the Accumulation of Antimony in Rice

The decrease of biomass and chlorophyll content of rice after AMF inoculation were mainly related to the change of Sb content and its existing form in rice after AMF inoculation. To verify

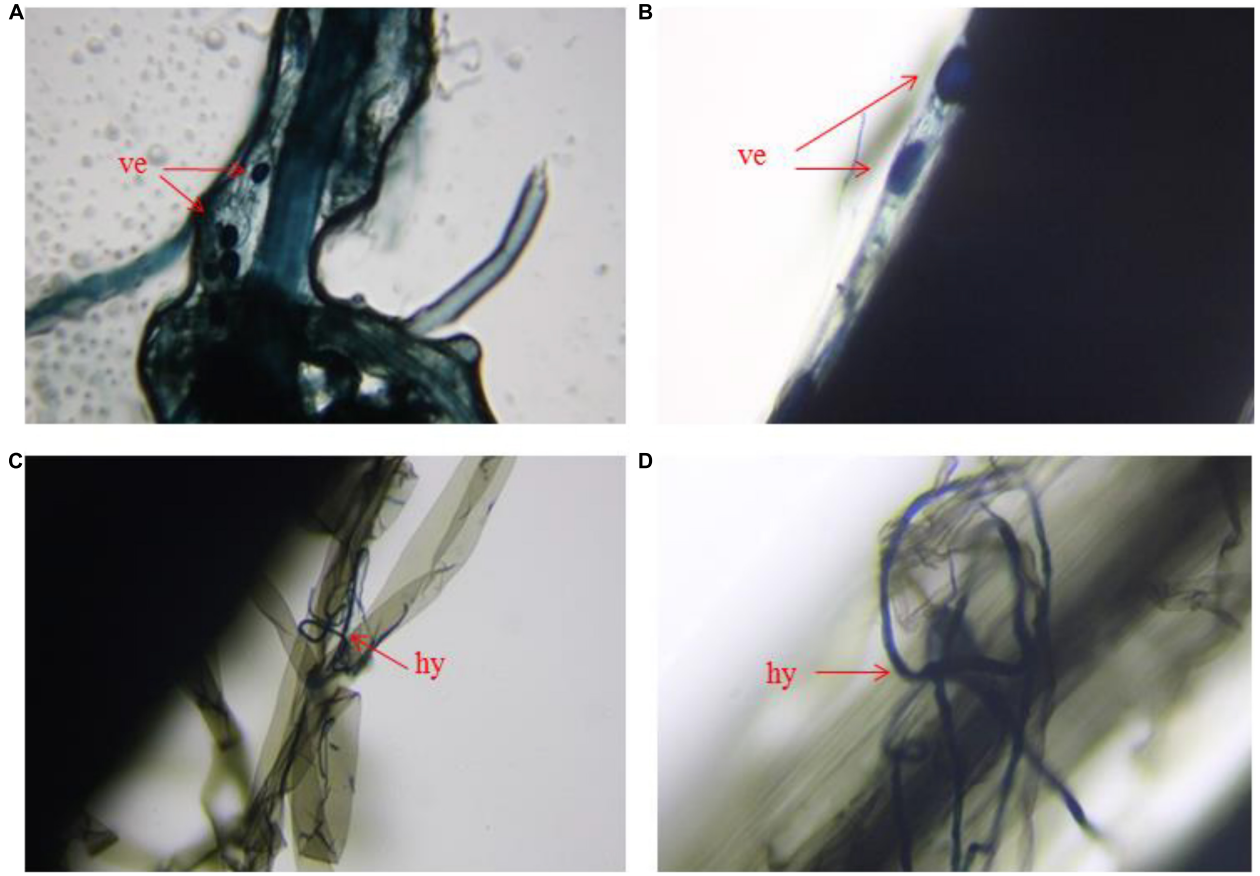

FIGURE 2 | Microstructure of arbuscular mycorrhizal fungi infect the root of rice. **(A,B)** Vesicle in roots of arbuscular mycorrhizal fungi, **(C,D)** hypha of arbuscular mycorrhizal fungi in roots. ve represents vesicle, hy represents hypha.

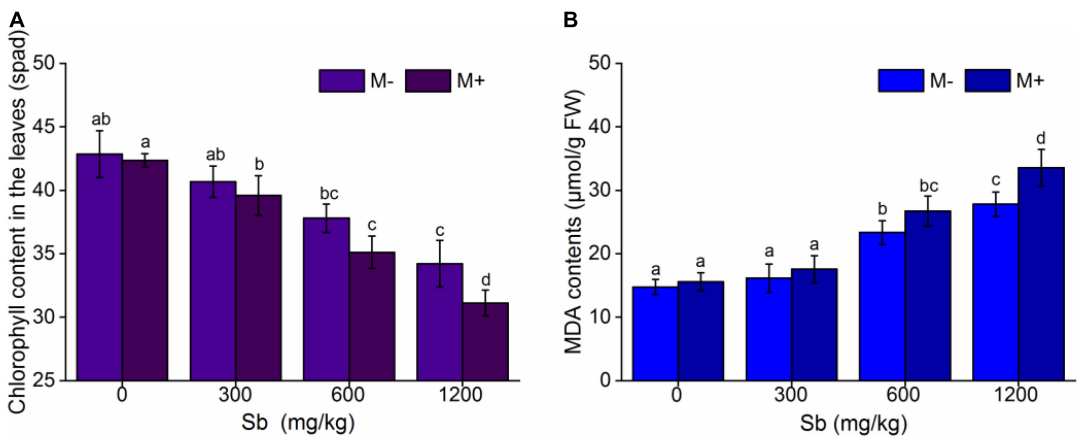

FIGURE 3 | Effects of AMF on chlorophyll contents and MDA contents of rice leaf. **(A)** Chlorophyll content in the leaves, **(B)** MDA content in the leaves. FW represents fresh weight. Error bar was calculated from three parallel samples. Error bars sharing no common letter indicate that chlorophyll content and MDA content are significantly different at $P < 0.05$ level for treatments. The data are means ± SDs ($n = 3$).

the above hypothesis, we further studied the distribution and morphology of Sb in rice with or without AMF inoculation. The study found that Sb concentration of different tissues of rice increased with increasing Sb content, while inoculation with AMF accelerated the Sb absorption of rice at the same concentrations (**Figure 4** and **Supplementary Table 4**). As shown

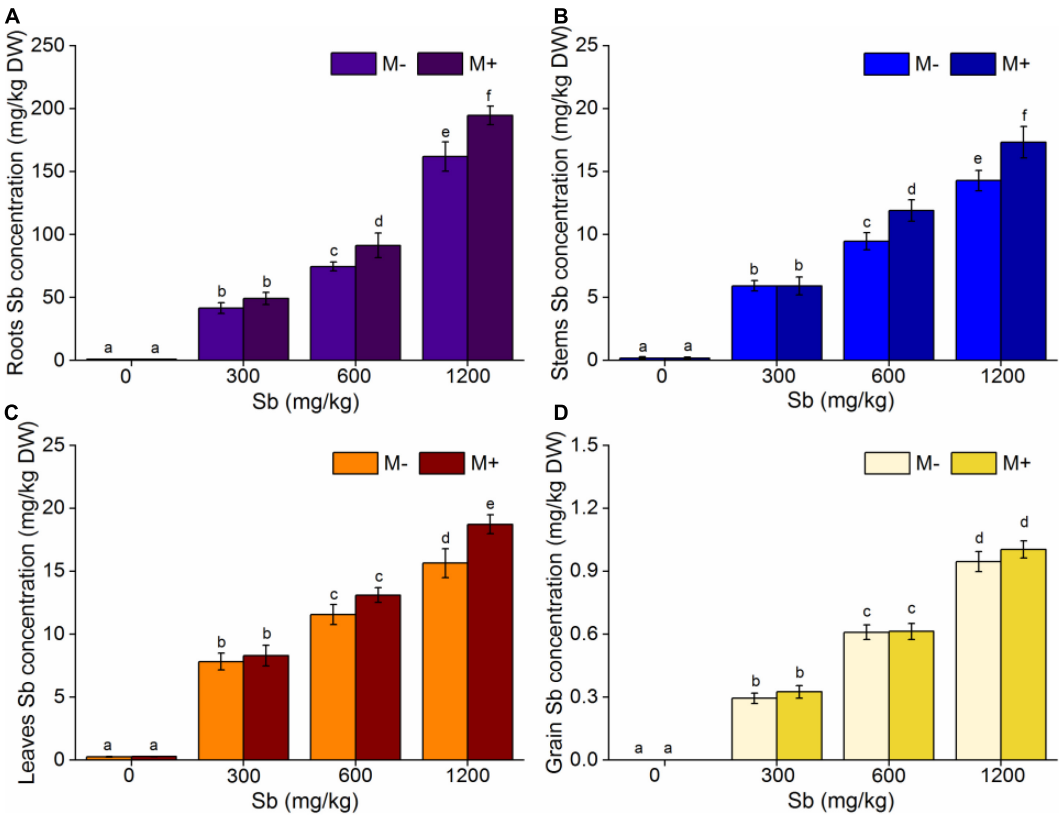

FIGURE 4 | Effects of AMF on Sb concentrations of rice. **(A)** Roots Sb concentration, **(B)** stems Sb concentration, **(C)** leaves Sb concentration, **(D)** grain Sb concentration. Error bar was calculated from three parallel samples. Error bars sharing no common letter indicate that Sb concentration are significantly different at $P < 0.05$ level for treatments. The data are means ± SDs ($n = 3$).

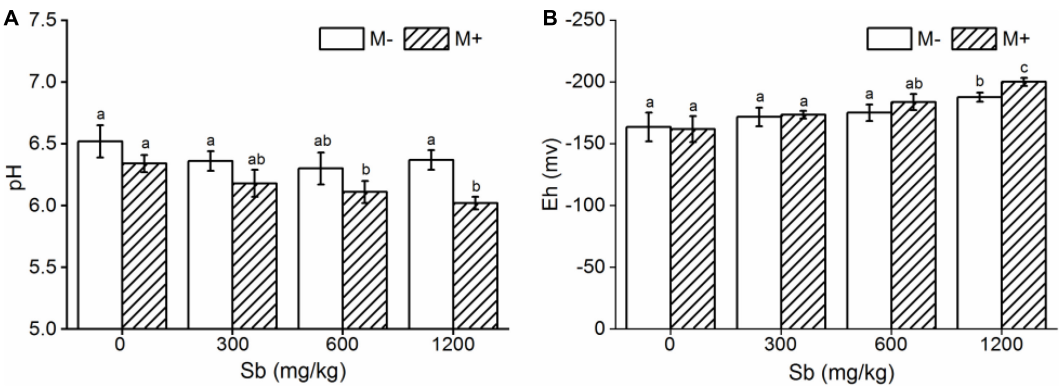

FIGURE 5 | Effects of AMF on pH and Eh in rhizosphere soil. **(A)** pH, **(B)** Eh. Error bar was calculated from three parallel samples. Error bars sharing no common letter indicate that pH and Eh are significantly different at $P < 0.05$ level for treatments. The data are means ± SDs ($n = 3$).

in **Figure 4**, AMF had an insignificant effect on Sb absorption in rice at lower Sb concentrations (0 and 300 mg/kg). However, with the increase in Sb content, the concentrations of Sb in the AMF inoculated group was significantly higher than that in the non-inoculated group. When the concentration of Sb reached 600 mg/kg, the accumulation capacity of Sb in the roots, stems, and leaves of the M+ group was, respectively, 1.18, 1.21, and 1.13 times that of the M− group (**Figures 4A–C**). When the concentration of Sb increased to 1,200 mg/kg, the ability of AMF to enhance the metal accumulation for each rice part was further enhanced. The accumulation of Sb in the roots, stems, and leaves of the M+ group was, respectively, 1.20, 1.21, and 1.20 times higher than that of the M− group. Notably, the absorption ability of Sb for grain after inoculation with AMF was

not obviously enhanced statistically (**Figure 4D**). This may be because Sb in the soil enters rice through the roots and migrates to different parts of the rice plant. The rice grains were the most link of the Sb migration and transfer pathway. Therefore, both the accumulation of Sb and the effect of AMF inoculation on the concentrations of Sb in grain were insignificant compared to those in other rice parts. Although AMF inoculation had no significant effect on the accumulation of Sb in grain, this negative effect still resulted in a significant decrease in the biomass of the grain and reduced the bioavailability of rice at high Sb concentrations (**Supplementary Figure 2**).

Symbiotic nets can be formed between rice roots and extraradical mycelium of AMF, and the symbiotic net can extend the contact area of plants with Sb in the soil, making Sb available for uptake by rice roots (Cejpková et al., 2016). This phenomenon was also confirmed in our microscope experiment (**Figure 2** and **Supplementary Figure 3**), which caused further metal entering the rice and accumulating in various plant parts under conditions of AMF inoculation. In addition, the change of physical and chemical properties of rhizosphere soil was another reason for accelerating Sb accumulation by AMF inoculation. First, the addition of AMF significantly increased the acidity of the soil (**Figure 5A** and **Supplementary Table 5**), which was due to the fact that AMF exude amino acids, acetic acid, and citric acid and activate the acid phosphatase of plants (Willamson and Alexander, 1975; Wei et al., 2016). The increase in soil acidity will promote the transformation of Sb from carbonate mineral to a soluble state, making it easier for Sb to enter various rice parts from the roots (He, 2007; Ning et al., 2015). Second, at the same time, inoculation with AMF can also significantly increase the electronegativity of the soil (**Figure 5B**), which directly affects the speciation state of the metalloid Sb in soil, in particular the conversion between Sb(V) and Sb(III), while the toxicity of Sb(III) was approximately 10-fold higher than the toxicity of Sb(V) (Chai et al., 2016). To further verify this phenomenon, we measured the content of different speciation of Sb in rhizosphere soil. As shown in **Figure 6**, when the amount of Sb added to the soil was 300, 600, and 1,200 mg/kg, the ratio of Sb(III) in the M+ group was 52.81, 54.54, and 59.52%, respectively. Compared with this, the ratio of Sb(III) in the M− group was 48.76, 51.28, and 52.12%, respectively, and lower than that in the M+ group. More Sb(III) was absorbed by rice than Sb(V) due to molecule configuration. Additionally, Sb(III) was in the form of neutral $Sb(OH)_3$ in the soil, whereas Sb(V) was in the form of $Sb(OH)_6^-$ (Nakamaru and Altansuvd, 2014). $Sb(OH)_3$ can enter the roots through aquaporins, which does not consume ATP (Feng et al., 2013). In contrast, plants might uptake $Sb(OH)_6^-$ through low selectively anion transporters, such as Cl^- and NO_3^- transporters, which requires ATP (Tschan et al., 2009). Furthermore, the negatively charged cell wall would hinder the transportation of similarly charged $Sb(OH)_6^-$ to plants (Ren et al., 2014; Zhu et al., 2020). The combination of these factors made it easier for Sb(III) to enter rice than Sb(V). In conclusion, after inoculation with AMF, the contact area of rice root increased to absorb heavy metal, and soil properties changed. This influenced the presence of Sb, making it easier and more toxic to enter rice. These phenomena will lead to further enhancement of the metal poisoning in rice and cause a decrease in biomass, as shown in section of effects of AMF inoculation on biomass and chlorophyll content of rice.

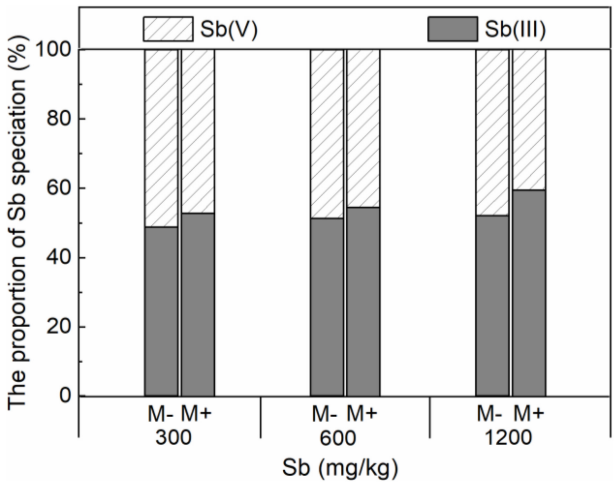

FIGURE 6 | Effects of AMF on the proportion of Sb speciation in roots of rice.

Effect of Arbuscular Mycorrhizal Fungi on Oxidative Stress Reactions in Rice

In order to further verify that AMF inoculation was mainly due to increasing the content of Sb in rice, thus increasing the stress effect of heavy metals on rice, we further examined the antioxidant enzyme activity of the M+ and M− groups. Further analysis of the antioxidant enzymes revealed that AMF inoculation increased the degree of heavy metal contamination in rice and led to weak growth (**Figure 7**). When the plant is in a stable state, the antioxidant enzymes in its body are in a dynamic balance. When the plant is attacked by harmful factors such as heavy metals, the antioxidant enzyme activity will increase to alleviate abiotic stress, so antioxidant enzyme activity is an important factor in assessing the response to heavy metal stress (Meghnous et al., 2019; Rajabpoor et al., 2019).

In the present study, we measured the changes of three typical antioxidant enzymes, including SOD, CAT, and POD, in rice with and without AMF inoculation. As shown in **Figure 7** and **Supplementary Table 3**, with the increased concentration of Sb, the response activities of the three antioxidant enzymes increased to different degrees, while inoculation with AMF decreased the corresponding values of the activities of the three antioxidant enzymes compared to non-inoculation AMF group. This phenomenon indicated that inoculation with AMF inhibited rice from activating the antioxidant enzymes to respond to heavy metal stress. In addition, the response of different antioxidant enzymes was different. For SOD (**Figure 7A**), the enzyme activity increased linearly with the increase in Sb concentration, because SOD was the first enzyme to defend against reactive oxygen species (ROS), and it could reduce the conversion of superoxide radicals ($O_2^{\cdot -}$) to hydrogen peroxide (H_2O_2) (Meier et al., 2011).

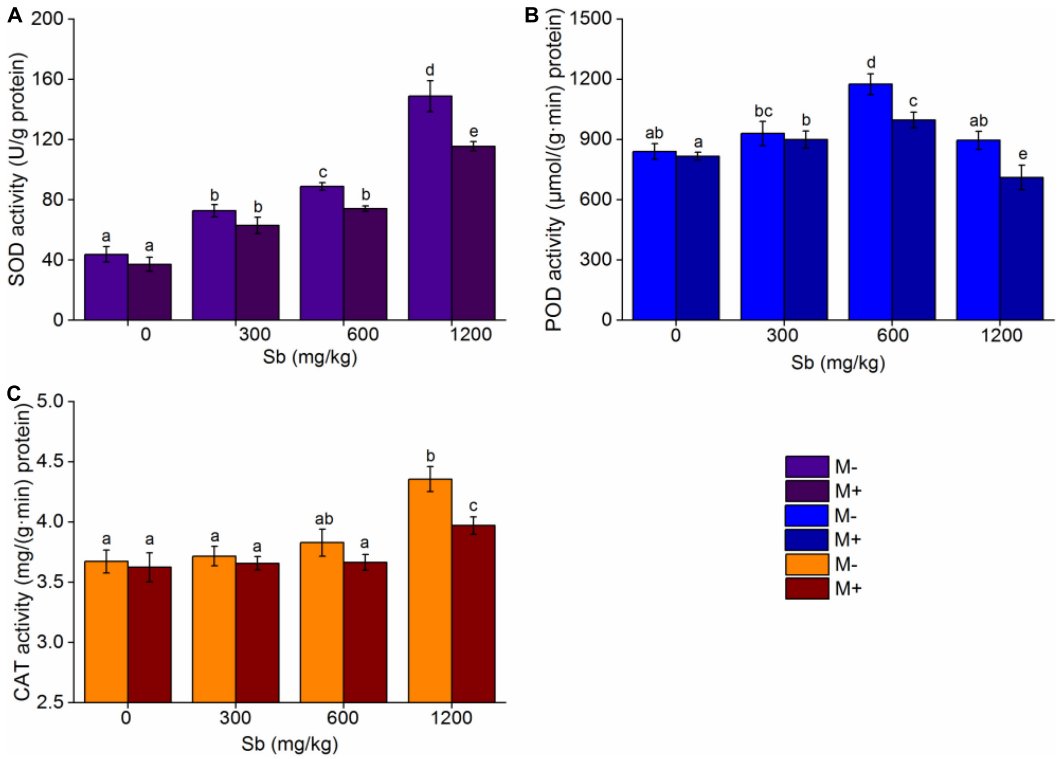

FIGURE 7 | Effects of AMF on antioxidant enzymes of rice. **(A)** SOD, **(B)** POD, **(C)** CAT. Error bar was calculated from three parallel samples. Error bars sharing no common letter indicate that SOD, CAT, and POD activity are significantly different at $P < 0.05$ level for treatments. The data are means ± SDs ($n = 3$).

When the concentration of Sb increased to 1,200 mg/kg, the enzyme activity of SOD was 3.40 times that of those without heavy metal addition, while the same enzyme activity of SOD was 3.11 times that without Sb addition after AMF inoculation. For POD (**Figure 7B**), the enzyme activity also increased linearly with the increase in Sb concentration; however, the increase in POD activity did not appear until the Sb concentration increased to 600 mg/kg, which may be because lower Sb concentrations could not activate the function of POD, which was to relieve the H_2O_2 produced by SOD (Bowler et al., 1992; Chai et al., 2016), so their activity response with the increase in metal concentration was behind that of SOD. Notably, the activity of POD for both the M+ and M− groups rapidly declined when the concentration of Sb was 1,200 mg/kg, because the tolerance of POD to Sb reached its limit, thus resulting in a significant decrease in enzyme activity (Hou et al., 2007; Chai et al., 2016). Interestingly, as shown in **Figure 7C**, when the concentration of Sb was below 1,200 mg/kg, the enzyme activity of CAT was not significantly changed, but when the concentration of Sb increased to 1,200 mg/kg, the enzyme activity of CAT increased rapidly. This may have occurred because the function of CAT and POD are to degrade hydrogen peroxide produced by SOD, and the response sensitivity of CAT may be poorer than that of POD (Kassa-Laouar et al., 2019). Therefore, when POD reached the upper limit of Sb tolerance, the stress response function of CAT was more activated. In addition, inoculation with AMF simultaneously reduced SOD, CAT, and POD activity in comparison to non-inoculated groups at the same Sb concentration, indicating that inoculation with AMF decreased antioxidant enzyme activity, resulting in more residual ROS in the leaves of rice, accelerating ROS damage to rice cells, and inhibiting rice growth.

CONCLUSION

This research elucidated that AMF plays a negative role in Sb transport in soil–rice systems. The presence of AMF increased the uptake of Sb in rice, thus aggravating the invasion of heavy metals. As a result, the chloroplast membrane of plants rupture, resulting in reducing photosynthesis and eventually leading to a significant reduction in the biomass of all parts of the plant, aboveground and underground. This was further corroborated by the decreased activity of various antioxidant enzymes caused by the enhanced stress response. Consequently, the presence of AMF would accelerate the invasion of Sb in rice. These phenomena will help us better understand the migration and transformation of Sb in soil-rice system in real natural environment. Such altered contaminant-accumulating capacities may significantly affect the availability and food safety of rice. Our research will further focus on screening the related proteins of Sb transport and regulatory network of Sb membrane protein to elucidate the molecular mechanism of AMF affecting Sb uptake and transport in rice roots. This aspect should be given consideration in the assessment

of the effect of AMF on rice uptake of Sb, avoiding the health risks of rice consumption.

DATA AVAILABILITY STATEMENT

The original contributions presented in the study are included in the article/**Supplementary Material**, further inquiries can be directed to the corresponding author/s.

AUTHOR CONTRIBUTIONS

MZ and XIL: conceptualization, methodology, data analysis and processing, visualization, and writing. XUL: sampling, investigation, and formal analysis. YM, RZ, HS, and HL: sampling and investigation. ZF: methodology and data analysis. YW and FW: research design, supervision, and funding acquisition. All authors contributed to the article and approved the submitted version.

FUNDING

This work was supported by the National Natural Science Foundation of China (Nos. 41907305, 41977294, and 52091544) and the Ministry of Science and Technology of the People's Republic of China (No. 2020YF C1807700).

ACKNOWLEDGMENTS

We thank Letpub company for supporting in the language of this study.

SUPPLEMENTARY MATERIAL

The Supplementary Material for this article can be found online at: https://www.frontiersin.org/articles/10.3389/fmicb.2022.814323/full#supplementary-material

REFERENCES

Bowler, C., Montagu, M., and Inze, D. (1992). Superoxide-dismutase and stress tolerance. *Annu. Rev. Plant Physiol. Plant Mol. Biol.* 43, 83–116. doi: 10.1146/annurev.arplant.43.1.83

Cejpková, J., Gryndler, M., Hršelová, H., Kotrba, P., Řanda, Z., Synková, I., et al. (2016). Bioaccumulation of heavy metals, metalloids, and chlorine in ectomycorrhizae from smelter-polluted area. *Environ. Pollut.* 218, 176–185. doi: 10.1016/j.envpol.2016.08.009

Chai, L. Y., Mubarak, H., Yang, Z. H., Yong, W., Tang, C. J., and Mirza, N. (2016). Growth, photosynthesis, and defense mechanism of antimony (Sb)-contaminated *Boehmeria nivea* L. *Environ. Sci. Pollut. Res.* 23, 7470–7481. doi: 10.1007/s11356-015-5987-0

Chakraborty, S., Mukherjee, A., and Das, T. K. (2013). Biochemical characterization of a lead-tolerant strain of aspergillus foetidus: an implication of bioremediation of lead from liquid media. *Int. Biodeter. Biodegradation* 84, 134–142. doi: 10.1016/j.ibiod.2012.05.031

Chen, B. D., Li, X. L., Tao, H. Q., Christie, P., and Wong, M. H. (2003). The role of arbuscular mycorrhiza in zinc uptake by red clover growing in a calcareous soil spiked with various quantities of zinc. *Chemosphere* 50, 839–846. doi: 10.1016/S0045-6535(02)00228-X

Chen, J. X., Xuan, J. X., Du, C. X., and Xie, J. X. (1997). Effect of potassium nutrition of rice on rhizosphere redox status. *Plant Soil* 188, 131–137. doi: 10.1023/A:1004264411323

Chen, X. W., Wu, F. Y., Li, H., Chan, W. F., Wu, S. C., and Wong, M. H. (2017). Mycorrhizal colonization status of lowland rice (*Oryza sativa* L.) in the southeastern region of China. *Environ. Sci. Pollut. Res.* 24, 5268–5276. doi: 10.1007/s11356-016-8287-4

Citterio, S., Prato, N., Fumagalli, P., Aina, R., Massa, N., Santagostino, A., et al. (2005). The arbuscular mycorrhizal fungus *Glomus mosseae* induces growth and metal accumulation changes in *Cannabis sativa* L. *Chemosphere* 59, 21–29. doi: 10.1016/j.chemosphere.2004.10.009

Fan, J. X., Wang, Y. J., Fan, T. T., Dang, F., and Zhou, D. M. (2016). Effect of aqueous Fe(II) on Sb(V) sorption on soil and goethite. *Chemosphere* 147, 44–51. doi: 10.1016/j.chemosphere.2015.12.078

Felip, M., and Catalan, J. (2000). The relationship between phytoplankton biovolume and chlorophyll in a deep oligotrophic lake: decoupling in their spatial and temporal maxima. *J. Plankton. Res.* 22, 91–105. doi: 10.1093/plankt/22.1.91

Feng, R. Y., Wei, C. Y., Tu, S. X., Ding, Y. Z., Wang, R. G., and Guo, J. K. (2013). The uptake and detoxification of antimony by plants: a review. *Environ. Exp. Bot.* 96, 28–34. doi: 10.1016/j.envexpbot.2013.08.006

Filella, M., Belzile, N., and Chen, Y. W. (2002). Antimony in the environment: a review focused on natural waters I. occurrence. *Earth Sci. Rev.* 57, 125–176. doi: 10.1016/S0012-8252(01)00070-8

Giannopolitis, C. N., and Ries, S. K. (1977). Superoxide dismutases I. occurrence in higher plants. *Plant Physiol.* 59, 309–314. doi: 10.1104/pp.59.2.309

Guo, Y., George, E., and Marschner, H. (1996). Contribution of an arbuscular mycorrhizal fungus to the uptake of cadmium and nickel in bean and maize plants. *Plant Soil* 184, 195–205. doi: 10.1007/BF00010449

He, L., Yang, H. S., Yu, Z. X., Tang, J. J., Xu, L. G., and Chen, X. (2014). Arbuscular mycorrhizal fungal phylogenetic groups differ in affecting host plants along heavy metal levels. *J. Environ. Sci.* 26, 2034–2040. doi: 10.1016/j.jes.2014.07.013

He, M. C. (2007). Distribution and phytoavailability of antimony at an antimony mining and smelting area, Hunan, China. *Environ. Geochem. Health* 29, 209–219. doi: 10.1007/s10653-006-9066-9

He, M. C., and Yang, J. R. (1999). Effects of different forms of antimony on rice during the period of germination and growth and antimony concentration in rice tissue. *Sci. Total Environ.* 243, 149–155. doi: 10.1016/S0048-9697(99)00370-8

Hernández-Ortega, H. A., Alarcón, A., Ferrera-Cerrato, R., Zavaleta-Mancera, H. A., López-Delgado, H. A., and Mendoza-López, M. R. (2012). Arbuscular mycorrhizal fungi on growth, nutrient status, and total antioxidant activity of *Melilotus albus* during phytoremediation of a diesel-contaminated substrate. *J. Environ. Manage* 95, S319–S324. doi: 10.1016/j.jenvman.2011.02.015

Hou, W. H., Chen, X., Song, G. L., Wang, Q. H., and Chang, C. C. (2007). Effects of copper and cadmium on heavy metal polluted waterbody restoration by duckweed (*Lemna minor*). *Plant Physiol. Biochem.* 45, 62–69. doi: 10.1016/j.plaphy.2006.12.005

Johnson, B. N. C., Graham, J. H., and Smith, F. A. (1997). Functioning of mycorrhizal associations along the mutualism-parasitism continuum. *New Phytol.* 135, 575–585. doi: 10.1046/j.1469-8137.1997.00729.x

Kassa-Laouar, M., Mechakra, A., Rodrigue, A., Meghnous, O., Bentellis, A., and Rached, O. (2019). Antioxidative enzyme responses to antimony stress of *serratia marcescens*-an endophytic bacteria of *Hedysarum pallidum* roots. *Pol. J. Environ. Stud.* 29, 141–152. doi: 10.15244/pjoes/100494

Knörzer, O. C., Burner, J., and Böger, P. (1996). Alterations in the antioxidative system of suspension-cultured soybean cells (*Glycine max*) induced by oxidative stress. *Physiol. Plant* 97, 388–396. doi: 10.1034/j.1399-3054.1996.970225.x

Li, J. Y., Zheng, B. H., He, Y. Z., Zhou, Y. Y., Chen, X., Ruan, S., et al. (2018). Antimony contamination, consequences and removal techniques: a review. *Ecotoxicol. Environ. Saf.* 156, 125–134. doi: 10.1016/j.ecoenv.2018.03.024

Liao, J. P., Lin, X. G., Cao, Z. H., Shi, Y. Q., and Wong, M. H. (2003). Interactions between arbuscular mycorrhizae and heavy metals under sand

culture experiment. *Chemosphere* 50, 847–853. doi: 10.1016/S0045-6535(02)00229-1

Long, J. M., Zhou, D. S., Li, B. Y., Zhou, Y. M., Li, Y., and Lei, M. (2020). The effect of an antimony resistant bacterium on the iron plaque fraction and antimony uptake by rice seedlings. *Environ. Pollut*. 258:113670. doi: 10.1016/j.envpol.2019.113670

Meena, K. K., Sorty, A. M., Bitla, U. M., Choudhary, K., Gupta, P., Pareek, A., et al. (2017). Abiotic stress responses and microbe-mediated mitigation in plants: the omics strategies. *Front. Plant Sci*. 8:172. doi: 10.3389/fpls.2017.00172

Meghnous, O., Dehimat, L., Doumas, P., Kassa-Laouar, M., Mosbah, F., and Rached, O. (2019). Oxidative and antioxidative responses to antimony stress by endophytic fungus *Aspergillus tubingensis* isolated from antimony accumulator *Hedysarum pallidum* Desf. *Biologia* 74, 1711–1720. doi: 10.2478/s11756-019-00305-z

Meier, S., Azcón, R., Cartes, P., Borie, F., and Cornejo, P. (2011). Alleviation of Cu toxicity in *Oenothera picensis* by copper-adapted arbuscular mycorrhizal fungi and treated agrowaste residue. *Appl. Soil Ecol*. 48, 117–124. doi: 10.1016/j.apsoil.2011.04.005

Nakamaru, Y. M., and Altansuvd, J. (2014). Speciation and bioavailability of selenium and antimony in non-flooded and wetland soils: a review. *Chemosphere* 111, 366–371. doi: 10.1016/j.chemosphere.2014.04.024

Ning, Z. P., Xiao, T. F., and Xiao, E. Z. (2015). Antimony in the soil-plant system in an Sb mining/smelting area of southwest China. *Int. J. Phytoremediation* 17, 1081–1089. doi: 10.1080/15226514.2015.1021955

Okkenhaug, G., Zhu, Y. G., He, J. W., Li, X., Luo, L., and Mulder, J. (2012). Antimony (Sb) and arsenic (As) in Sb mining impacted paddy soil from Xikuangshan, China: differences in mechanisms controlling soil sequestration and uptake in rice. *Environ. Sci. Technol*. 46, 3155–3162. doi: 10.1021/es2022472

Parvin, S., Geel, M. V., Yeasmin, T., Lievens, B., and Honnay, O. (2019). Variation in arbuscular mycorrhizal fungal communities associated with lowland rice (*Oryza sativa*) along a gradient of soil salinity and arsenic contamination in Bangladesh. *Sci. Total Environ*. 686, 546–554. doi: 10.1016/j.scitotenv.2019.05.450

Pierart, A., Dumat, C., Maes, A. Q., and Sejalon-Delmas, N. (2018). Influence of arbuscular mycorrhizal fungi on antimony phyto-uptake and compartmentation in vegetables cultivated in urban gardens. *Chemosphere* 191, 272–279. doi: 10.1016/j.chemosphere.2017.10.058

Rajabpoor, S., Ghaderian, S. M., and Schat, H. (2019). Effects of antimony on enzymatic and non-enzymatic antioxidants in a metallicolous and a non-metallicolous population of *Salvia spinosa* L. *Plant Physiol. Biochem*. 144, 386–394. doi: 10.1016/j.plaphy.2019.10.011

Redecker, D., Schüβler, A., Stockinger, H., Stürmer, S. L., Morton, J. B., and Walker, C. (2013). An evidence-based consensus for the classification of arbuscular mycorrhizal fungi (*Glomeromycota*). *Mycorrhiza* 23, 515–531. doi: 10.1007/s00572-013-0486-y

Ren, J. H., Ma, L. Q., Sun, H. J., Cai, F., and Luo, J. (2014). Antimony uptake, translocation and speciation in rice plants exposed to antimonite and antimonate. *Sci. Total Environ*. 475, 83–89. doi: 10.1016/j.scitotenv.2013.12.103

Saerens, A., Ghosh, M., Verdonck, J., and Godderis, L. (2019). Risk of cancer for workers exposed to antimony compounds: a systematic review. *Int. J. Environ. Res. Public Health* 16:4474. doi: 10.3390/ijerph16224474

Schnorr, T. M., Steenland, K., Thun, M. J., and Rinsky, R. A. (1995). Mortality in a cohort of antimony smelter workers. *Am. J. Ind. Med*. 27, 759–770. doi: 10.1002/ajim.4700270510

Shen, Y. Q., Wei, Y., Chen, Z. P., Zeng, Q. R., and Hou, H. (2017). Effects of arbuscular mycorrhizal fungi on growth, antimony uptake and antioxidant enzymes of maize under antimony stress. *Res. Environ. Sci*. 30, 712–719. doi: 10.13198/j.issn.1001-6929.2017.02.10

Solís-Domínguez, F. A., Valentín-Vargas, A., Chorover, J., and Maier, R. M. (2011). Effect of arbuscular mycorrhizal fungi on plant biomass and the rhizosphere microbial community structure of mesquite grown in acidic lead/zinc mine tailings. *Sci. Total Environ*. 409, 1009–1016. doi: 10.1016/j.scitotenv.2010.11.020

Sun, F., Yang, L. T., Xie, X. N., Liu, G. L., and Li, Y. R. (2013). Effect of chilling stress on physiological metabolism in chloroplasts of seedlings of sugarcane varieties with different chilling resistance. *Acta. Agron. Sin*. 38, 732–739. doi: 10.3724/SP.J.1006.2012.00732

Sun, W. M., Sun, X. X., Li, B. Q., Haggblom, M. M., Han, F., Xiao, E. Z., et al. (2019). Bacterial response to antimony and arsenic contamination in rice paddies during different flooding conditions. *Sci. Total Environ*. 675, 273–285. doi: 10.1016/j.scitotenv.2019.04.146

Tschan, M., Robinson, B. H., and Schulin, R. (2009). Antimony in the soil-plant system-a review. *Environ. Chem*. 6, 106–115. doi: 10.1071/EN08111

Vierheilig, H., Schweiger, P., and Brundrett, M. (2005). An overview of methods for the detection and observation of arbuscular mycorrhizal fungi in roots. *Physiol. Plant* 125, 393–404. doi: 10.1111/j.1399-3054.2005.00564.x

Wang, F. Y., and Shi, Z. Y. (2008). Biodiversity of arbuscular mycorrhizal fungi in China: a review. *Adv. Environ. Biol*. 2, 31–39.

Wei, Y., Chen, Z. P., Wu, F. C., Hou, H., Li, J. N., Shangguan, Y. X., et al. (2015). Molecular diversity of arbuscular mycorrhizal fungi at a large-scale antimony mining area in southern China. *J. Environ. Sci (China)*. 29, 18–26. doi: 10.1016/j.jes.2014.10.002

Wei, Y., Su, Q., Sun, Z. J., Shen, Y. Q., Li, J. N., and Zhu, X. L. (2016). The role of arbuscular mycorrhizal fungi in plant uptake, fractions, and speciation of antimony. *Appl. Soil Ecol*. 107, 244–250. doi: 10.1016/j.apsoil.2016.04.021

Willamson, B., and Alexander, I. J. (1975). Acid phosphatase localised in the sheath of beech mycorrhiza. *Soil Biol. Biochem*. 7, 195–198. doi: 10.1016/0038-0717(75)90037-1

Wu, C. C., Li, F., Xu, H., Zeng, W. M., Yu, R. L., and Wu, X. L. (2019). The potential role of brassinosteroids (BRs) in alleviating antimony (Sb) stress in arabidopsis thaliana. *Plant Physiol. Biochem*. 141, 51–59. doi: 10.1016/j.plaphy.2019.05.011

Wu, F. C., Fu, Z. Y., Liu, B. J., Mo, C. L., Chen, B., and Corns, W. (2011). Health risk associated with dietary co-exposure to high levels of antimony and arsenic in the world's largest antimony mine area. *Sci. Total Environ*. 409, 3344–3351. doi: 10.1016/j.scitotenv.2011.05.033

Xi, L., Shen, Y. Q., Zhao, X., Zhou, M., Mi, Y. D., Li, X. R., et al. (2021). Effects of arbuscular mycorrhizal fungi on frond antimony enrichment, morphology, and proteomics in *Pteris cretica* var. nervosa during antimony phytoremediation. *Sci. Total Environ*. 15:149904. doi: 10.1016/j.scitotenv.2021.149904

Zhang, Q. M., Gong, M. G., Liu, K. Y., Chen, Y. L., Yuan, J. F., and Chang, Q. S. (2020). *Rhizoglomus intraradices* improves plant growth, root morphology and phytohormone balance of *Robinia pseudoacacia* in arsenic-contaminated soils. *Front. Microbiol*. 11:1428. doi: 10.3389/fmicb.2020.01428

Zhang, Y. X., Song, B., Zhu, L. L., and Zhou, Z. Y. (2020). Evaluation of the metal(loid)s phytoextraction potential of wild plants grown in three antimony mines in southern China. *Int. J. Phytoremediation* 23, 1–10. doi: 10.1080/15226514.2020.1857685

Zhu, Y. M., Yang, J. G., Wang, L. Z., Lin, Z. T., Dai, J. X., Wang, R. J., et al. (2020). Factors influencing the uptake and speciation transformation of antimony in the soil-plant system, and the redistribution and toxicity of antimony in plants. *Sci. Total Environ*. 738:140232. doi: 10.1016/j.scitotenv.2020.140232

Conflict of Interest: The authors declare that the research was conducted in the absence of any commercial or financial relationships that could be construed as a potential conflict of interest.

Publisher's Note: All claims expressed in this article are solely those of the authors and do not necessarily represent those of their affiliated organizations, or those of the publisher, the editors and the reviewers. Any product that may be evaluated in this article, or claim that may be made by its manufacturer, is not guaranteed or endorsed by the publisher.

frontiers | Frontiers in Microbiology

REVIEW
published: 05 April 2022
doi: 10.3389/fmicb.2022.845725

A Review on Microorganisms in Constructed Wetlands for Typical Pollutant Removal: Species, Function, and Diversity

Jianwu Wang[1,2], Yuannan Long[1,2], Guanlong Yu[1,2,3], Guoliang Wang[1,2], Zhenyu Zhou[1,2], Peiyuan Li[1,2], Yameng Zhang[1,2], Kai Yang[1,2] and Shitao Wang[1,2]*

[1]School of Hydraulic and Environmental Engineering, Changsha University of Science & Technology, Changsha, China, [2]Key Laboratory of Dongting Lake Aquatic Eco-Environmental Control and Restoration of Hunan Province, Changsha, China, [3]Engineering and Technical Center of Hunan Provincial Environmental Protection for River-Lake Dredging Pollution Control, Changsha, China

OPEN ACCESS

Edited by:
Tian Li,
Nankai University, China

Reviewed by:
Junyuan Guo,
Chengdu University of Information Technology, China
Zhiqiang Shen,
Chinese Research Academy of Environmental Sciences, China
Jiachao Zhang,
Hunan Agricultural University, China
Yan Cheng,
Guilin University of Technology, China

***Correspondence:**
Yuannan Long
lynzhb@csust.edu.cn

Specialty section:
This article was submitted to Microbiotechnology, a section of the journal Frontiers in Microbiology

Received: 30 December 2021
Accepted: 01 March 2022
Published: 05 April 2022

Citation:
Wang J, Long Y, Yu G, Wang G, Zhou Z, Li P, Zhang Y, Yang K and Wang S (2022) A Review on Microorganisms in Constructed Wetlands for Typical Pollutant Removal: Species, Function, and Diversity. Front. Microbiol. 13:845725. doi: 10.3389/fmicb.2022.845725

Constructed wetlands (CWs) have been proven as a reliable alternative to traditional wastewater treatment technologies. Microorganisms in CWs, as an important component, play a key role in processes such as pollutant degradation and nutrient transformation. Therefore, an in-depth analysis of the community structure and diversity of microorganisms, especially for functional microorganisms, in CWs is important to understand its performance patterns and explore optimized strategies. With advances in molecular biotechnology, it is now possible to analyze and study microbial communities and species composition in complex environments. This review performed bibliometric analysis of microbial studies in CWs to evaluate research trends and identify the most studied pollutants. On this basis, the main functional microorganisms of CWs involved in the removal of these pollutants are summarized, and the effects of these pollutants on microbial diversity are investigated. The result showed that the main phylum involved in functional microorganisms in CWs include *Proteobacteria*, *Bacteroidetes*, *Actinobacteria* and *Firmicutes*. These functional microorganisms can remove pollutants from CWs by catalyzing chemical reactions, biodegradation, biosorption, and supporting plant growth, etc. Regarding microbial alpha diversity, heavy metals and high concentrations of nitrogen and phosphorus significantly reduce microbial richness and diversity, whereas antibiotics can cause large fluctuations in alpha diversity. Overall, this review can provide new ideas and directions for the research of microorganisms in CWs.

Keywords: constructed wetlands, functional microorganisms, microbial diversity, pollutant removal, wastewater treatment

INTRODUCTION

Constructed wetlands (CWs) are passive biological engineering systems that use natural processes for wastewater treatment (Chen et al., 2021b; Zheng et al., 2021a). They have been widely used since the 1960s because of their simple operation, ease of maintenance, low cost, and environmental friendliness, providing a viable alternative to traditional

wastewater treatment technologies (Zhao et al., 2016; Zheng et al., 2021a,b). They are mainly composed of substrate, plants, and microorganisms that purifying wastewater through the interaction of physical, chemical, and biological processes (Zhao et al., 2020c). Previous studies have shown that CWs can remove most environmental pollutants, including COD, N, P (Lin et al., 2002; Li et al., 2013; Zhao et al., 2019), heavy metals (Zhang et al., 2021e), and antibiotics (Liu et al., 2019), as well as some increasingly emerging pollutants (e.g., pesticides, flame retardants and persistent organic pollutants; Rajan et al., 2019; Long et al., 2021; Vymazal et al., 2021). Consequently, CWs are widely used in the treatment of domestic sewage, industrial wastewater, mine drainage, land leachate, polluted lake water, effluent from the livestock industry and other wastewater (Lin et al., 2002; Zhao et al., 2020c).

In CWs, microorganisms play a key role in pollutants removal, such as the degradation of organic pollutants and the conversion of various nutrients (Wang et al., 2020d). They can even use antibiotics as their sole carbon source (Ricken et al., 2013; Bessa et al., 2017). Regarding heavy metal compounds, which are generally difficult to biodegrade, microorganisms can also remove them from wastewater through biosorption, bioaccumulation and speciation transformation (Si et al., 2019). In addition, microorganisms can improve the tolerance and removal efficiency of CWs to pollutants by enhancing phytoremediation (Syranidou et al., 2018; Vassallo et al., 2020). In this context, in order to further optimize CWs, it is necessary to investigate the functional microorganisms associated with pollutant removal.

In recent years, advances in molecular biotechnology have largely facilitated intensive studies of microbial community structure and diversity (Arroyo et al., 2013). The advent of methods such as 16S sequencing, metagenomics sequencing, and high-throughput sequencing technologies has not only allowed a more accurate assessment of microbial diversity but only the analysis of the relative abundances of different microbial species and of the overall community structure (Zhao et al., 2016; Sanchez, 2017). In CWs, the diversity of microbial communities and the richness of certain species are key factors for efficient wastewater treatment (Zhao et al., 2020c). Therefore, in addition to the need for a summary of functional microorganisms, there is also a great need to study and analyze the effects of different pollutants on microbial diversity.

In recent year, various types of bibliometric analysis have been applied in different fields (Zhao et al., 2020b; Chen et al., 2021a; Kilicaslan et al., 2021). As a quantitative analysis technique, bibliometrics can reveal the current status and trends of a given research field by studying the distribution, quantitative relationships, and changing relationships of literature and information (Mao et al., 2015, 2018b; Liang and Gong, 2017). Overall, bibliometrics is a highly effective method of summarization and analysis and has become a useful tool when dealing with large amounts of scientific data (Mao et al., 2018a). This can help us to study the current state of research and trends in the field of microorganisms in CWs.

In this context, the purpose of this review is to first analyze, *via* bibliometrics, microbial-related articles in the field of CWs and several typical pollutants that are closely associated with microorganisms. Subsequently, the main functional microorganisms associated with the removal of targeted pollutants in CWs are systematically summarized and the effects of these pollutants on the diversity of microbial communities in CWs are discussed. This review will help us to further understand and explore the mechanisms of pollutant removal by microorganisms in CWs and the effects of pollutants in wastewater on microorganisms.

BIBLIOMETRICS

Here, the bibliometrics approach is divided into two main parts: plotting of the publication trends of articles related to CWs and microorganisms using the Origin 2021 software and analyzing the keywords found in the publications in terms of microorganisms using the VOSviewer software.

DATA COLLECTION

Respective data were obtained from the Web of Science (WOS) Core Collection database. And this review only considered the Science Citation Index Expanded (SCI-Expanded). To fully study the changes in the number of publications over the years, only publications from 1900 (the earliest time point that that can be set in the online SCI-Expanded database) to December 2020 were considered.

A search for CWs with the keywords "constructed wetland*" or "artificial wetland*" or "man-made wetland*" or "treatment wetland*" or "engineered wetland*" or "reed bed*" yielded 9,628 documents (the starting year is 1991, as the earliest record of microbial publications is from this year). The keywords "bacteri* OR microb* OR microorganism*" were searched for microbial, yielding a total of 2,764 documents. The year of publication and the bibliographic information of these publications (including authors, titles, source publications, abstracts, and references cited) were exported for subsequent analysis.

BIBLIOMETRIC ANALYSIS

The first aspect is the investigation of the general trend of microbial research by determining the change of articles involving microorganisms in CWs over time. For this, the yearly number of publications was counted and the articles about CWs and microorganisms were indicated separately by different colors to obtain the percentage of articles about microorganisms in the field of CWs (**Figure 1**). As can be seen in **Figure 1**, there is an overall upward trend in the number of yearly publications on CWs and microorganisms. Furthermore, an increasing number of publications involving CWs are related to microorganisms. These results reflect the wide use and study

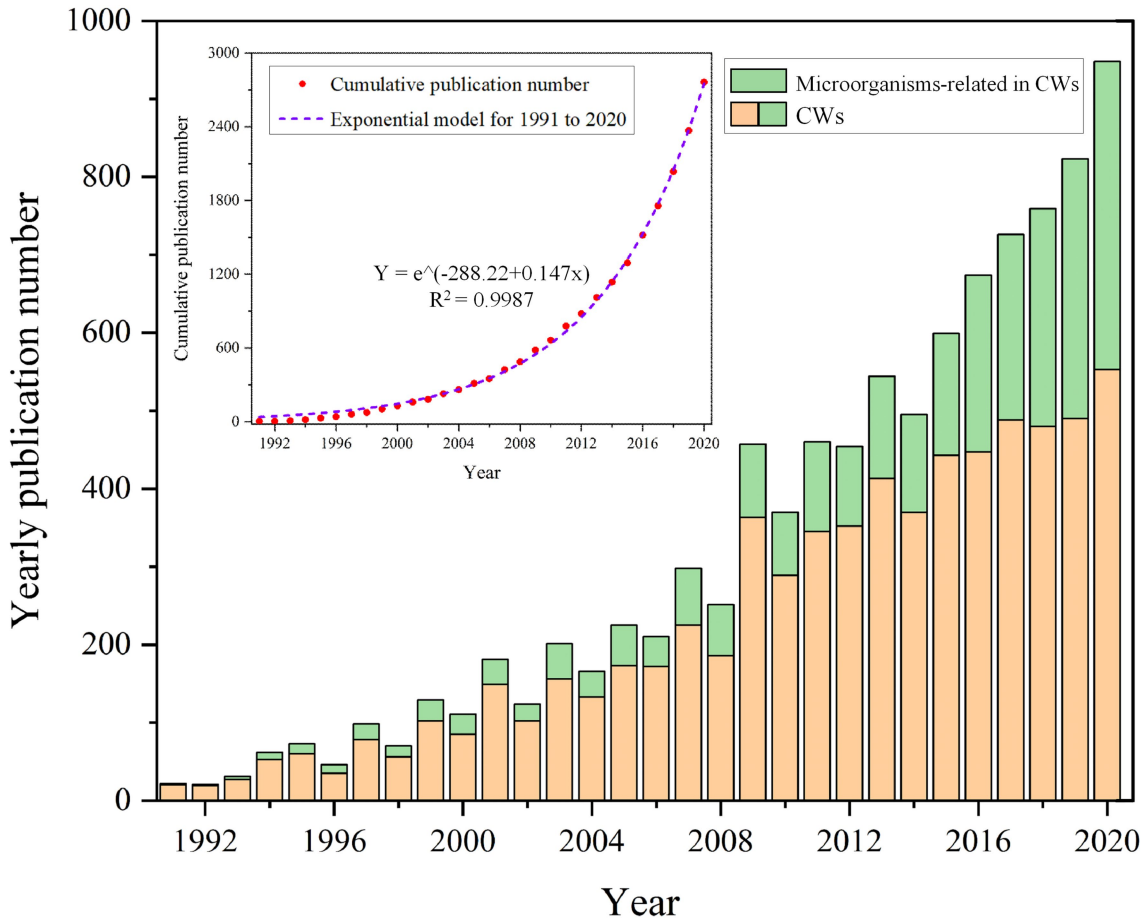

FIGURE 1 | Yearly publications about CWs and microorganisms (cumulative publications curve about microorganisms).

of CWs in an increasing number of countries as well as reflecting the increasing importance of microorganisms. Particularly in recent years with the advances in the molecular characterization of microbial communities, such as denaturing gradient gel electrophoresis or terminal fragment length polymorphism of PCR-amplified 16S ribosomal RNA gene fragments, as well as metagenomics, have greatly contributed to the development of microbial ecology research (Zhao et al., 2016; Sanchez, 2017; Rajan et al., 2019). This can be corroborated with the increasing trend of cumulative publication volume of microbial articles in **Figure 1**. We fit the cumulative publication volume of microbial articles and found that it in line with the exponential function, with an R^2 value of 0.9987, indicating an exponentially increasing publication trend.

The second aspect is the analysis of keyword co-occurrence by the VOSviewer software, with the aim to understand the connection among author keywords. After exporting the publications related to microbial from the WOS platform in plain text form, they were analyzed using the keyword co-occurrence function of the VOSviewer software and subsequently merged through the thesaurus file. The final results are shown in **Figure 2**. This figure shows the top 50 keywords in terms of the number of occurrences number; the high numbers indicate that there are more studies related to them, facilitating the subsequent analysis and summary. Different circles in the figure represent different keywords, and the circle size indicates the number of times the keywords appear, the larger the circle, the more times it appears. The line between the circles indicates that two keywords have appeared together in an article, and the more times they appear together, the thicker the line is. By selecting the keyword "microorganisms," we could observe the connection between this one and other keywords. Among these keywords, we intercepted the top 10 keywords in terms of number; of these 5 were related to the type of contaminants, namely nitrogen, phosphorus, heavy metals, antibiotics, and nutrients. However, among them, nutrients mainly contain nitrogen and phosphorus (Li et al., 2013), and therefore, this review finally identified nitrogen, phosphorus, heavy metals, and antibiotics as four typical contaminants for a functional microbial summary and diversity analysis.

FUNCTIONAL MICROORGANISMS

As mentioned above, four pollutants typical for CWs, namely nitrogen, phosphorus, heavy metals, and antibiotics, were

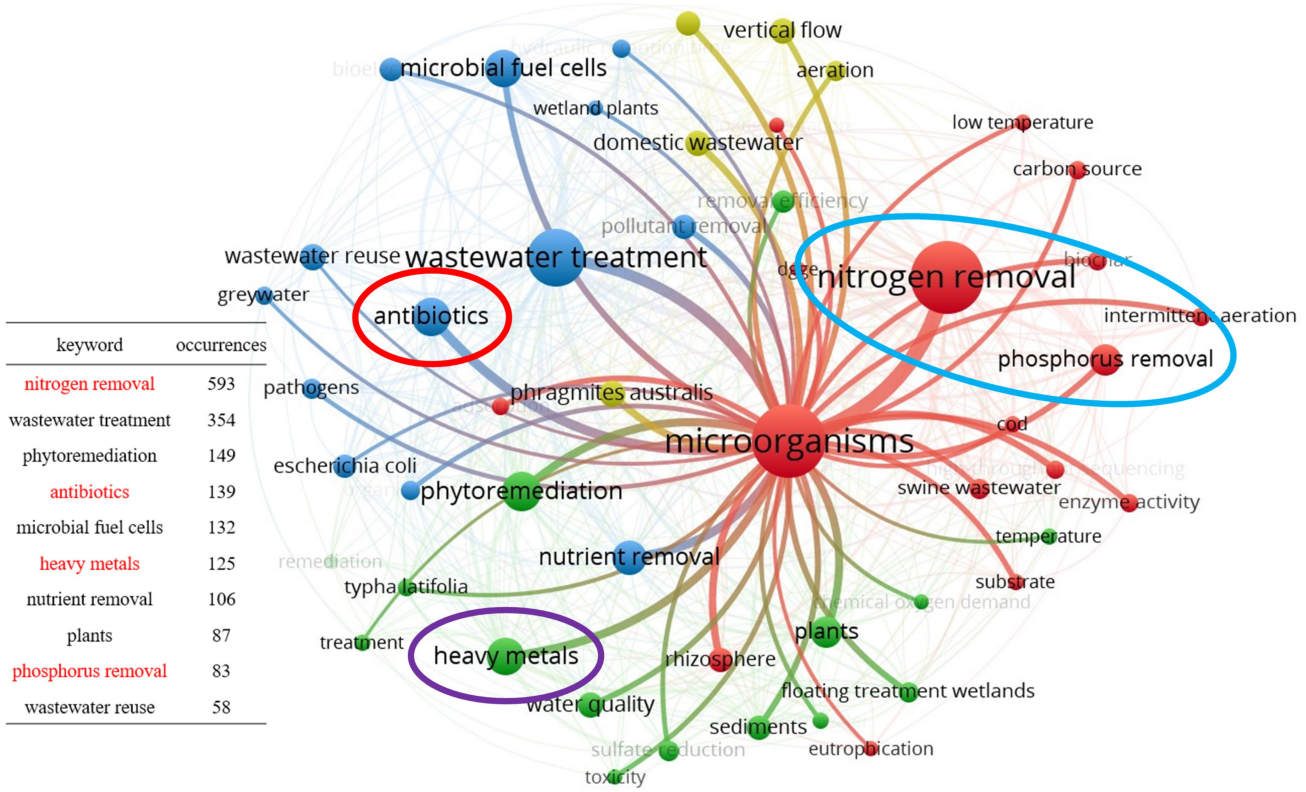

FIGURE 2 | Keyword co-occurrence network visualization map for publications involving microorganisms in CWs.

identified. Many functional microorganisms play an important role in the treatment of these polluted water. This review provides a summary and functional analysis of these microorganisms. Because the microbial species present in CWs are highly diverse, only the more abundant functional species reported were considered. In addition, only the phylum and genus are summarized and analyzed in this review, as most studies have analyzed microbial species at these two levels.

FUNCTIONAL MICROORGANISMS IN NITROGEN REMOVAL

Excess nitrogen discharge into water bodies tends to cause eutrophication and black-odorous, which deteriorates water quality and in turn poses a serious threat to humans and aquatic organisms (Wang et al., 2020d; Zhang et al., 2021c). Biological processes are the key processes in the nitrogen removal mechanisms of CWs, with Tan et al. (2021a) reporting that microorganisms can remove almost 90% of the nitrogen. The main pathways of nitrogen removal by microorganisms in CWs are shown in **Figure 3**.

Current research generally agrees that nitrogen removal by microorganisms in CWs is mainly accomplished through ammonification, nitrification and denitrification (Hu et al., 2016; Xie et al., 2016; Zhao et al., 2018). Ammonification is the process of converting organic nitrogen (Org-N) in wastewater into NH_4^+, which is then removed in other processes (e.g., nitrification, volatilization, and plant uptake; Lee et al., 2014; Xie et al., 2016). As shown in **Table 1**, the popular genera of ammonifying bacteria include *Chitinophaga*, *Isoptericola*, *Bacillus*, and *Sinorhizobium*. Regarding nitrification and denitrification, the microorganisms use NH_4^+ as electron donor during nitrification and oxidize it to NO_2^- and further to NO_3^-, which is then used as electron acceptor during denitrification and reduced to N_2O or N_2 (Tan et al., 2021b; Zhang et al., 2021c). The microorganisms involved in nitrification can be divided into two categories, ammonia-oxidizing bacteria (AOB) and archaea (AOA) which convert ammonium to nitrite, and nitrite-oxidizing bacteria (NOB) which convert nitrite to nitrate (Zhang et al., 2021b,c). In particular, AOA has a higher adaptability to low ammonia and high salt environments compared to AOB (Wang et al., 2019b; Zhao et al., 2021). This can help the AOA to become the predominant group more quickly and speed up the process of nitrification, as ammonia oxidation is the first and rate-limiting step in nitrification (Wang et al., 2019b). The popular phyla involved in nitrification include *Proteobacteria*, *Nitrospirae*, *Nitrospinae*, and *Thaumarchaeota*. Of these, the *Thaumarchaeota* phylum contains all the currently known AOA (Wang et al., 2019b). Regarding denitrification, *Proteobacteria*, *Bacteroidetes*, *Firmicutes*, and *Actinobacteria* are popular denitrifying bacteria in CWs.

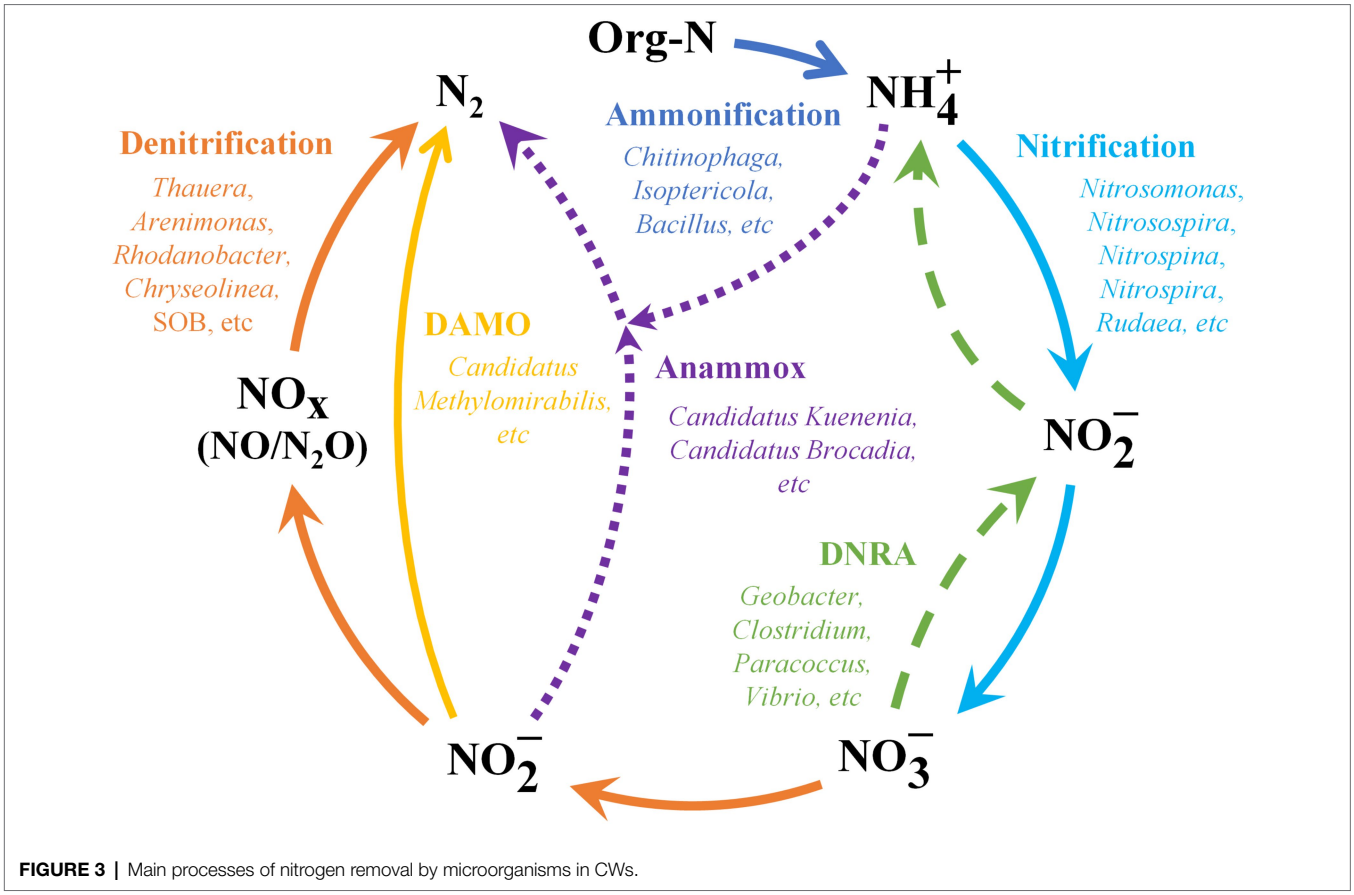

FIGURE 3 | Main processes of nitrogen removal by microorganisms in CWs.

However, nitrifying bacteria in CWs microbial communities usually face problems of low abundance and weak competitiveness (Tan et al., 2021a). This will result in a longer start-up period required for stable NH_4^+ oxidation, making nitrification a limiting step for nitrogen removal (Tan et al., 2021a). In this context, recent studies have highlighted the importance of heterotrophic nitrification and aerobic denitrification (HN-AD) bacteria (Liu et al., 2020b; Tan et al., 2021a; Wang et al., 2022). These bacteria can be responsible for NH_4^+ and NO_3^- transformation in the start-up phase of CWs, converting the nitrogen in the aqueous solution to nitrogen gas for complete denitrification (Tan et al., 2021a). Moreover, they grow more rapidly and can dominate quickly (Tan et al., 2021a). The discovery of HN-AD bacteria has changed the traditional theory that nitrification can only be carried out by autotrophic bacteria and denitrification can only take place under anaerobic conditions, which makes it more advantageous in nitrogen removal and organic matter removal (Wang et al., 2022). The HN-AD bacteria reported in the studies mainly included the genera *Dechloromonas*, *Ferribacterium*, *Hydrogenophaga*, *Zoogloea*, and *Aeromonas*. Regarding the denitrification process, new nitrogen removal pathways have also been detected, such as sulfur autotrophic denitrification (SAD) and denitrifying anaerobic methane oxidation (DAMO; Huang et al., 2020b; Wang et al., 2020a). During SAD, sulfur-oxidizing bacteria (SOB) reduce NO_3^- to N_2, using elemental S, S^{2-}, and $S_2O_3^{2-}$ as electron donors and NO_3^- as electron acceptors under anaerobic or anoxic conditions (Li et al., 2020a; Wang et al., 2020a). Hence, this pathway may dominate in removing nitrogen of low C/N ratio water due to available electron donors from sulfur and its compounds (Wang et al., 2020a). Most sulfur autotrophic denitrifying bacteria belong to the phylum *Proteobacteria*, with the popular genera being *Thiobacillus* and *Sulfurimonas*. Regarding DAMO, which can reduce NO_2^- to N_2 under anaerobic conditions using methane (CH_4) as the electron donor and sole source of carbon (Huang et al., 2020b; Zhang et al., 2020). DAMO can alleviate the greenhouse effect and contribute to reduce the unnecessary byproduct N_2O in the nitrogen removal process, thus allowing for more environmental benefits (Huang et al., 2020b; Zhang et al., 2020).

In addition to the traditional nitrification–denitrification process of nitrogen removal, there exists a novel pathway—anaerobic ammonia oxidation (anammox; Hu et al., 2016; Kraiema et al., 2019). In this pathway, nitrite is used as an electron acceptor under anaerobic conditions to convert ammonia directly to N_2 (Zhao et al., 2018; Kraiema et al., 2019). This makes it an alternative denitrification pathway at low oxygen levels and low C/N ratios (Hu et al., 2016). At present, almost all reported anammox bacteria belong to the phylum *Planctomycetes* (Jia et al., 2021; Zhang et al., 2021c). Regarding nitrate, among the different nitrogenous pollutants, nitrate nitrogen is more likely to leach and eventually deteriorate water

TABLE 1 | Functional microorganisms in CWs for nitrogen removal.

Function		Phyla	Genera (Notes)	Nitrogen transformation process	References
Ammonification		*Bacteroidetes, Actinobacteria, Firmicutes, Proteobacteria*	*Chitinophaga, Isoptericola, Bacillus, Sinorhizobium*	$Org\text{-}N \rightarrow NH_4^+$	Xie et al., 2016
Nitrification	Ammonia oxidizing archaea (AOA)	*Thaumarchaeota*	*Nitrososphaera*, *Nitrosopumilus*, *Candidatus Nitrosotalea*, *Candidatus_Nitrosoarchaeum*, *Candidatus_Nitrosopumilus* *Nitrosomonas*, *Nitrosospira*	$NH_4^+ \rightarrow NO_2^-$	Wang et al., 2019b; Zhao et al., 2021
	Ammonia oxidizing bacteria (AOB)	*Proteobacteria*	(Belongs to *Betaproteobacteria*) *Rudaea,* (Belongs to *Gammaproteobacteria*) *Nitrobacter* (Belongs to *Alphaproteobacteria*)		Zhao et al., 2016; Huang et al., 2019a
	Nitrite oxidizing bacteria (NOB)	*Proteobacteria*	*Nitrosococcus* (Belongs to *Gammaproteobacteria*)	$NO_2^- \rightarrow NO_3^-$	
		Nitrospirae	*Nitrospira*		Zhao et al., 2021
		Nitrospinae	*Nitrospina*		
		Chloroflexi	*Nitrolancea*		Wang et al., 2020d
Denitrification	Traditional denitrification or dissimilatory nitrate to ammonium (DNRA)	*Proteobacteria*	*Bradyrhizobium*, *Hyphomicrobium*, *Rhizobium*, *Rhodobacter*, *Rhodoplanes*, *Paracoccus*, *Methylobacterium*, *Gemmobacter*, *Brevundimonas*, *Roseobacter*, *Azospirillum*	$NO_2^-/NO_3^- \rightarrow N_2\uparrow$ (Traditional denitrification) $NO_2^-/NO_3^- \rightarrow NH_4^+$ (DNRA)	Gao et al., 2017; Zhao et al., 2018, 2019, 2020d, 2021; Aguilar et al., 2019; Liu et al., 2020b; Wang et al., 2020d; Jia et al., 2021; Tan et al., 2021b; Zhang et al., 2021d
			(Belongs to *Alphaproteobacteria*) *Thauera*, *Comamonas*, *Sulfuritalea*, *Denitratisoma*, *Azoarcus*, *Ralstonia*, *Ferribacterium*		
			(Belongs to *Betaproteobacteria*) *Enterobacter*, *Thermomonas, Arenimonas*, *Rhodanobacter*, *Silanimonas*, *Dokdonella*, *Halomonas*, *Zobellella*, *Thiothrix*, *Vibrio*		
			(Belongs to *Gammaproteobacteria*) *Desulfovibrio*, *Geobacter*, *Sulfuricurvum*		
		Actinobacteria	*Propionicella*, *Micropruina*		Zhao et al., 2019
		Bacteroidetes	*Maritimimonas*, *Chryseolinea*, *Prolixibacter*, *Paludibacter*, *Terrimonas*		Si et al., 2018; Ajibade et al., 2021; Kowal et al., 2021; Zhao et al., 2021
		Firmicutes	*Clostridium*		Zhao et al., 2019
		Calditrichaeota	*Calorithrix*		Zhao et al., 2021
	Sulfur autotrophic denitrification (SAD)	*Proteobacteria*	*Thiobacillus, Thiomonas* (Belongs to *Betaproteobacteria*) *Thiohalophilus, Thioalbus* (Belongs to *Gammaproteobacteria*) *Sulfurimonas, Sulfurovum*	$S + NO_3^- + NH_4^+ \rightarrow N_2\uparrow + SO_4^{2-}$	Wang et al., 2020a; Zhao et al., 2021
		Bacteroidetes	(Belongs to *Epsilonproteobacteria*) *Flavobacteriaceae*		Wang et al., 2020a
	Denitrifying anaerobic methane oxidation (DAMO)	*candidate division NC10*	*Candidatus Methylomirabilis*	$CH_4 + NO_2^- \rightarrow N_2\uparrow + CO_2\uparrow$	Zhang et al., 2020
Heterotrophic nitrification and aerobic denitrification (HN-AD)		*Proteobacteria*	*Zoogloea, Dechloromonas, Acidovorax, Hydrogenophaga, Ferritrophicum, Propionivibrio* (Belongs to *Betaproteobacteria*) *Pseudomonas, Acinetobacter, Aeromonas, Klebsiella*	$NH_4^+/NO_3^-/NO_2^- \rightarrow N_2\uparrow$	Liu et al., 2020b; Tan et al., 2021a; Wang et al., 2022
		Bacteroidetes	(Belongs to *Gammaproteobacteria*) *Flavobacterium, Pedobacter*		Zhao et al., 2016
		Firmicutes	*Bacillus*		
Anaerobic ammonia oxidation (anammox)		*Planctomycetes*	*Candidatus_Scalindua, Candidatus Kuenenia, Candidatus Brocadia*	$NH_4^+ + NO_2^- \rightarrow N_2\uparrow$	Zhao et al., 2021

quality (Li et al., 2021b). Therefore, nitrate removal is important to protect freshwater systems and underground water quality (Li et al., 2021b). In addition to denitrification, there is an alternative pathway for the reduction of nitrate, namely the dissimilatory nitrate reduction to ammonium (DNRA; Rahman et al., 2019). DNRA reduces NO_3^- to available NH_4^+ for use by other microorganisms, such as AOB and AOA (Zhang et al., 2021b,c). It has been reported to be more favorable than denitrification under high salinity conditions in sulfide-rich marine and coastal ecosystems (Zhang et al., 2021c). Many studies have found that some denitrifying genera able to execute the DNRA process, such as *Vibrio*, *Clostridium*, and *Desulfovibrio* (Zhang et al., 2021a,c). However, it is still difficult to distinguish denitrifying bacteria from DNRA bacteria, which requires further development of molecular biotechnology. However, currently, denitrifying bacteria and DNRA bacteria are not well distinguished, which requires further development of molecular biotechnology.

Based on the summary in **Table 1**, the phylum *Proteobacteria* contains a large number of species involved in nitrogen transformation. This phylum is widely distributed in CWs and is the most dominant phylum in most systems, playing an important role in nitrogen removal from different wastewaters (Gao et al., 2017; Si et al., 2018; Zhao et al., 2018). The genera *Nitrosomonas*, *Nitrobacter*, and *Nitrosospira* are associated with nitrification. The genera *Tauera*, *Thiobacillus*, *Thermomonas*, and *Arenimonass* are frequently detected among denitrifying bacteria. The class *Alphaproteobacteria*, *Betaproteobacteria*, and *Gammaproteobacteria* are the dominant class related to nitrogen removal in CWs. They contain large numbers of nitrifying bacteria, AOB, and NOB, which play important ecological functions in CWs and are largely involved in the nitrogen removal (Aguilar et al., 2019; Ajibade et al., 2021).

In addition, there is now a growing number of studies linking functional genes to the functional and quantitative analysis of nitrogen removal microorganisms (Zhao et al., 2020d; Tan et al., 2021b; Zhang et al., 2021b). For example, the abundance of *nrfA*- and *nirK*-carrying microorganisms influenced the denitrification performance of CWs (Zhao et al., 2020d); the abundance of the nitrification functional genes *amoA*-AOA, *amoA*-AOB, and *nxrA* represented the growth status of nitrifying bacteria (Zhao et al., 2021). Currently, the functional gene pools associated with the various processes of nitrogen removal (e.g., nitrification, denitrification, anammox, and DNRA) have been summarized (Tan et al., 2021a,b; Zhang et al., 2021b). Functional genes can essentially analyze the function of microorganisms and provide a feasible approach for us to further study functional microorganisms in CWs.

FUNCTIONAL MICROORGANISMS IN PHOSPHORUS REMOVAL

Phosphorus is one of the main elements causing eutrophication in water bodies (Du et al., 2017; Wang et al., 2021b). Excess phosphorus discharged into the aquatic environment from domestic, agricultural, and industrial sources can also harm aquatic life by altering the pH, lowering oxygen levels, and promoting algal growth (Du et al., 2017; Wang et al., 2021b). Microorganisms play an important role in the removal of phosphorus from CWs and can influence the form of the phosphorus (Wang et al., 2021b). The main microorganisms associated with phosphorus removal in CWs are shown in **Table 2**.

Biological phosphorus removal in CWs is mainly achieved by phosphorus-accumulating organisms (PAOs), which can absorb phosphate from wastewater and store it in cells under alternating aerobic and anaerobic conditions (Du et al., 2017; Shi et al., 2017; Tian et al., 2017). Under anaerobic conditions, PAOs break down intracellular polyphosphate and take up volatile fatty acids from the environment, which is then stored in the form of polyhydroxyalkanoates (Lv et al., 2021). Under aerobic conditions, PAOs rely on polyhydroxyalkanoates for energy provision and absorb phosphate to form polyphosphate storage (Tian et al., 2017). In general, the amount of phosphorus uptake by PAOs will be greater than the amount of phosphorus released, thus realizing the phosphorus removal process of microorganisms in CWs (Du et al., 2017; Shi et al., 2017; Tian et al., 2017). The main phylum is *Proteobacteria*, which are largely involved in phosphorus removal (Si et al., 2018, 2019; Huang et al., 2020a). Of these, *Alphaproteobacteria*, *Betaproteobacteria*, and *Gammaproteobacteria* contain most of the microbial species associated with biological phosphorus removal (Shi et al., 2017; Huang et al., 2020a; Wei et al., 2020; Lv et al., 2021). The families *Rhodobacteraceae* and *Rhizobiaceae* of the class *Alphaproteobacteria* can absorb volatile fatty acids under aerobic conditions and convert them into poly-β-hydroxyalkanoates, facilitating total phosphorus removal in CWs (Lv et al., 2021). The class *Betaproteobacteria* mainly contains the genera *Candidatus Accumulibacter*, *Dechloromonas*, and *Rhodocyclus*. Of these, the genus *Candidatus Accumulibacter* is considered a typical PAOs and the dominant PAOs in full-scale wastewater treatment plants and laboratory-scale reactors (Huang et al., 2019a). The genus *Dechloromonas* can reduce perchlorate, accumulate polyphosphate, and absorb carbon under anaerobic conditions (Huang et al., 2020a). *Rhodocyclus* have also been shown to have a significant contribution to phosphorus removal (Li et al., 2017). Regarding *Gammaproteobacteria*, three genera, namely *Klebsiella*, *Pseudomonas*, and *Acinetobacter* have been identified in relevant studies (Tian et al., 2017). Of these, *Pseudomonas* has a strong ability to absorb phosphorus from wastewater and store it in its cells as polyphosphate, making it an effective phosphorus-removal microorganism (Huang et al., 2020a). Tian et al. (2017) report that it can remove up to 80.6% of total phosphorus from domestic wastewater. Regarding the genus *Acinetobacter*, it is the first bacteria isolated from biomass with a high phosphorus removal capacity (Du et al., 2017). In addition to *Proteobacteria*, other taxa, such as *Gemmatimonadacea*, that can take up excess phosphate under aerobic conditions (Wang et al., 2021b).

The phosphorus removal efficiency of PAOs mainly depends on the accumulation and consumption of intracellular polyphosphate (Tian et al., 2017), which is directly related to the activities of the enzymes exopolyphosphatase (ppx) and polyphosphate kinase (ppk; Du et al., 2017). The ppx and ppk can catalyze anaerobic phosphorus release and aerobic phosphorus

TABLE 2 | Functional microorganisms in CWs for phosphorus removal.

Function	Phyla	Genera (Notes)	Morphology of the removed phosphorus	References
PAO	*Proteobacteria*	*Rhodobacteraceae* (family), *Rhizobiaceae* (family)	Phosphate	Lv et al., 2021
		(Belongs to *Alphaproteobacteria*) *Candidatus Accumulibacter*, *Dechloromonas*, *Rhodocyclus*		Li et al., 2017; Huang et al., 2019a, 2020a; Zheng et al., 2021a
		(Belongs to *Betaproteobacteria*) *Pseudomonas*, *Klebsiella*, *Acinetobacter*		Du et al., 2017; Tian et al., 2017; Huang et al., 2020a; Zheng et al., 2021a
		(Belongs to *Gammaproteobacteria*) *Rhodocyclaceae* (family), *Gemmatimonadacea* (family), *Gemmatimonas*		Wei et al., 2020; Wang et al., 2021b
PSB	*Actinobacteria, Proteobacteria*	*Corynebacterium*, *Enterobacter*	Convert insoluble phosphorus into soluble phosphorus	Wang et al., 2021b
DNPAO	*Proteobacteria*	*Paracoccus* (Belongs to *Alphaproteobacteria*), *Pseudomonadaceae* (family), Pseudomonas, Dechloromonas	Polyphosphate	Huang et al., 2019a; Lv et al., 2021; Wang et al., 2021b
	Chloroflexi	*Anaerolineae* (class)		Lv et al., 2021
Solubilize vast tricalcium phosphate through secreting organic acids	*Proteobacteria*	*Delftia* (Belongs to *Betaproteobacteria*)	Phosphate	Li et al., 2020b
Associated with the P element cycle	*Proteobacteria*	*Brevundimonas*, *Pseudorhodoferax*, *Variovorax*, *Panacagrimonas*	Organic phosphoric acid esters/ Insoluble phosphate	Wu et al., 2020
	Chlorobi, Firmicutes, Spirochaetes	*Chlorobaculum*, *Bacillus*, *Leptospira*		Wu et al., 2020

uptake, respectively, to achieve biological phosphorus removal (Tan et al., 2021b). However, high temperatures inhibit their activities; according to a previous study, the optimum temperature ranges from 20.0–35.0°C (Du et al., 2017).

In addition to PAOs, phosphorus-solubilizing bacteria (PSB) and denitrifying phosphorus-accumulating organisms (DNPAO) have also been found in CWs. Example are the genera *Corynebacterium* and *Enterobacter*, which are PSB that secrete organic acids (e.g., oxalic and citric acids) to convert insoluble phosphorus in the soil into soluble phosphorus for plant uptake (Wang et al., 2021b). Regarding DNPAO, it can use NO_3^-/NO_2^- as electron acceptors to absorb polyphosphate under anoxic conditions (Wang et al., 2020b). *Alphaproteobacteria* (e.g., the genus *Paracoccus*) and *Anaerolineae* have been reported to be DNPAO (Lv et al., 2021). The genera *Brevundimonas* and *Chlorobaculum* produce organophosphate hydrolases that hydrolyze organophosphate esters, and *Variovorax* can use insoluble phosphate as a phosphorus source for growth (Wu et al., 2020).

FUNCTIONAL MICROORGANISMS IN HEAVY METAL REMOVAL

Heavy metals are widely distributed in aquatic systems, difficult to degrade, and can accumulate in the food chain, making them hazardous environmental pollutants (Yu et al., 2020; Chen et al., 2021b). In CWs, microorganisms can be effective in removing heavy metals through mechanisms, such as biosorption, biomineralization, and valence transformation (Si et al., 2019; González Henao and Ghneim-Herrera, 2021). **Figure 4** shows the main pathways of heavy metal removal by microorganisms in CWs. The relevant microbial phyla and genera are summarized in **Table 3**.

Among heavy-metal polluted water, mining-impacted water, especially acid mine drainage (AMD), has attracted widespread attention worldwide (Chen et al., 2021b). The AMD generated during and after mining and smelting activities is characterized by high acidity and sulfate and toxic metallic ion enrichment (Chen et al., 2021b,c). Therefore, for AMD remediation, bacterial sulfate reduction in CWs is a key process as it reduces the acidity of AMD and removes heavy metals by immobilizing them as sulfides, hydroxides, and carbonate precipitates (Chen et al., 2021c). The bacteria involved in sulfate reduction are known as sulfate-reducing bacteria (SRB) and they can drive simultaneous sulfate and metal removal as well as acidity neutralization (Habe et al., 2020; Chen et al., 2021b). The majority of SRB belong to the class *Deltaproteobacteria* in the phylum *Proteobacteria*. Among them, the more popular ones include the genera *Desulfovibrio*, *Desulfobacter*, *Desulfobulbus*, and *Desulfurobacterium*. In addition to SRB, other functional microorganisms with complementary ecological niches are also important for the effective remediation of AMD (Chen et al., 2021b,c). For example, members of the genus *Propioniciclava* can use a variety of carbohydrates to produce acetate and propionic acids, driving dissimilatory SBR metabolism (Torregrosa et al., 2019). Regarding the genus *Cellulomonas*, it can protect SRB

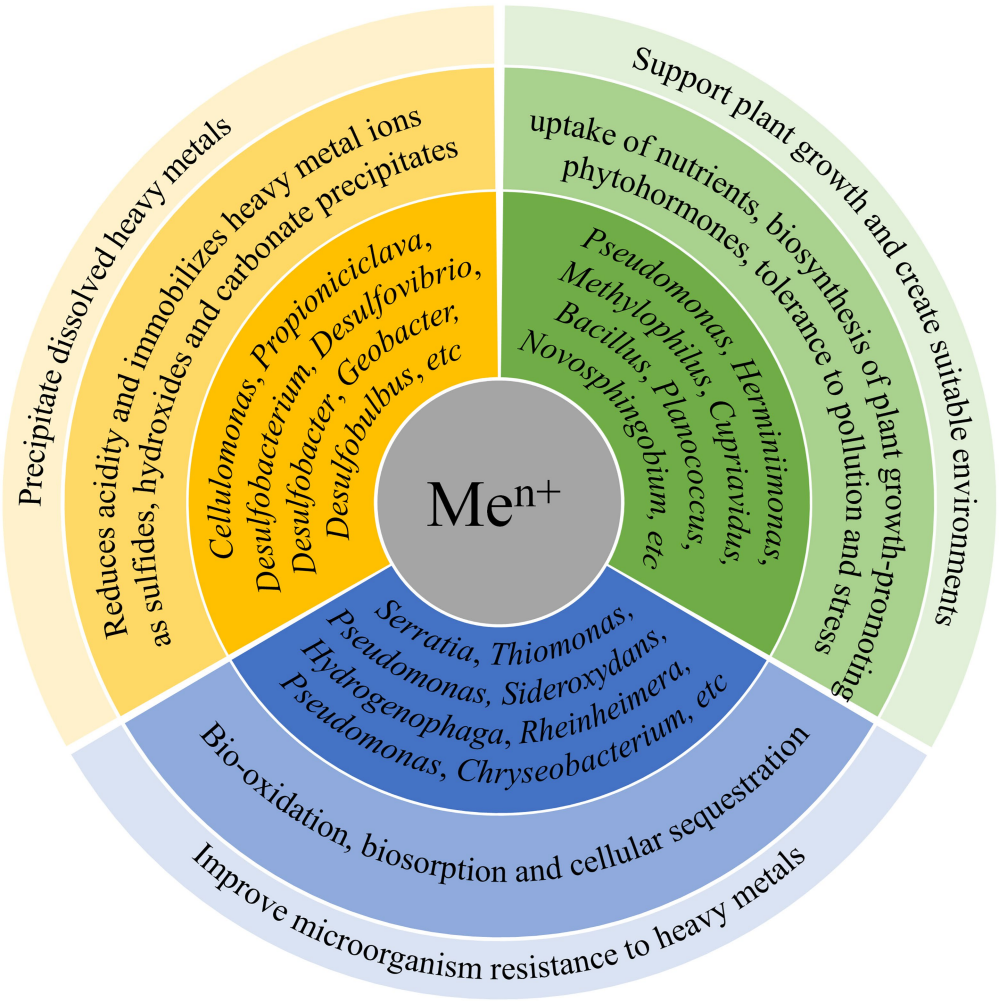

FIGURE 4 | Main mechanisms of heavy metal removal by microorganisms in CWs.

community from oxygen exposure and also generate low-molecular-weight compounds through saccharification and fermentation to act as electron donors for SRB (Chen et al., 2021b). Therefore, these phyla and genera, which are mainly involved in organic decomposition and sulfate reduction, are the key microbial groups participating in the treatment of AMD in CWs.

Ironically, metal ions generally negatively impact microorganisms by disrupting cell membranes, inhibiting enzyme activity, destroying DNA, and disturbing cellular function (Yu et al., 2020), making tolerance important for the removal of heavy metals by microorganisms. Fe^{2+} can be oxidized to Fe^{3+} by the genera *Thiomonas* and *Sideroxydans*, making it easier to precipitate and thus less hazardous (Chen et al., 2021c). Yu et al. (2020) also found that the genera *Serratia* and *Pseudomonas* screened using Cd^{2+} and Zn^{2+} concentrations gradients showed resistant to these two heavy metals resulting in an increase in removal rates of 10.13 and 8.57%, respectively. The extracellular polymeric substances synthesized by *Pseudomonas* can bind heavy metals and block their diffusion within the biofilm, achieving extracellular sequestration, thereby protecting cells from heavy metal stress (Teitzel and Parsek, 2003; Giovanella et al., 2017). In addition, the cell surface of *Pseudomonas* and *Serratia* could also enhance the adsorption of Cd^{2+} and Zn^{2+} due to the presence of anionic functional groups (Cristani et al., 2012; Limcharoensuk et al., 2015). These findings lead us to infer that the cultivation of resistant microorganisms is a viable approach in heavy metal removal from wastewater and deserves further investigation. However, the way in which *Serratia* reduces the hazard of heavy metals is through secreting several proteins and enzymes such as heavy metal-binding proteins, transporter proteins, amino acids, histidine-binding proteins, and redox enzymes, which can efflux metal ions (Chen et al., 2019). This cannot contribute to heavy metal removal by CWs. Therefore, resistant microorganisms are not exactly the same as functional microorganisms and further research into the mechanisms of heavy metal removal by microorganisms is required to make a determination. Yu et al. (2020) found that functional microorganisms also evolved in the control group that was not inoculated with resistant

TABLE 3 | Functional microorganisms in CWs for heavy metal removal.

Pollutant type	Phyla		Genera (Notes)	Removal principle	References
MIW, Especially AMD (Mainly contains Fe^{2+}, Cd^{2+}, Zn^{2+}, Cu^{2+}, Cr^{2+} and other heavy metals)	SRB	*Proteobacteria*	*Desulfobacterium*, *Desulforhabdus*, *Desulfobacca*, *Desulforegula*, *Desulfomonile*, *Desulfofustis*, *Desulfovibrio*, *Desulfobacter*, *Desulfobulbus*, *Desulfococcus*, *Desulfocapsa*, *Desulfatirhabdium* (Belongs to *Deltaproteobacteria*)	$SO_4^{2-} + 2CH_2O \rightarrow H_2S + 2HCO_3^-$ (H_2S is dissociated into $HS^- + H^+$) $H_2S + Me^{2+} \rightarrow MeS \downarrow + 2H^+$ (Me^{2+} refers to heavy metal ions)	Chen et al., 2016, 2021c; Sanchez, 2017; Urakawa et al., 2017
		Firmicutes	*Desulfotomaculum*, *Desulfosporosinus*		Urakawa et al., 2017; Habe et al., 2020
		Aquificae	*Desulfurobacterium*		Urakawa et al., 2017
	Others	*Actinobacteria*, *Proteobacteria*	*Cellulomonas*, *Propioniciclava*, *Geobacter*		Chen et al., 2021b,c
Fe^{2+}	*Proteobacteria*		*Thiomonas*, *Sideroxydans*	Bio-oxidation	Chen et al., 2021c
Cd^{2+}, Zn^{2+}	*Proteobacteria*		*Serratia*, *Pseudomonas*	Biosorption/Cellular sequestration	Yu et al., 2020
Cu^{2+}	*Fusobacteria, Bacteroidetes, Proteobacteria*		*Hydrogenophaga*, *Rheinheimera*	Resistant to heavy metals	Guo et al., 2021
Cd^{2+}	*Proteobacteria, Bacteroidetes*		*Pseudomonas*, *Chryseobacterium*		Zhang et al., 2021e
Fe^{2+}, Se^{4+}	*Firmicutes, Proteobacteria*		*Bacillus*, *Planococcus*, *Pseudomonas*	Support plant growth	Vassallo et al., 2020
Zn^{2+}, Ni^{2+}, Cd^{2+}	*Proteobacteria*		*Herminiimonas*, *Methylophilus*, *Cupriavidus*, *Novosphingobium*		Syranidou et al., 2018

microorganisms, albeit over a longer period. Most likely, the microbial community structure in the system was spontaneously altered, facilitating resistance to heavy metal stress. In contrast, systems inoculated with resistant microorganisms can experience a less pronounced microbial community evolution to obtain a dominant strain when encountering environments with heavy metals, saving time for biofilm stabilization (Rahman, 2020).

The interactions between microorganisms and plants also greatly affects the removal of heavy metals (González Henao and Ghneim-Herrera, 2021). Microorganisms and plants have long been growing together and microorganisms have more or less established associations with plants (Vassallo et al., 2020). In particular, rhizobacteria and endophytic bacteria can support plant growth through uptake of nutrients (e.g., N, P, Mg, Fe, and Ca), biosynthesis of plant growth-promoting phytohormones, and tolerance to pollution and stress (Syranidou et al., 2018; Vassallo et al., 2020). This can alleviate the toxic stress of heavy metals on plants and can also facilitate the accumulation of heavy metals by plants (Syranidou et al., 2018; Vassallo et al., 2020). In turn, the main function of plants in CWs is to provide additional oxygen and organic matter for microbial growth (Zhou et al., 2013). Thus, good plant growth also provides a more suitable environment for microbial growth (Sturz et al., 2000). This mutualistic interaction facilitates heavy metal removal by CWs. Syranidou et al. (2016) found that inoculation of the *Juncus acutus* with a selected endophytic bacterial consortium removed emergent pollutants and metals faster and more efficiently compared to uninoculated plants. Similarly, Vassallo et al. (2020) isolated eight bacterial strains (belonging to the genera *Bacillus*, *Planococcus*, and *Pseudomonas*) from samples taken from the roots of *Phragmites australis*. They grew well in wastewater with high concentrations of heavy metals (45 mg/l for Fe and 0.09 mg/l for Se), and the higher the concentration of heavy metals, the faster they grow (Vassallo et al., 2020). In conclusion, rhizobacteria and endophytic bacteria have been shown to be reliable functional microorganisms for heavy metal removal as they have sufficient resistance to heavy metals and can enhance phytoremediation efficacy.

FUNCTIONAL MICROORGANISMS IN ANTIBIOTIC REMOVAL

Antibiotics are compounds that inhibit the growth of microorganisms (Chen et al., 2020; Xu et al., 2020). They are widely used in human and animal medicine and as animal growth promotors (Chen et al., 2020; Xu et al., 2020). Based on previous studies, antibiotics are now widely present in

aquatic environment and that their presence and persistence often cause toxic effects, posing a significant threat to humans, animals, and aquatic habitats (Huang et al., 2017; Shan et al., 2020; Lu et al., 2021). Antibiotic contamination can also lead to the spread of resistance genes, thereby increasing the resistance of microorganisms and reducing the therapeutic potential against human and animal pathogens (Troiano et al., 2018; Chen et al., 2020; Shan et al., 2020). It has been reported that CWs are highly suitable for antibiotic removal, with removal efficiencies as high as 91.8 to 99.5% (Xu et al., 2020). The removal of antibiotics in CWs has undergone a series of complex physical, chemical and biological processes, such as adsorption, precipitation, and microbial degradation (Wang et al., 2019a). Among them, microorganisms are considered to be the driving force for the degradation of antibiotics in CWs (Wang et al., 2019a; Shan et al., 2020; Zheng et al., 2021b). The main functional microorganisms involved in antibiotics removal in CWs are summarized in **Table 4**.

Sulfonamides (SAs), including sulfamethoxazole (SMX) and sulfadiazine (SDZ), are widely used in animal agriculture and human health care and are the most common residual antibiotics in almost all environmental compartments (Ouyang et al., 2021). They can significantly inhibit bacterial populations, such as *Desulfarculus*, denitrifying bacteria, and *Syntrophobacter*, affecting the sulfur and nitrogen cycles (Man et al., 2020). Microbial-mediated degradation can significantly contribute to the removal of SAs in CWs, both under aerobic and anaerobic conditions (Chen et al., 2020). For example, under aerobic conditions, *Bacillus* and *Geobacter* can degrade SAs (Chen et al., 2020). The genus *Bacillus*, belonging to the phylum *Firmicutes*, can be enriched under SAs stress, degrading SMX to NH_4^+ and further to NO_3^- (Liu et al., 2018). *Geobacter*, a member of the phylum *Proteobacteria*, is considered a potential SDZ degrader (Zhang et al., 2019a). The genus *Microbacterium* in the phylum *Actinobacteria* can also use SMX as the sole carbon source under aerobic conditions (Sauvetre et al., 2020; Ouyang et al., 2021). The molecular mechanism of SMX catabolism by *Microbacterium* is initiated by ipso-hydroxylation, followed by NADH-dependent hydroxylation of the carbon atom attached to the sulfonyl group, which leads to the release of sulfite, 3-amino-5-methylisoxazole, and benzoquinone imine, of which the latter is converted to 4-aminophenol (Ricken et al., 2013). As for the genus *Bradyrhizobium* can accelerate SAs removal under anaerobic conditions (Chen et al., 2020). In CWs, the three main phyla involved in the degradation of SAs are *Proteobacteria*, *Actinobacteria* and *Firmicutes*, and some key genera, such as *Pseudomonas*, may metabolize glucose and subsequently attenuate SMX by co-metabolism of organic matter and SMX (Zheng et al., 2021b). In addition, *Desulfovibrio* also plays a key role in SMX transformation and can transform SMX alone (Ouyang et al., 2021).

In addition to SAs, common antibiotics include fluoroquinolones (FQ) and cephalosporin (CP), two of which are the most widely used antimicrobials drugs worldwide (Alexandrino et al., 2017). Among them, FQ include ciprofloxacin (CIP), ofloxacin (OFL), and enrofloxacin (ENR); CP include ceftiofur (CEF). For these types of antibiotics, Amorim et al. (2014) investigated the soil bacterium *Labrys portucalensis F11* in minimal medium supplemented with acetate as an additional carbon source and demonstrated its ability to degrade a range of FQ (e.g., CIP). Similarly, Lin et al. (2016) suggested that the genus *Arthrobacter* can dissipate FQ (e.g., OFL) as an additional carbon and energy source. The genus *Dysgonomonas* has also been shown to biodegrade ENR and CEF (Alexandrino et al., 2017).

In addition, the first Watch List of the EU Water Framework Directive [European Commission (EC)2015] identifies the anti-inflammatory diclofenac (DCF) and the antibiotic SMX as two emerging contaminants (Sauvetre et al., 2020). For DCF, Bessa et al. (2017) demonstrated that strain *Brevibacterium* sp. *D4* could biodegrade 35% of 10 mg/l of DCF as the sole carbon source. Moreira et al. (2018) also reported that the bacterial strain *Labrys. portucalensis F11* degraded 70% of 34 μM of DCF, supplied as the sole carbon source, after 30 days of cultivation. Regarding the microorganisms associated with the degradation of other antibiotics, such as ampicillin, tetracycline, triclosan (TCS), and ceftiofur (CEF) are listed in **Table 4**.

As shown in **Table 4**, the vast majority of functional microorganisms related to antibiotic removal belong to the *Proteobacteria*, *Acidobacteria*, and *Bacteroidetes* phyla, probably due to the presence of degradation genes (Liu et al., 2019). According to Huang et al. (2017), the phylum most significantly related to antibiotic removal is *Proteobacteria* phylum, followed by *Bacteroidetes* and *Actinobacteria*. Of these, *Betaproteobacteria* of the phylum *Proteobacteria* have been shown to be effective in addressing the global antibiotic resistance issue (Alexandrino et al., 2017; Shan et al., 2020).

However, functional microorganisms may develop antibiotic resistance in the process of degrading antibiotics and may even cover functions other than antibiotic resistance (Alonso et al., 2001; Troiano et al., 2018). Antibiotic resistance may be inherent to microorganisms or may arise through horizontal gene transfer from donor bacteria, phages, or free DNA (Alonso et al., 2001; Troiano et al., 2018; Santos et al., 2019a). An increase in antibiotic resistant microorganisms may lead to a decrease in the therapeutic potential of antibiotics, thus making it more difficult to treat microorganisms' infections (Santos et al., 2019a). Notably, an induction of antibiotic resistance genes has been reported with the effective removal of antibiotics by CWs (Liu et al., 2019). Therefore, it is a great challenge for CWs to avoid the induction of antibiotic resistance genes while effectively removing antibiotics.

EMERGING POLLUTANTS

In addition to the above four typical pollutants, CWs are also used to remove some emerging pollutants, such as hormones, pesticides, food additives, flame retardants, nanoparticles, and persistent organic pollutants (e.g., polychlorobiphenyls and polycyclic aromatic hydrocarbons; Rajan et al., 2019; Vymazal et al., 2021; Yin et al., 2021). Biodegradation is generally considered as one of the important processes responsible for these emerging pollutants removal

TABLE 4 | Functional microorganisms in CWs for antibiotic removal.

Antibiotic Category		Phyla	Genera (Notes)	Removal principle	References
SAs	SMX	*Proteobacteria*	*Sphingomonas*, *Bradyrhizobium*, *Sphingorhabdus*, *Reyranella*, *Ochrobactrum, Sphingobium*, *Hyphomicrobium*	Biodegradation or use of antibiotics as carbon source	Syranidou et al., 2017; Man et al., 2020; Sauvetre et al., 2020; Zheng et al., 2021b
			(Belongs to *Alphaproteobacteria*) *Acidovorax*, *Ralstonia*, *Azonexus*		Syranidou et al., 2017; Chen et al., 2020
			(Belongs to *Betaproteobacteria*) *Desulfovibrio* (Belongs to *Deltaproteobacteria*) *Pseudomonas*, *Luteimonas*, *Enterobacter*, *Acinetobacter*		Ouyang et al., 2021
			(Belongs to *Gammaproteobacteria*)		Wegrzyn and Felis, 2018; Ouyang et al., 2021; Zheng et al., 2021b
		Actinobacteria	*Rhodococcus*, *Microbacterium*, *Arthrobacter*, *Gordonia*, *Nocardioides*, *Streptomyces*		Syranidou et al., 2017; Wegrzyn and Felis, 2018; Sauvetre et al., 2020; Ouyang et al., 2021
		Firmicutes	*Bacillus*, *Virgibacillus*		Syranidou et al., 2017; Chen et al., 2020
	SDZ	*Proteobacteria*	*Geobacter* (Belongs to *Deltaproteobacteria*) *Labrys*, *Bradyrhizobium*		Chen et al., 2020
	CIP	*proteobacteria*	(Belongs to *Alphaproteobacteria*) *Pseudoxanthomonas*		Syranidou et al., 2017; Santos et al., 2019b; Chen et al., 2020
			(Belongs to *Gammaproteobacteria*)		Santos et al., 2019b
FQ		*Actinobacteria, Bacteroidetes*	*Nocardioides*, *Dysgonomonas* *Rhizobacter*, *Uliginosibacterium*		Alexandrino et al., 2017; Santos et al., 2019b
	OFL	*Proteobacteria*	(Belongs to *Betaproteobacteria*)		Lu et al., 2021
		Actinobacteria, Bacteroidetes	*Arthrobacter*, *Bacteroides*		Tong et al., 2020; Lu et al., 2021
	ENR	*Bacteroidetes*	*Alkaliflexus*, *Dysgonomonas*		Alexandrino et al., 2017; Santos et al., 2019b
DCF		*Proteobacteria*	*Labrys*, *Sphingobium* (Belongs to *Alphaproteobacteria*)		Wegrzyn and Felis, 2018; Sauvetre et al., 2020
		Actinobacteria	*Microbacterium*, *Brevibacterium*, *Streptomyces*		Wegrzyn and Felis, 2018; Sauvetre et al., 2020
		Fungi	*Trametes*		Wegrzyn and Felis, 2018
Ampicillin		*Proteobacteria*	*Luteimonas*, *Pseudoxanthomonas* (Belongs to *Gammaproteobacteria*)		Santos et al., 2019b; Zheng et al., 2021b
Tetracycline		*Proteobacteria*	*Novosphingobium* *Pseudomonas*, *Alcaligenes*, *Stenotrophomonas*, *Methylococcales* (order)		Santos et al., 2019b; Lu et al., 2021
TCS		*Proteobacteria*			Liu et al., 2016
CEF		*Bacteroidetes*	(Belongs to *Gammaproteobacteria*) *Dysgonomonas*		Alexandrino et al., 2017

(Vymazal et al., 2021). Zhang et al. (2021e) found that *Firmicutes*, *Clostridia*, and *Acetobacterium* were able to tolerate abiotic stresses and thus degrade chlorpyrifos into carbon sources. Liu et al. (2020b) demonstrated that *Pseudomonas*, *Duganella*, and *Sphingobium* are resistant to the threat of organophosphate flame retardants [tris (2-chloroethyl) phosphate, tris (1-chloro-2-propyl) phosphate, and tricresyl phosphate] and have the ability to biodegrade. Ahmad et al. (2019) also showed that various genera, such as *Flavobacteriaceae*, *Novosphingobium*, and *Mycobacterium* can degrade polycyclic aromatic hydrocarbons in a diverse environment. However, there is still relatively little research on these emerging pollutants removed by microorganisms in CWs, so this section is not the focus of this review and more research is needed in the future to focus on the degradation and removal mechanisms of these emerging pollutants by microorganisms.

MICROBIAL ALPHA DIVERSITY ANALYSIS

In addition to the composition and structure of microorganisms, the diversity of microbial communities can also influence the performance of CWs in removing pollutants (Zhang et al., 2019b). Therefore, this review explored the effect of four typical pollutants on the microbial diversity of CWs by counting the values of microbial diversity in different studies. As alpha diversity can reflect the species diversity of microbial communities within a given region, this review has chosen to represent the diversity of microbial communities through the value of alpha diversity (Pitacco et al., 2019; Laliberte et al., 2020).

To better reflect the influence of pollutant concentration on microbial diversity, the pollutants nitrogen and phosphorus were classified into high and low concentrations. Since CWs are generally used for deep treatment of the tailwater of wastewater treatment plants, wastewater with total nitrogen concentrations exceeding 20 mg/l and total phosphorus concentrations exceeding 1.5 mg/l was designated as high concentrations with reference to the Discharge Standard of Pollutants for Municipal Wastewater Treatment Plant (GB 18918–2002) - level B standard. **Table 5** shows the specific values of microbial alpha diversity in CWs considering the four typical pollutants (nitrogen, phosphorus, heavy metals, and antibiotics). To better visualize and compare, box plots (**Figure 5**) were generated using the median value of alpha diversity in **Table 5** as the data.

EFFECTS OF NITROGEN AND PHOSPHORUS ON ALPHA DIVERSITY

As shown in **Figure 5**, nitrogen and phosphorus have similar effects on alpha diversity, so we put them together for analysis. Regarding richness, at high concentrations of nitrogen and phosphorus, both the Chao1 index and the ACE index were significantly lower than at low concentrations, suggesting that microbial richness is severely reduced in environments with high concentrations of these pollutants. Most likely, microorganisms not involved in pollutant removal are eliminated or suppressed in these extreme environments, resulting in fewer microbial species (Xiao et al., 2020). The closer data for high concentrations of nitrogen and phosphorus also indicate that certain specific microbial species may have formed, resulting in similar richness levels in different studies. On the contrary, at low concentrations of nitrogen and phosphorus, although the values of both Chao1 and ACE indexes were higher, the data were more scattered. This may be due to the dominance of other influencing factors, such as C/N ratio (Jia et al., 2021) and substrate type (Ajibade et al., 2021).

Regarding diversity, it is evident from the Simpson index that high concentrations of nitrogen lead to a decrease in diversity, i.e., to the emergence of dominant populations. This corresponds with the richness analysis. Apparently, high nitrogen concentrations facilitate the growth of microorganisms associated with nitrogen cycling and suppress the growth of microorganisms of other functions (Xiao et al., 2020). Interestingly, the Shannon index was high but the Simpson index was low for high phosphorus concentrations, with the opposite pattern for low phosphorous levels. This may be explained by the high sensitivity of the Shannon index to community richness (Zhang et al., 2019b). Low phosphorous concentrations allow for a consistently high level of species diversity, reflecting no large differences in abundance among microorganisms with different functions in the absence of significantly prominent contaminants.

The combined richness and diversity indices show that high concentrations of nitrogen and phosphorus lead to varying reductions in both indices, reflecting the presence of significantly dominant populations. These populations are the functional microorganisms that play an important role in the removal of nitrogen and phosphorus.

EFFECTS OF HEAVY METALS ON ALPHA DIVERSITY

Heavy metals can significantly decrease microbial richness. This can be explained by the toxicity of heavy metals to microorganisms and the inability of microorganisms to directly degrade heavy metals (Bianchi et al., 2020). In this sense, the presence of heavy metals had a selection effect on microorganisms in CWs, and microbial succession occurred in CWs over time, where the enrichment and structural optimization of dominant species may lead to the reduction in richness and diversity (Xiao et al., 2021). However, in contrast to the case of high concentrations of nitrogen and phosphorus, the difference between the data for heavy metals is larger, resulting in a larger box in the box plot. The most likely reasons for this are that the toxicity of different types of heavy metals to microorganisms may vary and that different microorganisms have different resistance levels to heavy metals.

TABLE 5 | Alpha diversity of microorganisms in CWs treated different pollutant.

Alpha Diversity	Richness		Diversity		Concentration of pollutants (mg/l)	References
Pollutant type	**Chao1**	**ACE**	**Shannon**	**Simpson**		
High concentration of nitrogen	266.500 ± 62.500	269.000 ± 59.000	3.39500 ± 0.58500		NH_4^+ = 35.000, TN = 40.000	Zhao et al., 2016
	621.250 ± 115.150		4.07000 ± 0.71000		NO_3^- = 4.395 ± 0.695, NH_4^+ = 79.945 ± 1.805, TN = 87.100 ± 2.620	Li et al., 2019
	841.500 ± 163.500	1048.950 ± 190.230	6.72500 ± 0.17500	0.96814 ± 0.00316	NH_4^+ = 89.200	Xu et al., 2021
	1237.117 ± 230.722	1224.746 ± 245.1905	6.66750 ± 1.25450	0.96100 ± 0.02800	NH_4^+ = 18.000, NO_3^- = 6.000, TN = 24.000	Xia et al., 2020
	1296.915 ± 59.345	1292.191 ± 62.723	5.27000 ± 0.17400	0.98615 ± 0.00345	NO_3^- = 50.000	Zhao et al., 2019
	1375.965 ± 257.945	1422.860 ± 244.730	5.78500 ± 0.78500		NH_4^+ = 226.284	Lv et al., 2021
	1586.500 ± 214.500		7.67250 ± 0.13250		NH_4^+ = 20.140 ± 0.420, NO_3^- = 39.290 ± 0.730	Deng et al., 2019
	1725.500 ± 108.500	1725.500 ± 108.500	7.84500 ± 0.09500	0.97331 ± 0.00690	NH_4^+ = 115.000, NO_3^- = 182.000	Zhao et al., 2020d
	1755.075 ± 92.235		7.68319 ± 0.43451	0.97313 ± 0.00814	NH_4^+ = 26.250 ± 11.250, NO_3^- = 10.500 ± 4.500, TN = 43.750 ± 18.750	Xiao et al., 2020
	2001.110 ± 883.090	2091.605 ± 913.475	7.15500 ± 2.15500	0.89171 ± 0.10240	NH_4^+ = 112.580	Wang et al., 2021b
	2274.150 ± 56.660		7.76500 ± 0.20500	0.97500 ± 0.00500	NH_4^+ = 15.170 ± 0.804, TN = 21.910 ± 1.190	Huang et al., 2018
	2299.615 ± 366.595		5.31000 ± 0.42100	0.96165 ± 0.02155	NH_4^+ = 20.000, NO_3^- = 1.200, TN = 35.000	Yang et al., 2021
	4398.800 ± 804.200	4960.050 ± 535.150	5.48500 ± 1.35500	0.93350 ± 0.06250	NH_4^+ = 29.900, TN = 39.000	Zheng et al., 2020
	4422.000 ± 315.000		6.51850 ± 0.25450	0.99235 ± 0.00295	NH_4^+ = 18.680, TN = 60.360	Pelissari et al., 2018
	2133.745 ± 127.930	2144.504 ± 139.730	5.84550 ± 0.15450	0.99150 ± 0.00250	NH_4^+ = 5.315 ± 2.345, TN = 13.425 ± 5.785	Li et al., 2021a
	2346.600 ± 216.230	2330.600 ± 228.940	6.28000 ± 0.23000		NH_4^+ = 1.290 ± 0.020, NO_3^- = 7.380 ± 0.130, NO_2^- = 0.110 ± 0.010, TN = 14.680 ± 0.250	Jia et al., 2021
	2468.095 ± 837.095	2602.635 ± 971.635	8.0350 ± 1.0650	0.94488 ± 0.03924	TN = 20.000	Huang et al., 2019a
	2686.500 ± 317.500	2655.500 ± 303.500	6.24500 ± 0.74500	0.97360 ± 0.02460	NH_4^+ = 0.170, TN = 2.480	Wang et al., 2020c
Low concentration of nitrogen	3119.050 ± 215.950	3110.500 ± 252.140	5.60500 ± 0.27500	0.98225 ± 0.00595	NO_3^- = 12.000, NH_3^+ = 8.000	Ajibade et al., 2021
	3574.000 ± 75.000		10.89500 ± 0.03500	0.99874 ± 0.00002	NH_4^+ = 4.000, NO_3^- = 10.000	Qin et al., 2021
	4592.500 ± 269.500	4765.500 ± 259.500	6.47000 ± 0.22000	0.98900 ± 0.00100	NH_4^+ = 1.630 ± 0.090, NO_3^- = 10.410 ± 1.660, TN = 12.680 ± 1.320	Tong et al., 2019
	4932.250 ± 175.350		9.80000 ± 0.33000	1.00000 ± 0.00000	NH_4^+ = 9.110, NO_3^- = 9.530, TN = 19.050	Wei et al., 2020
	6924.040 ± 1255.720	8110.050 ± 935.750	7.16000 ± 0.20000	0.99730 ± 0.00170	NH_4^+ = 0.960	Zhao et al., 2020c
	4393.430		9.00625	0.99018	NH_4^+ = 1.500, NO_3^- = 10.500	Zhang et al., 2021e
	7972.000 ± 186.000		6.81750 ± 0.35750	0.92500 ± 0.01500	NH_4^+ = 2.408 ± 2.350, NO_3^- = 1.885 ± 0.925, NO_2^- = 0.105 ± 0.091	Ma et al., 2018
High concentration of phosphorus	621.250 ± 115.150		4.07000 ± 0.71000		TP = 10.525 ± 0.715	Li et al., 2019
	841.500 ± 163.500	1048.950 ± 190.230	6.72500 ± 0.17500	0.96814 ± 0.00316	PO_4^{3-} = 44.000	Xu et al., 2021
	1375.965 ± 257.945	1422.860 ± 244.730	5.78500 ± 0.78500		PO_4^{3-} = 19.554	Lv et al., 2021
	1725.500 ± 108.500	1725.500 ± 108.500	7.84500 ± 0.09500	0.97331 ± 0.00690	PO_4^{3-} = 4.387	Zhao et al., 2020d
	1755.075 ± 92.235		7.68319 ± 0.43451	0.97313 ± 0.00813	TP = 5.250 ± 2.250	Xiao et al., 2020
	1788.145 ± 157.145		7.47000 ± 0.50000	0.95000 ± 0.04000	TP = 3.000	Huang et al., 2020a
	2001.110 ± 883.090	2091.605 ± 913.475	7.15500 ± 2.15500	0.89171 ± 0.10240	PO_4^{3-} = 17.500	Wang et al., 2021b
	2274.150 ± 56.660		7.76500 ± 0.20500	0.97500 ± 0.00500	TP = 2.810 ± 0.170	Huang et al., 2018
	2299.615 ± 366.595		5.31000 ± 0.42100	0.96165 ± 0.02155	TP = 5.000	Yang et al., 2021
	2468.095 ± 837.095	2602.635 ± 971.635	8.03500 ± 1.06500	0.94488 ± 0.03924	TP = 3.000	Huang et al., 2019a
	4398.800 ± 804.200	4960.050 ± 535.150	5.48500 ± 1.35500	0.93350 ± 0.06250	TP = 3.600 ± 0.900	Zheng et al., 2020

(Continued)

TABLE 5 | Continued

Alpha Diversity	Richness		Diversity		Concentration of pollutants (mg/l)	References
Pollutant type	**Chao1**	**ACE**	**Shannon**	**Simpson**		
	4592.500 ± 269.500	4765.500 ± 259.500	6.47000 ± 0.22000	0.98900 ± 0.00100	PO_4^{3-} = 0.800 ± 0.070	Tong et al., 2019
	2346.600 ± 216.230	2330.600 ± 228.940	6.28000 ± 0.23000		TP = 0.210 ± 0.010	Jia et al., 2021
	2133.745 ± 127.930	2144.504 ± 139.730	5.84550 ± 0.15450	0.99150 ± 0.00250	TP = 0.505 ± 0.325	Li et al., 2021a
Low concentration of phosphorus	2686.500 ± 317.500	2655.500 ± 303.500	6.24500 ± 0.74500	0.97360 ± 0.02460	TP = 0.260	Wang et al., 2020c
	7492.815 ± 1030.225	10929.450 ± 1071.540	5.74500 ± 0.46500	0.98350 ± 0.00890	TP = 0.550 ± 0.300	Kang et al., 2017
	2355.050 ± 745.750	2442.000 ± 656.000	4.95600 ± 0.93300		TP = 1.200 ± 0.300	Wang et al., 2020a
	1796.650 ± 461.450	2269.500 ± 380.500	4.03650 ± 0.52850			
	4393.430		9.00625	0.99018	TP = 1.500	Zhang et al., 2021e
	7972.000 ± 186.000		6.81750 ± 0.35750	0.92500 ± 0.01500	PO_4^{3-} = 0.407 ± 0.025	Ma et al., 2018
Heavy Metal	961.900	969.000	7.08000	0.97900	Control group (NH_4^+ = 114.600, PO_4^{3-} = 17.900)	Liu et al., 2020a
	510.000 ± 109.600	527.600 ± 108.600	4.79950 ± 1.34850	0.87500 ± 0.09600	Ni = 2.000, 5.000, 10.000, 30.000	
	5296.025 ± 164.585		9.86543 ± 0.10423	0.99410 ± 0.00457	Control group (NH_4^+ = 141.580, NH_2^- = 17.140, NO_3^- = 43.330, PO_4^{3-} = 13.170)	Xiao et al., 2021
	2443.830 ± 238.130		8.89639 ± 0.67463	0.99107 ± 0.00491	Ni = 0.100, 1.000	
	516.425 ± 201.145	509.965 ± 192.635	5.14000 ± 0.43000	0.90500 ± 0.01500	Control group (NO_3^- = 50.500, NH_4^+ = 75.428, PO_4^{3-} = 6.581)	Wang et al., 2020b
	532.555 ± 132.355	545.470 ± 135.490	5.32000 ± 0.25000	0.93000 ± 0.02000	Zn = 24.769	
	3186.590 ± 456.720	3177.470 ± 474.670	6.56500 ± 0.36500	0.99425 ± 0.00325	Control group (NO_3^- = 4.195, NH_4^+ = 2.904, PO_4^{3-} = 1.727)	Wang et al., 2021a
	2602.910 ± 851.850	2621.995 ± 887.785	6.03500 ± 0.36500	0.98605 ± 0.00755	Cr = 0.100 mmol/l	
	1288.690 ± 581.040	1353.650 ± 622.490	7.69500 ± 1.47500	0.96500 ± 0.02500	Control group (NO_3^- = 50.500, NH_4^+ = 75.428, PO_4^{3-} = 6.581)	Zhao et al., 2020a
	1353.210 ± 806.080	1327.970 ± 478.900	7.12500 ± 1.77500	0.93000 ± 0.06000	Pb = 5.000	
	73.350 ± 42.150		2.76750 ± 0.72550	0.88450 ± 0.09650	As = 20.000, Zn = 15.000	Arroyo et al., 2013
	1962.290 ± 48.290	2032.945 ± 118.605	7.48500 ± 0.75500	0.96200 ± 0.01600	Cu = 2.000 ± 0.170, Zn = 4.000 ± 0.210, Cd = 0.100 ± 0.010, Co = 2.000 ± 0.230, Ni = 0.500 ± 0.040, Pb = 0.500 ± 0.270	Si et al., 2019
	3387.500 ± 461.500	3491.000 ± 453.000	7.12000 ± 0.82000	0.97500 ± 0.01500	Cu = 4.880 ± 0.080, Zn = 5.060 ± 0.210, Cd = 5.170 ± 0.170, Cr = 5.650 ± 0.580	Chen et al., 2021c
	1469.050 ± 182.450	1540.050 ± 182.300	7.44500 ± 0.39500	0.98500 ± 0.00500	Cr = 0.500, 1.000, 2.000, 4.000, 8.000, 16.000	Zhang et al., 2019b
	4217.190		8.77863	0.98390	Cd = 200.000 μg/l	Zhang et al., 2021e
	4019.520		8.88151	0.98791	Cd = 200.000 μg/l, chlorpyrifos = 200.000 μg/l	
Antibiotic	4592.500 ± 269.500	4765.500 ± 259.500	6.47000 ± 0.22000	0.98900 ± 0.00100	Control group (NO_3^- = 10.410 ± 1.660, NH_4^+ = 1.630 ± 0.090, TN = 12.680 ± 1.320, PO_4^{3-} = 0.800 ± 0.070)	Tong et al., 2019
	4088.500 ± 702.500	4184.000 ± 755.000	6.35000 ± 0.26000	0.98700 ± 0.00400	Ofloxacin = 0.100, 10.000, 1000.000 μg/l	
	1415.915 ± 733.675	1471.010 ± 759.730	4.61000 ± 0.73000	0.95220 ± 0.03370	Control group (NO_3^- = 10.590, NH_4^+ = 20.630, TN = 32.340, PO_4^{3-} = 4.310)	Zheng et al., 2021b
	1794.070 ± 641.170	1805.390 ± 620.340	5.17000 ± 0.51000	0.98010 ± 0.00720	Sulfamethoxazole = 100.000 μg/l	
	485.356 ± 186.811	497.745 ± 173.830	3.72600 ± 0.64200	0.93750 ± 0.02150	Control group (NO_3^- = 50.000, NH_4^+ = 76.420, TN = 12.680 ± 1.320, PO_4^{3-} = 6.600)	Lu et al., 2021

(Continued)

TABLE 5 | Continued

Alpha Diversity	Richness		Diversity		Concentration of pollutants (mg/l)	References
Pollutant type	Chao1	ACE	Shannon	Simpson		
	509.085 ± 253.085	528.041 ± 240.405	3.48900 ± 1.31900	0.80000 ± 0.18100	Levofloxacin = 0.100, 0.200, 0.300, 0.500, 1.000, 10.000, 100.000 μg/l	
	3425.000 ± 275.000	3420.000 ± 220.000	7.63000 ± 0.16000	0.93450 ± 0.00850	Ciprofloxacin = 99.400 ± 8.300 μg/l, Azithromycin = 1313.900 ± 63.600 μg/l, Oxytetracycline =972.350 ± 39.950 μg/l	Wang et al., 2019a
	6048.560 ± 1435.820	7528.120 ± 1563.730	6.06500 ± 0.53500	0.98371 ± 0.00952	Triclosan = 60.000 μg/l	Liu et al., 2016
	3804.525 ± 72.185		7.87500 ± 0.53500	0.97140 ± 0.01420	ciprofloxacin hydrochloride = 50.000 μg/l, Sulfamethoxazole = 50.000 μg/l	Yuan et al., 2020
	1748.150 ± 55.850		6.53450 ± 0.73150	0.94500 ± 0.02800	Sulfadiazine = 4.000	Song et al., 2018
	2987.970 ± 261.210	2965.010 ± 250.950	6.38100 ± 0.30700		Enrofloxacin = 46.550 ± 20.850 ng/l, Sulfamethoxazole =1 37.600 ± 73.600 ng/l	Huang et al., 2019b

Alpha diversity is mainly related to two factors. One is richness, i.e., the number of species; and the other is evenness, i.e., the relative abundance of different species. The Chao1 and ACE indices reflect richness; and the Shannon and Simpson indices are a combination of richness and evenness that reflects diversity. Higher values of these indices represent a higher richness or diversity of microbial communities.

Regarding the effect on diversity, although the median of heavy metals can be high, the data are scattered, with a relatively large gap between the maximum and the minimum values. The occurrence of low values is easy to understand because heavy metals screen and selectively enrich microbial communities (Jia et al., 2021; Xiao et al., 2021), and most studies on heavy metals select microorganisms isolated from plant roots or screened from wastewater with high concentrations of heavy metals as functional microorganisms, resulting in the formation of dominant populations and in a lower diversity index. The high values can be explained by the microbial community being under pressure from heavy metals and the species within the community all evolving towards high heavy metal resistance (Yu et al., 2020). As a result, the abundance of different species is gradually increasing and the community as a whole is more even, so that there are no clearly dominant populations. In addition, during the treatment of heavy metals, key microorganisms require a variety of other microorganisms to cooperate and complement them (Chen et al., 2021b), which can also lead to a higher diversity. For example, the section "Functional Microorganisms in Heavy Metal Removal" mentioned a variety of microorganisms that can enhance the metabolism of SRB or provide them with electron donors, thus enhancing the bacterial sulfate reduction process. Abed et al. (2018) suggested that although SRB play a key role in AMD remediation, they account for only a small fraction of the total bacteria in the CWs.

Since nitrogen and phosphorus are essential elements for CWs, we also counted the microbial alpha diversity of the control group. We found that after the addition of heavy metals, the richness and diversity of microbial community in CWs decreased to varying degrees. This suggests that heavy metals exert more selective pressure on microorganisms compared to nitrogen and phosphorus, resulting in lower richness and more pronounced dominant populations. The experiments by Zhang et al. (2021e) also demonstrated that the combined pollution of antibiotics and heavy metals had a greater effect on microbial richness than that of a single contaminant, resulting in a decrease in richness values; the higher values of diversity may be due to the variety of pollutants and the need for a wider variety of functional microorganisms to deal with these pollutants.

Overall, the addition of heavy metals causes different degrees of reduction in the alpha diversity of microbial communities in CWs; in particular, the effect on microbial richness is obvious. This is can be seen in **Table 5**. And the higher the concentration of heavy metals, the greater the impact on alpha diversity.

EFFECT OF ANTIBIOTICS ON ALPHA DIVERSITY

Antibiotics, due to their mechanism of action, result in lower richness values appear in microbial communities (Tong et al., 2019). However, the median value of the richness of antibiotics is located at a high level. In this case, the increase in microbial richness may be attributed to antibiotics acting as signaling molecules that stimulate the metabolic activity of microorganisms and thereby stimulate the growth of certain microbial species (Li et al., 2021c). With prolonged incubation time, microorganisms were able to gradually adapt to the environment and accumulate,

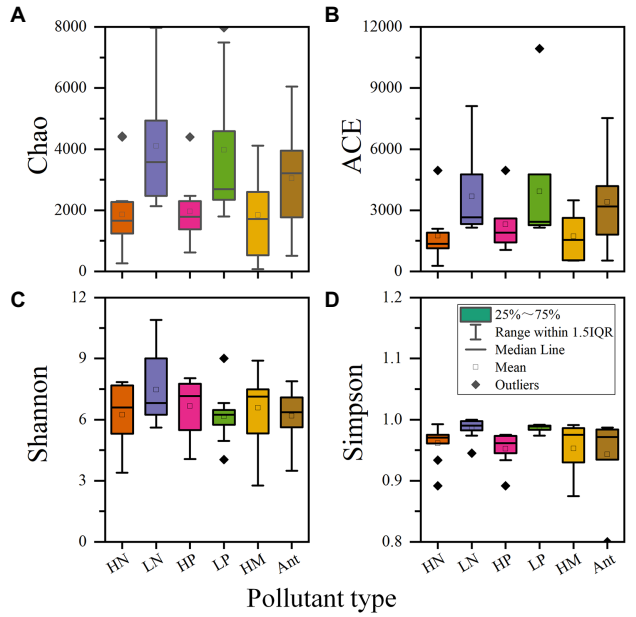

FIGURE 5 | Effects of four typical pollutants on microbial alpha diversity in CWs. **(A)** Chao index; **(B)** ACE index; **(C)** Shannon index; **(D)** Simpson index (HN: high concentration of nitrogen; LN: low concentration of nitrogen; HP: high concentration of phosphorus; LP: low concentration of phosphorus; HM: heavy metal; Ant: antibiotic).

leading to an increase in the richness of the microbial community. This is similar to the effect of heavy metals on microbial richness, but the difference is that the functional microorganisms involved in antibiotic removal can use antibiotics as carbon sources, resulting in a higher microbial richness (Zheng et al., 2021b). Based on the data presented in **Table 5**, in some studies, after the addition of antibiotics, the richness values were even higher than those in the control group.

Regarding diversity, different antibiotics correspond to different functional microorganisms and therefore easily lead to the formation of dominant population (Yuan et al., 2020). This explains the low values of both diversity indices in the presence of antibiotics.

Overall, antibiotics, like heavy metals, can have a significant impact on microbial alpha diversity, resulting in large differences among the various studies considered here. This reflects the fact that microbial communities may both take longer to remain stable and acquire the corresponding resistance or ability to remove contaminants in the presence of antibiotics or heavy metals (Yu et al., 2020; Zheng et al., 2021b).

CONCLUSION AND PERSPECTIVES

The microbial community, as an important component of CWs, plays a critical role in the removal of pollutants. According to the results of this review, research on microorganisms is gaining increased attention with the advancement of molecular bioanalysis techniques, and studies on microorganisms in CWs have gained considerable importance. This review provided a summary of the functional microorganisms involved in the removal of nitrogen, phosphorus, heavy metals, and antibiotics, the most frequently studied typical pollutants in CWs. This can help researchers to find links between functional microorganisms and pollutants, as well as facilitate the discovery of more relevant functional microorganisms. By summarizing the main functional microorganisms in CWs, we found that the phylum *Proteobacteria* is the dominant one, containing microorganisms with a wide range of functions. In addition, the phyla *Bacteroidetes*, *Actinobacteria*, and *Firmicutes* are also frequently detected in CWs. These functional microorganisms can remove pollutants from CWs by catalyzing chemical reactions, biodegradation, biosorption, and supporting plant growth, etc. The complexity of the microbial community structure and limitations of microbial analysis techniques make it difficult to draw other general conclusions. Regarding the effects of different pollutants on microbial diversity, we found that different microorganisms respond in different ways. When CWs contain high nitrogen and phosphorus levels, functional microorganisms associated with nitrogen and phosphorus removal become dominant in the system, and numerous cross-over phyla or genera of functional microorganisms have been identified. This indicates that research on nitrogen and phosphorous in CWs is advanced and that the removal mechanisms are well understood. In the case of heavy metals or antibiotics, the system can evolve microorganisms adapted to these substances. However, because studies on these two pollutants are scarce, the results cannot be generalized. Overall, heavy metals and high concentrations of nitrogen and phosphorus decrease both microbial richness and diversity in CWs, whereas antibiotics cause large fluctuations in alpha diversity.

Research on the microbial treatment of pollutants in CWs has achieved tremendous breakthroughs and advances with the development of various technologies, but some aspects deserve further investigations:

- Functional microorganisms in CWs should be studied and analyzed more frequently. They play an important role in the removal of pollutants but are often not the dominant microbes. Many studies have focused on the analysis of the overall microbial profile in the system, whereas research on the profile of functional microorganisms in the system is still lacking. In the future, it may be possible to focus on functional microorganisms and to investigate more deeply the composition and diversity of these microorganisms and the influence of different factors on their growth and development.
- Plant-microbe interactions are critical in the removal of contaminants in CWs, and many functional microorganisms associated with the removal of heavy metals, antibiotics, and organic pollution are rhizobacteria or endophytic bacteria isolated from plants. Therefore, further research on plant-associated microorganisms can deepen our understanding of the role of specific microorganisms and plants acting together in the removal of contaminants from CWs.
- There is a lack of studies on microorganisms involved in heavy metal, antibiotics, and some emerging pollutants (such as pesticides, flame retardants, and Polychlorobiphenyls) removal, and often, some specific strains are cultured or

isolated to improve the removal efficiency. Therefore, research on these aspects needs to be intensified.
- In the future, more emphasis should be placed on the study of microorganisms at the genetic level, determining their functional enzymes or functional genes. However, such an approach is dependent on the technological advances.

AUTHOR CONTRIBUTIONS

JW was responsible for data curation and formal analysis. JW and YL wrote the manuscript. GY contributed to conceptualization, the formal analysis, and visualization. GW, ZZ, PL, YZ, KY, and SW provided feedback on the manuscript. YL supervised, validated, reviewed, and edited the manuscript. All authors contributed to the article and approved the submitted version.

FUNDING

This work was supported by the National Natural Science Foundation of China (grant no. 52079010), the Natural Science Foundation of Hunan Province (no. 2021JJ30728), the Scientific Research Fund of Hunan Provincial Education Department (Project Contract No.: 19A032), and the Scientific Research Projects of Ecology and Environment Department of Hunan (no. HBKT-2021012).

REFERENCES

Abed, R. M. M., Al-Kharusi, S., Gkorezis, P., Prigent, S., and Headley, T. (2018). Bacterial communities in the rhizosphere of Phragmites australis from an oil-polluted wetland. *Arch. Agron. Soil Sci.* 64, 360–370. doi: 10.1080/03650340.2017.1352087

Aguilar, L., Gallegos, A., Arias, C. A., Ferrera, I., Sanchez, O., Rubio, R., et al. (2019). Microbial nitrate removal efficiency in groundwater polluted from agricultural activities with hybrid cork treatment wetlands. *Sci. Total Environ.* 653, 723–734. doi: 10.1016/j.scitotenv.2018.10.426

Ahmad, M., Yang, Q., Zhang, Y., Ling, J., Sajjad, W., Qi, S., et al. (2019). The distinct response of phenanthrene enriched bacterial consortia to different PAHs and their degradation potential: a mangrove sediment microcosm study. *J. Hazard. Mater.* 380:120863. doi: 10.1016/j.jhazmat.2019.120863

Ajibade, F. O., Wang, H. C., Guadie, A., Ajibade, T. F., Fang, Y. K., Sharif, H. M. A., et al. (2021). Total nitrogen removal in biochar amended non-aerated vertical flow constructed wetlands for secondary wastewater effluent with low C/N ratio: microbial community structure and dissolved organic carbon release conditions. *Bioresour. Technol.* 322:124430. doi: 10.1016/j.biortech.2020.124430

Alexandrino, D. A. M., Mucha, A. P., Almeida, C. M. R., Gao, W., Jia, Z. J., and Carvalho, M. F. (2017). Biodegradation of the veterinary antibiotics enrofloxacin and ceftiofur and associated microbial community dynamics. *Sci. Total Environ.* 581, 359–368. doi: 10.1016/j.scitotenv.2016.12.141

Alonso, A., Sanchez, P., and Martínez, J. L. (2001). Environmental selection of antibiotic resistance genes. *Environ. Microbiol.* 3, 1–9. doi: 10.1046/j.1462-2920.2001.00161.x

Amorim, C. L., Moreira, I. S., Maia, A. S., Tiritan, M. E., and Castro, P. M. (2014). Biodegradation of ofloxacin, norfloxacin, and ciprofloxacin as single and mixed substrates by Labrys portucalensis F11. *Appl. Microbiol. Biotechnol.* 98, 3181–3190. doi: 10.1007/s00253-013-5333-8

Arroyo, P., Ansola, G., and Miera, L. E. S. D. (2013). Effects of substrate, vegetation and flow on arsenic and zinc removal efficiency and microbial diversity in constructed wetlands. *Ecol. Eng.* 51, 95–103. doi: 10.1016/j.ecoleng.2012.12.013

Bessa, V. S., Moreira, I. S., Tiritan, M. E., and Castro, P. M. L. (2017). Enrichment of bacterial strains for the biodegradation of diclofenac and carbamazepine from activated sludge. *Int. Biodeterior. Biodegrad.* 120, 135–142. doi: 10.1016/j.ibiod.2017.02.008

Bianchi, E., Biancalani, A., Berardi, C., Antal, A., Fibbi, D., Coppi, A., et al. (2020). Improving the efficiency of wastewater treatment plants: bio-removal of heavy-metals and pharmaceuticals by Azolla filiculoides and Lemna minuta. *Sci. Total Environ.* 746:141219. doi: 10.1016/j.scitotenv.2020.141219

Chen, J. Q., Deng, S. J., Jia, W., Li, X., and Chang, J. J. (2021b). Removal of multiple heavy metals from mining-impacted water by biochar-filled constructed wetlands: adsorption and biotic removal routes. *Bioresour. Technol.* 331:125061. doi: 10.1016/j.biortech.2021.125061

Chen, J. Q., Li, X., Jia, W., Shen, S. L., Deng, S. J., Ji, B. H., et al. (2021c). Promotion of bioremediation performance in constructed wetland microcosms for acid mine drainage treatment by using organic substrates and supplementing domestic wastewater and plant litter broth. *J. Hazard. Mater.* 404:124125. doi: 10.1016/j.jhazmat.2020.124125

Chen, C., Li, C., Reniers, G., and Yang, F. (2021a). Safety and security of oil and gas pipeline transportation: a systematic analysis of research trends and future needs using WoS. *J. Clean. Prod.* 279:123583. doi: 10.1016/j.jclepro.2020.123583

Chen, J. F., Tong, T. L., Jiang, X. S., and Xie, S. G. (2020). Biodegradation of sulfonamides in both oxic and anoxic zones of vertical flow constructed wetland and the potential degraders. *Environ. Pollut.* 265:115040. doi: 10.1016/j.envpol.2020.115040

Chen, Y., Wen, Y., Zhou, Q., Huang, J. G., Vymazal, J., and Kuschk, P. (2016). Sulfate removal and sulfur transformation in constructed wetlands: the roles of filling material and plant biomass. *Water Res.* 102, 572–581. doi: 10.1016/j.watres.2016.07.001

Chen, Y., Zhu, Q., Dong, X., Huang, W., Du, C., and Lu, D. (2019). How Serratia marcescens HB-4 absorbs cadmium and its implication on phytoremediation. *Ecotoxicol. Environ. Saf.* 185:109723. doi: 10.1016/j.ecoenv.2019.109723

Cristani, M., Naccari, C., Nostro, A., Pizzimenti, A., Trombetta, D., and Pizzimenti, F. (2012). Possible use of Serratia marcescens in toxic metal biosorption (removal). *Environ. Sci. Pollut. Res. Int.* 19, 161–168. doi: 10.1007/s11356-011-0539-8

Deng, C. R., Huang, L., Liang, Y. K., Xiang, H. Y., Jiang, J., Wang, Q. H., et al. (2019). Response of microbes to biochar strengthen nitrogen removal in subsurface flow constructed wetlands: microbial community structure and metabolite characteristics. *Sci. Total Environ.* 694:133687. doi: 10.1016/j.scitotenv.2019.133687

Du, L., Chen, Q. R., Liu, P. P., Zhang, X., Wang, H. H., Zhou, Q. H., et al. (2017). Phosphorus removal performance and biological dephosphorization process in treating reclaimed water by integrated vertical-flow constructed wetlands (IVCWs). *Bioresour. Technol.* 243, 204–211. doi: 10.1016/j.biortech.2017.06.092

Gao, L., Zhou, W. L., Huang, J. C., He, S. B., Yan, Y. J., Zhu, W. Y., et al. (2017). Nitrogen removal by the enhanced floating treatment wetlands from the secondary effluent. *Bioresour. Technol.* 234, 243–252. doi: 10.1016/j.biortech.2017.03.036

Giovanella, P., Cabral, L., Costa, A. P., de Oliveira Camargo, F. A., Gianello, C., and Bento, F. M. (2017). Metal resistance mechanisms in gram-negative bacteria and their potential to remove hg in the presence of other metals. *Ecotoxicol. Environ. Saf.* 140, 162–169. doi: 10.1016/j.ecoenv.2017.02.010

González Henao, S., and Ghneim-Herrera, T. (2021). Heavy metals in soils and the remediation potential of bacteria associated With the plant microbiome. *Front. Environ. Sci.* 9:604216. doi: 10.3389/fenvs.2021.604216

Guo, X., Zhu, L., Zhong, H., Li, P., Zhang, C. J., and Wei, D. (2021). Response of antibiotic and heavy metal resistance genes to tetracyclines and copper in substrate-free hydroponic microcosms with Myriophyllum aquaticum. *J. Hazard. Mater.* 413:125444. doi: 10.1016/j.jhazmat.2021.125444

Habe, H., Sato, Y., Aoyagi, T., Inaba, T., Hori, T., Hamai, T., et al. (2020). Design, application, and microbiome of sulfate-reducing bioreactors for

treatment of mining-influenced water. *Appl. Microbiol. Biotechnol.* 104, 6893–6903. doi: 10.1007/s00253-020-10737-2

Hu, Y., He, F., Ma, L., Zhang, Y., and Wu, Z. B. (2016). Microbial nitrogen removal pathways in integrated vertical-flow constructed wetland systems. *Bioresour. Technol.* 207, 339–345. doi: 10.1016/j.biortech.2016.01.106

Huang, J., Cao, C., Yan, C. N., Guan, W. Z., and Liu, J. L. (2018). Comparison of &ITIris pseudacorus&IT wetland systems with unplanted systems on pollutant removal and microbial community under nanosilver exposure. *Sci. Total Environ.* 624, 1336–1347. doi: 10.1016/j.scitotenv.2017.12.222

Huang, T., Liu, W., Zhang, Y., Zhou, Q. H., Wu, Z. B., and He, F. (2020b). A stable simultaneous anammox, denitrifying anaerobic methane oxidation and denitrification process in integrated vertical constructed wetlands for slightly polluted wastewater. *Environ. Pollut.* 262:114363. doi: 10.1016/j.envpol.2020.114363

Huang, J., Xiao, J., Chen, M., Cao, C., Yan, C. N., Ma, Y. X., et al. (2019a). Fate of silver nanoparticles in constructed wetlands and its influence on performance and microbiome in the ecosystems after a 450-day exposure. *Bioresour. Technol.* 281, 107–117. doi: 10.1016/j.biortech.2019.02.013

Huang, J., Xiao, J., Guo, Y., Guan, W. Z., Cao, C., Yan, C. N., et al. (2020a). Long-term effects of silver nanoparticles on performance of phosphorus removal in a laboratory-scale vertical flow constructed wetland. *J. Environ. Sci.* 87, 319–330. doi: 10.1016/j.jes.2019.07.012

Huang, X. F., Ye, G. Y., Yi, N. K., Lu, L. J., Zhang, L., Yang, L. Y., et al. (2019b). Effect of plant physiological characteristics on the removal of conventional and emerging pollutants from aquaculture wastewater by constructed wetlands. *Ecol. Eng.* 135, 45–53. doi: 10.1016/j.ecoleng.2019.05.017

Huang, X., Zheng, J. L., Liu, C. X., Liu, L., Liu, Y. H., Fan, H. Y., et al. (2017). Performance and bacterial community dynamics of vertical flow constructed wetlands during the treatment of antibiotics-enriched swine wastewater. *Chem. Eng. J.* 316, 727–735. doi: 10.1016/j.cej.2017.02.029

Jia, W., Yang, Y. C., Yang, L. Y., and Gao, Y. (2021). High-efficient nitrogen removal and its microbiological mechanism of a novel carbon self-sufficient constructed wetland. *Sci. Total Environ.* 775:145901. doi: 10.1016/j.scitotenv.2021.145901

Kang, Y., Zhang, J., Xie, H. J., Guo, Z. Z., Ngo, H. H., Guo, W. S., et al. (2017). Enhanced nutrient removal and mechanisms study in benthic fauna added surface-flow constructed wetlands: The role of Tubifex tubifex. *Bioresour. Technol.* 224, 157–165. doi: 10.1016/j.biortech.2016.11.035

Kilicaslan, O. F., Nabi, V., Yardibi, F., Tokgoz, M. A., and Kose, O. (2021). Research tendency in lumbar spinal stenosis over the past decade: a Bibliometric analysis. *World Neurosurg.* 149, e71–e84. doi: 10.1016/j.wneu.2021.02.086

Kowal, P., Ciesielski, S., Godzieba, M., Fitobor, K., Gajewska, M., and Kolecka, K. (2021). Assessment of diversity and composition of bacterial community in sludge treatment reed bed systems. *Sci. Total Environ.* 756:144060. doi: 10.1016/j.scitotenv.2020.144060

Kraiema, K., Kallali, H., Wahab, M. A., Fra-vazquez, A., Mosquera-Corral, A., and Jedidi, N. (2019). Comparative study on pilots between ANAMMOX favored conditions in a partially saturated vertical flow constructed wetland and a hybrid system for rural wastewater treatment. *Sci. Total Environ.* 670, 644–653. doi: 10.1016/j.scitotenv.2019.03.220

Laliberte, E., Schweiger, A. K., and Legendre, P. (2020). Partitioning plant spectral diversity into alpha and beta components. *Ecol. Lett.* 23, 370–380. doi: 10.1111/ele.13429

Lee, S., Maniquiz-Redillas, M. C., Choi, J., and Kim, L. H. (2014). Nitrogen mass balance in a constructed wetland treating piggery wastewater effluent. *J. Environ. Sci.* 26, 1260–1266. doi: 10.1016/s1001-0742(13)60597-5

Li, Q. X., Bu, C. N., Ahmad, H. A., Guimbaud, C., Gao, B. Y., Qiao, Z. M., et al. (2021b). The distribution of dissimilatory nitrate reduction to ammonium bacteria in multistage constructed wetland of Jining, Shandong. *China. Environ. Sci. Pollut. Res.* 28, 4749–4761. doi: 10.1007/s11356-020-10709-z

Li, M., Duan, R., Hao, W., Li, Q. C., Arslan, M., Liu, P. P., et al. (2020a). High-rate nitrogen removal from carbon limited wastewater using sulfur-based constructed wetland: impact of sulfur sources. *Sci. Total Environ.* 744:140969. doi: 10.1016/j.scitotenv.2020.140969

Li, H., Li, Y., Gong, Z., and Li, X. (2013). Performance study of vertical flow constructed wetlands for phosphorus removal with water quenched slag as a substrate. *Ecol. Eng.* 53, 39–45. doi: 10.1016/j.ecoleng.2013.01.011

Li, H. F., Liu, F., Luo, P., Chen, X., Chen, J. L., Huang, Z. R., et al. (2019). Stimulation of optimized influent C:N ratios on nitrogen removal in surface flow constructed wetlands: Performance and microbial mechanisms. *Sci. Total Environ.* 694:9. doi: 10.1016/j.scitotenv.2019.07.381

Li, X. H., Lu, S. Y., Liu, S. D., Zheng, Q., Shen, P., and Wang, X. H. (2020b). Shifts of bacterial community and molecular ecological network at the presence of fluoroquinolones in a constructed wetland system. *Sci. Total Environ.* 708:135156. doi: 10.1016/j.scitotenv.2019.135156

Li, W., Shi, C., Yu, Y., Ruan, Y., Kong, D., Lv, X., et al. (2021c). Interrelationships between tetracyclines and nitrogen cycling processes mediated by microorganisms: a review. *Bioresour. Technol.* 319:124036. doi: 10.1016/j.biortech.2020.124036

Li, X., Zhang, M. M., Liu, F., Li, Y. Y., Li, Y., Xiao, R. L., et al. (2017). Bacterial community dynamics in a Myriophyllum elatinoides purification system for swine wastewater in sediments. *Appl. Soil Ecol.* 119, 56–63. doi: 10.1016/j.apsoil.2017.05.019

Li, J., Zheng, L., Ye, C. B., Ni, B. S., Wang, X. Z., and Liu, H. (2021a). Evaluation of an intermittent-aeration constructed wetland for removing residual organics and nutrients from secondary effluent: performance and microbial analysis. *Bioresour. Technol.* 329:124897. doi: 10.1016/j.biortech.2021.124897

Liang, L., and Gong, P. (2017). Climate change and human infectious diseases: A synthesis of research findings from global and spatio-temporal perspectives. *Environ. Int.* 103, 99–108. doi: 10.1016/j.envint.2017.03.011

Limcharoensuk, T., Sooksawat, N., Sumarnrote, A., Awutpet, T., Kruatrachue, M., Pokethitiyook, P., et al. (2015). Bioaccumulation and biosorption of cd(2+) and Zn(2+) by bacteria isolated from a zinc mine in Thailand. *Ecotoxicol. Environ. Saf.* 122, 322–330. doi: 10.1016/j.ecoenv.2015.08.013

Lin, H., Jin, D., Freitag, T. E., Sun, W., Yu, Q., Fu, J., et al. (2016). A compositional shift in the soil microbiome induced by tetracycline, sulfamonomethoxine and ciprofloxacin entering a plant-soil system. *Environ. Pollut.* 212, 440–448. doi: 10.1016/j.envpol.2016.02.043

Lin, Y.-F., Jing, S.-R., Lee, D.-Y., and Wang, T.-W. (2002). Nutrient removal from aquaculture wastewater using a constructed wetlands system. *Aquaculture* 209, 169–184. doi: 10.1016/S0044-8486(01)00801-8

Liu, X. H., Guo, X. C., Liu, Y., Lu, S. Y., Xi, B. D., Zhang, J., et al. (2019). A review on removing antibiotics and antibiotic resistance genes from wastewater by constructed wetlands: performance and microbial response. *Environ. Pollut.* 254:112996. doi: 10.1016/j.envpol.2019.112996

Liu, Q., Li, M., Liu, X., Zhang, Q., Liu, R., Wang, Z., et al. (2018). Removal of sulfamethoxazole and trimethoprim from reclaimed water and the biodegradation mechanism. *Front. Env. Sci. Eng.* 12:6. doi: 10.1007/s11783-018-1048-5

Liu, R. C., Li, S. S., Yu, N. L., Zhao, C. K., Gao, X. L., and Gao, C. J. (2020a). Performance evaluation and microbial community shift of sequencing batch reactors under different nickel (Ni(II)) concentrations. *Environ. Technol. Inno.* 19:100991. doi: 10.1016/j.eti.2020.100991

Liu, T., Lu, S. Y., Wang, R. W., Xu, S. R., Qin, P., and Gao, Y. S. (2020b). Behavior of selected organophosphate flame retardants (OPFRs) and their influence on rhizospheric microorganisms after short-term exposure in integrated vertical-flow constructed wetlands (IVCWs). *Sci. Total Environ.* 710:136403. doi: 10.1016/j.scitotenv.2019.136403

Liu, J. N., Wang, J. M., Zhao, C. C., Hay, A. G., Xie, H. J., and Zhan, J. (2016). Triclosan removal in wetlands constructed with different aquatic plants. *Appl. Microbiol. Biotechnol.* 100, 1459–1467. doi: 10.1007/s00253-015-7063-6

Long, Y., Zhou, Z., Yin, L., Wen, X., Xiao, R., Du, L., et al. (2021). Microplastics removal and characteristics of constructed wetlands WWTPs in rural area of Changsha, China: A different situation from urban WWTPs. *Sci. Total Environ.* 811:152352. doi: 10.1016/j.scitotenv.2021.152352

Lu, H. B., Wang, T., Lu, S. Y., Liu, H. Q., Wang, H. H., Li, C. J., et al. (2021). Performance and bacterial community dynamics of hydroponically grown Iris pseudacorus L. during the treatment of antibiotic-enriched wastewater at low/normal temperature. *Ecotoxicol. Environ. Saf.* 213:111997. doi: 10.1016/j.ecoenv.2021.111997

Lv, R. Y., Wu, D. N., Ding, J. W., Yuan, X. C., Zhou, G. Y., Zhang, Y. J., et al. (2021). Long-term performance and microbial mechanism in intertidal wetland sediment introduced constructed wetlands treating saline wastewater. *J. Clean. Prod.* 310:127409. doi: 10.1016/j.jclepro.2021.127409

Ma, X. N., Song, X. Q., Li, X., Fu, S. Z., Li, M., and Liu, Y. (2018). Characterization of microbial communities in pilot-scale constructed wetlands with Salicornia for treatment of marine aquaculture effluents. *Archaea* 2018:12. doi: 10.1155/2018/7819840

Man, Y., Wang, J. X., Tam, N. F. Y., Wan, X., Huang, W. D., Zheng, Y., et al. (2020). Responses of rhizosphere and bulk substrate microbiome to wastewater-borne sulfonamides in constructed wetlands with different plant species. *Sci. Total Environ.* 706:135955. doi: 10.1016/j.scitotenv.2019.135955

Mao, G., Huang, N., Chen, L., and Wang, H. (2018a). Research on biomass energy and environment from the past to the future: a bibliometric analysis. *Sci. Total Environ.* 635, 1081–1090. doi: 10.1016/j.scitotenv.2018.04.173

Mao, G., Shi, T., Zhang, S., Crittenden, J., Guo, S., and Du, H. (2018b). Bibliometric analysis of insights into soil remediation. *J. Soils Sediments* 18, 2520–2534. doi: 10.1007/s11368-018-1932-4

Mao, G., Zou, H., Chen, G., Du, H., and Zuo, J. (2015). Past, current and future of biomass energy research: A bibliometric analysis. *Renew. Sust. Energ. Rev.* 52, 1823–1833. doi: 10.1016/j.rser.2015.07.141

Moreira, I. S., Bessa, V. S., Murgolo, S., Piccirillo, C., Mascolo, G., and Castro, P. M. L. (2018). Biodegradation of Diclofenac by the bacterial strain Labrys portucalensis F11. *Ecotoxicol. Environ. Saf.* 152, 104–113. doi: 10.1016/j.ecoenv.2018.01.040

Ouyang, W. Y., Birkigt, J., Richnow, H. H., and Adrian, L. (2021). Anaerobic transformation and detoxification of Sulfamethoxazole by sulfate-reducing enrichments and Desulfovibrio vulgaris. *Environ. Sci. Technol.* 55, 271–282. doi: 10.1021/acs.est.0c03407

Pelissari, C., Guivernau, M., Vinas, M., Garcia, J., Velasco-Galilea, M., Souza, S. S., et al. (2018). Effects of partially saturated conditions on the metabolically active microbiome and on nitrogen removal in vertical subsurface flow constructed wetlands. *Water Res.* 141, 185–195. doi: 10.1016/j.watres.2018.05.002

Pitacco, V., Mistri, M., Aleffi, I. F., Lardicci, C., Prato, S., Tagliapietra, D., et al. (2019). Spatial patterns of macrobenthic alpha and beta diversity at different scales in Italian transitional waters (Central Mediterranean). *Estuar. Coast. Shelf Sci.* 222, 126–138. doi: 10.1016/j.ecss.2019.04.026

Qin, S., Zhang, X., He, S., and Huang, J. (2021). Improvement of nitrogen removal with iron scraps in floating treatment wetlands. *Environ. Sci. Pollut. Res.* 28, 17878–17890. doi: 10.1007/s11356-020-12177-x

Rahman, Z. (2020). An overview on heavy metal resistant microorganisms for simultaneous treatment of multiple chemical pollutants at co-contaminated sites, and their multipurpose application. *J. Hazard. Mater.* 396:122682. doi: 10.1016/j.jhazmat.2020.122682

Rahman, M. M., Roberts, K. L., Grace, M. R., Kessler, A. J., and Cook, P. L. M. (2019). Role of organic carbon, nitrate and ferrous iron on the partitioning between denitrification and DNRA in constructed stormwater urban wetlands. *Sci. Total Environ.* 666, 608–617. doi: 10.1016/j.scitotenv.2019.02.225

Rajan, R. J., Sudarsan, J. S., and Nithiyanantham, S. (2019). Microbial population dynamics in constructed wetlands: review of recent advancements for wastewater treatment. *Environ. Eng. Res.* 24, 181–190. doi: 10.4491/eer.2018.127

Ricken, B., Corvini, P. F., Cichocka, D., Parisi, M., Lenz, M., Wyss, D., et al. (2013). Ipso-hydroxylation and subsequent fragmentation: a novel microbial strategy to eliminate sulfonamide antibiotics. *Appl. Environ. Microbiol.* 79, 5550–5558. doi: 10.1128/AEM.00911-13

Sanchez, O. (2017). Constructed wetlands revisited: microbial diversity in the -omics era. *Microb. Ecol.* 73, 722–733. doi: 10.1007/s00248-016-0881-y

Santos, F., Almeida, C. M. R., Ribeiro, I., and Mucha, A. P. (2019a). Potential of constructed wetland for the removal of antibiotics and antibiotic resistant bacteria from livestock wastewater. *Ecol. Eng.* 129, 45–53. doi: 10.1016/j.ecoleng.2019.01.007

Santos, F., de Almeida, C. M. R., Ribeiro, I., Ferreira, A. C., and Mucha, A. P. (2019b). Removal of veterinary antibiotics in constructed wetland microcosms response of bacterial communities. *Ecotoxicol. Environ. Saf.* 169, 894–901. doi: 10.1016/j.ecoenv.2018.11.078

Sauvetre, A., Wegrzyn, A., Yang, L. H., Vestergaard, G., Miksch, K., Schroder, P., et al. (2020). Enrichment of endophytic Actinobacteria in roots and rhizomes of Miscanthus x giganteus plants exposed to diclofenac and sulfamethoxazole. *Environ. Sci. Pollut. Res.* 27, 11892–11904. doi: 10.1007/s11356-020-07609-7

Shan, A. Q., Wang, W. J., Kang, K. J., Hou, D. D., Luo, J. P., Wang, G., et al. (2020). The removal of antibiotics in relation to a microbial Community in an Integrated Constructed Wetland for tail water decontamination. *Wetlands* 40, 993–1004. doi: 10.1007/s13157-019-01262-8

Shi, X., Fan, J. L., Zhang, J., and Shen, Y. H. (2017). Enhanced phosphorus removal in intermittently aerated constructed wetlands filled with various construction wastes. *Environ. Sci. Pollut. Res.* 24, 22524–22534. doi: 10.1007/s11356-017-9870-z

Si, Z. H., Song, X. S., Wang, Y. H., Cao, X., Zhao, Y. F., Wang, B. D., et al. (2018). Intensified heterotrophic denitrification in constructed wetlands using four solid carbon sources: Denitrification efficiency and bacterial community structure. *Bioresour. Technol.* 267, 416–425. doi: 10.1016/j.biortech.2018.07.029

Si, Z. H., Wang, Y. H., Song, X. S., Cao, X., Zhang, X., and Sand, W. (2019). Mechanism and performance of trace metal removal by continuous-flow constructed wetlands coupled with a micro-electric field. *Water Res.* 164:114937. doi: 10.1016/j.watres.2019.114937

Song, H. L., Li, H., Zhang, S., Yang, Y. L., Zhang, L. M., Xu, H., et al. (2018). Fate of sulfadiazine and its corresponding resistance genes in up-flow microbial fuel cell coupled constructed wetlands: effects of circuit operation mode and hydraulic retention time. *Chem. Eng. J.* 350, 920–929. doi: 10.1016/j.cej.2018.06.035

Sturz, A. V., Christie, B. R., and Nowak, J. (2000). Bacterial Endophytes: potential role in developing sustainable Systems of Crop Production. *Crit. Rev. Plant Sci.* 19, 1–30. doi: 10.1080/07352680091139169

Syranidou, E., Christofilopoulos, S., Gkavrou, G., Thijs, S., Weyens, N., Vangronsveld, J., et al. (2016). Exploitation of Endophytic bacteria to enhance the phytoremediation potential of the wetland helophyte Juncus acutus. *Front. Microbiol.* 7:1016. doi: 10.3389/fmicb.2016.01016

Syranidou, E., Christofilopoulos, S., Politi, M., Weyens, N., Venieri, D., Vangronsveld, J., et al. (2017). Bisphenol-A removal by the halophyte Juncus acutus in a phytoremediation pilot: characterization and potential role of the endophytic community. *J. Hazard. Mater.* 323, 350–358. doi: 10.1016/j.jhazmat.2016.05.034

Syranidou, E., Thijs, S., Avramidou, M., Weyens, N., Venieri, D., Pintelon, I., et al. (2018). Responses of the Endophytic bacterial communities of Juncus acutus to pollution With metals, emerging organic pollutants and to bioaugmentation With indigenous strains. *Front. Plant Sci.* 9:1526. doi: 10.3389/fpls.2018.01526

Tan, X., Yang, Y. L., Liu, Y. W., Li, X., and Zhu, W. B. (2021a). Quantitative ecology associations between heterotrophic nitrification-aerobic denitrification, nitrogen-metabolism genes, and key bacteria in a tidal flow constructed wetland. *Bioresour. Technol.* 337:125449. doi: 10.1016/j.biortech.2021.125449

Tan, X., Yang, Y. L., Liu, Y. W., Yin, W. C., and Fan, X. Y. (2021b). The synergy of porous substrates and functional genera for efficient nutrients removal at low temperature in a pilot-scale two-stage tidal flow constructed wetland. *Bioresour. Technol.* 319:124135. doi: 10.1016/j.biortech.2020.124135

Teitzel, G. M., and Parsek, M. R. (2003). Heavy metal resistance of biofilm and planktonic Pseudomonas aeruginosa. *Appl. Environ. Microbiol.* 69, 2313–2320. doi: 10.1128/AEM.69.4.2313-2320.2003

Tian, J., Yu, C. L., Liu, J. F., Ye, C. R., Zhou, X. J., and Chen, L. Z. (2017). Performance of an ultraviolet Mutagenetic polyphosphate-accumulating bacterium PZ2 and its application for wastewater treatment in a newly designed constructed wetland. *Appl. Biochem. Biotechnol.* 181, 735–747. doi: 10.1007/s12010-016-2245-y

Tong, X. N., Wang, X. Z., He, X. J., Wang, Z., and Li, W. X. (2020). Effects of antibiotics on microbial community structure and microbial functions in constructed wetlands treated with artificial root exudates. *Environ. Sci.* 22, 217–226. doi: 10.1039/c9em00458k

Tong, X. N., Wang, X. Z., He, X. J., Xu, K. Q., and Mao, F. J. (2019). Effects of ofloxacin on nitrogen removal and microbial community structure in constructed wetland. *Sci. Total Environ.* 656, 503–511. doi: 10.1016/j.scitotenv.2018.11.358

Torregrosa, M., Schwarz, A., Nancucheo, I., and Balladares, E. (2019). Evaluation of the bio-protection mechanism in diffusive exchange permeable reactive barriers for the treatment of acid mine drainage. *Sci. Total Environ.* 655, 374–383. doi: 10.1016/j.scitotenv.2018.11.083

Troiano, E., Beneduce, L., Gross, A., and Ronen, Z. (2018). Antibiotic-resistant bacteria in Greywater and Greywater-irrigated soils. *Front. Microbiol.* 9:2666. doi: 10.3389/fmicb.2018.02666

Urakawa, H., Dettmar, D. L., and Thomas, S. (2017). The uniqueness and biogeochemical cycling of plant root microbial communities in a floating treatment wetland. *Ecol. Eng.* 108, 573–580. doi: 10.1016/j.ecoleng.2017.06.066

Vassallo, A., Miceli, E., Fagorzi, C., Castronovo, L. M., Del Duca, S., Chioccioli, S., et al. (2020). Temporal evolution of bacterial Endophytes associated to the roots ofPhragmites australisExploited in Phytodepuration of wastewater. *Front. Microbiol.* 11:1652. doi: 10.3389/fmicb.2020.01652

Vymazal, J., Zhao, Y. Q., and Mander, U. (2021). Recent research challenges in constructed wetlands for wastewater treatment: A review. *Ecol. Eng.* 169:106318. doi: 10.1016/j.ecoleng.2021.106318

Wang, S. Q., Cui, Y. B., Li, A. M., Wang, D., Zhang, W. J., and Chen, Z. B. (2019a). Seasonal dynamics of bacterial communities associated with antibiotic removal and sludge stabilization in three different sludge treatment wetlands. *J. Environ. Manag.* 240, 231–237. doi: 10.1016/j.jenvman.2019.03.092

Wang, Q., Ding, J. W., Xie, H. J., Hao, D. R., Du, Y. D., Zhao, C. C., et al. (2021b). Phosphorus removal performance of microbial-enhanced constructed wetlands that treat saline wastewater. *J. Clean. Prod.* 288:125119. doi: 10.1016/j.jclepro.2020.125119

Wang, H. J., Li, Y. Y., Zhang, S. Q., Li, D., Liu, X. C., Wang, W. J., et al. (2020a). Effect of influent feeding pattern on municipal tailwater treatment during a sulfur-based denitrification constructed wetland. *Bioresour. Technol.* 315:123807. doi: 10.1016/j.biortech.2020.123807

Wang, Q., Lv, R. Y., Rene, E. R., Qi, X. Y., Hao, Q., Du, Y. D., et al. (2020b). Characterization of microbial community and resistance gene (CzcA) shifts in up-flow constructed wetlands-microbial fuel cell treating Zn (II) contaminated wastewater. *Bioresour. Technol.* 302:122867. doi: 10.1016/j.biortech.2020.122867

Wang, Y., Shen, L. Y., Wu, J., Zhong, F., and Cheng, S. P. (2020d). Step-feeding ratios affect nitrogen removal and related microbial communities in multi-stage vertical flow constructed wetlands. *Sci. Total Environ.* 721:137689. doi: 10.1016/j.scitotenv.2020.137689

Wang, W. D., Su, Y., Wang, B. L., Wang, Y., Zhuang, L. J., and Zhu, G. B. (2019b). Spatiotemporal shifts of ammonia-oxidizing archaea abundance and structure during the restoration of a multiple pond and plant-bed/ditch wetland. *Sci. Total Environ.* 684, 629–640. doi: 10.1016/j.scitotenv.2019.04.415

Wang, T., Xiao, L., Lu, H., Lu, S., Li, J., Guo, X., et al. (2022). Nitrogen removal from summer to winter in a field pilot-scale multistage constructed wetland-pond system. *J. Environ. Sci.* 111, 249–262. doi: 10.1016/j.jes.2021.03.028

Wang, W. G., Zhao, Y. H., Jiang, G. M., and Wang, Y. Y. (2020c). The nutrient removal ability and microbial communities in a pilot-scale horizontal subsurface flow constructed wetland fed by slightly polluted Lake water. *Wetlands* 40, 2085–2096. doi: 10.1007/s13157-020-01327-z

Wang, B. C., Zhu, S. X., Li, W. J., Tang, Q., and Luo, H. Y. (2021a). Effects of chromium stress on the rhizosphere microbial community composition of Cyperus alternifolius. *Ecotoxicol. Environ. Saf.* 218:112253. doi: 10.1016/j.ecoenv.2021.112253

Wegrzyn, A., and Felis, E. (2018). Isolation of bacterial Endophytes from Phalaris arundinacea and their potential in Diclofenac and Sulfamethoxazole degradation. *Pol. J. Microbiol.* 67, 321–331. doi: 10.21307/pjm-2018-039

Wei, F., Zhou, Q. W., Wu, W. H., Bian, Z. F., Feng, X. Y., Li, J. Y., et al. (2020). Investigating the influence of iron-carbon microelectrolysis on the performance and microbial community of constructed wetlands. *Water Environ. J.* 34, 414–424. doi: 10.1111/wej.12538

Wu, Q., Xiao, J. J., Fu, L. J., Ma, M. X., and Peng, S. (2020). Microporous intermittent aeration vertical flow constructed wetlands for eutrophic water improvement. *Environ. Sci. Pollut. Res.* 27, 16574–16583. doi: 10.1007/s11356-020-08067-x

Xia, Z. G., Liu, G. C., She, Z. L., Gao, M. C., Zhao, Y. G., Guo, L., et al. (2020). Performance and bacterial communities in unsaturated and saturated zones of a vertical-flow constructed wetland with continuous-feed. *Bioresour. Technol.* 315:123859. doi: 10.1016/j.biortech.2020.123859

Xiao, J., Huang, J., Huang, M. J., Chen, M., and Wang, M. Y. (2020). Application of basalt fiber in vertical flow constructed wetland for different pollution loads wastewater: performance, substrate enzyme activity and microorganism community. *Bioresour. Technol.* 318:124229. doi: 10.1016/j.biortech.2020.124229

Xiao, J., Huang, J., Wang, M. Y., Huang, M. J., and Wang, Y. (2021). The fate and long-term toxic effects of NiO nanoparticles at environmental concentration in constructed wetland: enzyme activity, microbial property, metabolic pathway and functional genes. *J. Hazard. Mater.* 413:125295. doi: 10.1016/j.jhazmat.2021.125295

Xie, E., Ding, A. Z., Zheng, L., Lu, C. L., Wang, J. S., Huang, B. B., et al. (2016). Seasonal variation in populations of nitrogen-transforming bacteria and correlation with nitrogen removal in a full-scale horizontal flow constructed wetland treating Polluted River water. *Geomicrobiol J.* 33, 338–346. doi: 10.1080/01490451.2015.1052115

Xu, J. M., Liu, X. H., Lv, Y., Guo, X. C., and Lu, S. Y. (2020). Response of Cyperus involucratus to sulfamethoxazole and ofloxacin-contaminated environments: growth physiology, transportation, and microbial community. *Ecotoxicol. Environ. Saf.* 206:111332. doi: 10.1016/j.ecoenv.2020.111332

Xu, Z., Wu, C., Ban, Y., and Zhang, S. (2021). Effects of different shunt rate on the purification of hybrid constructed wetland. *Water Air Soil Pollut.* 232, 1–14. doi: 10.1007/s11270-021-05019-0

Yang, X. Y., He, Q., Guo, F. C., Sun, X. H., Zhang, J. M., and Chen, Y. (2021). Impacts of carbon-based nanomaterials on nutrient removal in constructed wetlands: microbial community structure, enzyme activities, and metabolism process. *J. Hazard. Mater.* 401:123270. doi: 10.1016/j.jhazmat.2020.123270

Yin, L., Wen, X., Huang, D., Du, C., Deng, R., Zhou, Z., et al. (2021). Interactions between microplastics/nanoplastics and vascular plants. *Environ. Pollut.* 290:117999. doi: 10.1016/j.envpol.2021.117999

Yu, G. L., Wang, G. L., Li, J. B., Chi, T. Y., Wang, S. T., Peng, H. Y., et al. (2020). Enhanced Cd2+ and Zn2+ removal from heavy metal wastewater in constructed wetlands with resistant microorganisms. *Bioresour. Technol.* 316:123898. doi: 10.1016/j.biortech.2020.123898

Yuan, Y. R., Yang, B. S., Wang, H., Lai, X. S., Li, F., Salam, M. M. A., et al. (2020). The simultaneous antibiotics and nitrogen removal in vertical flow constructed wetlands: E ffects of substrates and responses of microbial functions. *Bioresour. Technol.* 310:123419. doi: 10.1016/j.biortech.2020.123419

Zhang, M. P., Huang, J. C., Sun, S. S., Rehman, M. M. U., and He, S. B. (2020). Depth-specific distribution and significance of nitrite-dependent anaerobic methane oxidation process in tidal flow constructed wetlands used for treating river water. *Sci. Total Environ.* 716:137054. doi: 10.1016/j.scitotenv.2020.137054

Zhang, M., Huang, J. C., Sun, S., Rehman, M. M. U., He, S., and Zhou, W. (2021a). Nitrogen removal through collaborative microbial pathways in tidal flow constructed wetlands. *Sci. Total Environ.* 758:143594. doi: 10.1016/j.scitotenv.2020.143594

Zhang, M. P., Huang, J. C., Sun, S. S., Rehman, M. M. U., He, S. B., and Zhou, W. L. (2021b). Dissimilatory nitrate reduction processes and corresponding nitrogen loss in tidal flow constructed wetlands. *J. Clean. Prod.* 295:126429. doi: 10.1016/j.jclepro.2021.126429

Zhang, Y., Li, Y., Wang, J., Wang, X., Liu, Y., Wang, S., et al. (2021e). Interactions of chlorpyrifos degradation and cd removal in iron-carbon-based constructed wetlands for treating synthetic farmland wastewater. *J. Environ. Manag.* 299:113559. doi: 10.1016/j.jenvman.2021.113559

Zhang, S., Song, H. L., Cao, X., Li, H., Guo, J., Yang, X. L., et al. (2019a). Inhibition of methanogens decreased sulfadiazine removal and increased antibiotic resistance gene development in microbial fuel cells. *Bioresour. Technol.* 281, 188–194. doi: 10.1016/j.biortech.2019.02.089

Zhang, M. P., Wang, Z. J., Huang, J. C., Sun, S. S., Cui, X. J., Zhou, W. L., et al. (2021c). Salinity-driven nitrogen removal and its quantitative molecular mechanisms in artificial tidal wetlands. *Water Res.* 202:117446. doi: 10.1016/j.watres.2021.117446

Zhang, Q., Yang, Y. Q., Chen, F. R., Zhang, L. L., Ruan, J. J., Wu, S. J., et al. (2021d). Effects of hydraulic loading rate and substrate on ammonium removal in tidal flow constructed wetlands treating black and odorous water bodies. *Bioresour. Technol.* 321:124468. doi: 10.1016/j.biortech.2020.124468

Zhang, X., Zhao, S., Gao, J., Lei, Y., Yuan, Y., Jiang, Y., et al. (2019b). Microbial action and mechanisms for Cr(VI) removal performance by layered double hydroxide modified zeolite and quartz sand in constructed wetlands. *J. Environ. Manag.* 246, 636–646. doi: 10.1016/j.jenvman.2019.06.017

Zhao, Y. F., Cao, X., Song, X. S., Zhao, Z. M., Wang, Y. H., Si, Z. H., et al. (2018). Montmorillonite supported nanoscale zero-valent iron immobilized in sodium alginate (SA/Mt-NZVI) enhanced the nitrogen removal in vertical flow constructed wetlands (VFCWs). *Bioresour. Technol.* 267, 608–617. doi: 10.1016/j.biortech.2018.07.072

Zhao, L., Fu, G. P., Wu, J. F., Pang, W. C., and Hu, Z. L. (2021). Bioaugmented constructed wetlands for efficient saline wastewater treatment with multiple denitrification pathways. *Bioresour. Technol.* 335:125236. doi: 10.1016/j.biortech.2021.125236

Zhao, Y., Ji, B., Liu, R., Ren, B., and Wei, T. (2020b). Constructed treatment wetland: glance of development and future perspectives. *Water Cycle* 1, 104–112. doi: 10.1016/j.watcyc.2020.07.002

Zhao, Y. F., Mao, W., Pang, L. X., Li, R. J., and Li, S. Q. (2020c). Influence of Phragmites communis and Zizania aquatica on rhizosphere soil enzyme activity and bacterial community structure in a surface flow constructed wetland treating secondary domestic effluent in China. *Environ. Sci. Pollut. Res.* 27, 26141–26152. doi: 10.1007/s11356-020-08904-z

Zhao, C., Shang, D., Zou, Y., Du, Y., Wang, Q., Xu, F., et al. (2020a). Changes in electricity production and microbial community evolution in constructed wetland-microbial fuel cell exposed to wastewater containing Pb(II). *Sci. Total Environ.* 732:139127. doi: 10.1016/j.scitotenv.2020.139127

Zhao, Y. F., Song, X. S., Cao, X., Wang, Y. H., Zhao, Z. M., Si, Z. H., et al. (2019). Modified solid carbon sources with nitrate adsorption capability combined with nZVI improve the denitrification performance of constructed wetlands. *Bioresour. Technol.* 294:122189. doi: 10.1016/j.biortech.2019.122189

Zhao, X. Y., Yang, J. X., Bai, S. W., Ma, F., and Wang, L. (2016). Microbial population dynamics in response to bioaugmentation in a constructed wetland system under 10 degrees C. *Bioresour. Technol.* 205, 166–173. doi: 10.1016/j.biortech.2016.01.043

Zhao, Y. F., Zhao, Z. M., Song, X. S., Jiang, X. Y., Wang, Y. H., Cao, X., et al. (2020d). Effects of nZVI dosing on the improvement in the contaminant removal performance of constructed wetlands under the dye stress. *Sci. Total Environ.* 703:134789. doi: 10.1016/j.scitotenv.2019.134789

Zheng, Y. C., Liu, Y., Qu, M. W., Hao, M. Q., Yang, D., Yang, Q., et al. (2021b). Fate of an antibiotic and its effects on nitrogen transformation functional bacteria in integrated vertical flow constructed wetlands. *Chem. Eng. J.* 417:129272. doi: 10.1016/j.cej.2021.129272

Zheng, Y. C., Yang, D., Dzakpasu, M., Yang, Q., Liu, Y., Zhang, H. F., et al. (2020). Effects of plants competition on critical bacteria selection and pollutants dynamics in a long-term polyculture constructed wetland. *Bioresour. Technol.* 316:123927. doi: 10.1016/j.biortech.2020.123927

Zheng, C. Q., Zhang, X. W., Gan, L., He, Z. F., Zhu, J. L., Zhang, W., et al. (2021a). Effects of biochar on the growth of Vallisneria natans in surface flow constructed wetland. *Environ. Sci. Pollut. Res.* 28, 66158–66170. doi: 10.1007/s11356-021-15399-9

Zhou, Y., Tigane, T., Li, X., Truu, M., Truu, J., and Mander, Ü. (2013). Hexachlorobenzene dechlorination in constructed wetland mesocosms. *Water Res.* 47, 102–110. doi: 10.1016/j.watres.2012.09.030

Conflict of Interest: The authors declare that the research was conducted in the absence of any commercial or financial relationships that could be construed as a potential conflict of interest.

Publisher's Note: All claims expressed in this article are solely those of the authors and do not necessarily represent those of their affiliated organizations, or those of the publisher, the editors and the reviewers. Any product that may be evaluated in this article, or claim that may be made by its manufacturer, is not guaranteed or endorsed by the publisher.

frontiers | Frontiers in Microbiology

ORIGINAL RESEARCH
published: 16 May 2022
doi: 10.3389/fmicb.2022.844663

Fungi and Archaea Control Soil N_2O Production Potential in Chinese Grasslands Rather Than Bacteria

Lei Zhong[1], *Jinwu Qing*[1], *Min Liu*[2], *Xiaoxian Cai*[1], *Gaoyuan Li*[1], *Frank yonghong Li*[3], *Guanyi Chen*[1], *Xingliang Xu*[2,4], *Kai Xue*[4,5]* *and Yanfen Wang*[4,5]

[1] School of Environmental Science and Engineering, Tianjin University, Tianjin, China, [2] Key Laboratory of Ecosystem Network Observation and Modeling, Institute of Geographic Sciences and Natural Resources, Chinese Academy of Sciences, Beijing, China, [3] School of Ecology and Environment, Inner Mongolia University, Hohhot, China, [4] Chinese Academy of Sciences (CAS) Center for Excellence in Tibetan Plateau Earth Sciences, Chinese Academy of Sciences, Beijing, China, [5] College of Life Sciences, University of Chinese Academy of Sciences, Beijing, China

Nitrous oxide (N_2O) is a powerful greenhouse gas and the predominant stratospheric ozone-depleting substance. Soil is a major source of N_2O but remains largely uncertain due to the complicated processes of nitrification and denitrification performed by various groups of microbes such as bacteria, fungi, and archaea. We used incubation experiments to measure the total fungal, archaeal, and bacterial N_2O production potential and the microbial functional genes in soils along 3,000 km Chinese grassland transect, including meadow steppe, typical steppe, desert steppe, alpine meadow, and alpine steppe. The results indicated that fungi, archaea, and bacteria contributed 25, 34, and 19% to nitrification and 46, 29, and 15% to denitrification, respectively. The AOA and AOB genes were notably correlated with the total nitrification enzyme activity (TNEA), whereas both *narG* and *nirK* genes were significantly correlated with total denitrification enzyme activity (TDEA) at $p < 0.01$. The correlations between AOA and ANEA (archaeal nitrification enzyme activity), AOB and BNEA (bacterial nitrification enzyme activity), and *narG*, *nirK*, and BDEA (bacterial denitrification enzyme activity) showed higher coefficients than those between the functional genes and TNEA/TDEA. The structural equation modeling (SEM) results showed that fungi are dominant in N_2O production processes, followed by archaea in the northern Chinese grasslands. Our findings indicate that the microbial functional genes are powerful predictors of the N_2O production potential, after distinguishing bacterial, fungal, and archaeal processes. The key variables of N_2O production and the nitrogen (N) cycle depend on the dominant microbial functional groups in the N-cycle in soils.

Keywords: nitrification, denitrification, fungi, archaea, bacteria

OPEN ACCESS

Edited by:
Xiaojing Li,
Agro-Environmental Protection Institute (CAAS), China

Reviewed by:
Kai Ding,
Institute of Urban Environment (CAS), China
Anne E. Taylor,
Oregon State University, United States

***Correspondence:**
Kai Xue
xuekai@ucas.ac.cn

Specialty section:
This article was submitted to Microbiotechnology, a section of the journal Frontiers in Microbiology

Received: *28 December 2021*
Accepted: *06 April 2022*
Published: *16 May 2022*

Citation:
Zhong L, Qing J, Liu M, Cai X, Li G, Li Fy, Chen G, Xu X, Xue K and Wang Y (2022) Fungi and Archaea Control Soil N_2O Production Potential in Chinese Grasslands Rather Than Bacteria. Front. Microbiol. 13:844663. doi: 10.3389/fmicb.2022.844663

INTRODUCTION

Net primary productivity is usually restricted by nitrogen bioavailability in the terrestrial ecosystem (LeBauer and Treseder, 2008). Nonetheless, a fraction of available N can be lost *via* the N_2O flux from the soil, further aggravating the limitation of N. The emission of N_2O from the soil is mainly caused by the activity of nitrifiers and denitrifiers and contributes to 57% of the global N_2O emissions (Tian et al., 2019). As a powerful greenhouse gas, the warming potential of N_2O

is 300-fold stronger than that of carbon dioxide (Ravishankara et al., 2009). Consequently, several studies have been conducted to explore the emission of N_2O from terrestrial soils to determine its production and budget on a regional scale (Ravishankara et al., 2009; Attard et al., 2011; Cantarel et al., 2012; Zhong et al., 2014; Tian et al., 2019). However, global N_2O budgets remain largely uncertain due to the complicated microbial processes involving N_2O flux from soils (Skiba and Smith, 2000).

The nitrification and denitrification processes have been gradually identified (Arnold, 1954); for example, ammonia is converted to nitrite and then to nitrate by nitrifiers during nitrification. Subsequently, NO_3^- can be reduced to NO_2^- and then to NO and is finally transformed into N_2O and N_2 by denitrifiers during denitrification (Offre et al., 2013). Initially, microbial nitrification and denitrification were hypothesized to be mainly controlled by bacteria through functional genes (**Table 1**) (Stein, 2020). Most of these studies have been conducted in croplands or grasslands, which were managed or intermediate environments because the environments are more suitable for bacterial growth (Francis et al., 2007; Klotz and Stein, 2008). Meanwhile, more and more researches have been conducted to determine the relationship between microbial functional gene abundance and N_2O emission to accurately predict soil N_2O fluxes (Saleh-Lakha et al., 2009; Li et al., 2021). However, consistent relationships are seldom observed between them, suggesting that the gene abundance was not facilitating the prediction of N_2O fluxes from the soil (He et al., 2010; Attard et al., 2011; Zhong et al., 2014; Kou et al., 2019).

Recent research has reported that fungi and archaea also participate in the production of N_2O, following similar pathways to those of bacterial nitrification/denitrification. However, the process of fungal nitrification is still unclear, and fungal denitrification does not involve the reduction of nitrous oxide due to the absence of the *nos* gene (Wankel et al., 2017). Since the ammonia-oxidizing archaea were first observed in the oceans, archaeal nitrification has gained widespread attention and proved crucial in many habitats (Treusch et al., 2005; Leininger et al., 2006; Francis et al., 2007). Furthermore, Zhu et al. (2015) has also demonstrated that fungi also play an important role in nitrification and dominate the heterotrophic nitrification of acidic soils. Furthermore, the contribution of fungal denitrification to the N_2O production potential ranged from 17.0 to 89.1% in dryland or soil with high organic matter content (Zhong et al., 2018). This indicates that fungi and archaea could also play important roles in nitrification and denitrification due to their various environmental adaptabilities. However, few studies have quantified the contribution of bacteria, fungi, and archaea to N_2O production and their driving factors (Xu et al., 2017; Kaurin et al., 2018). Thus, the knowledge of the driving mechanisms of N_2O flux is limited, and the functional genes involved in soil N_2O fluxes are not well known. This might explain why previous studies using only the bacterial functional genes were unable to reach total N_2O production in the soil (Zhong et al., 2018).

Grassland accounts for about 20% of the global terrestrial land (DAHV CISNR, 1996). Grassland, which is the third largest ecosystem, occupies 41.70% of the land in China, with the presence of diverse grasslands and soil types across the north and northwest parts of China under various climates (DAHV CISNR, 1996; Wang and Fang, 2009). This provides a unique platform to examine N_2O production and clarify the roles of various microbial functional groups on a large scale (Liao and Jia, 1996). Previous studies demonstrated that soil moisture was the major factor in the N-cycle in Chinese grasslands due to the arid and semiarid climates, but the dominant microbes in soil N_2O production remain unknown (Zhong et al., 2014). To understand the role of bacteria, fungi, and archaea in the soil N-cycle, we quantified their contributions to N_2O production *via* the nitrification and denitrification processes and determined the relationships between archaeal, fungal, or bacterial functional genes and N_2O production potential in Chinese grassland soils over a large space. Based on previous studies, we hypothesize the following: (1) fungi and archaea play a major role in soil N_2O production since climatic and edaphic conditions are more suitable for them in the grasslands of Northern China (Zhong et al., 2014, 2018); (2) the differentiation of the bacterial, fungal, and archaeal N_2O production processes can increase the predictive power of microbial functional genes in soil N_2O production. Finally, we have also clarified the driving factors responsible for the production of N_2O in Chinese grasslands and have demonstrated that integrating the roles of bacteria, fungi, and archaea will remarkably improve the evaluation of the soil N_2O budget.

MATERIALS AND METHODS

Chinese Grassland Transects and Soil Sampling

Soil samples were collected from four stations in the Inner Mongolia grassland and four in the Tibet grassland (**Supplementary Table S1**), spanning nearly 20° in latitude (31°26′N−50°21′N), 30° in longitude (89°02′E−119°07′E), and 4,000 m in altitude range (618–4,700 m above sea level). The mean annual air temperature (MAT) on the grasslands varied from −2.6 to 2.1°C and −2.1 to 1.1°C in Inner Mongolia and Tibet grasslands, respectively. The mean annual precipitation (MAP) varied from 223 to 385 mm and 310 to 630 mm in the Inner Mongolia and Tibet grasslands, respectively (**Supplementary Table S1**).

The main grassland types in Inner Mongolia were meadow, typical, and desert steppe, which were from northeast to southwest. The typical steppe, also known as true steppe or dry steppe, occupies the largest and most contiguous extent of all the steppe ecosystem types in China and holds the central position in the ecological sequence of Chinese steppe grassland ecosystems (Li et al., 2020). The major grassland types in the Tibet Plateau were alpine meadow steppe, alpine steppe, and alpine desert steppe. The details of dominant plant species and soil types were the same as mentioned by Kou et al., 2019.

The soil samples were collected in triplicate in August 2017. Each time, five samples were mixed in equal proportions by three soil cores (10 cm in diameter) at a depth of 0–10 cm taken from each plot located along a diagonal line. All soil samples were

TABLE 1 | Enzymes and functional genes involved in microbial production and consumption of N_2O.

Progress	Organism	Enzyme	General reaction	Gene name(s)
Nitrification	AOB, AOA, comammox	Ammonia monooxygenase	$NH_3 \rightarrow NO_2^-$	*amo*
	AOB, comammox, anammox	Hydroxylamine dehydrogenase	$NH_2OH \rightarrow NO$	*hao*
	Comammox, NOB	Nitrite oxidoreductase	$NO_2^- \rightarrow NO_3^-$	*nxr*
Denitrification	Denitrifiers, denitrifying methanotrophs, ANME-2d	Nitrate reductase (dissimilatory)	$NO_3^- \rightarrow NO_2^-$	*nar*
	Denitrifiers, denitrifying methanotrophs, NC10, AOB, AOA, comammox, NOB, anammox	Nitrite reductase (dissimilatory)	$NO_2^- \rightarrow NO$	*nirS*, *nirK*
	Denitrifiers, denitrifying methanotrophs, (some) AOB	Nitric oxide reductase	$NO \rightarrow N_2O$	*nor*
	Denitrifiers, nondenitrifying N_2O reducers	Nitrous oxide reductase	$N_2O \rightarrow N_2$	*nosZ*

sieved, homogenized, and then divided into two fractions: one was air-dried for chemical analyses, and the other was preserved at −20°C for 2 weeks for enzyme and gene abundance analysis.

DNA Extraction and Measurement

To determine the soil levels of NO_3^--N and NH_4^+-N, the soil sample was extracted with KCl solution (2 mol/L), and then an Automated Ion Analyzer (Quickchem FIA Star 5010, LACHAT) was utilized. Gravimetric soil moisture (SM) was determined by the percentage of moisture content in the soil after oven-drying at 105°C for 24 h. The soil level analyses of total nitrogen (TN) and total carbon (TC) were carried out by the Kjeldahl method and the H_2SO_4-$K_2Cr_2O_7$ oxidation, respectively (Nelson et al., 2015).

We extracted soil DNA using the MoBio–DNA Kit according to the manufacturers' instructions. The DNA samples were kept at −20°C before the determination. The population sizes of ammonia monooxygenase, *amoA*-AOA, *amoA*-AOB, bacterial *nirK*, *nirS*, and *nosZ* clade I and II genes and of fungal *nirK* (*FnirK*) were measured using Q-PCR in triplicates. The primers are shown in **Supplementary Table S2**, and the method has been described in the study by Zhong et al. (2017, 2018).

The Nitrification Enzyme Activities

To determine the N_2O production potential from the total and the individual potentials of bacteria, fungi, and archaea, we determined the total (TNEA), bacterial (BNEA), fungal (FNEA), and archaeal (ANEA) nitrification enzyme activities using an improved method of Dassonville et al. (2011). In a 250 ml bottle, we added 80 ml of solution of $(NH_4)_2SO_4$ (50 μg N- g^{-1} dry soil) to offer the NH_4^+-N as the raw material for the nitrification process, then an equivalent amount of 10 g of fresh soil to dry soil was added. Each soil sample was divided into four treatment groups with three replications [all inhibitors' concentrations were determined by inhibitor additivity ratios (IAR) evaluation]: (1) bactericide (streptomycin sulfate, $C_{42}H_{84}N_{14}O_{36}S_3$) at 3.0 mg g^{-1}; (2) fungicide (cycloheximide, $C_{15}H_{23}NO_4$) at 1.5 mg g^{-1} (Castaldi and Smith, 1998; Laughlin and Stevens, 2002); (3) sterilized group (0.3 MPa and 121°C for 30 min) (Heil et al., 2015); and (4) no-inhibitor control. Then they were kept on a shaker at 28°C (180 rpm) for incubation, and a 10 ml of sample (soil slurry) was taken and filtered at 0, 24, and 48 h. An automated discrete analyzer (Smartchem 200, LACHAT) was used to analyze the $NO_3^- + NO_2^-$ density. Here, we define the NEA as the nitrification enzymatic activity rate, and k is equal to the slope of the time-dependent linear rate of the $NO_2^- + NO_3^-$ generation. Thus, TNEA (total NEA) = k (no-inhibitor control); BNEA (bacteria NEA) = TNEA – k (bactericide group); FNEA (fungi NEA) = TNEA – k (fungicide group); ANEA (archaea NEA) = TNEA – BDEA – FDEA – k (sterilized group).

The Denitrification Enzyme Activities

To determine the N_2O production potential from the total and the individual potentials of the bacteria, fungi, and archaea, we determined the total (TDEA), bacterial (BDEA), fungal (FDEA), and archaeal (ADEA) denitrification enzyme activities using the method proposed by Patra et al. (2006) and Marusenko et al. (2013). In a 250 ml bottle, we added 80 ml of solution of KNO_3 (50 μg N- g^{-1} dry soil), glutamic acid (0.5 mg C- g^{-1} dry soil), and glucose (0.5 mg C- g^{-1} dry soil) as raw materials for the denitrification process, then an equivalent amount of 10 g of fresh soil to dry soil was added. Each soil sample was divided into four treatment groups with three replications (all inhibitors' concentrations were determined by IAR evaluation): (1) bactericide (streptomycin sulfate, $C_{42}H_{84}N_{14}O_{36}S_3$) at 3.0 mg g^{-1}; (2) fungicide (cycloheximide, $C_{15}H_{23}NO_4$) at 1.5 mg g^{-1}; (3) sterilized group (0.3 MPa and 121°C for 30 min); and (4) no-inhibitor control. Also, the air at the bottle headspaces was replaced by the N_2 gas and C_2H_2 (10% v/v) to suppress the N_2O-to-N_2 reduction and maintain an anaerobic denitrification process. Then they were kept in a shaker at 28°C (180 rpm) for incubation, and a 10 ml gas sample was taken at 0, 24, and 48 h during the period and then used to analyze the N_2O concentration *via* gas chromatography. Here, we define the DEA as the denitrification enzymatic activity rate, and k is equal to the slope of the time-dependent linear rate of the N_2O generation. Thus, TDEA (total DEA) = k (no-inhibitor control); BDEA (bacteria DEA) = TDEA – k (bactericide group); FDEA (fungi DEA) = TDEA – k (fungicide group); ADEA (archaea DEA) = TDEA – BDEA – FDEA – k (sterilized group).

Inhibitor Additivity Ratios Evaluation

The concentrations of inhibitors mentioned above were determined using IAR evaluation (Bailey et al., 2003; Zhong et al., 2022). Therefore, it is sure that the concentrations of

inhibitors are sufficient to achieve the best inhibition and target the microbe without affecting other types of microorganisms. The incubation experimental conditions of the IAR evaluation are the same as those of the enzyme activity experiment. The IAR is estimated using the equation: IAR = [(A – B) + (A – C)] / (A – D). A is the no-inhibitor group, B is the bactericide group, C is the fungicide group, and D is the bactericide and fungicide group. Their values are equal to the slope of the time-dependent linear rate of the $NO_3^- + NO_2^-$ density or N_2O generation. The results of IAR are shown in **Supplementary Table S3**.

Verification of the Archaeal Nitrification and Denitrification Enzyme Activity

The archaeal nitrification and denitrification enzyme activities were estimated by calculating the difference between all treatments due to the lack of specific inhibitors for archaea. Zhao et al. (2020) reported simvastatin as a specific inhibitor of archaea; hence, we compared the accuracy of determining the archaeal nitrification and denitrification enzyme activities by the two methods.

We experimented with the parts of the "The nitrification enzyme activities" and "The denitrification enzyme activities" sections and added another treatment (5), wherein simvastatin ($C_{25}H_{38}O_5$, an archaea code) at 12.5 mg g^{-1} in solution was used to inhibit the nitrification and denitrification activities of the soil archaea. The nitrification and denitrification enzyme activities of the soil archaea were estimated by the difference between the rates of denitrification enzyme activity under treatments (4), (3), (2), and (1) as ANEA1 and ADEA1 and between treatments (4) and (5) as ANEA2 and ADEA2. The results are presented in **Supplementary Figure S1** to document the accuracy of our method.

Statistical Analyses

The random forest (RF) analysis was used to explore the most important predictors influencing the N_2O production potentials from nitrification and denitrification, using the program "random forest" in the statistical package R (Liaw and Wiener, 2002). The details were described in the study by Archer, 2021 and Evans and Murphy, 2019.

For a better understanding of the chemical, physical, and biological traits of soil, as well as the N_2O generation potentials, the structural equation modeling (SEM) was used considering all variables (MAP, MAT, soil pH, TC, TN, NH_4^+-N, NO_3^--N, TNEA, FNEA, ANEA, BNEA, TDEA, FDEA, ADEA, and BDEA). For a better model fit, we represented NH_4^+, NO_3^-, TC, and TN by the soil factors (SC) through the principal component analysis (PCA) aided by SPSS 18 to reduce the model variable number. Given the small sample number for the variable number per modeling ($n = 32$), the estimates were likely conservative and fit (Shipley et al., 2004; Kang and Shipley, 2009). The gene abundance was examined for statistical significance *via* one-way ANOVA; significant differences among 8 locations were further examined at a 0.05 level through Duncan's multirange test. The gene abundance was also examined for statistical significance using the Mann–Whitney U test, with significant differences between Tibet and Inner Mongolia ($p < 0.05$). The SEM model was employed in IBM® SPSS® AmosTM 20. The chi-squared (χ^2) test was applied to determine the difference between actual observed data and predicted by the model, and a p-value > 0.05 indicated no significant difference between the predicted and actual observed data. The coefficients were estimated by standardized coefficients then examined by analyzing correlation matrices and were considered significant when $p < 0.05$ (Petersen et al., 2012).

RESULTS

The Abundance of the N-Cycle Genes Across the Grassland Transect

The abundance of the functional microbial groups (bacteria: AOB, *narG*, *nirK*, *nirS*, *nosZ*, and *nosZ* clade II genes; archaea: AOA gene; and fungi: *nirK* gene) related to the N-cycle was measured (**Table 2**). However, the fungal *nirK* gene was not detected (**Supplementary Table S2**; **Table 2**). Across the grassland transect, there is a significant difference between Tibet and Inner Mongolia on AOA, AOB, *narG*, *nirK*, and *nirS* ($p < 0.05$, **Table 2**). The AOB and *narG* gene abundances ranged between 0 to 2.6×10^8 and 7.9×10^3 to 1.8×10^7 copies g $soil^{-1}$, respectively. The *nirK* and *nirS* genes copies ranged from 1.9×10^3 copies g $soil^{-1}$ at the Sonid Zuoq site to 1.8×10^7 copies g $soil^{-1}$ at the Hezuo site and from 1.8×10^3 copies g $soil^{-1}$ at the Sonid Zuoq site to 3.6×10^6 copies g $soil^{-1}$ at the Hulunbuir site, respectively. The abundances of the *nosZ* and *nosZ* clade II genes ranged from 4.7×10^6 to 2.4×10^7 and 0 to 6.8×10^5 copies g $soil^{-1}$, but the AOA gene abundance ranged from 1.6×10^4 to 9.6×10^8 copies g $soil^{-1}$ across all the sites. Among 8 sites, Sonid Zuoq site is the significantly lowest ($p < 0.05$) on all gene abundance; Hezuo site is the significantly highest ($p < 0.05$) on AOA, AOB, and *narG*; Haibei site is the significantly highest ($p < 0.05$) on *nirK*; Hulunbuir site is the significantly highest ($p < 0.05$) on *nirS*; Xilin Hot site is the significantly highest ($p < 0.05$) on *nosZ*; and Haibei, Hezuo, and Nagqu are significantly higher than Sonid Zuoq on *nosZ* clade II ($p < 0.05$). The fungal *nirK* gene was not determined in any of the sites across the grassland transect.

Nitrification and Denitrification Enzyme Activities Across the Grassland Transect

Across the Chinese grassland transect, the TNEA and TDEA in the soils varied from 0.03 to 3.34 and 0.05 to 4.77 μg N g^{-1} h^{-1}, respectively. The BNEA, FNEA, and ANEA varied from 0 to 0.88, 0 to 1.17, and 0.03 to 0.56 μg N g^{-1} h^{-1}, respectively. In comparison, the BDEA, FDEA, and ADEA varied from 0 to 0.92, 0 to 2.62, and 0.04 to 0.81 μg N g^{-1} h^{-1}, respectively. In the Tibetan grasslands, the NEA and DEA from bacteria, fungi, and archaea were much higher than in the Inner Mongolia grasslands, except for FNEA and BNEA in Baingoin (**Figure 1**).

The verification of the archaeal nitrification and denitrification enzyme activity showed no significant difference ($p > 0.05$) between these two methods, which agreed with our design and the results of the ANEA and ADEA methods.

TABLE 2 | Copy numbers of soil microbial functional nitrification and denitrification genes in grasslands.

	Gene copies g^{-1} soil	AOA*	AOB*	*narG**	*nirK**	*nirS*	*nosZ*	*nosZ* clade II
Tibet	Baingoin	4.2E8 ± 4.1E7**c**	1.3E6 ± 7.9E5**a**	5.1E6 ± 4.7E5**cd**	3.0E6 ± 5.6E5**cd**	3.0E5 ± 4.2E4**b**	3.2E4 ± 2.1E3**c**	6.3E6 ± 5.3E6**ab**
	Nagqu	6.6E8 ± 2.6 E7**d**	5.9E7 ± 2.2E7**b**	4.5E6 ± 6.0E5**cd**	5.0E6 ± 1.2E6**de**	3.6E5 ± 1.6E4**b**	1.9E5 ± 3.8E4**d**	1.6E7 ± 4.5E6**b**
	Hezuo	9.0E8 ± 7.6 E7**e**	2.6E8 ± 4.8E7**d**	1.8E7 ± 2.5E6**e**	8.1E6 ± 1.4E6**e**	1.6E6 ± 9.7E4**c**	4.3E5 ± 2.2E4**f**	1.8E7 ± 1.1E6**b**
	Haibei	9.6E8 ± 3.2 E7**e**	1.5E8 ± 1.2E7**c**	1.4E7 ± 2.5E6**e**	1.3E7 ± 1.8E6**f**	1.3E6 ± 2.4E5**c**	5.1E5 ± 3.9E4**g**	2.4E7 ± 1.3E7**b**
Inner magnolia	Duolun	1.6E4 ± 8.0 E3**a**	3.9E7 ± 1.2E7**b**	1.1E6 ± 9.7E5**b**	5.3E5 ± 1.1E5**b**	1.6E6 ± 5.4E5**c**	1.7E4 ± 4.0E3**b**	4.7E6 ± 1.9E6**ab**
	Sonid Zuoq	3.2E5 ± 7.4 E4**a**	0.0 ± 0.0**a**	7.9E3 ± 2.6E2**a**	1.9E3 ± 6.0E2**a**	1.8E3 ± 1.8E2**a**	0.0 ± 0.0**a**	5.1E3 ± 2.2E2**a**
	Xilin Hot	1.9E8 ± 1.8 E7**b**	7.0E7 ± 2.9E7**b**	6.8E6 ± 1.4E5**d**	2.2E6 ± 1.2E6**bc**	2.3E5 ± 5.2E4**b**	6.8E5 ± 3.0E4**h**	7.6E6 ± 3.0E6**ab**
	Hulunbuir	2.2E8 ± 4.7 E6**b**	1.6E6 ± 1.0E6**a**	3.1E6 ± 2.0E5**bc**	1.3E6 ± 2.1E5**bc**	3.6E6 ± 4.2E5**d**	3.3E5 ± 2.8E4**e**	5.7E6 ± 3.3E6**ab**

*The values represent means ± 1 SEM (n = 4) and followed by a different letter are significantly different between different sites (p < 0.05). With * mark means that there is a significant difference between Tibet and Inner Mongolia via the Mann–Whitney U test (p < 0.05).*

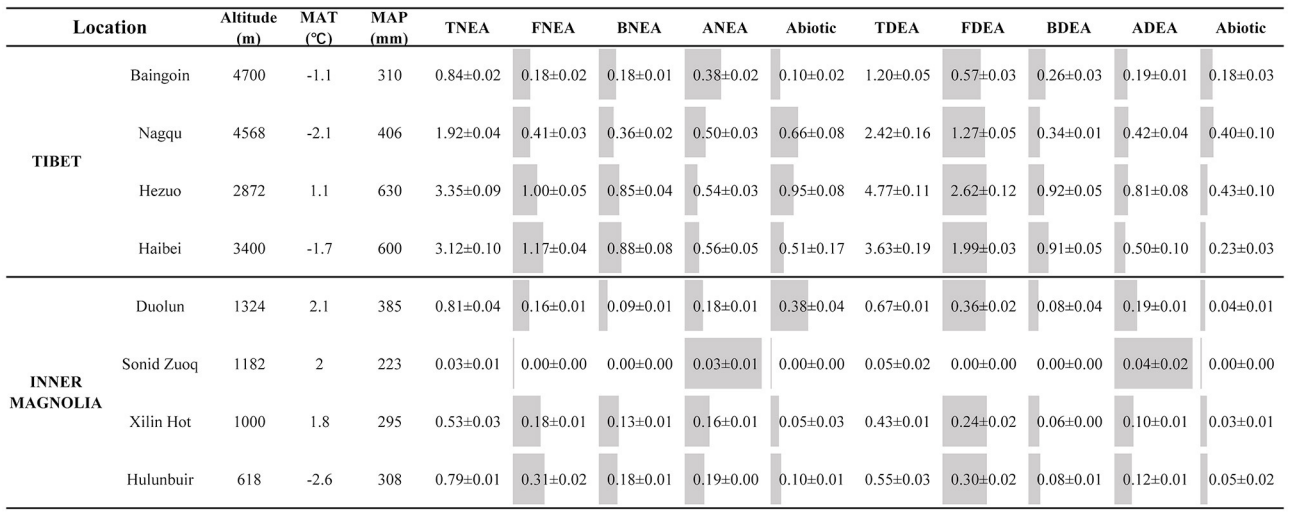

FIGURE 1 | The activities of nitrification and denitrification enzymes from fungi (FNEA and FDEA), bacteria (BNEA and BDEA), and archaea (ANEA and ADEA) and total nitrification and denitrification enzymes activities (TNEA and TDEA) at different sampling sites in grassland soils. The values represent means ± 1 SEM ($n = 4$). The length of the gray bar means the contribution percentage of fungi, bacteria, archaea, and abiotic on the total nitrification or denitrification enzymes activities (0% equal to 0 cm, 100% equal to cell width).

Correlations Between the Soil Factors and Gene Abundance, and Between the Gene Abundance and Enzyme Activities

The results revealed that the gene abundance was strongly associated with enzyme activities at the regional level, which is among 8 sites' regions (**Figure 2**). The abundance of AOA, AOB, *narG*, and *nirK* genes significantly correlated with all factors, except for the pH and AOA. The abundance of *nirS* significantly correlated with TC and TN. The *nosZ* gene was significantly correlated with TC, TN, NH_4^+-N, and NO_3^--N, whereas that of *nosZ* clade II was significantly correlated with SM, TC, TN, and NO_3^--N (**Figure 3C**).

Significant linear correlations were observed between the AOB genes, BNEA ($R^2 = 0.81$, $p < 0.01$) and TNEA ($R^2 = 0.51$, $p < 0.01$); between the AOA genes, ANEA ($R^2 = 0.71$, $p < 0.01$) and TNEA ($R^2 = 0.52$, $p < 0.01$); between the *narG* genes, BDEA ($R^2 = 0.72$, $p < 0.01$) and TNEA ($R^2 = 0.53$, $p < 0.01$); and between the *nirK* genes, BDEA ($R^2 = 0.61$, $P < 0.01$) and TNEA ($R^2 = 0.39$, $p < 0.01$). The predictive power of function genes was noticeable base on the significant linear correlations especially between microbial function genes with corresponding strain enzyme activities, e.g., AOA with ANEA. The *nirS*, *nosZ* +*nosZ* clade II gene abundances were not significantly correlated with BDEA or TDEA (**Figure 2**).

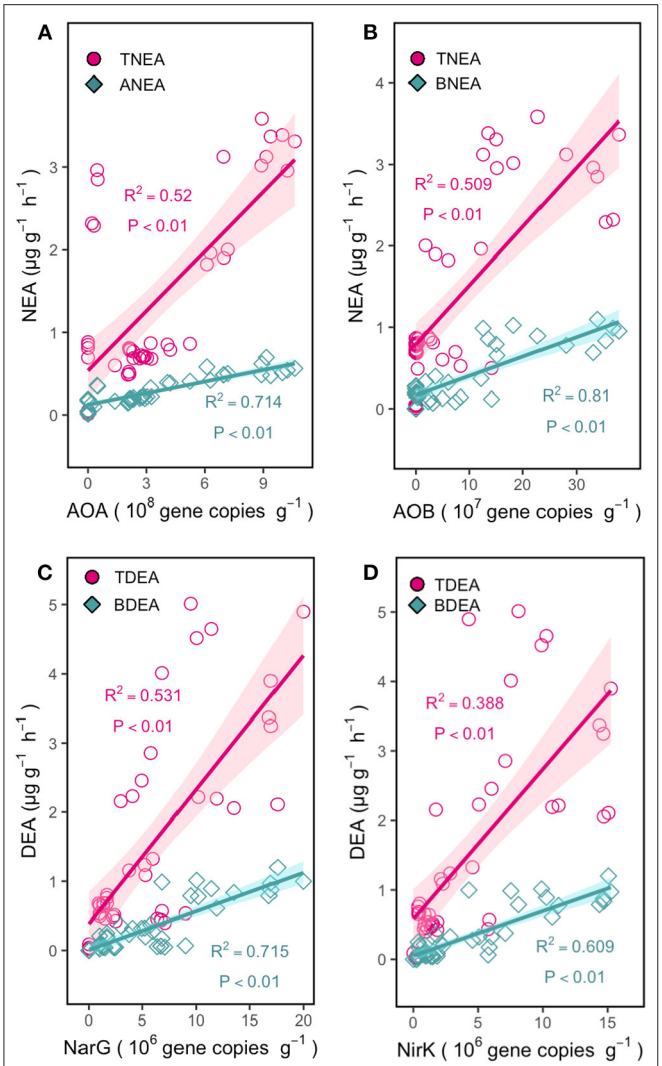

FIGURE 2 | Relationships between the abundance of AOA and TNEA or ANEA **(A)**; AOB and TNEA or BNEA **(B)**; *narG* and TDEA or BDEA **(C)**; *nirK* and TDEA or BDEA **(D)** in grassland soils. The R^2 values are the coefficients of determination.

Factors Controlling the Nitrification and Denitrification Process

The RF results showed that MAP was the foremost factor influencing the TNEA, FNEA, ANEA, TDEA, and FDEA. The TC, TN, and NH_4^+-N were also important influencers of BNEA, while the TC, TN, and NO_3^--N influenced BDEA. The AOA, AOB, and *nirK* genes were the foremost factor for ANEA, BNEA, and BDEA, respectively (**Figures 3A**, **4B**).

The soil factors (SC) were the data of TN, TC, NH_4^+-N, and NO_3^--N by principal component analysis (**Supplementary Figure S2**). The first principal components explained 68.9% of the total variance, suggesting that they could sufficiently describe the change in these data as soil factors. The primary model is presented in **Supplementary Figure S3**. The bacterial nitrification and denitrification could be assessed indirectly by quantifying the functional genes such as AOB, *narG*, and *nirK*. However, this approach could not assess the fungal or archaeal nitrification and denitrification because there were no fungal or archaeal functional genes related to nitrification and denitrification. As a result, to equally evaluate the relative importance of bacteria, fungi, and archaea to TNEA and TDEA, we did not include functional genes in the structural equation modeling.

The SEM results demonstrated fitting of the conceptual models for both TNEA and TDEA (**Figure 4A**, TNEA: $\chi^2 = 4.138$, d.f. $= 7$, $p = 0.598$; **Figure 4B**, TDEA: $\chi^2 = 5.365$, d.f. $= 7$, $p = 0.721$) to the observation data in the conventional system. For TNEA, FNEA was the foremost factor, followed by ANEA and BNEA. FNEA was explained by MAP and SC; BNEA was explained by SC, MAP, and soil pH. Similarly, for TDEA, FDEA was the most important controlling factor, followed by ADEA and BDEA. FDEA was explained by MAP, while BDEA was explained by SC. ANEA and ADEA had no relationship with other factors.

DISCUSSION

The Nitrification and Denitrification Gene Abundance

It was shown that the abundances of nitrification and denitrification genes revealed significant spatial heterogeneity in the Chinese grassland (**Table 2**). The abundances of the genes were higher in the Tibetan grassland as compared to the Inner Mongolian grassland, with the highest being at the Hezuo and Haibei sites and the lowest at the Sonid Zuoq site. This was in line with a previous study that also reported that the denitrification genes were the highest in the Tibetan grassland in China (Kou et al., 2019). This suggested that spatial heterogeneity may be a major driver of the changes in genes related to the nitrogen cycle. In our study, the relationship between soil moisture and AOA gene was the highest compared to that with other soil factors, whereas the bacterial nitrification and denitrification genes were more related to soil nutrients such as NH_4^+-N, NO_3^--N, TC, or TN content, compared to soil moisture and pH (**Figure 3C**). All these relationships proved that the soil properties were crucial in driving the variation in the genes involved in the nitrogen cycle, but the driving factors were different for different functional genes because the responses to the changes in environmental factors may be different (Che et al., 2018; Zhong et al., 2018).

The Contribution of Bacteria, Fungi, and Archaea to Nitrous Oxide Production Potential

Previous studies have demonstrated that fungi are powerful nitrifiers and denitrifiers in arid, semiarid, or acidic soils (Laughlin and Stevens, 2002; Marusenko et al., 2013; Zhu et al., 2015; Zhong et al., 2018), with some evidence demonstrating nitrification and denitrification by archaea (Jung et al., 2011; Li et al., 2020). However, the researchers only compared the relative importance of the bacterial and fungal N_2O production potential or between AOA and AOB genes. The contribution of bacteria,

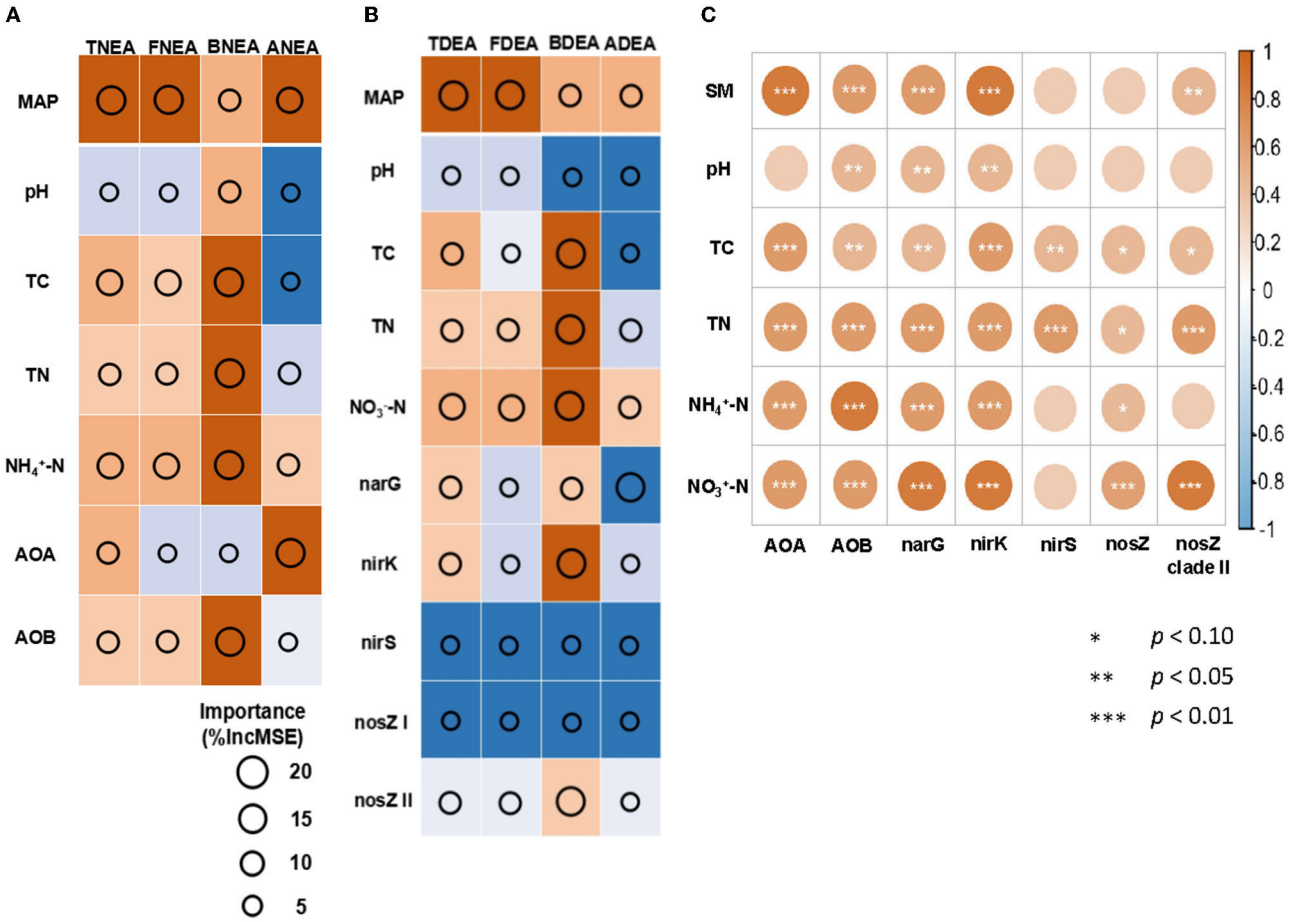

FIGURE 3 | Random forest (RF) models to identify the significant environmental factors and the abundance of nitrification genes controlling TNEA, FNEA, BENA, and ANEA **(A)**; the abundance of denitrification genes controlling TDEA, FDEA, BDEA, and ADEA **(B)**. The relationships between the physical and chemical properties of the soil and gene abundance **(C)**. The importance is calculated as the percentage (%) increase in the mean square error in RF models (%IncMSE). For **(A,B)**, the size of the circles indicates the importance of the environmental factors or the gene abundance for TNEA and TDEA. The text colored in orange represents adjusted $p < 0.05$; in blue represents adjusted $p > 0.05$, with the darker color indicating the lower or higher p-value, respectively. For **(C)**, the color shade indicated the coefficients of determination, * indicates $p < 0.10$, ** indicates $p < 0.05$, and *** indicates $p < 0.01$.

fungi, and archaea to N_2O production is still unclear. Here, we used soils collected along the Chinese grassland transect and incubated them to quantify their contributions. We observed that the fungi, archaea, and bacteria contributed 25, 34, and 19% to the nitrification potential and 46, 29, and 15% to the denitrification potential, respectively (**Figure 1**). It was confirmed that the first hypothesis is true: fungi and archaea play a major role in soil N_2O production and further suggested that fungi play a major role in N_2O production, followed by archaea and bacteria (**Figure 4**). However, fungal *nirK* and archaea denitrification genes were not found, but fungi and archaea are the important contributors to the denitrification progress, which proved that the existing primers we used (**Supplementary Table S2**) are not suitable in Chinese north grasslands soil; those primers are only successfully proved in agricultural soil (Duan et al., 2018; Lourenço et al., 2022; Zhong et al., 2022). It is partly in agreement with those studies that showed that the AOA was more important in nitrification than AOB in temperate grasslands (Che et al., 2018), and fungi dominated the nitrous oxide production processes in Tibet grasslands (Zhong et al., 2018). However, some researchers have found that AOA produce less N_2O than bacteria (Giguere et al., 2017; Waggoner et al., 2021), which is in contrast with our result. We believe that the different soil conditions can explain it; AOB has higher activities than AOA under high inorganic nutrients environment or artificial pasture (Zhong et al., 2014).

Regarding the Chinese north grasslands, minor contributions from bacterial nitrifiers and denitrifiers are ascribed to the low contents of inorganic nutrients or arid environment conditions in the temperate grasslands (Zhong et al., 2014), as well as the cold climate or high organic matter content in the alpine grasslands (Zhong et al., 2018). This is because bacteria generally have high gene abundance and activities in soils with high content of inorganic nutrients or relatively high moisture (Di et al., 2009; Yang et al., 2017). The average archaeal nitrification

rates were higher than fungal nitrification because FNEA and BNEA were closer to 0% and dominated by archaea due to the extreme drought at Sonid Zuoq (**Supplementary Table S1**). If the Sonid Zuoq site is excluded, the average FNEA would be higher than the archaeal nitrification across the Chinese grassland transect. Therefore, fungi and archaea are more important than bacteria for N_2O production process in both temperate and alpine grasslands.

The Prediction Ability of the Functional Gene Abundance to the Potential of Nitrous Oxide Emissions

Compared to the previous studies that used only bacterial functional genes, this study demonstrates that the gene abundance is a powerful predictor in the N_2O production process after integrating the bacterial and fungal genes. The archaeal processes of nitrification and denitrification (**Figure 2**), i.e., the correlations between the AOA and ANEA, AOB and BNEA, and *narG*, *nirK*, and BDEA were much higher than those between AOA, AOB, and TNEA or between *narG*, *nirK*, and TDEA (**Figure 2**). The RF model also confirms these results and shows the same trend (**Figure 3**). It is in line with previous research, which reported that the abundances of bacterial nitrifiers and denitrifiers are weak indicators for predicting the rates of total nitrification and denitrification (Attard et al., 2011; Zhong et al., 2014; Kou et al., 2019). The microbial functional groups and soil N transformation rates and/or N_2O emissions lack significant relationships, which is ascribed to using only the bacterial functional genes (Attard et al., 2011; Zhong et al., 2014; Kou et al., 2019). However, the contribution of bacteria to the N_2O potential is often much lower than those of fungi and archaea, as the latter have different adaptation strategies to environmental changes compared to bacteria, i.e., inorganic nutrients can significantly increase the abundance and activity of the AOB gene but have no effects on the AOA gene in an agroecosystem (Xiang et al., 2017). Besides, warming can increase the bacteria but decrease the fungal N_2O production potential in alpine grasslands (Zhong et al., 2018). All these studies show no or low correlation between the microbial functional genes and the total nitrification and denitrification rates. However, after we distinguished the bacterial, fungal, and archaeal N_2O production processes, the results of correlations analysis found a significant relationship between function genes with enzyme activities. Therefore, we confirm that the functional genes are powerful indexes to the potential of nitrous oxide prediction after distinguishing the bacterial, fungal, and archaeal N_2O production processes.

The Driving Factors Dominant the Nitrous Oxide Production Processes

To clarify the driving factors of bacterial, fungal, and archaeal N_2O production, the soil nitrous oxide production pathways were investigated by SEM analysis. It indicated that fungi represent a major source of N_2O production, followed by archaea. Several previous studies suggest that MAP or soil moisture play an important role in driving nitrification and denitrification in regions across the Chinese grassland transect, but they considered only the climate or soil properties (Wang et al., 2006; Zhong et al., 2014). Our results provide a different explanation: the MAP or soil moisture drives the N_2O production process, where fungi and archaea are the dominant microbes in the N_2O production process because they have also been reported to be the factors in the MAP in Chinese grassland.

The RF and SEM analysis confirmed that the MAP was the most important factor for fungal and archaeal nitrification and denitrification (**Figures 3**, **4**), which was the major contributor to the N_2O production potential. This indicates that MAP is a major driving factor in the N_2O production in Chinese grassland. On the other hand, our study also demonstrated that mainly bacterial nitrification and denitrification were explained by different factors compared to the processes of archaea and fungi. The BNEA and BDEA were largely controlled by SC instead of MAP at the regional scale (**Figures 3**, **4**). This finding was different from that observed in most studies on arid or semiarid grasslands, which reported that the bacterial functional genes, communities, or activities were mainly controlled by the MAP or soil moisture, as the grassland ecosystem was considered to be limited by water (Zhong et al., 2014, 2017). This might be explained by the higher sensitivity of bacterial nitrification and denitrification to changes in nutrient composition compared to soil moisture, even in semi-arid or alpine environmental conditions (Xiang et al., 2017). Therefore, our results highlight that it is necessary to describe the dominant microorganisms of the N_2O production process to know its driving mechanism in the ecosystem, which is fungi in our research.

Based on the above results, if the role of fungi and archaea in N_2O production is not accounted for, the evaluations of the budget of N_2O from the soil will be highly uncertain. Several classical models like DAYCENT or DNDC simulated the emission of N_2O with nitrification and denitrification modules (Ri et al., 2003; Del Grosso et al., 2005). Wu et al. (2015) used the SPACSYS model further to simulate the autotrophic/heterotrophic nitrification and denitrification and used its responses to environmental factors or nutrient availability to simulate of the N_2O flux. All these ecosystem-modeling procedures in the soil make a unique pool; therefore, it ignored the microbial type and generally assumed that the variations in the biogeochemical process can predict system behavior based on a simple hypothesis, which simply takes all microbes as one pool and regardless of how the identity and abundance of microbial communities' changes. In our view, this "black box" may be valid only if the N-cycle process was dominated and made up largely by bacteria; otherwise, it might be a major reason behind the uncertainty of these models (Allison and Martiny, 2008). The modeling of N_2O emission should further distinguish the bacterial, fungal, and archaeal nitrification and denitrification modules to improve the accuracy of the models (**Figure 5**). If so, the abundance of the microbial functional genes related to N_2O production can significantly improve the accuracy of N_2O prediction and can also be an important module of the models. On the contrary, while our study provides a novel insight into the models of N_2O emission, it has several limitations. First, we only demonstrated that the microbial functional genes were powerful indicators

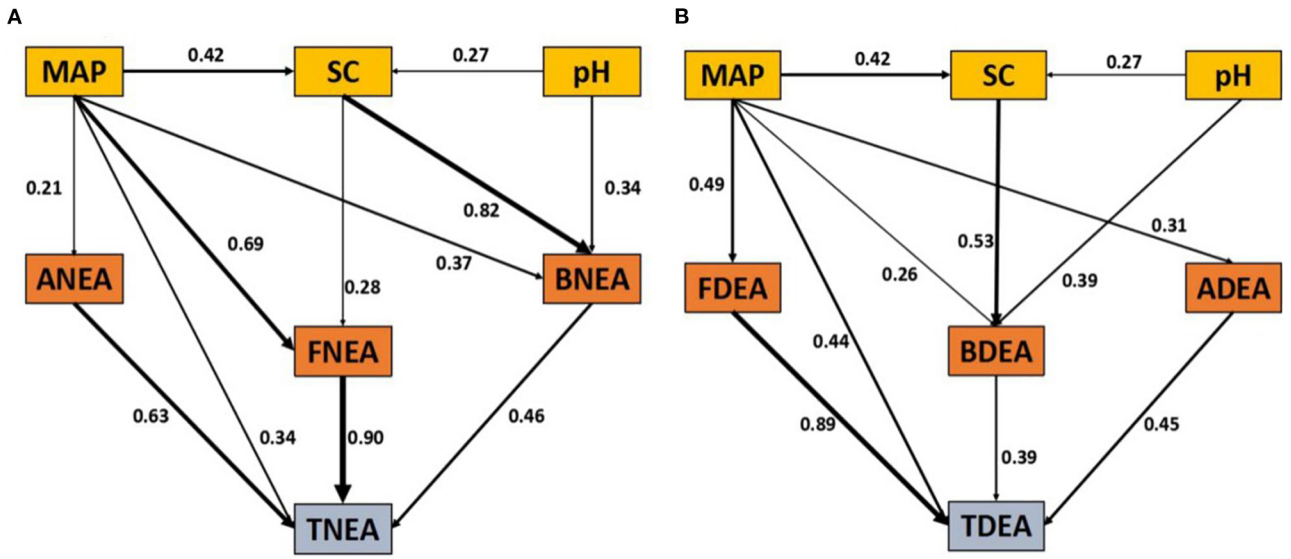

FIGURE 4 | Path plot of the final model, which depicts the pattern observations in both TNEA **(A)** and TDEA **(B)**. The coefficients related with arrows represent the coefficients for multiple linear regressions. SC, soil condition; MAP, mean annual precipitation; pH, soil pH. The number of the pathway is the coefficient with significant levels denoted ($p < 0.05$).

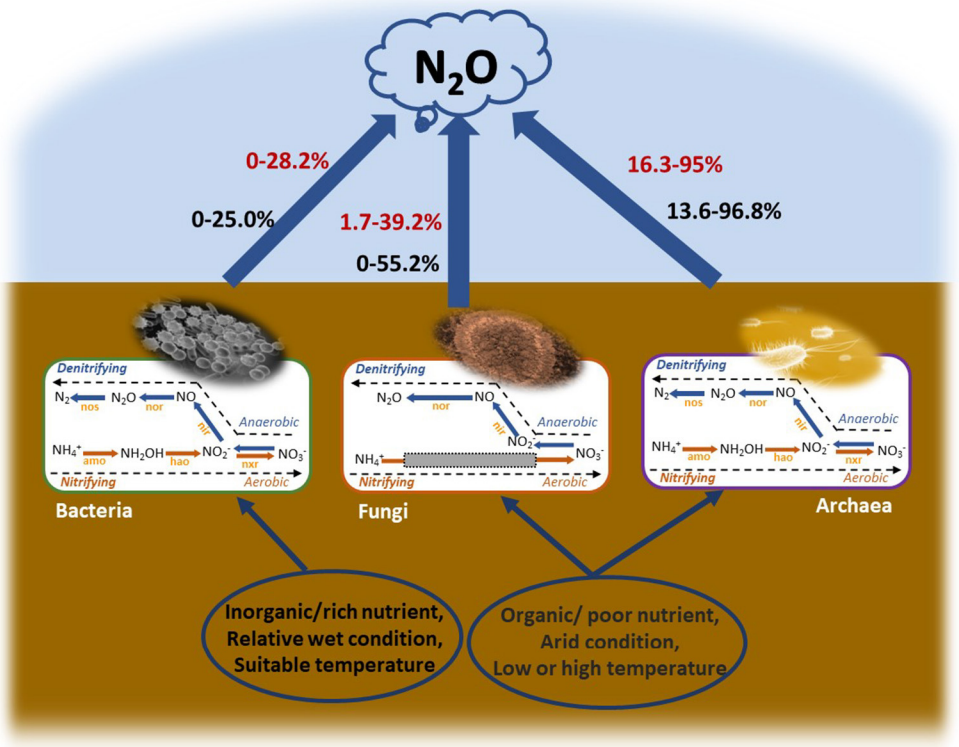

FIGURE 5 | Contribution and mechanisms of bacteria, fungi, and archaea to the N_2O production potential. The red color of the numbers represents the contribution of BNEA, FNEA, or ANEA to TNEA. The black color of the numbers represents the contribution of BDEA, FDEA, or ADEA to TDEA.

for predicting N_2O production potential after distinguishing the bacterial, fungal, and archaeal nitrification and denitrification. Improving the method to distinguish the N_2O flux of bacteria, fungi, and archaea is important for improving the model. Secondly, irrespective of the metagenomic sequencing, geochip, or Q-PCR, the results were mainly based on the bacterial microbial functional genes. In contrast, the fungal, and particularly the archaeal functional genes, were studied less due to the lack of the primers for fungal *nirK* genes suitable for grassland soil and the lack of clarity regarding fungal nitrification (Vogel et al., 2009; Gao et al., 2020), and also lack of clarity regarding archaea denitrification, which only a few cultured archaea are capable of denitrification (Torregrosa-Crespo et al., 2016). Therefore, it is important to reveal the fungal nitrification process and design more primers for the fungal and archaeal functional genes related to the N_2O production process and then promote the microbial module to improve the accuracy of the models further.

CONCLUSION

We demonstrate that fungi and archaea play dominant roles in the N_2O production process in the grasslands of North China. It is suggested that the microbial functional genes are powerful indicators for predicting N_2O production potential after distinguishing the bacterial, fungal, and archaeal N_2O production processes. Besides, the key controlling variable on N_2O production and N-cycle depends on the dominant microorganisms of the N-cycle in soils. Therefore, accurate predictions for N_2O production and contribution to the development of the ecosystem N-cycle models will benefit from distinguishing the bacterial, fungal, and archaeal N-cycle process.

DATA AVAILABILITY STATEMENT

The raw data supporting the conclusions of this article will be made available by the authors, without undue reservation.

AUTHOR CONTRIBUTIONS

LZ: conceptualization, methodology, and writing—original draft. JQ: investigation and writing—review and editing. ML: visualization. XC and GL: writing—review and editing. FL: data curation. GY: resources. XX: formal analysis. KX and YW: methodology, validation, and supervision. All authors contributed to the article and approved the submitted version.

FUNDING

This research was funded by the Tianjin Science and Technology Committee (Grant No. 19JCQNJC13900) and the National Natural Science Foundation of China (No. 41601245).

SUPPLEMENTARY MATERIAL

The Supplementary Material for this article can be found online at: https://www.frontiersin.org/articles/10.3389/fmicb.2022.844663/full#supplementary-material

REFERENCES

Allison, S. D., and Martiny, J. B. H. (2008). Resistance, resilience, and redundancy in microbial communities. *Proc. Natl. Acad. Sci. U. S. A.* 105, 11512–11519. doi: 10.1073/pnas.0801925105

Archer, E. (2021). *Estimate Permutation p-Values for Random Forest Importance Metrics [R package rfPermute version 2.5]*. Available online at: https://CRAN.R-project.org/package=rfPermute (accessed March 10, 2022).

Arnold, P. W. (1954). Losses of nitrous oxide from soil. *J. Soil Sci.* 5, 16–128. doi: 10.1111/j.1365-2389.1954.tb02180.x

Attard, E., Recous, S., Chabbi, A., Berranger, C., de, Guillaumaud, N., Labreuche, J., et al. (2011). Soil environmental conditions rather than denitrifier abundance and diversity drive potential denitrification after changes in land uses. *Glob. Chang. Biol.* 17, 1975–1989. doi: 10.1111/j.1365-2486.2010.02340.x

Bailey, V. L., Smith, J. L., and Bolton, H. (2003). Novel antibiotics as inhibitors for the selective respiratory inhibition method of measuring fungal:bacterial ratios in soil. *Biol. Fertil. Soils* 38, 154–160. doi: 10.1007/s00374-003-0620-7

Cantarel, A. A. M., Bloor, J. M. G., Pommier, T., Guillaumaud, N., Moirot, C., Soussana, J. F., et al. (2012). Four years of experimental climate change modifies the microbial drivers of N2O fluxes in an upland grassland ecosystem. *Glob. Chang. Biol.* 18, 2520–2531. doi: 10.1111/j.1365-2486.2012.02692.x

Castaldi, S., and Smith, K. A. (1998). Effect of cycloheximide on N2O and NO3/- production in a forest and an agricultural soil. *Biol. Fertil. Soils* 27, 27–34. doi: 10.1007/s003740050395

Che, R., Qin, J., Tahmasbian, I., Wang, F., Zhou, S., Xu, Z., et al. (2018). Litter amendment rather than phosphorus can dramatically change inorganic nitrogen pools in a degraded grassland soil by affecting nitrogen-cycling microbes. *Soil Biol. Biochem.* 120, 145–152. doi: 10.1016/j.soilbio.2018.02.006

DAHV and CISNR (1996). *Rangeland Resources of China*. Beijing: China Agricultural Science and Technology. Department of Animal Husbandry and Veterinary, Institute of Grasslands, Chinese Academy of Agricultural Sciences, Commission for Integrated Survey of Natural Resources, Chinese Academy of Sciences.

Dassonville, N., Guillaumaud, N., Piola, F., Meerts, P., and Poly, F. (2011). Niche construction by the invasive Asian knotweeds (species complex Fallopia): impact on activity, abundance and community structure of denitrifiers and nitrifiers. *Biol. Invasions* 13, 1115–1133. doi: 10.1007/s10530-011-9954-5

Del Grosso, S. J., Mosier, A. R., Parton, W. J., and Ojima, D. S. (2005). DAYCENT model analysis of past and contemporary soil N2O and net greenhouse gas flux for major crops in the USA. *Soil Tillage Res.* 83, 9–24. doi: 10.1016/j.still.2005.02.007

Di, H. J., Cameron, K. C., Shen, J. P., Winefield, C. S., Ocallaghan, M., Bowatte, S., et al. (2009). Nitrification driven by bacteria and not archaea in nitrogen-rich grassland soils. *Nat. Geosci.* 2, 621–624. doi: 10.1038/ngeo613

Duan, P., Zhang, X., Zhang, Q., Wu, Z., and Xiong, Z. (2018). Field-aged biochar stimulated N2O production from greenhouse vegetable production soils by nitrification and denitrification. *Sci. Total Environ.* 642, 1303–1310. doi: 10.1016/j.scitotenv.2018.06.166

Evans, J. S., and Murphy, M. A. (2019). *rfUtilities: Random Forests Model Selection and Performance Evaluation*. Available online at: https://cran.r-project.org/web/packages/rfUtilities/index.html (accessed October 3, 2019).

Francis, C. A., Beman, J. M., and Kuypers, M. M. M. (2007). New processes and players in the nitrogen cycle: the microbial ecology of anaerobic and archaeal ammonia oxidation. *ISME J.* 1, 19–27. doi: 10.1038/ismej.2007.8

Gao, Q., Wang, G., Xue, K., Yang, Y., Xie, J., Yu, H., et al. (2020). Stimulation of soil respiration by elevated CO2 is enhanced under nitrogen limitation in a decade-long grassland study. *Proc. Natl. Acad. Sci. U. S. A.* 117, 33317–33324. doi: 10.1073/pnas.2002780117

Giguere, A. T., Taylor, A. E., Suwa, Y., Myrold, D. D., and Bottomley, P. J. (2017). Uncoupling of ammonia oxidation from nitrite oxidation: impact upon nitrous

oxide production in non-cropped Oregon soils. *Soil Biol. Biochem*. 104, 30–38. doi: 10.1016/j.soilbio.2016.10.011

He, Z., Xu, M., Deng, Y., Kang, S., Kellogg, L., Wu, L., et al. (2010). Metagenomic analysis reveals a marked divergence in the structure of belowground microbial communities at elevated CO2. *Ecol. Lett.* 13, 564–575. doi: 10.1111/j.1461-0248.2010.01453.x

Heil, J., Liu, S., Vereecken, H., and Brüggemann, N. (2015). Abiotic nitrous oxide production from hydroxylamine in soils and their dependence on soil properties. *Soil Biol. Biochem.* 84, 107–115. doi: 10.1016/j.soilbio.2015.02.022

Jung, M. Y., Park, S. J., Min, D., Kim, J. S., Rijpstra, W. I. C., Damst,é, J. S. S., et al. (2011). Enrichment and characterization of an autotrophic ammonia-oxidizing archaeon of mesophilic crenarchaeal group I.1a from an agricultural soil. *Appl. Environ. Microbiol.* 77, 8635–8647. doi: 10.1128/AEM.05787-11

Kang, C., and Shipley, B. (2009). A new inferential test for path models based on directed acyclic graphs. *Struct. Equ. Model. Multidisci. J.* 16, 537–538. doi: 10.1080/10705510903008279

Kaurin, A., Miheli,č, R., Kastelec, D., Grčman, H., Bru, D., Philippot, L., et al. (2018). Resilience of bacteria, archaea, fungi and N-cycling microbial guilds under plough and conservation tillage, to agricultural drought. *Soil Biol. Biochem.* 120, 233–245. doi: 10.1016/j.soilbio.2018.02.007

Klotz, M. G., and Stein, L. Y. (2008). Nitrifier genomics and evolution of the nitrogen cycle. *FEMS Microbiol. Lett.* 278, 146–156. doi: 10.1111/j.1574-6968.2007.00970.x

Kou, Y., Li, C., Li, J., Tu, B., Wang, Y., and Li, X. (2019). Climate and soil parameters are more important than denitrifier abundances in controlling potential denitrification rates in Chinese grassland soils. *Sci. Total Environ.* 669, 62–69. doi: 10.1016/j.scitotenv.2019.03.093

Laughlin, R. J., and Stevens, R. J. (2002). Evidence for fungal dominance of denitrification and codenitrification in a grassland soil. *Soil Sci. Soc. Am. J.* 66, 1540–1548. doi: 10.2136/sssaj2002.1540

LeBauer, D. S., and Treseder, K. K. (2008). Nitrogen limitation of net primary productivity in terrestrial ecosystems is globally distributed. *Ecology* 89, 371–379. doi: 10.1890/06-2057.1

Leininger, S., Urich, T., Schloter, M., Schwark, L., Qi, J., Nicol, G. W., et al. (2006). Archaea predominate among ammonia-oxidizing prokaryotes in soils. *Nature* 442, 806–809. doi: 10.1038/nature04983

Li, Z., Li, L., Xia, S., Zhang, R., Zhang, R., Chen, P., et al. (2021). K fertilizer alleviates N2O emissions by regulating the abundance of nitrifying and denitrifying microbial communities in the soil-plant system. *J. Environ. Manage.* 291, 112579. doi: 10.1016/j.jenvman.2021.112579

Li, L., Chen, J., Han, X., Zhang, W., and Shao, C. (2020). "Typical steppe ecosystem," in *Grassland Ecosystems of China. Ecosystems of China*. Gan, J editor. Vol. 2. (Singapore: Springer).

Liao, G. F., and Jia, Y. L. (1996). *Rangeland Resources of China*. Beijing: Chinese Science and Technology Press, 7–12.

Liaw, A., and Wiener, M. (2002). Classification and regression by randomForest. *R news* 2, 18–22.

Lourenço, K. S., Costa, O. Y., de, A., Cantarella, H., and Kuramae, E. E. (2022). Ammonia-oxidizing bacteria and fungal denitrifier diversity are associated with N2O production in tropical soils. *Soil Biol. Biochem*. 166, 108563. doi: 10.1016/j.soilbio.2022.108563

Marusenko, Y., Huber, D. P., and Hall, S. J. (2013). Fungi mediate nitrous oxide production but not ammonia oxidation in aridland soils of the southwestern US. *Soil Biol. Biochem.* 63: 24–36 doi: 10.1016/j.soilbio.2013.03.018

Nelson, D. W., and Sommers, L. E. (2015). *Total Carbon, Organic Carbon, and Organic Matter*, Madison.

Offre, P., Spang, A., and Schleper, C. (2013). Archaea in biogeochemical cycles. *Annu. Rev. Microbiol.* 67, 437–457. doi: 10.1146/annurev-micro-092412-155614

Patra, A. K., Abbadie, L., Clays-Josserand, A., Degrange, V., Grayston, S. J., Guillaumaud, N., et al. (2006). Effects of management regime and plant species on the enzyme activity and genetic structure of N-fixing, denitrifying and nitrifying bacterial communities in grassland soils. *Environ. Microbiol.* 8, 1005–1016. doi: 10.1111/j.1462-2920.2006.00992.x

Petersen, D. G., Blazewicz, S. J., Firestone, M., Herman, D. J., Turetsky, M., and Waldrop, M. (2012). Abundance of microbial genes associated with nitrogen cycling as indices of biogeochemical process rates across a vegetation gradient in Alaska. *Environ. Microbiol.* 14, 993–1008. doi: 10.1111/j.1462-2920.2011.02679.x

Ravishankara, A. R., Daniel, J. S., and Portmann, R. W. (2009). Nitrous oxide (N2O): The dominant ozone-depleting substance emitted in the 21st century. *Science* 326, 123–125. doi: 10.1126/science.1176985

Ri, X., Wang, Y., Zheng, X., Ji, B., and Wang, M. (2003). A comparison between measured and modeled N2O emissions from Inner Mongolian semiarid grassland. *Plant Soil* 255, 513–528. doi: 10.1023/A:1026076914167

Saleh-Lakha, S., Shannon, K. E., Henderson, S. L., Zebarth, B. J., Burton, D. L., Goyer, C., et al. (2009). Effect of nitrate and acetylene on nirS, cnorB, and nosZ expression and denitrification activity in P*seudomonas mandelii*. *Appl. Environ. Microbiol.* 75, 5082–5087. doi: 10.1128/AEM.00777-09

Shipley, B. (2004). *Cause and Correlation in Biology A User's Guide to Path Analysis, Structural Equations and Causal Inference*, Cambridge: Cambridge University Press.

Skiba, U., and Smith, K. A. (2000). The control of nitrous oxide emissions from agricultural and natural soils. *Chemosphere Global Change Sci.* 2, 379–386. doi: 10.1016/S1465-9972(00)00016-7

Stein, L. Y. (2020). The long-term relationship between microbial metabolism and greenhouse gases. *Trends Microbiol.* 28, 500–511. doi: 10.1016/j.tim.2020.01.006

Tian, H., Yang, J., Xu, R., Lu, C., Canadell, J. G., Davidson, E. A., et al. (2019). Global soil nitrous oxide emissions since the preindustrial era estimated by an ensemble of terrestrial biosphere models: Magnitude, attribution, and uncertainty. *Glob. Chang. Biol.* 25, 640–659. doi: 10.1111/gcb.14514

Torregrosa-Crespo, J., Martínez-Espinosa, R. M., Esclapez, J., Bautista, V., Pire, C., Camacho, M., et al. (2016). Anaerobic metabolism in haloferax genus: denitrification as case of study. *Adv. Microb. Physiol.* 68, 41–85. doi: 10.1016/bs.ampbs.2016.02.001

Treusch, A. H., Leininger, S., Kletzin, A., Schuster, S. C., Klenk, H. P., and Schleper, C. (2005). Novel genes for nitrite reductase and Amo-related proteins indicate a role of uncultivated mesophilic crenarchaeota in nitrogen cycling. *Environ. Microbiol.* 7, 1985–1995. doi: 10.1111/j.1462-2920.2005.00906.x

Vogel, T. M., Simonet, P., Jansson, J. K., Hirsch, P. R., Tiedje, J. M., van Elsas, J. D., et al. (2009). TerraGenome: a consortium for the sequencing of a soil metagenome. *Nat. Rev. Microbiol.* 7, 252. doi: 10.1038/nrmicro2119

Waggoner, A. L., Bottomley, P. J., Taylor, A. E., and Myrold, D. D. (2021). Soil nitrification response to dairy digestate and inorganic ammonium sources depends on soil pH and nitrifier abundances. *Soil Sci. Soc. Am. J.* 85, 1990–2006. doi: 10.1002/saj2.20325

Wang, C., Wan, S., Xing, X., Zhang, L., and Han, X. (2006). Temperature and soil moisture interactively affected soil net N mineralization in temperate grassland in Northern China. *Soil Biol. Biochem.* 38, 1101–1110. doi: 10.1016/j.soilbio.2005.09.009

Wang, W., and Fang, J. (2009). Soil respiration and human effects on global grasslands. *Glob. Planet. Change* 67, 20–28. doi: 10.1016/j.gloplacha.2008.12.011

Wankel, S. D., Ziebis, W., Buchwald, C., Charoenpong, C., Beer, D.i., de, Dentinger, J., et al. (2017). Evidence for fungal and chemodenitrification based N2O flux from nitrogen impacted coastal sediments. *Nat. Commun.* 8, 1–11. doi: 10.1038/ncomms15595

Wu, L., Rees, R. M., Tarsitano, D., Zhang, X., Jones, S. K., and Whitmore, A. P. (2015). Simulation of nitrous oxide emissions at field scale using the SPACSYS model. *Sci. Total Environ.* 530–531, 76–86. doi: 10.1016/j.scitotenv.2015.05.064

Xiang, X., He, D., He, J. S., Myrold, D. D., and Chu, H. (2017). Ammonia-oxidizing bacteria rather than archaea respond to short-term urea amendment in an alpine grassland. *Soil Biol. Biochem.* 107, 218–225. doi: 10.1016/j.soilbio.2017.01.012

Xu, X., Liu, X., Li, Y., Ran, Y., Liu, Y., Zhang, Q., et al. (2017). High temperatures inhibited the growth of soil bacteria and archaea but not that of fungi and altered nitrous oxide production mechanisms from different nitrogen sources in an acidic soil. *Soil Biol. Biochem.* 107, 168–179. doi: 10.1016/j.soilbio.2017.01.003

Yang, L., Zhang, X., and Ju, X. (2017). Linkage between N2O emission and functional gene abundance in an intensively managed calcareous fluvo-aquic soil. *Sci. Rep.* 7, 43283. doi: 10.1038/srep43283

Zhao, J., Bello, M. O., Meng, Y., Prosser, J. I., and Gubry-Rangin, C. (2020). Selective inhibition of ammonia oxidising archaea by simvastatin stimulates growth of ammonia oxidising bacteria. *Soil Biol. Biochem.* 141, 107673. doi: 10.1016/j.soilbio.2019.107673

Zhong, L., Du, R., Ding, K., Kang, X., Li, F. Y., Bowatte, S., et al. (2014). Effects of grazing on N2O production potential and abundance of nitrifying and denitrifying microbial communities in meadow-steppe grassland in northern China. *Soil Biol. Biochem.* 69, 1–10. doi: 10.1016/j.soilbio.2013.10.028

Zhong, L., Li, G., Qing, J., Li, J., Xue, J., Yan, B., et al. (2022). Biochar can reduce N2O production potential from rhizosphere of fertilized agricultural soils by suppressing bacterial denitrification. *Eur. J. Soil Biol.* 109, 103391. doi: 10.1016/j.ejsobi.2022.103391

Zhong, L., Wang, S., Xu, X., Wang, Y., Rui, Y., Zhou, X., et al. (2018). Fungi regulate the response of the N2O production process to warming and grazing in a Tibetan grassland. *Biogeosciences* 15, 4447–4457. doi: 10.5194/bg-15-4447-2018

Zhong, L., Zhou, X., Wang, Y., Li, F. Y., Zhou, S., Bai, Y., et al. (2017). Mixed grazing and clipping is beneficial to ecosystem recovery but may increase potential N2O emissions in a semi-arid grassland. *Soil Biol. Biochem.* 114, 42–51. doi: 10.1016/j.soilbio.2017.07.002

Zhu, T., Meng, T., Zhang, J., Zhong, W., Müller, C., and Cai, Z. (2015). Fungi-dominant heterotrophic nitrification in a subtropical forest soil of China. *J. Soils Sediments* 15, 705–709. doi: 10.1007/s11368-014-1048-4

Conflict of Interest: The authors declare that the research was conducted in the absence of any commercial or financial relationships that could be construed as a potential conflict of interest.

The reviewer KD declared a shared affiliation with the author ML, XX, and YW at the time of the review.

Publisher's Note: All claims expressed in this article are solely those of the authors and do not necessarily represent those of their affiliated organizations, or those of the publisher, the editors and the reviewers. Any product that may be evaluated in this article, or claim that may be made by its manufacturer, is not guaranteed or endorsed by the publisher.

Advantages of publishing in Frontiers

OPEN ACCESS
Articles are free to read for greatest visibility and readership

FAST PUBLICATION
Around 90 days from submission to decision

HIGH QUALITY PEER-REVIEW
Rigorous, collaborative, and constructive peer-review

TRANSPARENT PEER-REVIEW
Editors and reviewers acknowledged by name on published articles

Frontiers
Avenue du Tribunal-Fédéral 34
1005 Lausanne | Switzerland

Visit us: www.frontiersin.org
Contact us: frontiersin.org/about/contact

REPRODUCIBILITY OF RESEARCH
Support open data and methods to enhance research reproducibility

DIGITAL PUBLISHING
Articles designed for optimal readership across devices

FOLLOW US
@frontiersin

IMPACT METRICS
Advanced article metrics track visibility across digital media

EXTENSIVE PROMOTION
Marketing and promotion of impactful research

LOOP RESEARCH NETWORK
Our network increases your article's readership